

## ABSTRACT

Title of Document: CURVED INTEGRAL ABUTMENT BRIDGES  
Narong Thanasattayawibul, Doctor of Philosophy, 2006

Directed By: Professor Amde M. Amde  
Department of Civil and Environmental Engineering

Traditionally, expansion joints, expansion bearings, and other structural release mechanisms have been used on long, multi-span highway bridges to accommodate thermal movements of the bridge superstructure. However, joint systems are a major cause of extensive maintenance and expensive rehabilitation work on bridges.

Straight integral abutment bridges (straight IAB's) and IAB's with varying skew angles have been studied by many researchers in recent years. This study focuses on horizontally curved steel I-girder IAB's with a degree of curvature ranging from 0 degree to 172 degrees based on a 1200 ft bridge length. A three-dimensional non-linear finite element model is used to perform parametric study to investigate the effect of different parameters on the behavior of curved steel I-girder IAB's. Parameters that are used in this study include: bridge length, temperature, soil profile type, span length, radius, and pile type.

Over 1,700 finite element bridge models were studied, and each model considered the complete bridge including the superstructure, substructure and soil. The behavior of piles in curved IAB's was also studied. Recommendations are made for design of IAB bridges as well as piles in IAB's.

CURVED INTEGRAL ABUTMENT BRIDGES

By

Narong Thanasattayawibul

Dissertation submitted to the Faculty of the Graduate School of the  
University of Maryland, College Park, in partial fulfillment  
of the requirements for the degree of  
Doctor of Philosophy  
2006

Advisory Committee:  
Professor Amde M. Amde, Chair/Advisor  
Professor M. Sherif Aggour  
Professor Donald W. Vannoy  
Affiliate Associate Professor Chung C. Fu  
Professor Sung W. Lee

© Copyright by  
Narong Thanasattayawibul  
[2006]

## DEDICATION

To my father Sakol, my mother Chusri, my sisters, Doungsamorn and Porntip.

## ACKNOWLEDGEMENTS

I would like to express my deep gratitude to Professor Amde M. Amde whom under his supervision this study was performed. His technical and advice proved to be superior. Without his financial support, this research would not have had the depth and breadth it has achieved.

I would like to thank to the members of my doctoral committee, Professor M. Sherif Aggour, Professor Donald W. Vannoy, Affiliate Associate Professor Chung C. Fu, and Professor Sung W. Lee for kindly serving on my committee.

# TABLE OF CONTENTS

DEDICATION.....	ii
ACKNOWLEDGEMENTS.....	iii
LIST OF TABLES.....	vii
LIST OF FIGURES.....	xv
1 INTRODUCTION.....	1
1.1 Introduction.....	1
1.2 Background.....	6
1.2.1 Design of Integral Abutment Bridges.....	7
1.2.2 Performance of Integral Abutment Bridges.....	8
1.3 Statement of the Problem.....	12
1.3.1 Secondary Effects.....	13
1.3.2 Thermal Gradients.....	13
1.3.3 Straight Bridges with Integral Abutments.....	14
1.3.4 Skewed Bridges with Integral Abutments.....	15
1.4 Objectives and Scope.....	17
2 TEMPERATURE IN COMPOSITE BRIDGES.....	18
2.1 Introduction.....	18
2.2 Thermal Movements.....	19
2.3 Analysis of Thermal Movements.....	21
2.3.1 Radiation.....	21
2.3.2 Convection.....	24
2.3.3 Conduction.....	24
2.4 Solar Radiation.....	25
2.5 Diurnal Air Temperature Variation.....	28
2.6 Temperature Distributions.....	29
2.7 Thermal Stresses.....	36
2.8 Thermal Responses.....	38
2.9 Thermal Responses in Curved Bridges.....	40
3 HORIZONTALLY CURVED STEEL I-GIRDER BRIDGES.....	44
3.1 Introduction.....	44
3.2 Types of Curved Framing.....	46
3.3 Effect of Cross-Bracing.....	49
3.4 Effect of Curvature.....	49

4	PILE FOUNDATIONS.....	51
4.1	Introduction.....	51
4.2	Timber Piles.....	53
4.3	Concrete Piles.....	54
	4.3.1 Precast and Prestressed Concrete Piles.....	54
	4.3.2 Cast-in-Place Concrete Piles.....	56
4.4	Steel Piles.....	57
5	SOIL MODELING.....	59
5.1	Introduction.....	59
5.2	Soil Representation.....	60
5.3	Soil Characteristics.....	64
5.4	Modified Ramberg-Osgood Model.....	64
5.5	Cyclic Model.....	70
6	THE THREE-DIMENSIONAL MODEL.....	72
6.1	Introduction.....	72
6.2	Model Geometry.....	73
6.3	Soil Properties.....	81
6.4	Loading Conditions.....	85
6.5	The Complete Three-Dimensional Model.....	86
6.6	Nonlinearity.....	88
	6.6.1 Material Nonlinearity.....	88
	6.6.2 Geometric Nonlinearity.....	89
	6.6.3 Solution of Nonlinear Problems in ANSYS.....	90
7	PARAMETRIC STUDY OF STRESS INTENSITY IN THE PILES.....	93
7.1	Effect of Bridge Length Variation.....	95
7.2	Effect of Temperature Increase.....	112
	7.2.1 Curved Integral Abutment Bridges with 50 ft Spans.....	112
	7.2.2 Curved Integral Abutment Bridges with 100 ft Spans.....	117
	7.2.3 Conclusions.....	121
7.3	Effect of Soil Profile Variation.....	129
	7.3.1 Curved Integral Abutment Bridges with 50 ft Spans.....	129
	7.3.2 Curved Integral Abutment Bridges with 100 ft Spans.....	136
	7.3.3 Stress Increase in Piles in Varying Depths of Predrilled Holes.....	141
	7.3.4 Conclusions.....	145
7.4	Effect of Span Length Variation.....	157
	7.4.1 Conclusions.....	164
7.5	Effect of Radius Variation.....	173
	7.5.1 Curved Integral Abutment Bridges with 50 ft Spans.....	173
	7.5.2 Curved Integral Abutment Bridges with 100 ft Spans.....	179
	7.5.3 Conclusions.....	185
7.6	Effect of Pile Type.....	208
	7.6.1 Conclusions.....	214



8	PARAMETRIC STUDY OF LATERAL DISPLACEMENT OF CURVED INTEGRAL ABUTMENT BRIDGES.....	218
8.1	Effect of Bridge Length Variation.....	219
8.2	Effect of Temperature Increase.....	231
8.2.1	Curved Integral Abutment Bridges with 50 ft Spans.....	231
8.2.2	Curved Integral Abutment Bridges with 100 ft Spans.....	235
8.2.3	Conclusions.....	239
8.3	Effect of Soil Profile Variation.....	247
8.3.1	Curved Integral Abutment Bridges with 50 ft Spans.....	247
8.3.2	Curved Integral Abutment Bridges with 100 ft Spans.....	253
8.3.3	Conclusions.....	258
8.4	Effect of Span Length Variation.....	269
8.4.1	Conclusions.....	275
8.5	Effect of Radius Variation.....	283
8.5.1	Curved Integral Abutment Bridges with 50 ft Spans.....	283
8.5.2	Curved Integral Abutment Bridges with 100 ft Spans.....	289
8.5.3	Conclusions.....	294
8.6	Effect of Pile Type.....	316
9	PILES IN CURVED INTEGRAL ABUTMENT BRIDGES.....	317
9.1	Stress in Piles.....	317
9.1.1	Location of Partially Plastic Hinges.....	317
9.1.2	Stress in Piles at Different Locations in the Abutment.....	330
9.2	Displacement of Piles.....	337
9.3	Conclusions.....	359
10	CONCLUSIONS AND RECOMMENDATION.....	361
	BIBLIOGRAPHY.....	370

## LIST OF TABLES

Table 5.1 – Parameters for Soil Springs.....	61
Table 5.2 – Analytical Forms of $p$ - $y$ Curves.....	65
Table 5.3 – Analytical Forms of $f$ - $z$ Curves.....	67
Table 5.4 – Analytical Forms of $q$ - $z$ Curves.....	68
Table 5.5 – Parameters used in the Modified Ramberg-Osgood Models for Clay and Sand.....	69
Table 7.1 – Materials, Material Properties, and Loads.....	94
Table 7.2 – Information of Curved Integral Abutment Bridges.....	96
Table 7.3 – Highest Stress Intensity (psi) in End-Bearing Piles in Very Stiff Clay Soil Profile of Curved Integral Abutment Bridges of Different Radii.....	98
Table 7.4 – Highest Stress Intensity (psi) in End-Bearing Piles in 9 ft Deep Predrilled Holes of Curved Integral Abutment Bridges of Different Radii.....	98
Table 7.5 – Stress Reduction (%) of End-Bearing Piles in Varying Depths of Predrilled Holes of Bridges with 100 ft Spans and Bridge Length of 100 ft and 200 ft.....	111
Table 7.6 – Stress Increase (%) of End-Bearing Piles in Very Stiff Clay Soil Profile of Bridges with 50 ft Spans due to a 30° F Temperature Increase.....	113
Table 7.7 – Stress Increase (%) of End-Bearing Piles in Varying Depths of Predrilled Holes of Bridges with 50 ft Spans due to a 30° F Temperature Increase.....	114
Table 7.8 – Mean and Standard Deviation of Stress Increase (%) of End-Bearing Piles of Bridges with 50 ft Spans due to a 30° F Temperature Increase.....	115
Table 7.9 – Mean and Standard Deviation of Stress Increase (%) of End-Bearing Piles of Bridges of Different Radii with 50 ft Spans due to a 30° F Temperature Increase.....	116
Table 7.10 – Stress Increase (%) of End-Bearing Piles in Very Stiff Clay Soil Profile of Bridges with 100 ft Spans due to a 30° F Temperature Increase.....	118

Table 7.11 – Stress Increase (%) of End-Bearing Piles in Varying Depths of Predrilled Holes of Bridges with 100 ft Spans due to a 30° F Temperature Increase.....	119
Table 7.12 – Mean and Standard Deviation of Stress Increase (%) of End-Bearing Piles of Bridges with 100 ft Spans due to a 30° F Temperature Increase....	120
Table 7.13 – Mean and Standard Deviation of Stress Increase (%) of End-Bearing Piles of Bridges of Different Radii with 100 ft Spans due to a 30° F Temperature Increase.....	120
Table 7.14 – Difference in Stress Increase (%) of End-Bearing Piles between Bridges with 50 ft and 100 ft Spans due to a 30° F Temperature Increase.....	128
Table 7.15 – Stress Reduction (%) of End-Bearing Piles in Varying Depths of Predrilled Holes of Bridges with 50 ft Spans ( $\Delta T_{\text{slab}} = 90^\circ \text{ F}$ , $\Delta T_{\text{the rest}} = 60^\circ \text{ F}$ ).....	130
Table 7.16 – Mean and Standard Deviation of Stress Reduction (%) of End-Bearing Piles in Varying Depths of Predrilled Holes of Bridges with 50 ft Spans....	134
Table 7.17 – Mean and Standard Deviation of Stress Reduction (%) of End-Bearing Piles in Varying Depths of Predrilled Holes of Bridges of Different Radii with 50 ft Spans.....	135
Table 7.18 – Stress Reduction (%) of End-Bearing Piles in Varying Depths of Predrilled Holes of Bridges with 100 ft Spans ( $\Delta T_{\text{slab}} = 90^\circ \text{ F}$ , $\Delta T_{\text{the rest}} = 60^\circ \text{ F}$ ).....	136
Table 7.19 – Mean and Standard Deviation of Stress Reduction (%) of End-Bearing Piles in Varying Depths of Predrilled Holes of Bridges with 100 ft Spans...	140
Table 7.20 – Mean and Standard Deviation of Stress Reduction (%) of End-Bearing Piles in Varying Depths of Predrilled Holes of Bridges of Different Radii with 100 ft Spans.....	141
Table 7.21 – Stress Increase (%) of End-Bearing Piles in Varying Depths of Predrilled Holes of Bridges of Different Radii ( $\Delta T_{\text{slab}} = 90^\circ \text{ F}$ , $\Delta T_{\text{the rest}} = 60^\circ \text{ F}$ ).....	142
Table 7.22 – Stress Reduction (%) of End-Bearing Piles in Very Stiff Clay Soil Profile due to the Increase in the Number of Spans.....	158
Table 7.23 – Stress Reduction (%) of End-Bearing Piles in 9 ft Deep Predrilled Holes due to the Increase in the Number of Spans.....	159

Table 7.24 – Difference in Stress Reduction (%) between End-Bearing Piles in Predrilled Holes and End-Bearing Piles without Predrilled Holes due to the Increase in the Number of Spans.....	160
Table 7.25 – Difference in Stress Reduction (%) of End-Bearing Piles between Bridges of Different Radii due to the Increase in the Number of Spans ( $\Delta T_{\text{slab}} = 90^{\circ} \text{ F}$ , $\Delta T_{\text{the rest}} = 60^{\circ} \text{ F}$ ).....	161
Table 7.26 – Mean and Standard Deviation of Stress Reduction (%) of End-Bearing Piles in Various Soil Profile Types of Bridges of Different Radii due to the Increase in the Number of Spans.....	162
Table 7.27 – Difference in Stress Reduction (%) of End-Bearing Piles between $\Delta T_{\text{slab}} = 120^{\circ} \text{ F}$ , $\Delta T_{\text{the rest}} = 90^{\circ} \text{ F}$ and $\Delta T_{\text{slab}} = 90^{\circ} \text{ F}$ , $\Delta T_{\text{the rest}} = 60^{\circ} \text{ F}$ due to the Increase in the Number of Spans.....	163
Table 7.28 – Mean and Standard Deviation of Stress Reduction (%) of End-Bearing Piles in Various Soil Profile Types due to the Increase in the Number of Spans ( $\Delta T_{\text{slab}} = 90^{\circ} \text{ F}$ , $\Delta T_{\text{the rest}} = 60^{\circ} \text{ F}$ ).....	166
Table 7.29 – Mean and Standard Deviation of Stress Reduction (%) of End-Bearing Piles in Various Soil Profile Types due to the Increase in the Number of Spans ( $\Delta T_{\text{slab}} = 120^{\circ} \text{ F}$ , $\Delta T_{\text{the rest}} = 90^{\circ} \text{ F}$ ).....	167
Table 7.30 – Stress Decrease (%) of End-Bearing Piles in Very Stiff Clay Soil Profile of Bridges with 50 ft Spans due to Change in Radius.....	173
Table 7.31 – Stress Increase (%) of End-Bearing Piles in Very Stiff Clay Soil Profile of Bridges with 50 ft Spans due to Change in Radius ( $\Delta T_{\text{slab}} = 90^{\circ} \text{ F}$ , $\Delta T_{\text{the rest}} = 60^{\circ} \text{ F}$ ).....	174
Table 7.32 – Stress Decrease (%) of End-Bearing Piles in 9 ft Deep Predrilled Holes of Bridges with 50 ft Spans due to Change in Radius.....	175
Table 7.33 – Stress Increase (%) of End-Bearing Piles in 9 ft Deep Predrilled Holes of Bridges with 50 ft Spans due to Change in Radius ( $\Delta T_{\text{slab}} = 90^{\circ} \text{ F}$ , $\Delta T_{\text{the rest}} = 60^{\circ} \text{ F}$ ).....	176
Table 7.34 – Difference in Stress Increase (%) between End-Bearing Piles in Varying Depths of Predrilled Holes and End-Bearing Piles without Predrilled Holes of Bridges with 50 ft Spans due to Change in Radius ( $\Delta T_{\text{slab}} = 90^{\circ} \text{ F}$ , $\Delta T_{\text{the rest}} = 60^{\circ} \text{ F}$ ).....	178
Table 7.35 – Stress Decrease (%) of End-Bearing Piles in Very Stiff Clay Soil Profile of Bridges with 100 ft Spans due to Change in Radius.....	179

Table 7.36 – Stress Increase (%) of End-Bearing Piles in Very Stiff Clay Soil Profile of Bridges with 100 ft Spans due to Change in Radius ( $\Delta T_{\text{slab}} = 90^{\circ} \text{ F}$ , $\Delta T_{\text{the rest}} = 60^{\circ} \text{ F}$ ).....	180
Table 7.37 – Stress Decrease (%) of End-Bearing Piles in 9 ft Deep Predrilled Holes of Bridges with 100 ft Spans due to Change in Radius.....	181
Table 7.38 – Stress Increase (%) of End-Bearing Piles in 9 ft Deep Predrilled Holes of Bridges with 100 ft Spans due to Change in Radius ( $\Delta T_{\text{slab}} = 90^{\circ} \text{ F}$ , $\Delta T_{\text{the rest}} = 60^{\circ} \text{ F}$ ).....	182
Table 7.39 – Difference in Stress Increase (%) between End-Bearing Piles in Varying Depths of Predrilled Holes and End-Bearing Piles without Predrilled Holes of Bridges with 100 ft Spans due to Change in Radius ( $\Delta T_{\text{slab}} = 90^{\circ} \text{ F}$ , $\Delta T_{\text{the rest}} = 60^{\circ} \text{ F}$ ).....	184
Table 7.40 – Difference in Stress Increase (%) of End-Bearing Piles between Bridges with 50 ft and 100 ft Spans due to Change in Radius ( $\Delta T_{\text{slab}} = 90^{\circ} \text{ F}$ , $\Delta T_{\text{the rest}} = 60^{\circ} \text{ F}$ ).....	187
Table 7.41 – Mean and Standard Deviation of Stress Increase (%) of End-Bearing Piles Compared to Friction Piles of Bridges with 50 ft spans.....	208
Table 7.42 – Mean and Standard Deviation of Stress Increase (%) of End-Bearing Piles Compared to Friction Piles of Bridges with 100 ft spans.....	209
Table 7.43 – Location of Partially Plastic Hinges in Piles.....	212
Table 8.1 – Highest Lateral Displacement (inches) of Curved Integral Abutment Bridges of Different Radii with End-Bearing Piles in Very Stiff Clay Soil Profile.....	221
Table 8.2 – Highest Lateral Displacement (inches) of Curved Integral Abutment Bridges of Different Radii with End-Bearing Piles in 9 ft Deep Predrilled Holes.....	221
Table 8.3 – Mean and Standard Deviation of Lateral Displacement Increase (%) of Bridges with 50 ft Spans and End-Bearing Piles due to a 30° F Temperature Increase.....	233
Table 8.4 – Mean and Standard Deviation of Lateral Displacement Increase (%) of Bridges of Different Radii with 50 ft Spans and End-Bearing Piles due to a 30° F Temperature Increase.....	234

Table 8.5 – Mean and Standard Deviation of Lateral Displacement Increase (%) of Bridges with 100 ft Spans and End-Bearing Piles due to a 30° F Temperature Increase.....	237
Table 8.6 – Mean and Standard Deviation of Lateral Displacement Increase (%) of Bridges of Different Radii with 100 ft Spans and End-Bearing Piles due to a 30° F Temperature Increase.....	238
Table 8.7 – Difference in Lateral Displacement Increase (%) between Bridges with 50 ft and 100 ft Spans and End-Bearing Piles due to a 30° F Temperature Increase.....	246
Table 8.8 – Lateral Displacement Reduction (%) of Bridges with 50 ft Spans and End-Bearing Piles in Varying Depths of Predrilled Holes Filled with Loose Sand ( $\Delta T_{\text{slab}} = 90^\circ \text{ F}$ , $\Delta T_{\text{the rest}} = 60^\circ \text{ F}$ ).....	249
Table 8.9 – Mean and Standard Deviation of Lateral Displacement Reduction (%) of Bridges with 50 ft Spans and End-Bearing Piles in Varying Depths of Predrilled Holes Filled with Loose Sand.....	251
Table 8.10 – Mean and Standard Deviation of Lateral Displacement Reduction (%) of Bridges of Different Radii with 50 ft Spans and End-Bearing Piles in Varying Depths of Predrilled Holes Filled with Loose Sand.....	252
Table 8.11 – Lateral Displacement Reduction (%) of Bridges with 100 ft Spans and End-Bearing Piles in Varying Depths of Predrilled Holes Filled with Loose Sand ( $\Delta T_{\text{slab}} = 90^\circ \text{ F}$ , $\Delta T_{\text{the rest}} = 60^\circ \text{ F}$ ).....	254
Table 8.12 – Mean and Standard Deviation of Lateral Displacement Reduction (%) of Bridges with 100 ft Spans and End-Bearing Piles in Varying Depths of Predrilled Holes Filled with Loose Sand.....	256
Table 8.13 – Mean and Standard Deviation of Lateral Displacement Reduction (%) of Bridges of Different Radii with 100 ft Spans and End-Bearing Piles in Varying Depths of Predrilled Holes Filled with Loose Sand.....	257
Table 8.14 – Lateral Displacement Reduction (%) of Bridges and End-Bearing Piles in Very Stiff Clay Soil Profile due to the Increase in the Number of Spans.....	270
Table 8.15 – Lateral Displacement Reduction (%) of Bridges and End-Bearing Piles in 9 ft Deep Predrilled Holes due to the Increase in the Number of Spans.....	271

Table 8.16 – Mean and Standard Deviation of Lateral Displacement Reduction (%) of Bridges of Different Radii and End-Bearing Piles in Various Soil Profile Types due to the Increase in the Number of Spans.....	273
Table 8.17 – Difference in Lateral Displacement Reduction (%) of Bridges and End-Bearing Piles due to the Increase in the Number of Spans between $\Delta T_{\text{slab}} = 120^{\circ} \text{ F}$ , $\Delta T_{\text{the rest}} = 90^{\circ} \text{ F}$ and $\Delta T_{\text{slab}} = 90^{\circ} \text{ F}$ , $\Delta T_{\text{the rest}} = 60^{\circ} \text{ F}$ ....	274
Table 8.18 – Mean and Standard Deviation of Lateral Displacement Reduction (%) of Bridges and End-Bearing Piles in Various Soil Profile Types due to the Increase in the Number of Spans ( $\Delta T_{\text{slab}} = 90^{\circ} \text{ F}$ , $\Delta T_{\text{the rest}} = 60^{\circ} \text{ F}$ ).....	276
Table 8.19 – Mean and Standard Deviation of Lateral Displacement Reduction (%) of Bridges and End-Bearing Piles in Various Soil Profile Types due to the Increase in the Number of Spans ( $\Delta T_{\text{slab}} = 120^{\circ} \text{ F}$ , $\Delta T_{\text{the rest}} = 90^{\circ} \text{ F}$ ).....	277
Table 8.20 – Lateral Displacement Decrease (%) of Bridges with 50 ft Spans and End-Bearing Piles in Very Stiff Clay Soil Profile due to Change in Radius.....	284
Table 8.21 – Lateral Displacement Increase (%) of Bridges with 50 ft Spans and End-Bearing Piles in Very Stiff Clay Soil Profile due to Change in Radius at 1200 ft Length ( $\Delta T_{\text{slab}} = 90^{\circ} \text{ F}$ , $\Delta T_{\text{the rest}} = 60^{\circ} \text{ F}$ ).....	284
Table 8.22 – Lateral Displacement Decrease (%) of Bridges with 50 ft Spans and End-Bearing Piles in Very Stiff Clay Soil Profile due to Change in Various Radii to Infinity at 1200 ft Length ( $\Delta T_{\text{slab}} = 90^{\circ} \text{ F}$ , $\Delta T_{\text{the rest}} = 60^{\circ} \text{ F}$ ).....	284
Table 8.23 – Lateral Displacement Decrease (%) of Bridges with 50 ft Spans and End-Bearing Piles in 9 ft Deep Predrilled Holes due to Change in Radius.....	285
Table 8.24 – Lateral Displacement Increase (%) of Bridges with 50 ft Spans and End-Bearing Piles in 9 ft Deep Predrilled Holes due to Change in Radius at 1200 ft Length ( $\Delta T_{\text{slab}} = 90^{\circ} \text{ F}$ , $\Delta T_{\text{the rest}} = 60^{\circ} \text{ F}$ ).....	286
Table 8.25 – Lateral Displacement Decrease (%) of Bridges with 50 ft Spans and End-Bearing Piles in 9 ft Deep Predrilled Holes due to Change in Various Radii to Infinity at 1200 ft Length ( $\Delta T_{\text{slab}} = 90^{\circ} \text{ F}$ , $\Delta T_{\text{the rest}} = 60^{\circ} \text{ F}$ ).....	286
Table 8.26 – Difference in Lateral Displacement Increase (%) due to Change in Radius of Bridges with 50 ft Spans and End-Bearing Piles in Varying Depths of Predrilled Holes or End-Bearing Piles without Predrilled Holes ( $\Delta T_{\text{slab}} = 90^{\circ} \text{ F}$ , $\Delta T_{\text{the rest}} = 60^{\circ} \text{ F}$ ).....	288

Table 8.27 – Lateral Displacement Decrease (%) of Bridges with 100 ft Spans and End-Bearing Piles in Very Stiff Clay Soil Profile due to Change in Radius.....	289
Table 8.28 – Lateral Displacement Increase (%) of Bridges with 100 ft Spans and End-Bearing Piles in Very Stiff Clay Soil Profile due to Change in Radius at 1200 ft Length ( $\Delta T_{\text{slab}} = 90^{\circ} \text{ F}$ , $\Delta T_{\text{the rest}} = 60^{\circ} \text{ F}$ ).....	290
Table 8.29 – Lateral Displacement Decrease (%) of Bridges with 100 ft Spans and End-Bearing Piles in Very Stiff Clay Soil Profile due to Change in Various Radii to Infinity at 1200 ft Length ( $\Delta T_{\text{slab}} = 90^{\circ} \text{ F}$ , $\Delta T_{\text{the rest}} = 60^{\circ} \text{ F}$ ).....	290
Table 8.30 – Lateral Displacement Decrease (%) of Bridges with 100 ft Spans and End-Bearing Piles in 9 ft Deep Predrilled Holes due to Change in Radius.....	291
Table 8.31 – Lateral Displacement Increase (%) of Bridges with 100 ft Spans and End-Bearing Piles in 9 ft Deep Predrilled Holes due to Change in Radius at 1200 ft Length ( $\Delta T_{\text{slab}} = 90^{\circ} \text{ F}$ , $\Delta T_{\text{the rest}} = 60^{\circ} \text{ F}$ ).....	291
Table 8.32 – Lateral Displacement Decrease (%) of Bridges with 100 ft Spans and End-Bearing Piles in 9 ft Deep Predrilled Holes due to Change in Various Radii to Infinity at 1200 ft Length ( $\Delta T_{\text{slab}} = 90^{\circ} \text{ F}$ , $\Delta T_{\text{the rest}} = 60^{\circ} \text{ F}$ ).....	291
Table 8.33 – Difference in Lateral Displacement Increase (%) due to Change in Radius of Bridges with 100 ft Spans and End-Bearing Piles in Varying Depths of Predrilled Holes or End-Bearing Piles without Predrilled Holes ( $\Delta T_{\text{slab}} = 90^{\circ} \text{ F}$ , $\Delta T_{\text{the rest}} = 60^{\circ} \text{ F}$ ).....	293
Table 8.34 – Difference in Maximum Lateral Displacement (inch) of Curved Integral Abutment Bridges between Friction and End-Bearing Piles.....	316
Table 9.1 – Location of Partially Plastic Hinges in End-Bearing Piles in Various Soil Profile Types of Bridges with 800 ft Radius and 800 ft Length ( $\Delta T_{\text{slab}} = 120^{\circ} \text{ F}$ , $\Delta T_{\text{the rest}} = 90^{\circ} \text{ F}$ ).....	325
Table 9.2 – Stress Reduction (%) of End-Bearing Piles in Various Soil Profile Types of Bridges with 800 ft Radius and 800 ft Length due to the Increase in the Number of Spans ( $\Delta T_{\text{slab}} = 120^{\circ} \text{ F}$ , $\Delta T_{\text{the rest}} = 90^{\circ} \text{ F}$ ).....	326
Table 9.3 – Equivalent Stress in End-Bearing Piles in Various Soil Profile Types of Bridges with 800 ft Radius and 800 ft Length ( $\Delta T_{\text{slab}} = 120^{\circ} \text{ F}$ , $\Delta T_{\text{the rest}} = 90^{\circ} \text{ F}$ ).....	328



Table 9.4 – Equivalent Stress Decrease (%) of End-Bearing Piles in 9 ft Deep Predrilled Holes between Piles at Different Locations in the Abutment ( $\Delta T_{\text{slab}} = 120^{\circ} \text{ F}$ , $\Delta T_{\text{the rest}} = 90^{\circ} \text{ F}$ ).....	334
Table 9.5 – Location of Partially Plastic Hinges in End-Bearing Piles in 9 ft Deep Predrilled Holes at Different Locations in the Abutment ( $\Delta T_{\text{slab}} = 120^{\circ} \text{ F}$ , $\Delta T_{\text{the rest}} = 90^{\circ} \text{ F}$ ).....	334
Table 9.6 – Equivalent Stress in End-Bearing Piles in 9 ft Deep Predrilled Holes at Different Locations in the Abutment of Bridges with 800 ft Radius and 800 ft Length ( $\Delta T_{\text{slab}} = 120^{\circ} \text{ F}$ , $\Delta T_{\text{the rest}} = 90^{\circ} \text{ F}$ ).....	336
Table 9.7 – Displacements and Point of Fixity of End-Bearing Piles in Various Soil Profile Types of Bridges with 800 ft Radius and 800 ft Length ( $\Delta T_{\text{slab}} = 120^{\circ} \text{ F}$ , $\Delta T_{\text{the rest}} = 90^{\circ} \text{ F}$ ).....	348
Table 9.8 – Difference in Longitudinal and Lateral Displacements of End-Bearing Piles in Various Soil Profile Types of Bridges with 800 ft Radius and 800 ft Length ( $\Delta T_{\text{slab}} = 120^{\circ} \text{ F}$ , $\Delta T_{\text{the rest}} = 90^{\circ} \text{ F}$ ).....	350
Table 9.9 – Difference in Displacements and Point of Fixity of End-Bearing Piles in Various Soil Profile Types between Bridges with 100 ft and 50 ft Spans with 800 ft Radius and 800 ft Length ( $\Delta T_{\text{slab}} = 120^{\circ} \text{ F}$ , $\Delta T_{\text{the rest}} = 90^{\circ} \text{ F}$ ).....	350
Table 9.10 – Displacements and Point of Fixity of End-Bearing Piles in 9 ft Deep Predrilled Holes at Different Locations in the Abutment of Bridges with 800 ft Radius and 800 ft Length ( $\Delta T_{\text{slab}} = 120^{\circ} \text{ F}$ , $\Delta T_{\text{the rest}} = 90^{\circ} \text{ F}$ ).....	352
Table 9.11 – Difference in Displacements and Point of Fixity of End-Bearing Piles in 9 ft Deep Predrilled Holes at Different Locations in the Abutment between Bridges with 100 ft and 50 ft Spans with 800 ft Radius and 800 ft Length ( $\Delta T_{\text{slab}} = 120^{\circ} \text{ F}$ , $\Delta T_{\text{the rest}} = 90^{\circ} \text{ F}$ ).....	352
Table 10.1 – Summary of Curved Integral Abutment Bridges.....	367

# LIST OF FIGURES

Figure 1.1 – Bridge with Expansion Joints.....	1
Figure 1.2 – Damaged Expansion Joints and Their Effects on the Substructure .....	2
Figure 1.3 – Bridge with Integral Abutments.....	3
Figure 1.4 – Integral Abutment Details.....	4
Figure 1.5 – Semi-Integral Abutment Details: Ohio.....	5
Figure 1.6 – Pile Orientations in the Skewed Bridges.....	16
Figure 2.1 – Variation in Solar Radiation for Various Latitudes.....	22
Figure 2.2 – Solar Radiation Reaching the Surface of a Bridge.....	23
Figure 2.3 – Variation in Solar Radiation for a Clear Day.....	23
Figure 2.4 – Geometry Defining Incidence Angle of Solar Radiation.....	27
Figure 2.5 – Temperature Distribution on a Composite Steel Girder on a Hot Summer Day.....	30
Figure 2.6 – Vertical Temperature Distribution Proposed by Berwanger.....	33
Figure 2.7 – Typical Variation in Temperature for Steel Bridge with Composite Deck.....	35
Figure 2.8 – Factors Affecting Thermal Response.....	39
Figure 2.9 – Displacements for: (a) Support Condition I; (b) Support Condition II.....	41
Figure 2.10 - Thermal Movements of a Curved Bridge.....	43
Figure 2.11 - Typical Orientation and Placement of Bridge Bearings on a Curved Bridge.....	43
Figure 3.1 – Curved Girders Tied Together with Diaphragms and Lateral Bracing.....	46
Figure 3.2 – Curved Girders Tied Together with Diaphragms.....	47

Figure 3.3 – Curved Girders Tied Together with Diaphragms and Lateral Bracing in Alternate Bays.....	48
Figure 4.1 – Typical Pile Configurations.....	52
Figure 4.2 – Typical Details of Precast Piles.....	55
Figure 4.3 – Typical Prestressed Concrete Piles.....	55
Figure 5.1 – Soil-Pile Interaction.....	60
Figure 5.2 – Reduction Factor $\alpha$ .....	63
Figure 5.3 – The Modified Ramberg-Osgood Curve for a Typical $p$ - $y$ Curve.....	67
Figure 5.4 – Effect of the Shape Parameter ( $n$ ) on Modified Ramberg-Osgood Equation.....	70
Figure 6.1 – Typical Section of the Three-Dimensional Model.....	73
Figure 6.2 – Concrete Slab Nodes Shown in Typical Section.....	74
Figure 6.3 – Nodes Distribution for Steel Girders and Cross Bracings Shown in Typical Section.....	74
Figure 6.4 – Plan View of the Mesh Layout for a Single Span Model.....	75
Figure 6.5 – Isometric View of the Mesh Layout for a Single Span Model.....	76
Figure 6.6 – Isometric View of the Mesh at Each Abutment.....	77
Figure 6.7 – Mesh in a Steel Pile.....	78
Figure 6.8 – Spring Model for Soil.....	80
Figure 6.9 – Soil Properties and Layout for the Different Soil Profile Models.....	82
Figure 6.10 – Normalized $p$ - $y$ Curve for HP 10x42 Steel Piles in Very Stiff Clay....	83
Figure 6.11 – Normalized $f$ - $z$ Curve for HP 10x42 Steel Pile in Very Stiff Clay.....	84
Figure 6.12 – Normalized $q$ - $z$ Curve for HP 10x42 Steel Pile in Very Stiff Clay.....	84
Figure 6.13 – The Three-Dimensional Model Components.....	86

Figure 6.14 – Undeformed Shape of a Curved Integral Abutment Bridge with 400 ft Radius and 4 - 50 ft Spans with Piles in Very Stiff Clay Soil Profile with 9 ft Deep Predrilled Holes Filled with Loose Sand.....	87
Figure 6.15 – Deformed Shape of a Curved Integral Abutment Bridge with 400 ft Radius and 4 - 50 ft Spans with Piles in Very Stiff Clay Soil Profile with 9 ft Deep Predrilled Holes Filled with Loose Sand.....	88
Figure 6.16 – Traditional Newton-Raphson Method vs. Arc-Length Method.....	91
Figure 6.17 – Load Steps, Substeps, and Time.....	92
Figure 7.1 – Curved Integral Abutment Bridges of Different Radii.....	97
Figure 7.2 – Maximum Stress Intensity in End-Bearing Piles in Very Stiff Clay Soil Profile of Bridges with 50 ft Spans.....	102
Figure 7.3 – Maximum Stress Intensity in End-Bearing Piles in 5 ft Deep Predrilled Holes of Bridges with 50 ft Spans.....	103
Figure 7.4 – Maximum Stress Intensity in End-Bearing Piles in 9 ft Deep Predrilled Holes of Bridges with 50 ft Spans.....	104
Figure 7.5 – Maximum Stress Intensity in End-Bearing Piles in 15 ft Deep Predrilled Holes of Bridges with 50 ft Spans.....	105
Figure 7.6 – Maximum Stress Intensity in End-Bearing Piles in Very Stiff Clay Soil Profile of Bridges with 100 ft Spans.....	106
Figure 7.7 – Maximum Stress Intensity in End-Bearing Piles in 5 ft Deep Predrilled Holes of Bridges with 100 ft Spans.....	107
Figure 7.8 – Maximum Stress Intensity in End-Bearing Piles in 9 ft Deep Predrilled Holes of Bridges with 100 ft Spans.....	108
Figure 7.9 – Maximum Stress Intensity in End-Bearing Piles in 15 ft Deep Predrilled Holes of Bridges with 100 ft Spans.....	109
Figure 7.10 – Highest Stress Intensity in End-Bearing Piles at Different Bridge Lengths of Curved Integral Abutment Bridges of Different Radii.....	110
Figure 7.11 – Stress Reduction (%) of End-Bearing Piles in Varying Depths of Predrilled Holes of Bridges with 100 ft Spans and Bridge Length of 100 ft and 200 ft.....	111

Figure 7.12 – Stress Increase (%) of End-Bearing Piles of Bridges with 50 ft Spans due to a 30° F Temperature Increase.....	123
Figure 7.13 – Stress Increase (%) of End-Bearing Piles of Bridges with 100 ft Spans due to a 30° F Temperature Increase.....	125
Figure 7.14 – Mean of Stress Increase (%) of End-Bearing Piles of Bridges with 50 ft and 100 ft Spans due to a 30° F Temperature Increase.....	127
Figure 7.15 – Mean of Stress Increase (%) of End-Bearing Piles of Bridges of Different Radii due to a 30° F Temperature Increase.....	127
Figure 7.16 – Difference in Stress Increase (%) of End-Bearing Piles between Bridges with 50 ft and 100 ft Spans due to a 30° F Temperature Increase.....	128
Figure 7.17 – Stress Reduction (%) of End-Bearing Piles in 5 ft Deep Predrilled Holes of Bridges with 50 ft Spans.....	148
Figure 7.18 – Stress Reduction (%) of End-Bearing Piles in 9 ft Deep Predrilled Holes of Bridges with 50 ft Spans.....	149
Figure 7.19 – Stress Reduction (%) of End-Bearing Piles in 15 ft Deep Predrilled Holes of Bridges with 50 ft Spans.....	150
Figure 7.20 – Mean of Stress Reduction (%) of End-Bearing Piles in Varying Depths of Predrilled Holes of Bridges with 50 ft and 100 ft Spans.....	151
Figure 7.21 – Mean of Stress Reduction (%) of End-Bearing Piles in Varying Depths of Predrilled Holes of Bridges of Different Radii with 50 ft Spans.....	152
Figure 7.22 – Stress Reduction (%) of End-Bearing Piles in 5 ft Deep Predrilled Holes of Bridges with 100 ft Spans.....	153
Figure 7.23 – Stress Reduction (%) of End-Bearing Piles in 9 ft Deep Predrilled Holes of Bridges with 100 ft Spans.....	154
Figure 7.24 – Stress Reduction (%) of End-Bearing Piles in 15 ft Deep Predrilled Holes of Bridges with 100 ft Spans.....	155
Figure 7.25 – Mean of Stress Reduction (%) of End-Bearing Piles in Varying Depths of Predrilled Holes of Bridges of Different Radii with 100 ft Spans.....	156
Figure 7.26 – Stress Reduction (%) of End-Bearing Piles in Very Stiff Clay Soil Profile due to the Increase in the Number of Spans.....	168

Figure 7.27 – Stress Reduction (%) of End-Bearing Piles in 9 ft Deep Predrilled Holes due to the Increase in the Number of Spans.....	169
Figure 7.28 – Mean of Stress Reduction (%) of End-Bearing Piles in Various Soil Profile Types of Bridges of Different Radii due to the Increase in the Number of Spans.....	170
Figure 7.29 – Mean of Stress Reduction of End-Bearing Piles in Various Soil Profile Types due to the Increase in the Number of Spans.....	171
Figure 7.30 – Difference in Stress Reduction (%) of End-Bearing Piles between $\Delta T_{\text{slab}} = 120^{\circ} \text{ F}$ , $\Delta T_{\text{the rest}} = 90^{\circ} \text{ F}$ and $\Delta T_{\text{slab}} = 90^{\circ} \text{ F}$ , $\Delta T_{\text{the rest}} = 60^{\circ} \text{ F}$ due to the Increase in the Number of Spans.....	172
Figure 7.31 – Stress Increase (%) of End-Bearing Piles in Very Stiff Clay Soil Profile of Bridges with 50 ft Spans due to Change in Radius from 400 ft to a Larger Radius.....	188
Figure 7.32 – Stress Increase (%) of End-Bearing Piles in Very Stiff Clay Soil Profile of Bridges with 50 ft Spans due to Change in Radius from 600 ft to a Larger Radius.....	189
Figure 7.33 – Stress Increase (%) of End-Bearing Piles in Very Stiff Clay Soil Profile of Bridges with 50 ft Spans due to Change in Radius from 800 ft to a Larger Radius.....	190
Figure 7.34 – Stress Increase (%) of End-Bearing Piles in Very Stiff Clay Soil Profile of Bridges with 50 ft Spans due to Change in Radius from 1200 ft to a Larger Radius.....	191
Figure 7.35 – Stress Increase (%) of End-Bearing Piles in Very Stiff Clay Soil Profile of Bridges with 50 ft Spans due to Change in Radius from Different Values to Infinity.....	192
Figure 7.36 – Stress Increase (%) of End-Bearing Piles in 9 ft Deep Predrilled Holes of Bridges with 50 ft Spans due to Change in Radius from 400 ft to a Larger Radius.....	193
Figure 7.37 – Stress Increase (%) of End-Bearing Piles in 9 ft Deep Predrilled Holes of Bridges with 50 ft Spans due to Change in Radius from 600 ft to a Larger Radius.....	194
Figure 7.38 – Stress Increase (%) of End-Bearing Piles in 9 ft Deep Predrilled Holes of Bridges with 50 ft Spans due to Change in Radius from 800 ft to a Larger Radius.....	195

Figure 7.39 – Stress Increase (%) of End-Bearing Piles in 9 ft Deep Predrilled Holes of Bridges with 50 ft Spans due to Change in Radius from 1200 ft to a Larger Radius.....	196
Figure 7.40 – Stress Increase (%) of End-Bearing Piles in 9 ft Deep Predrilled Holes of Bridges with 50 ft Spans due to Change in Radius from Different Values to Infinity.....	197
Figure 7.41 – Stress Increase (%) of End-Bearing Piles in Very Stiff Clay Soil Profile of Bridges with 100 ft Spans due to Change in Radius from 400 ft to a Larger Radius.....	198
Figure 7.42 – Stress Increase (%) of End-Bearing Piles in Very Stiff Clay Soil Profile of Bridges with 100 ft Spans due to Change in Radius from 600 ft to a Larger Radius.....	199
Figure 7.43 – Stress Increase (%) of End-Bearing Piles in Very Stiff Clay Soil Profile of Bridges with 100 ft Spans due to Change in Radius from 800 ft to a Larger Radius.....	200
Figure 7.44 – Stress Increase (%) of End-Bearing Piles in Very Stiff Clay Soil Profile of Bridges with 100 ft Spans due to Change in Radius from 1200 ft to a Larger Radius.....	201
Figure 7.45 – Stress Increase (%) of End-Bearing Piles in Very Stiff Clay Soil Profile of Bridges with 100 ft Spans due to Change in Radius from Different Values to Infinity.....	202
Figure 7.46 – Stress Increase (%) of End-Bearing Piles in 9 ft Deep Predrilled Holes of Bridges with 100 ft Spans due to Change in Radius from 400 ft to a Larger Radius.....	203
Figure 7.47 – Stress Increase (%) of End-Bearing Piles in 9 ft Deep Predrilled Holes of Bridges with 100 ft Spans due to Change in Radius from 600 ft to a Larger Radius.....	204
Figure 7.48 – Stress Increase (%) of End-Bearing Piles in 9 ft Deep Predrilled Holes of Bridges with 100 ft Spans due to Change in Radius from 800 ft to a Larger Radius.....	205
Figure 7.49 – Stress Increase (%) of End-Bearing Piles in 9 ft Deep Predrilled Holes of Bridges with 100 ft Spans due to Change in Radius from 1200 ft to a Larger Radius.....	206

Figure 7.50 – Stress Increase (%) of End-Bearing Piles in 9 ft Deep Predrilled Holes of Bridges with 100 ft Spans due to Change in Radius from Different Values to Infinity.....	207
Figure 7.51 – Equivalent Stress Contour of Piles in 9 ft Deep Predrilled Holes of Bridges with 800 ft Radius and 800 ft Length ( $\Delta T_{\text{slab}} = 120^{\circ} \text{ F}$ , $\Delta T_{\text{the rest}} = 90^{\circ} \text{ F}$ ).....	210
Figure 7.52 – Comparison of Equivalent Stress in Friction and End-Bearing Piles in 9 ft Deep Predrilled Holes of Bridges with 800 ft Radius and 800 ft Length ( $\Delta T_{\text{slab}} = 120^{\circ} \text{ F}$ , $\Delta T_{\text{the rest}} = 90^{\circ} \text{ F}$ ).....	211
Figure 7.53 – Equivalent Stress Contour with Deformed and Undeformed Shapes of Piles in 9 ft Deep Predrilled Holes of Bridges with 800 ft Radius and 800 ft Length ( $\Delta T_{\text{slab}} = 120^{\circ} \text{ F}$ , $\Delta T_{\text{the rest}} = 90^{\circ} \text{ F}$ ).....	212
Figure 7.54 – Deformed and Undeformed Shapes at the End Span of Bridges with 800 ft Radius and 800 ft Length and with Piles in 9 ft Deep Predrilled Holes ( $\Delta T_{\text{slab}} = 120^{\circ} \text{ F}$ , $\Delta T_{\text{the rest}} = 90^{\circ} \text{ F}$ ).....	215
Figure 7.55 – Deformed and Undeformed Shapes of Friction and End-Bearing Piles in 9 ft Deep Predrilled Holes of Bridges with 800 ft Radius and 800 ft Length ( $\Delta T_{\text{slab}} = 120^{\circ} \text{ F}$ , $\Delta T_{\text{the rest}} = 90^{\circ} \text{ F}$ ).....	216
Figure 7.56 – Vertical Displacement of Friction and End-Bearing Piles in 9 ft Deep Predrilled Holes of Bridges with 800 ft Radius and 800 ft Length ( $\Delta T_{\text{slab}} = 120^{\circ} \text{ F}$ , $\Delta T_{\text{the rest}} = 90^{\circ} \text{ F}$ ).....	217
Figure 8.1 – Maximum Lateral Displacement of Bridges with 50 ft Spans and End-Bearing Piles in Very Stiff Clay Soil Profile.....	222
Figure 8.2 – Maximum Lateral Displacement of Bridges with 50 ft Spans and End-Bearing Piles in 5 ft Deep Predrilled Holes.....	223
Figure 8.3 – Maximum Lateral Displacement of Bridges with 50 ft Spans and End-Bearing Piles in 9 ft Deep Predrilled Holes.....	224
Figure 8.4 – Maximum Lateral Displacement of Bridges with 50 ft Spans and End-Bearing Piles in 15 ft Deep Predrilled Holes.....	225
Figure 8.5 – Maximum Lateral Displacement of Bridges with 100 ft Spans and End-Bearing Piles in Very Stiff Clay Soil Profile.....	226
Figure 8.6 – Maximum Lateral Displacement of Bridges with 100 ft Spans and End-Bearing Piles in 5 ft Deep Predrilled Holes.....	227



Figure 8.7 – Maximum Lateral Displacement of Bridges with 100 ft Spans and End-Bearing Piles in 9 ft Deep Predrilled Holes.....	228
Figure 8.8 – Maximum Lateral Displacement of Bridges with 100 ft Spans and End-Bearing Piles in 15 ft Deep Predrilled Holes.....	229
Figure 8.9 – Highest Lateral Displacement of Curved Integral Abutment Bridges of Different Radii at Different Bridge Lengths.....	230
Figure 8.10 – Lateral Displacement Increase (%) of Bridges with 50 ft Spans and End-Bearing Piles due to a 30° F Temperature Increase.....	241
Figure 8.11 – Lateral Displacement Increase (%) of Bridges with 100 ft Spans and End-Bearing Piles due to a 30° F Temperature Increase.....	243
Figure 8.12 – Mean of Lateral Displacement Increase (%) of Bridges with 50 ft and 100 ft Spans and End-Bearing Piles due to a 30° F Temperature Increase...	245
Figure 8.13 – Mean of Lateral Displacement Increase (%) of Bridges of Different Radii and End-Bearing Piles due to a 30° F Temperature Increase.....	245
Figure 8.14 – Difference in Lateral Displacement Increase (%) between Bridges with 50 ft and 100 ft Spans and End-Bearing Piles due to a 30° F Temperature Increase.....	246
Figure 8.15 – Lateral Displacement Reduction (%) of Bridges with 50 ft Spans and End-Bearing Piles in 5 ft Deep Predrilled Holes.....	260
Figure 8.16 – Lateral Displacement Reduction (%) of Bridges with 50 ft Spans and End-Bearing Piles in 9 ft Deep Predrilled Holes.....	261
Figure 8.17 – Lateral Displacement Reduction (%) of Bridges with 50 ft Spans and End-Bearing Piles in 15 ft Deep Predrilled Holes.....	262
Figure 8.18 – Mean of Lateral Displacement Reduction (%) of Bridges with 50 ft and 100 ft Spans and End-Bearing Piles in Varying Depths of Predrilled Holes.....	263
Figure 8.19 – Mean of Lateral Displacement Reduction (%) of Bridges of Different Radii with 50 ft Spans and End-Bearing Piles in Varying Depths of Predrilled Holes.....	264
Figure 8.20 – Lateral Displacement Reduction (%) of Bridges with 100 ft Spans and End-Bearing Piles in 5 ft Deep Predrilled Holes.....	265

Figure 8.21 – Lateral Displacement Reduction (%) of Bridges with 100 ft Spans and End-Bearing Piles in 9 ft Deep Predrilled Holes.....	266
Figure 8.22 – Lateral Displacement Reduction (%) of Bridges with 100 ft Spans and End-Bearing Piles in 15 ft Deep Predrilled Holes.....	267
Figure 8.23 – Mean of Lateral Displacement Reduction (%) of Bridges of Different Radii with 100 ft Spans and End-Bearing Piles in Varying Depths of Predrilled Holes.....	268
Figure 8.24 – Lateral Displacement Reduction (%) of Bridges and End-Bearing Piles in Very Stiff Clay Soil Profile due to the Increase in the Number of Spans.....	278
Figure 8.25 – Lateral Displacement Reduction (%) of Bridges and End-Bearing Piles in 9 ft Deep Predrilled Holes due to the Increase in the Number of Spans.....	279
Figure 8.26 – Mean of Lateral Displacement Reduction (%) of Bridges of Different Radii and End-Bearing Piles in Various Soil Profile Types due to the Increase in the Number of Spans.....	280
Figure 8.27 – Mean of Lateral Displacement Reduction (%) of Bridges and End-Bearing Piles in Various Soil Profile Types due to the Increase in the Number of Spans.....	281
Figure 8.28 – Difference in Lateral Displacement Reduction (%) of Bridges and End-Bearing Piles due to the Increase in the Number of Spans between $\Delta T_{\text{slab}} = 120^{\circ} \text{ F}$ , $\Delta T_{\text{the rest}} = 90^{\circ} \text{ F}$ and $\Delta T_{\text{slab}} = 90^{\circ} \text{ F}$ , $\Delta T_{\text{the rest}} = 60^{\circ} \text{ F}$ .....	282
Figure 8.29 – Lateral Displacement Increase (%) of Bridges with 50 ft Spans and End-Bearing Piles in Very Stiff Clay Soil Profile due to Change in Radius from 400 ft to a Larger Radius.....	296
Figure 8.30 – Lateral Displacement Increase (%) of Bridges with 50 ft Spans and End-Bearing Piles in Very Stiff Clay Soil Profile due to Change in Radius from 600 ft to a Larger Radius.....	297
Figure 8.31 – Lateral Displacement Increase (%) of Bridges with 50 ft Spans and End-Bearing Piles in Very Stiff Clay Soil Profile due to Change in Radius from 800 ft to a Larger Radius.....	298
Figure 8.32 – Lateral Displacement Increase (%) of Bridges with 50 ft Spans and End-Bearing Piles in Very Stiff Clay Soil Profile due to Change in Radius from 1200 ft to a Larger Radius.....	299

Figure 8.33 – Lateral Displacement Increase (%) of Bridges with 50 ft Spans and End-Bearing Piles in Very Stiff Clay Soil Profile due to Change in Radius from Different Values to Infinity.....	300
Figure 8.34 – Lateral Displacement Increase (%) of Bridges with 50 ft Spans and End-Bearing Piles in 9 ft Deep Predrilled Holes due to Change in Radius from 400 ft to a Larger Radius.....	301
Figure 8.35 – Lateral Displacement Increase (%) of Bridges with 50 ft Spans and End-Bearing Piles in 9 ft Deep Predrilled Holes due to Change in Radius from 600 ft to a Larger Radius.....	302
Figure 8.36 – Lateral Displacement Increase (%) of Bridges with 50 ft Spans and End-Bearing Piles in 9 ft Deep Predrilled Holes due to Change in Radius from 800 ft to a Larger Radius.....	303
Figure 8.37 – Lateral Displacement Increase (%) of Bridges with 50 ft Spans and End-Bearing Piles in 9 ft Deep Predrilled Holes due to Change in Radius from 1200 ft to a Larger Radius.....	304
Figure 8.38 – Lateral Displacement Decrease (%) of Bridges with 50 ft Spans and End-Bearing Piles in 9 ft Deep Predrilled Holes due to Change in Radius from Different Values to Infinity.....	305
Figure 8.39 – Lateral Displacement Increase (%) of Bridges with 100 ft Spans and End-Bearing Piles in Very Stiff Clay Soil Profile due to Change in Radius from 400 ft to a Larger Radius.....	306
Figure 8.40 – Lateral Displacement Increase (%) of Bridges with 100 ft Spans and End-Bearing Piles in Very Stiff Clay Soil Profile due to Change in Radius from 600 ft to a Larger Radius.....	307
Figure 8.41 – Lateral Displacement Increase (%) of Bridges with 100 ft Spans and End-Bearing Piles in Very Stiff Clay Soil Profile due to Change in Radius from 800 ft to a Larger Radius.....	308
Figure 8.42 – Lateral Displacement Increase (%) of Bridges with 100 ft Spans and End-Bearing Piles in Very Stiff Clay Soil Profile due to Change in Radius from 1200 ft to a Larger Radius.....	309
Figure 8.43 – Lateral Displacement Increase (%) of Bridges with 100 ft Spans and End-Bearing Piles in Very Stiff Clay Soil Profile due to Change in Radius from Different Values to Infinity.....	310

Figure 8.44 – Lateral Displacement Increase (%) of Bridges with 100 ft Spans and End-Bearing Piles in 9 ft Deep Predrilled Holes due to Change in Radius from 400 ft to a Larger Radius.....	311
Figure 8.45 – Lateral Displacement Increase (%) of Bridges with 100 ft Spans and End-Bearing Piles in 9 ft Deep Predrilled Holes due to Change in Radius from 600 ft to a Larger Radius.....	312
Figure 8.46 – Lateral Displacement Increase (%) of Bridges with 100 ft Spans and End-Bearing Piles in 9 ft Deep Predrilled Holes due to Change in Radius from 800 ft to a Larger Radius.....	313
Figure 8.47 – Lateral Displacement Increase (%) of Bridges with 100 ft Spans and End-Bearing Piles in 9 ft Deep Predrilled Holes due to Change in Radius from 1200 ft to a Larger Radius.....	314
Figure 8.48 – Lateral Displacement Decrease (%) of Bridges with 100 ft Spans and End-Bearing Piles in 9 ft Deep Predrilled Holes due to Change in Radius from Different Values to Infinity.....	315
Figure 9.1 – Equivalent Stress Contour in End-Bearing Piles of Bridges with 800 ft Radius and 800 ft Length ( $\Delta T_{\text{slab}} = 120^{\circ} \text{ F}$ , $\Delta T_{\text{the rest}} = 90^{\circ} \text{ F}$ ).....	318
Figure 9.2 – Equivalent Stress Contour in End-Bearing Piles in Various Soil Profile Types of Bridges with 800 ft Radius and 800 ft Length ( $\Delta T_{\text{slab}} = 120^{\circ} \text{ F}$ , $\Delta T_{\text{the rest}} = 90^{\circ} \text{ F}$ ).....	319
Figure 9.3 – Equivalent Stress and Location of Partially Plastic Hinges in End-Bearing Piles in Various Soil Profile Types of a Bridge with 800 ft Radius and 16 - 50 ft Spans ( $\Delta T_{\text{slab}} = 120^{\circ} \text{ F}$ , $\Delta T_{\text{the rest}} = 90^{\circ} \text{ F}$ ).....	320
Figure 9.4 – Equivalent Stress and Location of Partially Plastic Hinges in End-Bearing Piles in Various Soil Profile Types of a Bridge with 800 ft Radius and 8 - 100 ft Spans ( $\Delta T_{\text{slab}} = 120^{\circ} \text{ F}$ , $\Delta T_{\text{the rest}} = 90^{\circ} \text{ F}$ ).....	321
Figure 9.5 – Comparison of Equivalent Stress and Location of Partially Plastic Hinges in End-Bearing Piles in Various Soil Profile Types between Bridges with 50 ft and 100 ft Spans with 800 ft Radius and 800 ft Length ( $\Delta T_{\text{slab}} = 120^{\circ} \text{ F}$ , $\Delta T_{\text{the rest}} = 90^{\circ} \text{ F}$ ).....	322
Figure 9.6 – Equivalent Stress Contour with Deformed and Undeformed Shapes of End-Bearing Piles in Various Soil Profile Types of Bridges with 800 ft Radius and 800 ft Length ( $\Delta T_{\text{slab}} = 120^{\circ} \text{ F}$ , $\Delta T_{\text{the rest}} = 90^{\circ} \text{ F}$ ).....	323

Figure 9.7 – Equivalent Stress Contour in End-Bearing Piles in 9 ft Deep Predrilled Holes of Bridges with 800 ft Radius and 800 ft Length ( $\Delta T_{\text{slab}} = 120^{\circ} \text{ F}$ , $\Delta T_{\text{the rest}} = 90^{\circ} \text{ F}$ ).....	330
Figure 9.8 – Equivalent Stress in End-Bearing Piles in 9 ft Deep Predrilled Holes at Different Locations in the Abutment of a Bridge with 800 ft Radius and 16 - 50 ft Spans ( $\Delta T_{\text{slab}} = 120^{\circ} \text{ F}$ , $\Delta T_{\text{the rest}} = 90^{\circ} \text{ F}$ ).....	331
Figure 9.9 – Equivalent Stress in End-Bearing Piles in 9 ft Deep Predrilled Holes at Different Locations in the Abutment of a Bridge with 800 ft Radius and 8 - 100 ft Spans ( $\Delta T_{\text{slab}} = 120^{\circ} \text{ F}$ , $\Delta T_{\text{the rest}} = 90^{\circ} \text{ F}$ ).....	332
Figure 9.10 – Comparison of Equivalent Stress in End-Bearing Piles in 9 ft Deep Predrilled Holes at Different Locations in the Abutment between Bridges with 50 ft and 100 ft Spans with 800 ft Radius and 800 ft Length ( $\Delta T_{\text{slab}} = 120^{\circ} \text{ F}$ , $\Delta T_{\text{the rest}} = 90^{\circ} \text{ F}$ ).....	333
Figure 9.11 – Deformed and Undeformed Shapes of Bridges with 800 ft Radius and 800 ft Length with End-Bearing Piles in 9 ft Deep Predrilled Holes ( $\Delta T_{\text{slab}} = 120^{\circ} \text{ F}$ , $\Delta T_{\text{the rest}} = 90^{\circ} \text{ F}$ ).....	337
Figure 9.12 – Front View of Deformed and Undeformed Shapes at the Right Abutment of Bridges with 800 ft Radius and 800 ft Length with End-Bearing Piles in 9 ft Deep Predrilled Holes ( $\Delta T_{\text{slab}} = 120^{\circ} \text{ F}$ , $\Delta T_{\text{the rest}} = 90^{\circ} \text{ F}$ ).....	338
Figure 9.13 – Zoom View of Deformed and Undeformed Shapes at the Right Abutment of Bridges with 800 ft Radius and 800 ft Length with End-Bearing Piles in 9 ft Deep Predrilled Holes ( $\Delta T_{\text{slab}} = 120^{\circ} \text{ F}$ , $\Delta T_{\text{the rest}} = 90^{\circ} \text{ F}$ ).....	339
Figure 9.14 – Top View of Deformed and Undeformed Shapes at the Right Abutment of Bridges with 800 ft Radius and 800 ft Length with End-Bearing Piles in 9 ft Deep Predrilled Holes ( $\Delta T_{\text{slab}} = 120^{\circ} \text{ F}$ , $\Delta T_{\text{the rest}} = 90^{\circ} \text{ F}$ ).....	340
Figure 9.15 – Deformed and Undeformed Shapes of Abutment with End-Bearing Piles in Very Stiff Clay Soil Profile of Bridges with 800 ft Radius and 800 ft Length ( $\Delta T_{\text{slab}} = 120^{\circ} \text{ F}$ , $\Delta T_{\text{the rest}} = 90^{\circ} \text{ F}$ ).....	342
Figure 9.16 – Deformed and Undeformed Shapes of Abutment with End-Bearing Piles in 9 ft Deep Predrilled Holes of Bridges with 800 ft Radius and 800 ft Length ( $\Delta T_{\text{slab}} = 120^{\circ} \text{ F}$ , $\Delta T_{\text{the rest}} = 90^{\circ} \text{ F}$ ).....	343
Figure 9.17 – Deformed and Undeformed Shapes of End-Bearing Piles in Very Stiff Clay Soil Profile of a Bridge with 800 ft Radius and 16 - 50 ft Spans ( $\Delta T_{\text{slab}} = 120^{\circ} \text{ F}$ , $\Delta T_{\text{the rest}} = 90^{\circ} \text{ F}$ ).....	344

Figure 9.18 – Deformed and Undeformed Shapes of End-Bearing Piles in Very Stiff Clay Soil Profile of a Bridge with 800 ft Radius and 8 - 100 ft Spans ( $\Delta T_{\text{slab}} = 120^{\circ} \text{ F}$ , $\Delta T_{\text{the rest}} = 90^{\circ} \text{ F}$ ).....	345
Figure 9.19 – Deformed and Undeformed Shapes of End-Bearing Piles in 9 ft Deep Predrilled Holes of a Bridge with 800 ft Radius and 16 - 50 ft Spans ( $\Delta T_{\text{slab}} = 120^{\circ} \text{ F}$ , $\Delta T_{\text{the rest}} = 90^{\circ} \text{ F}$ ).....	346
Figure 9.20 – Deformed and Undeformed Shapes of End-Bearing Piles in 9 ft Deep Predrilled Holes of a Bridge with 800 ft Radius and 8 - 100 ft Spans ( $\Delta T_{\text{slab}} = 120^{\circ} \text{ F}$ , $\Delta T_{\text{the rest}} = 90^{\circ} \text{ F}$ ).....	347
Figure 9.21 – Top View of Deformed and Undeformed Shapes of End-Bearing Piles in Various Soil Profile Types of Bridges with 800 ft Radius and 800 ft Length ( $\Delta T_{\text{slab}} = 120^{\circ} \text{ F}$ , $\Delta T_{\text{the rest}} = 90^{\circ} \text{ F}$ ).....	353
Figure 9.22 – Deformed and Undeformed Shapes of End-Bearing Piles in Various Soil Profile Types of Bridges with 800 ft Radius and 800 ft Length ( $\Delta T_{\text{slab}} = 120^{\circ} \text{ F}$ , $\Delta T_{\text{the rest}} = 90^{\circ} \text{ F}$ ).....	354
Figure 9.23 – Lateral Displacement of End-Bearing Piles in Various Soil Profile Types of Bridges with 800 ft Radius and 800 ft Length ( $\Delta T_{\text{slab}} = 120^{\circ} \text{ F}$ , $\Delta T_{\text{the rest}} = 90^{\circ} \text{ F}$ ).....	355
Figure 9.24 – Longitudinal Displacement of End-Bearing Piles in Various Soil Profile Types of Bridges with 800 ft Radius and 800 ft Length ( $\Delta T_{\text{slab}} = 120^{\circ} \text{ F}$ , $\Delta T_{\text{the rest}} = 90^{\circ} \text{ F}$ ).....	356
Figure 9.25 – Lateral Displacement of End-Bearing Piles in 9 ft Deep Predrilled Holes at Different Locations in the Abutment of Bridges with 800 ft Radius and 800 ft Length ( $\Delta T_{\text{slab}} = 120^{\circ} \text{ F}$ , $\Delta T_{\text{the rest}} = 90^{\circ} \text{ F}$ ).....	357
Figure 9.26 – Longitudinal Displacement of End-Bearing Piles in 9 ft Deep Predrilled Holes at Different Locations in the Abutment of Bridges with 800 ft Radius and 800 ft Length ( $\Delta T_{\text{slab}} = 120^{\circ} \text{ F}$ , $\Delta T_{\text{the rest}} = 90^{\circ} \text{ F}$ ).....	358

# CHAPTER 1

## INTRODUCTION

### 1.1 Introduction

Over the years, many types of expansion joints, expansion bearings, and other structural release mechanisms have been used on long, multi-span highway bridges to accommodate thermal movements. The desirable characteristics of an expansion joint are water-tightness, smooth ride ability, low noise level, wear resistance, and resistance to damage caused by snowplow blades. The performances of many joint systems, however, are disappointing. When subjected to traffic and to bridge movement, these joints fail in one or more important aspects, notably water-tightness [1.1]. They often leak and allow water contaminated with salt and debris to be spilled onto the substructure and the underside of the deck. An example of a bridge with expansion joints is shown in Figure 1.1. Examples of damaged expansion joints and their effects on the substructure are shown in Figure 1.2.

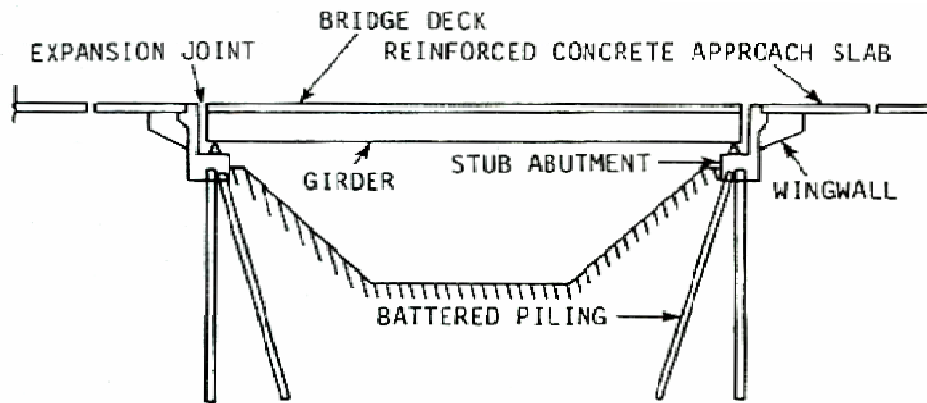
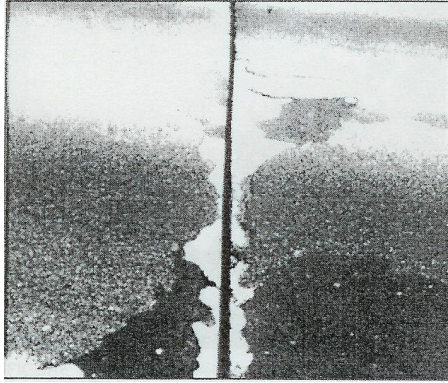
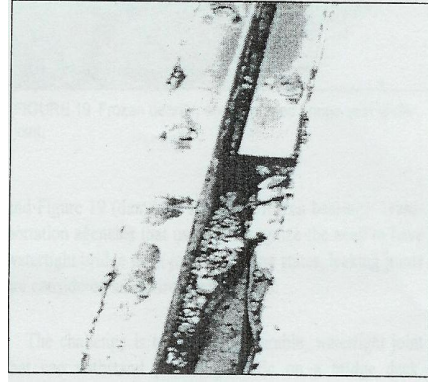


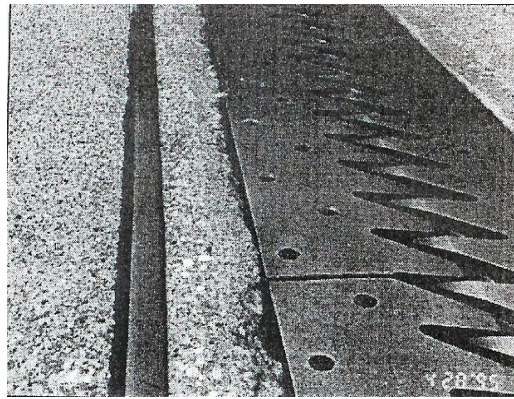
Figure 1.1 – Bridge with Expansion Joints



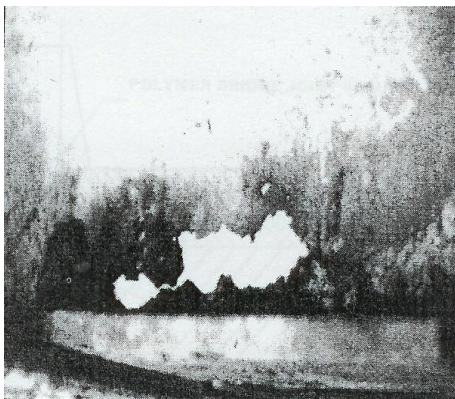
**a) Damaged Butt Joints**



**b) Damaged Joint Armor**



**c) Damaged Concrete around Finger Joint**



**d) Corroded Steel Beam End**



**e) Frozen Bearing and Damaged Bridge Seat under Joint**

**Figure 1.2 – Damaged Expansion Joints and Their Effects on the Substructure  
[Source: 1.2]**



The rehabilitation or retrofitting of bridge deck joints was studied by Amde et al. [1.3]. The concept of integral and semi-integral abutment bridges was developed in an attempt to eliminate joints in these locations.

Integral abutment bridges (Fig. 1.3) are single- or multiple-span structures with flexible foundations (single row of steel piles) in which the girders are integrated with the abutments. Expansion joints and moveable bearings at the end of the deck are replaced with control joints at the end of the approach slab, where joint leakage will not adversely affect the structure. The effect of longitudinal forces in the structure is minimized by making the foundation flexible and less resistant to longitudinal movement [1.4, 1.5, Amde et al. [1.6-1.8]]. The approach slab to bridges was studied by Amde et al. [1.9-1.16]. Figure 1.4 shows integral abutment details used by six transportation departments [1.4].

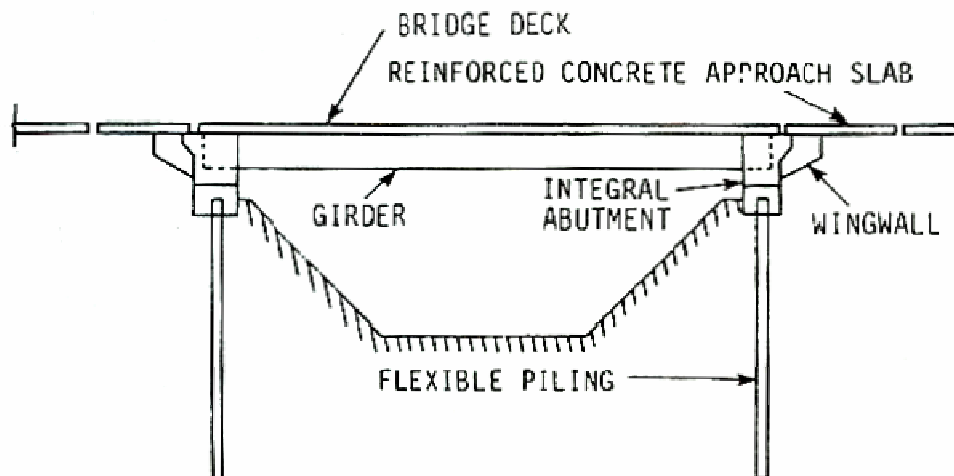
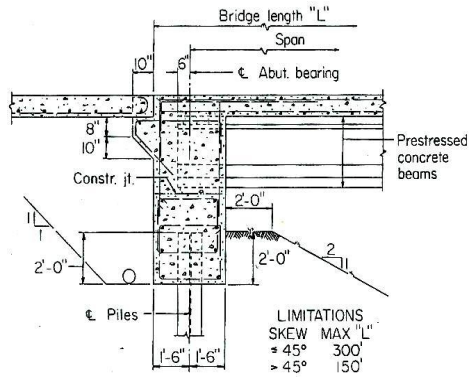
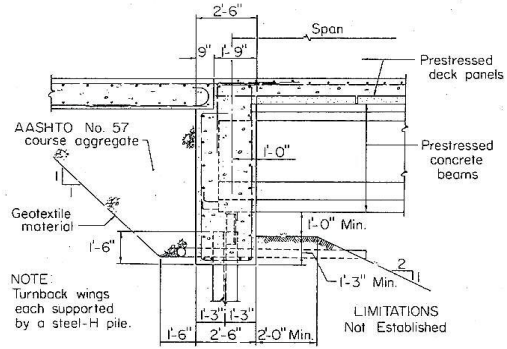


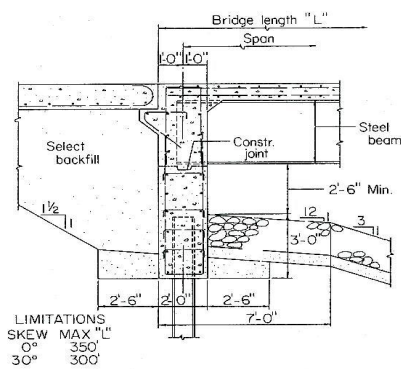
**Figure 1.3 – Bridge with Integral Abutments**



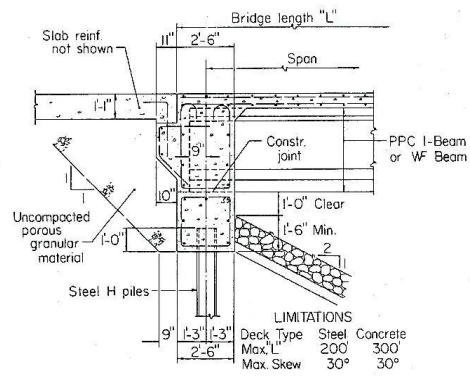
a) Iowa



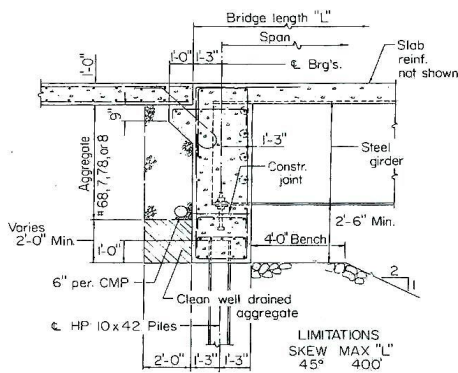
b) Pennsylvania



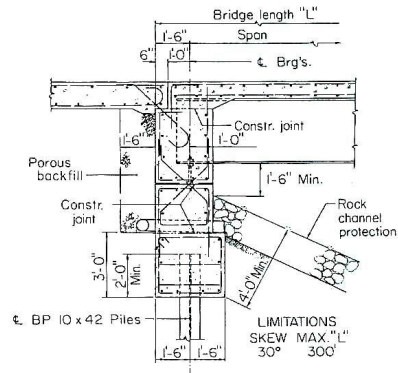
c) North Dakota



d) Illinois



e) Tennessee



f) Ohio

Figure 1.4 – Integral Abutment Details [Source: 1.4]

Semi-integral abutment bridges are single- or multiple-span structures with rigid foundations (spread footings) which are designed to minimize the transfer of rotational displacement to the pilings. Rotation is generally accomplished by using a flexible bearing surface at a selected horizontal interface in the abutment, since allowing rotation at the pile top generally reduces pile loads. A control joint is provided at the end of the approach slab that is detailed to slide in between the wing walls [1.4, 1.5, Amde et al. [1.6-1.16], 1.17-1.20]. Figure 1.5 shows semi-integral abutment details used by Ohio Department of Transportation [1.4].

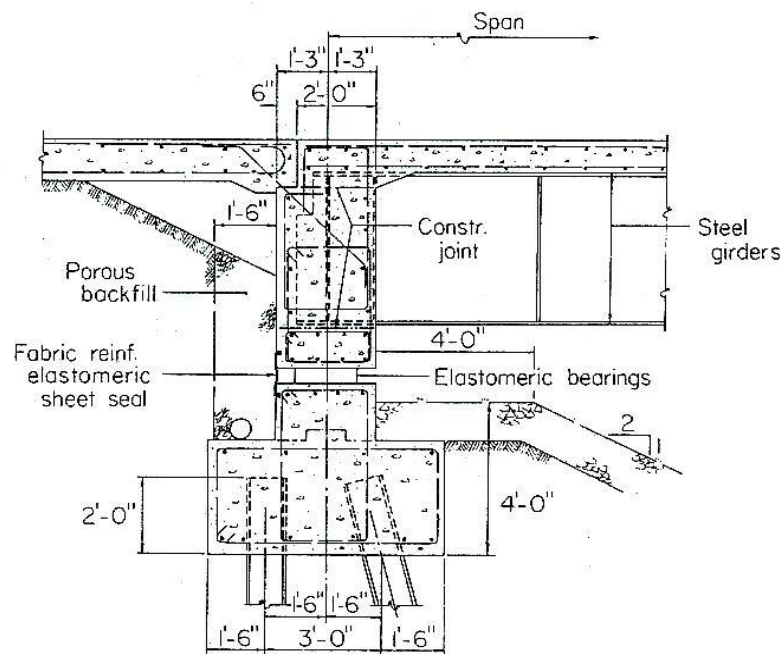


**Figure 1.5 – Semi-Integral Abutment Details: Ohio [Source: 1.4]**

Integral abutment bridges are more economical than semi-integral abutment bridges because of both the elimination of bearings and abutment footings and the use of smaller and lighter abutments. These economic advantages have been recognized by bridge design engineers for many years [1.4, 1.5, Amde et al. [1.6-1.8, 1.21, 1.22]].

## **1.2 Background**

The development of integral abutment bridges began on an experimental basis during the 1930s in the United States, New Zealand, and Australia. At first, these bridges were relatively short, ranging in length from 50 ft (15.24 m) to 100 ft (30.48 m). Because rational design guidelines were not available, any subsequent increase in allowable length was based empirically on reports of successful performance of a prototype in the field. As a result, each highway agency has developed its own unique length limitations and other design criteria for its integral abutment bridges.

In 1980, a Federal Highway Administration (FHWA) technical advisory (“Integral, no-joint structures” 1980) was issued, recommending the following length limits for integral abutment bridges:

- 300 ft (91.4 m) for steel;
- 500 ft (152.4 m) for poured-in-place concrete;
- 600 ft (182.9 m) for prestressed concrete.

These tentative FHWA length recommendations have indeed been exceeded by some highway agencies, notably Tennessee and Missouri [1.22].

### **1.2.1 Design of Integral Abutment Bridges**

The design of abutment-superstructure continuity connections and transverse wingwalls can be standardized for a wide range of bridge applications. A nominal amount of reinforcement will be suitable to resist the slight live and dead loads typical of such applications plus a wide range of secondary effects (shrinkage, creep, thermal gradient, passive pressure, etc.). Also, a nominal amount of reinforcement can be provided for transverse wingwalls to resist the maximum anticipated passive pressure. Once these standard details are established, each bridge abutment can be configured and reinforced for the vertical reactions associated with various roadway widths and span lengths. In general, this consists of no more than the determination of an appropriate pile load, spacing and pile cap reinforcement [Amde et al. [1.6-1.16, 1.21, 1.22], 1.23, 1.24].

The design of piers is similarly accomplished. Essentially all horizontal superstructure loads are distributed to approach embankments, and moments resulting from pier-superstructure continuity are negligible. Therefore, piers of integral bridges (capped-pile or free-standing types with movable bearings) need to be designed only for vertical superstructure and pier loads and for lateral loads that may be applied directly to the piers (stream flow, stream debris, earth pressure, wind). Where these lateral pier loads are small, as usually the case, most piers, like abutments, can be designed specifically for vertical loads alone [Amde et al. [1.6-1.16, 1.21, 1.22], 1.23, 1.24].

For flexible piers that receive much of their lateral support from their connection to the superstructure, construction procedures are necessary to ensure that

these piers are not laterally loaded until after they have been connected to the superstructure and after the continuity connections to the superstructure abutment have been completed [Amde et al. [1.6-1.16, 1.21, 1.22], 1.23, 1.24]. The steel H or HP piles are the types most frequently used, but cast-in-place, prestressed, pipe and concrete-filled steel-sheet piles have also been used. The design of piles in integral abutment bridges has been presented by Amde et al. [1.25-1.30], and Abendroth et al. [1.31].

### **1.2.2 Performance of Integral Abutment Bridges**

Many researchers have studied the performance of integral abutment bridges [1.5, Amde et al. [1.7-1.9, 1.21, 1.22], 1.32-1.37]. Integral abutment bridges perform adequately well; however, many of them operate at high stress levels. For instance, an abutment supported on a single row of piles is considered flexible enough to accommodate longitudinal thermal cycling of the superstructure and dynamic end rotations induced by the movement of vehicle traffic. The steel piles of such an abutment are routinely subjected to axial and flexural stresses approaching, equaling, or exceeding yield stresses. The stress at the top of the pile is sufficient to initiate a yield stress in the steel but not sufficient to cause the formation of a plastic hinge [Amde et al. [1.25-1.30], 1.38]. However, for longer integral abutment bridges, such piling stresses, if large enough, they will result in the formation of plastic hinges that will limit the flexural resistance of the piles to additional superstructure elongation. Lack of movement of the abutments can cause higher stresses in the deck than it is designed to sustain as the bridge attempts to expand or contract but is restrained

[1.23, 1.32]. At the same time, the laterally supported piles should retain their capacity to sustain vertical loads.

Even though there are similarities between the integral abutment details used by various transportation departments (Fig. 1.4), there also are important differences. Most critical are the wide variety of methods engineers have used to deal with passive pressure and with pile stresses.

To minimize passive pressure developed in abutment backfill by an expanding integral bridge, a number of controls, devices and procedures are used [1.39]. These include:

- limiting bridge length, structure skew and the vertical penetration of abutments into embankments;
- using select granular backfill and uncompacted backfill;
- providing approach slabs to prevent vehicular compaction of backfill or to permit the use of backfill voids behind abutments;
- using embankment benches to shorten wingwalls and using suspended turn-back wingwalls;
- and using semi-integral abutment designs to eliminate passive pressure below bridge seats.

Longitudinal forces in superstructures are related to the resistance of abutment pile foundations to longitudinal movement. Therefore, pile stresses are dealt with by [1.39]:

- limiting the foundation of integral bridges to a single row of slender vertical piles;

- limiting the pile types;
- orienting the weak axis of H-piles normal to the direction of movement;
- using pre-bored holes filled with fine granular material for piles;
- providing an abutment hinge to control pile flexure;
- limiting structure skew;
- and using semi-integral abutment designs for longer bridges to minimize foundation restraint to longitudinal movement.

The main advantages of integral abutment bridges over bridges with expansion joints [1.4, 1.5, Amde et al. [1.6-1.8, 1.40], 1.33] are:

- No cost for maintenance or replacement of faulty expansion joints.
- Low initial cost of design, manufacture, and installation due to the simplicity of the abutment and wingwall design.
- Fewer piles are required for foundation support and no battered piles are needed.
- Low maintenance cost.
- Improved seismic performance.
- Greater end-span ratios are achievable.
- Smooth, uninterrupted deck of the integral bridge is aesthetically pleasing and improves vehicular riding quality.

The disadvantages of integral abutment bridges [1.23, 1.33] are:

- Increased earth load can cause abutment cracking.
- Cracks developed in the asphalt backface of the abutments, as a result of which a bump at the end of bridge or approach slab could appear.



- Integral abutment bridges are limited to pile supported abutments, and drill shafts cannot be used.
- Lack of rational methods for predicting behavior. Also, thermal stresses are unknown.
- Temporary shoring will be required in precast bridges.
- Crane cannot go close to place precast beams, since backfill is put in after the beams have been placed. Therefore, cranes with large booms are required.
- Longer than normal approach slab is required.
- Limits future modifications, such as widening.
- Cracks in slab, end diaphragm or wingwalls are possible.
- Erosion of the approach embankment caused by water intrusion.
- Field problems exist when constructing a bridge on a steep slope.

However, in most cases, the integral abutment bridges have not caused major structural damage or affected the long-term serviceability of these structures.

The following are some comments made about construction and maintenance problems using integral abutments [1.32, 1.41]:

- Field placement of precast beams could be a problem, since cranes cannot get close to the abutments because the backfill is not placed until after the beams are placed.
- The proper compaction of backfill is critical.
- Careful consideration at the end of the bridge is necessary.

- The effects of elastic-shortening after post-tensioning should be carefully considered.
- Wingwalls may need to be designed for heavier loads to prevent cracking.
- Adequate pressure relief joints should be provided in the approach slab to avoid overstressing of the abutments.
- Positive tie connection between the approach slab and abutment may be necessary to avoid opening in cold weather.

### **1.3 Statement of the Problem**

Integral abutment bridges have reduced maintenance, improved riding quality, lower impact loads, reduced snow plow damage and structural continuity for live load and seismic resistance. However, the thermal movements of the bridge must still be accommodated. Because the entire bridge is tied together, there are restraint forces from the abutments and piers. The general design philosophy is to build flexibility into the support structures to the extent feasible while providing sufficient strength for restraint forces that cannot be completely eliminated. However, the magnitude of expected thermal movements and the effective stiffnesses of restraining elements considered in determining design forces are uncertain. The design of these bridges has, for the most part, been based on judgment and empirical rules rather than on scientific and engineering understanding of material and structural responses [1.24, 1.42].

### **1.3.1 Secondary Effects**

Like most of their jointed bridge counterparts, integral bridges are subjected to secondary effects due to shrinkage, creep, thermal gradients, differential settlement, and differential deflections. They are also subjected to passive pressure effects when abutment backfill is compressed during superstructure elongation and to pavement relief joint pressures when moisture and sustained high temperatures trigger pavement growth. The stress levels generated by these secondary effects are generally well understood but as of yet, not well quantified. However, they can be controlled and be provided for to such an extent that, except for continuity connections at supports, they usually need not be considered when designing short single span or multiple span continuous bridges of less than 300 ft (91 m) long [1.43].

### **1.3.2 Thermal Gradients**

The simultaneous axial load due to thermal effects could be either tension or compression induced by the resistance of abutments to longitudinal bridge movements and by the extreme low or high ambient temperatures, respectively.

When the sun is shining on the bridge, the exposed concrete surface has temperature increase at a higher rate than the remaining concrete. Hence, the sun causes unequal temperature within the concrete. After sundown, the concrete temperature is influenced by the current temperature of the concrete and the air temperature. By daybreak, the air will have had the best possible chance to equalize the temperature throughout the concrete [1.38].

In the summer, the bridge deck was heated and cooled not only by the surrounding air but also, more significantly, by the solar radiation affecting the top of the bridge deck. Solar radiation drives the bridge behavior during the summer months by creating a thermal gradient across the width and depth of the bridge. In the winter, the bridge deck was heated and cooled by the air surrounding all sides of the bridge. Solar radiation played a much smaller part in bridge deck temperatures during the winter because of the tilt of the earth [1.32].

Burke [1.43] recommended a number of primary limitations to minimize secondary effects:

- Bridge length – less than 300 ft (91 m).
- Bridge spans – less than 80 ft (24 m).
- Skew – less than 30 degrees.
- Curvature – less than 5 degrees.
- Settlement of supports should be limited to less than one thousandth of the span length.

### **1.3.3 Straight Bridges with Integral Abutments**

Straight integral abutment bridges subjected to thermal gradient were studied by many researchers [1.24, 1.32, 1.38, 1.42]. They concluded that thermal gradient had a relatively small effect on the movements of the abutments and piers of short bridges (less than 300 ft). Its effect on long bridges might be significant.

Arockiasamy et al. [1.44] studied the secondary effects considering creep, shrinkage, and temperature with emphasis on predrilled holes, types of soil (previously studied

by Amde et al. [1.25-1.30, 1.40, 1.45]), water table level and pile orientation. They found that water table elevation had very little significance on the response of laterally loaded piles and also confirmed the current practice of orienting the piles supporting the integral abutments along the weak axis. Faraji et al. [1.46] studied the reaction of the soil behind the abutments and next to the foundation piles, especially during thermal expansion. Results from this study showed that the level of soil compaction behind the abutment wall was a vitally important factor affecting the overall bridge behavior.

#### **1.3.4 Skewed Bridges with Integral Abutments**

The skewed bridges with integral abutments were studied by Greimann and Amde [1.47], and Haj-Najib [1.48]. The survey questions were sent to several states about the direction of thermal expansion and contraction of the integral abutments of skewed bridges and their pile orientations in the integral abutments. Figure 1.6 shows pile orientations in the skewed bridges that were used in the questionnaire.

The pile orientations in the integral abutments on skewed bridges shown in Figure 1.6 can be classified into two parts:

- a) the web of the pile perpendicular or parallel to the roadway centerline—e.g., types 1a and 1b, respectively;
- b) the web of the pile parallel and perpendicular to the centerline of the abutment—e.g., types 2a and 2b, respectively.

One major difference between skewed and nonskewed bridges with integral abutments is that when both are subjected to thermal expansion and contraction, the

skewed bridges will have thermal-induced biaxial bending stresses on piles if pile orientation 2a or 2b is specified. This becomes a three-dimensional analysis problem. For types 1a and 1b, pile orientations will have the same thermal effects as with nonskewed integral-abutment bridges.

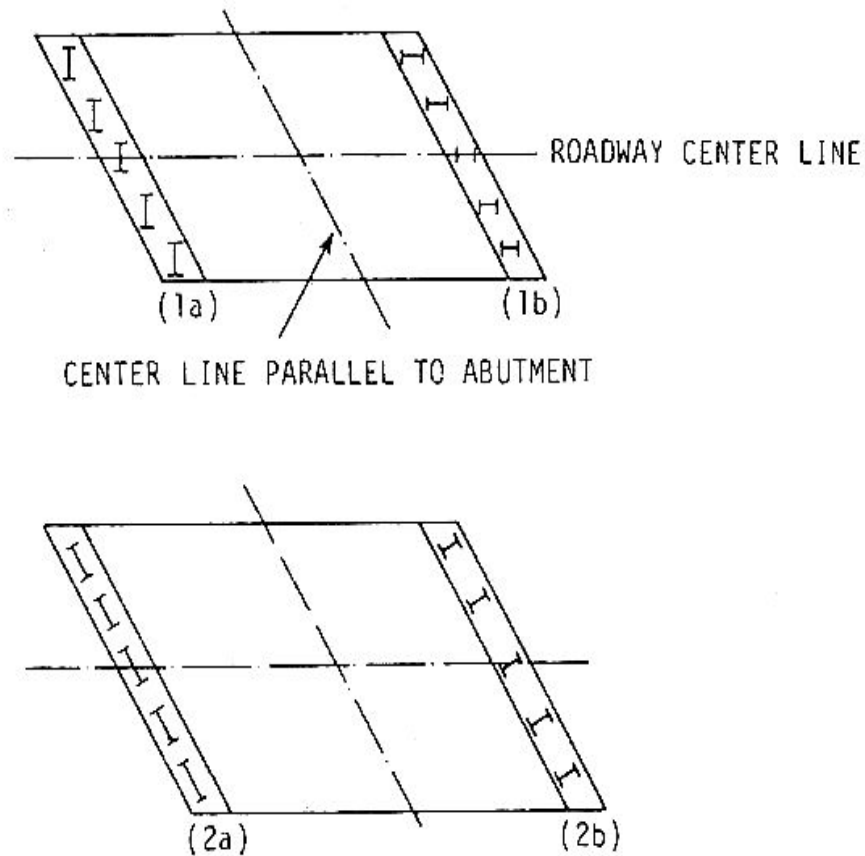


**Figure 1.6 – Pile Orientations in the Skewed Bridges [Source: 1.47]**

They concluded that if the bridge design has a small skew ( $\leq 10^\circ$ ) and a relatively small anticipated movement at each abutment ( $\pm 0.375$  in.), no special consideration need be given beyond that of a  $0^\circ$  skew condition. For a long skewed bridge with integral abutment, temperature-induced stresses become very critical to

the piling load capacities. If pile orientations 2a and 2b are adopted, the thermal expansion or contraction along the roadway center can be divided into two components, one parallel to the pile web (transverse) and the other perpendicular to it (longitudinal). Thus, the piles in integral abutment skewed bridges will be subjected to biaxial bending due to thermal movement. It is also possible that in long skewed bridges, diagonal thermal expansion and contraction will cause serious problems. For large skewed bridges ( $\pm 40^\circ$ ), use shear keys on the bottom of the pile cap to prevent lateral movement of the pile cap.

Girton et al. [1.42] presented the design recommendation for integral-abutment piles after studying the behaviors of two skewed bridges in Iowa subjected to air temperatures. Field experimental and analytical studies of the straight and skewed bridges were also studied by Oesterle et al. [1.24, 1.49].

#### **1.4 Objectives and Scope**

This research is focused on horizontally curved steel I-girder integral abutment bridges. A three-dimensional finite element model is used to perform a parametric study to investigate the effect of different parameters on the behavior of horizontally curved steel I-girder integral abutment bridges. Parameters that are used in this study are: bridge length, temperature, soil profile type, span length, radius, and pile type. The finite element model considers the complete bridge including the superstructure, substructure and soil. The results of the study are used to make recommendations on the design and construction of horizontally curved steel I-girder integral abutment bridges.

## CHAPTER 2

### TEMPERATURE IN COMPOSITE BRIDGES

#### 2.1 Introduction

Thermal effects in bridges are caused by both short-term daily temperature changes and the more lengthy seasonal temperature change. There are many factors involved in the longitudinal deformation of a bridge, but among the major factors to be considered are thermally induced movements. Thermal effects are considered more frequently for steel bridges than for concrete bridges. Nonuniform temperature distributions throughout the depth of a bridge can create local stresses of considerable magnitude. Seasonal temperature changes cause bigger movements than daily changes. A combination of thermal strain and thermal stress is usually present because the materials are never completely free to move nor are they completely restrained [2.1].

There are two basic temperature cycles [2.2]: the daily cycle and the yearly cycle. The daily cycle usually begins with a low temperature being attained just before sunrise. The sun's appearance causes a steady rise in temperature until the daily peak temperature is reached, usually in midafternoon to a few hours before sunset, and then air temperature drops rapidly to a low reached to sunrise the next morning. The basic daily temperature cycle can be altered by clouds which shade the area or release some from of precipitation. Either of these conditions can result in a sudden drop of temperature. New air masses moving into a locality from a cooler or warmer region can also make the usual daily temperature cycle. The yearly



temperature cycle results from changes in position and distance of the earth relative to the sun. As the sun changes position and distance from the earth, the maximum solar radiation incident on the surface occurs on the longest day of the year, and the maximum ambient air temperature typically occurs several days later. Both temperature cycles are important. The daily cycle provides rapid temperature variations throughout the different parts of the structure, while the yearly cycle induces the greatest overall movements.

## **2.2 Thermal Movements**

Thermal movements were measured and studied in some detail for a number of bridges in England by Emerson [2.3-2.5]. This experimental work showed that thermal movements can be divided into two parts. First, there is a daily temperature cycle and the movements associated with this cycle. These daily movements tend to be much larger for steel bridges than for concrete bridges, because the steel may experience the full daily range of air temperature while the average temperature of the concrete has much less variation. Concrete bridges have much greater thermal mass, and so they do not fully adapt to short term temperature changes as does steel. Direct radiation of the sun may cause daily local temperatures which greatly exceeds the air temperature for both steel and concrete. Steel that is exposed to this direct radiation may quickly assume a similar temperature throughout the section because of the conductivity and relatively low thermal mass of the steel. Concrete bridge decks are commonly exposed to direct solar radiation and this affects their daily temperature cycle. However, the average temperatures of the bridge deck seldom approach the

ambient temperatures because of the thickness of the deck [2.6]. Daily temperature cycles of concrete decks exposed to solar radiation are often larger than the air temperature cycles, especially when decks are thin [2.7].

The second part of the thermal movements is caused by the annual temperature cycle. This component is usually considerably larger than the movement due to the daily cycle. Concrete bridges will experience smaller annual movements than steel bridges because the extreme high and low annual temperatures are of short duration. The mass of the concrete bridge prevents it from responding to very short duration temperature changes, but the relative difference of the annual cycle movements for concrete and steel bridges is much smaller than the relative difference of the daily temperature cycle movements. Movements in concrete bridges are dependent upon a smaller range such as a three day running average of the air temperature [2.6].

The bridge bearings and expansion joints are designed for thermal movements. In other cases the bridge piers and abutments may be integrally constructed with the superstructure [Amde et al. [1.25-1.30], 1.36, 2.8], and thermal movements may be accommodated by deflection of the piers or movement of the abutment into the backfill. In a few cases, the bridge will restrict all movement and the thermal forces will be resisted within the structure. Extremely large forces,  $F_T$ , are possible if all movement is restrained. If the movement is restrained in one direction only, the force is [2.6]:

$$F_T = AE \left( \frac{\Delta L}{L} \right) \dots\dots\dots(2.1)$$

where  $A$  = cross sectional area of the restrained elements;

$E$  = the elastic modulus.

## **2.3 Analysis of Thermal Movements**

Analysis of thermal movement is the determination of the temperatures within the bridge as a function of time. Temperature calculations are based on 3 basic heat flow components: radiation, convection, and conduction [2.6, 2.9]. Accurate determination of the temperature of the bridge requires consideration of all 3 components of heat flow, and it requires other information including the cloud cover, air temperature, wind speed, the angles of the sun, the orientation of the structure with respect to the sun, and the geometry and materials of bridge [2.6].

### **2.3.1 Radiation**

Heat transfer by radiation is generally considered to be the most important of three mechanisms. During the daylight hours when the structure is exposed to the sun, especially during the warm summer months, a net gain of heat energy occurs through the depth of structure, primarily as a result of the solar radiation impinging on the surfaces of the structures. Conversely, a net loss of heat energy occurs during the night as a result of the additional radiation in the surrounding environment due to the heat energy stored in the structure. During the summer, the temperature in the top surface of the bridge deck is warmer than the soffit, which results in a positive gradient. Negative gradient develops on typical winter nights when the top surface is cooler than the soffit. The intensity of the solar radiation reaching the surface of the earth is dependent on the angle at which the radiation passes through the atmosphere

and on the length of daylight time [2.9]. This intensity is dependent on latitude and has an annual variation, as shown in Figure 2.1.

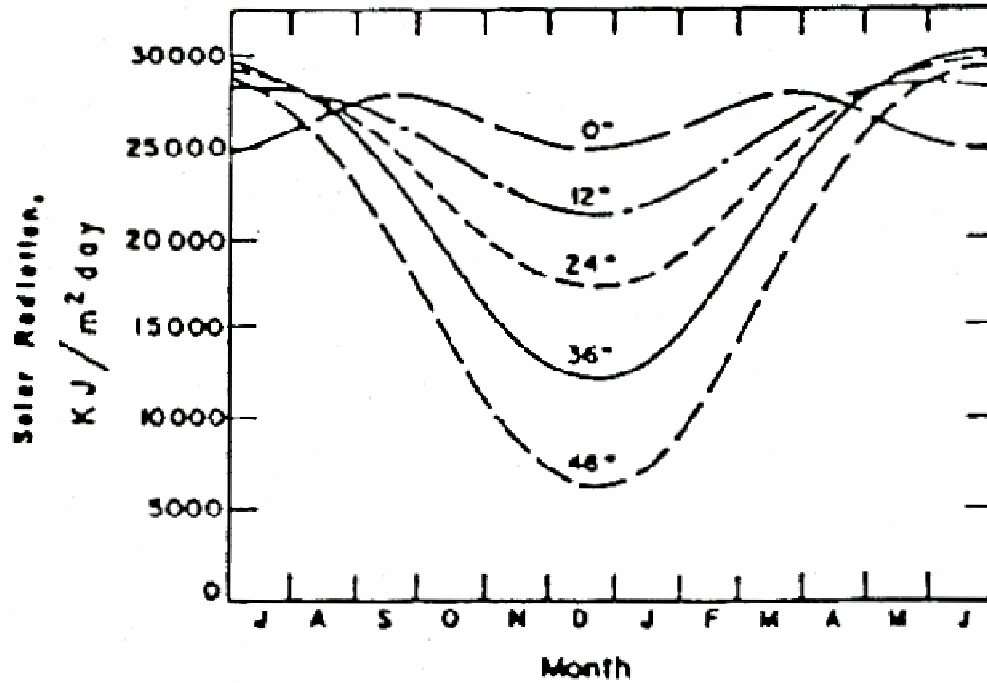


Figure 2.1 – Variation in Solar Radiation for Various Latitudes [Source: 2.10]

In addition, the intensity of the solar radiation reaching the surface of a bridge is dependent on several other factors, each pertaining to the condition of the earth’s atmosphere. These factors are shown diagrammatically in Figure 2.2. The intensity of solar radiation varies daily, as shown in Figure 2.3. Moreover, because of the poor thermal conductivity of concrete, these diurnal variations result in temperature gradients within the bridge superstructures [2.9].

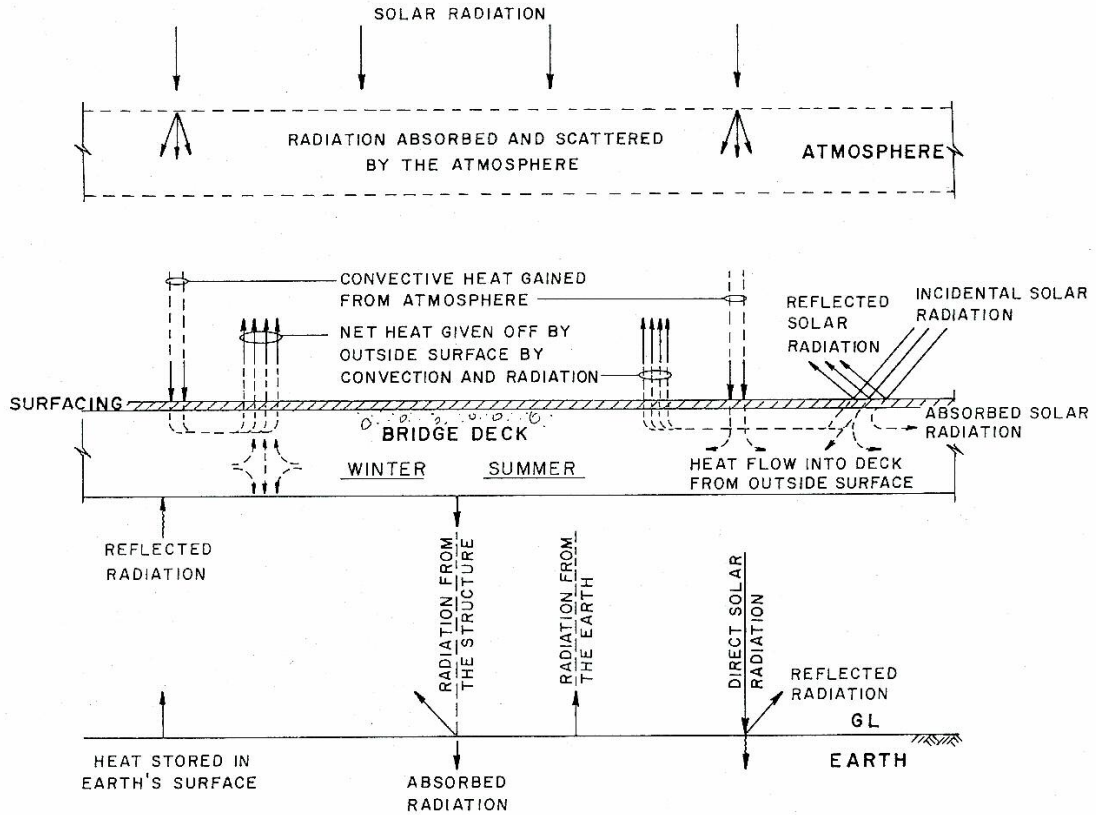


Figure 2.2 – Solar Radiation Reaching the Surface of a Bridge [Source: 2.9]

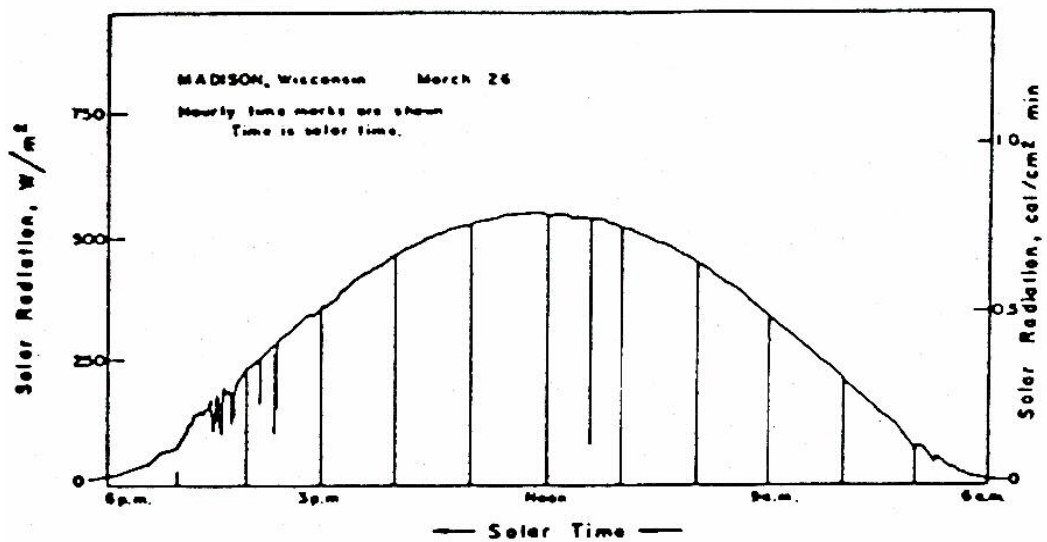


Figure 2.3 – Variation in Solar Radiation for a Clear Day [Source: 2.10]

As shown in Figure 2.2, the radiation which penetrates the atmosphere and reaches the surface of a bridge deck has two primary effects. It may be reflected or it may penetrate the surface, be absorbed and be converted to heat. The amount of absorbed radiation in a bridge structure is dependent on the type of surfacing. Various media absorb different quantities of radiation. Colored bodies are distinguished by their selective absorption of different wavelengths of light. A body which absorbs all wavelengths is defined as a “blackbody.” Concrete structures function as “gray bodies” because they absorb only a certain amount of wavelength and reflect the remainder [2.9].

### **2.3.2 Convection**

Convection is the transfer of heat from a solid (the bridge) to moving air or fluid. This heat flow is influenced by the air temperature and is largely driven by the wind or by air currents caused by moving traffic. Convection tends to reduce the extremely high temperatures, caused by radiation, of the bridge during the summer, and it may lower the extremely low temperatures which occur during cold winters [2.6].

### **2.3.3 Conduction**

Conduction is the flow of heat within the bridge, since all solid bodies are moving toward a uniform equilibrium temperature in the absence of other outside influences [2.6].

## 2.4 Solar Radiation

Solar radiation is the predominant source of temperature change in most bridges after initial hydration of the cement paste. The deck absorbs part of the radiant energy from the sun, and the remainder is reflected. A dark surface absorbs more radiation energy than a light surface, and a rough surface gains more radiation than a smooth surface. Bridges directly exposed to sunlight will have larger diurnal temperature cycles than shaded bridges in the same geographical region.

Asphaltic concrete overlays are usually much darker in color than portland cement concrete surfaces. An asphaltic concrete overlay absorbs more radiation than a portland cement surface and typically insulates the underlying concrete deck against temperature changes. Consequently, except for overlays thinner than 2 in., asphaltic concrete overlays typically reduce the effects of radiation [2.7].

The rate of solar energy incident upon a surface normal to the sun rays is [2.11]:

$$I_n = I_{sc}K_T \dots \dots \dots (2.2)$$

in which  $I_{sc}$  = rate at a point on the outer edge of the earth's atmosphere. This rate is called a solar constant;

$K_T$  = a transmission coefficient accounting for the attenuation of solar radiation by the atmosphere.

$$K_T = 0.9^{k_a t_u / \sin(\theta_a + 5^\circ)} \dots \dots \dots (2.3)$$

in which  $k_a$  = ratio of atmospheric pressure to pressure at sea level.  $k_a$  is equal to 1.0 at sea level, and 0.94, 0.89, 0.84, and 0.79 for altitudes of 500, 1,000, 1,500, and 2,000 m accordingly;

$t_u$  = a turbidity factor accounting for the effect of clouds and air pollution. It can be assumed to have values ranging from two (for a clear-sky situation) to eight (when air pollution is present) [2.12];

$\theta_a$  = solar altitude.

When the sun rays make an angle  $\theta$  with normal to the surface, the rate of solar radiation becomes:

$$I = I_n \cos \theta \dots\dots\dots(2.4)$$

The angle  $\theta$  can be described in terms of several angles defining the position of the sun relative to an observer on the earth and the orientation of the surface relative to the surface of the earth as follows [2.13] (see Fig. 2.4):

$$\cos \theta = \sin \delta \sin \varphi \cos \beta - \sin \delta \cos \varphi \sin \beta \cos \gamma + \cos \delta \cos \varphi \cos \beta \cos \tau + \cos \delta \sin \varphi \sin \beta \cos \gamma \cos \tau + \cos \delta \sin \beta \sin \gamma \sin \tau \dots\dots\dots(2.5)$$

in which  $\varphi$  = latitude of the location (north positive);

$\delta$  = solar declination, i.e., the angular position of the sun at solar noon with respect to the plane of the equator (north positive);

$\beta$  = angle between the horizontal and the surface;

$\gamma$  = surface azimuth angle, i.e., the angle between the normal to the surface and the local meridian, the zero point being south, east being positive and west being negative;

$\tau$  = hour angle, solar noon being zero, and each hour equaling  $15^\circ$  of longitude with mornings positive and afternoon negative.





Also, Eq. (2.4) does not apply to a shaded surface. The height of the shade of the overhanging slab on the web of a bridge (Fig. 2.4) is given by:

$$l_{sh} = l_c \frac{\tan \theta_a}{\sin(90 + \gamma - \gamma') \sin \beta - \cos \beta \tan \theta_a} \dots\dots\dots(2.9)$$

in which  $l_c$  = length of the overhanging slab;

$\beta$  = angle between the web and the horizontal;

$\gamma'$  = azimuth angle of the sun [2.15]:

$$\gamma' = \sin^{-1} \left( \frac{\cos \delta \sin \tau}{\cos \theta_a} \right) \dots\dots\dots(2.10)$$

## 2.5 Diurnal Air Temperature Variation

The diurnal variation of ambient air temperature is assumed to follow a sinusoidal cycle [2.11, 2.16] between the minimum air temperature,  $\min T_a$ , and the maximum air temperature,  $\max T_a$ . Thus:

$$T_a(t) = A \sin \frac{2\pi(t - \xi)}{24} + B \dots\dots\dots(2.11)$$

in which  $t$  = hour of the day;

$A$  = amplitude of the sine wave, or one-half the daily range of air

temperature, i.e.,  $A = \frac{1}{2} (\max T_a - \min T_a)$ ;

$B$  = average daily temperature, i.e.,  $B = \frac{1}{2} (\max T_a + \min T_a)$ ;

$\xi$  = a lag factor equal to 9.0, assuming the minimum air temperature to occur at 3:00 a.m. and the maximum air temperature to occur at 3:00 p.m.

## **2.6 Temperature Distributions**

The bottom elements of a bridge will ordinarily have the same temperature as that of the air [2.17]. The upper elements and the exterior beams will vary in temperature depending upon the amount of solar radiation received, the wind and the amount and type of precipitation [2.2]. The top of the deck slab is warmer than the bottom of the bridge when the sun shines on the exposed decks. The top will cool faster than the girders when a rain or snow storm first begins. A uniform temperature can exist just before sunrise when the air temperature has remained nearly constant for several hours. Thus, a variety of temperature distributions are possible throughout the depth of a bridge [2.1].

The horizontal movements of the bridge are primarily related to the average bridge temperature. This average temperature is an integration of the true temperature distribution over the total bridge at a given time. The true distribution may have a minor effect on the thermal movements, but it has a major influence on the temperature dependent deflections and rotations of the bridge girders and the thermal stress in the structure. Figure 2.5 shows a typical distribution of temperature in a steel girder-composite deck bridge during a hot summer day. The steel girder experiences very little temperature variation through its thickness or depth unless there are unusual circumstances such as the sun shining on a portion of a girder or local shading of a portion of the bridge [2.6].

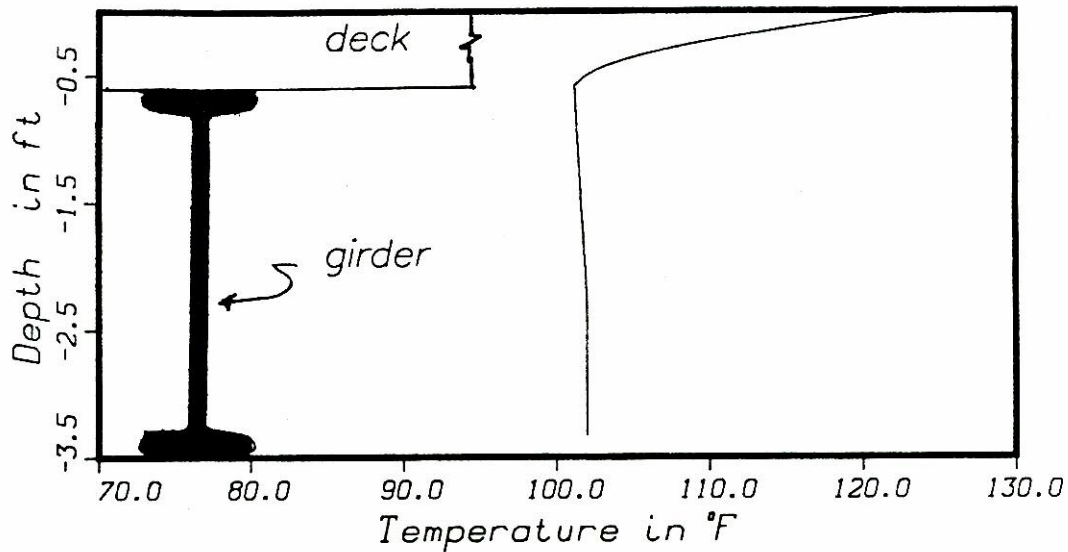


**Figure 2.5 – Temperature Distribution on a Composite Steel Girder on a Hot Summer Day [Source: 2.6]**

Temperature distributions in composite steel bridges were studied by many researchers. Narouka, Hirai, and Yamaguti [2.18] conducted several tests on a composite steel bridge and verified that there were nonlinear temperature gradients through the depth of the concrete deck. The maximum measured temperature gradient was about 16° F. Barber [2.19] presented a formula to estimate the maximum pavement surface temperature. The formulation included the relationships between pavement temperature, air temperature, wind speed, intensity of solar radiation, and the thermal properties of the pavement materials.

Zuk [2.17] attempted to predict the maximum bridge surface temperature for the Virginia area by using a modification of the equation originally presented by Barber [2.19]. He also presented an equation for determining the maximum temperature differential between the top and bottom of a composite steel bridge. Good correlation was reported between the measured and computed values. Field

tests further confirmed the accuracy of Zuk's equation in determining the nonlinear temperature distribution through the concrete deck. Temperature distribution in the steel beams was either uniform or varied. The computed maximum temperature differential was 24° F, compared to the measured temperature differential of 23° F. In addition, good correlation was obtained between the calculated maximum deck temperature of 102° F and the measured value of 98° F.

Zuk [2.20] found that the temperature differentials between the top and bottom of the concrete deck slab can be as high as 40° F (22° C) during the summer and as low as -10° F (-6° C) in the winter. In another study, Zuk [2.17] obtained field data on the vertical temperature distribution in a composite bridge over the Hardware River near Charlottesville, North Carolina. The results revealed that the maximum temperature differences between the top and bottom of the concrete deck slab ranged from +20 to + 35° F (11 to 19° C) during the day, and -3 to -7° F (-2 to -4° C) during the night. The vertical temperature distribution was almost linear in the concrete deck slab with very small variation through the depth of the steel girder and can be considered uniform and equal to the ambient temperature gradient.

Zuk [2.17] developed coefficients for the calculation of the maximum bridge surface temperature under two conditions. For a normal concrete deck in the Middle Atlantic States, the maximum surface temperature, in degrees Fahrenheit, is:

$$T_m = T_{avg} + 0.18L_a + 0.667 (0.50T_r + 0.054L) \dots\dots\dots(2.12)$$

in which  $T_m$  = the maximum surface temperature, °F;

$T_{avg}$  = the average daily temperature, °F;

$T_r$  = the daily range in air temperature, °F;

$L_a$  = the solar radiation received on a horizontal surface, in gram-calories per square centimeter per day.

The maximum surface temperature of a bitumen covered deck would be:

$$T_m = T_{avg} + 0.027L_a + 0.65 (0.50T_r + 0.081L) \dots \dots \dots (2.13)$$

The constants in both equations would vary depending on the local conditions. The Langleys of solar radiation,  $L_a$ , can be determined from U.S. Weather Bureau maps or can be measured with a pyrliometer.

An approximate equation for the maximum differential between the top and bottom temperatures of a composite steel and concrete bridge was also developed by Zuk [2.17]:

$$\Delta T_m = T_m - T_{avg} - \lambda T_r \dots \dots \dots (2.14)$$

in which  $\lambda$  = the factor indicating the phase lag between the maximum surface temperature and the maximum ambient temperature. For the Middle Atlantic States, a lag factor of 1/4 was found to be appropriate for the summer and a factor of 1/2 for the winter. Comparisons of the recorded temperature variation through the thickness of the slab with the calculated values showed fair agreement.

Berwanger [2.2] found that three temperature distributions were typical of those most likely to occur in a composite concrete deck and steel girder bridge as shown in Figure 2.6. The temperature of the bottom of the slab was assumed to be the same as that of the steel girder. The first case involved a uniform temperature throughout the slab which is not realistic since it contradicts other findings [2.20]. Cases two and three had a nonlinear temperature variation in the slab, one with the

top of the slab warmer than the bottom (positive gradient), and one with it cooler (negative gradient).

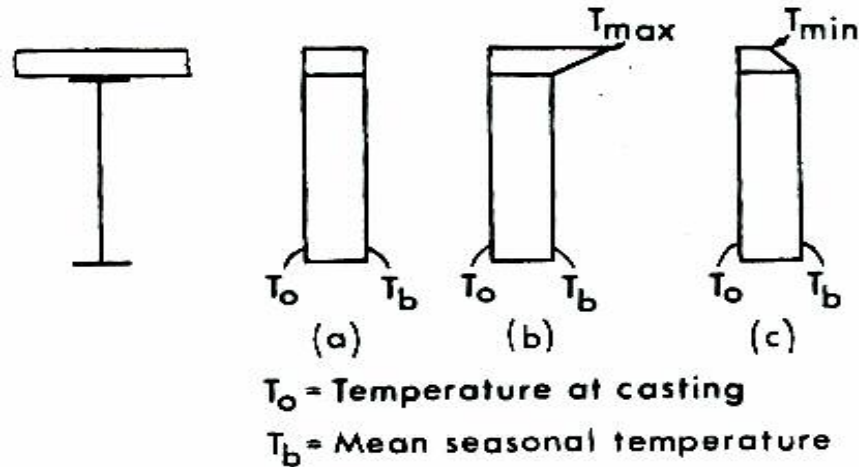


**Figure 2.6 – Vertical Temperature Distribution Proposed by Berwanger [2.2]**

Emanuel and Hulseay [2.16] studied the temperature distributions in composite bridges. They concluded that the magnitude of stress in a composite-girder bridge depends upon the temperature distribution, the internal induced forces produced by differences in thermal coefficients of expansion, and the boundary support conditions.

Chuchward and Sokal [2.21] studied the empirical relationships between the thermal loadings (such as the effective temperature) and the climatic parameters (such as ambient temperature and solar radiation). Application of such empirical relationships was limited to bridges of similar construction located in regions with similar climatic conditions.

The transient thermal behavior of continuous composite steel beam-reinforced concrete slab highway bridges was investigated both analytically and experimentally by Berwanger [2.22]. Temperatures and deformations were measured during transient

cooling of a 0.354 scale model of a three-span continuous bridge. A numerical procedure was presented for the solution of transient temperatures in composite slab-steel beam highway bridges. The two-dimensional finite element analysis predicted the temperature distributions of the cross section to  $\pm 0.5^\circ \text{F}$  ( $\pm 0.3^\circ \text{C}$ ). A linear temperature rectangular finite element was used. Statistical analyses indicated a better than 0.99 probability of correlation between the predicted and measured temperatures.

Ho and Liu [2.23] studied thermal loadings on highway bridges. These thermal loadings were treated as random variables. Values of such loadings for a 50-year return period were determined based on an analysis of the statistics of extremes. Calibration of the mathematical model was based on a comparison of the statistics of the measured and calculated thermal loadings and not, as is often the case, by comparing the analytical results with field data observed on any one particular day (or days). An explanation of Evan's method, which is used to calculate the first four moments of a random function, was also given, based on the idea of Gaussian quadrature. This method is an essential tool in the statistical study of the extreme values of thermal loadings. It was noted that the extreme values are random variables and that study of such values must be based on the methods of the statistics of extremes. Emphasis was placed on the statistical aspect of the thermal loadings rather than on the numerical modeling of the heat flow problem.

Extensive calculations and field measurements of bridge temperatures were performed by Moorthy and Roeder [2.24, 2.25]. Figure 2.7 shows the computed local bridge temperatures through the depth of a composite steel girder bridge at 4 p.m. on a hot summer day and at 3 a.m. on a cold winter night. These temperatures were



computed by consideration of conduction, convection, and radiation heat flow combined with the environmental conditions for the given date. Local bridge temperatures vary widely with time through the bridge cross section, but the average temperature of the bridge cross section,  $T_{Avg}$ , controls bridge movements [2.26].

$T_{Avg}$  is a weighted average of the bridge temperature over the bridge cross-section based upon equilibrium:

$$T_{Avg} = \frac{\sum A_i E_i \alpha_i T_i}{\sum A_i E_i \alpha_i} \dots\dots\dots(2.15)$$

- where
- $i$  = the segments of the bridge cross section;
  - $A_i$  = cross-sectional area of the  $i$  th segment;
  - $E_i$  = elastic modulus of the  $i$  th segment;
  - $\alpha_i$  = coefficient of thermal expansion of the  $i$  th segment;
  - $T_i$  = temperature of the  $i$  th segment.

Minimum values of  $T_{Avg}$  occur in the early morning hours of the coldest winter nights, and maximum  $T_{Avg}$  values occur in midafternoon of the hottest summer days.

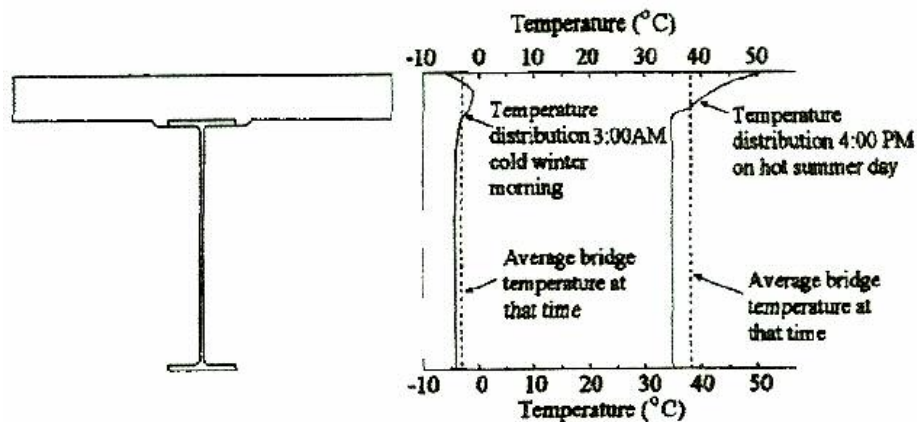


**Figure 2.7 – Typical Variation in Temperature for Steel Bridge with Composite Deck [Source: 2.25]**

## 2.7 Thermal Stresses

Thermal stresses are known to cause considerable damage in bridges. In composite concrete slab-on-steel beam bridges, these stresses can be significant when compared to dead or live load stresses. Such stresses also tend to magnify the development of cracks in the concrete deck slab leading to corrosion of the steel beams, the steel reinforcing and hence the spalling of the concrete, as well as to deterioration of the concrete by allowing the seepage of salt-laden water [2.27].

Bridge structures are subject to complex thermal stresses which vary continuously with time. The magnitude of these stresses depends upon the temperature variation within the structure and this depends upon the geographic location and the orientation of the bridge, climatological condition, cross section geometry and thermal properties of the material and the exposed surfaces.

Uniform temperature changes in a homogenous and isotropic material cause axial deformation. A varying temperature distribution through a bridge produces flexural deformation. In composite bridges, the concrete deck is anchored to steel girders by shear connectors. Theoretically, there is no movement between the steel girder and concrete deck at the interface. Thus the differing coefficients of thermal expansion of the steel and concrete will create additional stresses as the two materials try to match the movements of each other [2.2]. Internal thermal stresses are normally affected more by large temperature differentials than by the large overall temperature changes between summer and winter that will cause general expansion or contraction of a bridge [2.17].

For most bridges, daily temperature changes produce larger thermal stresses than seasonal temperature changes. Thermal stresses and risk of transverse deck cracking are greatest when daily temperature cycles are large, solar radiation is high, and large seasonal temperature differences exist. These conditions vary greatly by geographical location, and are unavoidable [2.7].

For steel girders supporting a concrete deck, stresses from seasonal temperature changes cause stress when the concrete has a different thermal expansion rate than the steel. Because most concretes have a lower coefficient of thermal expansion than steel has, seasonal temperature decreases will generally cause compressive stresses in the deck, and temperature increases will cause tensile stresses in the deck [2.7].

Several authors studied thermal stresses in composite steel bridges. Zuk [2.28] developed a rigorous method for computing thermal stresses and deflections in statically determinate composite steel bridges. This method made it possible to estimate the stresses and strains resulting from linear temperature gradients over the bridge cross section. Lui and Zuk [2.29] extended this work to include the temperature effects in simply supported, prestressed concrete bridges. This method included the change in prestressing force caused by the change in temperature of the tendon. Temperatures of the tendon were assumed to experience the same temperature as the surrounding concrete. Results of the study indicated that the change in the prestressing force varied from -3 to 5 percent of the initial prestress. Temperature-induced stresses were computed to be approximately 200 psi in compression and 100 psi in tension.

Zuk [2.20] presented a simple empirical formula for use as a design check of thermal stresses in simply supported composite highway bridges. The formula related the thermal stresses at the bottom of the girder to the temperature difference between the top and bottom of the slab and the depth of the bridge.

Berwanger [2.2] developed an equation which more fully considered the factors affecting thermal stresses found in composite reinforced concrete slab and steel beam bridges. In calculating the induced thermal stresses, he took into account the temperature differentials throughout the depth of the bridge and the difference between the coefficients of thermal expansion of the steel beams and concrete slab, as well as the different coefficients of thermal expansion of the reinforcing steel and the concrete slab.

Houk [2.30] conducted tests on small unreinforced beams to study the effects of volume changes thermally induced in massive concrete structures at locations of high restraint. Tensile and compressive strains were measured at the outer fibers of plain concrete beams. He found that the magnitudes of these thermal stress-strain values to be significant near test failure. Strains developed by the temperature changes would approach those measured at failure of the beam in loading.

## **2.8 Thermal Responses**

Thermal response of bridge decks is a complex transient phenomenon influenced by many parameters, as indicated for a typical section in Figure 2.8. In addition to the fundamental influence of the time-dependent solar radiation, response

is affected by ambient temperature and wind speed fluctuations, material properties, surface characteristics, and section geometry [2.31].

The increase of the deck surface temperature results in a tendency for the superstructure to hog upwards between the abutments, which if restrained by internal supports induce sagging bending moments. These can be of comparable magnitude to those resulting from design live load [2.32]. Although longitudinal flexural stresses induced by restraint of vertical temperature gradients are the most significant effect of thermal loading, a number of other aspects are important. Restraint of thermal hogging curvatures involves a redistribution of support reactions with increased shear force in the end spans, and the possibility of bearing failure at the abutments [2.31].

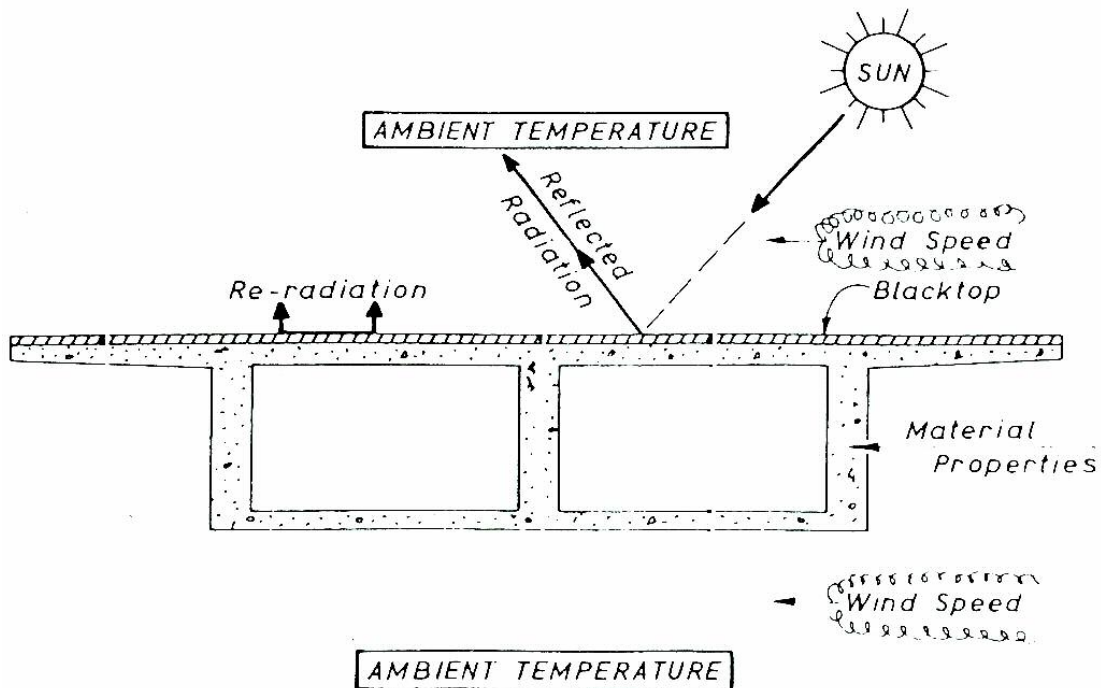


**Figure 2.8 – Factors Affecting Thermal Response [Source: 2.31]**

## 2.9 Thermal Responses in Curved Bridges

Field observations have shown that curved bridges have thermal movements which are neither on the tangent nor the chord. In some cases, the radial component of movement is of similar magnitude to the chord or to tangential movement [2.6].

Juhl [2.33] proposed an approximate method for the computation of the displacements of boundary points of curved bridges. The application of the method was demonstrated for a circular slab. In the example, two different lateral support conditions (Fig. 2.9) were chosen to demonstrate how these conditions affect the directions of the boundary displacements. Condition I had one interior bearing with lateral movements restricted in all directions and, with a rocker bearing at one end, allowing lateral displacements in only one direction. Condition II was provided by three rocker bearings with only one lateral direction of movement each. It was found that the shapes of the deformed plates under the two support conditions with equal and uniform temperature change were identical, and they were affined to the original shape. Only the locations of the two plates were different after the temperature change as shown in Figure 2.9.

Scale for displacements  
 $u$  and  $v$ , 1 in. =  $20 \frac{\text{in.}}{E\delta}$

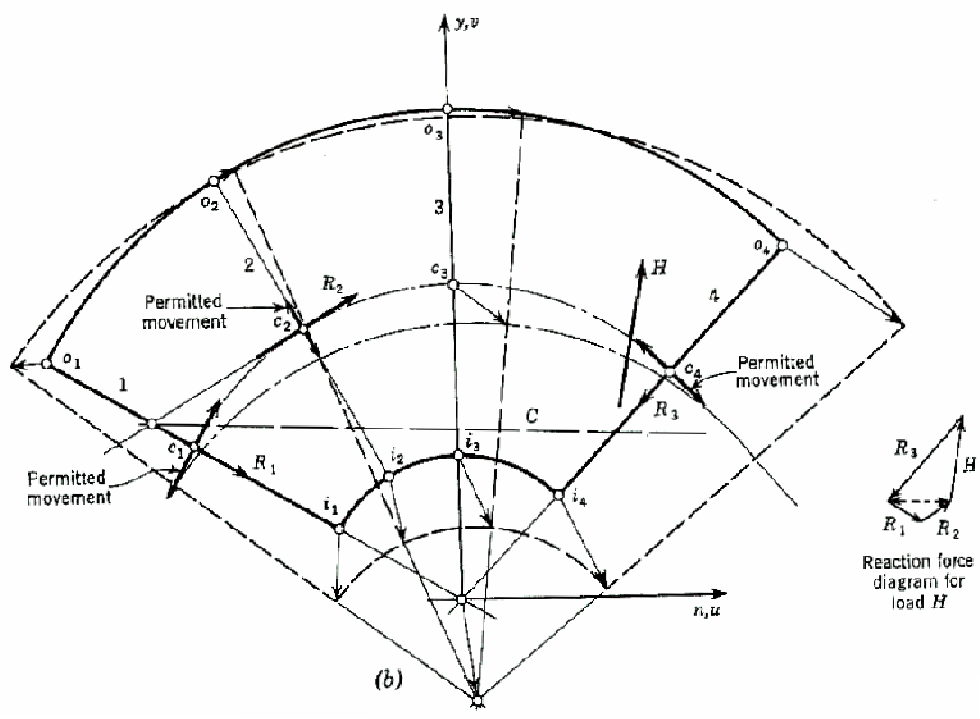
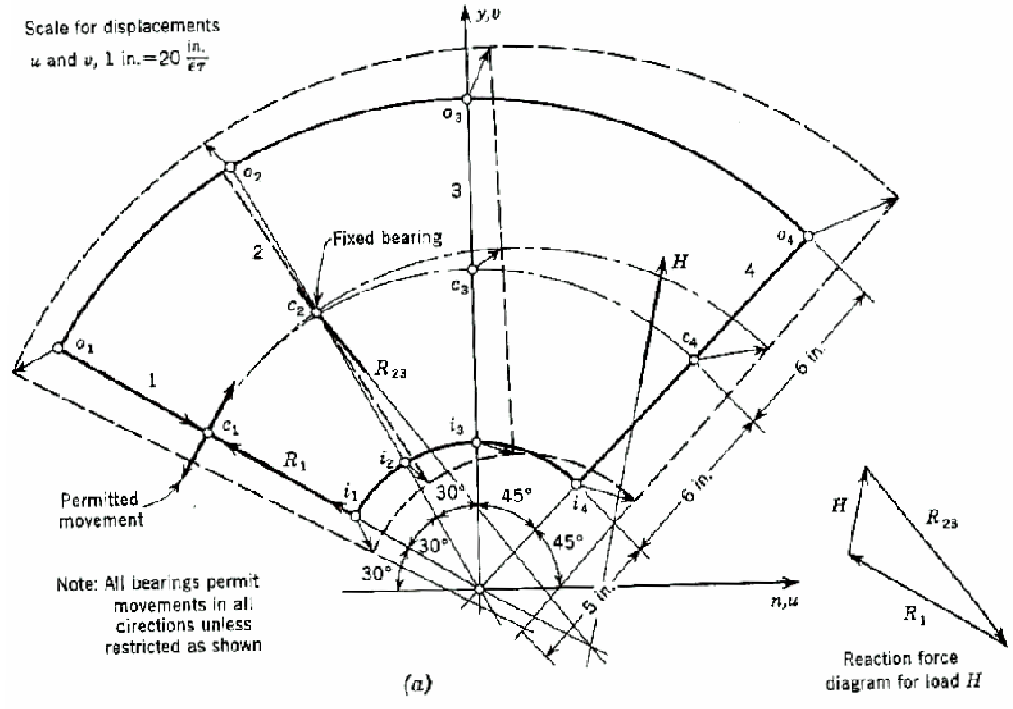


Figure 2.9 – Displacements for: (a) Support Condition I;  
 (b) Support Condition II [Source: 2.33]

If the curved bridge is a line element with uniform temperature and rigidly fixed at one location, theoretical calculations show that the movement at free supports will be on the chord from the fixed point. However, theoretical calculations show that real bridges often do not obey this simplistic relation. Curved bridges always have at least two girders, and they cease to behave as a line element when this occurs. In addition, the fixed location of the curved girders is often at a pier which is not rigid, and as a result, it may have thermal deflection which complicates the direction of movement. The net effect of these observations is that any directional guiding devices at moveable bearings of a curved bridge are almost certain to be oriented in a less than optimal direction [2.6]. Roeder and Moorty [2.6] conducted a study on a three span, four girder curved bridge predicted to have the thermal movements shown in Figure 2.10. The dashed outline in Figure 2.10 is the undeformed shape of the bridge. This figure shows that there is considerable movement of the bridge even at the “fixed” support due to deflection of the piers. The radial movements that would be obtained by orienting the bearing along the chord of this bridge were slightly larger than those obtained by orienting the bearings along the tangent (Fig. 2.11). Thus, guiding devices on curved bridges must be relatively strong or the piers and supporting elements must be relatively flexible if damage is to be avoided.



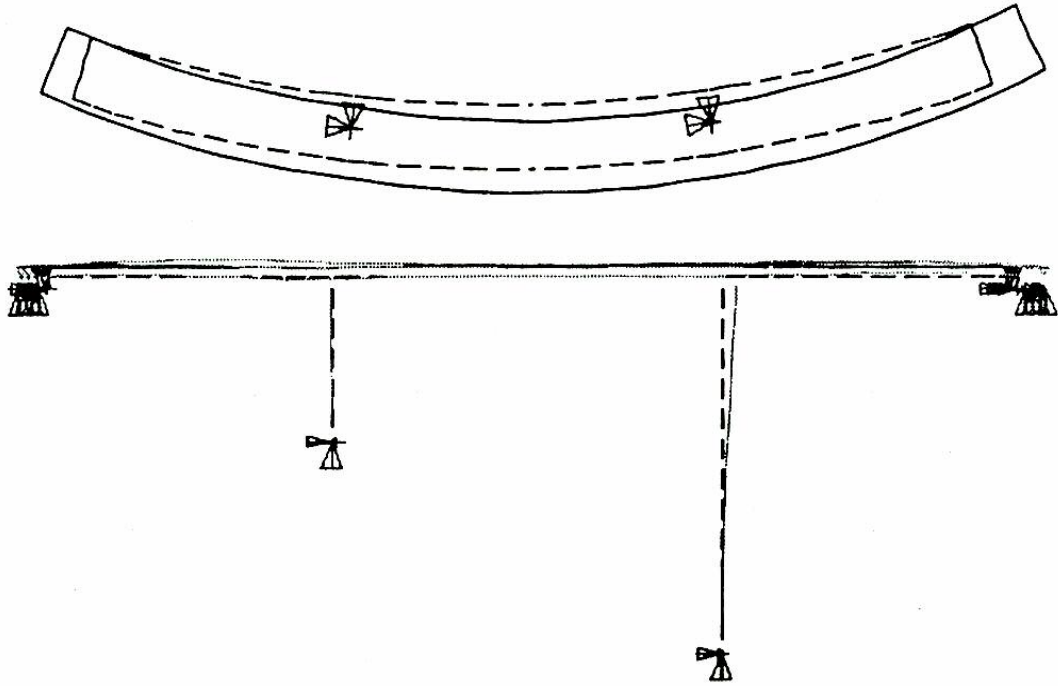


Figure 2.10 – Thermal Movements of a Curved Bridge [Source: 2.6]

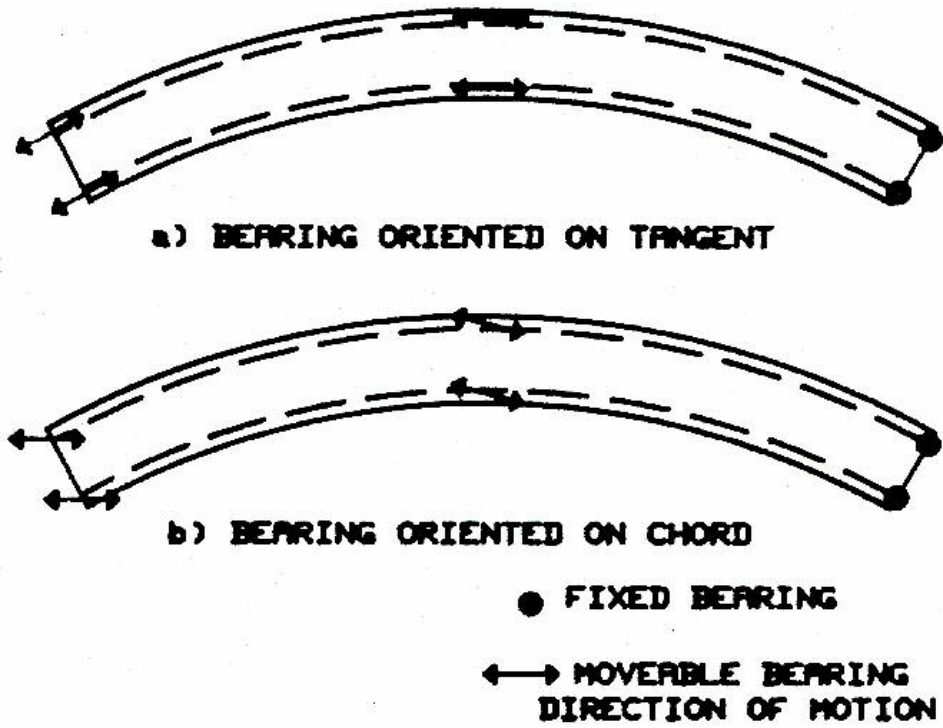


Figure 2.11 – Typical Orientation and Placement of Bridge Bearings on a Curved Bridge [Source: 2.6]

## CHAPTER 3

### HORIZONTALLY CURVED STEEL I-GIRDER BRIDGES

#### 3.1 Introduction

The location of highway bridges used to be determined by the most convenient crossing site with little regard to the general alignment of the roadway. After the bridge location was established, the highway designer or surveyor laid out the highway according to the bridge.

During the last several decades, this situation has reversed and now bridges must fit the highway alignment that has been predetermined by many other considerations. The increasingly frequent occurrence of structures on curved alignment is presenting real challenges to engineers, especially in the design of urban freeways where multi-level interchanges must be built within tight geometric restrictions.

The present-day emphasis on good appearance is also an important factor. Welding has helped to produce structures with smooth surfaces, interrupted by a minimum amount of detail. Outside transverse stiffeners are no longer used on many highway girders. The use of curved supporting beams or girders in a structure on curved alignment is a natural outgrowth of this trend toward aesthetic design.

Compared with girders composed of straight segments and along with aesthetic considerations, curved girders offer certain technical advantages in which structures must be built to fit curved highway alignment. The roadway slab design and construction become much simpler because the stringer spacing and parapet

overhang from the exterior stringer are constant over the entire length of structure. This provides for equally spaced slab reinforcement, a more uniform stress distribution, and panel forms which can be re-used as pouring of the deck slab progresses.

In addition, curved girders permit the designer to make use of its continuous construction and its inherent advantages in situations which might otherwise be limited to simple spans. Continuous spans make the use of materials more efficient and permit the elimination of many undesirable expansion details. A stiffer structure is obtained, and in some cases, more vertical clearance is available due to the use of shallower girders.

Curved girders also permit the designer increased flexibility when possible locations of the substructures are often limited because of required clearances. The use of straight girders to span the same distance could mean a complicated framing system to support the deck. When high substructures are involved, the use of longer spans may also result in savings.

The major advantages of curved girders are structural efficiency, appearance and simplicity in certain phases of design, detailing, and construction [3.1].

### 3.2 Types of Curved Framing

Curved girder framing may be categorized into two types: closed framing and open framing. In the closed framing type, curved girders are tied together by diaphragms or floorbeams and horizontal lateral bracing at the girder flanges levels (Fig. 3.1). Torsion is resisted by individual curved girders and interaction of these girders through diaphragms or floorbeams and lateral bracing [3.1].

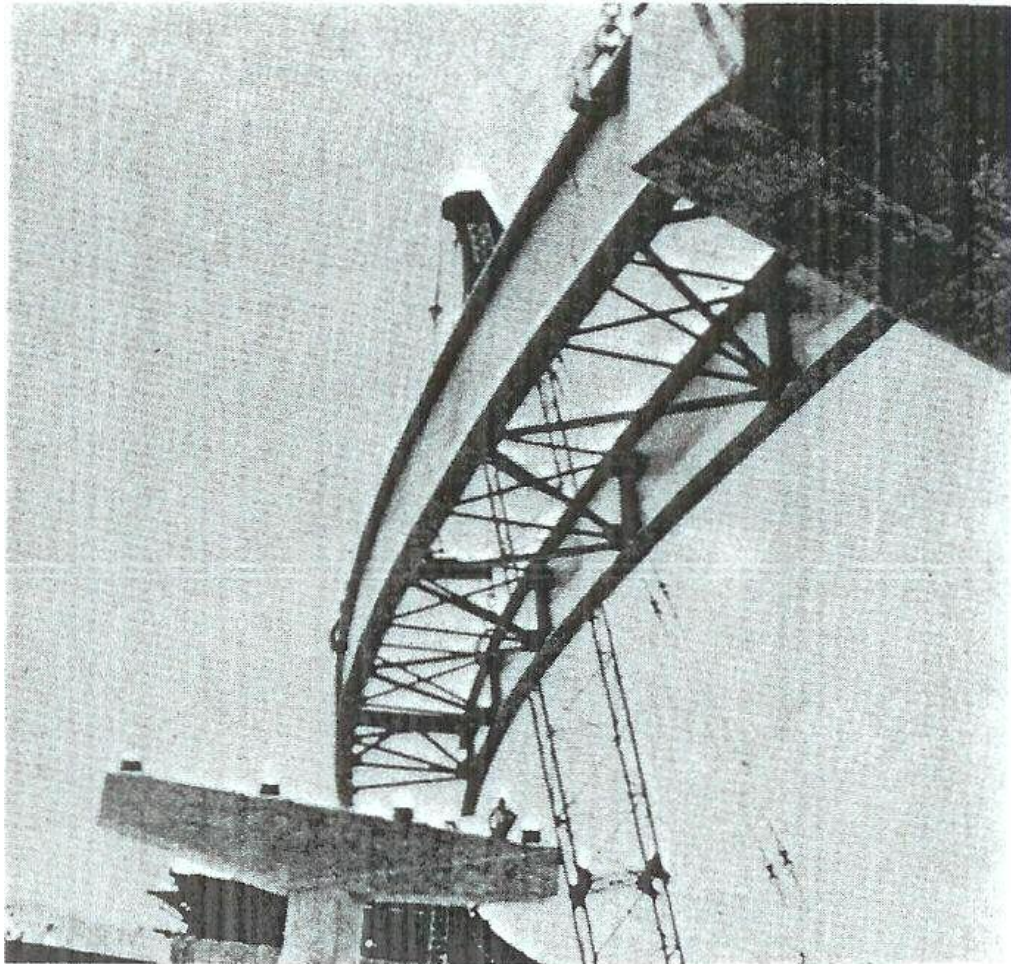


**Figure 3.1 – Curved Girders Tied together with Diaphragms and Lateral Bracing [Source: 3.1]**

In the open framing type, curved girders are tied together by diaphragms or floorbeams only, with no horizontal lateral bracing (Fig. 3.2). In this case, torsion must be resisted by individual curved girders and interaction of curved girders through diaphragms or floorbeams [3.1].

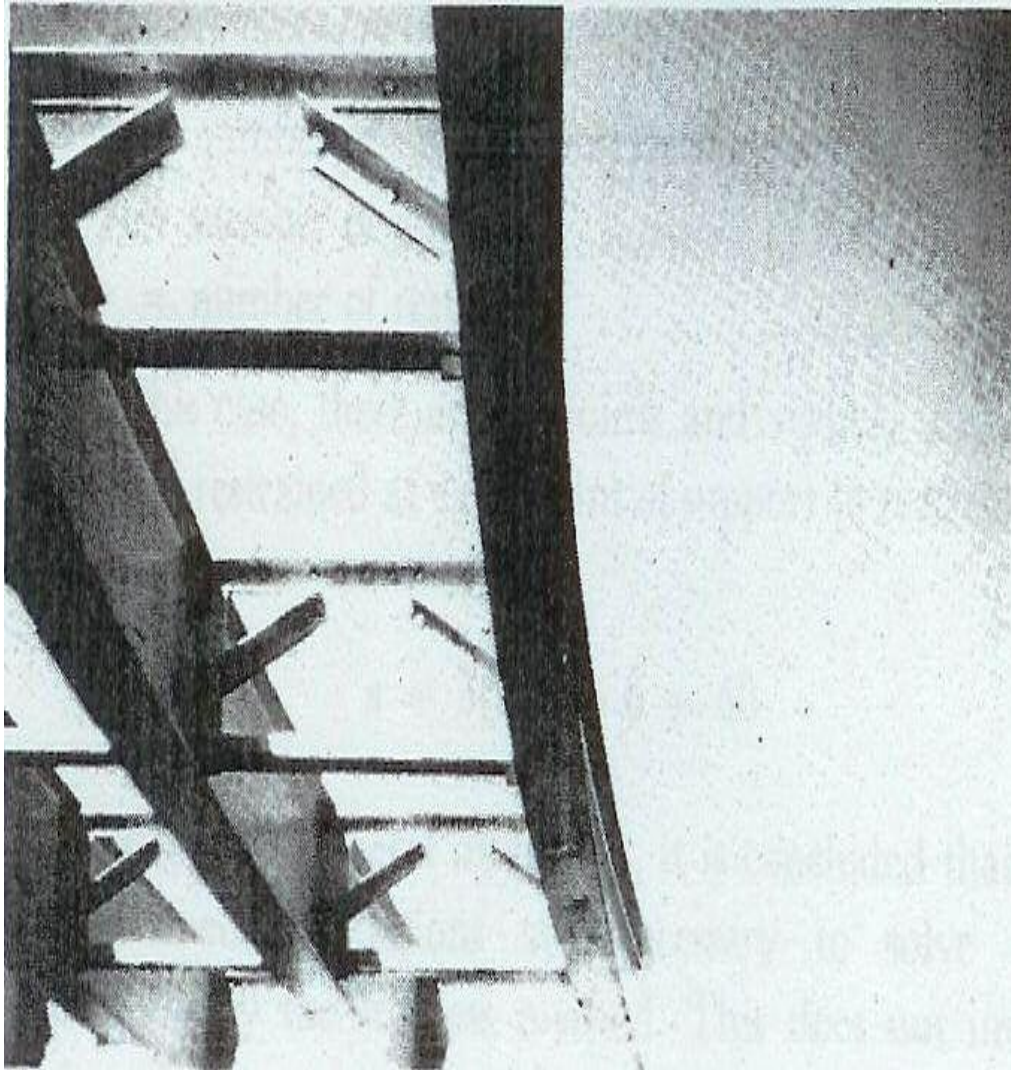


**Figure 3.2 – Curved Girders Tied together with Diaphragms [Source: 3.1]**

A combination of closed and open framing can be used to form a third type of curved framing. For example, in Figure 3.3, the exterior girders of a four-girder curved bridge are tied to the adjacent interior girders by diaphragms and horizontal lateral bracing, while the interior girders are tied to each other by diaphragms only [3.1].

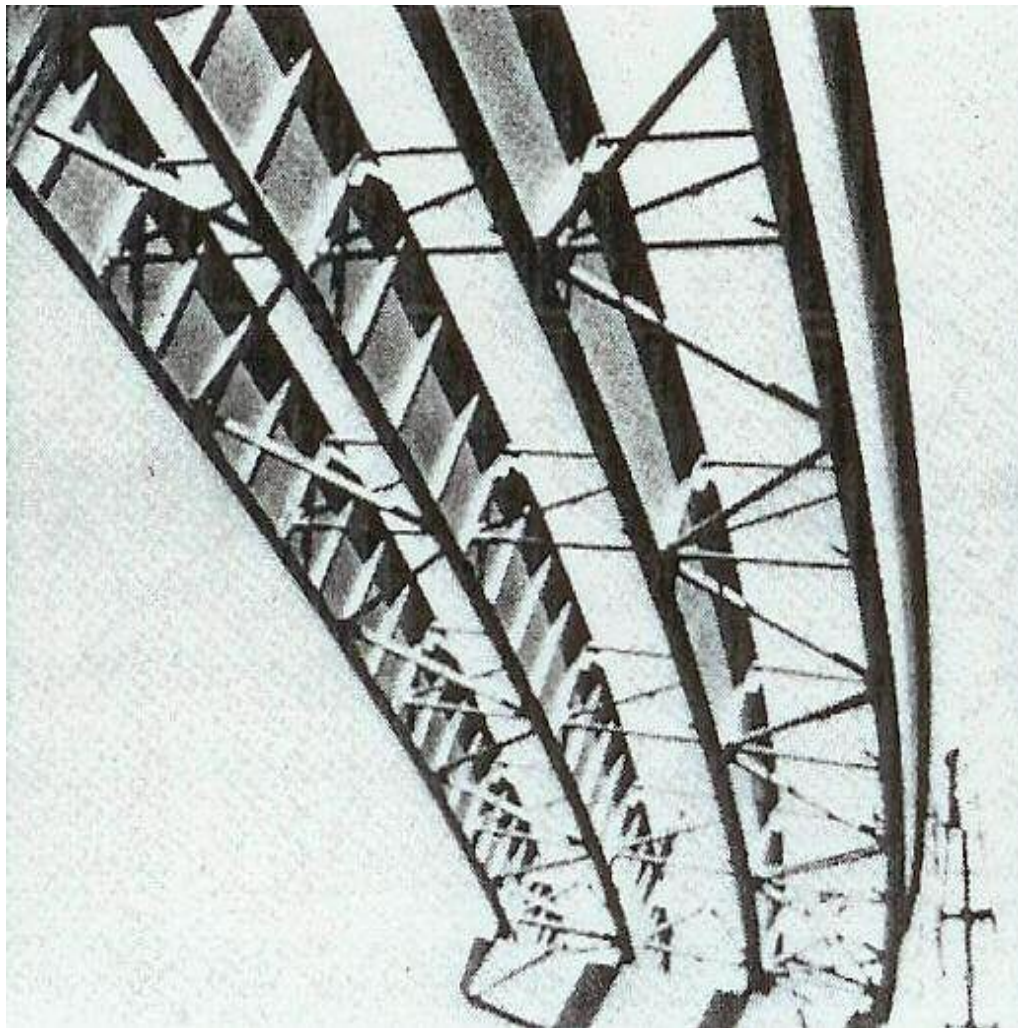


**Figure 3.3 – Curved Girders Tied Together with Diaphragms and Lateral Bracing in Alternate Bays [Source: 3.1]**

### **3.3 Effect of Cross-Bracing**

In straight right-angled bridges, cross frame and diaphragms act as secondary members in maintaining structural integrity. There is growing sentiment in the bridge engineering community to eliminate, or at least minimize, the number of cross frames due to the added cost and adverse fatigue problems. However, in horizontally curved and skewed bridges, the interaction of bending and torsion causes these components to become major load-carrying elements (primary members) [3.2, 3.3].

Yoo and Littrell [3.2] studied the role of cross-bracing in unifying individual curved members. They found that maximum bending stress and maximum deck deflections stabilized with minimal bracing but warping stresses were sensitive to the number of braced intervals. The cross section of the plate girders will deform (warp) considerably under dead and live loads if not adequately braced. Cross-sectional deformation leads to high warping stresses that may exceed the magnitude of the longitudinal bending stresses.

Davidson et al. [3.3] investigated the effects of cross frames on the curved girder system and compared them to the straight girder system. They found that span length, radius of curvature, flange width, and cross-frame spacing have the greatest effect on the warping-to-bending stress ratio.

### **3.4 Effect of Curvature**

Compared with straight bridges, certain girders in curved bridges experience a much larger bending moment. Depending on the overall geometry of a curved bridge, the distribution of bending moment among girders may be quite different from the

distribution of moments among girders of a comparable straight bridge. While girders in a straight bridge each carry about the same amount of bending moment, the outer girders in curved bridges often experience a much larger bending moment than the inner girders [3.4]. The overall sum of moments for all girders is the same for bridges with the same span length regardless of the curvature angle. This is because the overall static moment of a simply supported system is constant for the same load and span length. Because of the nonuniform distribution of bending moment among girders, it is imperative to accurately determine the maximum bending moment for all girders in curved bridges and check their design for any potential overstress condition. The accurate determination of the bending moment distribution can be achieved by the aid of a three-dimensional structural analysis. Horizontally curved bridges may also develop a significant torsional moment in their girders. This may especially be prevalent when the curvature angle is large, roughly 30-40° [3.4]. The magnitude of these internal forces depends on the angle of curvature, the span length and the geometry of girders.

Desantiago et al. [3.5] studied the behavior of horizontally curved bridges. The analyses used a typical truckload and also the dead load as the primary forces on bridges. When the horizontal angle of curvature is large (about 20-30°), the analyses revealed that bending moment in girders of a curved bridge can be about 23.5% higher compared with moments in girders of a straight bridge of similar span and design configuration. The torsional moment was founded to be about 10.3% of the maximum bending moment of comparable straight bridges.



## **CHAPTER 4**

### **PILE FOUNDATIONS**

#### **4.1 Introduction**

Piles are structural members of timber, concrete, and steel that are used to transmit surface loads to lower levels in the soil mass. This transfer may be by vertical distribution of the load along the pile shaft or a direct application of load to a lower stratum through the pile point. A vertical distribution of the load is made using a friction (or floating) pile and a direct load application is made by a point, or end-bearing, pile. This distinction is purely one of convenience since all piles carry load as a combination of side resistance and point bearing except when the pile penetrates an extremely soft soil to a solid base.

Piles are commonly used (refer to Fig. 4.1) for the following purposes:

- To carry the superstructure loads into or through a soil stratum. Both vertical and lateral loads may be involved.
- To resist uplift, or overturning, forces, such as for basement mats below the water table or to support tower legs subjected to overturning from lateral loads such as wind.
- To compact loose, cohesionless deposits through a combination of pile volume displacement and driving vibrations. These piles may be later pulled.
- To control settlements when spread footings or a mat is on a marginal soil or is underlain by a highly compressible stratum.

- To stiffen the soil beneath machine foundations to control both amplitudes of vibration and the natural frequency of the system.
- As an additional safety factor beneath bridge abutments and/or piers, particularly if scour is a potential problem.
- In offshore construction to transmit loads above the water surface through the water and into the underlying soil. This case is one in which partially embedded piling is subjected to vertical (and buckling) as well as lateral loads [4.1].

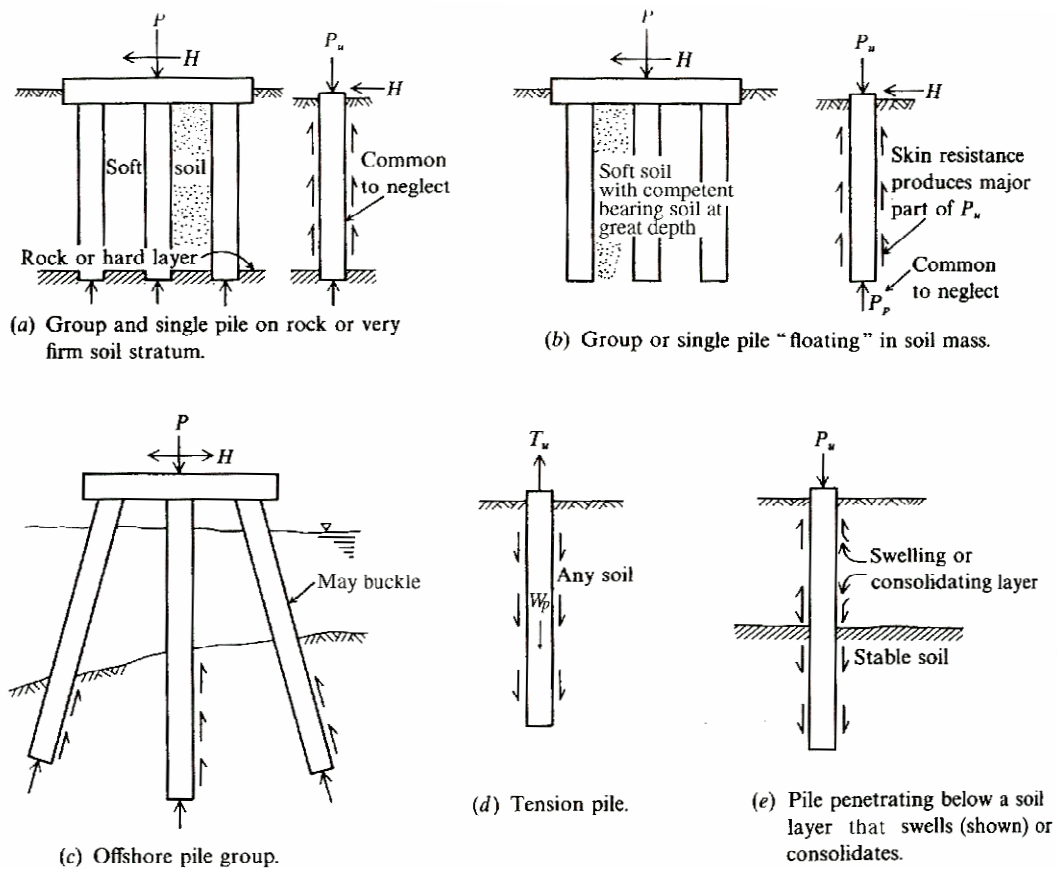


**Figure 4.1 – Typical Pile Configurations [Source: 4.1]**

## 4.2 Timber Piles

These are the oldest type of pile foundations in bridge work. They are obtained from straight and slender sections of tree trunks with no defects and a uniform taper. Timber piles situated wholly below the permanent groundwater table are resistance to fungal decay. However, when the project is above the groundwater, piles must be treated with preservatives to retard deterioration. The life of timber piles above the water table can be considerably increased by treating with creosote, oil-borne preservatives, and salt. Creosote application by pressure treatment is the most effective method of protection and almost the generally accepted preservation.

The advantages of timber piles are:

- They are light and easy to handle.
- They have a high strength-to-weight ratio, and
- They are durable when placed below the groundwater table.

Conversely, their disadvantages are:

- Their structural capacity is relatively low compared to other types.
- They are prone to damage during driving, especially in dense soil.
- They need protection when placed above the groundwater table, and
- They are difficult to splice when extra length is needed [4.2].

The allowable design load based on pile material is:

$$P_a = A_p f_a \dots\dots\dots(4.1)$$

where

$A_p$  = average pile cross-sectional area at the pile cap;

$f_a$  = allowable design stress value for the type of timber.

### **4.3 Concrete Piles**

This type includes precast concrete piles, prestressed concrete piles, cast in place concrete piles. Their advantages are:

- They have relatively large axial capacity and suitability to soil and water conditions that require long piles.
- They have ability to withstand aggressive ground or marine environment with proper design.
- They offer resistance during hard driving, and
- They also have all the advantages inherent in prestressing.

Conversely, concrete piles may suffer damage during handling and driving, and cutting off excess length or splicing after driving is difficult and costly [4.2].

#### **4.3.1 Precast and Prestressed Concrete Piles**

Piles are formed in a central casting yard to the specified length, cured, and then shipped to the construction site. If space is available and a sufficient quantity of piles needed, a casting yard may be provided at the site to reduce transportation costs.

Precast piles may be made using ordinary reinforcement as in Figure 4.2 or they may be prestressed as in Figure 4.3. Precast piles using ordinary reinforcement are designed to resist bending stresses during pickup and transport to the site and bending moments from lateral loads and to provide sufficient resistance to vertical loads and any tension forces developed during driving. Temporary stresses from handling and driving (tensile) may be used that are on the order of 50 percent larger

than the allowable concrete design stresses. The minimum pile reinforcement should be 1 percent [4.1].

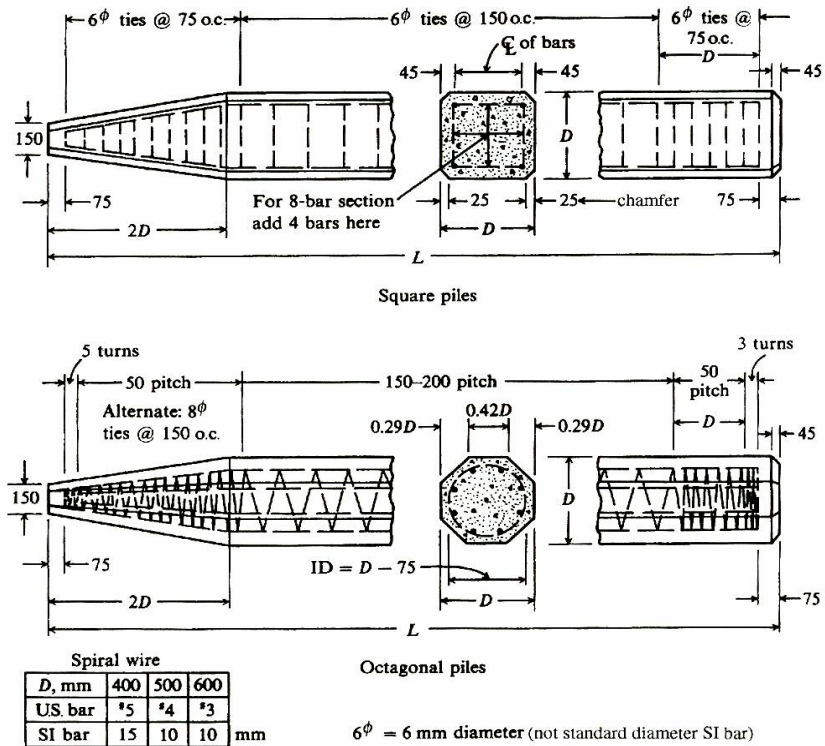
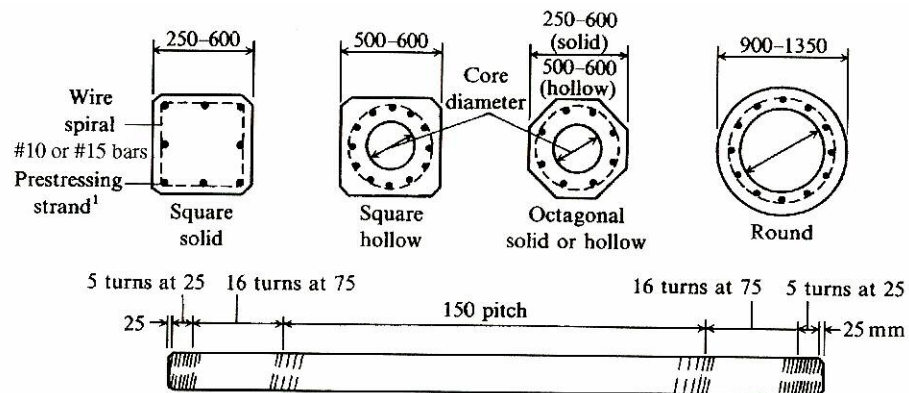


Figure 4.2 – Typical Details of Precast Piles [Source: 4.1]



<sup>1</sup> Strand: 9.5–12.7 mm ( $\frac{3}{8}$  to  $\frac{1}{2}$  in.) nominal diam.,  $f_u = 1860$  MPa

Figure 4.3 – Typical Prestressed Concrete Piles [Source: 4.1]

Prestressed piles are formed by tensioning high-strength steel ( $f_{ult}$  of 1700 to 1860 MPa) prestress cables to a value on the order of 0.5 to 0.7  $f_{ult}$ , and casting the concrete pile about the cable. The allowable design load based on pile material for prestressed piles, and including prestress loss due to load and creep, can be computed as:

$$P_a = A_g (0.33 f'_c - 0.27 f_{pe}) \dots \dots \dots (4.2)$$

where  $A_p$  = gross (total) concrete area;

$f_{pe}$  = effective prestress after all losses (about 5 MPa is usual).

#### 4.3.2 Cast-in-Place Concrete Piles

A cast-in-place is formed by drilling a hole in the ground and filling it with concrete. The hole may be drilled (as in caissons), or formed by driving a shell or casing into the ground. The casing may be driven using a mandrel, after which withdrawal of the mandrel empties the casing. The casing may also be driven with a driving tip on the point, providing a shell that is ready for filling with concrete immediately, or the casing may be driven open-end, the soil entrapped in the casing being jetted out after the driving is completed [4.1].

The allowable design load for all concrete piles (not prestressed) is:

$$P_a = A_c f_c + A_s f_s \dots \dots \dots (4.3)$$

where  $A_c, A_s$  = area of concrete and steel shell, respectively;

$f_c, f_s$  = allowable material stresses.

#### 4.4 Steel Piles

These members are usually rolled HP shapes or pipe piles. Wide-flange beams or I beams may also be used; however, the H shape is especially proportioned to withstand the hard driving stress to which the pile may be subjected. In the HP pile, the flanges and web are of equal thickness; the standard W and I shapes usually have a thinner web [4.1].

Steel H-piles are suitable for penetrating rock and other hard materials. During driving they displace a minimum soil mass, and therefore the operation does not cause heave. The usual load range is 40 to 120 tons (156 to 1068 kN), and the common length range is 40 to 100 feet. Preferably, the flange width should be at least 85 percent of the depth of the pile section to ensure comparable strength in the weak axis.

Steel H-piles have the following advantages:

- They are robust and light.
- They come in various sizes and can easily be spliced.
- They provide ample axial capacity and resistance to buckling.
- They can penetrate hard layers, and
- They accommodate situations with close pile spacing.

Their inherent disadvantages are susceptibility to corrosion if left unprotected, small bearing resistance because of the small bearing area if left unplugged, and susceptibility to deflection if they hit hard layers and obstructions [4.2].

The allowable design load for a steel pile is:

$$P_a = A_s f_s \dots\dots\dots(4.4)$$

where  $A_s$  = cross-sectional area of pile;

$f_s$  = allowable steel stress.



## **CHAPTER 5**

### **SOIL MODELING**

#### **5.1 Introduction**

Soil consists primarily of solid particles, which may range in size from less than a micron to several millimeters. Most soils result from the breakdown of the rocks which form the crust of the Earth, by means of the natural processes of weathering due to the action of the sun, rain, water, ice and frost, and to chemical and biological activity.

Some soils (notably peat) do not result from the breakdown of rocks, but from the decay of organic matter. Like topsoil, these soils are not suitable for engineering purposes. Peat is very highly compressible, and will often have a mass density which is only slightly greater than that of water. Unlike topsoil, organic soils may be naturally buried below the surface, and their presence is not necessarily obvious [5.1].

Soil is made up essentially of solid particles, with spaces or voids in between. The voids are in general occupied partly by water and partly by air. So, it is very important to know the type of soils at the location of the substructure elements of a bridge especially around the piles, so the representation of this material can be as accurate as possible.

## 5.2 Soil Representation

The simplest model to represent the soil around a pile is as a Winkler foundation with distributed springs and dashpots that are constant or frequency dependent or with lumped springs concentrated at a finite number of nodes.

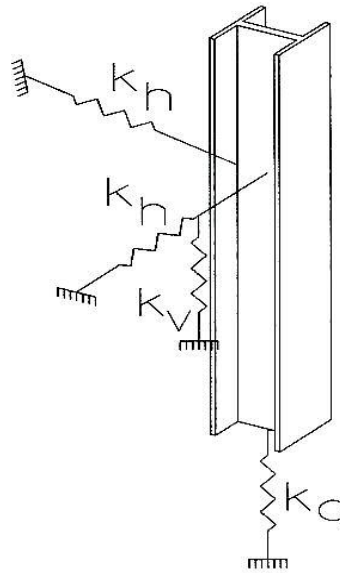


**Figure 5.1 – Soil-Pile Interaction**

The soil is idealized by three sets of springs: lateral springs, vertical springs, and a point spring as shown in Figure 5.1. Parameters needed to describe these relationships are the ultimate soil resistance and the initial stiffness. These parameters are shown in Table 5.1. Shear strength reduction factors are shown in Figure 5.2. The ultimate lateral soil resistance  $P_u$  and the initial stiffness  $k_h$  are assumed to be either constant with depth or linearly increasing with depth. The parameters for the vertical springs are the maximum skin friction developed between the pile and soil  $f_{max}$  and

the initial stiffness  $k_v$ . The point spring is described by the maximum bearing stress of the pile tip  $q_{max}$  and the initial point stiffness  $k_q$  [Greimann and Amde [5.2]].

**Table 5.1 – Parameters for Soil Springs [Source: 5.2]**

Parameter	Case	
	Clay	Sand
Lateral Springs		
$P_u$	$9c_u B$	$3\gamma B k_{px}$
$k_h$	$67c_u$	$n_h x$
Vertical Springs		
$f_{max}$ (H-Piles) , (klf)	The least of: $2(d + b_f)c_u$ $2(d + 2b_f)c_a$ $2(dc_u + b_f c_a)$	$0.02N[2(d + 2b_f)]$
$f_{max}$ (Others) , (klf)	The lesser of: $l_g c_a$ $l_g c_u$	$0.04Nl_g$
$k_v$	$\frac{10f_{max}}{z_c}$	$\frac{10f_{max}}{z_c}$
Point Spring		
$q_{max}$ , (ksf)	$9c_u$	$8N_{corr}$
$k_q$	$\frac{10q_{max}}{z_c}$	$\frac{10q_{max}}{z_c}$

where

$B$  = pile width;

$b_f$  = flange width of H-pile (ft);

$c_a$  = adhesion between soil and pile =  $\alpha c_u$  (psf);

$c_u$  = undrained cohesion of the clay soil =  $97.0N + 114.0$  (psf);

$d$  = section depth of H-pile or diameter of pipe pile (ft);

$J$  = 200 for loose sand; 600 for medium sand; 1,500 for dense sand;

$l_g$  = gross perimeter of the pile (ft);

$$k_p = \tan^2 \left( 45^\circ + \frac{\phi}{2} \right);$$

$N$  = average standard penetration blow count;

$N_{corr}$  = corrected standard penetration test (SPT) blow count at depth  
of pile tip

$$= N \text{ (uncorrected) if } N \leq 15;$$

$$= 15 + 0.5 (N-15) \text{ if } N > 15;$$

$$n_h = \text{constant of subgrade reaction} = \frac{J\gamma}{1.35};$$

$x$  = depth from soil surface;

$z_c$  = relative displacement required to develop  $f_{max}$  or  $q_{max}$

$$= 0.4 \text{ in. (0.033 ft.) for sand;}$$

$$= 0.2 \text{ in. (0.021 ft.) for clay;}$$

$\alpha$  = shear strength reduction factor;

$\gamma$  = effective unit soil weight;

$\phi$  = angle of internal friction.

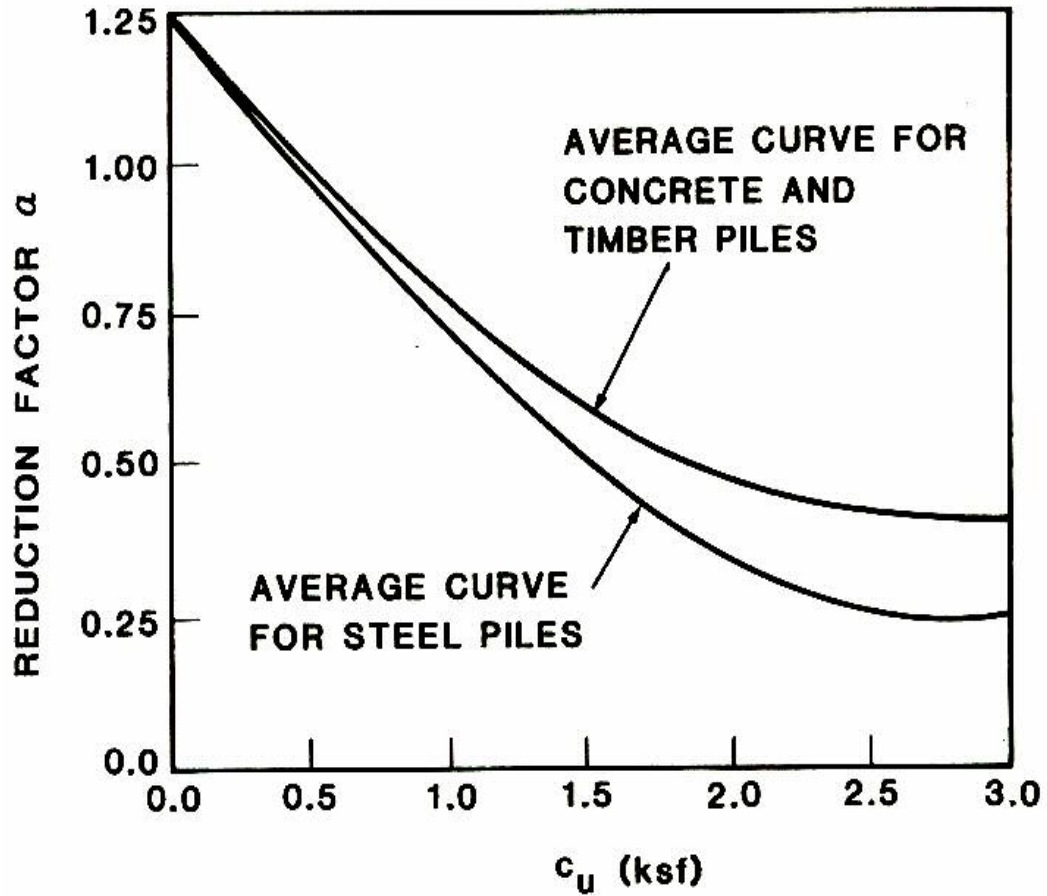


Figure 5.2 – Reduction Factor  $\alpha$  [Source: 5.2]

Spring constants are obtained from analytical considerations or from experimental data. The major advantage of this approach lies in its ability to simulate non-linearity, inhomogeneity, and hysteretic degradation of the soil surrounding the pile by simply changing the spring and dashpot constants.

### 5.3 Soil Characteristics

Three types of soil resistance-displacement models can describe the soil characteristics [Amde et al. [5.3]]: lateral resistance-displacement ( $p$ - $y$ ) curves; longitudinal load-slip ( $f$ - $z$ ) curves; and pile tip load-settlement ( $q$ - $z$ ) curves.

The  $p$ - $y$  curves represent the relationship between the lateral soil pressure against the pile (force per unit length of the pile) and the corresponding lateral pile displacement. The  $f$ - $z$  curves describe the relationship between skin friction (force per unit length of the pile) and the relative vertical displacement between the pile and the soil. Finally, the  $q$ - $z$  curves describe the relationship between the bearing stress at the pile tip and the pile tip settlement. The total pile tip force is  $q$  times the effective pile tip area. All three types of curves assume the soil behavior to be nonlinear, and can be developed from basic soil parameters.

### 5.4 Modified Ramberg-Osgood Model

The modified Ramberg-Osgood model [Amde et al. [5.3, 5.4]] is used to approximate the  $p$ - $y$ ,  $f$ - $z$  and  $q$ - $z$  soil displacement-resistance curves as follows:

$$P = \frac{k_h y}{\sqrt[n]{1 + \left| \frac{y}{y_u} \right|^n}} \dots\dots\dots(5.1)$$

$$y_u = \frac{P_u}{k_h} \dots\dots\dots(5.2)$$

where  $k_h$  = initial lateral stiffness;

$P$  = generalized soil resistance;

$P_u$  = ultimate lateral soil resistance;

$n$  = shape parameter;

$y$  = generalized displacement;

$y_u$  = ultimate lateral displacement.

The constants for equations 5.1 and 5.2 can be obtained from Table 5.2, which is specifically for  $p$ - $y$  curves, and for different types of soil.

**Table 5.2 – Analytical Forms of  $p$ - $y$  Curves [Source: 5.2-5.4]**

Case	Basic $p$ - $y$ Curve Equations	$P_u$ (Use Lesser Value)	$E_{si}$
Soft Clay (Static Load)	$\frac{P}{P_u} = 0.5(y/y_{50})^{1/3}$	$P_u = 9c_u B$ $P_u = (3 + \frac{\gamma}{c_u}x + \frac{0.5}{B}x)c_u B$	-
Stiff Clay (Static Load)	$\frac{P}{P_u} = 0.5(y/y_{50})^{1/4}$	$P_u = 9c_u B$ $P_u = (3 + \frac{\gamma}{c_u}x + \frac{0.5}{B}xc_u B)$	-
Very Stiff Clay (Static Load)	$\frac{P}{P_u} = 0.5(y/y_{50})^{1/2}$	$P_u = 9c_u B$ $P_u = (3 + \frac{\gamma}{c_u}x + \frac{2.0}{B}x)c_u B$	-
Sand (Static Load)	$\frac{P}{P_u} = \tanh(E_{si}y/P_u)$	$P_u = \gamma x [B(k_p - k_a) + \eta + \mu]$ $P_u = \gamma x (k_p^3 + 2k_p^2 k_o \tan \phi - k_a) B$ $\eta = x k_p \tan \alpha \tan \beta$ $\mu = x k_o \tan \beta (\tan \phi - \tan \alpha)$	$\frac{J\gamma x}{1.35}$

where  $c_u = \text{undrained cohesion indicated for an unconsolidated, undrained laboratory test;}$

$B = \text{pile width;}$

$\gamma = \text{effective unit soil weight;}$

$x = \text{depth from soil surface;}$

$\phi = \text{angle of internal friction;}$

$$k_p = \tan^2 \left( 45^\circ + \frac{\phi}{2} \right) = \frac{1 + \sin \phi}{1 - \sin \phi};$$

$$k_a = \tan^2 \left( 45^\circ - \frac{\phi}{2} \right) = \frac{1 - \sin \phi}{1 + \sin \phi};$$

$$k_o = 1 - \sin \phi;$$

$$\alpha = \frac{\phi}{2} \text{ for dense or medium sand; } = \frac{\phi}{3} \text{ for loose sand;}$$

$$\beta = 45^\circ + \frac{\phi}{2};$$

$J = 200 \text{ for loose sand; } 600 \text{ for medium sand; } 1,500 \text{ for dense sand;}$

$y_{50} = \text{displacement at one-half ultimate soil reaction;}$

$$= 2.5B\varepsilon_{50} \text{ for soft and stiff clay;}$$

$$= 2.0B\varepsilon_{50} \text{ for very stiff clay;}$$

$\varepsilon_{50} = \text{from laboratory triaxial test, or use}$

$$= 0.02 \text{ for soft clay; } 0.01 \text{ for stiff clay; } 0.005 \text{ for very stiff clay.}$$

(Axial strain at 0.5 times peak stress difference)



Figure 5.3 shows the modified Ramberg-Osgood curve for a typical p-y curve.

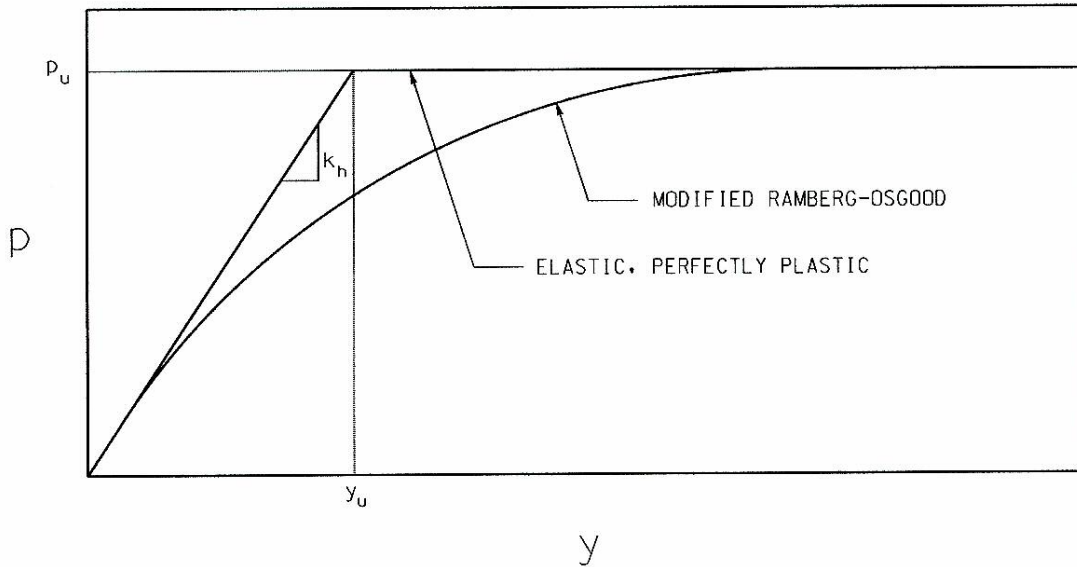


**Figure 5.3 – The Modified Ramberg-Osgood Curve for a Typical  $p$ - $y$  Curve**

Equation 5.1 can be used for the  $f$ - $z$  curves by using  $k_v$  (the initial vertical stiffness),  $z$  (vertical displacement) and  $f$  (the shear stress) instead of  $k_h$ ,  $y$  and  $P$  respectively. Table 5.3 shows the analytical forms of the  $f$ - $z$  curves for different types of soil.

**Table 5.3 – Analytical Forms of  $f$ - $z$  Curves [Source: 5.2-5.4]**

Case	Basic $f$ - $z$ Curve Equations	$f_{\max}$ (klf)	
		H Piles	Others
Clay (Static Load)	$\frac{f}{f_{\max}} = 2\sqrt{\frac{z}{z_c}} - \frac{z}{z_c}$	The least of: $2(d + b_f)c_u$ $2(d + 2b_f)c_a$ $2(dc_u + b_f c_a)$	The lesser of: $l_g c_a$ $l_g c_u$
Sand (Static Load)	$\frac{f}{f_{\max}} = 2\sqrt{\frac{z}{z_c}} - \frac{z}{z_c}$	$0.04N(d + 2b_f)$	$0.04Nl_g$

where  $b_f$  = flange width of H-pile (ft);

$c_a$  = adhesion between soil and pile =  $\alpha c_u$  (psf);

$c_u$  = undrained cohesion of the clay soil =  $97.0N + 114.0$  (psf);

$d$  = section depth of H-pile or diameter of pipe pile (ft);

$N$  = average standard penetration blow count;

$z_c$  = relative displacement required to develop  $f_{max}$

= 0.4 in. (0.033 ft.) for sand;

= 0.2 in. (0.021 ft.) for clay;

$\alpha$  = shear strength reduction factor;

$l_g$  = gross perimeter of the pile (ft).

For pile tip-settlement ( $q$ - $z$ ) curves, the equations listed in Tables 5.4 and 5.5 can be used to calculate the parameters  $k_q$  (the initial point stiffness),  $q_{max}$  (the maximum bearing stress) and  $n$  (the shape parameter) [Amde et al. [5.3, 5.4]].

**Table 5.4 – Analytical Forms of  $q$ - $z$  Curves [Source: 5.2-5.4]**

Case	Basic $q$ - $z$ Curve Equation	$q_{max}$ (ksf)
Clay (Static Load)	$\frac{q}{q_{max}} = \left( \frac{z}{z_c} \right)^{1/3}$	$9c_u$
Sand (Static Load)	$\frac{q}{q_{max}} = \left( \frac{z}{z_c} \right)^{1/3}$	$8N_{corr}$

where  $N_{corr}$  = corrected standard penetration test (SPT) blow count at depth  
of pile tip

$$= N \text{ (uncorrected) if } N \leq 15;$$

$$= 15 + 0.5 (N-15) \text{ if } N > 15;$$

$$c_u = \text{undrained cohesion of the clay soil} = 97.0N + 114.0 \text{ (psf);}$$

$N$  = average standard penetration blow count;

$z_c$  = relative displacement required to develop  $q_{max}$

$$= 0.4 \text{ in. (0.033 ft.) for sand;}$$

$$= 0.2 \text{ in. (0.021 ft.) for clay.}$$

**Table 5.5 – Parameters used in the Modified Ramberg-Osgood Models  
for Clay and Sand [Source: 5.2-5.5]**

Curve Type	Soil Type	Calculated		Used	
		$k_{(h, v, q)}$	n	$k_{(h, v, q)}$	n
$p$ - $y$	Soft Clay	$0.669 \frac{P_u}{y_{50}}$	1.5	$\frac{P_u}{y_{50}}$	1.0
	Stiff Clay	$0.915 \frac{P_u}{y_{50}}$	1.07	$\frac{P_u}{y_{50}}$	1.0
	Very Stiff Clay	$0.539 \frac{P_u}{y_{50}}$	2.56	$\frac{P_u}{2y_{50}}$	2.0
	Sand	-	-	$\frac{J\gamma x}{1.35}$	3.0
$f$ - $z$	All Soils	$7.32 \frac{f_{max}}{z_c}$	1.33	$10 \frac{f_{max}}{z_c}$	1.0
$q$ - $z$	All Soils	$7.32 \frac{q_{max}}{z_c}$	1.33	$10 \frac{q_{max}}{z_c}$	1.0

The effect of the shape parameter (n) is shown in Figure 5.4.

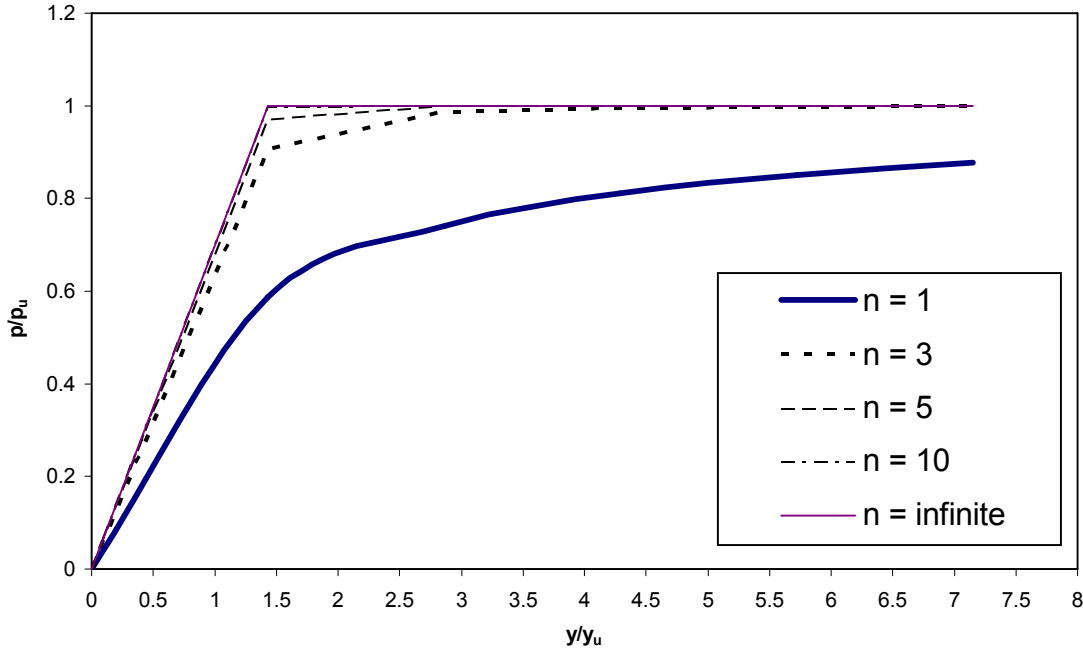


**Figure 5.4 – Effect of the Shape Parameter (n) on Modified Ramberg-Osgood Equation [Source: 5.5]**

**5.5 Cyclic Model**

Piles in integral abutment bridges move back and forth due to the bridge superstructure undergoes expansion and contraction due to annual temperature changes. A modified Ramberg-Osgood cyclic model for both symmetrical and irregular cyclic loading has been proposed [Amde et al. [5.3, 5.6]] for cyclic loading:

$$P = P_c + \frac{k_h(y - y_c)}{\left[ 1 + \left( \frac{1}{c} \left| \frac{y - y_c}{y_u} \right| \right)^n \right]^{1/n}} \dots\dots\dots(5.3)$$

where  $y_u = \frac{P_u}{k_h} \dots\dots\dots(5.4)$

$$c = \pm \left| 1 - \frac{P_c}{P_u} \right| \dots\dots\dots(5.5)$$

$k_h$  = initial lateral stiffness;

$P$  = generalized soil resistance;

$P_u$  = ultimate lateral soil resistance;

$n$  = shape parameter;

$y$  = generalized displacement;

$y_u$  = ultimate lateral displacement.

$c$  = amplification factor;

$P_c$  = the soil resistance at the previous reversal;

$y_c$  = the soil displacement at the previous reversal.

Soil resistance is represented in this study by a series of unconnected non-linear springs.

## CHAPTER 6

### THE THREE-DIMENSIONAL MODEL

#### 6.1 Introduction

A state of the art three-dimensional model is used for the analysis of integral abutment bridges. The model represents the complete bridge structure including all superstructure and substructure elements and the soil below the abutments. The model consists of shell elements for slabs, girders and piles, beam elements for cross bracings, solid elements for the abutments, and non-linear spring elements to represent the soil.

The model is analyzed using a finite element software, ANSYS, by ANSYS, Inc. The shell element type that is chosen for the slabs, girders and piles is SHELL 43, a 4-node plastic shell. The element has plasticity, creep, stress stiffening, large deflection, and large strain capabilities. The element has six degrees of freedom at each node: translations in the nodal x, y, and z directions and rotations about the nodal x, y, and z-axes.

Cross bracings are modeled using beam elements of type BEAM 4, 3D elastic beam. BEAM 4 is a uniaxial element with tension, compression, torsion, and bending capabilities. The element has six degrees of freedom at each node: translations in the nodal x, y, and z directions and rotations about the nodal x, y, and z axes.

Abutments are modeled using solid elements of type SOLID 45. The element has plasticity, creep, swelling, stress stiffening, large deflection, and large strain

capabilities. The element is defined by eight nodes having three degrees of freedom at each node: translations in the nodal x, y, and z directions.

Multipoint constraint elements, MPC184, with rigid beam option are used to connect all elements together. MPC184 comprises a general class of multipoint constraint elements that implement kinematic constraints using Lagrange multipliers. A rigid beam option has six degrees of freedom at each node: translations and rotations in x, y, and z directions.

Soil is modeled using spring elements, COMBIN39, a spring between a node and ground. The spring is a unidirectional element with nonlinear generalized force-deflection capability. The element has three degrees of freedom at each node: translations in the nodal x, y, and z directions.

## 6.2 Model Geometry

The superstructure of the model consists of 7 inches of concrete slab that sits on six steel girders spaced at 6 ft with 2 ft overhang on each side as shown in Figure 6.1. The girders are integrated into 3 ft wide and 7 ft 7 in. high abutments at both ends of the bridge.

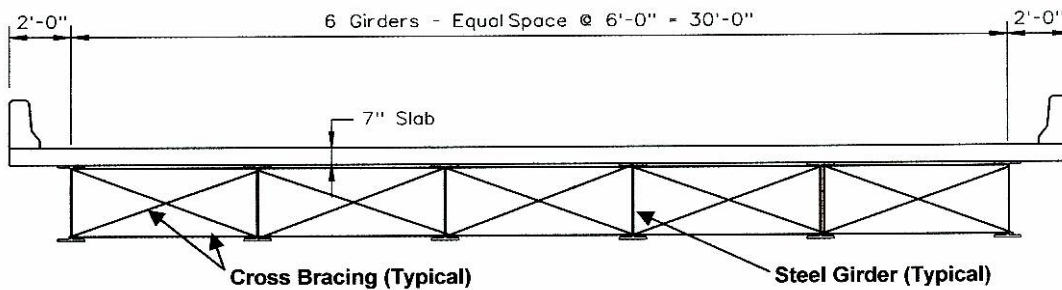


**Figure 6.1 – Typical Section of the Three-Dimensional Model**

The concrete slab is modeled using shell elements, and a node was placed at each end of the typical section, along the center line of each girder, along each end of the girders' top flange, and at a point half way between girders, as shown in Figure 6.2.

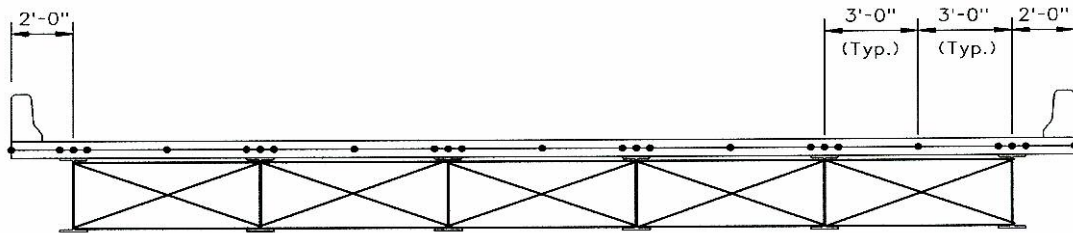


**Figure 6.2 – Concrete Slab Nodes Shown in Typical Section**

Steel girders and cross bracings are represented in the model. Shell elements are used to model the steel girders with nodes at each end of the flanges and the three nodes along the web where two of them are at the intersection of the web and the flanges. Beam elements are used to model the cross bracings with the same nodes at the intersection of web and flanges. The layout of nodes for the girders and cross bracings is shown in Figure 6.3.

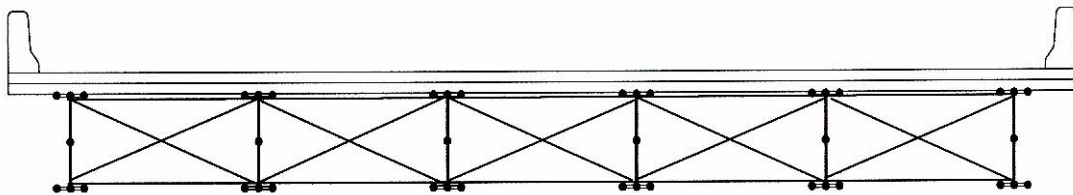


**Figure 6.3 – Nodes Distribution for Steel Girders and Cross Bracings Shown in Typical Section**



Cross-bracing spacing for each span length is provided as follow:

- For span length (L) 50 ft, spacing of L/5
- For span length (L) 100 ft, spacing of L/10

The nodes at the top of each girder are connected to the corresponding nodes in the concrete slab through a rigid connection. The nodes for the concrete slab, steel girders, and cross bracings are repeated along the bridge length. The 1.5 ft length of steel girders at each end of a bridge superstructure is embedded into the abutment. The plan and isometric views of the model indicating the mesh layout along the bridge length are shown in Figures 6.4 and 6.5.

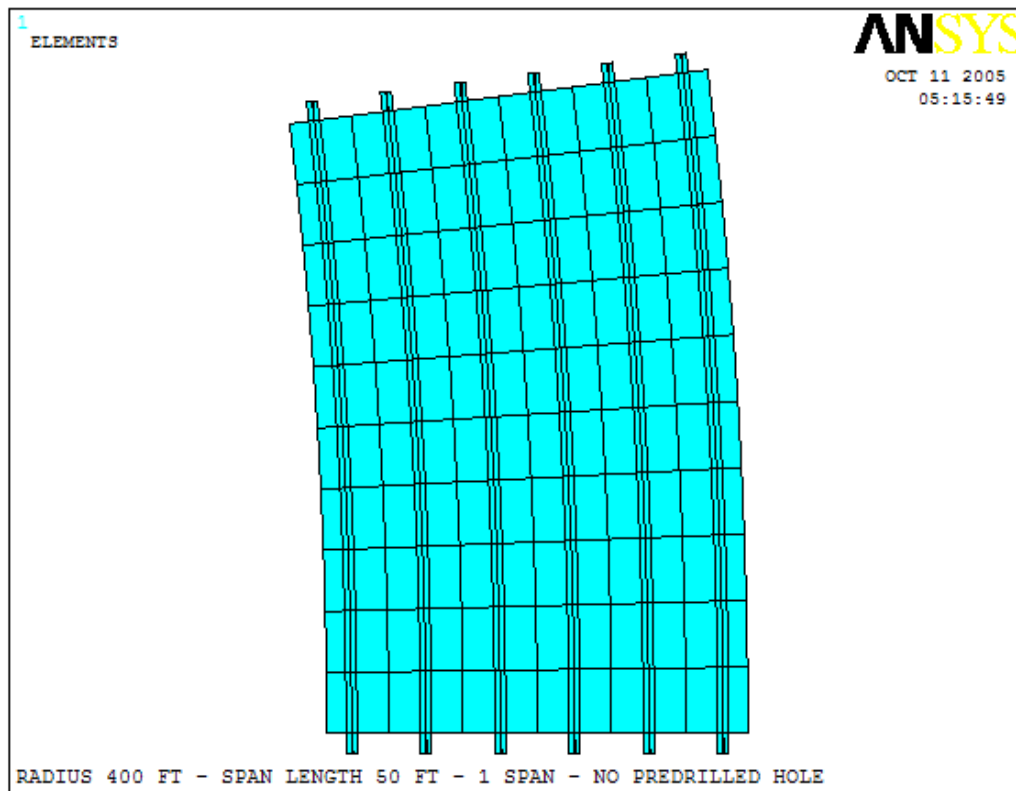


**Figure 6.4 – Plan View of the Mesh Layout for a Single Span Model**

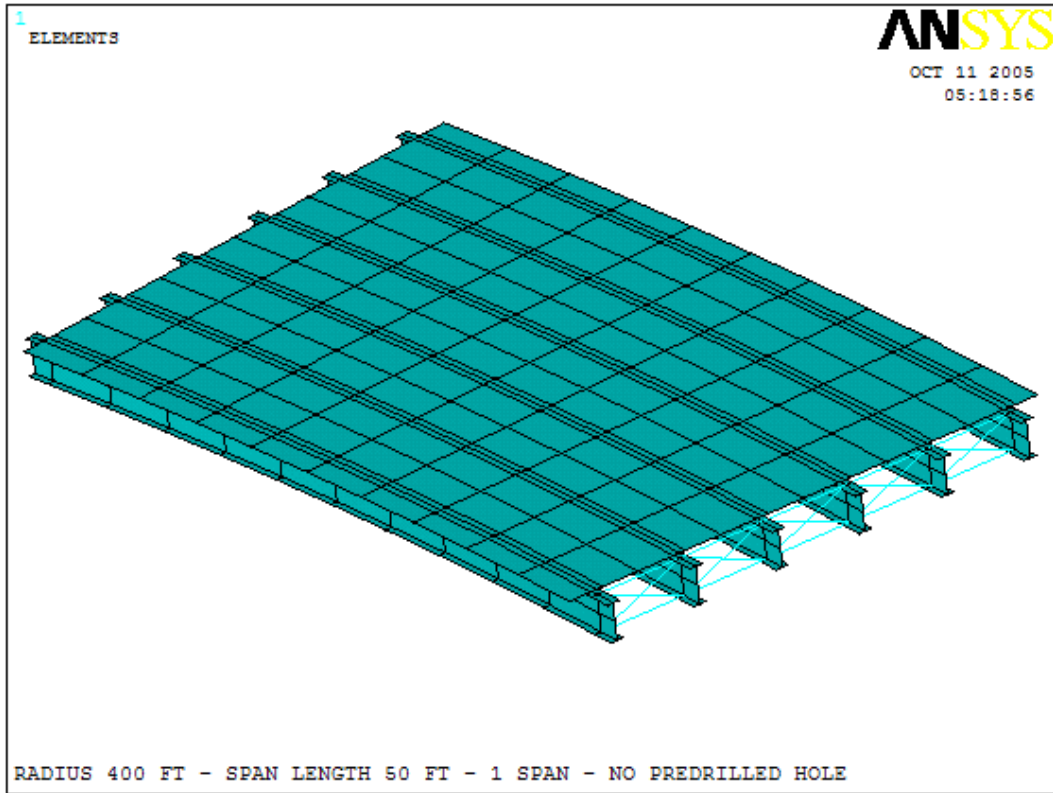


**Figure 6.5 – Isometric View of the Mesh Layout for a Single Span Model**

Each abutment is modeled using solid elements, and each element has eight nodes. The nodes are along the same lines in the superstructure and each layer along the abutment cross section has three nodes in which two of these nodes are at the edges and one along the abutment centerline. This layout for the abutment is shown in Figure 6.6 in an isometric view.

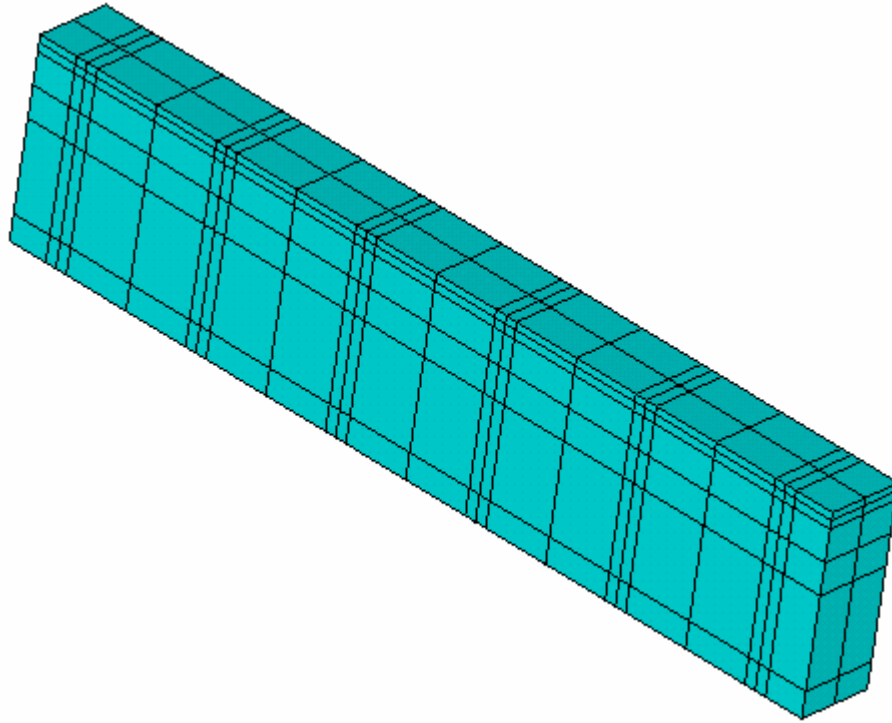
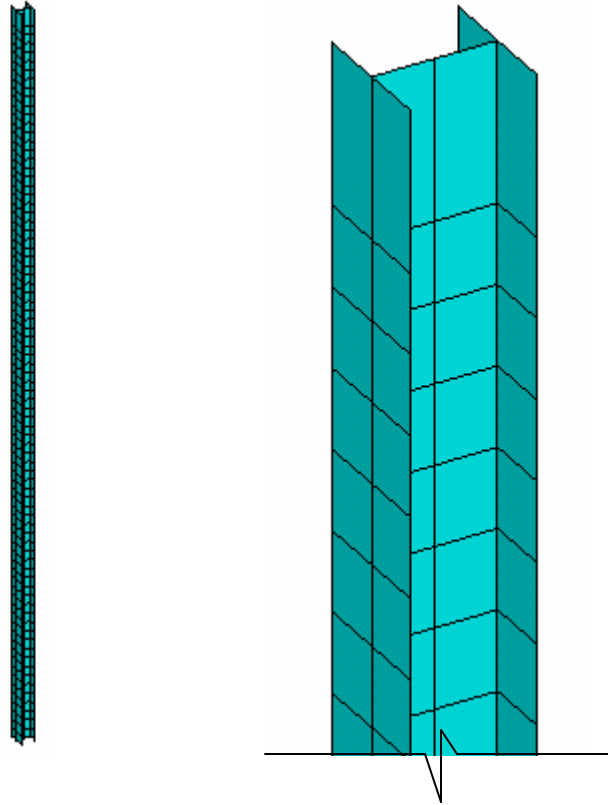


**Figure 6.6 – Isometric View of the Mesh at Each Abutment**

Piles are modeled using shell elements with nodes at each end of the flanges and three nodes along the web where two of them are at the intersection of the web and the flanges. Seven nodes represent each layer of each pile. The pile itself is divided into eighty layers at equal spaces and one layer at the top of the pile. The length of the pile in this analysis is 41 ft, where 1 ft is embedded into the abutment and the remaining 40 ft is driven into the soil and divided into eighty equally spaced layers of nodes producing vertical spacing of 6 inches between the layers. Figure 6.7 shows the mesh of a steel pile in the model.



**a) Isometric View**

**b) Zoom View**

**Figure 6.7 – Mesh in a Steel Pile**

Multipoint constraint elements, MPC184, with rigid beam option, are used to connect all elements together. The elements are placed in two locations. The first location is between the nodes at the top of each girder and the corresponding nodes in the concrete slab. The second location is at the top 1 ft length of piles which are embedded into the abutment.

Finally, the soil is represented as a three-dimensional model of non-linear springs, with their properties as specified in Chapter 5 and Section 6.3. There are three types of springs used in the model. The first type represents the displacement in lateral and longitudinal directions and consists of two springs. Both springs are at the center of the web. They will be modeled at each layer of the nodes along the pile starting at one layer below the bottom of the abutment and continuing all the way to one layer above the tip of the pile. The second type of springs represents friction along the pile and consists of a single spring at each node along the web of each pile starting one layer below the bottom of the abutment and ending one layer above the tip of the pile. The third and final type of springs is the tip spring that represents the settlement in the pile and consists of seven springs at each node at the tip of the pile. This spring representation of the tip of each pile allows for uniform resistance to pile settlement and is used in the analysis of friction piles. These pile tip-settlement springs are replaced with fixed end conditions when analyzing bridge models with end-bearing piles. Figure 6.8 shows the spring model of a steel pile.

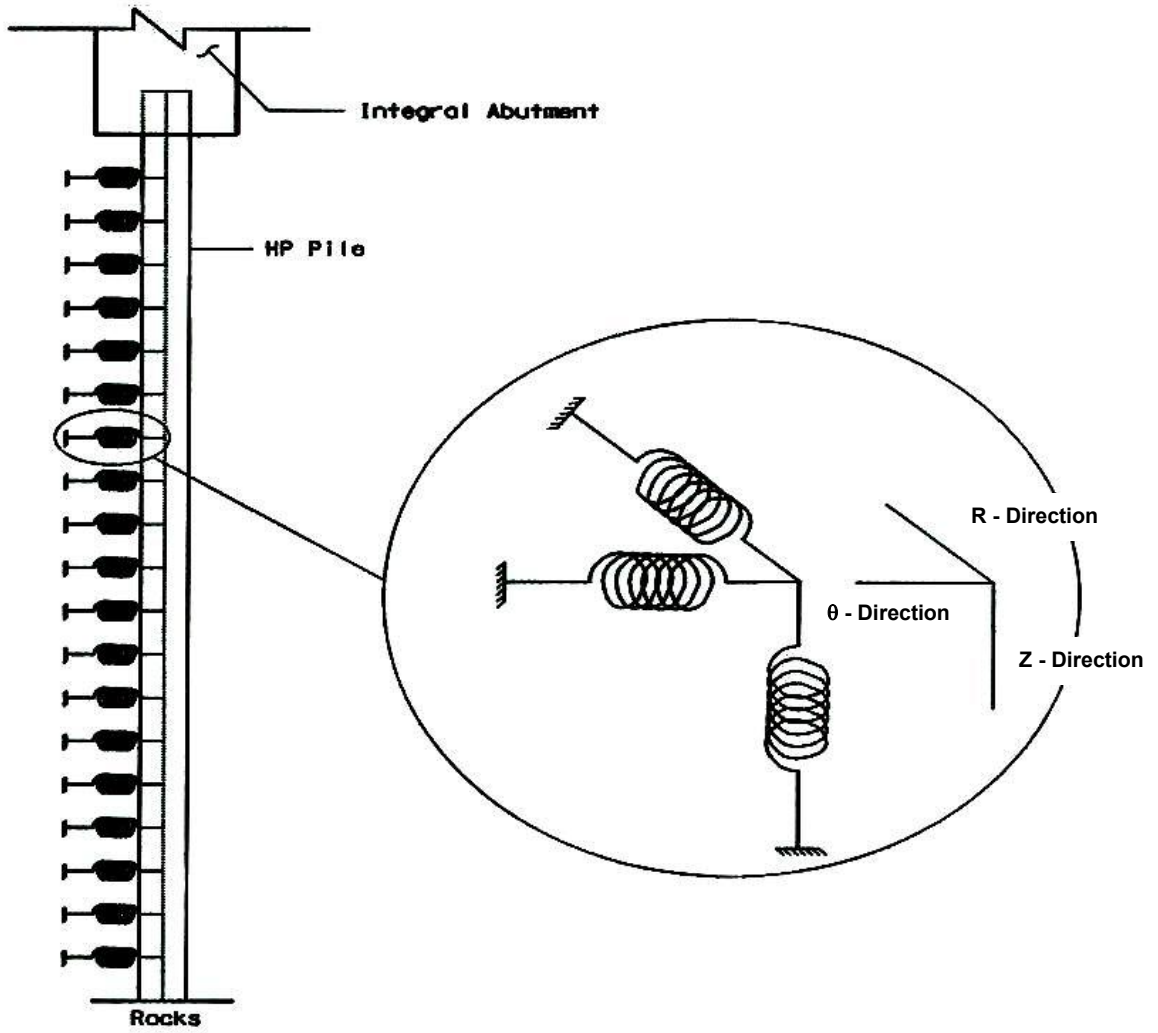


Figure 6.8 – Spring Model for Soil

### 6.3 Soil Properties

Four soil profiles were used in this investigation to study the effect of the soil profile on curved integral abutment bridges.

The first soil profile is one layer of very stiff clay that extends from the bottom of the abutment to the piles' tips. The other three soil profiles consist of two layers. The first layer consists of loose sand to represent a pile placed in a predrilled hole filled with loose sand. The depths of loose sand layer are 5 ft, 9ft and 15 ft. The second layer consists of very stiff clay that extends from the loose sand layer to the piles' tips. Figure 6.9 shows graphical representations for the four soil profiles.

The soil properties for the loose sand used in the analysis are:

1. The effective unit soil weight (submerged unit weight)  $\gamma' = 55$  pcf.
2. The angle of internal friction  $\Phi = 30^\circ$ .

The soil properties for the very stiff clay used in the analysis are:

1. The effective unit soil weight (submerged unit weight)  $\gamma' = 65$  pcf.
2. The undrained cohesion of the clay soil  $C_u = 5000$  psf.
3. The axial strain at 0.5 times peak stress difference  $\epsilon_{50} = 0.005$ .

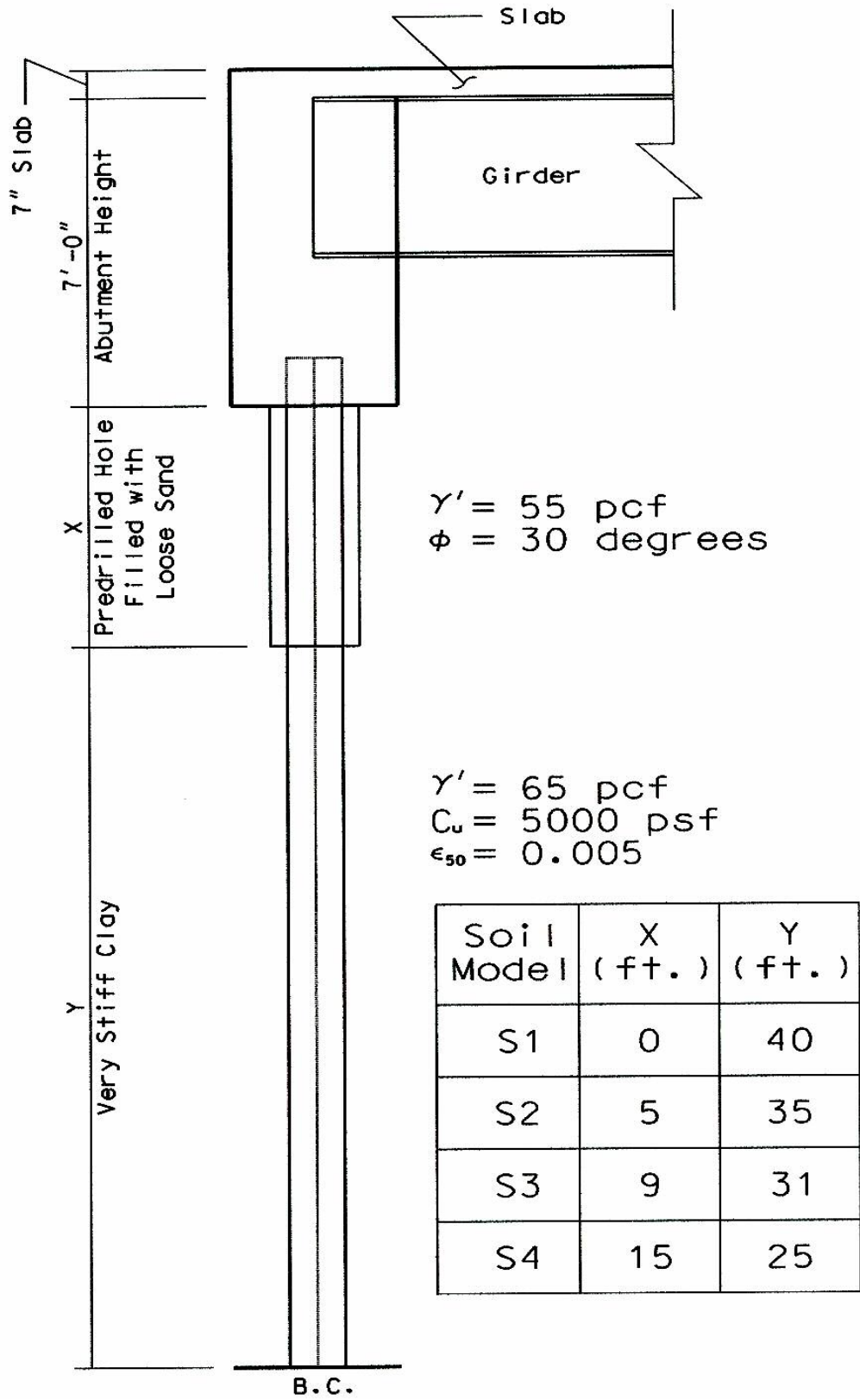


Figure 6.9 – Soil Properties and Layout for the Different Soil Profile Models



It is assumed that in all soil profiles, the soil behind the abutment is to be compacted dense sand. Since non-linear behavior of soil is considered, the spring stiffness is not constant and varies with displacement. A set of  $p$ - $y$  curves is generated using the modified Ramberg-Osgood model for different types of soil, particularly very stiff clay, loose sand, and dense sand. Similar curves for  $f$ - $z$ , load-slip, and  $q$ - $z$ , pile tip load settlement curves are also generated using the same modified Ramberg-Osgood model.

The modified Ramberg-Osgood model that is represented by Equation 5.1 is used for calculating load-displacement curves for different soil types and different HP steel piles used in the analysis at different depths. The numbers were modified to account for the spacing between springs in the model which is 0.5 ft.

A normalized  $p$ - $y$  curve for the very stiff clay type of soil is shown Figure 6.10, while Figures 6.11 and 6.12 show  $f$ - $z$  and  $q$ - $z$  curves for the same type of soil.

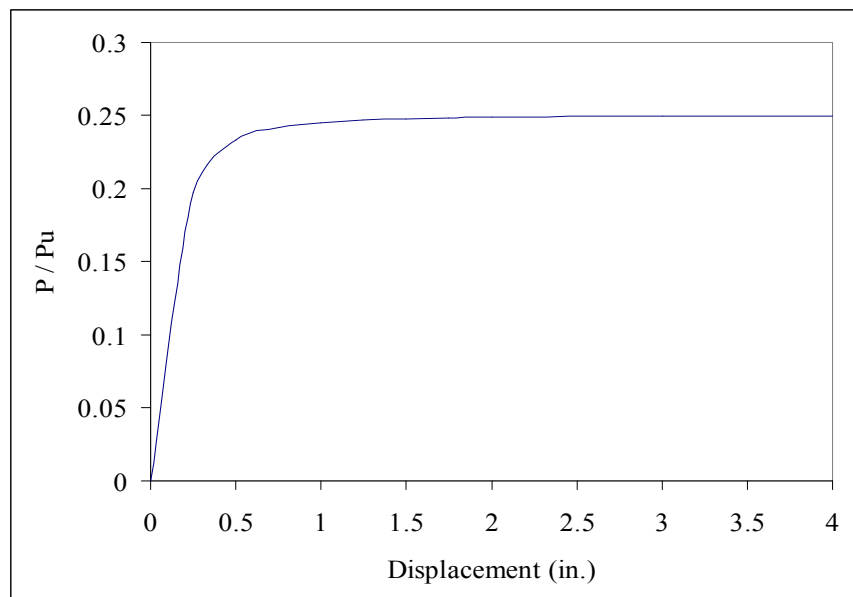


**Figure 6.10 – Normalized  $p$ - $y$  Curve for HP 10x42 Steel Piles in Very Stiff Clay**

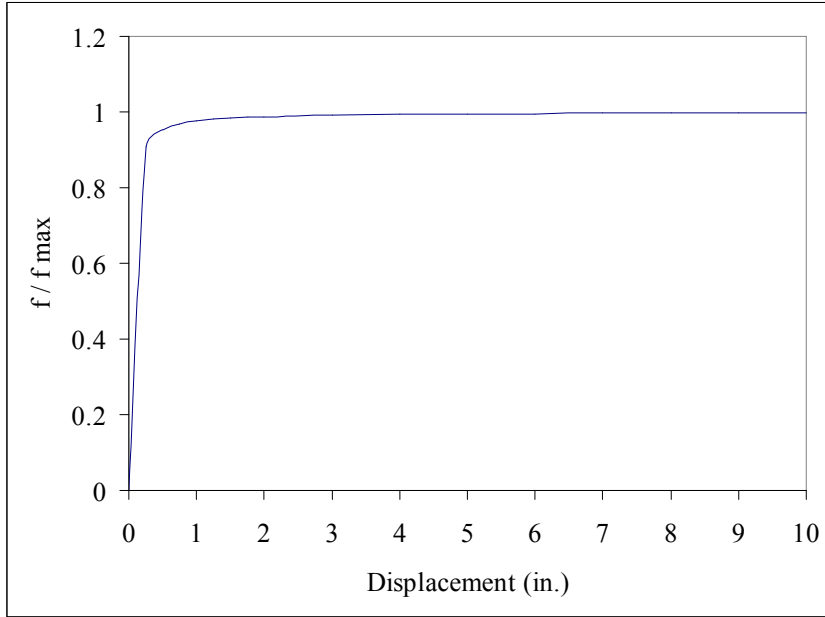


**Figure 6.11 – Normalized  $f$ - $z$  Curve for HP 10x42 Steel Pile in Very Stiff Clay**

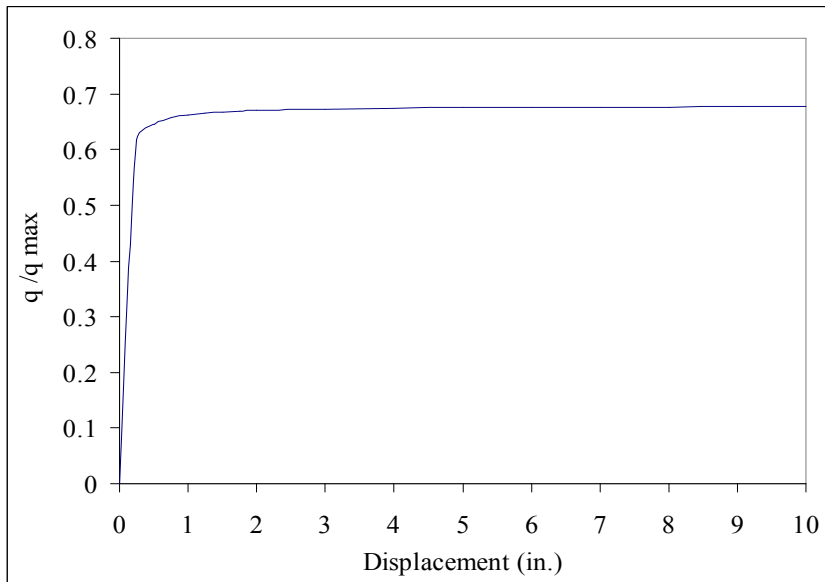


**Figure 6.12 – Normalized  $q$ - $z$  Curve for HP 10x42 Steel Pile in Very Stiff Clay**

The analyses include investigations for two types of piles, friction piles, and end-bearing piles. The assumption for the latter type is that the piles are driven to refusal and therefore sit on stiff rocks.

## 6.4 Loading Conditions

All models are analyzed using live load, dead load and temperature loads. Live loads in the models are based on AASHTO specifications for HS20-44 lane loading condition. Dead loads are considered the self-weight of the bridge, including superstructure and substructure. Temperature loading is taken as per AASHTO specifications for steel structures to vary from 0° F to 120° F for moderate climate.

Two temperature load cases are studied in this analysis. The first temperature load case is a temperature differential of 90° F for concrete slab and the top 3.5 inches of both abutments and the temperature differential of 60° F for the rest of the bridge structures which are steel girders, abutments and piles ( $\Delta T_{\text{slab}} = 90^\circ \text{ F}$ ,  $\Delta T_{\text{the rest}} = 60^\circ \text{ F}$ ). The second temperature load case is a temperature differential of 120° F for concrete slab and the top 3.5 inches of both abutments and the temperature differential of 90° F for the rest of the bridge structures which are steel girders, abutments and piles ( $\Delta T_{\text{slab}} = 120^\circ \text{ F}$ ,  $\Delta T_{\text{the rest}} = 90^\circ \text{ F}$ ). The temperature distribution will vary uniformly in both cases. Material coefficient of thermal expansion,  $\alpha$ , is as follows:

For normal weight concrete:  $\alpha = 0.0000060 \text{ in./in./}^\circ\text{F}$

For structural steel:  $\alpha = 0.0000065 \text{ in./in./}^\circ\text{F}$

Since the model represents a two-lane bridge based on its width, there is no need to include any reduction in load intensity as per AASHTO recommendations. Wind loads on both the superstructure and substructure elements are neglected.

## 6.5 The Complete Three-Dimensional Model

Figure 6.13 shows all elements used in the model in a sample bridge with end-bearing piles. The friction type piles are represented with a similar model with the exception of an additional set of springs added at the bottom to represent the load-settlement behavior of the pile.

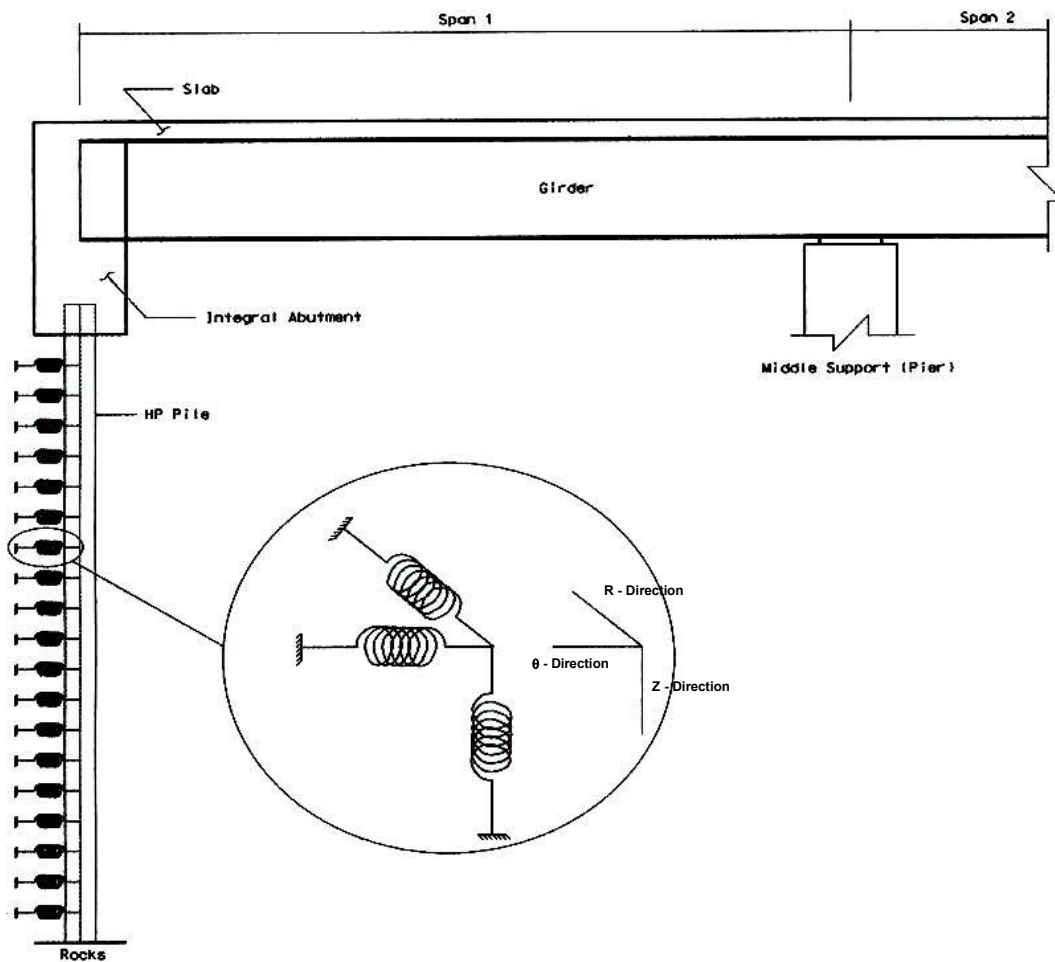
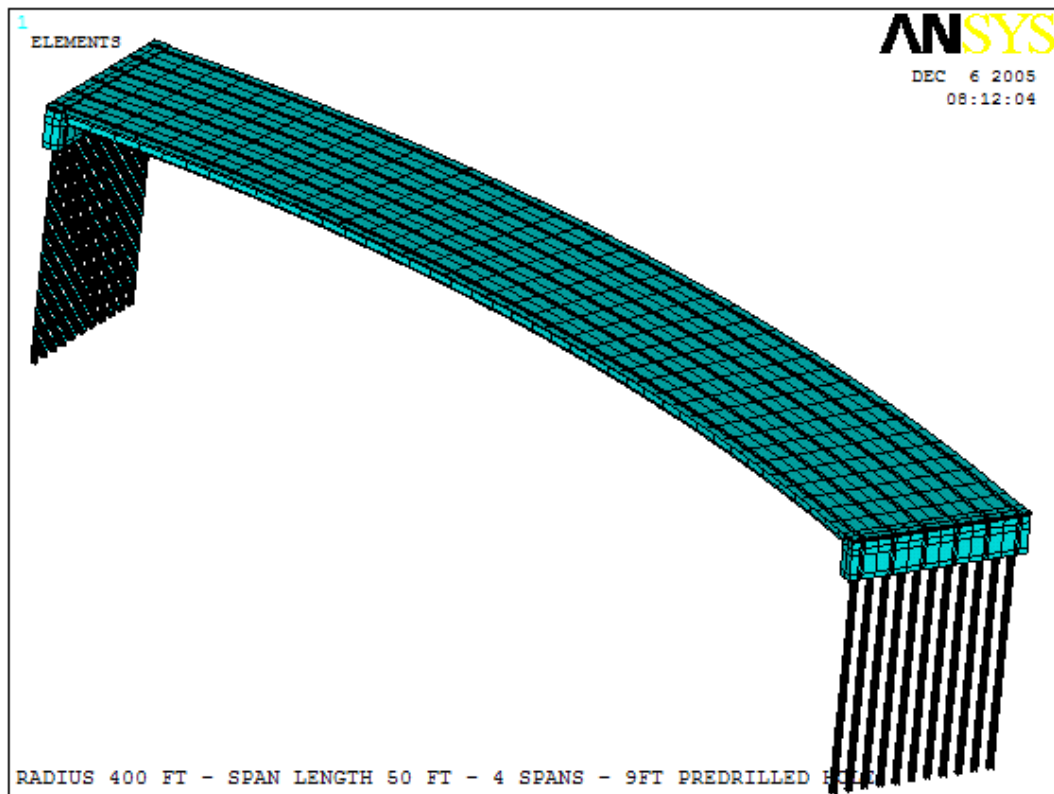
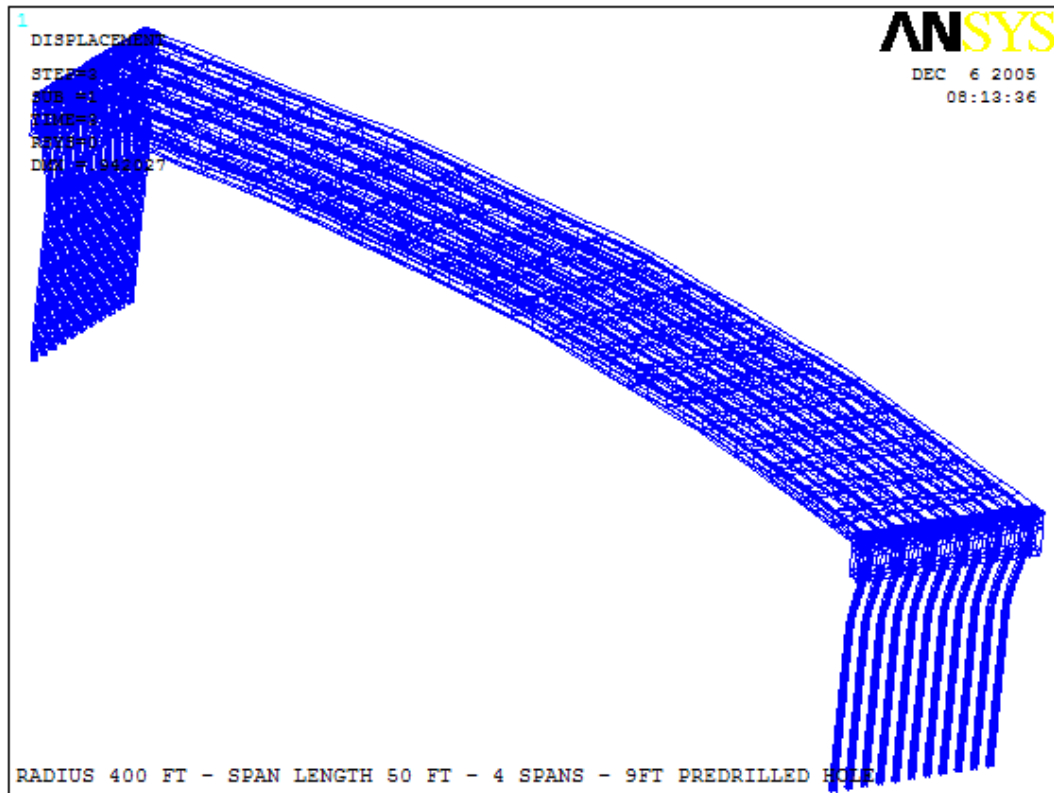


Figure 6.13 – The Three-Dimensional Model Components

Figures 6.14 and 6.15 are for an actual shape of a sample model used in the analysis before and after deformation (before and after applying forces). The sample shown in Figures 6.14 and 6.15 is for a curved integral abutment bridge with a 400 ft radius and 50 ft spans. The four spans add to a 200 ft long bridge model with 28.65 degree of curvature. Piles with end-bearing type are in very stiff clay soil profile with 9 ft deep predrilled holes filled with loose sand. The bridge is subjected to a thermal load of  $\Delta T_{\text{slab}}$  of 120° F and  $\Delta T_{\text{the rest}}$  of 90° F. A deflection scale factor of 40 is used to enlarge the displacement of the bridge structure.



**Figure 6.14 – Undeformed Shape of a Curved Integral Abutment Bridge with 400 ft Radius and 4 - 50 ft Spans with Piles in Very Stiff Clay Soil Profile with 9 ft Deep Predrilled Holes Filled with Loose Sand**



**Figure 6.15 – Deformed Shape of a Curved Integral Abutment Bridge with 400 ft Radius and 4 - 50 ft Spans with Piles in Very Stiff Clay Soil Profile with 9 ft Deep Predrilled Holes Filled with Loose Sand**

## 6.6 Nonlinearity

There are three sources of nonlinearity in structural mechanics simulations, material nonlinearity, boundary nonlinearity, and geometric nonlinearity. The two that are of interest in this study are the material and geometric nonlinearities.

### 6.6.1 Material Nonlinearity

Nonlinear stress-strain relationships are a common cause of nonlinear structural behavior. Many factors can influence a material's stress-strain properties,

including load history (as in elastoplastic response), environmental conditions (such as temperature), and the amount of time that a load is applied (as in creep response).

Most metals have a fairly linear stress/strain relationship at low strain values, but at higher strains, the metal yields resulting in a response which becomes nonlinear and irreversible.

### **6.6.2 Geometric Nonlinearity**

This source of nonlinearity is related to changes in the geometry of the model during the analysis. Geometric nonlinearity occurs whenever the magnitude of the displacement affects the response of the structure. Geometric nonlinearity can be caused by large deflections or rotations or by initial stresses or load stiffening.

Geometric nonlinearity occurs whenever the magnitude of the displacements affects the response of the structure. It includes the effects of large displacements, rotations and load stiffening. Nonlinear problems are solved iteratively using the Newton-Raphson method.

In ANSYS, the nonlinear analysis step is split into a number of increments. ANSYS iterates to find the approximate static equilibrium obtained at the end of each new load increment. ANSYS controls the load incrementation by using convergence controls throughout the simulation.

### **6.6.3 Solution of Nonlinear Problems in ANSYS**

ANSYS employs the "Newton-Raphson" approach to solve nonlinear problems. In this approach, the load is subdivided into a series of load increments. The load increments can be applied over several load steps.

Before each solution, the Newton-Raphson method evaluates the out-of-balance load vector, which is the difference between the restoring forces (the loads corresponding to the element stresses) and the applied loads. The program then performs a linear solution, using the out-of-balance loads, and checks for convergence. If convergence criteria are not satisfied, the out-of-balance load vector is reevaluated, the stiffness matrix is updated, and a new solution is obtained. This iterative procedure continues until the problem converges.

A number of convergence-enhancement and recovery features, such as line search, automatic load stepping, and bisection, can be activated to help the problem to converge. If convergence cannot be achieved, then the program attempts to solve with a smaller load increment.

In some nonlinear static analyses, if the Newton-Raphson method is used alone, the tangent stiffness matrix may become singular (or non-unique), causing severe convergence difficulties. Such occurrences include nonlinear buckling analyses in which the structure either collapses completely or "snaps through" to another stable configuration. For such situations, an alternative iteration scheme, the arc-length method, can be activated to help avoid bifurcation points and track unloading.



The arc-length method causes the Newton-Raphson equilibrium iterations to converge along an arc, thereby often preventing divergence, even when the slope of the load vs. deflection curve becomes zero or negative. This iteration method is represented schematically in Figure 6.16.

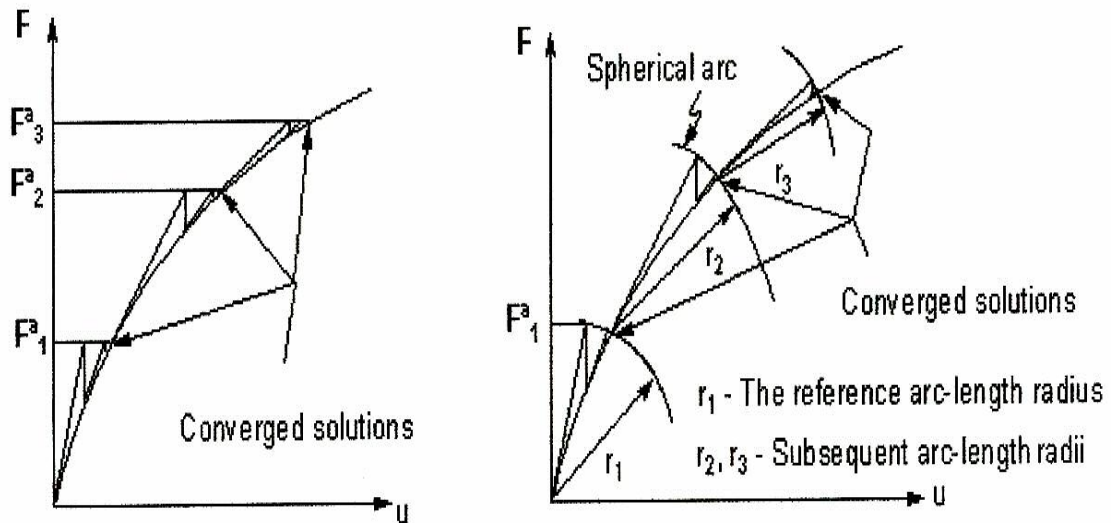


**Figure 6.16 – Traditional Newton-Raphson Method vs. Arc-Length Method**

To summarize, a nonlinear analysis is organized into three levels of operation:

- The top level consists of the load steps defined explicitly over a time span. Loads are assumed to vary linearly within load steps.
- Within each load step, the program can be directed to perform several solutions (substeps or time steps) to apply the load gradually.
- At each substep, the program will perform a number of equilibrium iterations to obtain a converged solution.

Figure 6.17 illustrates a typical load history for a nonlinear analysis. The ANSYS program gives a number of choices to designate convergence criteria: base convergence checking on forces, moments, displacements, or rotations, or on any combination of these items. Additionally, each item can have a different convergence tolerance value. For multiple-degree-of-freedom problems, it also has a choice of convergence norms.

The ANSYS program almost always employs a force-based (and, when applicable, moment-based) convergence tolerance. Displacement-based (and, when applicable, rotation-based) convergence checking can be added, if desired, but should usually not be used alone.

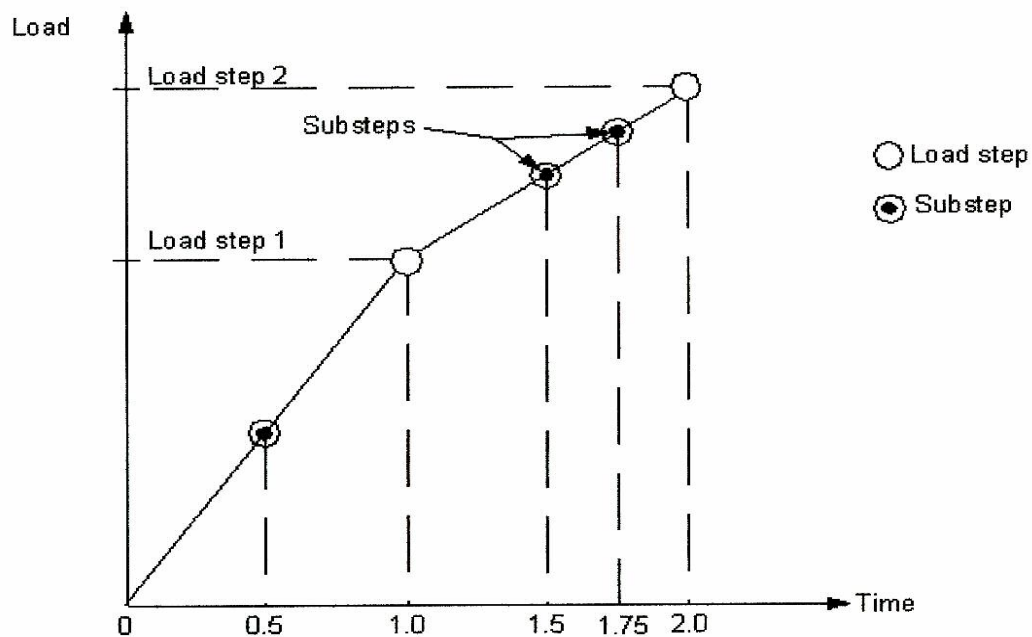


**Figure 6.17 – Load Steps, Substeps, and Time**

## CHAPTER 7

### PARAMETRIC STUDY OF STRESS INTENSITY IN THE PILES

Over 1,700 models were analyzed using the ANSYS program. These models were broken into two categories based on the following differential temperatures:

- $\Delta T_{\text{slab}} = 90^{\circ} \text{ F}$  and  $\Delta T_{\text{the rest}} = 60^{\circ} \text{ F}$
- $\Delta T_{\text{slab}} = 120^{\circ} \text{ F}$  and  $\Delta T_{\text{the rest}} = 90^{\circ} \text{ F}$

The maximum stress intensity (stress concentration) in the piles of curved integral abutment bridges (hereafter referred to as curved IAB's) was investigated using the following parameters:

1. Effect of bridge length variation (from 50 ft to 1200 ft)
2. Effect of temperature increase (from  $\Delta T_{\text{slab}} = 90^{\circ} \text{ F}$  and  $\Delta T_{\text{the rest}} = 60^{\circ} \text{ F}$  to  $\Delta T_{\text{slab}} = 120^{\circ} \text{ F}$  and  $\Delta T_{\text{the rest}} = 90^{\circ} \text{ F}$ )
3. Effect of soil profile variation (very stiff clay soil profile, and very stiff clay soil profile with varying depths (5ft, 9ft, and 15 ft) of predrilled holes filled with loose sand (hereafter referred to as predrilled holes))
4. Effect of span length variation (50 ft and 100 ft)
5. Effect of radius variation (400 ft, 600 ft, 800 ft, 1200 ft, 2400 ft and Infinity)
6. Effect of pile type (end-bearing and friction piles)

Curved IAB's with end-bearing piles were considered throughout this study except when the parameter being considered is the effect of pile type.

Materials used in this study were modeled using material nonlinearity. Steel was modeled with Bilinear Kinematic Hardening property with the tangent modulus equal to the elastic modulus. Materials, material properties, and loads used in this study are indicated in Table 7.1.

**Table 7.1 – Materials, Material Properties, and Loads**

<b>Materials</b>	<b>Value</b>
<b>Concrete</b>	
Slab (Thickness)	7 in.
Abutment (Width x Height)	3 ft x 7 ft 7 in.
<b>Steel</b>	
Girders	W30x132
Cross-Bracings	L6x6x1
Piles	HP10x42
<b>Soil</b>	See Chapter 5
<b>Material Properties</b>	
<b>Concrete</b>	
Modulus of elasticity	$3.6 \times 10^6$ psi
Weight	145 lb/ft <sup>3</sup>
Coefficient of thermal expansion	$6 \times 10^{-6}$ in./in./°F
<b>Steel</b>	
Modulus of elasticity	$29 \times 10^6$ psi
Weight	490 lb/ft <sup>3</sup>
Coefficient of thermal expansion	$6.5 \times 10^{-6}$ in./in./°F
<b>Soil</b>	See Section 6.3
<b>Loads</b>	
Dead Load	Self weight of bridge structure
Live Load	HS20-44 lane load
Thermal Load	$\Delta T_{\text{slab}} = 90^\circ \text{ F}$ and $\Delta T_{\text{the rest}} = 60^\circ \text{ F}$
	$\Delta T_{\text{slab}} = 120^\circ \text{ F}$ and $\Delta T_{\text{the rest}} = 90^\circ \text{ F}$

## **7.1 Effect of Bridge Length Variation**

The analysis presented herein investigates the maximum stress intensity (stress concentration) in the piles of curved IAB's with an increasing bridge length from 50 ft to 1200 ft. Several different models with different radii, span lengths, soil profiles and temperature levels were created to investigate the effect of bridge length variation on the maximum stress intensity developed in the piles. Table 7.2 shows the information of curved IAB's that were used in this study and that is also plotted in Figure 7.1.

Figures 7.2 to 7.9 indicate that the maximum stress intensity in the piles of curved IAB's increases as the bridge length is increased. The maximum stress intensity in the piles will reach its highest value at the bridge length indicated in Tables 7.3 and 7.4. Beyond that bridge length, the highest pile stress intensity value will start decreasing as the bridge length is increased to 1200 ft. Except in the case of straight IAB's (an infinite radius), the maximum stress intensity in the piles increases as the bridge length is increased.

Figures 7.2 to 7.5 also indicate that the maximum stress intensity in the piles of curved IAB's with a 400 ft radius and 50 ft spans is almost constant for bridge lengths from 800 ft to 1200 ft.

**Table 7.2 – Information of Curved Integral Abutment Bridges**

Span Length (ft)	Number of Spans	Bridge Length (ft)	Degree of Curve (Degrees) for Radius					
			400 ft	600 ft	800 ft	1200 ft	2400 ft	Infinity
50	1	50	7.162	4.775	3.581	2.387	1.194	0
	2	100	14.324	9.549	7.162	4.774	2.387	0
	3	150	21.486	14.324	10.743	7.162	3.581	0
	4	200	28.648	19.099	14.324	9.548	4.775	0
	6	300	42.972	28.648	21.486	14.322	7.162	0
	8	400	57.296	38.197	28.648	19.096	9.549	0
	12	600	85.944	57.296	42.972	28.644	14.324	0
	16	800	114.592	76.394	57.296	38.192	19.099	0
	20	1000	143.239	95.493	71.620	47.746	23.873	0
	24	1200	171.888	114.592	85.944	57.288	28.648	0
100	1	100	14.324	9.549	7.162	4.774	2.387	0
	2	200	28.648	19.099	14.324	9.548	4.775	0
	3	300	42.972	28.648	21.486	14.322	7.162	0
	4	400	57.296	38.197	28.648	19.096	9.549	0
	6	600	85.944	57.296	42.972	28.644	14.324	0
	8	800	114.592	76.394	57.296	38.192	19.099	0
	10	1000	143.239	95.493	71.620	47.746	23.873	0
	12	1200	171.888	114.592	85.944	57.288	28.648	0

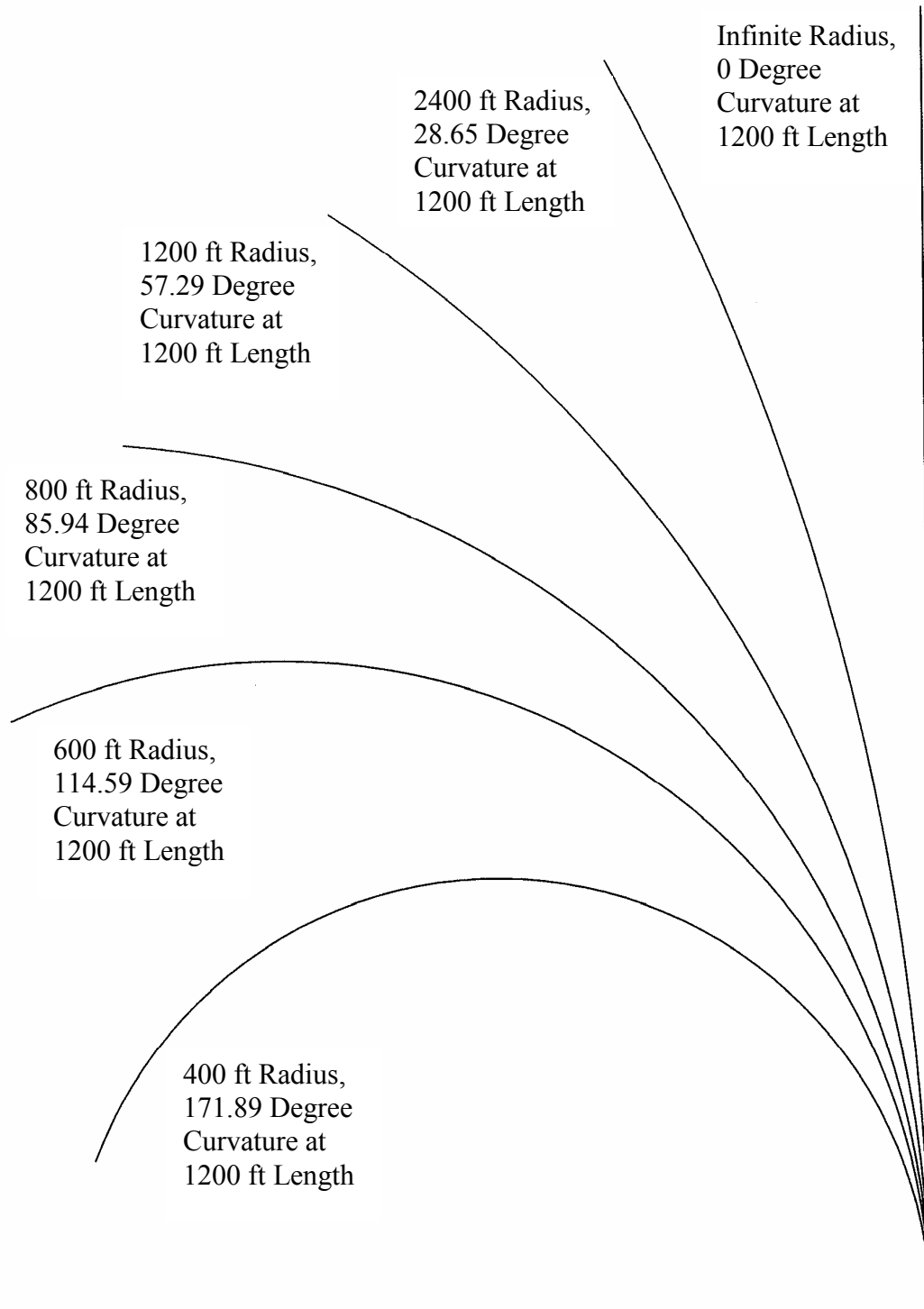


**Figure 7.1 – Curved Integral Abutment Bridges of Different Radii**

**Table 7.3 – Highest Stress Intensity (psi) in End-Bearing Piles in Very Stiff Clay Soil Profile of Curved Integral Abutment Bridges of Different Radii**

Span Length (ft)	Radius (ft)	Degree of Curve (Degrees)	Bridge Length (ft)	$\Delta T_{\text{slab}} = 90^\circ \text{ F}$ $\Delta T_{\text{the rest}} = 60^\circ \text{ F}$	$\Delta T_{\text{slab}} = 120^\circ \text{ F}$ $\Delta T_{\text{the rest}} = 90^\circ \text{ F}$
50	400	57.296	400	49074	65569
	600	38.197	400	58951	74408
	800	28.648	400	62759	77185
	1200	28.644	600	73091	88670
	2400	19.099	800	87174	106584
	Infinity	0	1200	115773	147777
100	400	57.296	400	63119	73934
	600	38.197	400	69421	80627
	800	28.648	400	71341	82833
	1200	28.644	600	79444	91734
	2400	19.099	800	90471	108421
	Infinity	0	1200	115477	145516

**Table 7.4 – Highest Stress Intensity (psi) in End-Bearing Piles in 9 ft Deep Predrilled Holes of Curved Integral Abutment Bridges of Different Radii**

Span Length (ft)	Radius (ft)	Degree of Curve (Degrees)	Bridge Length (ft)	$\Delta T_{\text{slab}} = 90^\circ \text{ F}$ $\Delta T_{\text{the rest}} = 60^\circ \text{ F}$	$\Delta T_{\text{slab}} = 120^\circ \text{ F}$ $\Delta T_{\text{the rest}} = 90^\circ \text{ F}$
50	400	57.296	400	36615	47960
	600	57.296	600	41617	56638
	800	42.972	600	43820	58858
	1200	38.192	800	48173	65019
	2400	23.873	1000	56786	77237
	Infinity	0	1200	71296	95200
100	400	57.296	400	62408	73925
	600	57.296	600	63746	77604
	800	42.972	600	66516	80940
	1200	38.192	800	68529	84920
	2400	23.873	1000	74314	93231
	Infinity	0	1200	86139	107998



The lengths of curved IAB's which have the highest stress intensity in the piles from Tables 7.3, 7.4, and Figures 7.2 to 7.9 are plotted in Figure 7.10. The maximum stress intensity in the piles in very stiff clay soil profile (no predrilled holes) of curved IAB's of all radii starts to increase from a 50 ft bridge length until it reaches its highest value at the bridge length indicated in Figure 7.10 (solid line). Beyond that bridge length, the highest pile stress intensity value will start decreasing as the bridge length is increased (dashed and dotted lines).

For piles in predrilled holes, the maximum stress intensity in the piles of curved IAB's of all radii starts to increase from a 50 ft bridge length until it reaches its highest value at the bridge length indicated in Figure 7.10 (dashed line). Beyond that bridge length, the highest pile stress intensity value will start decreasing as the bridge length is increased (dotted line).

Figure 7.10 also indicates that the highest stress intensity value in the piles of curved IAB's with radii of 400 ft and infinity (straight IAB's) is at the same bridge length (a 400 ft length for a 400 ft radius, and a 1200 ft length for an infinite radius) for piles in all soil profile types. The introduction of predrilled holes results in the highest stress intensity value in the piles of curved IAB's with radii of 600 ft, 800 ft, 1200 ft, and 2400 ft occurring at a bridge length of 200 ft longer than the highest stress intensity value in the piles without predrilled holes.

For piles in very stiff clay soil profile, curved IAB's of all radii have approximately the same maximum stress intensity value in the piles at the same bridge length for bridge lengths up to 300 ft. Beyond the 300 ft length, curved IAB's

with a smaller radius, for the most part, have a maximum stress intensity in the piles less than that of curved IAB's with a larger radius as the bridge length is increased.

For piles in predrilled holes, curved IAB's with a larger radius have a maximum stress intensity in the piles less than that of curved IAB's with a smaller radius for bridge lengths up to 400 ft. Beyond the 400 ft length, curved IAB's with a smaller radius, for the most part, have a maximum stress intensity in the piles less than that of curved IAB's with a larger radius as the bridge length is increased.

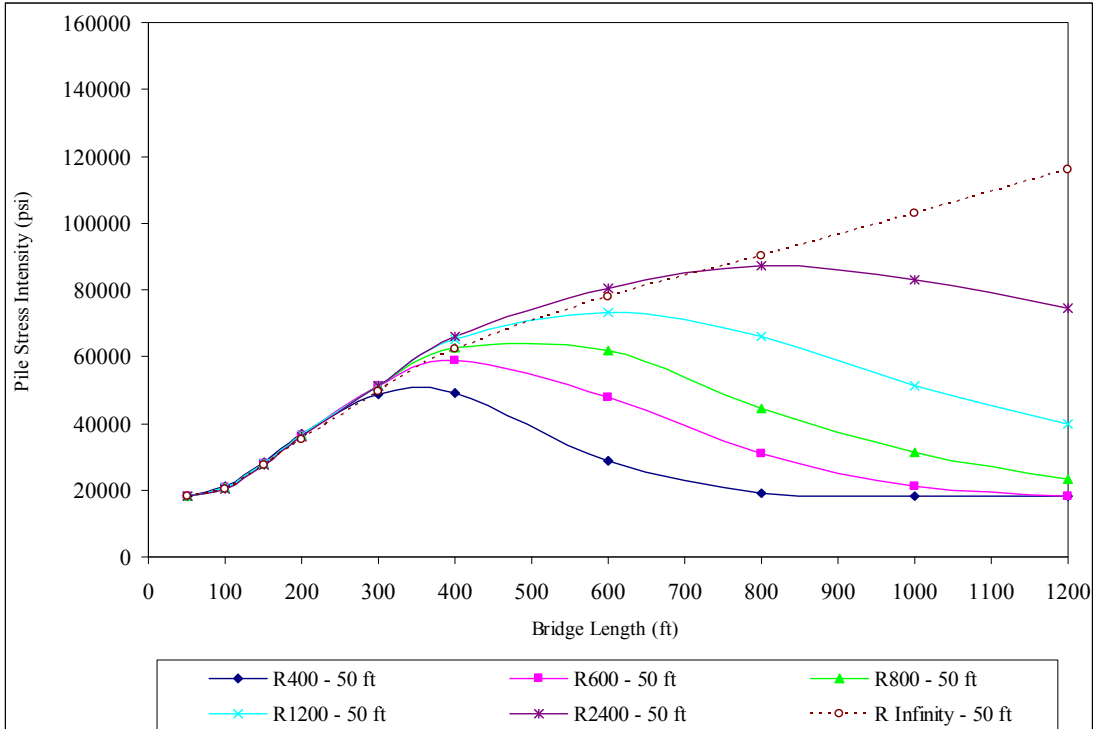
For curved IAB's with 100 ft spans and with piles in predrilled holes, curved IAB's with double spans (bridge length of 200 ft) can reduce the maximum stress intensity in the piles when compared with single span bridges (bridge length of 100 ft). The pile stress intensity reduction is in the range of 9.5% to 22% for  $\Delta T_{\text{slab}}$  of 90° F and  $\Delta T_{\text{the rest}}$  of 60° F and is in the range of 2.6% to 16.4% for  $\Delta T_{\text{slab}}$  of 120° F and  $\Delta T_{\text{the rest}}$  of 90° F as indicated in Table 7.5 and plotted in Figure 7.11.

Table 7.5 and Figure 7.11 indicate that for piles in predrilled holes, curved IAB's with a smaller radius have a pile stress intensity reduction less than that of curved IAB's with a larger radius when comparing curved IAB's with double spans (bridge length of 200 ft) with single span bridges (bridge length of 100 ft).

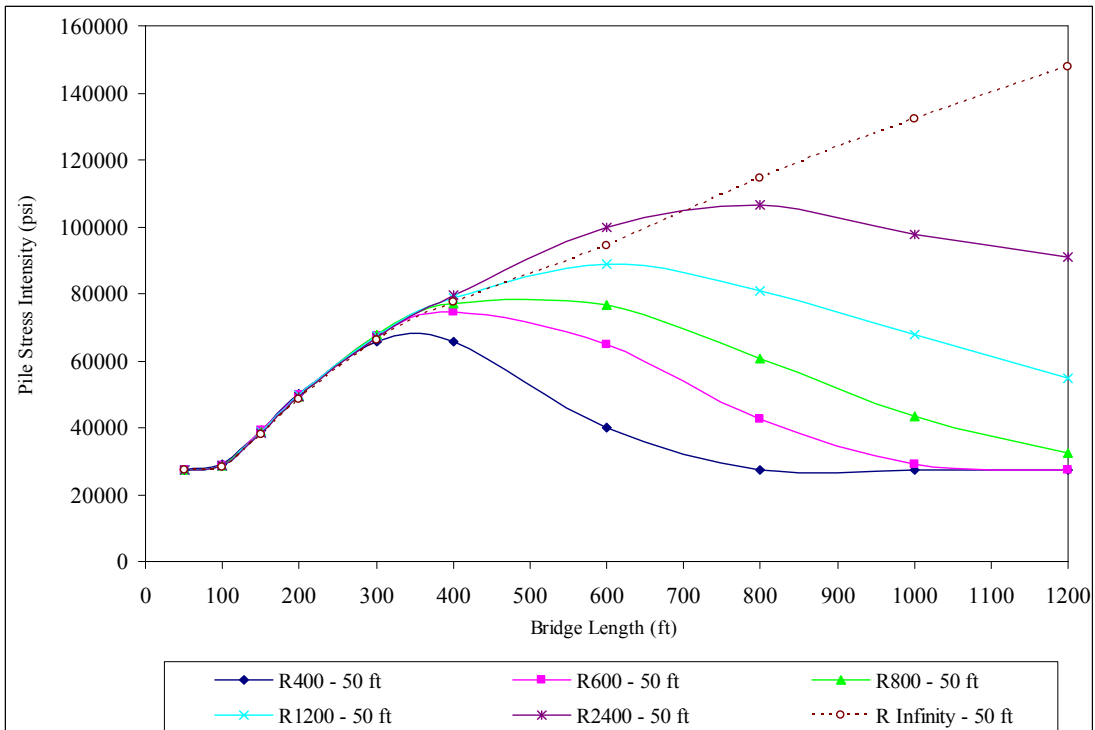
It is shown that a temperature increase results in a lower pile stress intensity reduction. Curved IAB's subjected to a high temperature load ( $\Delta T_{\text{slab}}$  of 120° F and  $\Delta T_{\text{the rest}}$  of 90° F) have a pile stress intensity reduction less than that of curved IAB's subjected to a low temperature load ( $\Delta T_{\text{slab}}$  of 90° F and  $\Delta T_{\text{the rest}}$  of 60° F).

It is also shown that 9 feet deep predrilled holes filled with loose sand have a significant reduction in the pile stress intensity when compared with 5 ft deep

predrilled holes filled with loose sand. The depth increase of predrilled holes deeper than 9 ft will further reduce the stress intensity in the piles, but the rate of reduction is much smaller than that of 9 ft deep predrilled holes.

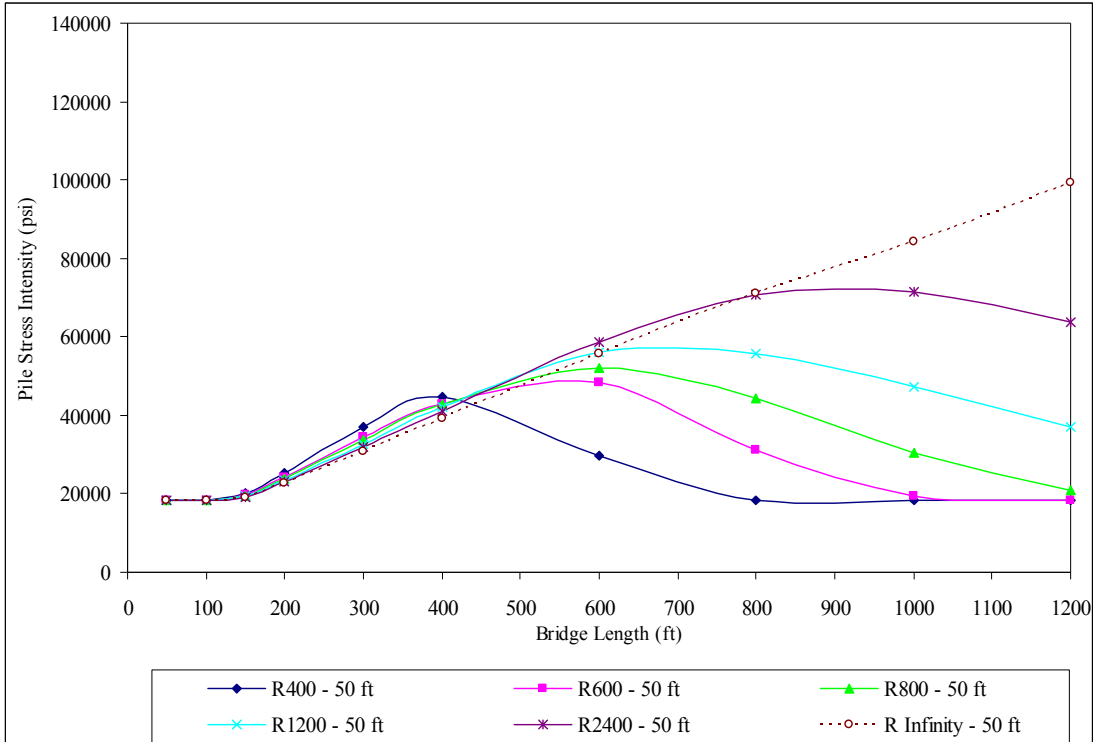


a)  $\Delta T_{\text{slab}} = 90^{\circ} \text{ F}$ ,  $\Delta T_{\text{the rest}} = 60^{\circ} \text{ F}$

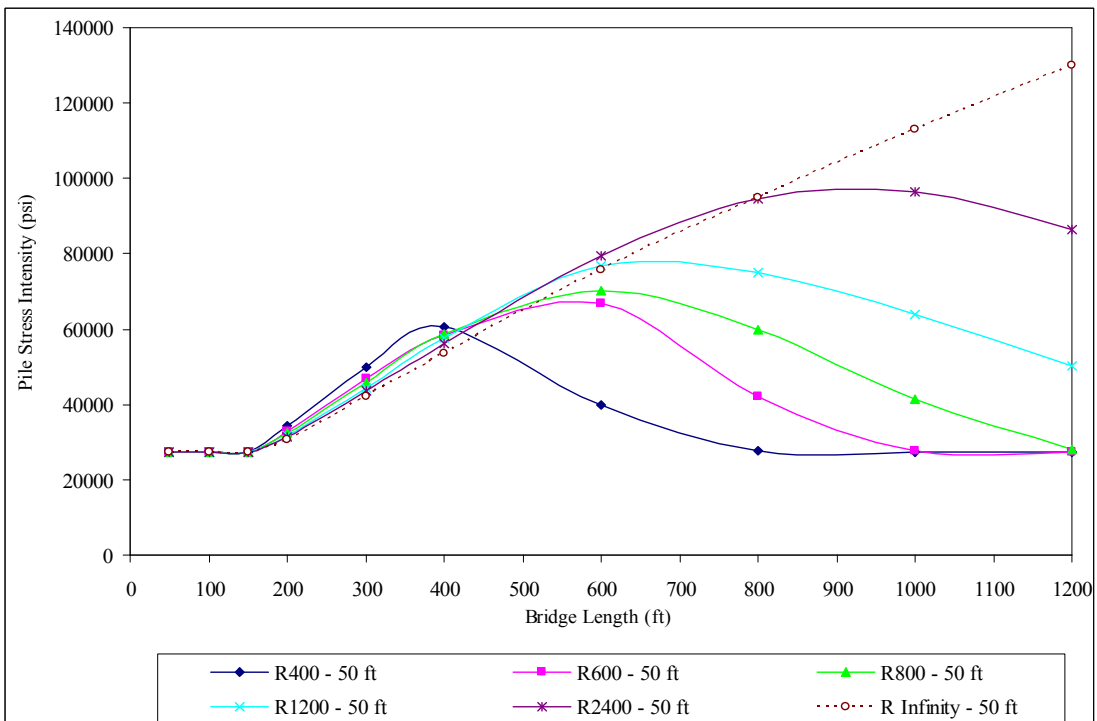


b)  $\Delta T_{\text{slab}} = 120^{\circ} \text{ F}$ ,  $\Delta T_{\text{the rest}} = 90^{\circ} \text{ F}$

**Figure 7.2 – Maximum Stress Intensity in End-Bearing Piles in Very Stiff Clay Soil Profile of Bridges with 50 ft Spans**

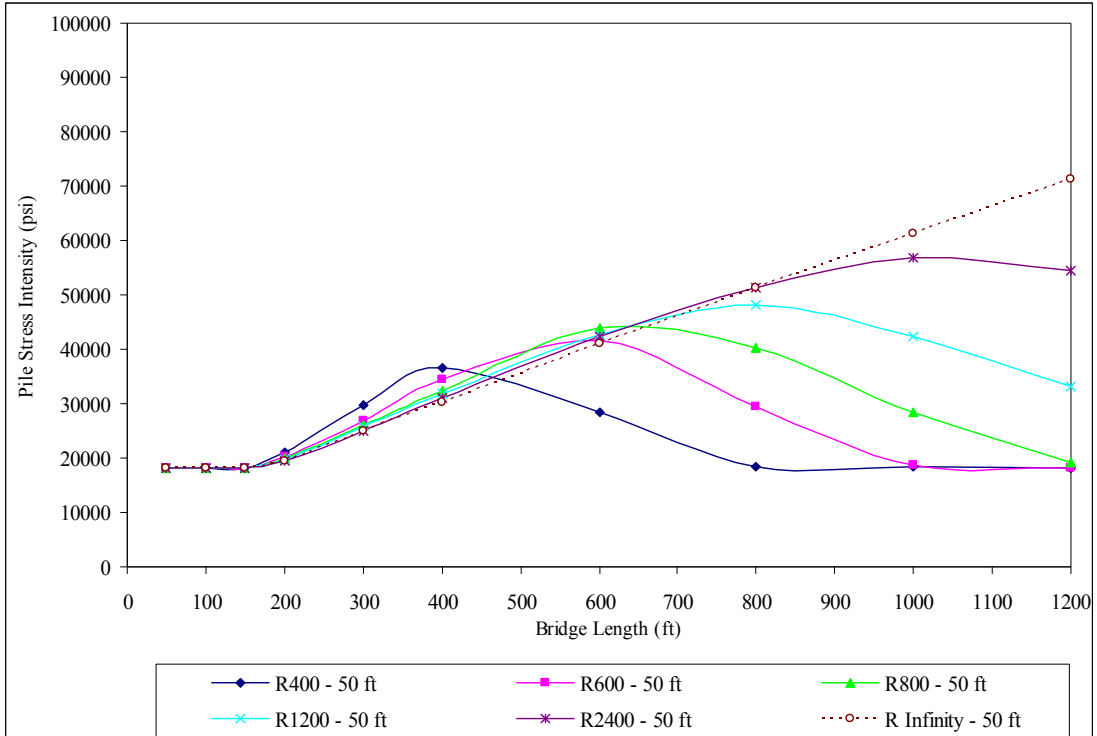


a)  $\Delta T_{\text{slab}} = 90^{\circ} \text{ F}$ ,  $\Delta T_{\text{the rest}} = 60^{\circ} \text{ F}$

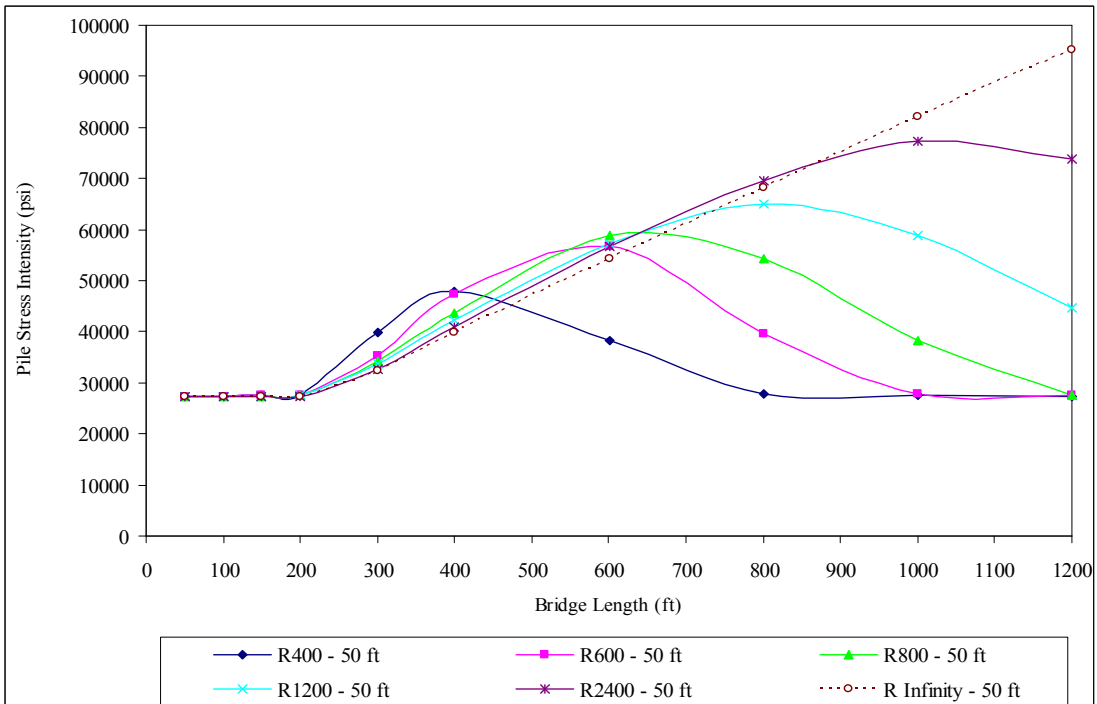


b)  $\Delta T_{\text{slab}} = 120^{\circ} \text{ F}$ ,  $\Delta T_{\text{the rest}} = 90^{\circ} \text{ F}$

**Figure 7.3 – Maximum Stress Intensity in End-Bearing Piles in 5 ft Deep Predrilled Holes of Bridges with 50 ft Spans**

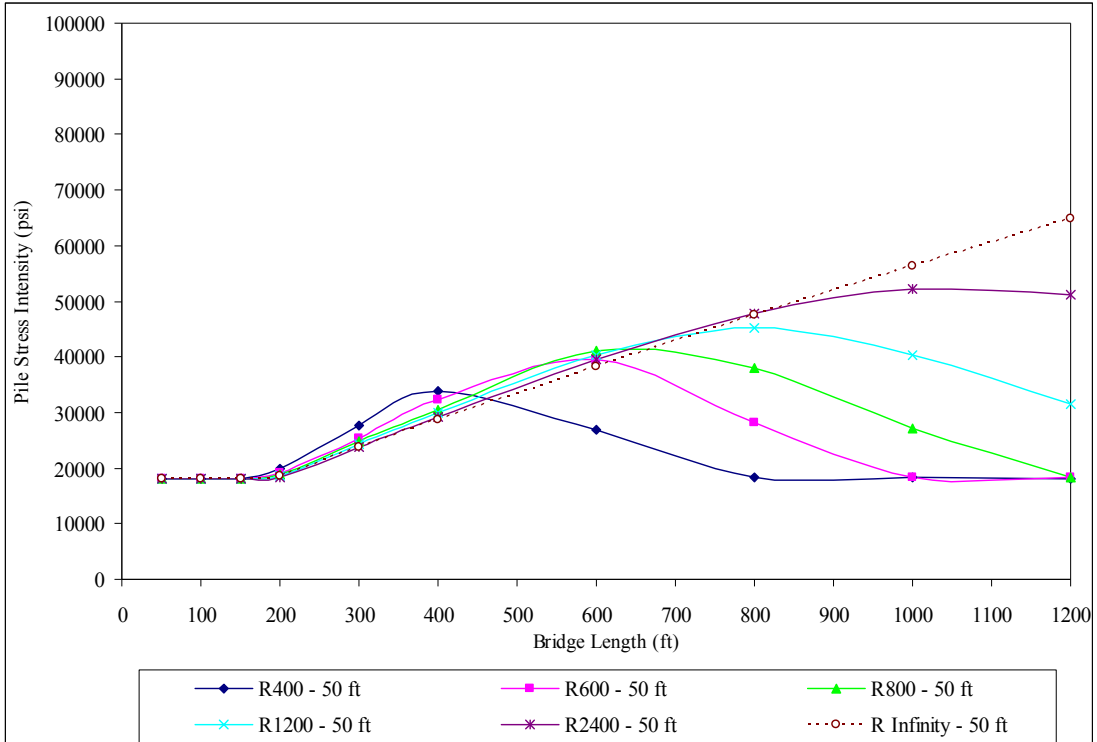


a)  $\Delta T_{\text{slab}} = 90^\circ \text{ F}$ ,  $\Delta T_{\text{the rest}} = 60^\circ \text{ F}$

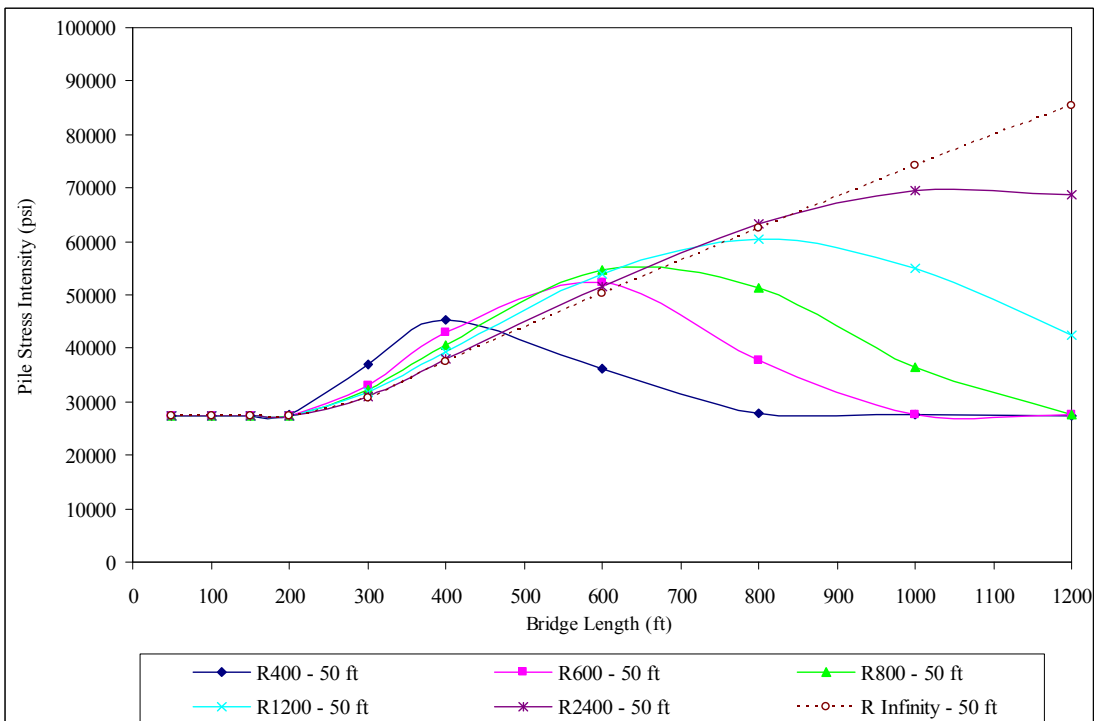


b)  $\Delta T_{\text{slab}} = 120^\circ \text{ F}$ ,  $\Delta T_{\text{the rest}} = 90^\circ \text{ F}$

**Figure 7.4 – Maximum Stress Intensity in End-Bearing Piles in 9 ft Deep Predrilled Holes of Bridges with 50 ft Spans**

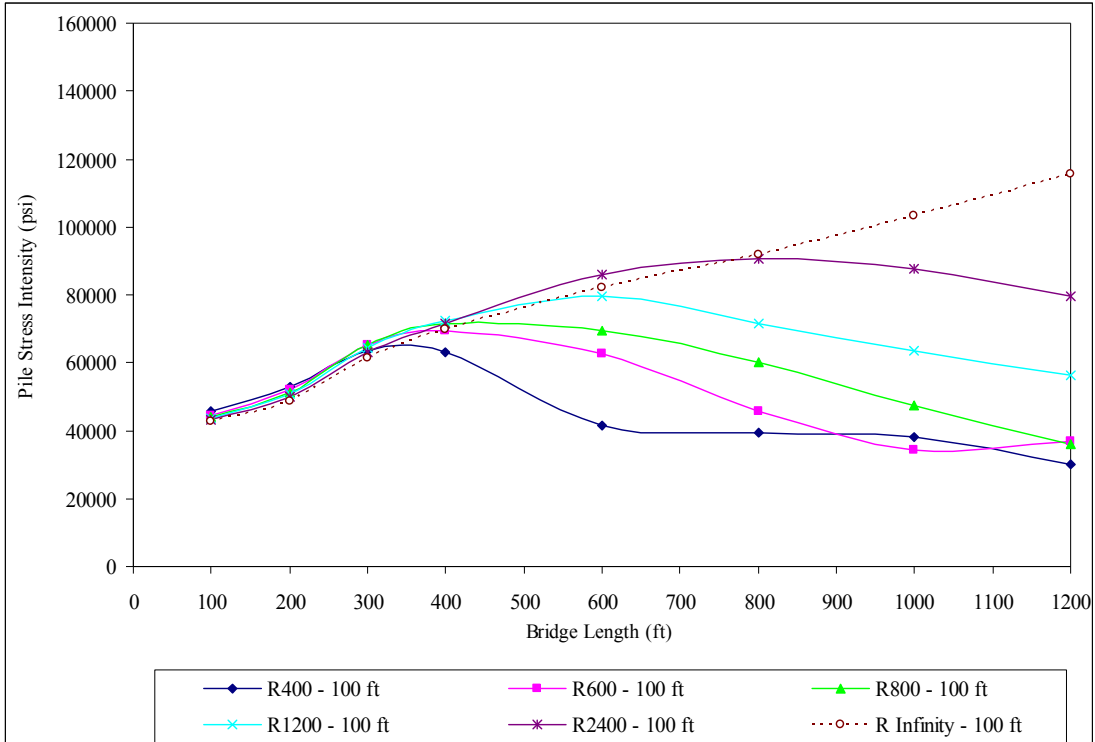


a)  $\Delta T_{\text{slab}} = 90^\circ \text{ F}$ ,  $\Delta T_{\text{the rest}} = 60^\circ \text{ F}$

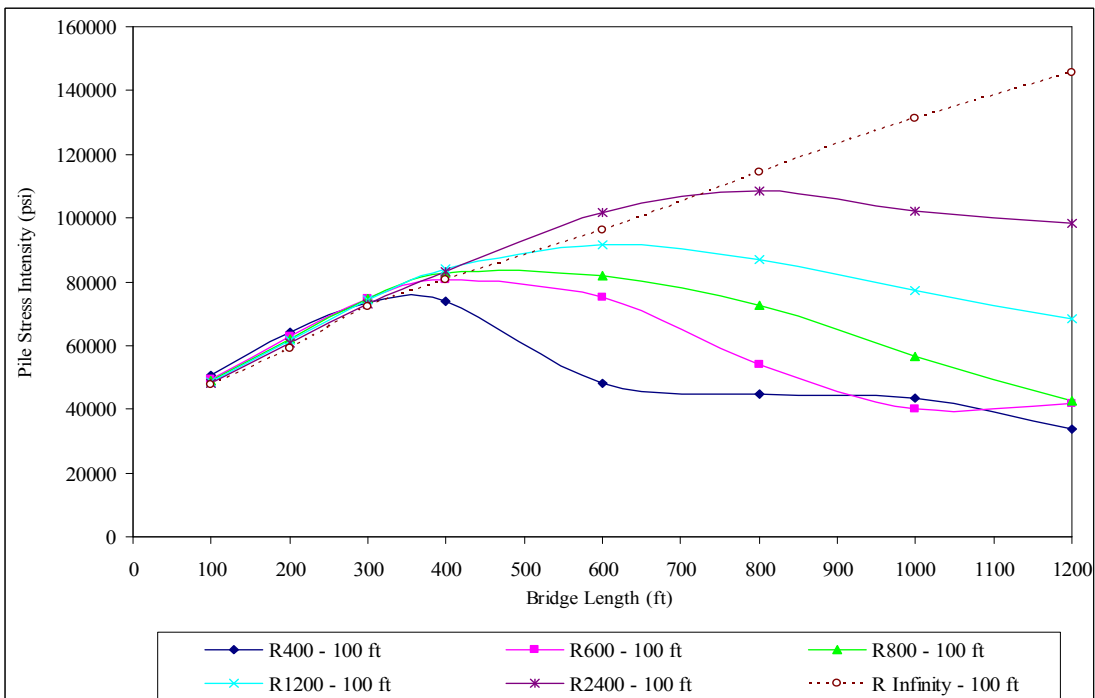


b)  $\Delta T_{\text{slab}} = 120^\circ \text{ F}$ ,  $\Delta T_{\text{the rest}} = 90^\circ \text{ F}$

**Figure 7.5 – Maximum Stress Intensity in End-Bearing Piles in 15 ft Deep Predrilled Holes of Bridges with 50 ft Spans**



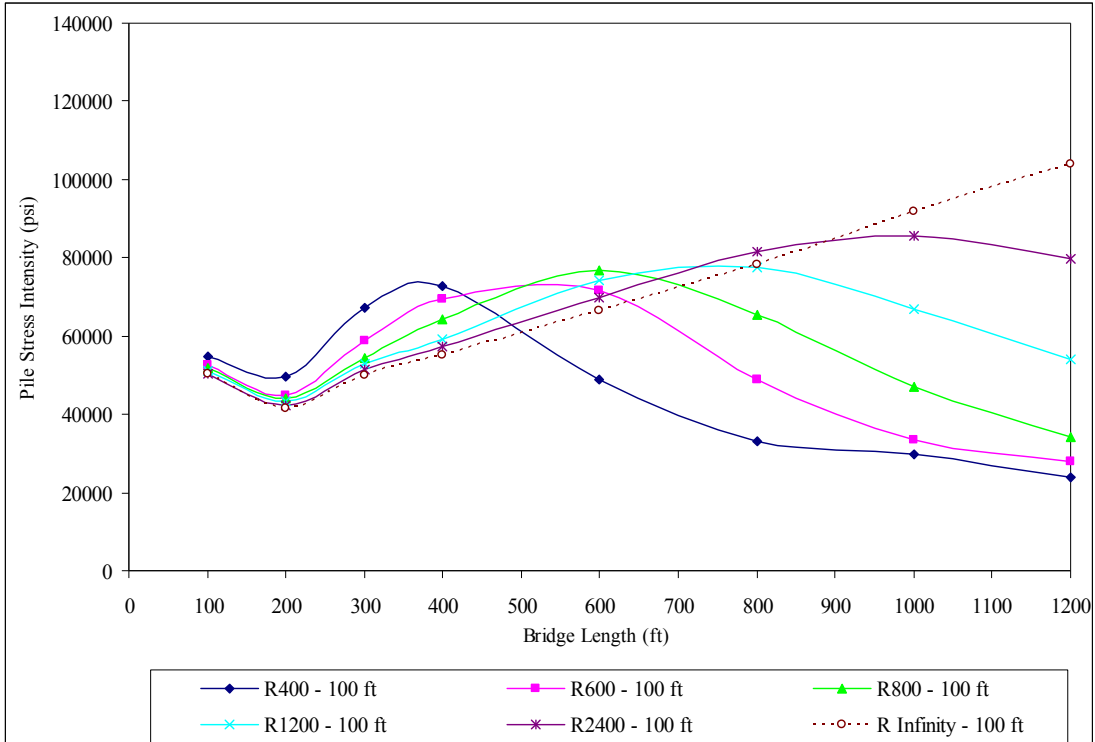
a)  $\Delta T_{\text{slab}} = 90^\circ \text{ F}$ ,  $\Delta T_{\text{the rest}} = 60^\circ \text{ F}$



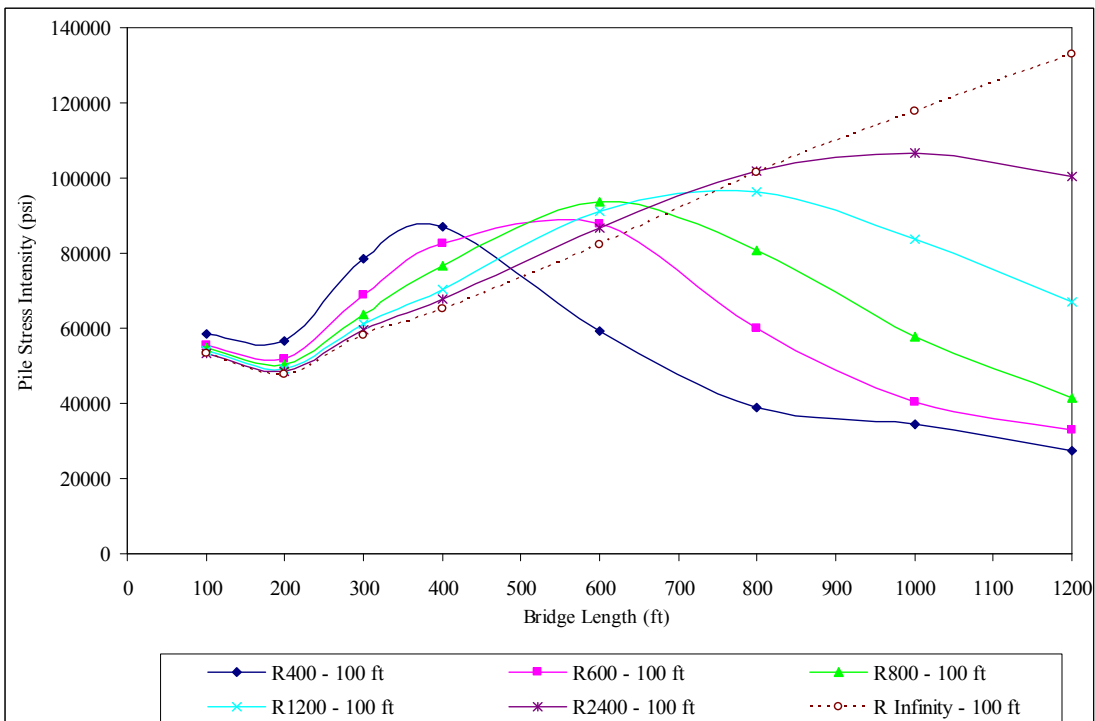
b)  $\Delta T_{\text{slab}} = 120^\circ \text{ F}$ ,  $\Delta T_{\text{the rest}} = 90^\circ \text{ F}$

Figure 7.6 – Maximum Stress Intensity in End-Bearing Piles in Very Stiff Clay Soil Profile of Bridges with 100 ft Spans



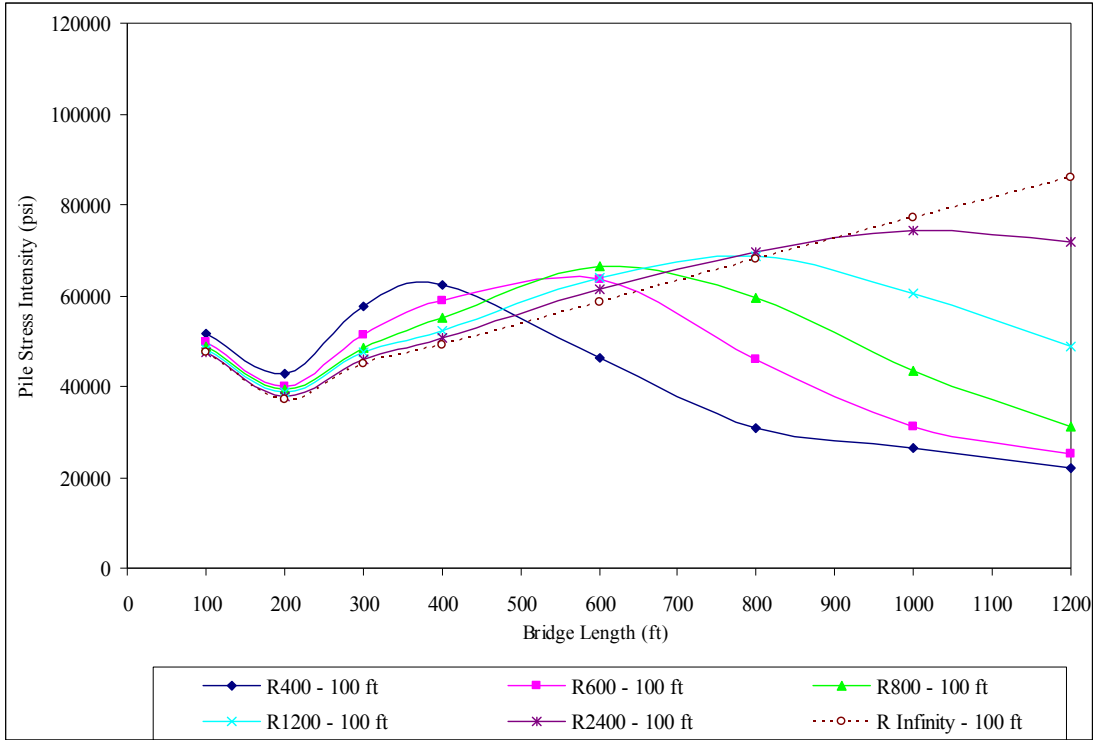


a)  $\Delta T_{\text{slab}} = 90^\circ \text{ F}$ ,  $\Delta T_{\text{the rest}} = 60^\circ \text{ F}$

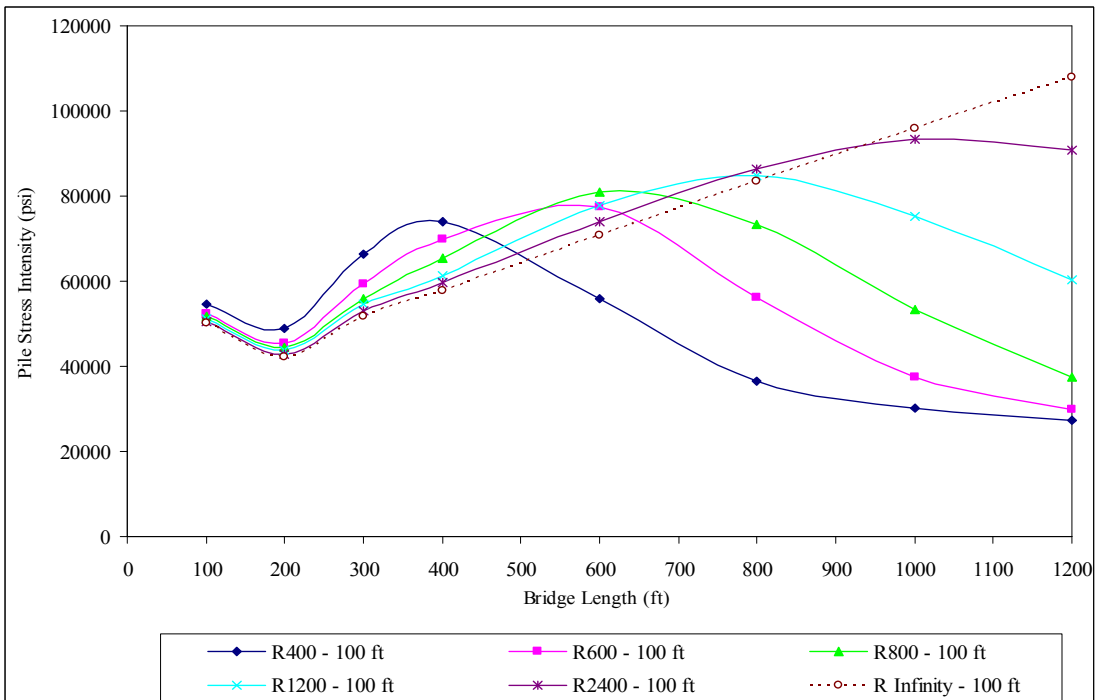


b)  $\Delta T_{\text{slab}} = 120^\circ \text{ F}$ ,  $\Delta T_{\text{the rest}} = 90^\circ \text{ F}$

**Figure 7.7 – Maximum Stress Intensity in End-Bearing Piles in 5 ft Deep Predrilled Holes of Bridges with 100 ft Spans**

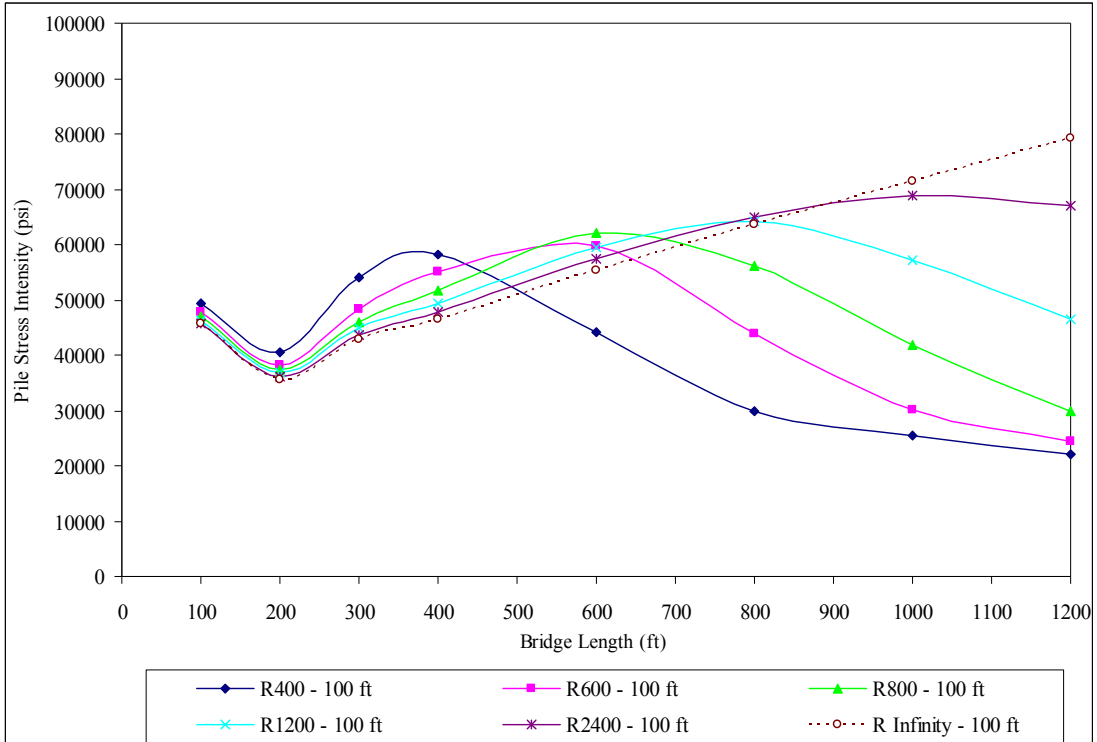


a)  $\Delta T_{\text{slab}} = 90^\circ \text{ F}$ ,  $\Delta T_{\text{the rest}} = 60^\circ \text{ F}$

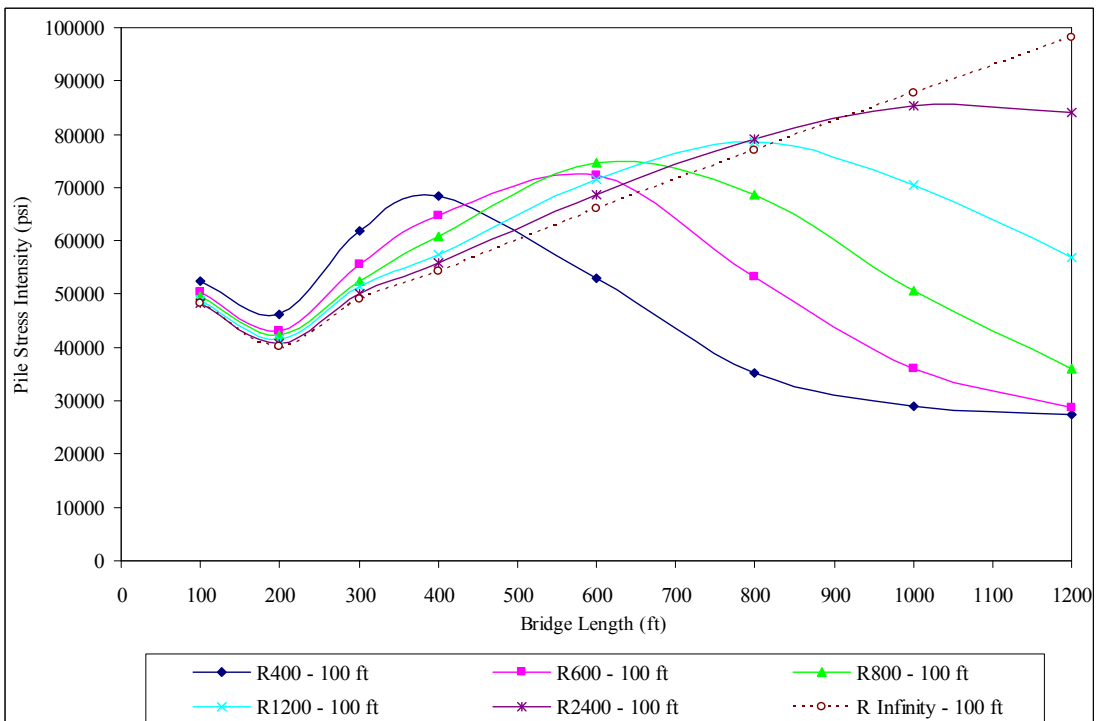


b)  $\Delta T_{\text{slab}} = 120^\circ \text{ F}$ ,  $\Delta T_{\text{the rest}} = 90^\circ \text{ F}$

**Figure 7.8 – Maximum Stress Intensity in End-Bearing Piles in 9 ft Deep Predrilled Holes of Bridges with 100 ft Spans**



a)  $\Delta T_{\text{slab}} = 90^\circ \text{ F}$ ,  $\Delta T_{\text{the rest}} = 60^\circ \text{ F}$



b)  $\Delta T_{\text{slab}} = 120^\circ \text{ F}$ ,  $\Delta T_{\text{the rest}} = 90^\circ \text{ F}$

**Figure 7.9 – Maximum Stress Intensity in End-Bearing Piles in 15 ft Deep Predrilled Holes of Bridges with 100 ft Spans**

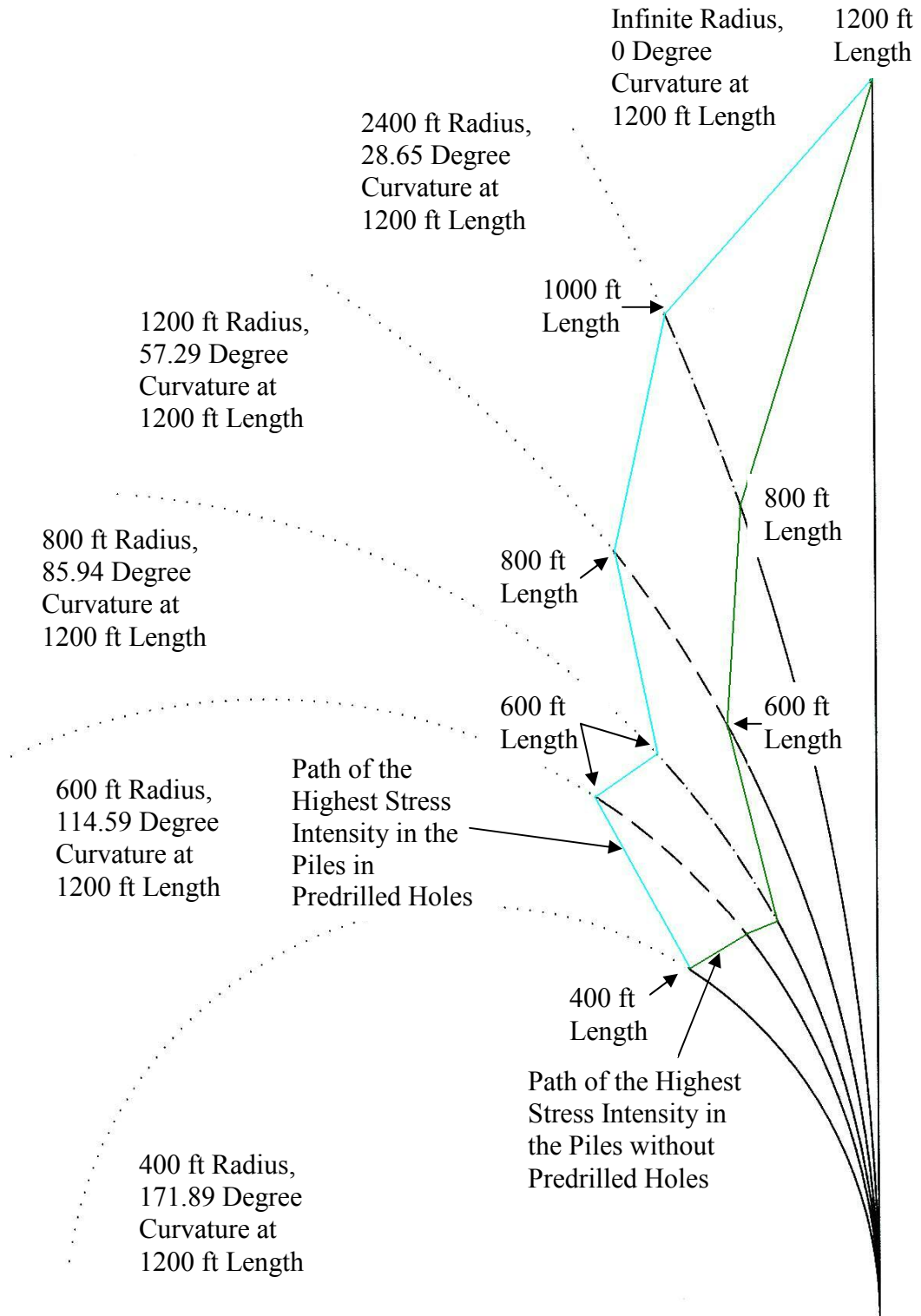


**Figure 7.10 – Highest Stress Intensity in End-Bearing Piles at Different Bridge Lengths of Curved Integral Abutment Bridges of Different Radii**

**Table 7.5 – Stress Reduction (%) of End-Bearing Piles in Varying Depths of Predrilled Holes of Bridges with 100 ft Spans and Bridge Length of 100 ft and 200 ft**

Radius (ft)	$\Delta T_{\text{slab}} = 90^\circ \text{ F}, \Delta T_{\text{the rest}} = 60^\circ \text{ F}$			$\Delta T_{\text{slab}} = 120^\circ \text{ F}, \Delta T_{\text{the rest}} = 90^\circ \text{ F}$		
	Depth of Predrilled Holes (ft)			Depth of Predrilled Holes (ft)		
	5	9	15	5	9	15
400	9.49	16.72	17.86	2.62	10.60	11.88
600	14.59	19.46	20.19	7.09	13.56	14.50
800	14.85	19.69	20.41	8.00	13.85	14.77
1200	15.14	19.93	20.64	8.53	14.12	15.03
2400	15.69	20.36	21.05	9.16	14.61	15.49
Infinity	17.21	21.60	22.01	10.57	15.85	16.41

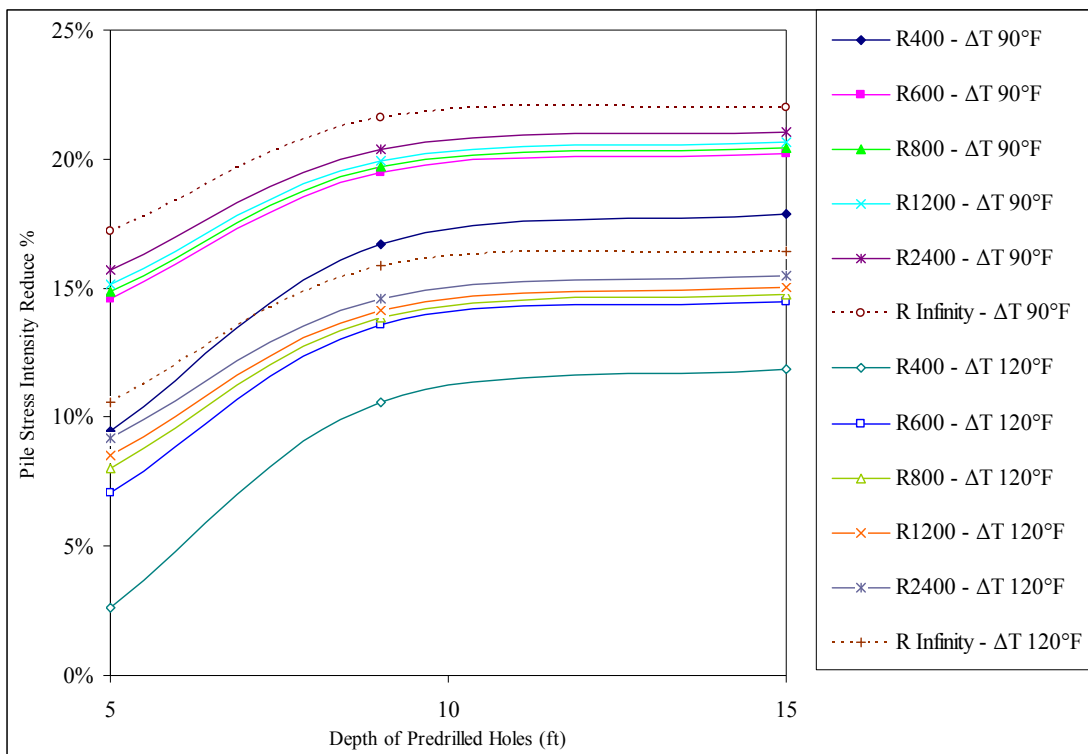


**Figure 7.11 – Stress Reduction (%) of End-Bearing Piles in Varying Depths of Predrilled Holes of Bridges with 100 ft Spans and Bridge Length of 100 ft and 200 ft**

## 7.2 Effect of Temperature Increase

The effect of a temperature increase from  $\Delta T_{\text{slab}}$  of 90° F and  $\Delta T_{\text{the rest}}$  of 60° F to  $\Delta T_{\text{slab}}$  of 120° F and  $\Delta T_{\text{the rest}}$  of 90° F (temperature increase of 30° F) in curved IAB's is investigated in this study to determine the maximum stress intensity (stress concentration) increase in the piles. All other parameters are held constant.

### 7.2.1 Curved Integral Abutment Bridges with 50 ft Spans

Figure 7.12 indicates that the highest pile stress intensity increase value due to the temperature increase of curved IAB's of all radii with piles in very stiff clay soil profile is approximately 50.5% at a 50 ft bridge length. It decreases to its lowest value at the bridge length indicated in Table 7.6. After it reaches its lowest value, the pile stress intensity increase rate starts increasing and continues to increase as the bridge length is increased to 1200 ft as indicated in Table 7.6.

For piles in predrilled holes, the highest pile stress intensity increase value due to the temperature increase of curved IAB's of all radii is approximately 50.5% for bridge lengths from 50 ft to 100 ft for piles in 5 ft deep predrilled holes and for bridge lengths from 50 ft to 150 ft for piles in 9 ft and 15 ft deep predrilled holes. Beyond these lengths, it decreases to the new pile stress intensity increase rate and remains nearly constant for the ranges of bridge lengths indicated in Figure 7.12 and Table 7.7.

It is shown that the pile stress intensity increase rates due to the temperature increase of curved IAB's of all radii with piles in predrilled holes are almost constant for several ranges of bridge lengths. For curved IAB's with a radius larger than

800 ft, the pile stress intensity increase rates are almost constant for bridge lengths in the range of 200 ft to 1200 ft for piles in 5 ft deep predrilled holes and in the range of 300 ft to 1200 ft for piles in 9 ft and 15 ft deep predrilled holes.

**Table 7.6 – Stress Increase (%) of End-Bearing Piles in Very Stiff Clay Soil Profile of Bridges with 50 ft Spans due to a 30° F Temperature Increase**

Radius (ft)	Bridge Length (ft)	Lowest Stress Increase (%)	Stress Increase (%) at 1200 ft Length
400	400	33.6	50.4
600	400	26.2	50.5
800	400	23.0	38.1
1200	400	21.1	36.7
2400	1000	17.6	21.7
Infinity	600	21.3	27.6

The mean of the pile stress intensity increase due to the temperature increase of curved IAB's of all radii with 50 ft spans is listed in Table 7.8 and plotted in Figure 7.14. It is shown that the highest mean of the pile stress intensity increase due to the temperature increase of curved IAB's of all radii with piles in all soil profile types is at a 50 ft bridge length. It continues to decrease to its lowest value at bridge lengths between 200 ft and 400 ft. Beyond these lengths, it starts increasing and continues to increase as the bridge length is increased to 1200 ft.

For curved IAB's of different radii with 50 ft spans, it is found that curved IAB's with a smaller radius have the mean of the pile stress intensity increase due to the temperature increase greater than that of curved IAB's with a larger radius as indicated in Table 7.9 and Figure 7.15. The mean of the pile stress intensity increase of curved IAB's with piles in predrilled holes is greater than that of curved IAB's

with piles without predrilled holes as indicated in Tables 7.8 and 7.9 as well as Figures 7.14 and 7.15.

**Table 7.7 – Stress Increase (%) of End-Bearing Piles in Varying Depths of Predrilled Holes of Bridges with 50 ft Spans due to a 30° F Temperature Increase**

Radius (ft)	Depth of Predrilled Holes (ft)	Approximate Stress Increase (%)	At Bridge Length (ft)
400	5	35.7	200 to 600
		50.4	800 to 1200
	9	32.6	200 to 600
		50.4	800 to 1200
	15	34.0	300 to 600
		50.4	800 to 1200
600	5	36.3	200 to 800
		50.4	1200
	9	35.2	200 to 800
		49.5	1000 to 1200
	15	32.8	300 to 800
		50.4	1000 to 1200
800	5	35.5	200 to 1200
	9	33.8	300 to 1000
		44.4	1200
	15	33.3	300 to 1000
		50.4	1200
	1200 to Infinity	5	35.3
9		33.5	300 to 1200
15		32.1	300 to 1200



**Table 7.8 – Mean and Standard Deviation of Stress Increase (%) of End-Bearing Piles of Bridges with 50 ft Spans due to a 30° F Temperature Increase**

Span Length (ft)	Description	Bridge Length (ft)	Depth of Predrilled Holes (ft)			
			0	5	9	15
50	MEAN	50	50.5	50.5	50.5	50.5
		100	38.6	50.5	50.5	50.5
		150	39.2	40.9	50.5	50.5
		200	36.1	35.1	37.4	44.7
		300	32.5	36.1	31.5	30.9
		400	24.8	37.0	32.9	32.0
		600	27.5	36.1	34.2	32.6
		800	31.6	37.0	37.3	36.3
		1000	33.9	38.7	40.3	39.5
		1200	37.5	39.6	41.6	41.9
	STD	50	0.0	0.0	0.0	0.0
		100	0.2	0.0	0.0	0.0
		150	0.5	2.2	0.0	0.0
		200	0.4	0.1	3.7	3.4
		300	1.5	0.2	1.5	1.4
		400	4.7	0.5	2.3	1.5
		600	7.6	1.3	1.1	1.5
		800	9.1	6.6	6.4	7.0
		1000	10.9	6.6	7.3	8.6
		1200	11.7	8.6	7.8	9.4

**Table 7.9 – Mean and Standard Deviation of Stress Increase (%) of End-Bearing Piles of Bridges of Different Radii with 50 ft Spans due to a 30° F Temperature Increase**

Span Length (ft)	Description	Radius (ft)	Depth of Predrilled Holes (ft)			
			0	5	9	15
50	MEAN	400	41.5	43.1	43.3	44.3
		600	38.4	41.5	42.6	42.7
		800	35.5	39.1	40.3	41.3
		1200	33.1	39.4	39.7	39.9
		2400	30.2	39.1	39.5	39.2
		Infinity	32.7	38.7	38.5	38.3
	STD	400	6.8	7.8	9.3	8.0
		600	7.5	6.6	8.0	8.8
		800	7.8	6.3	7.8	8.7
		1200	9.5	6.2	7.8	8.6
		2400	10.7	6.5	8.0	9.4
		Infinity	8.7	6.8	8.6	9.8

## 7.2.2 Curved Integral Abutment Bridges with 100 ft Spans

Figure 7.13 indicates that the lowest pile stress intensity increase value due to the temperature increase of curved IAB's of all radii with piles in very stiff clay soil profile is approximately 11% at a 100 ft bridge length and increases to approximately 21.3% at a 200 ft length. The pile stress intensity increase rate then decreases to approximately 15.5% at a 300 ft length. Beyond the 300 ft length, the pile stress intensity increase rate is as follows:

- For curved IAB's with a 400 ft radius, the pile stress intensity increase rate increases to 17.1% at a 400 ft length. Beyond the 400 ft length, it starts decreasing and continues to decrease as the bridge length is increased to 1200 ft.
- For curved IAB's with a 600 ft radius, the pile stress intensity increase rate increases to 19.6% at a 600 ft length. Beyond the 600 ft length, it starts decreasing and continues to decrease as the bridge length is increased to 1200 ft.
- For curved IAB's with a radius from 800 ft to infinity, the pile stress intensity increase rate continues to increase as the bridge length is increased from 300 ft to 1200 ft as indicated in Table 7.10.

For piles in predrilled holes, the lowest pile stress intensity increase value due to the temperature increase of curved IAB's of all radii is approximately 6% at a 100 ft bridge length. It increases to its highest value at the bridge length indicated in Table 7.11. After it reaches its highest value, some of the pile stress intensity increase

rates start decreasing and continue to decrease as the bridge length is increased to 1200 ft.

It is shown in Figure 7.13 that the pile stress intensity increase due to the temperature increase of curved IAB's with radii of 600 ft, 800 ft, and 1200 ft and with piles in all soil profile types decreases from bridge lengths of 1000 ft to 1200 ft.

**Table 7.10 – Stress Increase (%) of End-Bearing Piles in Very Stiff Clay Soil Profile of Bridges with 100 ft Spans due to a 30° F Temperature Increase**

Radius (ft)	Stress Increase (%) at 1200 ft Length
400	12.5
600	13.3
800	18.6
1200	21.1
2400	23.9
Infinity	26.0

The mean of the pile stress intensity increase due to the temperature increase of curved IAB's of all radii with 100 ft spans is listed in Table 7.12 and plotted in Figure 7.14. It is shown that the lowest mean of the pile stress intensity increase due to the temperature increase of curved IAB's of all radii with piles in all soil profile types is at a 100 ft bridge length. It continues to increase as the bridge length is increased to 1200 ft. At bridge lengths from 800 ft to 1200 ft, the mean of the pile stress intensity increase is almost constant.

For curved IAB's of different radii with 100 ft spans, it is found that curved IAB's with a smaller radius have the mean of the pile stress intensity increase due to the temperature increase less than that of curved IAB's with a larger radius as

indicated in Table 7.13 and Figure 7.15. The mean of the pile stress intensity increase of curved IAB's with piles in predrilled holes, in most cases except for bridge lengths between 100 ft and 300 ft, is greater than that of curved IAB's with piles without predrilled holes as indicated in Table 7.12 as well as Figures 7.14 and 7.15.

**Table 7.11 – Stress Increase (%) of End-Bearing Piles in Varying Depths of Predrilled Holes of Bridges with 100 ft Spans due to a 30° F Temperature Increase**

Radius (ft)	Depth of Predrilled Holes (ft)	Bridge Length (ft)	Highest Stress Increase (%)	Stress Increase (%) at 1200 ft Length
400	5	600	20.8	15.0
	9 and 15	1200	23.1	23.1
600	5, 9 and 15	800	22.0	17.0
800	5, 9 and 15	800	23.0	21.0
1200	5, 9 and 15	1000	24.5	23.2
2400	5, 9 and 15	1200	26.2	26.2
Infinity	5	800	29.7	28.1
	9	1200	25.4	25.4
	15	1200	23.7	23.7

**Table 7.12 – Mean and Standard Deviation of Stress Increase (%) of End-Bearing Piles of Bridges with 100 ft Spans due to a 30° F Temperature Increase**

Span Length (ft)	Description	Bridge Length (ft)	Depth of Predrilled Holes (ft)			
			0	5	9	15
100	MEAN	100	11.0	6.0	5.8	5.7
		200	21.4	14.5	13.6	13.2
		300	15.6	16.1	15.2	14.5
		400	16.2	18.9	18.0	17.2
		600	17.6	22.6	21.2	20.1
		800	19.6	23.7	22.3	21.3
		1000	19.2	22.8	21.9	21.0
	1200	19.2	22.1	22.7	22.0	
	STD	100	0.4	0.4	0.2	0.2
		200	0.3	0.5	0.3	0.3
		300	1.0	0.6	0.3	0.3
		400	0.6	0.5	0.5	0.4
		600	1.5	1.3	0.6	0.5
		800	3.9	3.7	2.1	1.7
1000		4.8	4.4	3.9	3.5	
1200	5.5	5.1	3.4	3.0		

**Table 7.13 – Mean and Standard Deviation of Stress Increase (%) of End-Bearing Piles of Bridges of Different Radii with 100 ft Spans due to a 30° F Temperature Increase**

Span Length (ft)	Description	Radius (ft)	Depth of Predrilled Holes (ft)			
			0	5	9	15
100	MEAN	400	14.8	15.9	16.4	16.0
		600	16.5	17.4	16.7	16.2
		800	17.5	18.3	17.6	16.9
		1200	17.9	18.8	18.2	17.4
		2400	18.1	19.2	18.6	17.6
		Infinity	20.1	20.6	18.1	17.3
	STD	400	3.4	4.3	5.1	5.1
		600	3.5	5.3	5.3	5.2
		800	3.4	5.9	5.9	5.7
		1200	4.0	6.7	6.6	6.2
		2400	3.9	7.0	7.1	6.5
		Infinity	5.6	8.4	6.5	6.0

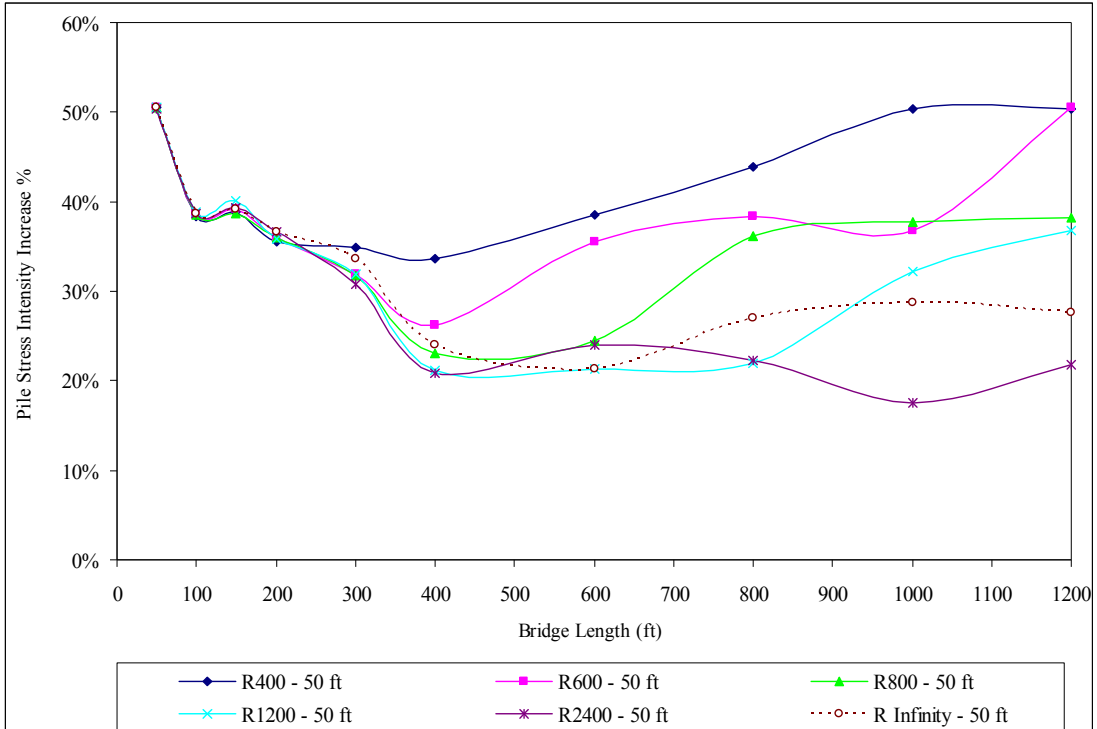
### 7.2.3 Conclusions

The following conclusions are drawn from the study of the effect of a temperature increase of 30° F in curved IAB's on the maximum stress intensity (stress concentration) increase in the piles investigated in this section:

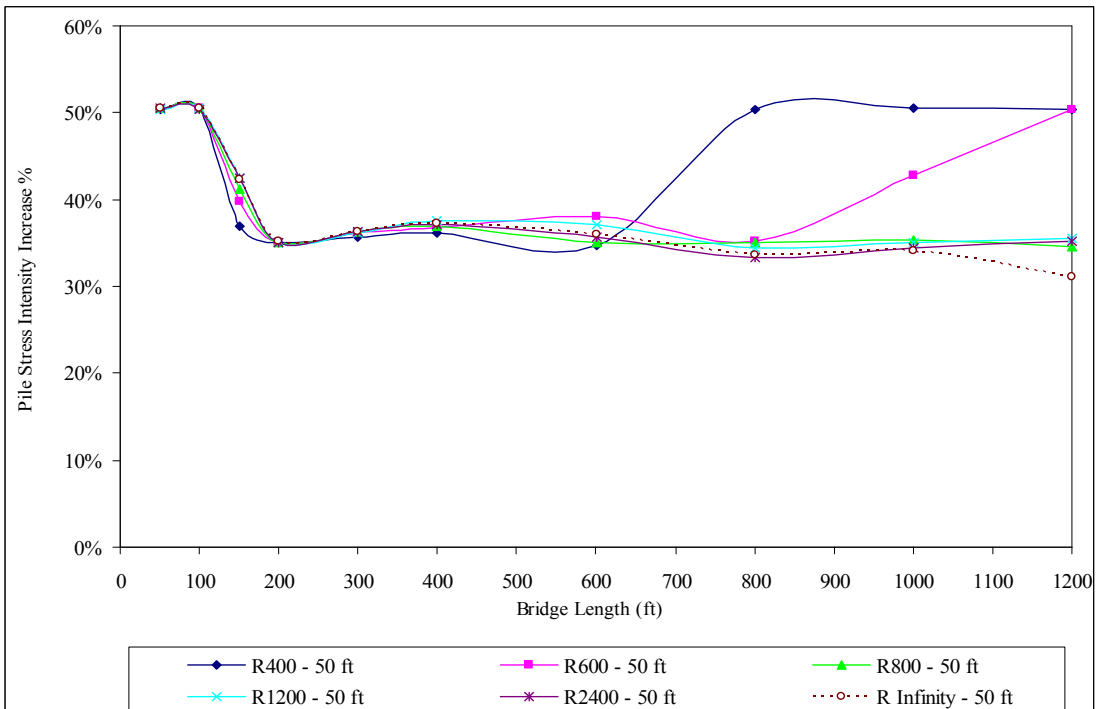
1. The mean of the pile stress intensity increase due to the temperature increase of curved IAB's with 50 ft spans indicates that curved IAB's with a smaller radius have a pile stress intensity increase greater than that of curved IAB's with a larger radius. For curved IAB's with 100 ft spans, curved IAB's with a smaller radius have a pile stress intensity increase less than that of curved IAB's with a larger radius.
2. For curved IAB's of all radii with 50 ft spans and with piles in all soil profile types, the highest mean of the pile stress intensity increase due to the temperature increase is at a 50 ft bridge length. It continues to decrease to its lowest value at bridge lengths between 200 ft and 400 ft. Beyond these lengths, it starts increasing and continues to increase as the bridge length is increased to 1200 ft.
3. For curved IAB's of all radii with 100 ft spans and with piles in all soil profile types, the lowest mean of the pile stress intensity increase due to the temperature increase is at a 100 ft bridge length. It continues to increase as the bridge length is increased to 1200 ft. At bridge lengths from 800 ft to 1200 ft, the mean of the pile stress intensity increase is almost constant.

4. Curved IAB's with piles in predrilled holes have a mean of the pile stress intensity increase due to the temperature increase greater than that of curved IAB's with piles without predrilled holes.
5. The comparison of the pile stress intensity increase due to the temperature increase between curved IAB's with 50 ft and 100 ft spans listed in Table 7.14 and plotted in Figure 7.16 indicates that the pile stress intensity increase of curved IAB's with 50 ft spans is greater than that of curved IAB's with 100 ft spans. Since the stress intensity in the piles is mainly due to the weight of the bridge structure itself, curved IAB's with the longer span lengths will result in a smaller stress intensity increase in the piles due to the temperature increase when compared to curved IAB's with the shorter span lengths.



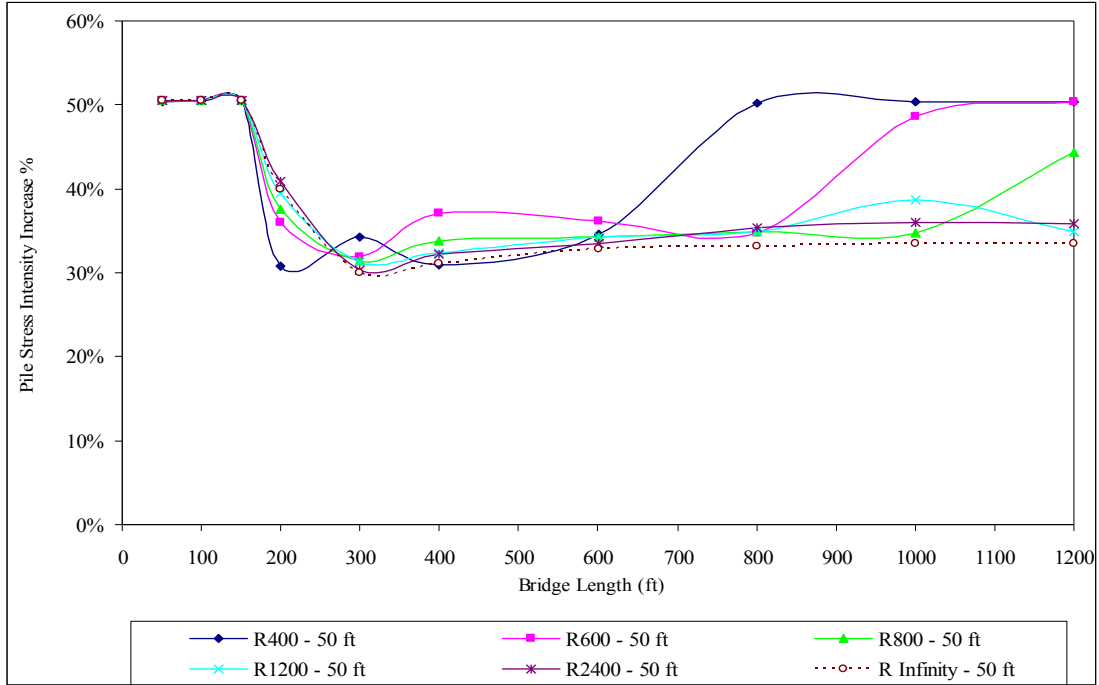


**a) Very Stiff Clay Soil Profile**

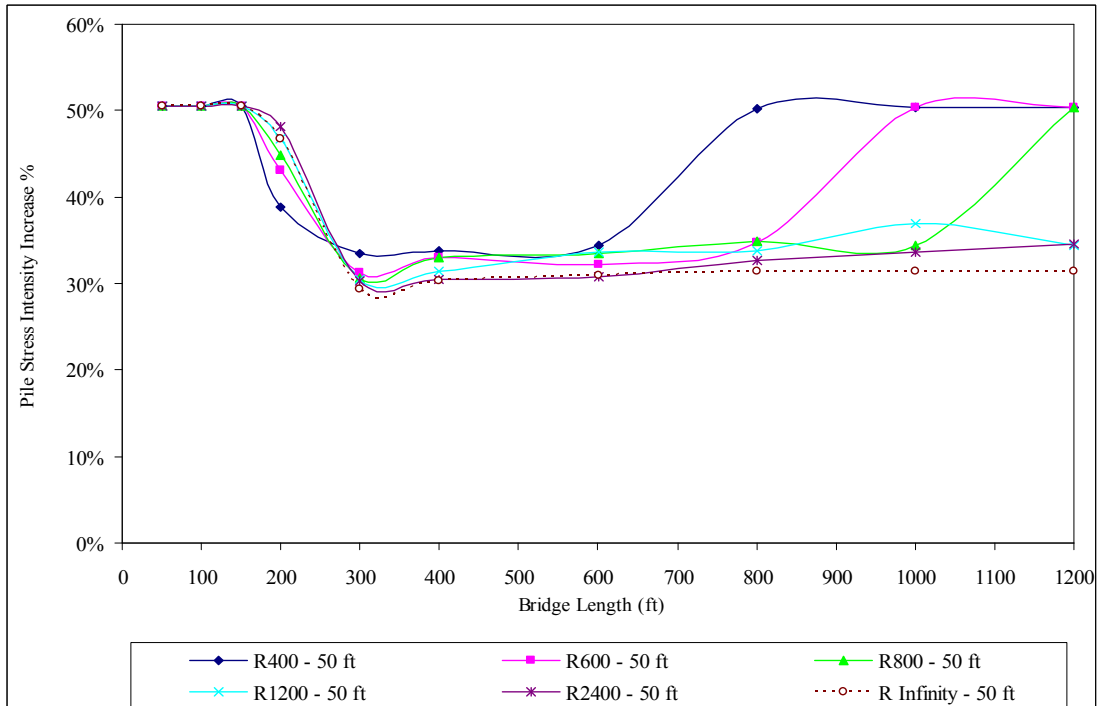


**b) Very Stiff Clay Soil Profile with 5 ft Deep Predrilled Holes Filled with Loose Sand**

**Figure 7.12 – Stress Increase (%) of End-Bearing Piles of Bridges with 50 ft Spans due to a 30° F Temperature Increase**

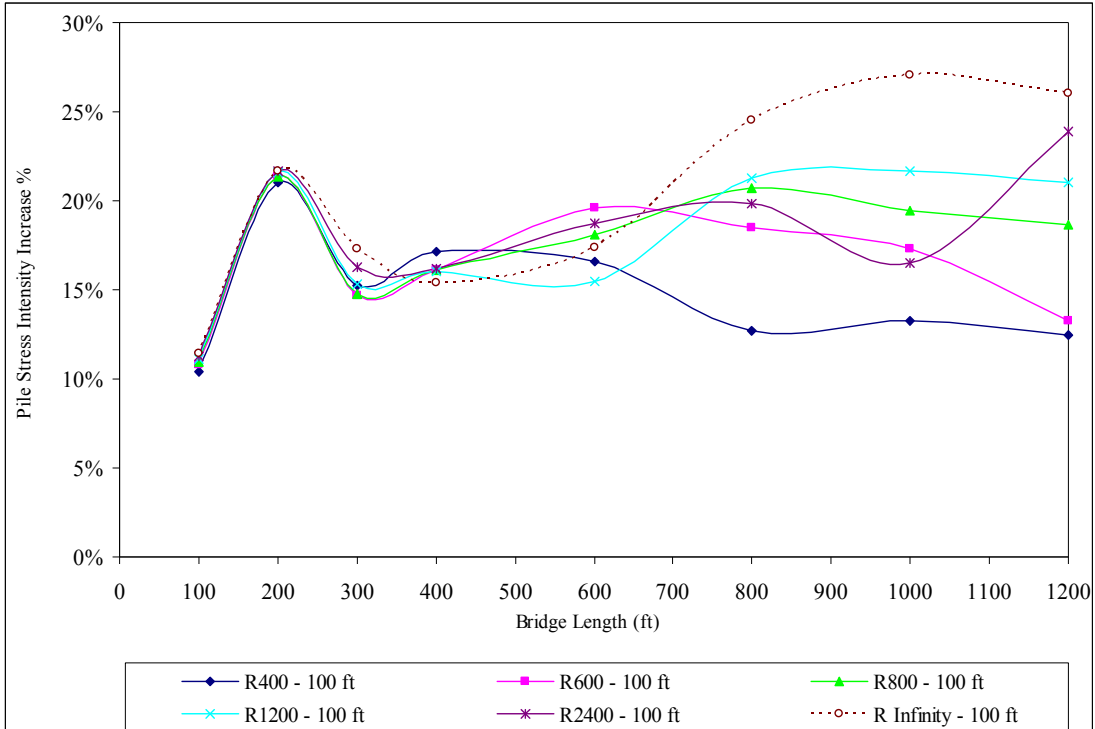


**c) Very Stiff Clay Soil Profile with 9 ft Deep Predrilled Holes Filled with Loose Sand**

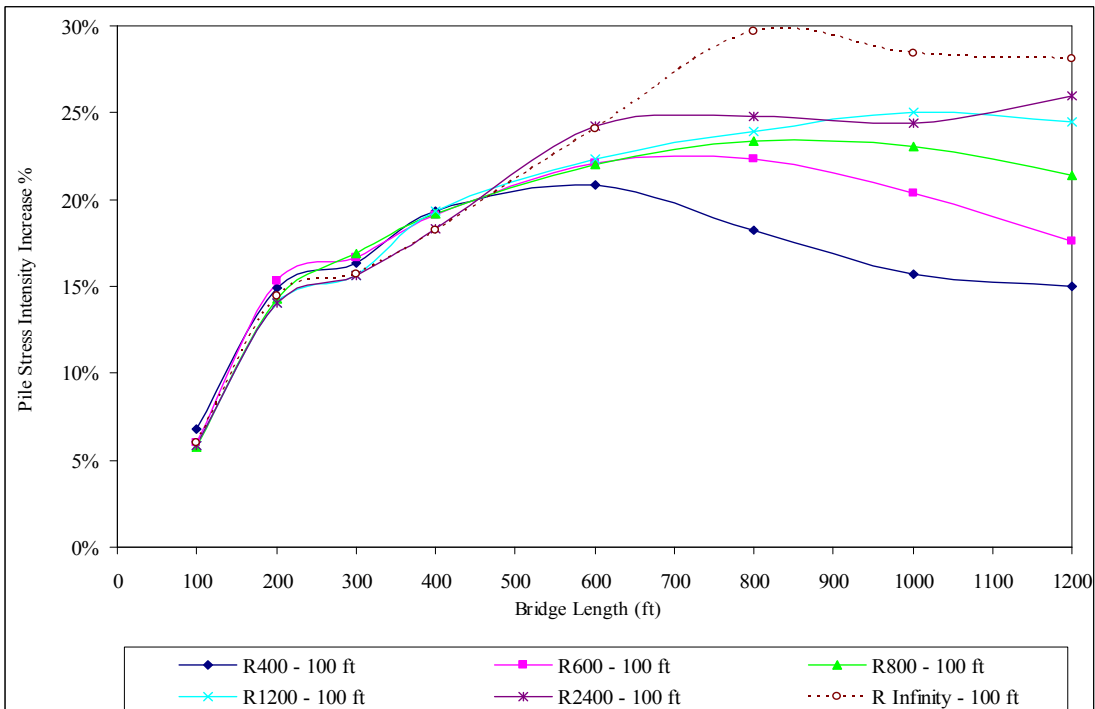


**d) Very Stiff Clay Soil Profile with 15 ft Deep Predrilled Holes Filled with Loose Sand**

**Figure 7.12 (Continued) – Stress Increase (%) of End-Bearing Piles of Bridges with 50 ft Spans due to a 30° F Temperature Increase**

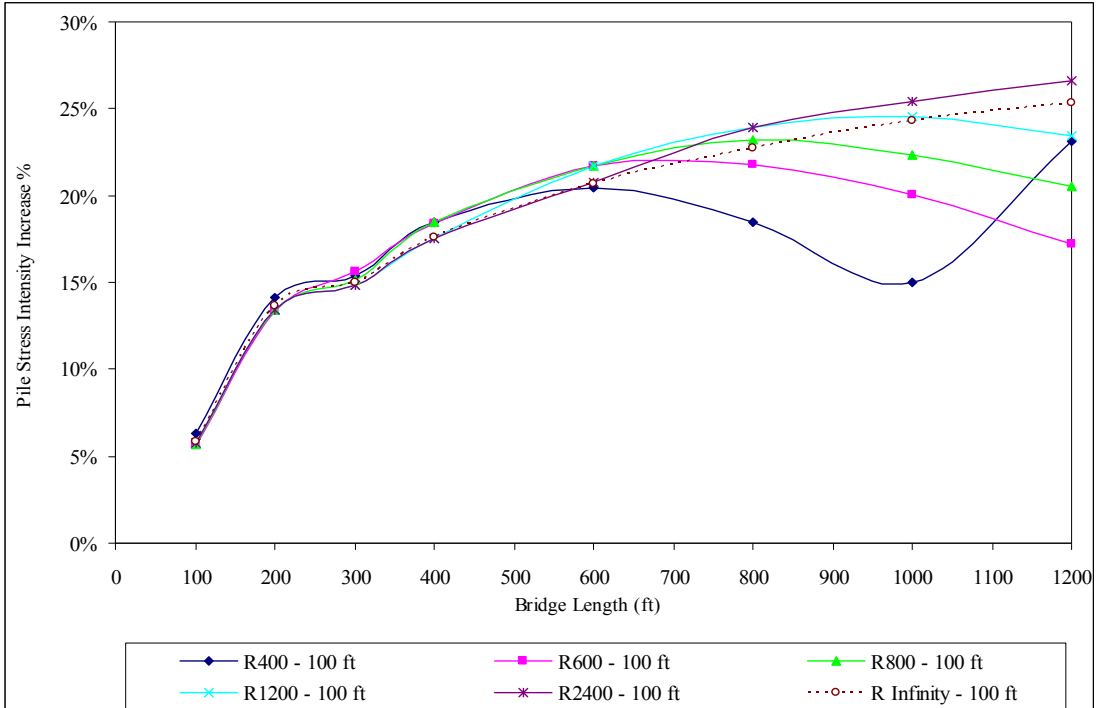


**a) Very Stiff Clay Soil Profile**

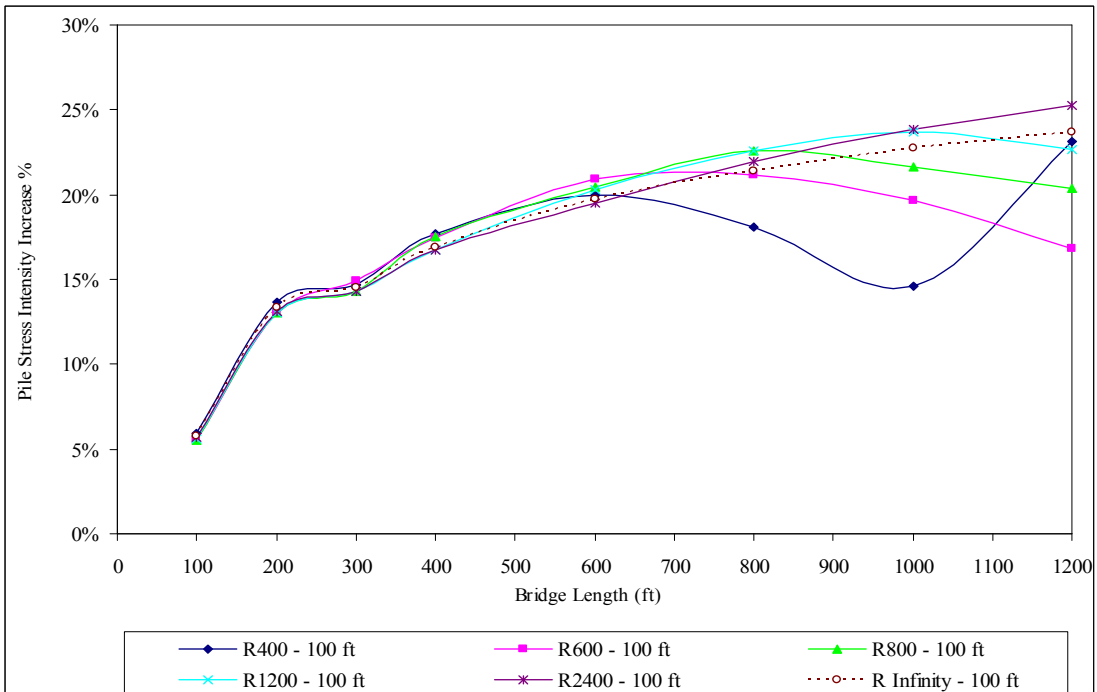


**b) Very Stiff Clay Soil Profile with 5 ft Deep Predrilled Holes Filled with Loose Sand**

**Figure 7.13 – Stress Increase (%) of End-Bearing Piles of Bridges with 100 ft Spans due to a 30° F Temperature Increase**



**c) Very Stiff Clay Soil Profile with 9 ft Deep Predrilled Holes Filled with Loose Sand**



**d) Very Stiff Clay Soil Profile with 15 ft Deep Predrilled Holes Filled with Loose Sand**

**Figure 7.13 (Continued) – Stress Increase (%) of End-Bearing Piles of Bridges with 100 ft Spans due to a 30° F Temperature Increase**

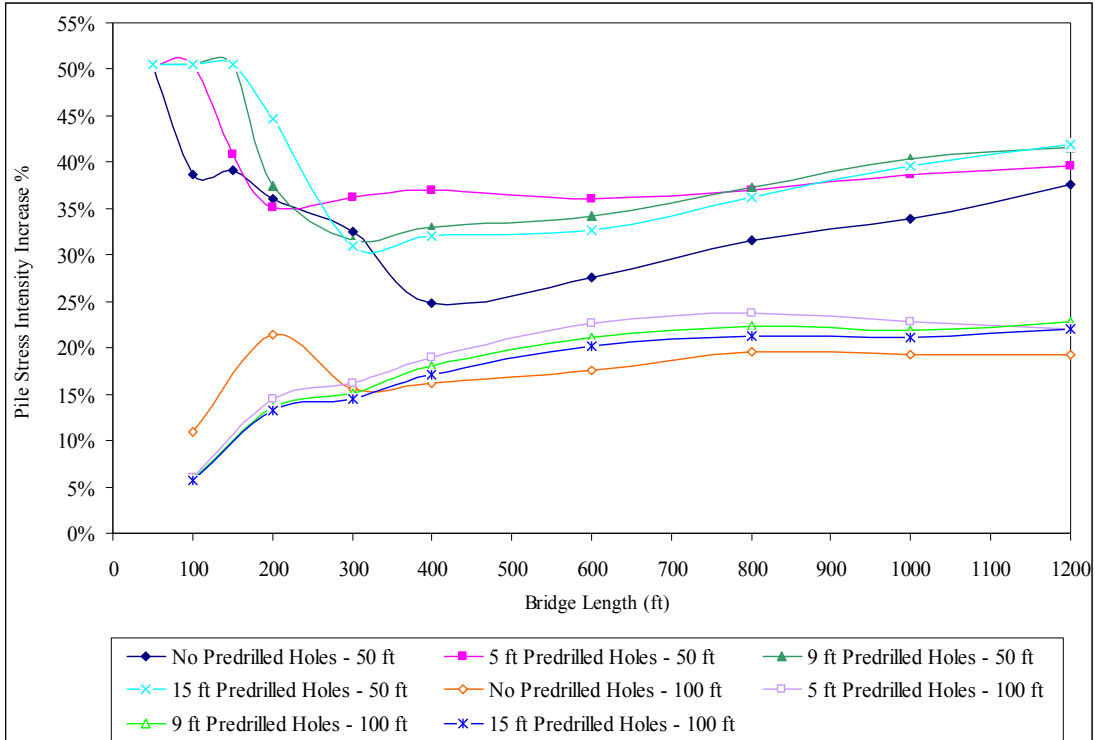


**Figure 7.14 – Mean of Stress Increase (%) of End-Bearing Piles of Bridges with 50 ft and 100 ft Spans due to a 30° F Temperature Increase**

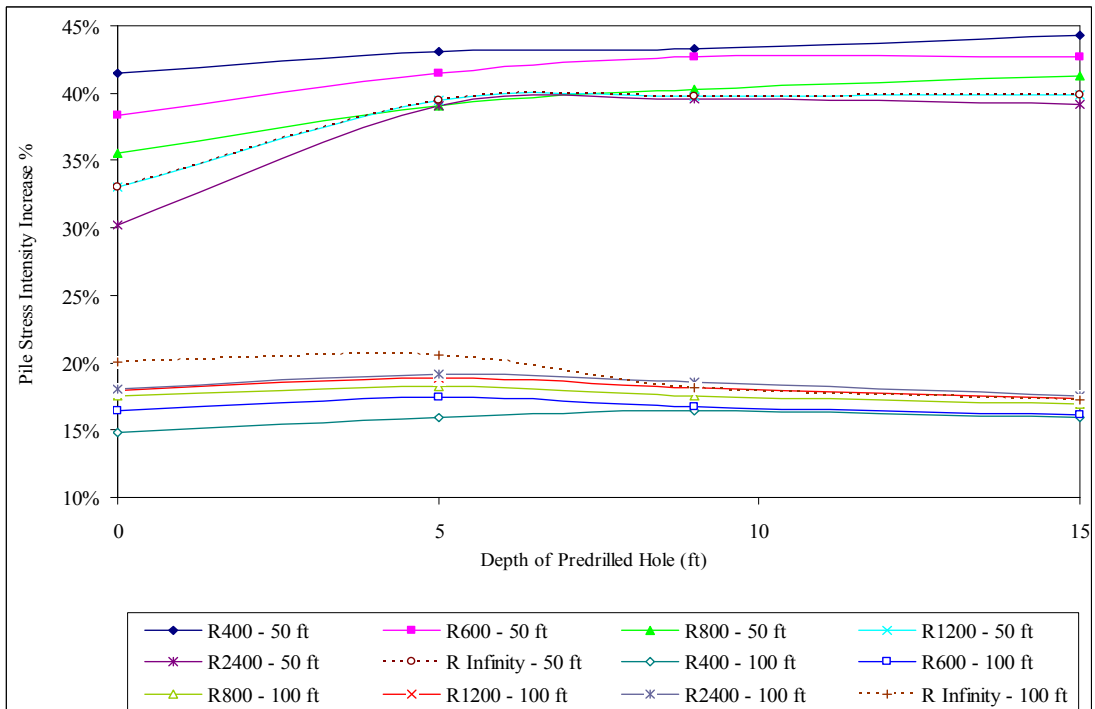


**Figure 7.15 – Mean of Stress Increase (%) of End-Bearing Piles of Bridges of Different Radii due to a 30° F Temperature Increase**

**Table 7.14 – Difference in Stress Increase (%) of End-Bearing Piles between Bridges with 50 ft and 100 ft Spans due to a 30° F Temperature Increase**

Description	Bridge Length (ft)	Depth of Predrilled Holes (ft)			
		0	5	9	15
MEAN	100	27.6	44.4	44.6	44.8
	200	14.7	20.5	23.9	31.5
	300	16.9	20.0	16.4	16.4
	400	8.6	18.1	14.9	14.8
	600	9.9	13.5	13.1	12.4
	800	12.0	13.3	14.9	15.0
	1000	14.7	15.9	18.4	18.5
	1200	18.3	17.5	18.8	19.9
STD	100	0.3	0.4	0.2	0.1
	200	0.2	0.5	3.9	3.6
	300	1.7	0.6	1.3	1.3
	400	4.4	0.8	2.2	1.1
	600	7.3	1.8	0.9	1.3
	800	12.2	9.7	8.3	8.5
	1000	13.5	10.8	10.9	11.7
	1200	17.0	13.4	10.6	11.6

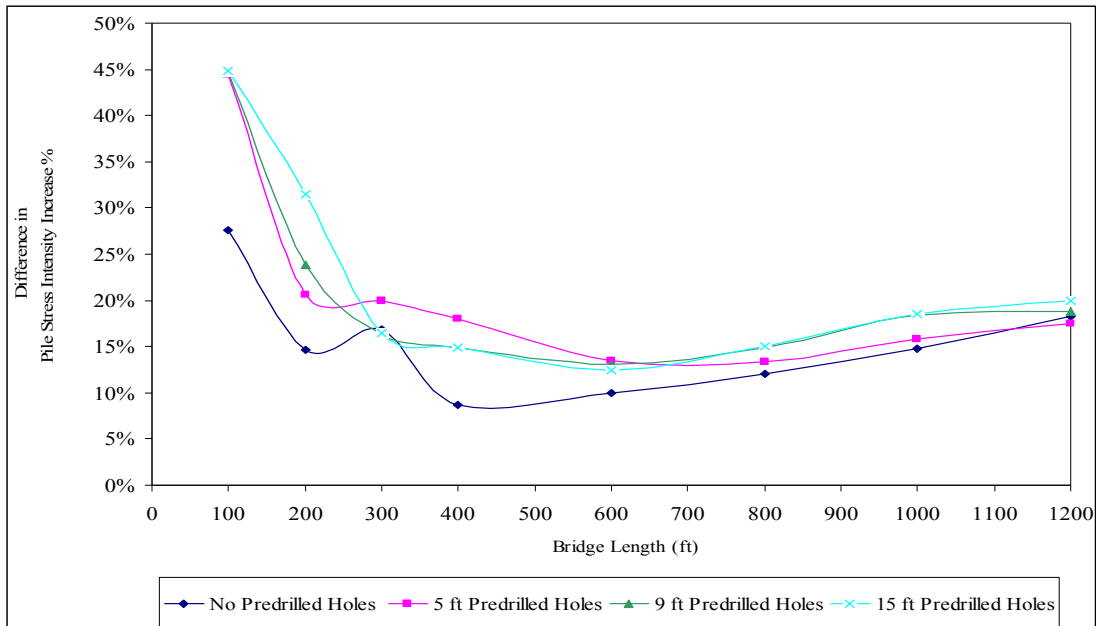


**Figure 7.16 – Difference in Stress Increase (%) of End-Bearing Piles between Bridges with 50 ft and 100 ft Spans due to a 30° F Temperature Increase**

### **7.3 Effect of Soil Profile Variation**

Four different soil profiles are investigated in this study. Piles are driven 40 ft below the bottom of the abutment in each one of these four soil profiles. The first soil profile is a single layer of 40 ft deep very stiff clay below the abutment (equivalent to 0 ft predrilled hole). The other three soil profiles each consist of two layers combined to a total of 40 ft deep below the abutment. The top layer is loose sand to simulate predrilled holes filled with loose sand, while the bottom layer is very stiff clay. The difference between these three soil profiles is the depth of the predrilled holes, which is 5 ft, 9 ft, and 15 ft respectively. All other parameters are held constant.

#### **7.3.1 Curved Integral Abutment Bridges with 50 ft Spans**

Figures 7.17 to 7.19 indicate that the pile stress intensity (stress concentration) reduction due to the introduction of predrilled holes for  $\Delta T_{\text{slab}}$  of 90° F and  $\Delta T_{\text{the rest}}$  of 60° F of curved IAB's of all radii is almost the same for bridge lengths from 50 ft to 150 ft. There is no pile stress intensity reduction at a 50 ft bridge length. The pile stress intensity reduction rate starts to increase from a 50 ft bridge length to its highest value at the bridge length indicated in Table 7.15. After it reaches its highest value, the pile stress intensity reduction rate starts to decrease to its lowest value at the bridge length indicated in Table 7.15. At the lowest value, some of the pile stress intensity reduction rates start increasing and continue to increase as the bridge length is increased to 1200 ft.

**Table 7.15 – Stress Reduction (%) of End-Bearing Piles in Varying Depths of Predrilled Holes of Bridges with 50 ft Spans ( $\Delta T_{\text{slab}} = 90^\circ \text{ F}$ ,  $\Delta T_{\text{the rest}} = 60^\circ \text{ F}$ )**

Radius (ft)	Highest Stress Reduction (%) at Bridge Length (ft)		Lowest Stress Reduction (%) at Bridge Length (ft)		Stress Reduction (%) at 1200 ft Length
400	31.2	200	-3.2	600	0.0
600	33.5	200	-1.4	600 to 800	-0.2
800	34.5	300	0.0	800	11.2
1200	36.1	300	7.6	1200	7.6
2400	37.9	400	13.7	1000	14.2
Infinity	37.6	300	14.3	1200	14.3

**a) 5 ft Deep Predrilled Holes Filled with Loose Sand**

Radius (ft)	Highest Stress Reduction (%) at Bridge Length (ft)		Lowest Stress Reduction (%) at Bridge Length (ft)		Stress Reduction (%) at 1200 ft Length
400	43.0	200	-0.4	1000	0.1
600	47.7	300	-0.3	1200	-0.3
800	49.1	300	9.5	800	18.5
1200	51.0	400	17.0	1200	17.0
2400	53.1	400	27.0	1200	27.0
Infinity	51.3	400	38.4	1200	38.4

**b) 9 ft Deep Predrilled Holes Filled with Loose Sand**

Radius (ft)	Difference between Depth of Predrilled Holes	
	9 ft – 5 ft	15 ft – 9 ft
400	0 to 16.2	0 to 5.6
600	0 to 14.8	0 to 4.3
800	0 to 16.4	0 to 5.1
1200	0 to 18.4	0 to 4.5
2400	0 to 22.3	0 to 5.7
Infinity	0 to 24.1	0 to 5.5

**c) Difference in Pile Stress Reduction (%)**



It is shown in Table 7.15 and Figures 7.17 to 7.19 that the highest pile stress intensity reduction value due to the introduction of predrilled holes is at bridge lengths between 200 ft and 400 ft. The pile stress intensity reduction rate of curved IAB's with a smaller radius decreases much more rapidly after reaching its highest value than that of curved IAB's with a larger radius as the bridge length is increased to 1200 ft.

A minus sign in Table 7.15 indicates that the introduction of predrilled holes does not reduce the stress intensity in the piles, but rather increases it. Curved IAB's with smaller radii (400 ft, and 600 ft) have a stress intensity increase in the piles at some bridge lengths when the predrilled holes are introduced.

According to Greimann, Amde, and Yang [1.45], the displacements of the piles decrease the vertical load carrying capacity of the piles. While the vertical load (self weight of a bridge superstructure) is constant, the displacements in lateral, longitudinal, and twisting of the piles in predrilled holes are greater than that of the piles without predrilled holes which result in the increase in the pile stress intensity at some bridge lengths of curved IAB's.

Therefore, it can be concluded that a difference in the arrangement of pile groups due to different bridge lengths of curved IAB's with different radii results in the stress intensity increase in the piles in predrilled holes at some bridge lengths when compared to the piles without predrilled holes.

The pile stress intensity increase due to the introduction of predrilled holes of curved IAB's with smaller radii (400 ft, and 600 ft) is relatively small which is in the range of 0.2% to 3.2% as indicated in Table 7.15 and Figures 7.17 to 7.19. As the

radius becomes larger (larger than 600 ft), there is no stress intensity increase in the piles due to the introduction of predrilled holes. It is indicated that the increase in the radius and in the depth of predrilled holes decreases the stress intensity increase in the piles due to the introduction of predrilled holes.

The mean of the pile stress intensity reduction due to the introduction of predrilled holes of curved IAB's of all radii with 50 ft spans is listed in Table 7.16 and plotted in Figure 7.20. It is shown that there is no pile stress intensity reduction at a 50 ft bridge length. The mean of the pile stress intensity reduction starts to increase from a 50 ft bridge length to its highest value at bridge lengths between 200 ft and 300 ft. Beyond these lengths, it starts decreasing and continues to decrease as the bridge length is increased to 1200 ft.

For curved IAB's of different radii with 50 ft spans, it is found that curved IAB's with a smaller radius have the mean of the pile stress intensity reduction due to the introduction of predrilled holes less than that of curved IAB's with a larger radius as indicated in Table 7.17 and Figure 7.21.

Tables 7.15c to 7.17 as well as Figures 7.17 to 7.21 indicate that piles in 9 ft deep predrilled holes have a pile stress intensity reduction in the range of 0% to 24% greater than those in 5 ft deep predrilled holes and in the range of 0% to 5.7% less than those in 15 ft deep predrilled holes. Therefore, it can be concluded that 9 feet deep predrilled holes filled with loose sand have a significant reduction in the pile stress intensity when compared with 5 ft deep predrilled holes filled with loose sand. The depth increase of predrilled holes deeper than 9 ft will further reduce the stress

intensity in the piles, but the rate of reduction is much smaller than that of 9 ft deep predrilled holes.

From the analyses, it is shown that a temperature increase results in a lower pile stress intensity reduction. The mean of the pile stress intensity reduction due to the introduction of predrilled holes of curved IAB's subjected to a temperature load of  $\Delta T_{\text{slab}}$  of 90° F and  $\Delta T_{\text{the rest}}$  of 60° F is greater than that of curved IAB's subjected to a temperature load of  $\Delta T_{\text{slab}}$  of 120° F and  $\Delta T_{\text{the rest}}$  of 90° F by 0% to 7.5%.

**Table 7.16 – Mean and Standard Deviation of Stress Reduction (%) of End-Bearing Piles in Varying Depths of Predrilled Holes of Bridges with 50 ft Spans**

Description	Bridge Length (ft)	$\Delta T_{\text{slab}} = 90^\circ \text{ F}$ $\Delta T_{\text{the rest}} = 60^\circ \text{ F}$			$\Delta T_{\text{slab}} = 120^\circ \text{ F}$ $\Delta T_{\text{the rest}} = 90^\circ \text{ F}$		
		Depth of Predrilled Holes (ft)					
		5	9	15	5	9	15
MEAN	50	0.1	0.3	0.3	0.1	0.3	0.3
	100	12.0	12.1	12.2	4.4	4.6	4.6
	150	30.0	34.6	34.6	29.2	29.3	29.3
	200	34.3	45.0	47.8	34.8	44.4	44.5
	300	33.8	47.7	50.6	32.0	48.1	51.2
	400	29.9	45.1	48.5	23.3	41.8	45.7
	600	15.1	29.9	33.9	9.8	26.8	31.9
	800	9.7	21.5	25.2	6.1	18.5	22.8
	1000	8.4	18.5	21.8	5.1	14.7	18.6
	1200	7.9	16.8	19.7	6.4	14.5	17.3
STD	50	0.0	0.0	0.0	0.0	0.0	0.0
	100	0.8	0.8	0.9	0.8	0.8	0.8
	150	0.7	0.7	0.7	0.6	0.7	0.7
	200	1.8	1.1	0.9	1.9	0.6	0.6
	300	5.1	4.4	3.8	4.5	4.5	3.8
	400	10.8	10.5	9.4	8.4	8.6	8.2
	600	14.0	19.3	18.7	9.9	16.3	15.8
	800	10.1	18.2	18.9	7.1	16.3	17.8
	1000	6.7	14.9	16.8	5.1	13.6	16.2
	1200	6.6	15.1	17.4	5.8	13.4	16.2

**Table 7.17 – Mean and Standard Deviation of Stress Reduction (%) of End-Bearing Piles in Varying Depths of Predrilled Holes of Bridges of Different Radii with 50 ft Spans**

Span Length (ft)	Description	Radius (ft)	$\Delta T_{\text{slab}} = 90^\circ \text{ F}$ $\Delta T_{\text{the rest}} = 60^\circ \text{ F}$			$\Delta T_{\text{slab}} = 120^\circ \text{ F}$ $\Delta T_{\text{the rest}} = 90^\circ \text{ F}$		
			Depth of Predrilled Holes (ft)					
			5	9	15	5	9	15
50	MEAN	400	10.7	16.0	17.9	9.7	15.0	16.3
		600	14.3	21.2	23.1	12.4	18.8	20.8
		800	17.2	25.6	28.2	15.1	23.2	25.3
		1200	20.4	29.7	32.1	16.5	26.2	28.8
		2400	22.7	34.3	36.9	17.1	29.4	32.5
		Infinity	23.3	36.0	38.6	19.8	33.1	35.9
	STD	400	13.0	17.9	19.0	13.3	18.2	18.9
		600	15.1	19.1	19.7	14.8	18.9	19.7
		800	14.3	18.0	18.3	13.5	17.7	18.1
		1200	13.5	17.6	18.2	13.5	17.8	18.1
		2400	12.9	17.4	18.4	14.5	18.2	19.0
		Infinity	12.6	17.0	18.4	12.9	17.7	19.2

### 7.3.2 Curved Integral Abutment Bridges with 100 ft Spans

Figures 7.22 to 7.24 indicate that the pile stress intensity (stress concentration) reduction due to the introduction of predrilled holes for  $\Delta T_{\text{slab}}$  of 90° F and  $\Delta T_{\text{the rest}}$  of 60° F of curved IAB's of all radii starts to increase from a 100 ft bridge length to bridge lengths between 200 ft and 400 ft. Beyond these lengths, the pile stress intensity reduction rate decreases at the bridge length indicated in Table 7.18 and then, some of the pile stress intensity reduction rates (curved IAB's with radii of 600 ft to 1200 ft) begin increasing. They continue to increase as the bridge length is increased to 1200 ft as indicated in Table 7.18. For curved IAB's with a 400 ft radius, after the pile stress intensity reduction rate reaches its lowest value, it continues to increase to its highest value at a 1000 ft length and decreases again at a 1200 ft length.

**Table 7.18 – Stress Reduction (%) of End-Bearing Piles in Varying Depths of Predrilled Holes of Bridges with 100 ft Spans ( $\Delta T_{\text{slab}} = 90^\circ \text{ F}$ ,  $\Delta T_{\text{the rest}} = 60^\circ \text{ F}$ )**

Radius (ft)	Bridge Length (ft)	Depth of Predrilled Holes (ft)		
		5	9	15
400	100	-19.2	-12.4	-7.9
	200	6.5	18.9	23.2
600 to Infinity	100	≈ -17.4	≈ -11.0	≈ -6.6
	200	≈ 14.3	≈ 23.5	≈ 27.1

**a) Pile Stress Reduction (%) at 100 ft Length and 200 ft Length**

**Table 7.18 (Continued) – Stress Reduction (%) of End-Bearing Piles in Varying Depths of Predrilled Holes of Bridges with 100 ft Spans**  
 ( $\Delta T_{\text{slab}} = 90^\circ \text{ F}$ ,  $\Delta T_{\text{the rest}} = 60^\circ \text{ F}$ )

Radius (ft)	Stress Reduction (%) at Bridge Length (ft)		Stress Reduction (%) at 1200 ft Length
400	-18.0	600	20.5
600	-14.6	600	23.7
800	-10.5	600	5.1
1200	-8.2	800	4.4
2400	-0.4	1200	-0.4
Infinity	10.0	1200	10.0

**b) 5 ft Deep Predrilled Holes Filled with Loose Sand**

Radius (ft)	Stress Reduction (%) at Bridge Length (ft)		Stress Reduction (%) at 1200 ft Length
400	-11.7	600	25.7
600	-1.7	600	31.2
800	1.3	800	13.4
1200	4.4	800	13.6
2400	9.8	1200	9.8
Infinity	25.4	1200	25.4

**c) 9 ft Deep Predrilled Holes Filled with Loose Sand**

Radius (ft)	Difference between Depth of Predrilled Holes	
	9 ft – 5ft	15 ft – 9 ft
400	5.2 to 16.5	0 to 6.6
600	6.3 to 14.9	2.3 to 6.3
800	6.3 to 14.8	3.0 to 6.4
1200	6.3 to 13.1	3.7 to 6.3
2400	6.3 to 13.3	3.7 to 6.2
Infinity	6.6 to 15.4	3.4 to 5.9

**d) Difference in Pile Stress Reduction (%)**

A minus sign in Table 7.18 indicates that the introduction of predrilled holes does not reduce the stress intensity in the piles, but rather increases it.

According to Greimann, Amde, and Yang [1.45], the displacements of the piles decrease the vertical load carrying capacity of the piles. While the vertical load (self weight of a bridge superstructure) is constant, the displacements in lateral, longitudinal, and twisting of the piles in predrilled holes are greater than that of the piles without predrilled holes which result in the increase in the pile stress intensity at some bridge lengths of curved IAB's.

Therefore, it can be concluded that a difference in the arrangement of pile groups due to different bridge lengths of curved IAB's with different radii results in the stress intensity increase in the piles in predrilled holes at some bridge lengths when compared to the piles without predrilled holes.

It is shown in Table 7.18 and Figures 7.22 to 7.24 that the increase in the radius and in the depth of predrilled holes decreases the stress intensity increase in the piles due to the introduction of predrilled holes.

The mean of the pile stress intensity reduction due to the introduction of predrilled holes of curved IAB's of all radii with 100 ft spans is listed in Table 7.19 and plotted in Figure 7.20. It is shown that the mean of the pile stress intensity reduction is in the range of -6.8% to -17.7% at a 100 ft bridge length. It continues to increase to its highest value at a 200 ft length and then starts decreasing and continues to decrease as the bridge length is increased to 600 ft. Beyond the 600 ft length, the mean of the pile stress intensity reduction increases and continues to increase as the bridge length is increased to 1200 ft. A minus sign indicates that the introduction of



predrilled holes does not reduce the stress intensity in the piles, but rather increases it as discussed above.

For curved IAB's of different radii with 100 ft spans, it is found that curved IAB's with a smaller radius have the mean of the pile stress intensity reduction due to the introduction of predrilled holes less than that of curved IAB's with a larger radius as indicated in Table 7.20 and Figure 7.25.

Tables 7.18d to 7.20 as well as Figures 7.20 and 7.22 to 7.25 indicate that piles in 9 ft deep predrilled holes have a pile stress intensity reduction in the range of 5.2% to 16.5% greater than those in 5 ft deep predrilled holes and in the range of 0% to 6.6% less than those in 15 ft deep predrilled holes. Therefore, it can be concluded that 9 feet deep predrilled holes filled with loose sand have a significant reduction in the pile stress intensity when compared with 5 ft deep predrilled holes filled with loose sand. The depth increase of predrilled holes deeper than 9 ft will further reduce the stress intensity in the piles, but the rate of reduction is much smaller than that of 9 ft deep predrilled holes.

From the analyses, it is shown that a temperature increase results in a lower pile stress intensity reduction, except at bridge lengths between 100 ft and 200 ft. The mean of the pile stress intensity reduction due to the introduction of predrilled holes of curved IAB's subjected to a temperature load of  $\Delta T_{\text{slab}}$  of 90° F and  $\Delta T_{\text{the rest}}$  of 60° F is less than that of curved IAB's subjected to a temperature load of  $\Delta T_{\text{slab}}$  of 120° F and  $\Delta T_{\text{the rest}}$  of 90° F by 4.1% for bridge lengths from 100 ft to 200 ft. It is greater than that of curved IAB's subjected to a temperature load of  $\Delta T_{\text{slab}}$  of 120° F and  $\Delta T_{\text{the rest}}$  of 90° F by 0% to 5.3% for bridge lengths from 300 ft to 1200 ft.

**Table 7.19 – Mean and Standard Deviation of Stress Reduction (%) of End-Bearing Piles in Varying Depths of Predrilled Holes of Bridges with 100 ft Spans**

Description	Bridge Length (ft)	$\Delta T_{\text{slab}} = 90^\circ \text{ F}$ $\Delta T_{\text{the rest}} = 60^\circ \text{ F}$			$\Delta T_{\text{slab}} = 120^\circ \text{ F}$ $\Delta T_{\text{the rest}} = 90^\circ \text{ F}$		
		Depth of Predrilled Holes (ft)					
		5	9	15	5	9	15
MEAN	100	-17.7	-11.3	-6.8	-12.5	-6.1	-1.7
	200	13.0	22.7	26.5	17.9	27.7	31.5
	300	12.3	22.6	26.8	11.9	22.9	27.5
	400	9.1	21.0	25.7	6.9	19.7	25.1
	600	0.1	11.2	16.6	-3.9	8.5	14.8
	800	2.7	12.6	17.4	-0.5	10.5	16.1
	1000	5.4	15.5	19.9	2.4	13.4	18.5
	1200	10.6	19.9	23.4	8.4	17.5	21.6
STD	100	0.8	0.6	0.6	1.5	1.1	1.0
	200	3.2	1.9	1.7	3.4	2.1	1.8
	300	9.5	6.7	5.9	10.1	7.1	6.2
	400	14.4	11.2	10.1	14.6	11.3	10.1
	600	16.7	16.7	16.2	16.3	17.2	16.7
	800	12.2	12.2	11.8	11.6	12.8	12.6
	1000	9.8	10.6	10.4	10.8	11.9	11.5
	1200	9.6	8.7	7.9	9.4	8.4	8.2

**Table 7.20 – Mean and Standard Deviation of Stress Reduction (%) of End-Bearing Piles in Varying Depths of Predrilled Holes of Bridges of Different Radii with 100 ft Spans**

Span Length (ft)	Description	Radius (ft)	$\Delta T_{\text{slab}} = 90^\circ \text{ F}$ $\Delta T_{\text{the rest}} = 60^\circ \text{ F}$			$\Delta T_{\text{slab}} = 120^\circ \text{ F}$ $\Delta T_{\text{the rest}} = 90^\circ \text{ F}$		
			Depth of Predrilled Holes (ft)					
			5	9	15	5	9	15
100	MEAN	400	0.9	10.5	14.5	0.1	9.5	13.8
		600	1.1	10.6	14.9	0.4	10.4	15.2
		800	1.1	10.9	15.4	0.5	10.9	15.8
		1200	3.8	13.7	18.3	3.2	13.6	18.8
		2400	8.3	18.2	23.0	7.6	18.0	23.4
		Infinity	11.4	21.7	26.2	11.3	23.2	28.1
	STD	400	17.7	16.7	15.4	17.5	16.0	14.8
		600	14.2	14.5	13.9	14.1	14.4	13.7
		800	12.3	12.8	12.4	12.6	12.8	12.3
		1200	13.1	13.4	13.0	13.1	13.1	12.5
		2400	12.7	13.4	13.2	12.2	12.8	12.3
		Infinity	12.4	13.5	13.5	10.4	11.7	11.9

### 7.3.3 Stress Increase in Piles in Varying Depths of Predrilled Holes

Varying depths of predrilled holes filled with loose sand can reduce the stress intensity in the piles of curved IAB's in most cases. In some cases, the stress intensity in the piles does not decrease but increases as indicated in Table 7.21.

Table 7.21 indicates that the pile stress intensity increase due to the introduction of predrilled holes of curved IAB's with 50 ft spans and radii of 400 ft, and 600 ft at some bridge lengths is relatively small. It is in the range of 0.2% to 3.2%. As the radius becomes larger (larger than 600 ft), there is no stress intensity increase in the piles due to the introduction of predrilled holes.

**Table 7.21 – Stress Increase (%) of End-Bearing Piles in Varying Depths of Predrilled Holes of Bridges of Different Radii ( $\Delta T_{\text{slab}} = 90^\circ \text{ F}$ ,  $\Delta T_{\text{the rest}} = 60^\circ \text{ F}$ )**

Radius (ft)	Depth of Predrilled Holes (ft)					
	5	Bridge Length (ft)	9	Bridge Length (ft)	15	Bridge Length (ft)
400	0 to 3.2	500 to 700	0.4	1000	0.3	1000
	0.2	1000				
600	0.8 to 1.4	600 to 800	0.3	1200	0.3	1200
	0.2	1200				
800 to Infinity	-					

**a) 50 ft Spans**

Radius (ft)	Depth of Predrilled Holes (ft)					
	5	Bridge Length (ft)	9	Bridge Length (ft)	15	Bridge Length (ft)
400	19.2	100	12.4	100	7.9	100
	0 to 18.0	250 to 700	0 to 11.7	400 to 700	3 to 6.6	500 to 650
600	17.8	100	11.5	100	7.0	100
	3.0 to 14.6	400 to 950	1 to 1.7	600 to 800	-	
800	17.4	100	11.1	100	6.6	100
	0 to 10.5	500 to 1000	-			
1200	17.2	100	10.9	100	6.4	100
	2 to 8.2	700 to 1100	-			
2400	16.9	100	10.6	100	6.1	100
	0.4	1200	-			
Infinity	17.9	100	11.2	100	6.8	100

**b) 100 ft Spans**

Curved IAB's with 100 ft spans have a pile stress intensity increase due to the introduction of predrilled holes at a 100 ft bridge length. The pile stress intensity increase rate begins to decrease as the bridge length is increased to the length indicated in Figures 7.22 to 7.24. It then starts to increase again at the bridge length range indicated in Table 7.21 b. It is shown that the stress intensity increase in the piles due to the introduction of predrilled holes decreases as the radius is increased.

The stress intensity increase in the piles of curved IAB's with 100 ft spans is greater than that of curved IAB's with 50 ft spans at some bridge lengths when varying depths of predrilled holes are used for piles. The increase in the span length results in the increase in lateral and longitudinal displacements of the piles as well as the self weight of a bridge superstructure which increase the stress intensity in the piles. Therefore, curved IAB's with the longer span lengths will result in a higher stress increase in the piles when compared to curved IAB's with the shorter span lengths.

According to Greimann, Amde, and Yang [1.45], the displacements of the piles decrease the vertical load carrying capacity of the piles. While the vertical load (self weight of a bridge superstructure) is constant, the displacements in lateral, longitudinal, and twisting of the piles in predrilled holes are greater than that of the piles without predrilled holes which result in the increase in the pile stress intensity at some bridge lengths of curved IAB's.

Therefore, it can be concluded that a difference in the arrangement of pile groups due to different bridge lengths of curved IAB's with different radii results in

the stress intensity increase in the piles in predrilled holes at some bridge lengths when compared to the piles without predrilled holes.

From the analyses, it can be concluded that the increase in the radius and in the depth of predrilled holes decreases the stress intensity increase in the piles due to the introduction of predrilled holes for curved IAB's with both 50 ft and 100 ft spans.

Curved IAB's with double spans (bridge length of 200 ft) and with piles in predrilled holes can reduce the maximum stress intensity in the piles when compared with single span bridges (bridge length of 100 ft). The pile stress intensity reduction is in the range of 9.5% to 22% for  $\Delta T_{\text{slab}}$  of 90° F and  $\Delta T_{\text{the rest}}$  of 60° F and is in the range of 2.6% to 16.4% for  $\Delta T_{\text{slab}}$  of 120° F and  $\Delta T_{\text{the rest}}$  of 90° F as indicated in Table 7.5 and Figure 7.11 in Section 7.1.

### 7.3.4 Conclusions

The following conclusions are drawn from the study of the effect of using varying depths of predrilled holes filled with loose sand instead of no predrilled holes on the maximum stress intensity (stress concentration) reduction in the piles of curved IAB's investigated in this section:

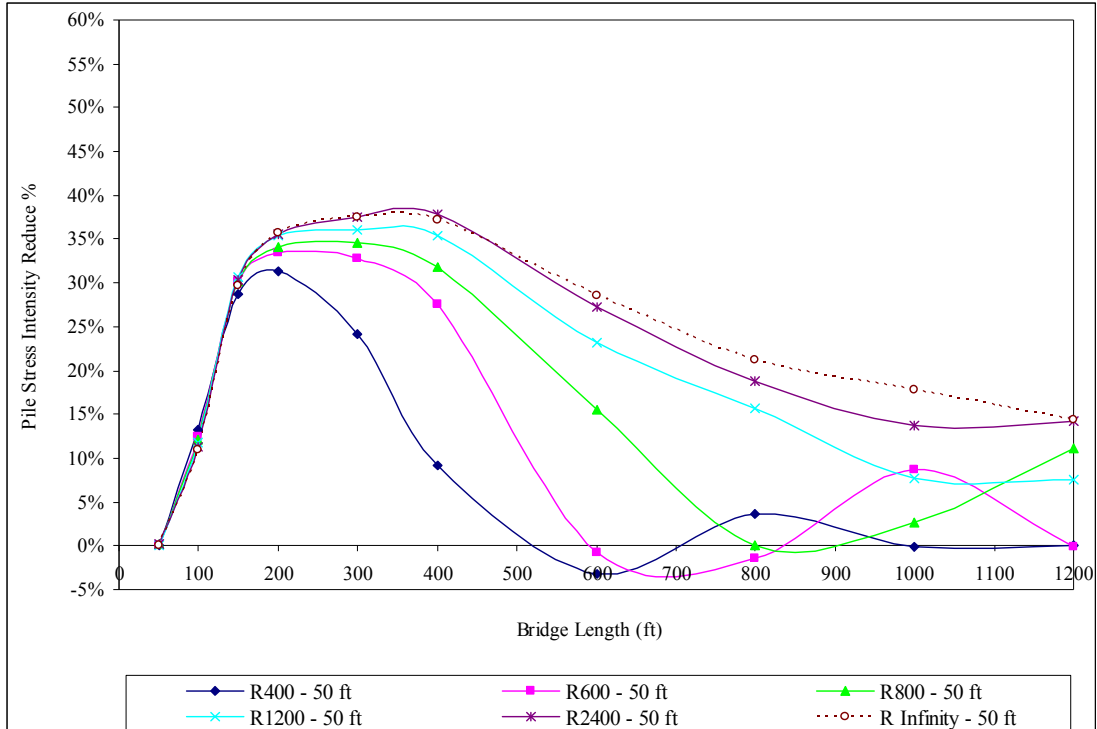
1. The pile stress intensity reduction due to the introduction of predrilled holes increases as the depth of the predrilled holes is increased.
2. Piles in 9 feet deep predrilled holes filled with loose sand have a significant reduction in the pile stress intensity when compared with piles in 5 ft deep predrilled holes filled with loose sand. The depth increase of predrilled holes deeper than 9 ft will further reduce the stress intensity in the piles, but the rate of reduction is much smaller than that of 9 ft deep predrilled holes.
3. Curved IAB's with a smaller radius have the mean of the pile stress intensity reduction less than that of curved IAB's with a larger radius.
4. The mean of the pile stress intensity reduction due to the introduction of predrilled holes of curved IAB's of all radii with 50 ft spans indicates that there is no pile stress intensity reduction at a 50 ft bridge length. The mean of the pile stress intensity reduction continues to increase to its highest value at bridge lengths between 200 ft and 300 ft. Beyond these lengths, it starts decreasing and continues to decrease as the bridge length is increased to 1200 ft.

5. For curved IAB's of all radii with 100 ft spans, the mean of the pile stress intensity reduction due to the introduction of predrilled holes is in the range of -6.8% to -17.7% at a 100 ft bridge length. It increases to its highest value at a 200 ft length and then starts decreasing and continues to decrease as the bridge length is increased to 600 ft. Beyond the 600 ft length, the mean of the pile stress intensity reduction increases and continues to increase as the bridge length is increased to 1200 ft. A minus sign indicates that the introduction of predrilled holes does not reduce the stress intensity in the piles, but rather increases it.
6. According to Greimann, Amde, and Yang [1.45], the displacements of the piles decrease the vertical load carrying capacity of the piles. While the vertical load (self weight of a bridge superstructure) is constant, the displacements in lateral, longitudinal, and twisting of the piles in predrilled holes are greater than that of the piles without predrilled holes which result in the increase in the pile stress intensity at some bridge lengths of curved IAB's. Therefore, it can be concluded that a difference in the arrangement of pile groups due to different bridge lengths of curved IAB's with different radii results in the stress intensity increase in the piles in predrilled holes at some bridge lengths when compared to the piles without predrilled holes. It is also shown that the increase in the radius and in the depth of predrilled holes

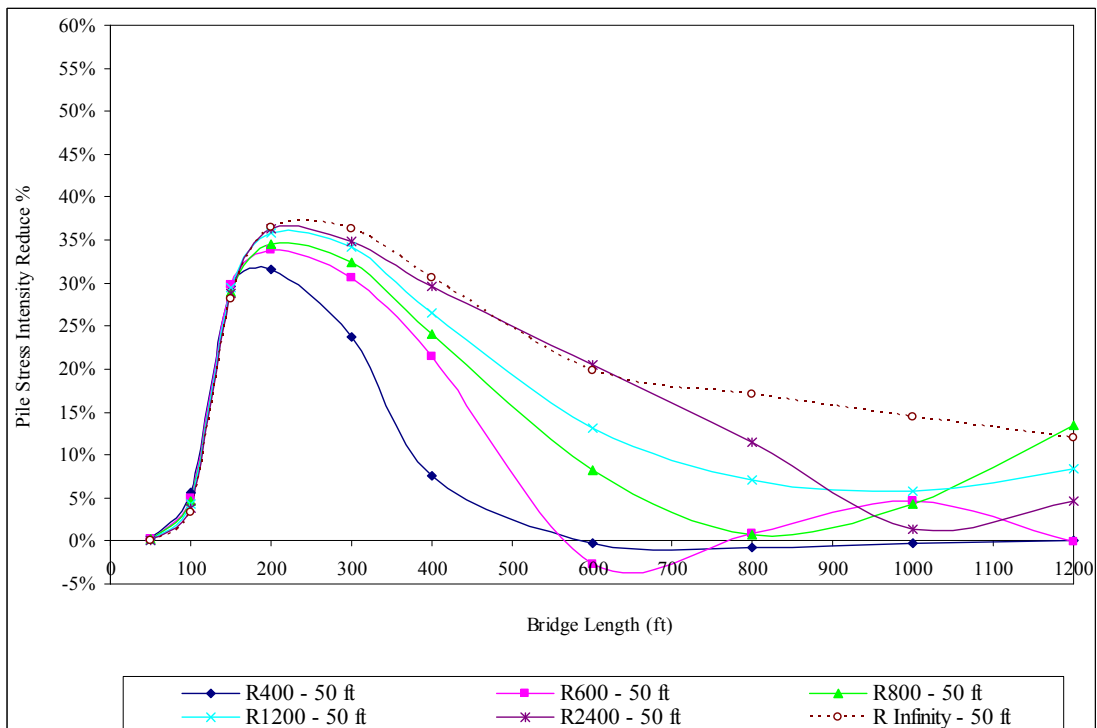


decreases the stress intensity increase in the piles due to the introduction of predrilled holes.

7. The comparison of the mean of the pile stress intensity reduction due to the introduction of the predrilled holes between curved IAB's with 50 ft and 100 ft spans in Tables 7.16, 7.17, 7.19, and 7.20 indicates that curved IAB's with 50 ft spans have the mean of the pile stress intensity reduction greater than that of curved IAB's with 100 ft spans. The pile stress intensity reduction is greater for bridge lengths from 100 ft to 300 ft by 22.6% to 24%. It is greater for bridge lengths from 400 ft to 1200 ft by 17% to 0%. The decrease in the span length results in the decrease in lateral and longitudinal displacements of the piles as well as the self weight of a bridge superstructure which decreases the stress intensity in the piles. Therefore, curved IAB's with the shorter span lengths will result in a smaller stress intensity increase in the piles when compared to curved IAB's with the longer span lengths.
8. A temperature increase results in a lower pile stress intensity reduction due to the introduction of predrilled holes in most cases, except curved IAB's with 100 ft spans at bridge lengths between 100 ft and 200 ft.

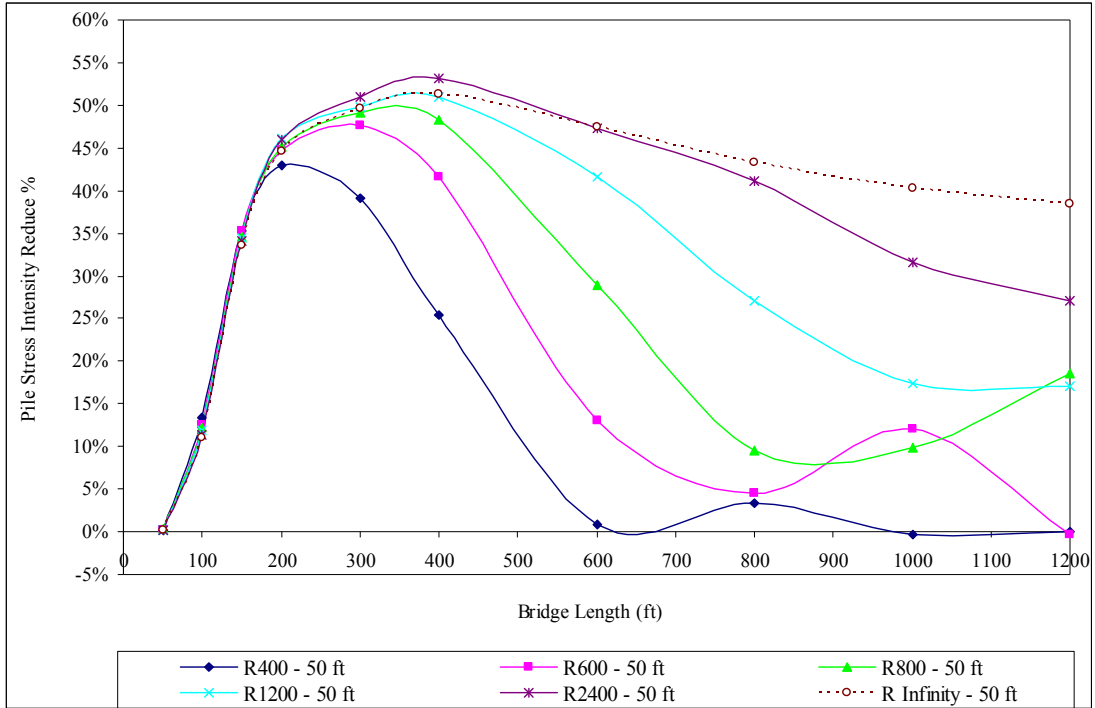


a)  $\Delta T_{\text{slab}} = 90^\circ \text{ F}$ ,  $\Delta T_{\text{the rest}} = 60^\circ \text{ F}$

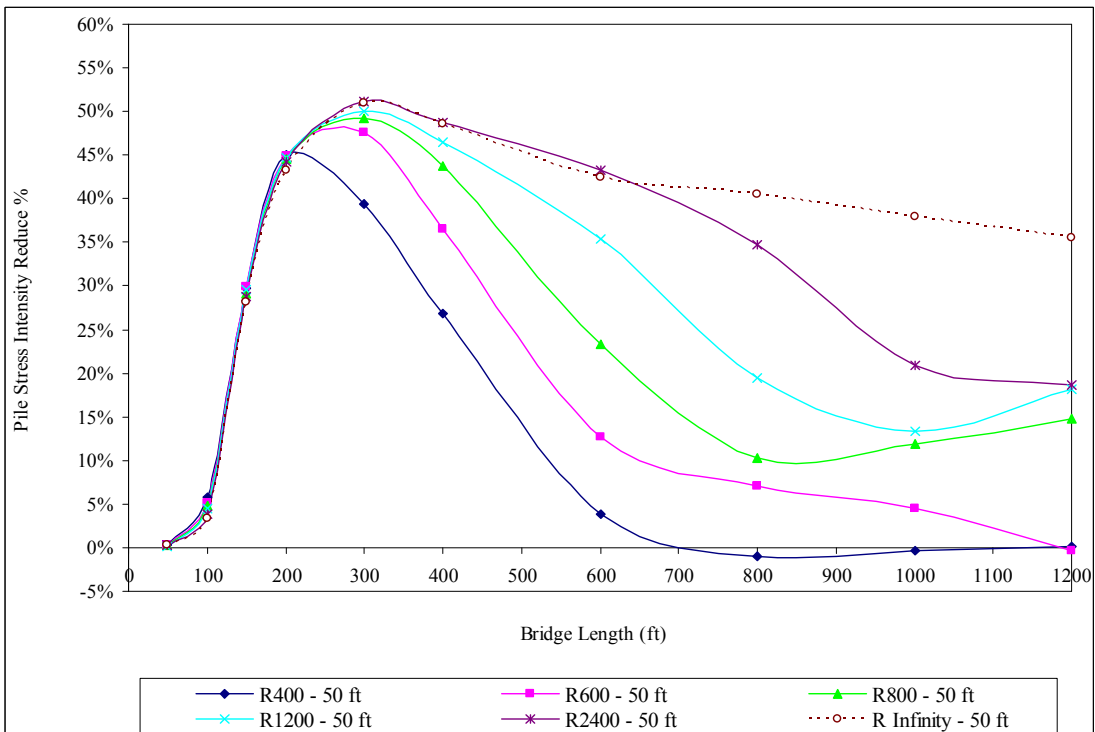


b)  $\Delta T_{\text{slab}} = 120^\circ \text{ F}$ ,  $\Delta T_{\text{the rest}} = 90^\circ \text{ F}$

**Figure 7.17 – Stress Reduction (%) of End-Bearing Piles in 5 ft Deep Predrilled Holes of Bridges with 50 ft Spans**

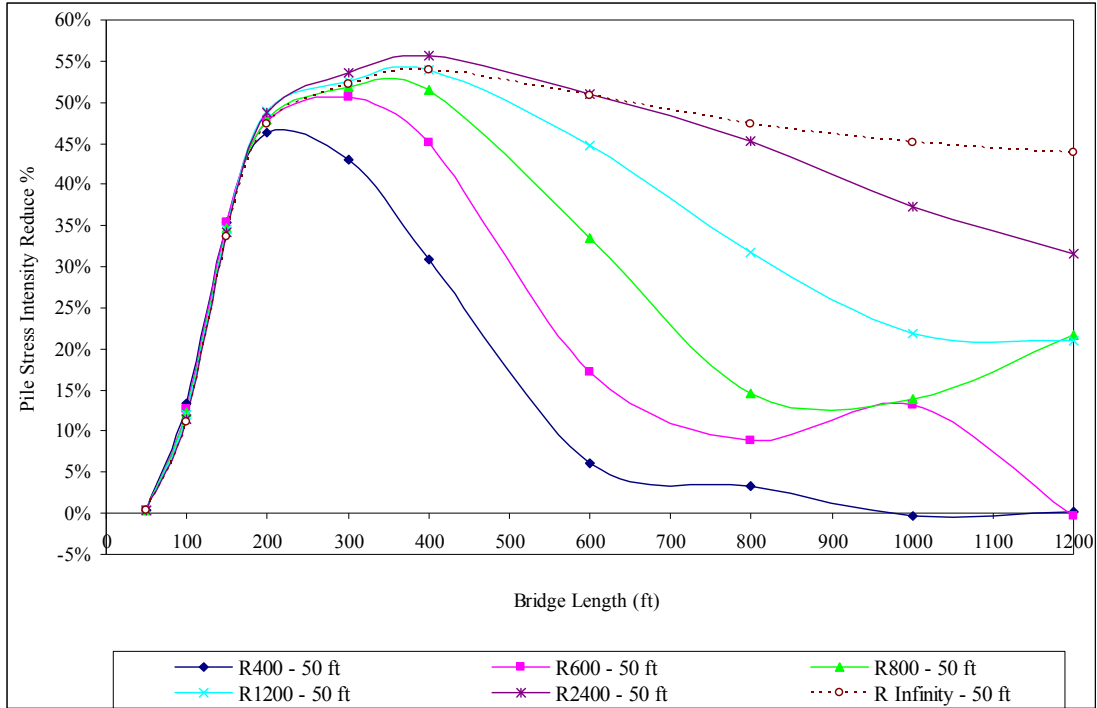


a)  $\Delta T_{\text{slab}} = 90^\circ \text{ F}$ ,  $\Delta T_{\text{the rest}} = 60^\circ \text{ F}$

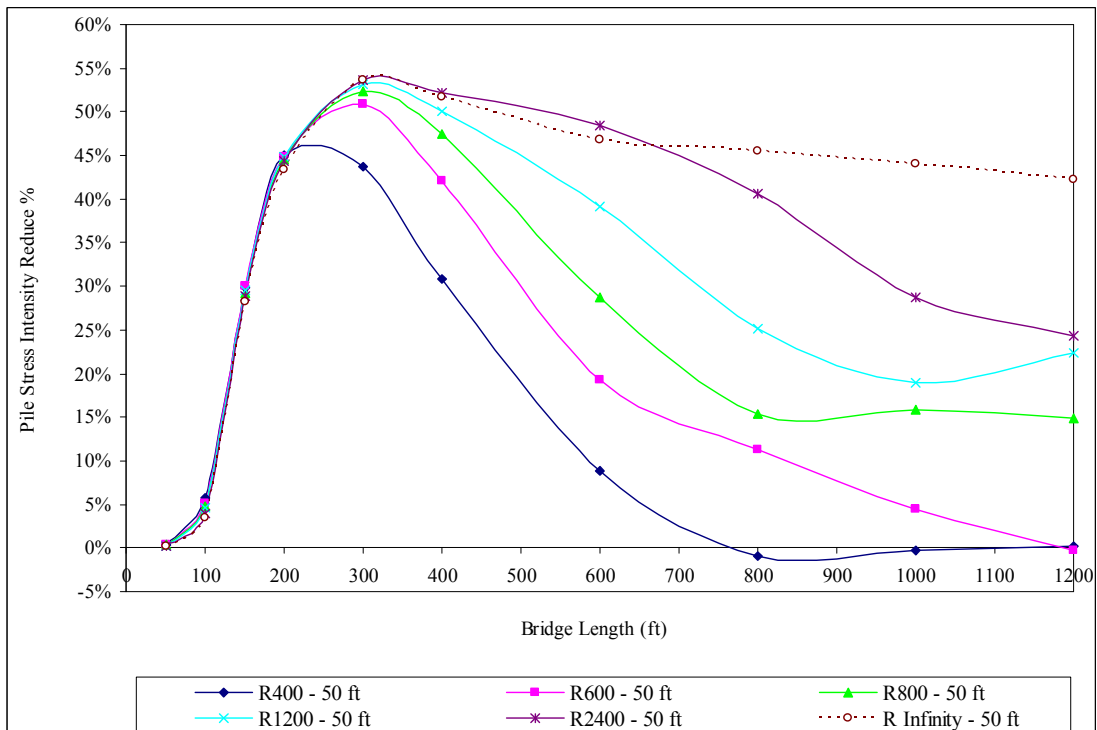


b)  $\Delta T_{\text{slab}} = 120^\circ \text{ F}$ ,  $\Delta T_{\text{the rest}} = 90^\circ \text{ F}$

**Figure 7.18 – Stress Reduction (%) of End-Bearing Piles in 9 ft Deep Predrilled Holes of Bridges with 50 ft Spans**

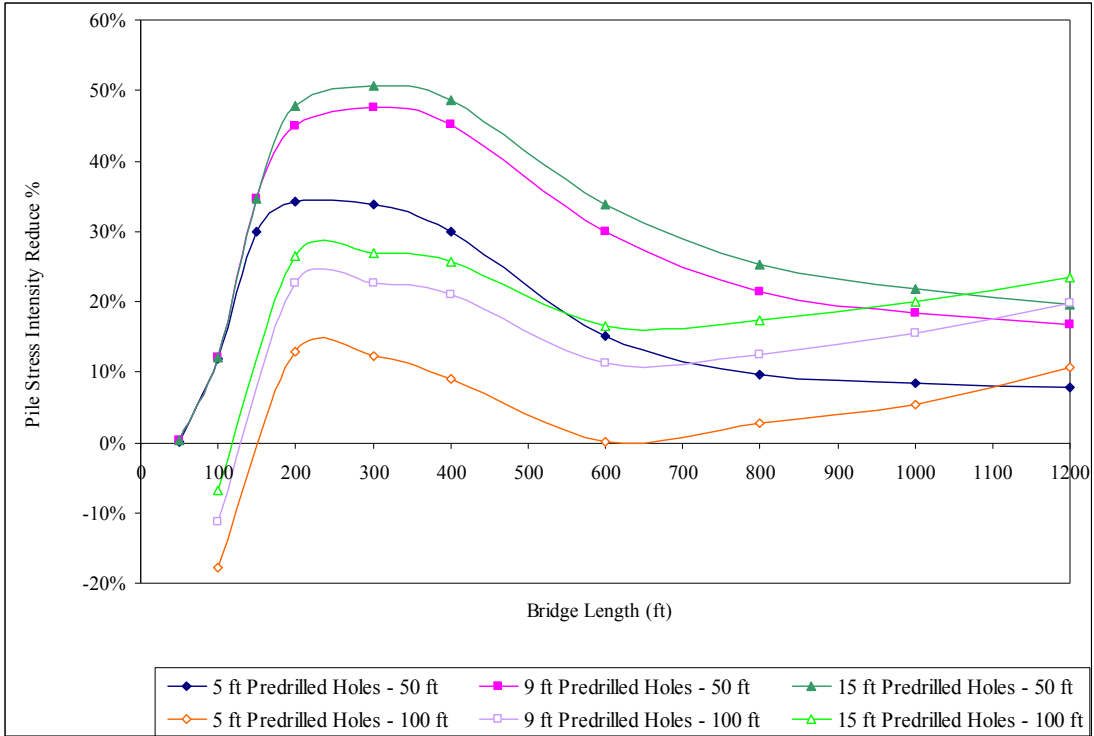


a)  $\Delta T_{\text{slab}} = 90^\circ \text{ F}$ ,  $\Delta T_{\text{the rest}} = 60^\circ \text{ F}$

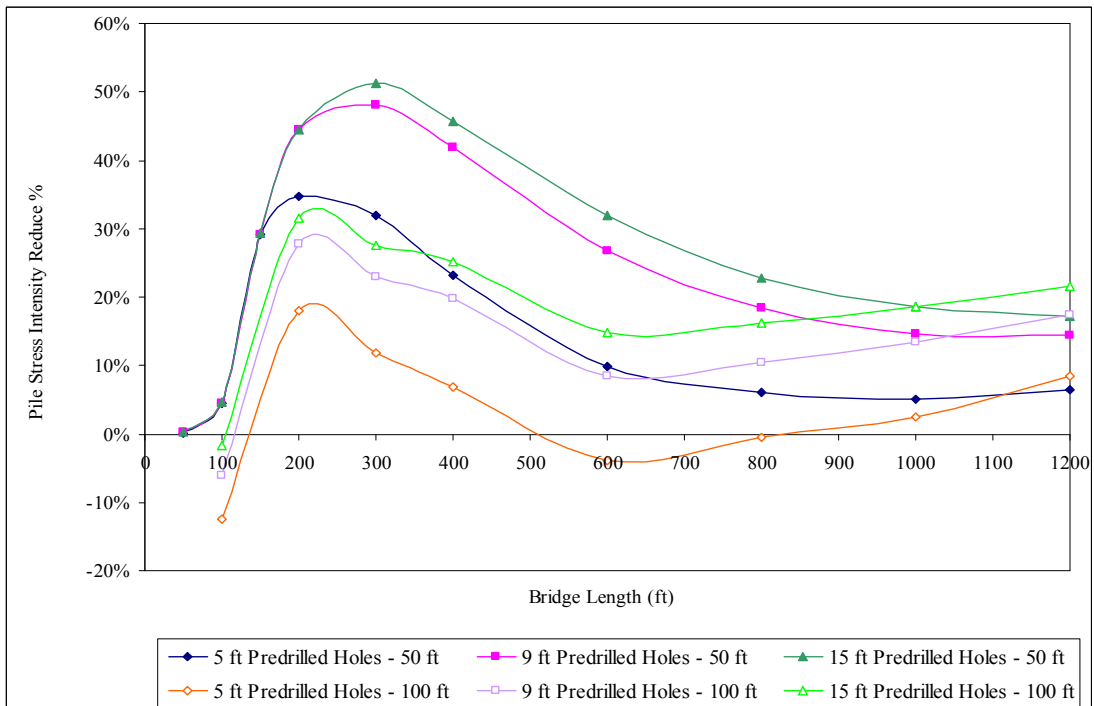


b)  $\Delta T_{\text{slab}} = 120^\circ \text{ F}$ ,  $\Delta T_{\text{the rest}} = 90^\circ \text{ F}$

**Figure 7.19 – Stress Reduction (%) of End-Bearing Piles in 15 ft Deep Predrilled Holes of Bridges with 50 ft Spans**

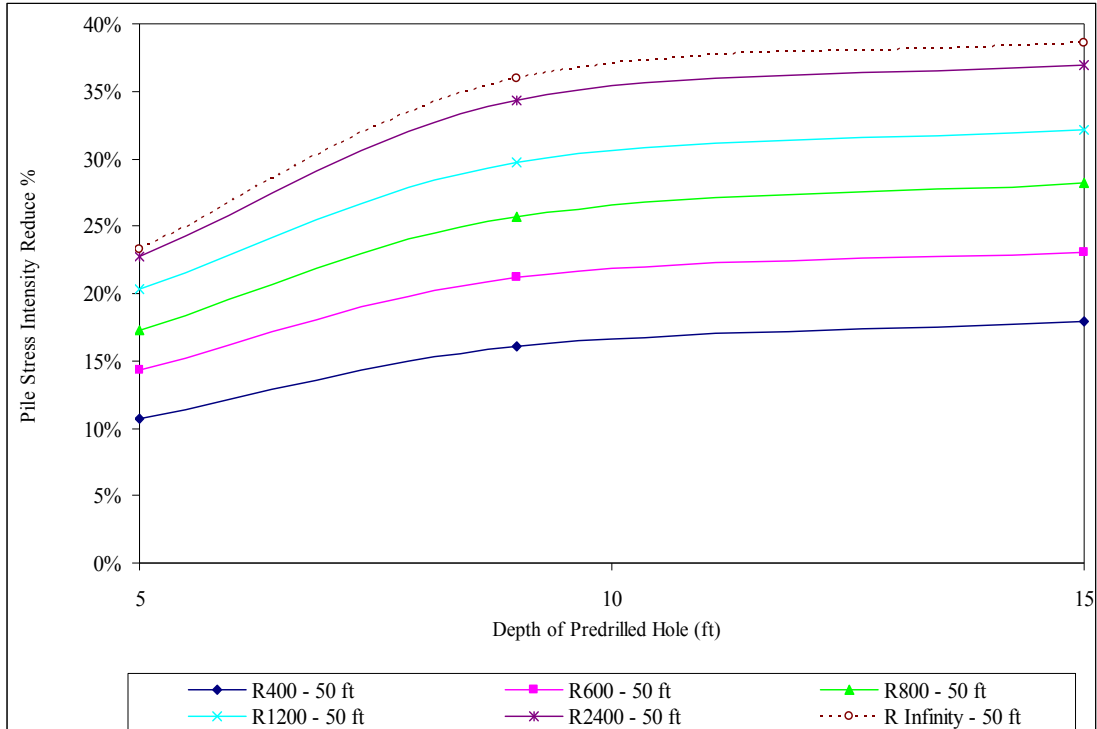


a)  $\Delta T_{\text{slab}} = 90^\circ \text{ F}$ ,  $\Delta T_{\text{the rest}} = 60^\circ \text{ F}$

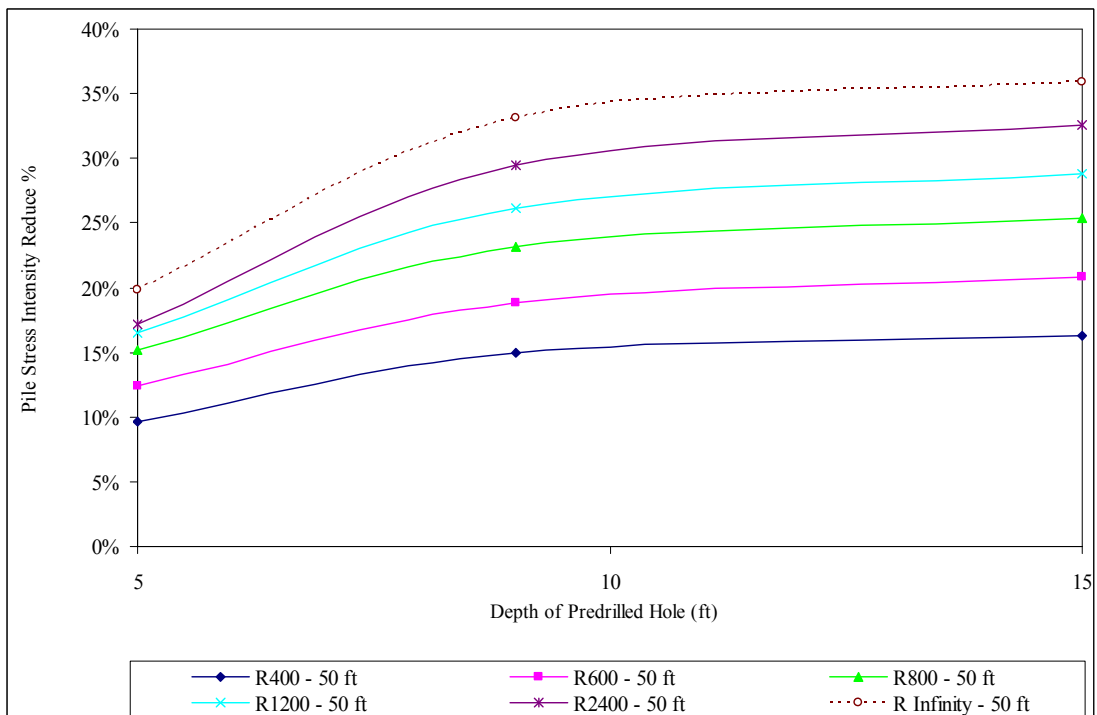


b)  $\Delta T_{\text{slab}} = 120^\circ \text{ F}$ ,  $\Delta T_{\text{the rest}} = 90^\circ \text{ F}$

Figure 7.20 – Mean of Stress Reduction (%) of End-Bearing Piles in Varying Depths of Predrilled Holes of Bridges with 50 ft and 100 ft Spans

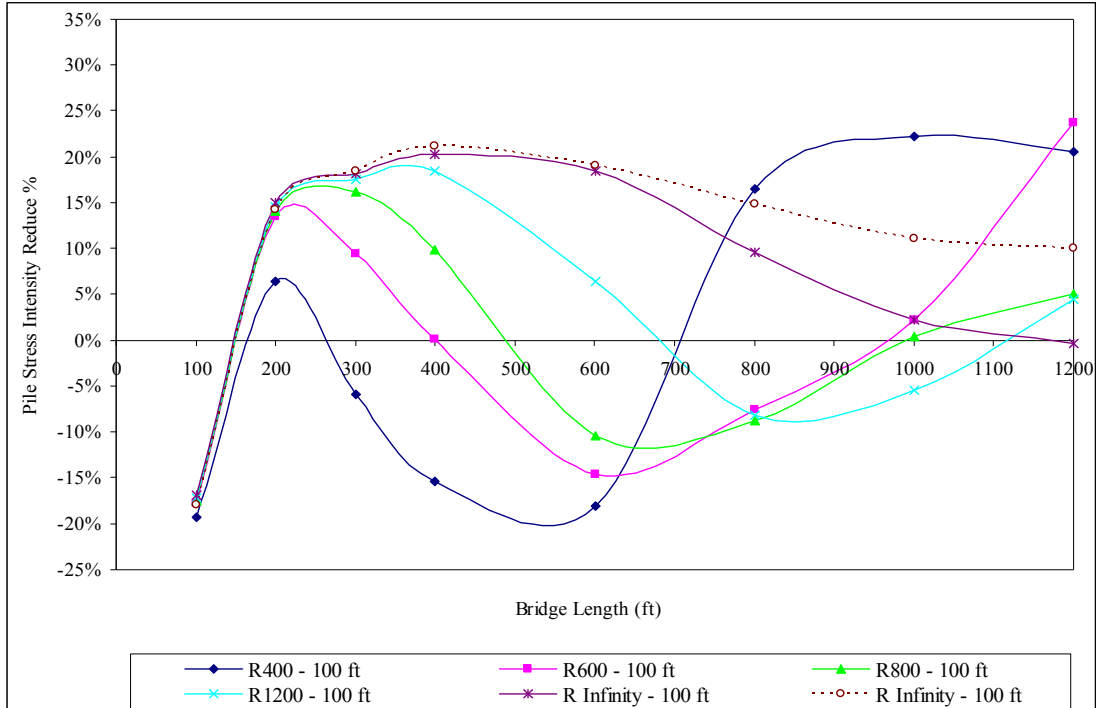


a)  $\Delta T_{\text{slab}} = 90^\circ \text{ F}, \Delta T_{\text{the rest}} = 60^\circ \text{ F}$

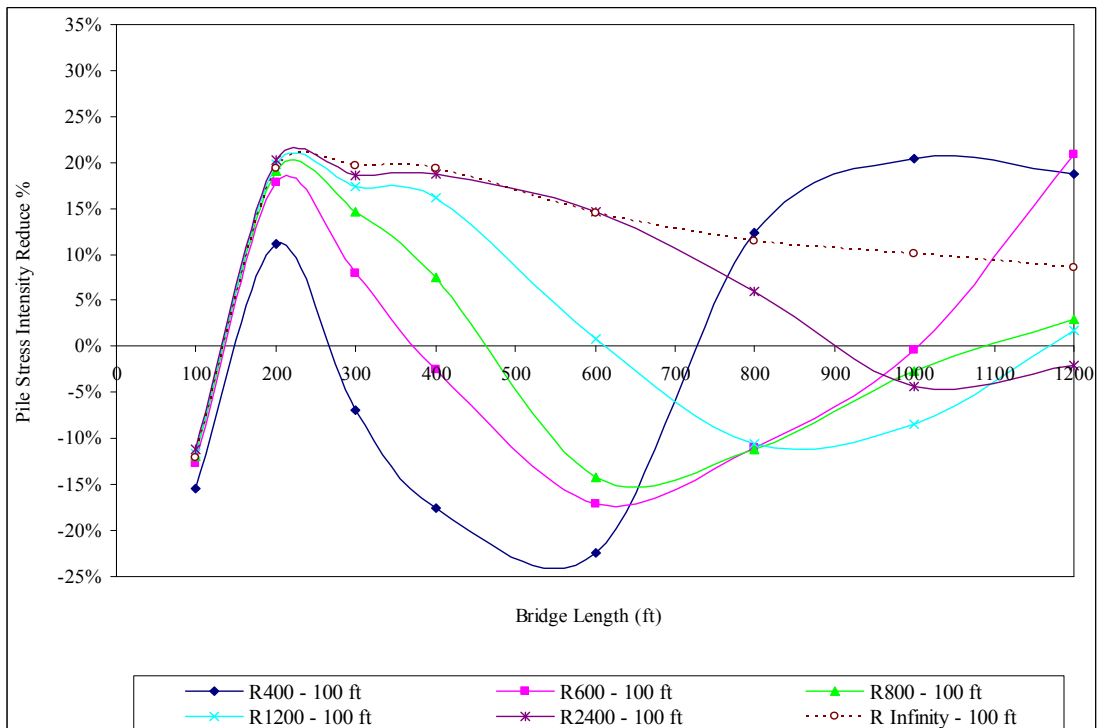


b)  $\Delta T_{\text{slab}} = 120^\circ \text{ F}, \Delta T_{\text{the rest}} = 90^\circ \text{ F}$

**Figure 7.21 – Mean of Stress Reduction (%) of End-Bearing Piles in Varying Depths of Predrilled Holes of Bridges of Different Radii with 50 ft Spans**

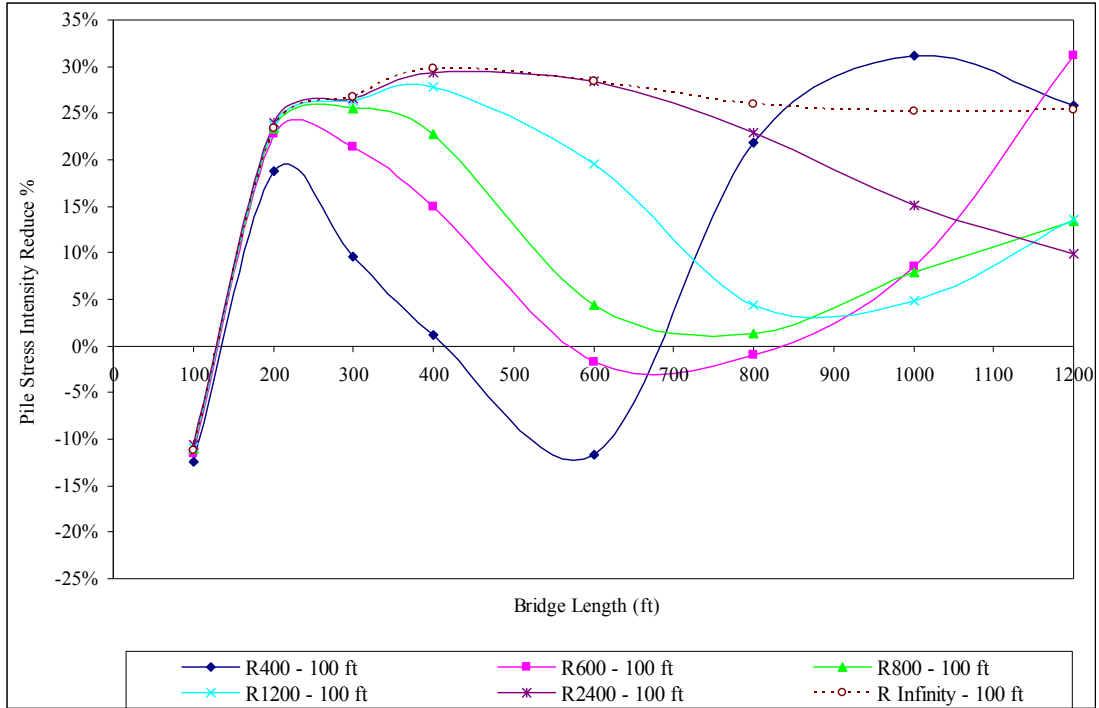


a)  $\Delta T_{\text{slab}} = 90^\circ \text{ F}$ ,  $\Delta T_{\text{the rest}} = 60^\circ \text{ F}$

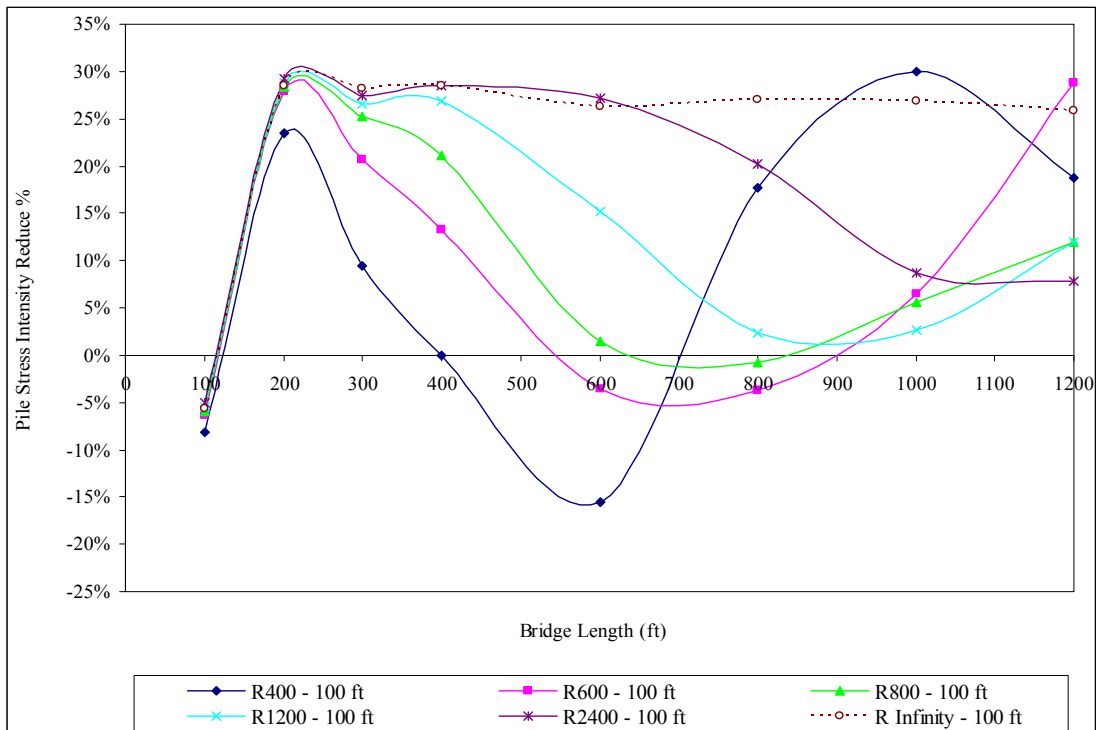


b)  $\Delta T_{\text{slab}} = 120^\circ \text{ F}$ ,  $\Delta T_{\text{the rest}} = 90^\circ \text{ F}$

**Figure 7.22 – Stress Reduction (%) of End-Bearing Piles in 5 ft Deep Predrilled Holes of Bridges with 100 ft Spans**



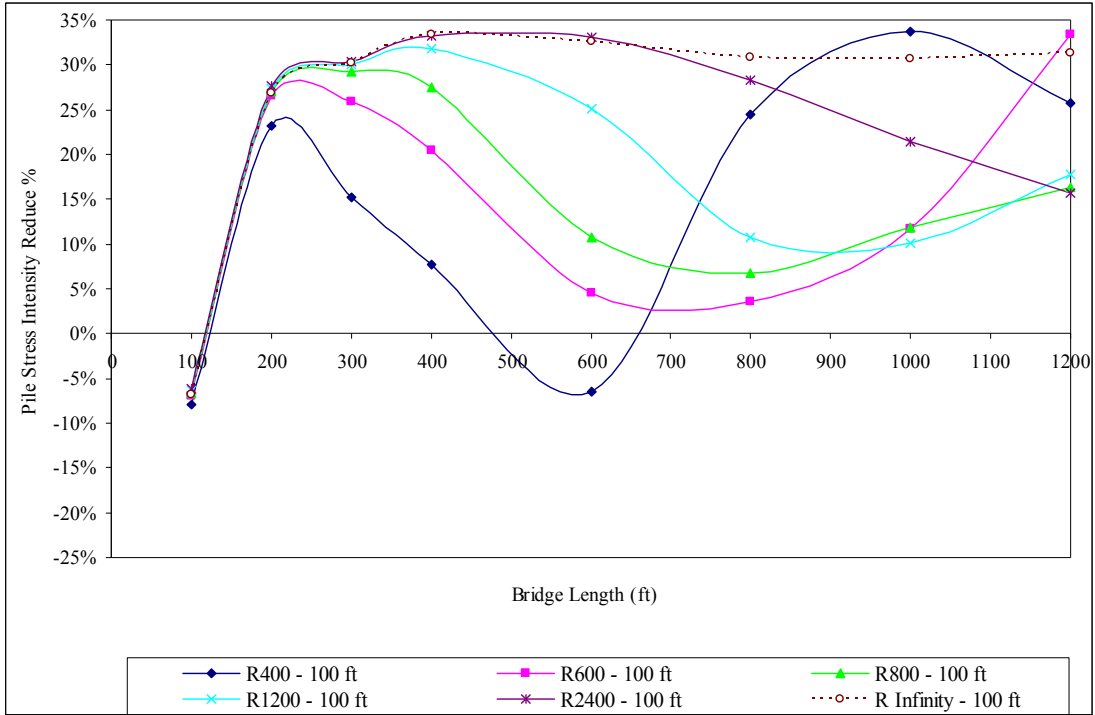
a)  $\Delta T_{\text{slab}} = 90^\circ \text{ F}$ ,  $\Delta T_{\text{the rest}} = 60^\circ \text{ F}$



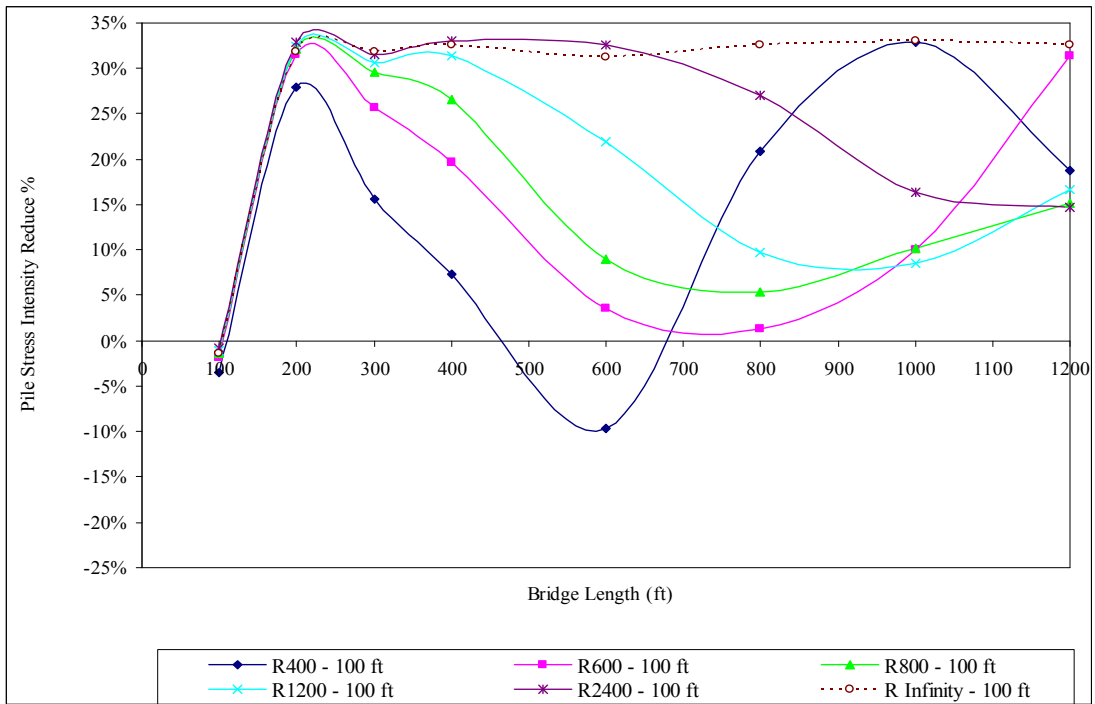
b)  $\Delta T_{\text{slab}} = 120^\circ \text{ F}$ ,  $\Delta T_{\text{the rest}} = 90^\circ \text{ F}$

Figure 7.23 – Stress Reduction (%) of End-Bearing Piles in 9 ft Deep Predrilled Holes of Bridges with 100 ft Spans



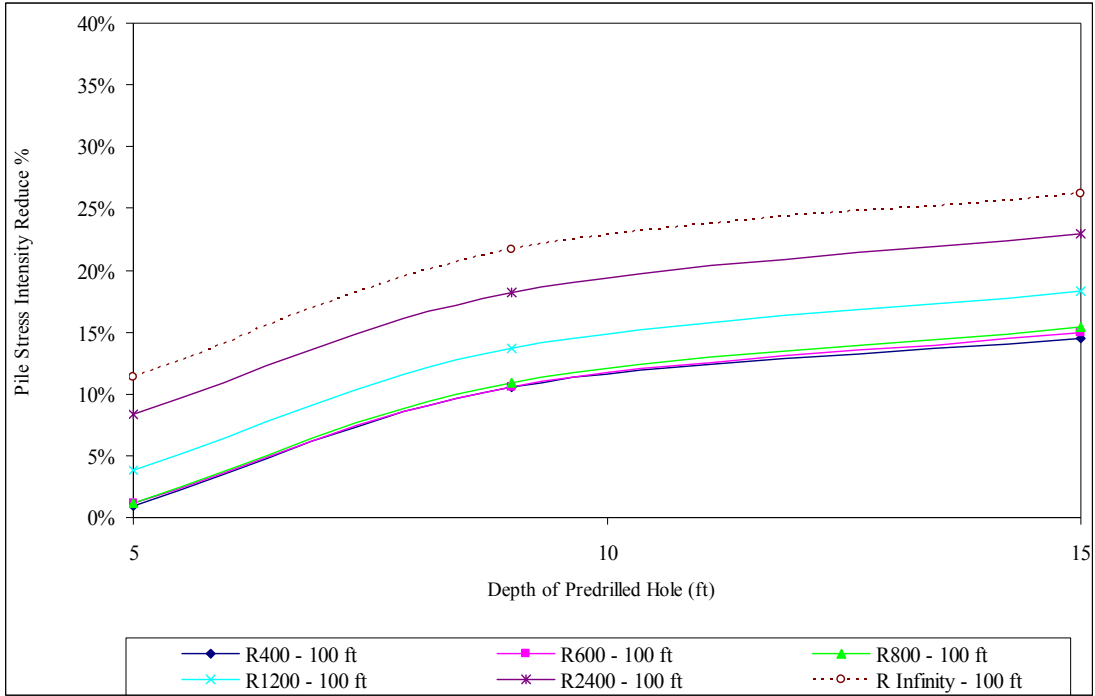


a)  $\Delta T_{\text{slab}} = 90^\circ \text{ F}$ ,  $\Delta T_{\text{the rest}} = 60^\circ \text{ F}$

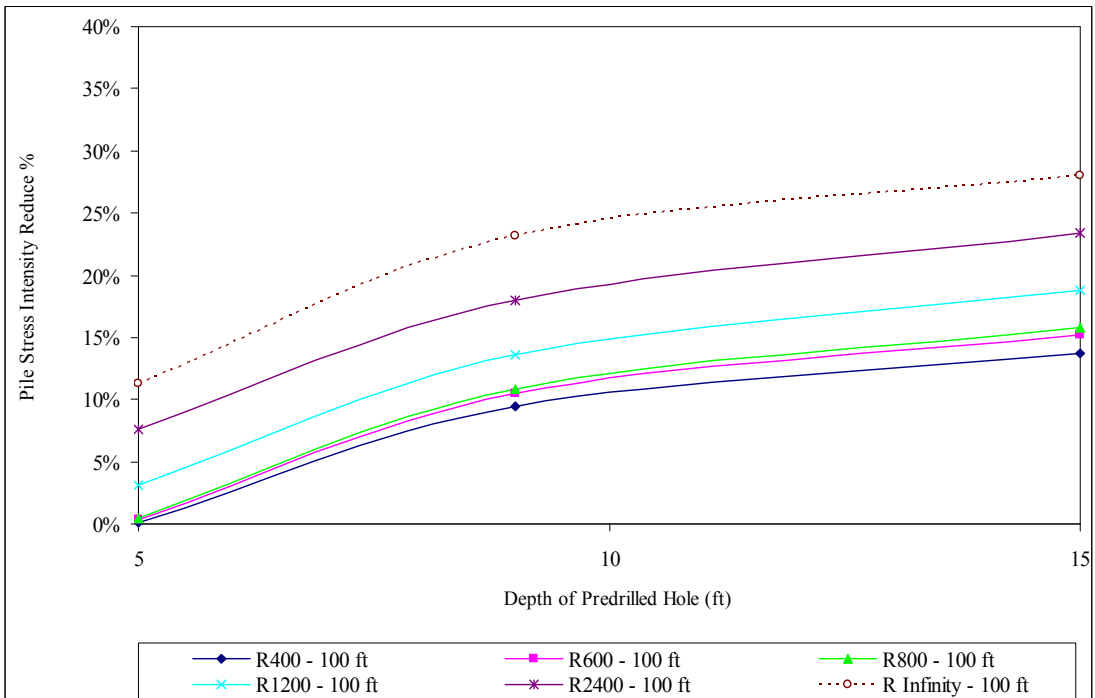


b)  $\Delta T_{\text{slab}} = 120^\circ \text{ F}$ ,  $\Delta T_{\text{the rest}} = 90^\circ \text{ F}$

Figure 7.24 – Stress Reduction (%) of End-Bearing Piles in 15 ft Deep Predrilled Holes of Bridges with 100 ft Spans



a)  $\Delta T_{\text{slab}} = 90^\circ \text{F}$ ,  $\Delta T_{\text{the rest}} = 60^\circ \text{F}$



b)  $\Delta T_{\text{slab}} = 120^\circ \text{F}$ ,  $\Delta T_{\text{the rest}} = 90^\circ \text{F}$

**Figure 7.25 – Mean of Stress Reduction (%) of End-Bearing Piles in Varying Depths of Predrilled Holes of Bridges of Different Radii with 100 ft Spans**

#### 7.4 Effect of Span Length Variation

The effect of span length variation from 100 ft to 50 ft on the maximum stress intensity (stress concentration) reduction in the piles of curved IAB's is discussed in this section. All other parameters are held constant.

For piles in very stiff clay soil profile as shown in Figure 7.26, the highest pile stress intensity reduction value due to the increase in the number of spans of curved IAB's of all radii is between 52.2% and 54.2% for  $\Delta T_{\text{slab}}$  of 90° F and  $\Delta T_{\text{the rest}}$  of 60° F and between 40.5% and 42.6% for  $\Delta T_{\text{slab}}$  of 120° F and  $\Delta T_{\text{the rest}}$  of 90° F at a 100 ft bridge length. It decreases to its lowest value at the bridge length indicated in Table 7.22. After it reaches its lowest value, some of the pile stress intensity reduction rates start increasing and continue to increase as the bridge length is increased to 1200 ft. Except curved IAB's with a 400 ft radius, after the pile stress intensity reduction rate reaches its lowest value, it starts to increase at a 1000 ft length and decreases again as the bridge length is increased to 1200 ft.

For piles in 9 ft deep predrilled holes filled with loose sand as shown in Figure 7.27, the highest pile stress intensity reduction value due to the increase in the number of spans of curved IAB's of all radii is between 61.8% and 64.7% for  $\Delta T_{\text{slab}}$  of 90° F and  $\Delta T_{\text{the rest}}$  of 60° F and between 45.6% and 50.8% for  $\Delta T_{\text{slab}}$  of 120° F and  $\Delta T_{\text{the rest}}$  of 90° F at a 100 ft bridge length. It decreases to its lowest value at the bridge length indicated in Table 7.23. After it reaches its lowest value, some of the pile stress intensity reduction rates start increasing and continue to increase as the bridge length is increased to 1200 ft.

**Table 7.22 – Stress Reduction (%) of End-Bearing Piles in Very Stiff Clay Soil Profile due to the Increase in the Number of Spans**

Radius (ft)	Bridge Length (ft)	$\Delta T_{\text{slab}} = 90^\circ \text{ F}$ $\Delta T_{\text{the rest}} = 60^\circ \text{ F}$	$\Delta T_{\text{slab}} = 120^\circ \text{ F}$ $\Delta T_{\text{the rest}} = 90^\circ \text{ F}$
400	300	23.6	10.6
600	400	15.1	7.7
800	600	11.4	6.6
1200	800	7.7	7.1
2400	800	3.6	1.7
Infinity	1200	-0.3	-1.6

**a) Lowest Pile Stress Reduction (%)**

Radius (ft)	Bridge Length (ft)	$\Delta T_{\text{slab}} = 90^\circ \text{ F}$ $\Delta T_{\text{the rest}} = 60^\circ \text{ F}$	$\Delta T_{\text{slab}} = 120^\circ \text{ F}$ $\Delta T_{\text{the rest}} = 90^\circ \text{ F}$
400	1200	39.0	18.4
600	1200	50.5	34.2
800	1200	34.6	23.9
1200	1200	29.2	20.0
2400	1200	6.2	7.8
Infinity	1200	-0.3	-1.6

**b) Pile Stress Reduction (%) at 1200 ft Length**

**Table 7.23 – Stress Reduction (%) of End-Bearing Piles in 9 ft Deep Predrilled Holes due to the Increase in the Number of Spans**

Radius (ft)	Bridge Length (ft)	$\Delta T_{\text{slab}} = 90^\circ \text{ F}$ $\Delta T_{\text{the rest}} = 60^\circ \text{ F}$	$\Delta T_{\text{slab}} = 120^\circ \text{ F}$ $\Delta T_{\text{the rest}} = 90^\circ \text{ F}$
400	1200	17.9	-0.2
600	1200	27.8	7.4
800	800	32.3	25.9
1200	1000	29.8	21.7
2400	1000	23.6	17.2
Infinity	1200	17.2	11.9

**a) Lowest Pile Stress Reduction (%)**

Radius (ft)	Bridge Length (ft)	$\Delta T_{\text{slab}} = 90^\circ \text{ F}$ $\Delta T_{\text{the rest}} = 60^\circ \text{ F}$	$\Delta T_{\text{slab}} = 120^\circ \text{ F}$ $\Delta T_{\text{the rest}} = 90^\circ \text{ F}$
400	1200	17.9	-0.2
600	1200	27.8	7.4
800	1200	38.5	26.3
1200	1200	32.0	25.7
2400	1200	24.1	18.6
Infinity	1200	17.2	11.9

**b) Pile Stress Reduction (%) at 1200 ft Length**

**Table 7.24 – Difference in Stress Reduction (%) between End-Bearing Piles in  
Predrilled Holes and End-Bearing Piles without Predrilled Holes  
due to the Increase in the Number of Spans**

Bridge Length (ft)	$\Delta T_{\text{slab}} = 90^\circ \text{ F}, \Delta T_{\text{the rest}} = 60^\circ \text{ F}$			$\Delta T_{\text{slab}} = 120^\circ \text{ F}, \Delta T_{\text{the rest}} = 90^\circ \text{ F}$		
	Depth of Predrilled Holes (ft)			Depth of Predrilled Holes (ft)		
	5	9	15	5	9	15
100	11.9	9.9	8.3	8.8	5.9	3.6
200	17.4	20.5	20.7	16.4	18.4	15.1
300	19.2	25.6	25.8	20.4	29.6	29.7
400	19.8	27.0	27.1	15.8	25.7	25.8
600	12.7	19.5	19.3	11.4	19.0	19.1
800	6.6	11.0	10.7	5.9	9.3	8.9
1000	3.5	5.2	4.7	2.4	2.3	1.6
1200	-1.0	-0.3	-0.5	-2.1	-2.2	-3.2

Table 7.24 and Figures 7.28 and 7.29 indicate that the pile stress intensity reduction due to the increase in the number of spans of curved IAB's with piles in predrilled holes is greater than that of curved IAB's with piles without predrilled holes. It is shown that piles in 9 feet deep predrilled holes filled with loose sand have a significant reduction in the pile stress intensity when compared with piles in 5 ft deep predrilled holes filled with loose sand. The depth increase of predrilled holes deeper than 9 ft will further reduce the stress intensity in the piles, but the rate of reduction is much smaller than that of 9 ft deep predrilled holes.

Figures 7.26 to 7.28 indicate that curved IAB's with a smaller radius, for the most part, have a pile stress intensity reduction due to the increase in the number of spans greater than that of curved IAB's with a larger radius in the range of 0% to the maximum value indicated in Table 7.25. The difference in the pile stress intensity reduction due to the increase in the number of spans between curved IAB's with

different radii is smaller when predrilled holes are used for the piles instead of the piles with no predrilled holes as indicated in Table 7.26 and Figure 7.28.

**Table 7.25 – Difference in Stress Reduction (%) of End-Bearing Piles between Bridges of Different Radii due to the Increase in the Number of Spans**  
 ( $\Delta T_{\text{slab}} = 90^\circ \text{ F}$ ,  $\Delta T_{\text{the rest}} = 60^\circ \text{ F}$ )

	Radius (ft) used for Stress Comparison				
	400	600	800	1200	2400
Radius (ft) (Compared to)	% More Than				
600	19.2	-	-	-	-
800	25.5	15.9	-	-	-
1200	43.9	24.8	18.4	-	-
2400	48.0	44.3	28.4	23.0	-
Infinity	51.9	50.7	34.9	29.4	6.5

**a) Very Stiff Clay Soil Profile**

	Radius (ft) used for Stress Comparison				
	400	600	800	1200	2400
Radius (ft) (Compared to)	% More Than				
600	4.1	-	-	-	-
800	8.0	5.4	-	-	-
1200	10.6	10.8	6.5	-	-
2400	14.0	16.9	14.4	7.9	-
Infinity	15.6	20.1	21.2	14.7	6.9

**b) Very Stiff Clay Soil Profile with 9 ft Deep Predrilled Holes Filled with Loose Sand**

**Table 7.26 – Mean and Standard Deviation of Stress Reduction (%) of End-Bearing Piles in Various Soil Profile Types of Bridges of Different Radii due to the Increase in the Number of Spans**

Description	Radius (ft)	$\Delta T_{\text{slab}} = 90^\circ \text{ F}$ $\Delta T_{\text{the rest}} = 60^\circ \text{ F}$				$\Delta T_{\text{slab}} = 120^\circ \text{ F}$ $\Delta T_{\text{the rest}} = 90^\circ \text{ F}$			
		Depth of Predrilled Holes (ft)							
		0	5	9	15	0	5	9	15
MEAN	400	38	43	42	41	25	30	29	28
	600	33	42	43	42	22	31	31	30
	800	28	40	42	42	19	31	33	32
	1200	22	36	40	40	15	27	31	30
	2400	16	30	38	37	11	21	29	28
	Infinity	15	27	36	36	9	19	27	27
STD	400	13	12	14	14	13	16	17	17
	600	14	10	11	11	12	10	12	13
	800	14	11	10	10	12	9	8	7
	1200	15	13	12	11	12	11	9	8
	2400	17	18	14	13	13	15	11	10
	Infinity	18	21	15	15	14	17	12	11

From the analyses, it is shown that a temperature increase results in a lower pile stress intensity reduction. The mean of the pile stress intensity reduction due to the increase in the number of spans of curved IAB's subjected to a temperature load of  $\Delta T_{\text{slab}}$  of  $120^\circ \text{ F}$  and  $\Delta T_{\text{the rest}}$  of  $90^\circ \text{ F}$  is less than that of curved IAB's subjected to a temperature load of  $\Delta T_{\text{slab}}$  of  $90^\circ \text{ F}$  and  $\Delta T_{\text{the rest}}$  of  $60^\circ \text{ F}$  in the range of 6.3% to 16.4% as indicated in Table 7.27 and plotted in Figure 7.30.



**Table 7.27 – Difference in Stress Reduction (%) of End-Bearing Piles between  $\Delta T_{\text{slab}} = 120^\circ \text{ F}$ ,  $\Delta T_{\text{the rest}} = 90^\circ \text{ F}$  and  $\Delta T_{\text{slab}} = 90^\circ \text{ F}$ ,  $\Delta T_{\text{the rest}} = 60^\circ \text{ F}$  due to the Increase in the Number of Spans**

Description	Bridge Length (ft)	Depth of Predrilled Holes (ft)			
		0	5	9	15
MEAN	100	-11.7	-14.7	-15.7	-16.4
	200	-8.6	-9.7	-10.7	-14.1
	300	-11.6	-10.3	-7.6	-7.7
	400	-6.3	-10.2	-7.6	-7.6
	600	-6.7	-8.0	-7.1	-6.9
	800	-6.4	-7.2	-8.1	-8.3
	1000	-7.6	-8.7	-10.4	-10.7
	1200	-9.4	-10.5	-11.3	-12.0
STD	100	0.1	0.6	0.5	0.5
	200	0.2	0.5	1.9	1.9
	300	0.9	0.8	0.4	0.4
	400	2.7	1.2	1.0	0.4
	600	4.0	0.9	0.3	0.5
	800	5.6	4.2	3.9	4.2
	1000	5.7	5.2	6.2	6.9
	1200	8.5	8.4	6.7	7.2

#### 7.4.1 Conclusions

The following conclusions are drawn from the study of the effect of span length variation from 100 ft to 50 ft on the maximum stress intensity (stress concentration) reduction in the piles of curved IAB's investigated in this section:

1. Curved IAB's with a smaller radius, for the most part, have a pile stress intensity reduction due to the increase in the number of spans greater than that of curved IAB's with a larger radius.
2. The pile stress intensity reduction due to the increase in the number of spans of curved IAB's with piles in predrilled holes is greater than that of curved IAB's with piles without predrilled holes. It is shown that piles in 9 feet deep predrilled holes filled with loose sand have a significant reduction in the pile stress intensity when compared with piles in 5 ft deep predrilled holes filled with loose sand. The depth increase of predrilled holes deeper than 9 ft will further reduce the stress intensity in the piles, but the rate of reduction is much smaller than that of 9 ft deep predrilled holes.
3. The difference in the pile stress intensity reduction due to the increase in the number of spans between curved IAB's with different radii is smaller when predrilled holes are used for the piles instead of the piles with no predrilled holes.
4. A temperature increase results in a lower pile stress intensity reduction due to the increase in the number of spans.

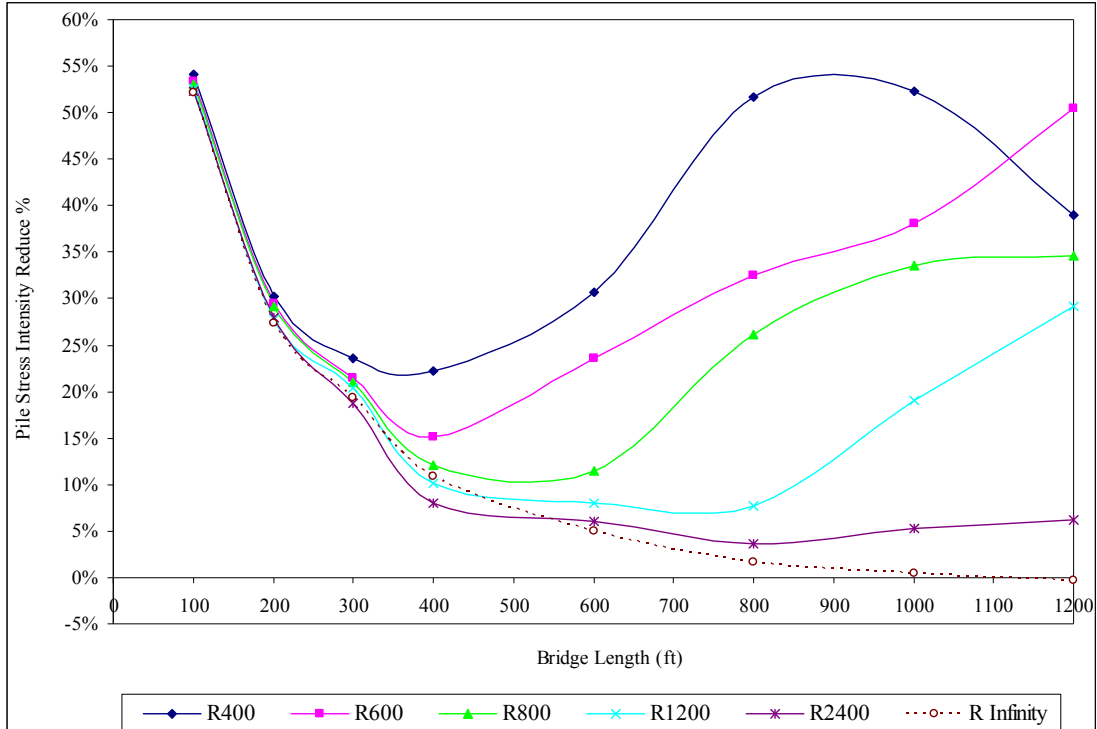
5. Tables 7.28 and 7.29 as well as Figure 7.29 indicate that the highest mean of the pile stress intensity reduction due to the increase in the number of spans of curved IAB's of all radii with piles in very stiff clay soil profile is at a 100 ft bridge length. It continues to decrease to its lowest value at a 400 ft length. Beyond the 400 ft length, it starts increasing and continues to increase as the bridge length is increased to 1200 ft.
6. For piles in predrilled holes, the highest mean of the pile stress intensity reduction due to the increase in the number of spans of curved IAB's of all radii is at a 100 ft bridge length. It starts decreasing and continues to decrease to its lowest value as the bridge length is increased to 1200 ft.

**Table 7.28 – Mean and Standard Deviation of Stress Reduction (%) of  
End-Bearing Piles in Various Soil Profile Types  
due to the Increase in the Number of Spans  
( $\Delta T_{\text{slab}} = 90^\circ \text{ F}$ ,  $\Delta T_{\text{the rest}} = 60^\circ \text{ F}$ )**

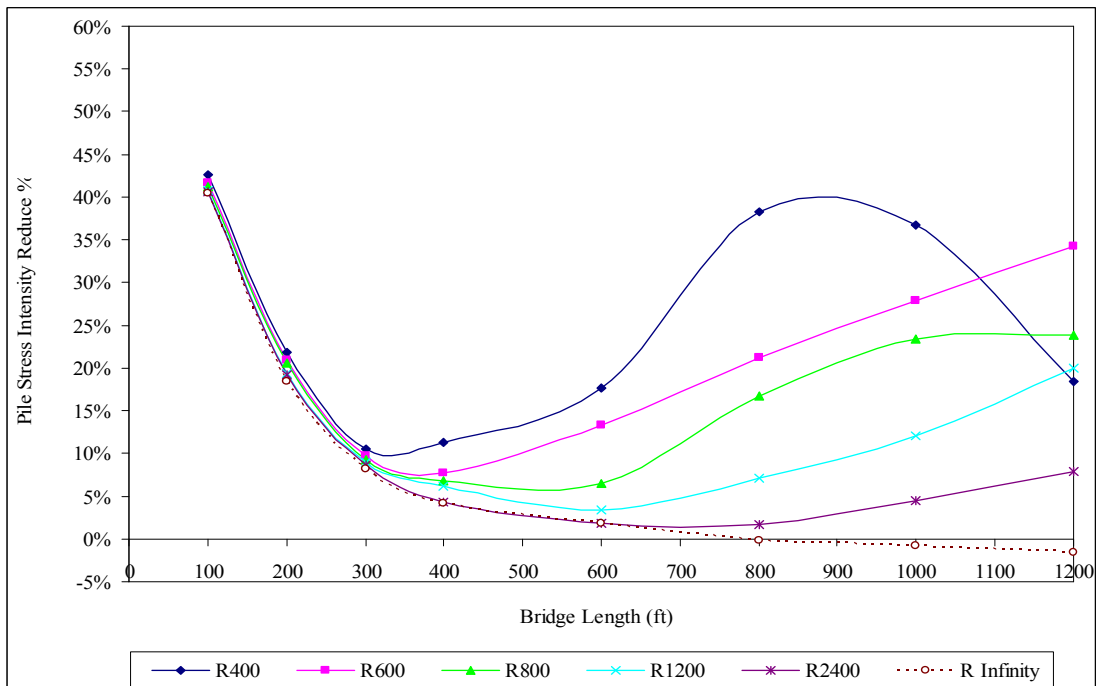
Description	Bridge Length (ft)	Depth of Predrilled Holes (ft)			
		0	5	9	15
MEAN	100	52.9	64.8	62.8	61.3
	200	28.7	46.1	49.2	49.3
	300	20.8	40.0	46.4	46.5
	400	13.1	32.8	40.1	40.2
	600	14.1	26.9	33.6	33.4
	800	20.6	27.2	31.6	31.3
	1000	24.8	28.3	30.0	29.5
	1200	26.5	25.5	26.3	26.0
STD	100	0.7	1.1	1.1	1.1
	200	1.1	1.3	1.1	1.1
	300	1.7	3.0	1.4	1.4
	400	5.1	4.8	1.5	1.4
	600	10.6	9.6	3.0	3.0
	800	19.7	13.6	5.9	5.2
	1000	20.1	13.4	7.3	6.7
	1200	19.7	12.5	8.2	8.1

**Table 7.29 – Mean and Standard Deviation of Stress Reduction (%) of End-Bearing Piles in Various Soil Profile Types due to the Increase in the Number of Spans ( $\Delta T_{\text{slab}} = 120^\circ \text{ F}$ ,  $\Delta T_{\text{the rest}} = 90^\circ \text{ F}$ )**

Description	Bridge Length (ft)	Depth of Predrilled Holes (ft)			
		0	5	9	15
MEAN	100	41.2	50.1	47.1	44.9
	200	20.1	36.4	38.5	35.2
	300	9.2	29.6	38.8	38.9
	400	6.8	22.6	32.5	32.6
	600	7.4	18.9	26.5	26.6
	800	14.2	20.0	23.5	23.0
	1000	17.2	19.6	19.6	18.9
	1200	17.1	15.0	14.9	14.0
STD	100	0.8	1.6	1.6	1.7
	200	1.3	1.7	3.0	2.9
	300	0.8	3.7	1.2	1.2
	400	2.6	6.0	1.6	1.1
	600	6.6	9.8	2.9	2.8
	800	14.5	10.6	4.1	3.8
	1000	14.5	10.8	7.3	7.9
	1200	12.5	12.7	10.5	10.5

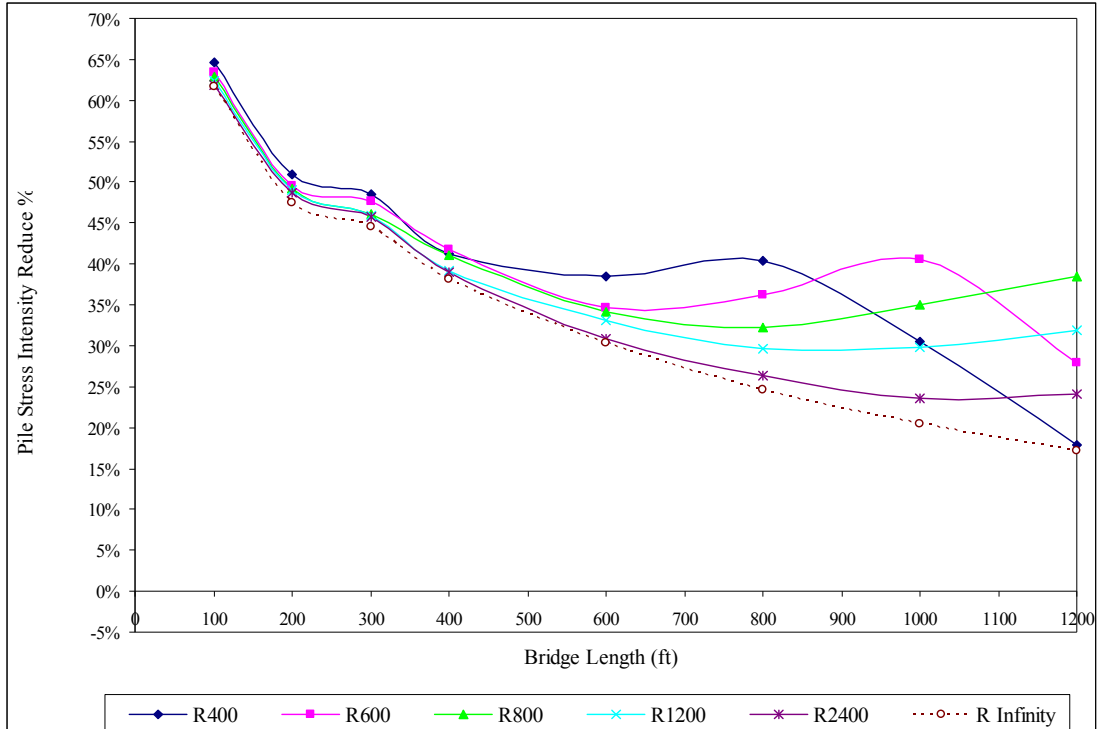


a)  $\Delta T_{\text{slab}} = 90^\circ \text{ F}$ ,  $\Delta T_{\text{the rest}} = 60^\circ \text{ F}$

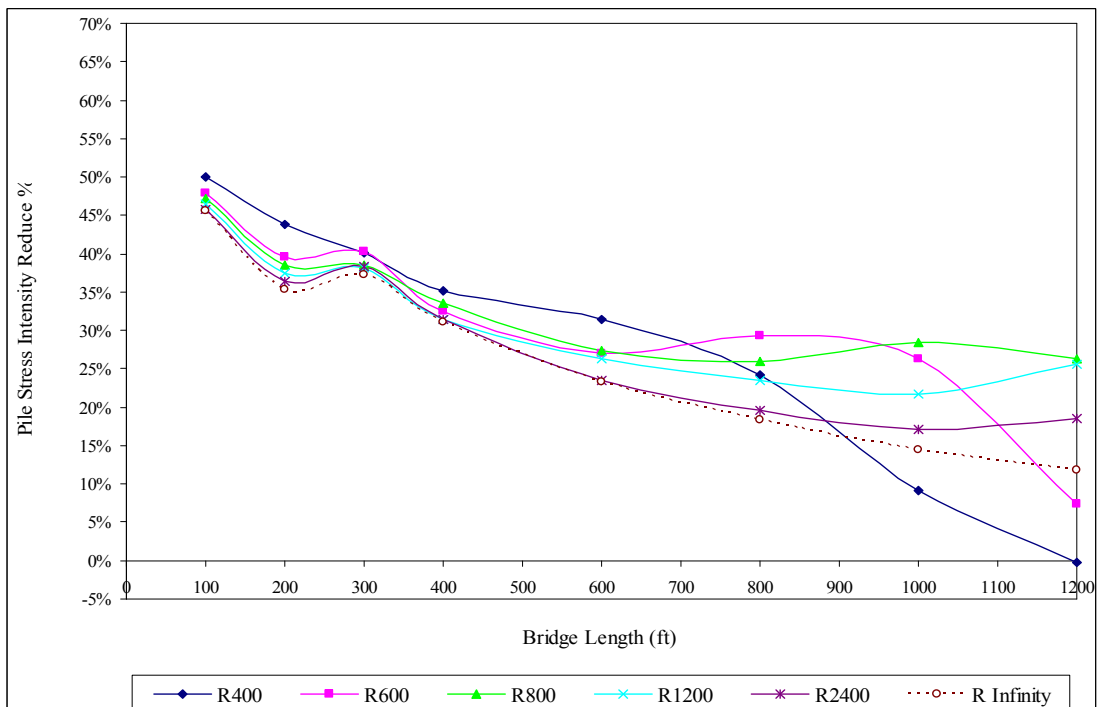


b)  $\Delta T_{\text{slab}} = 120^\circ \text{ F}$ ,  $\Delta T_{\text{the rest}} = 90^\circ \text{ F}$

**Figure 7.26 – Stress Reduction (%) of End-Bearing Piles in Very Stiff Clay Soil Profile due to the Increase in the Number of Spans**

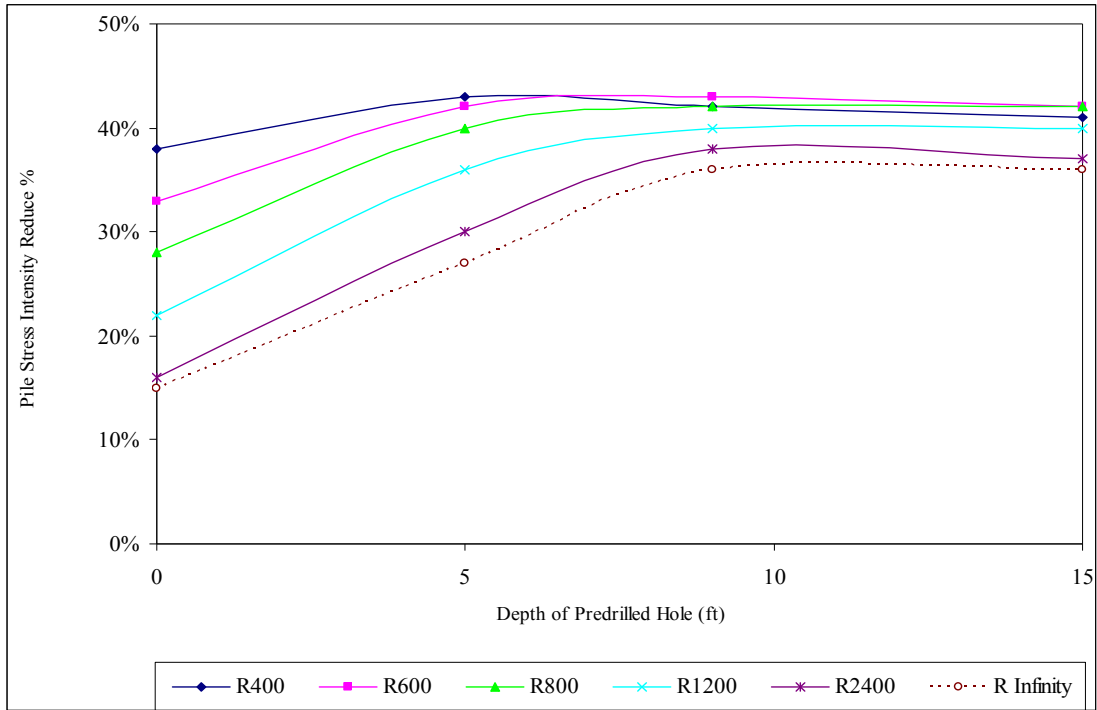


a)  $\Delta T_{\text{slab}} = 90^\circ \text{ F}$ ,  $\Delta T_{\text{the rest}} = 60^\circ \text{ F}$

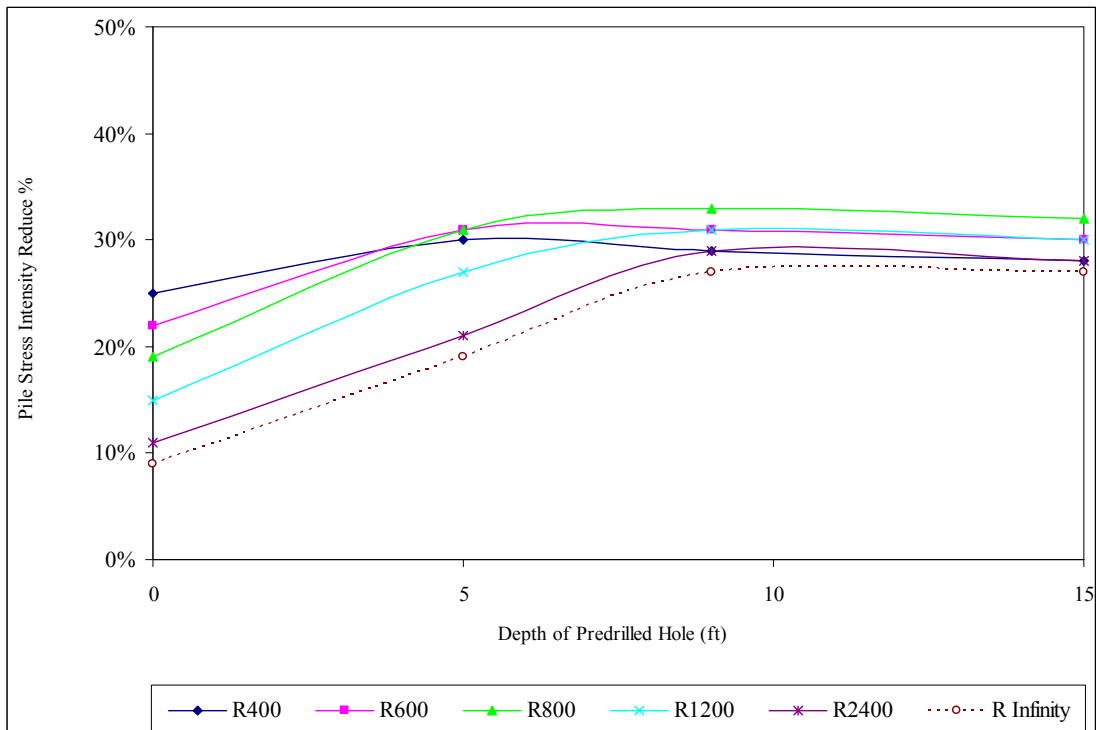


b)  $\Delta T_{\text{slab}} = 120^\circ \text{ F}$ ,  $\Delta T_{\text{the rest}} = 90^\circ \text{ F}$

**Figure 7.27 – Stress Reduction (%) of End-Bearing Piles in 9 ft Deep Predrilled Holes due to the Increase in the Number of Spans**



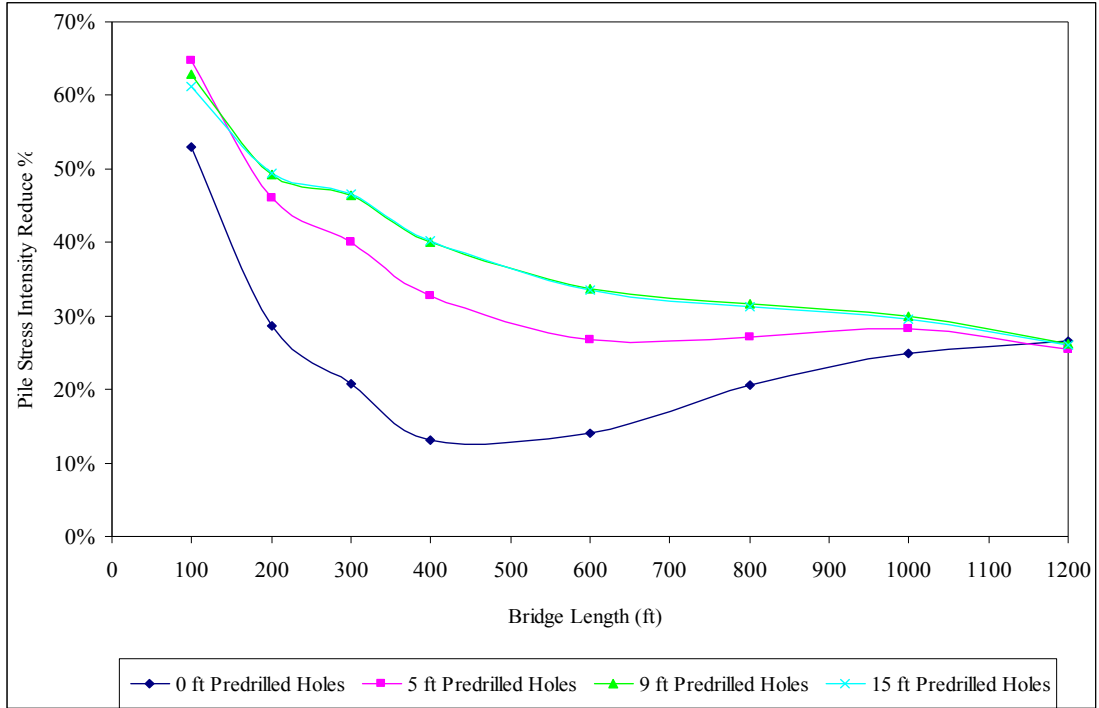
a)  $\Delta T_{\text{slab}} = 90^{\circ} \text{ F}$ ,  $\Delta T_{\text{the rest}} = 60^{\circ} \text{ F}$



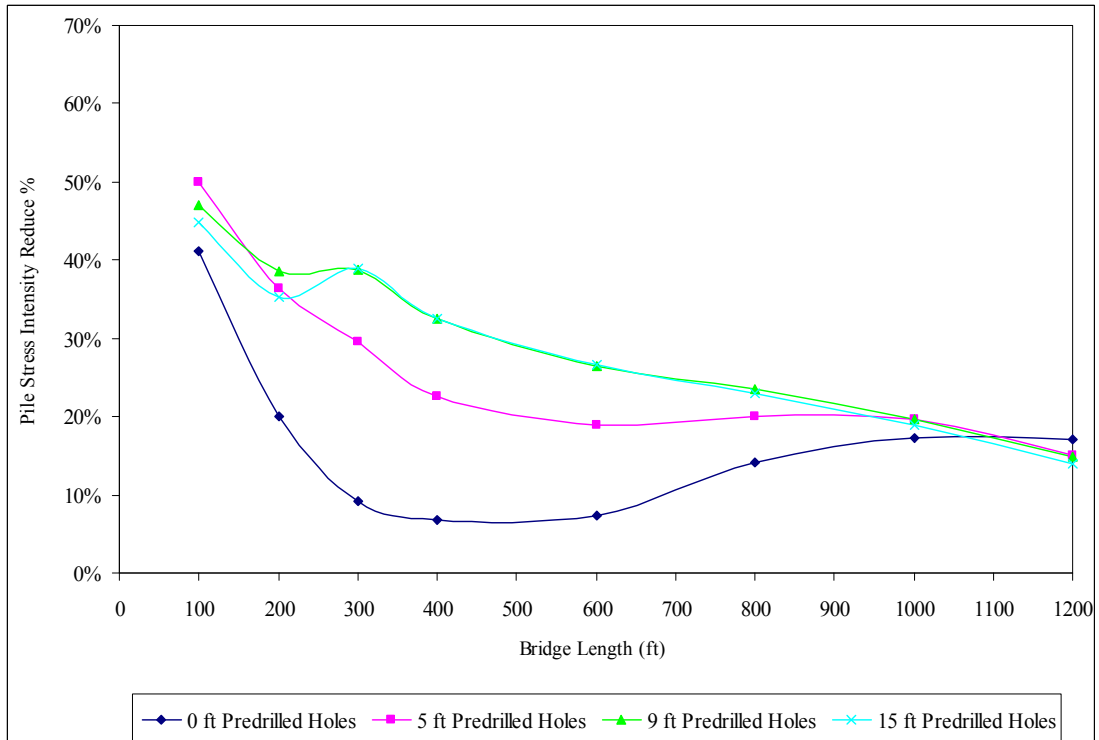
b)  $\Delta T_{\text{slab}} = 120^{\circ} \text{ F}$ ,  $\Delta T_{\text{the rest}} = 90^{\circ} \text{ F}$

**Figure 7.28 – Mean of Stress Reduction (%) of End-Bearing Piles in Various Soil Profile Types of Bridges of Different Radii due to the Increase in the Number of Spans**





a)  $\Delta T_{\text{slab}} = 90^\circ \text{F}$ ,  $\Delta T_{\text{the rest}} = 60^\circ \text{F}$



b)  $\Delta T_{\text{slab}} = 120^\circ \text{F}$ ,  $\Delta T_{\text{the rest}} = 90^\circ \text{F}$

**Figure 7.29 – Mean of Stress Reduction of End-Bearing Piles in Various Soil Profile Types due to the Increase in the Number of Spans**

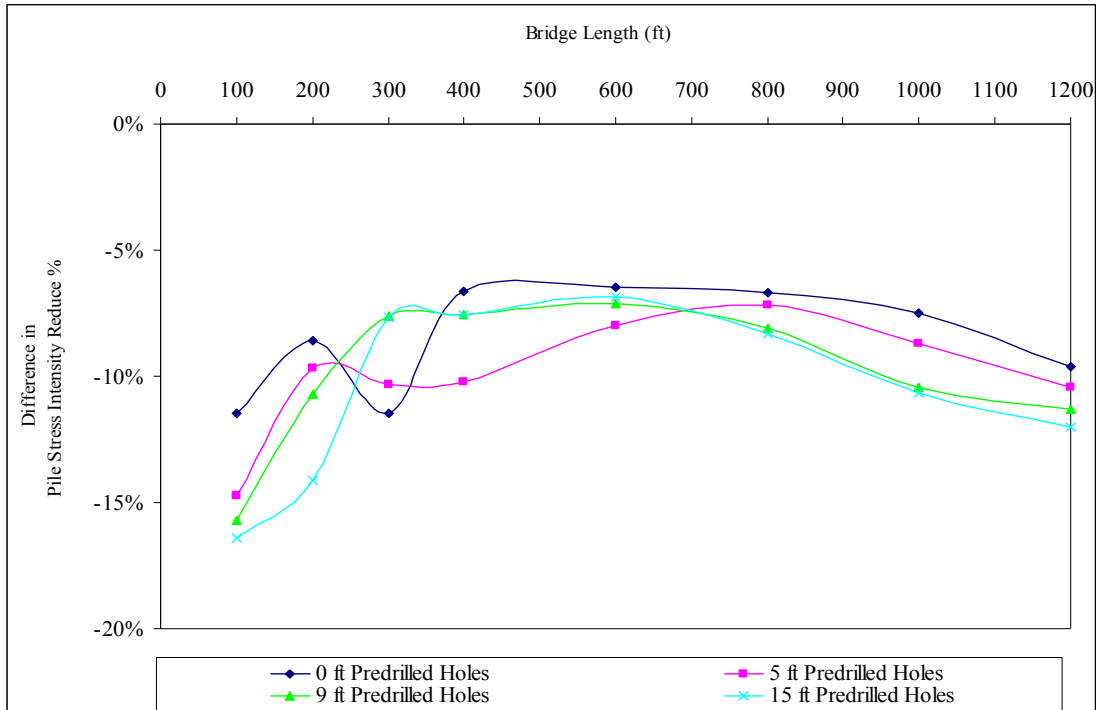


**Figure 7.30 – Difference in Stress Reduction (%) of End-Bearing Piles between  $\Delta T_{\text{slab}} = 120^\circ \text{ F}$ ,  $\Delta T_{\text{the rest}} = 90^\circ \text{ F}$  and  $\Delta T_{\text{slab}} = 90^\circ \text{ F}$ ,  $\Delta T_{\text{the rest}} = 60^\circ \text{ F}$  due to the Increase in the Number of Spans**

## 7.5 Effect of Radius Variation

The effect of radius variation on the maximum stress intensity (stress concentration) in the end-bearing piles of curved IAB's is discussed in this section. All other parameters are held constant.

### 7.5.1 Curved Integral Abutment Bridges with 50 ft Spans

Figures 7.31 to 7.35 indicate that the pile stress intensity of curved IAB's with piles in very stiff clay soil profile at two temperature levels decreases as the radius is increased for bridge lengths between 50 ft and 600 ft as indicated in Table 7.30. Curved IAB's with a smaller radius have a pile stress intensity decrease due to change in radius at a shorter bridge length range than that of curved IAB's with a larger radius.

**Table 7.30 – Stress Decrease (%) of End-Bearing Piles in Very Stiff Clay Soil Profile of Bridges with 50 ft Spans due to Change in Radius**

Radius Increase from X ft to Infinity		
Radius X (ft)	Stress Decrease (%)	Bridge Length (ft)
400	0.01 to 4.24	50 to 200
600	0.02 to 3.52	50 to 300
800	0.01 to 3.48	50 to 300
1200	0.01 to 4.06	50 to 400
2400	0.45 to 5.45	50 to 600

Beyond the lengths indicated in Table 7.30, the stress intensity in the piles starts to increase to its highest value as indicated in Table 7.31. After it reaches its

highest value, some of the pile stress intensity increase rates begin to decrease as the bridge length is increased to 1200 ft.

**Table 7.31 – Stress Increase (%) of End-Bearing Piles in Very Stiff Clay Soil Profile of Bridges with 50 ft Spans due to Change in Radius**  
 ( $\Delta T_{\text{slab}} = 90^\circ \text{ F}$ ,  $\Delta T_{\text{the rest}} = 60^\circ \text{ F}$ )

Increase Radius (ft)	400	600	800	1200	2400
To Radius (ft)					
600	66.7	-	-	-	-
800	132.6	48.3	-	-	-
1200	246.2	142.8	70.5	-	-
2400	356.2	309.1	218.0	86.5	-
Infinity	535.0	535.1	393.7	189.5	55.3

**a) Highest Pile Stress Increase (%)**

Increase Radius (ft)	400	600	800	1200	2400
To Radius (ft)					
600	600	-	-	-	-
800	800	1000	-	-	-
1200	800	1000	1200	-	-
2400	800	1200	1200	1200	-
Infinity	1200	1200	1200	1200	1200

**b) Bridge Length (ft) at Highest Pile Stress Increase**

Increase Radius (ft)	400	600	800	1200	2400
To Radius (ft)					
600	16.2	-	-	-	-
800	28.6	28.7	-	-	-
1200	119.3	119.4	70.5	-	-
2400	309.0	309.1	218.0	86.5	-
Infinity	535.0	535.1	393.7	189.5	55.3

**c) Pile Stress Increase (%) at 1200 ft Length**

For curved IAB's with piles in 9 ft deep predrilled holes filled with loose sand as shown in Figures 7.36 to 7.40, the pile stress intensity at two temperature levels decreases as the radius is increased for bridge lengths between 50 ft and 800 ft as indicated in Table 7.32. Curved IAB's with a smaller radius have a pile stress intensity decrease due to change in radius at a shorter bridge length range than that of curved IAB's with a larger radius.

**Table 7.32 – Stress Decrease (%) of End-Bearing Piles in 9 ft Deep Predrilled Holes of Bridges with 50 ft Spans due to Change in Radius**

Radius Increase from X ft to Infinity		
Radius X (ft)	Stress Decrease (%)	Bridge Length (ft)
400	0.01 to 17.01	50 to 450
600	0.01 to 11.72	50 to 600
800	0.01 to 6.60	50 to 650
1200	0.02 to 4.55	50 to 700
2400	0.01 to 3.61	50 to 800

Beyond the lengths indicated in Table 7.32, the stress intensity in the piles starts to increase to its highest value as indicated in Table 7.33. After it reaches its highest value, some of the pile stress intensity increase rates begin to decrease as the bridge length is increased to 1200 ft.

**Table 7.33 – Stress Increase (%) of End-Bearing Piles in 9 ft Deep Predrilled Holes of Bridges with 50 ft Spans due to Change in Radius**  
 ( $\Delta T_{\text{slab}} = 90^\circ \text{ F}$ ,  $\Delta T_{\text{the rest}} = 60^\circ \text{ F}$ )

Increase Radius (ft)	400	600	800	1200	2400
To Radius (ft)					
600	59.0	-	-	-	-
800	117.8	52.0	-	-	-
1200	160.8	128.0	73.6	-	-
2400	210.4	204.9	184.6	64.0	-
Infinity	291.4	290.0	273.0	114.8	31.0

**a) Highest Pile Stress Increase (%)**

Increase Radius (ft)	400	600	800	1200	2400
To Radius (ft)					
600	800	-	-	-	-
800	800	1000	-	-	-
1200	800	1000	1200	-	-
2400	1000	1000	1200	1200	-
Infinity	1200	1200	1200	1200	1200

**b) Bridge Length (ft) at Highest Pile Stress Increase**

Increase Radius (ft)	400	600	800	1200	2400
To Radius (ft)					
600	0.4	-	-	-	-
800	5.0	4.6	-	-	-
1200	82.2	81.5	73.6	-	-
2400	199.0	197.6	184.6	64.0	-
Infinity	291.4	290.0	273.0	114.8	31.0

**c) Pile Stress Increase (%) at 1200 ft Length**

Tables 7.30 and 7.32 indicate that the pile stress intensity decrease due to change in radius of curved IAB's with piles in 9 ft deep predrilled holes filled with loose sand occurs at the bridge length ranges of 200 ft to 350 ft longer than that of curved IAB's with piles without predrilled holes.

Tables 7.31 and 7.33, and Figures 7.31 to 7.40 indicate that the pile stress intensity increase due to change in radius of curved IAB's with a smaller radius range, for the most part, is less than that of curved IAB's with a larger radius range. The highest pile stress intensity increase value due to change in radius of curved IAB's from different radii to infinite radius is at a 1200 ft length. If the radius continues to increase from a radius larger than 2400 ft to infinity, the pile stress intensity increase due to change in radius will decrease until there is a relatively small increase in the pile stress intensity ( $\approx 0\%$ ).

The pile stress intensity increase due to change in radius of curved IAB's with piles in predrilled holes is less than that of curved IAB's with piles without predrilled holes. It is shown that piles in 9 feet deep predrilled holes filled with loose sand have a significant reduction in the pile stress intensity when compared with piles in 5 ft deep predrilled holes filled with loose sand. The depth increase of predrilled holes deeper than 9 ft will further reduce the stress intensity in the piles but the rate of reduction is much smaller than that of 9 ft deep predrilled holes as indicated in Table 7.34 and discussed in Section 7.3.

The pile stress intensity increase due to change in radius of curved IAB's subjected to a temperature load of  $\Delta T_{\text{slab}}$  of  $120^\circ\text{ F}$  and  $\Delta T_{\text{the rest}}$  of  $90^\circ\text{ F}$  is less than that of curved IAB's subjected to a temperature load of  $\Delta T_{\text{slab}}$  of  $90^\circ\text{ F}$  and  $\Delta T_{\text{the rest}}$

of 60° F by 1.2% to 16.6%. This is because with a temperature increase, the stress intensity increase in the piles of curved IAB's with a smaller radius is greater than that of curved IAB's with a larger radius as discussed in Section 7.2.1.

**Table 7.34 – Difference in Stress Increase (%) between End-Bearing Piles in Varying Depths of Predrilled Holes and End-Bearing Piles without Predrilled Holes of Bridges with 50 ft Spans due to Change in Radius**  
 ( $\Delta T_{\text{slab}} = 90^\circ \text{ F}$ ,  $\Delta T_{\text{the rest}} = 60^\circ \text{ F}$ )

To Radius (ft)		600	800	1200	2400	Infinity
Increase Radius (ft)	Depth of Predrilled Holes (ft)					
400	5	-24	-39	-65	-83	-102
	9	-26	-60	-104	-178	-244
	15	-25	-63	-105	-198	-278
600	5	-	-21	-36	-59	-92
	9	-	-24	-51	-111	-245
	15	-	-28	-54	-130	-280
800	5	-	-	-23	-37	-51
	9	-	-	-29	-68	-121
	15	-	-	-30	-72	-140
1200	5	-	-	-	-13	-22
	9	-	-	-	-28	-75
	15	-	-	-	-32	-84
2400	5	-	-	-	-	-6
	9	-	-	-	-	-24
	15	-	-	-	-	-28



### 7.5.2 Curved Integral Abutment Bridges with 100 ft Spans

Figures 7.41 to 7.45 indicate that the pile stress intensity of curved IAB's with piles in very stiff clay soil profile at two temperature levels decreases as the radius is increased for bridge lengths between 100 ft and 750 ft as indicated in Table 7.35.

Curved IAB's with a smaller radius have a pile stress intensity decrease due to change in radius at a shorter bridge length range than that of curved IAB's with a larger radius.

**Table 7.35 – Stress Decrease (%) of End-Bearing Piles in Very Stiff Clay Soil Profile of Bridges with 100 ft Spans due to Change in Radius**

Radius Increase from X ft to Infinity		
Radius X (ft)	Stress Decrease (%)	Bridge Length (ft)
400	1.14 to 8.01	100 to 300
600	0.16 to 6.27	100 to 350
800	1.05 to 5.41	100 to 400
1200	1.10 to 4.41	100 to 500
2400	0.83 to 4.40	100 to 750

Beyond the lengths indicated in Table 7.35, the stress intensity in the piles starts to increase to its highest value as indicated in Table 7.36. After it reaches its highest value, some of the pile stress intensity increase rates begin to decrease as the bridge length is increased to 1200 ft.

**Table 7.36 – Stress Increase (%) of End-Bearing Piles in Very Stiff Clay Soil  
Profile of Bridges with 100 ft Spans due to Change in Radius  
( $\Delta T_{\text{slab}} = 90^\circ \text{ F}$ ,  $\Delta T_{\text{the rest}} = 60^\circ \text{ F}$ )**

Increase Radius (ft)	400	600	800	1200	2400
To Radius (ft)					
600	51.1	-	-	-	-
800	67.7	38.1	-	-	-
1200	91.6	85.4	57.4	-	-
2400	166.0	155.7	121.7	40.8	-
Infinity	286.2	213.7	222.0	104.5	45.2

**a) Highest Pile Stress Increase (%)**

Increase Radius (ft)	400	600	800	1200	2400
To Radius (ft)					
600	600	-	-	-	-
800	600	1000	-	-	-
1200	600	1000	1200	-	-
2400	1200	1000	1200	1200	-
Infinity	1200	1200	1200	1200	1200

**b) Bridge Length (ft) at Highest Pile Stress Increase**

Increase Radius (ft)	400	600	800	1200	2400
To Radius (ft)					
600	23.1	-	-	-	-
800	20.0	-2.6	-	-	-
1200	88.9	53.4	57.4	-	-
2400	166.0	116.0	121.7	40.8	-
Infinity	286.2	213.7	222.0	104.5	45.2

**c) Pile Stress Increase (%) at 1200 ft Length**

For curved IAB's with piles in 9 ft deep predrilled holes filled with loose sand as shown in Figures 7.46 to 7.50, the pile stress intensity at two temperature levels decreases as the radius is increased for bridge lengths between 100 ft and 900 ft as indicated in Table 7.37. Curved IAB's with a smaller radius have a pile stress intensity decrease due to change in radius at a shorter bridge length range than that of curved IAB's with a larger radius.

**Table 7.37 – Stress Decrease (%) of End-Bearing Piles in 9 ft Deep Predrilled Holes of Bridges with 100 ft Spans due to Change in Radius**

Radius Increase from X ft to Infinity		
Radius X (ft)	Stress Decrease (%)	Bridge Length (ft)
400	3.46 to 21.70	100 to 500
600	1.53 to 16.82	100 to 650
800	1.44 to 11.70	100 to 700
1200	1.37 to 8.11	100 to 800
2400	0.21 to 4.24	100 to 900

Beyond the lengths indicated in Table 7.37, the stress intensity in the piles starts to increase to its highest value as indicated in Table 7.38. After it reaches its highest value, some of the pile stress intensity increase rates begin to decrease as the bridge length is increased to 1200 ft.

**Table 7.38 – Stress Increase (%) of End-Bearing Piles in 9 ft Deep Predrilled Holes of Bridges with 100 ft Spans due to Change in Radius**  
 ( $\Delta T_{\text{slab}} = 90^\circ \text{ F}$ ,  $\Delta T_{\text{the rest}} = 60^\circ \text{ F}$ )

Increase Radius (ft)	400	600	800	1200	2400
To Radius (ft)					
600	48.8	-	-	-	-
800	92.1	39.2	-	-	-
1200	129.5	93.1	57.0	-	-
2400	222.9	183.0	130.7	47.0	-
Infinity	288.0	240.0	177.2	76.6	20.2

**a) Highest Pile Stress Increase (%)**

Increase Radius (ft)	400	600	800	1200	2400
To Radius (ft)					
600	800	-	-	-	-
800	800	1000	-	-	-
1200	1000	1000	1200	-	-
2400	1200	1200	1200	1200	-
Infinity	1200	1200	1200	1200	1200

**b) Bridge Length (ft) at Highest Pile Stress Increase**

Increase Radius (ft)	400	600	800	1200	2400
To Radius (ft)					
600	14.1	-	-	-	-
800	40.0	22.6	-	-	-
1200	120.0	92.5	57.0	-	-
2400	222.9	183.0	130.7	47.0	-
Infinity	288.0	240.0	177.2	76.6	20.2

**c) Pile Stress Increase (%) at 1200 ft Length**

Tables 7.35 and 7.37 indicate that the pile stress intensity decrease due to change in radius of curved IAB's with piles in 9 ft deep predrilled holes filled with loose sand occurs at the bridge length ranges of 200 ft to 300 ft longer than that of curved IAB's with piles without predrilled holes.

Tables 7.36 and 7.38, and Figures 7.41 to 7.50 indicate that the pile stress intensity increase due to change in radius of curved IAB's with a smaller radius range, for the most part, is less than that of curved IAB's with a larger radius range. The highest pile stress intensity increase value due to change in radius of curved IAB's from different radii to infinite radius is at a 1200 ft length. If the radius continues to increase from a radius larger than 2400 ft to infinity, the pile stress intensity increase due to change in radius will decrease until there is a relatively small increase in the pile stress intensity ( $\approx 0\%$ ).

The pile stress intensity increase due to change in radius of curved IAB's with piles in predrilled holes is less than that of curved IAB's with piles without predrilled holes. It is shown that piles in 9 feet deep predrilled holes filled with loose sand have a significant reduction in the pile stress intensity when compared with piles in 5 ft deep predrilled holes filled with loose sand. The depth increase of predrilled holes deeper than 9 ft will further reduce the stress intensity in the piles, but the rate of reduction is much smaller than that of 9 ft deep predrilled holes as indicated in Table 7.39 and discussed in Section 7.3.

The pile stress intensity increase due to change in radius of curved IAB's subjected to a temperature load of  $\Delta T_{\text{slab}}$  of 120° F and  $\Delta T_{\text{the rest}}$  of 90° F is greater than that of curved IAB's subjected to a temperature load of  $\Delta T_{\text{slab}}$  of 90° F and

$\Delta T_{\text{the rest}}$  of 60° F by 0.3% to 8.7%. This is because with a temperature increase, the stress intensity increase in the piles of curved IAB's with a larger radius is greater than that of curved IAB's with a smaller radius as discussed in Section 7.2.2.

**Table 7.39 – Difference in Stress Increase (%) between End-Bearing Piles in Varying Depths of Predrilled Holes and End-Bearing Piles without Predrilled Holes of Bridges with 100 ft Spans due to Change in Radius**  
 ( $\Delta T_{\text{slab}} = 90^\circ \text{ F}$ ,  $\Delta T_{\text{the rest}} = 60^\circ \text{ F}$ )

To Radius (ft)		600	800	1200	2400	Infinity
Increase Radius (ft)	Depth of Predrilled Holes (ft)					
400	5	-15	-25	-40	-64	-62
	9	-15	-25	-54	-74	-71
	15	-16	-27	-57	-77	-73
600	5	-	-10	-23	-40	-42
	9	-	-9	-26	-47	-55
	15	-	-9	-27	-51	-65
800	5	-	-	-17	-32	-33
	9	-	-	-18	-33	-45
	15	-	-	-18	-35	-58
1200	5	-	-	-	-21	-27
	9	-	-	-	-24	-35
	15	-	-	-	-25	-37
2400	5	-	-	-	-	-15
	9	-	-	-	-	-25
	15	-	-	-	-	-27

### 7.5.3 Conclusions

The following conclusions are drawn from the study of the effect of radius variation on the maximum stress intensity (stress concentration) in the piles of curved IAB's investigated in this section:

1. The pile stress intensity of curved IAB's with both 50 ft and 100 ft spans and with piles in very stiff clay soil profile decreases as the radius is increased at bridge lengths between 50 ft and 750 ft. Beyond these lengths, the pile stress intensity starts to increase as the radius is increased.
2. Curved IAB's with piles in predrilled holes have a pile stress intensity decrease due to change in radius occurring at the bridge length ranges of 200 ft to 350 ft longer than that of curved IAB's with piles without predrilled holes.
3. Curved IAB's with a smaller radius have a pile stress intensity decrease due to change in radius at a shorter bridge length range than that of curved IAB's with a larger radius.
4. Curved IAB's with a smaller radius range, for the most part, have a pile stress intensity increase due to change in radius less than that of curved IAB's with a larger radius range.
5. The highest pile stress intensity increase value due to change in radius of curved IAB's from different radii to infinite radius is at a 1200 ft length.

6. If the radius continues to increase from a radius larger than 2400 ft to infinity, the pile stress intensity increase due to change in radius will decrease until there is a relatively small increase in the pile stress intensity ( $\approx 0\%$ ).
7. The introduction of predrilled holes can reduce the pile stress intensity increase due to change in radius of curved IAB's. It is shown that piles in 9 feet deep predrilled holes filled with loose sand have a significant reduction in the pile stress intensity when compared with piles in 5 ft deep predrilled holes filled with loose sand. The depth increase of predrilled holes deeper than 9 ft will further reduce the stress intensity in the piles, but the rate of reduction is much smaller than that of 9 ft deep predrilled holes.
8. Curved IAB's with 50 ft spans have a pile stress intensity increase due to change in radius greater than that of curved IAB's with 100 ft spans in the range of 0% to the maximum value indicated in Table 7.40. This is due to the maximum stress intensity in the piles of curved IAB's with 100 ft spans of different radii is closer than that of curved IAB's of different radii with 50 ft spans. This results in a smaller stress intensity increase in the piles when the radius increases, as shown in Figures 7.2 to 7.9 in Section 7.1.
9. A temperature increase results in a lower pile stress intensity increase in curved IAB's with 50 ft spans due to change in radius. For curved



IAB's with 100 ft spans, a temperature increase results in a higher pile stress intensity increase due to change in radius.

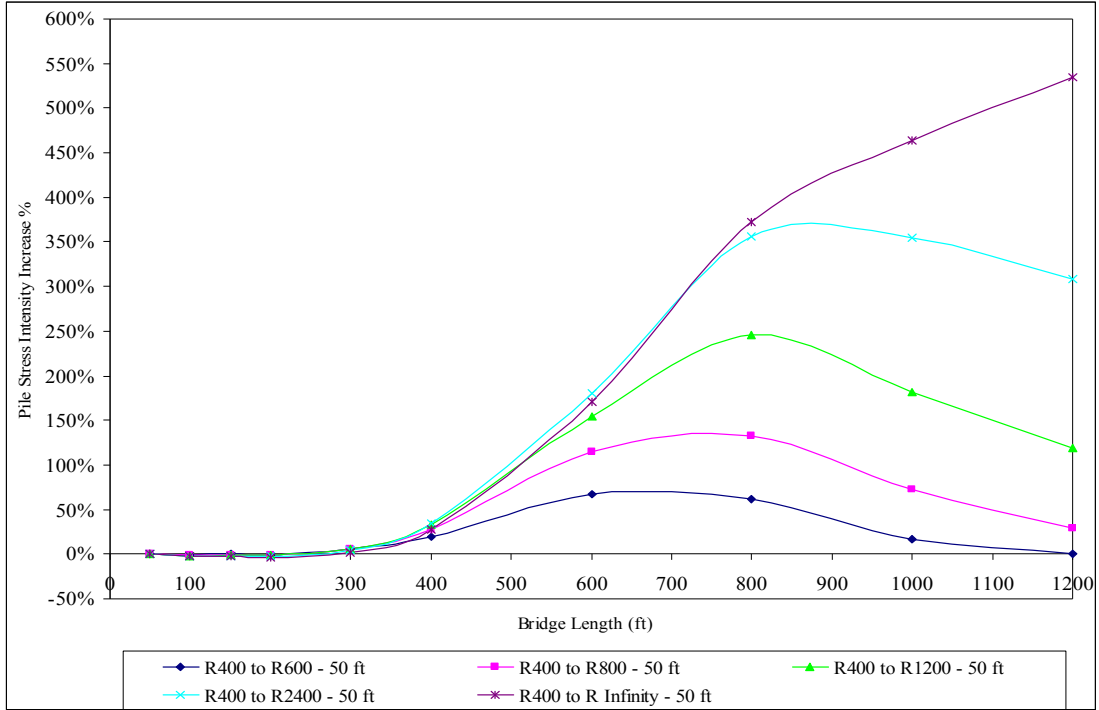
**Table 7.40 – Difference in Stress Increase (%) of End-Bearing Piles between Bridges with 50 ft and 100 ft Spans due to Change in Radius**  
 ( $\Delta T_{\text{slab}} = 90^\circ \text{ F}$ ,  $\Delta T_{\text{the rest}} = 60^\circ \text{ F}$ )

Increase Radius (ft)	400	600	800	1200	2400
To Radius (ft)					
600	45.8	-	-	-	-
800	80.4	31.2	-	-	-
1200	164.9	66.0	29.8	-	-
2400	227.5	193.1	96.3	45.7	-
Infinity	293.7	321.4	171.7	85.1	10.0

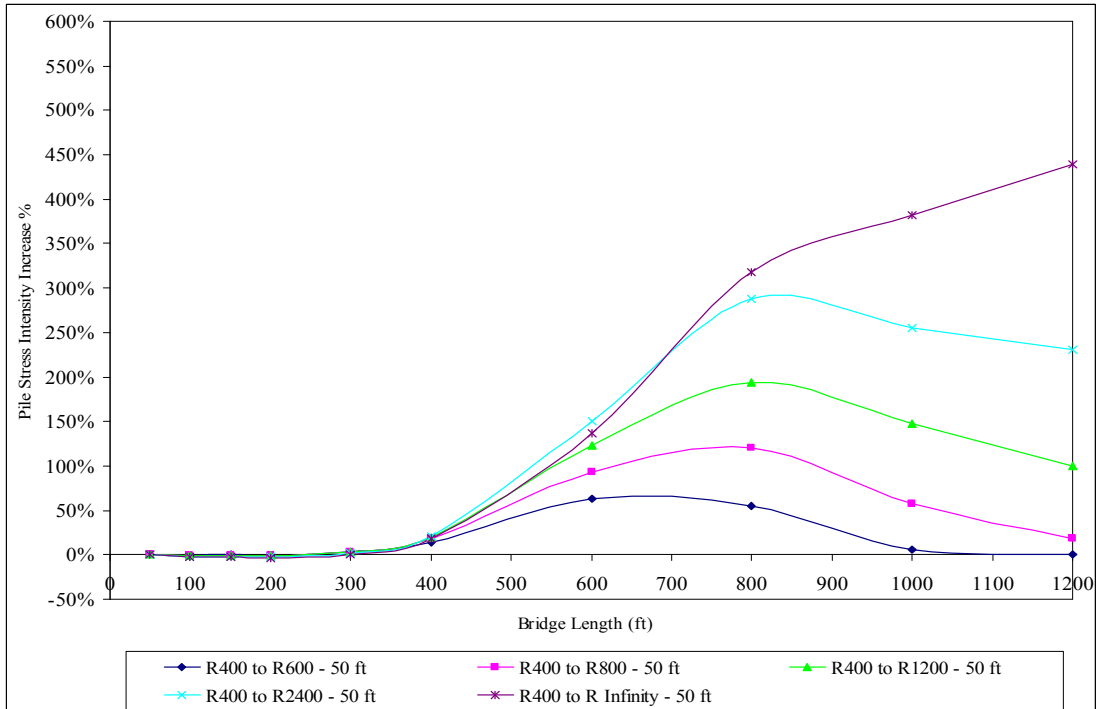
**a) Very Stiff Clay Soil Profile**

Increase Radius (ft)	400	600	800	1200	2400
To Radius (ft)					
600	10.2	-	-	-	-
800	25.7	12.7	-	-	-
1200	39.3	34.9	16.6	-	-
2400	52.7	67.6	53.9	17.0	-
Infinity	57.6	83.2	95.7	38.2	10.9

**b) Very Stiff Clay Soil Profile with 9 ft Deep Predrilled Holes Filled with Loose Sand**

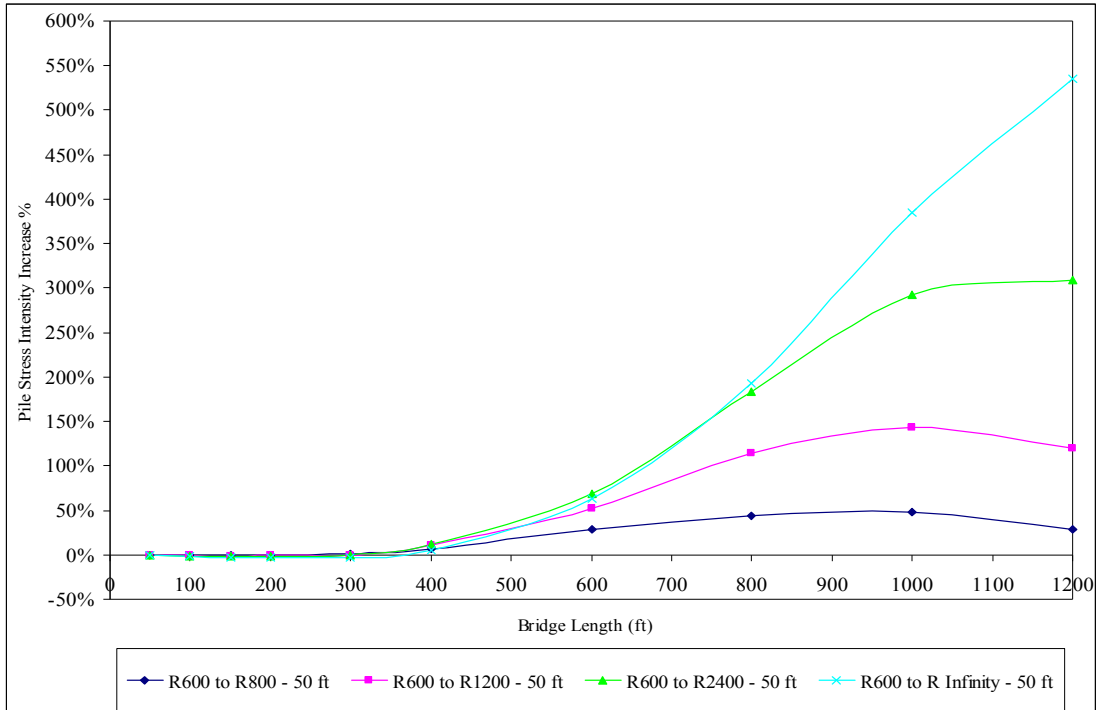


a)  $\Delta T_{\text{slab}} = 90^\circ \text{ F}$ ,  $\Delta T_{\text{the rest}} = 60^\circ \text{ F}$

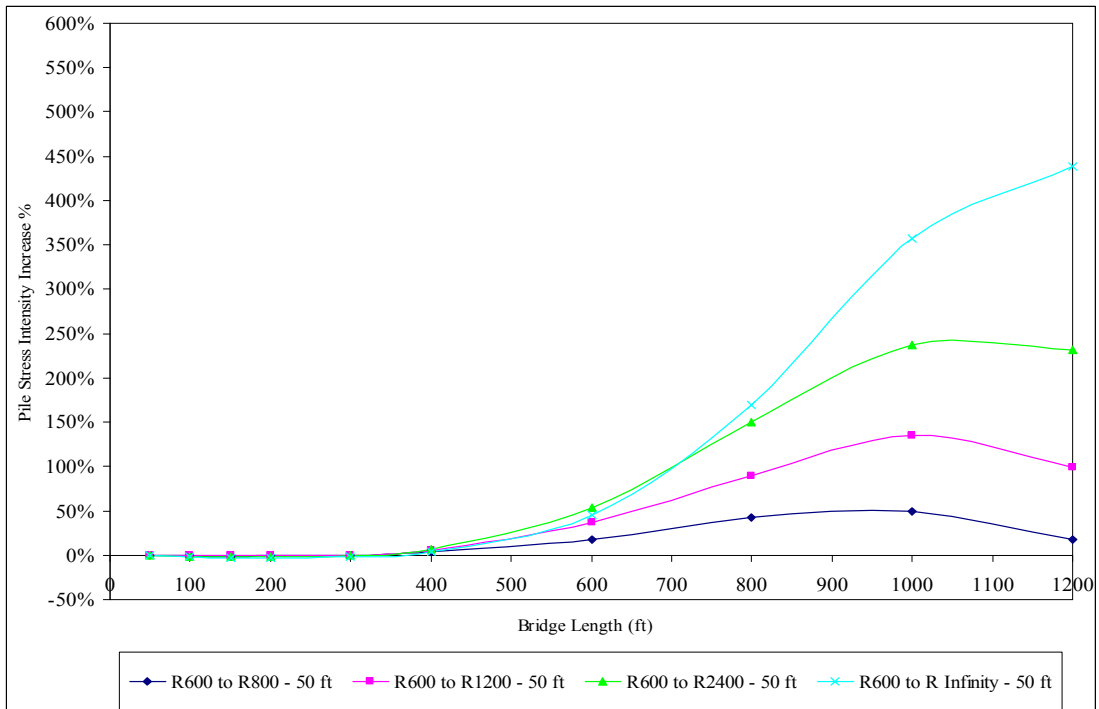


b)  $\Delta T_{\text{slab}} = 120^\circ \text{ F}$ ,  $\Delta T_{\text{the rest}} = 90^\circ \text{ F}$

**Figure 7.31 – Stress Increase (%) of End-Bearing Piles in Very Stiff Clay Soil Profile of Bridges with 50 ft Spans due to Change in Radius from 400 ft to a Larger Radius**

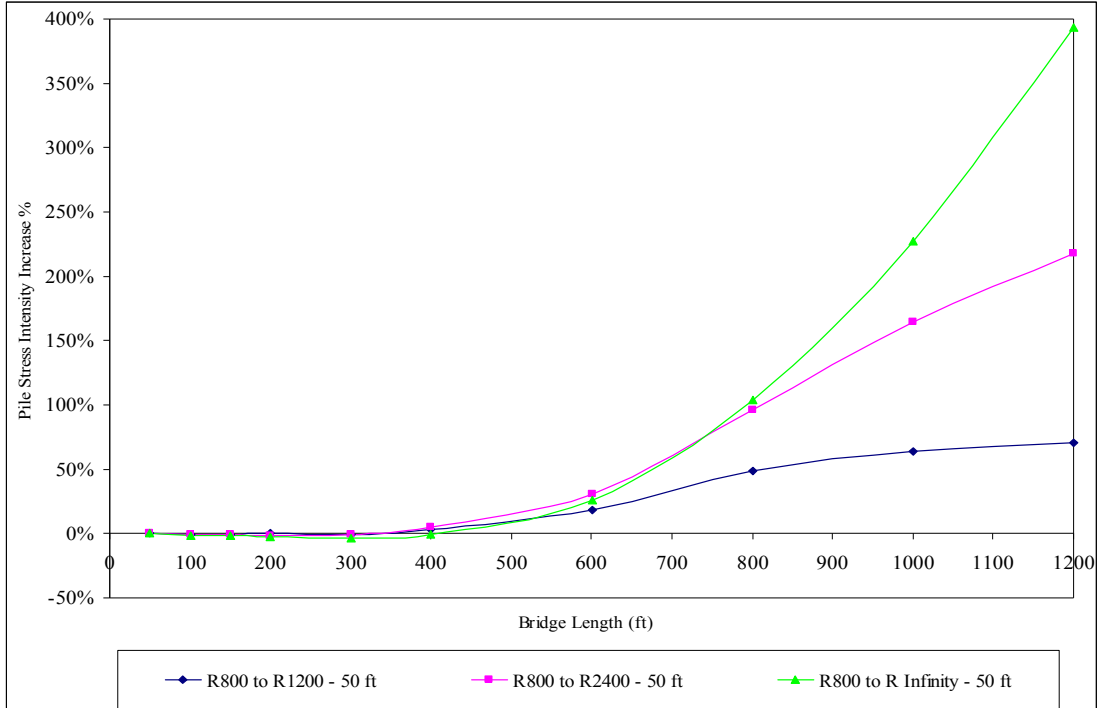


a)  $\Delta T_{\text{slab}} = 90^\circ \text{ F}, \Delta T_{\text{the rest}} = 60^\circ \text{ F}$

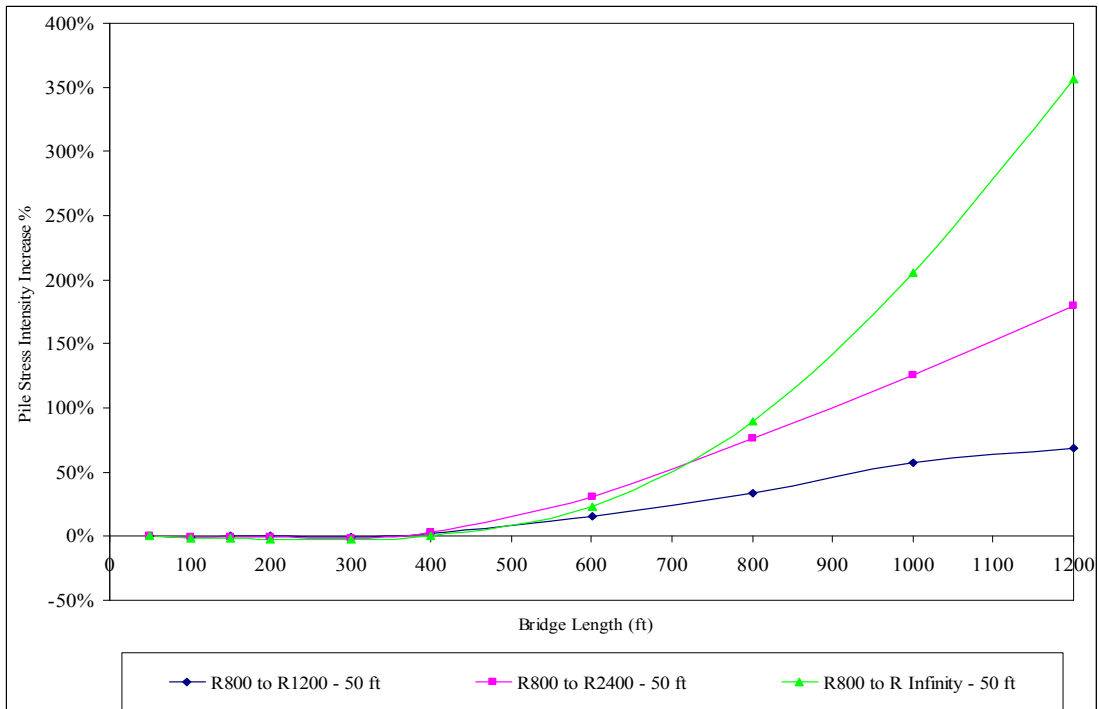


b)  $\Delta T_{\text{slab}} = 120^\circ \text{ F}, \Delta T_{\text{the rest}} = 90^\circ \text{ F}$

**Figure 7.32 – Stress Increase (%) of End-Bearing Piles in Very Stiff Clay Soil Profile of Bridges with 50 ft Spans due to Change in Radius from 600 ft to a Larger Radius**

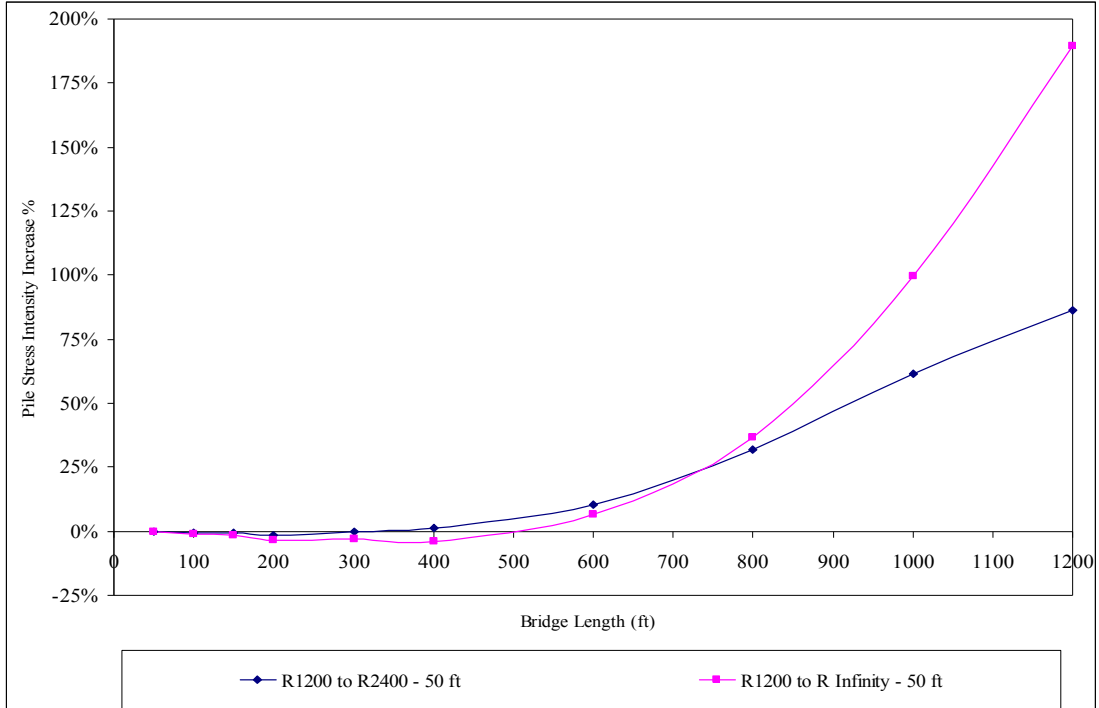


a)  $\Delta T_{\text{slab}} = 90^\circ \text{ F}$ ,  $\Delta T_{\text{the rest}} = 60^\circ \text{ F}$

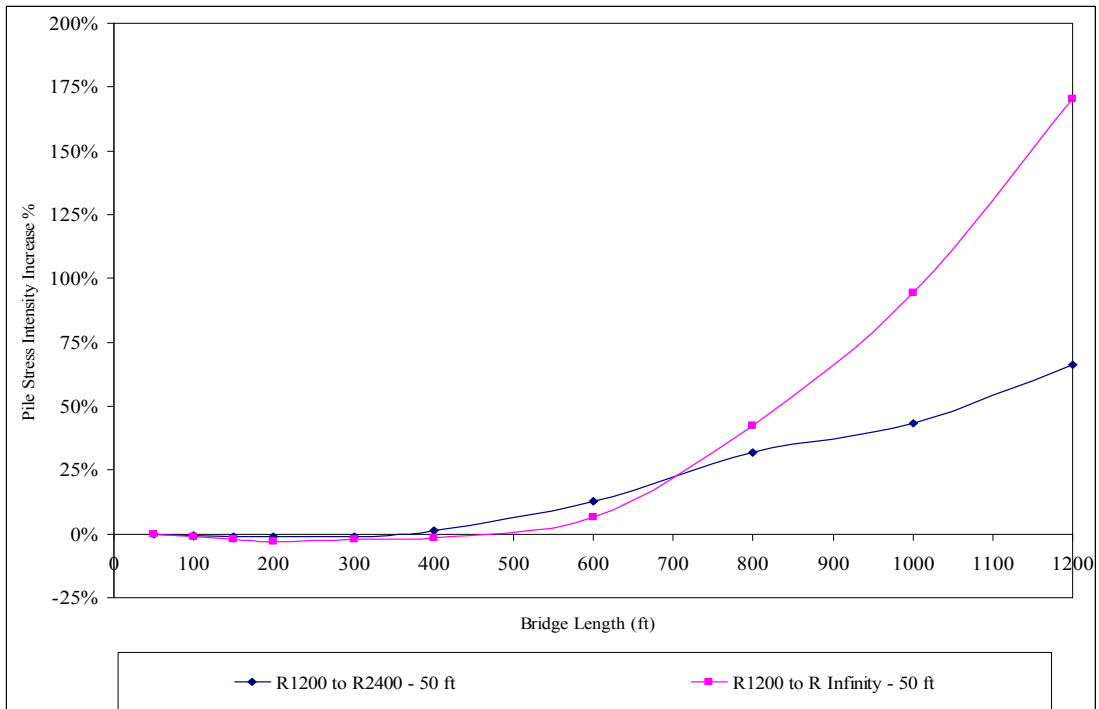


b)  $\Delta T_{\text{slab}} = 120^\circ \text{ F}$ ,  $\Delta T_{\text{the rest}} = 90^\circ \text{ F}$

**Figure 7.33 – Stress Increase (%) of End-Bearing Piles in Very Stiff Clay Soil Profile of Bridges with 50 ft Spans due to Change in Radius from 800 ft to a Larger Radius**

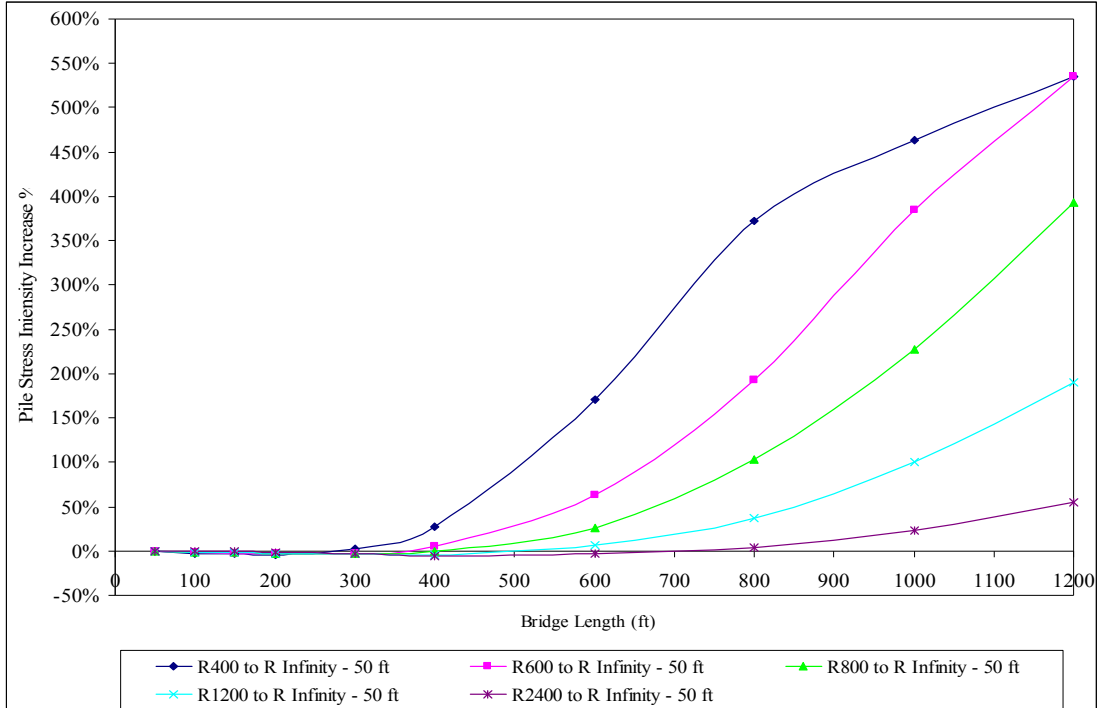


a)  $\Delta T_{\text{slab}} = 90^\circ \text{ F}$ ,  $\Delta T_{\text{the rest}} = 60^\circ \text{ F}$

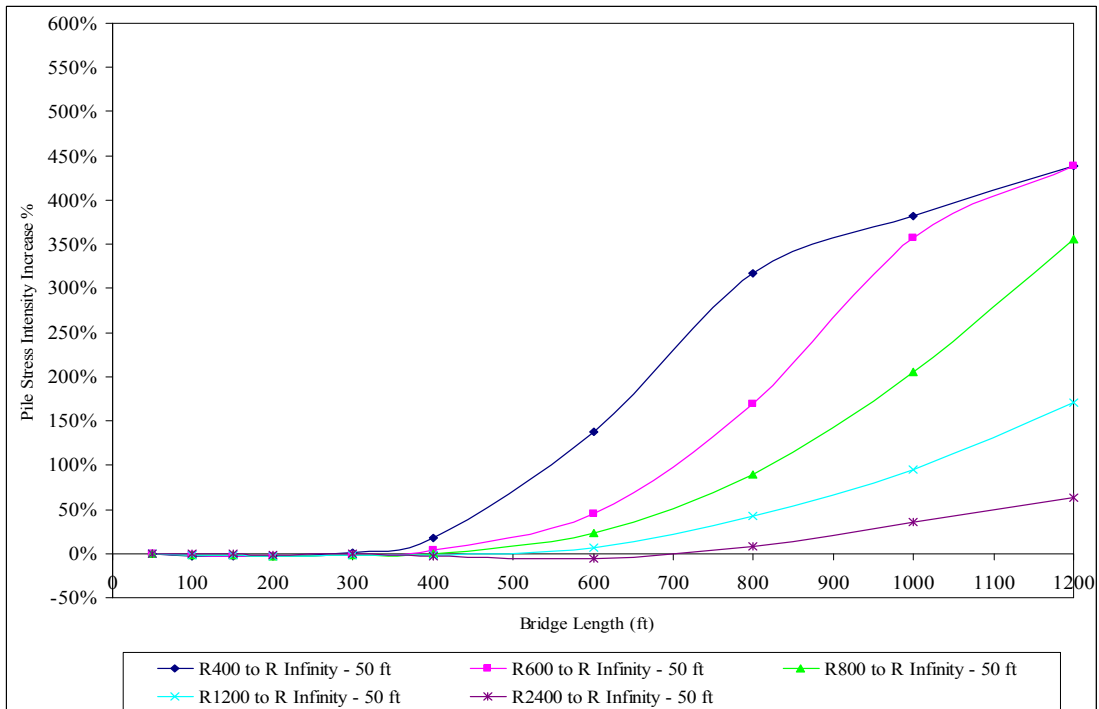


b)  $\Delta T_{\text{slab}} = 120^\circ \text{ F}$ ,  $\Delta T_{\text{the rest}} = 90^\circ \text{ F}$

**Figure 7.34 – Stress Increase (%) of End-Bearing Piles in Very Stiff Clay Soil Profile of Bridges with 50 ft Spans due to Change in Radius from 1200 ft to a Larger Radius**

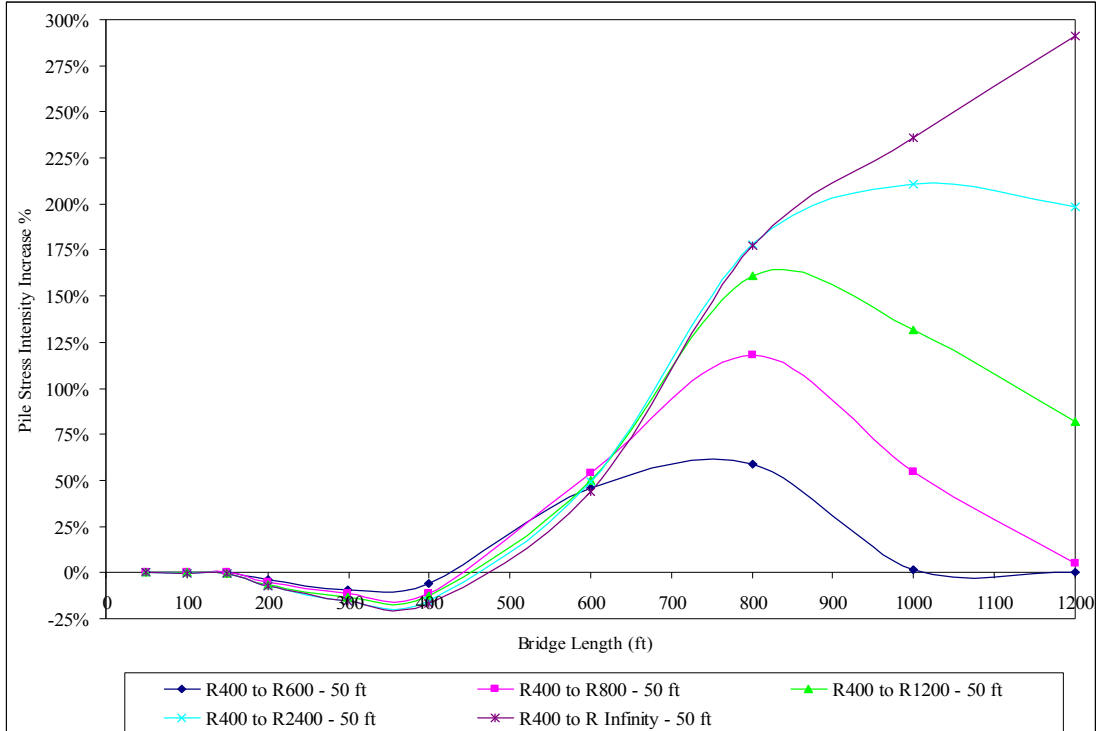


a)  $\Delta T_{\text{slab}} = 90^\circ \text{ F}$ ,  $\Delta T_{\text{the rest}} = 60^\circ \text{ F}$

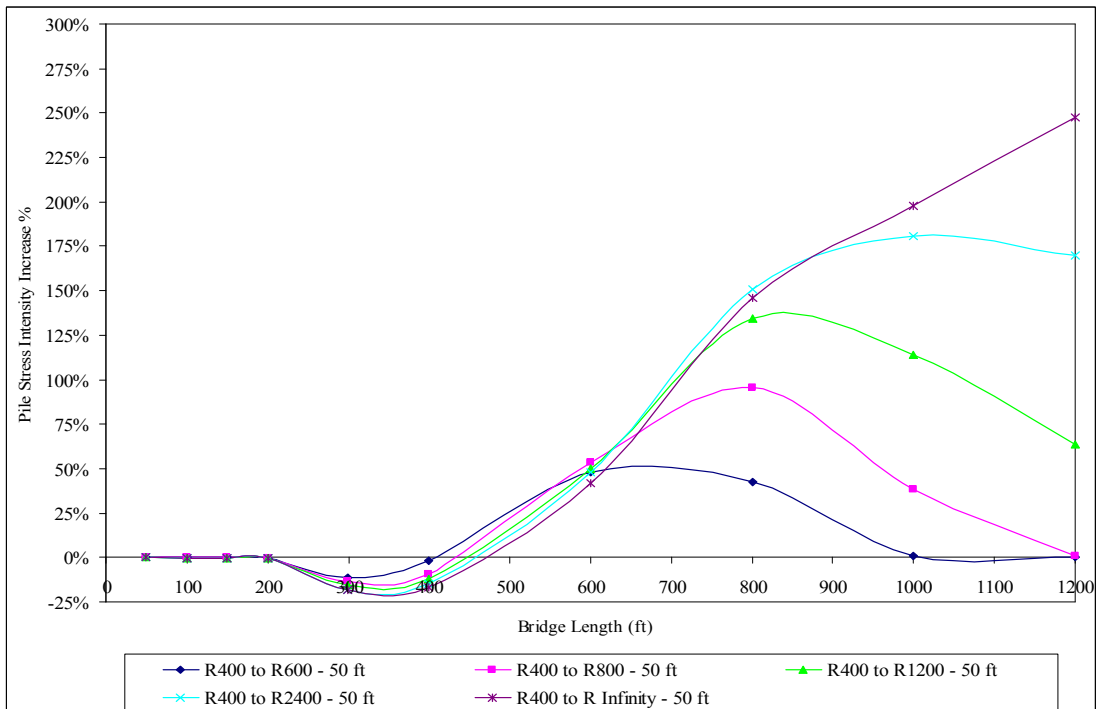


b)  $\Delta T_{\text{slab}} = 120^\circ \text{ F}$ ,  $\Delta T_{\text{the rest}} = 90^\circ \text{ F}$

**Figure 7.35 – Stress Increase (%) of End-Bearing Piles in Very Stiff Clay Soil Profile of Bridges with 50 ft Spans due to Change in Radius from Different Values to Infinity**

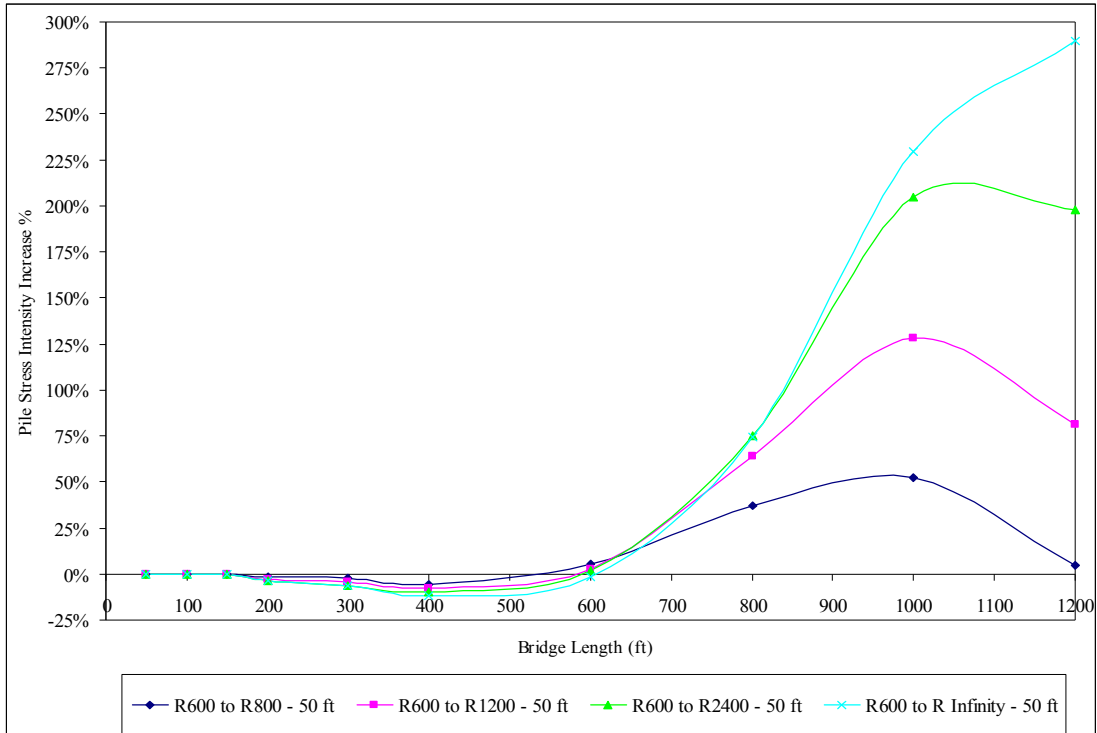


a)  $\Delta T_{\text{slab}} = 90^\circ \text{ F}$ ,  $\Delta T_{\text{the rest}} = 60^\circ \text{ F}$

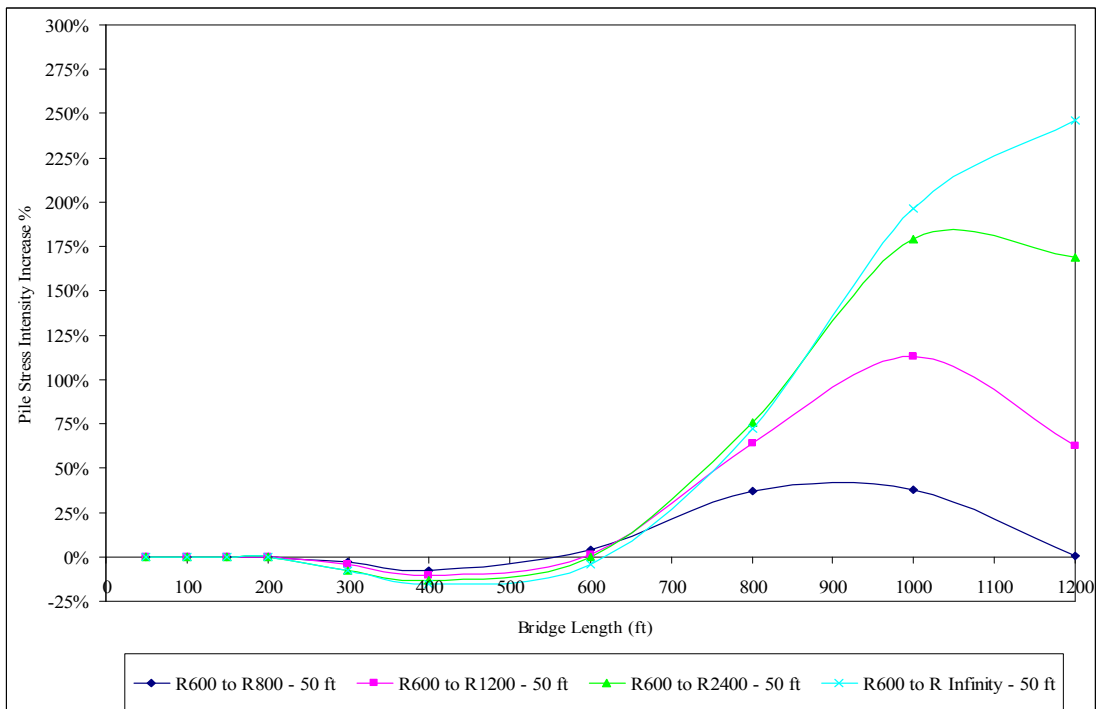


b)  $\Delta T_{\text{slab}} = 120^\circ \text{ F}$ ,  $\Delta T_{\text{the rest}} = 90^\circ \text{ F}$

**Figure 7.36 – Stress Increase (%) of End-Bearing Piles in 9 ft Deep Predrilled Holes of Bridges with 50 ft Spans due to Change in Radius from 400 ft to a Larger Radius**



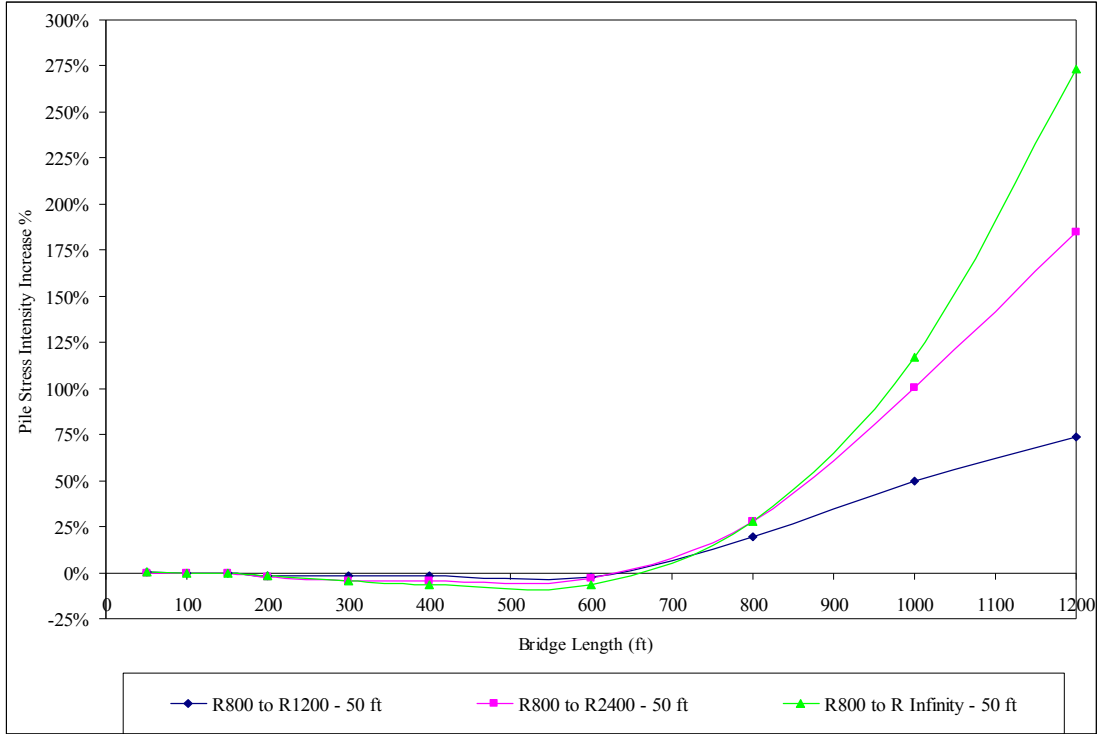
a)  $\Delta T_{\text{slab}} = 90^\circ \text{ F}$ ,  $\Delta T_{\text{the rest}} = 60^\circ \text{ F}$



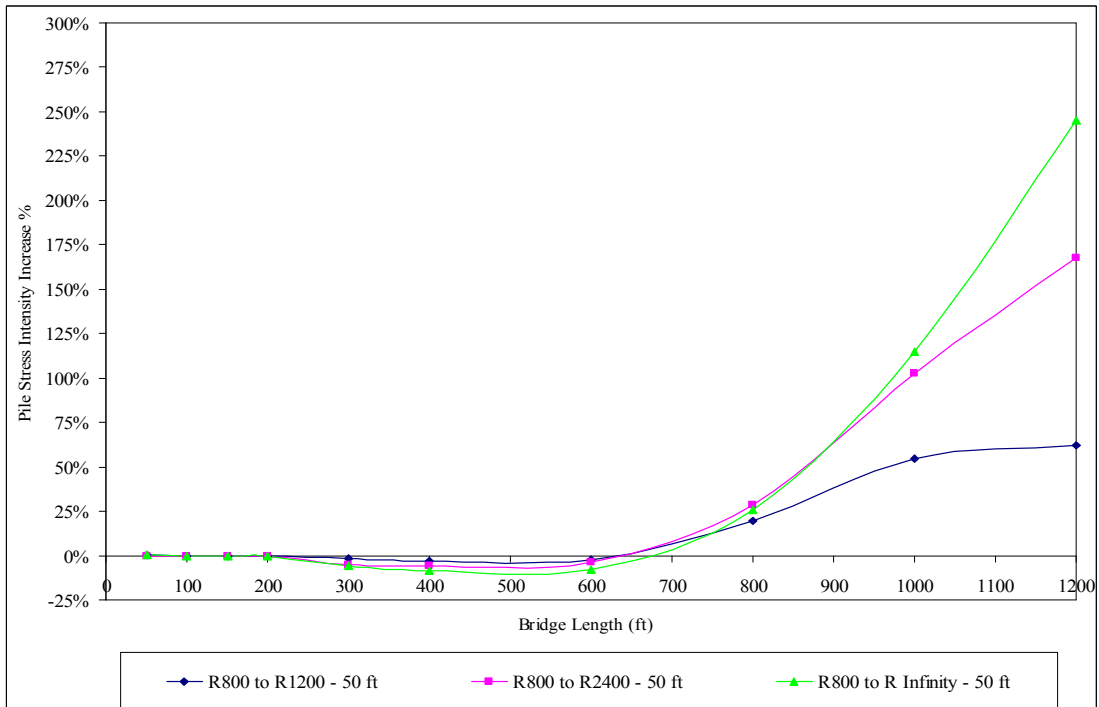
b)  $\Delta T_{\text{slab}} = 120^\circ \text{ F}$ ,  $\Delta T_{\text{the rest}} = 90^\circ \text{ F}$

**Figure 7.37 – Stress Increase (%) of End-Bearing Piles in 9 ft Deep Predrilled Holes of Bridges with 50 ft Spans due to Change in Radius from 600 ft to a Larger Radius**



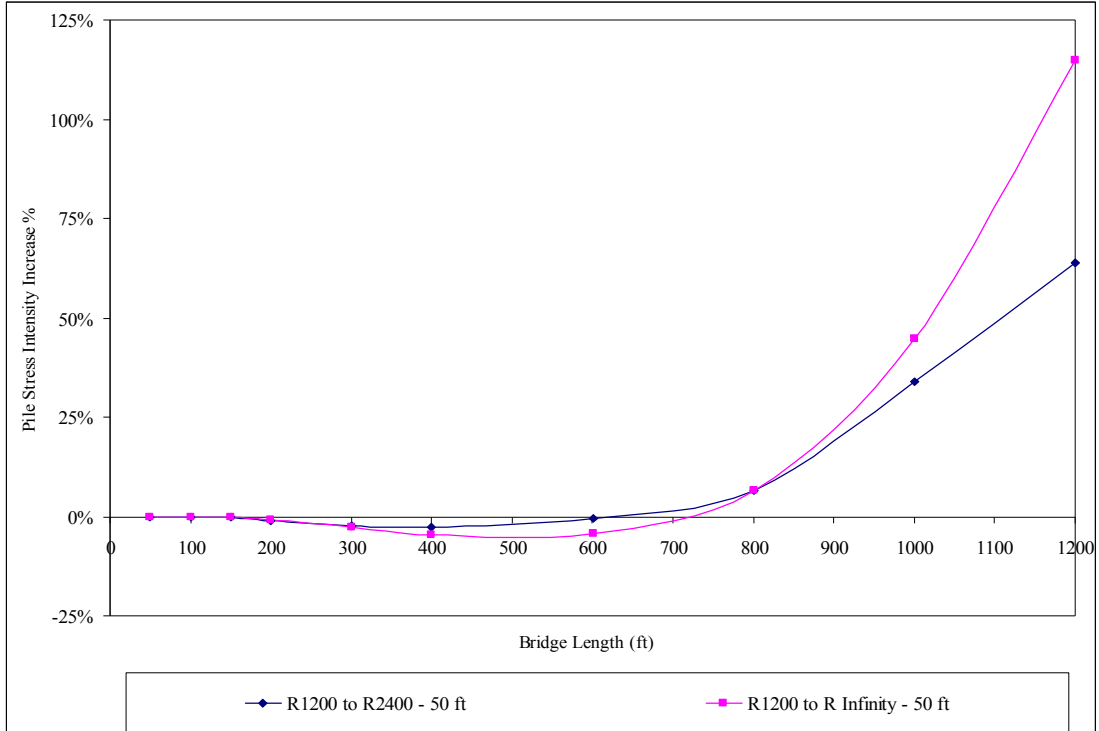


a)  $\Delta T_{\text{slab}} = 90^\circ \text{ F}, \Delta T_{\text{the rest}} = 60^\circ \text{ F}$

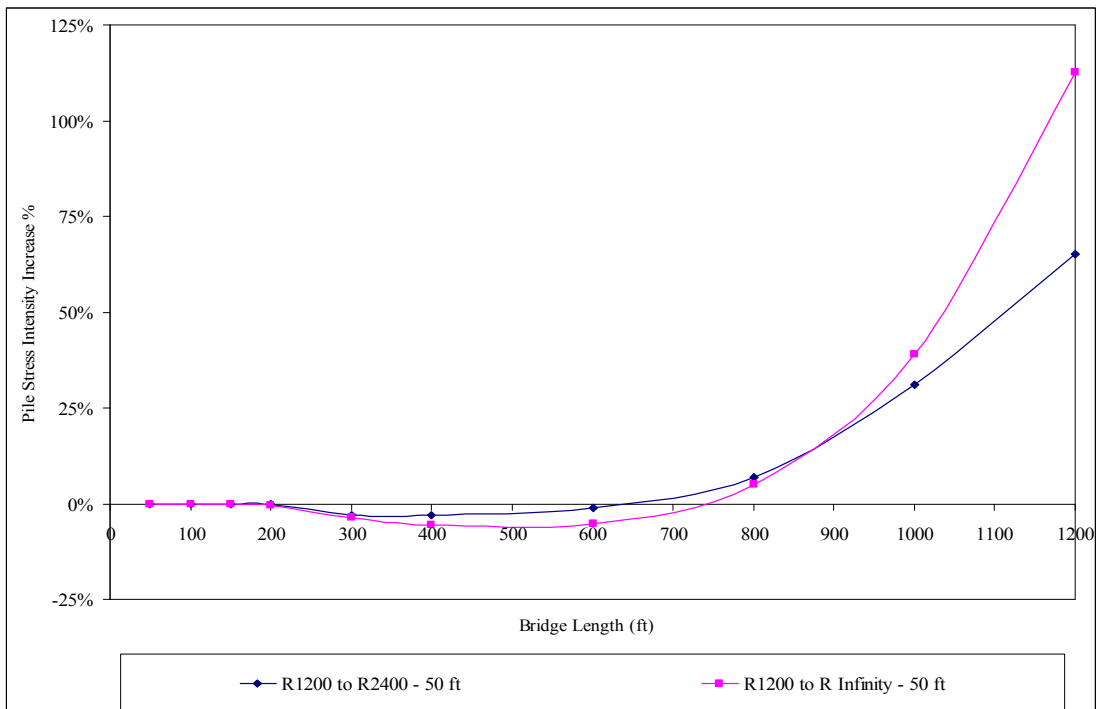


b)  $\Delta T_{\text{slab}} = 120^\circ \text{ F}, \Delta T_{\text{the rest}} = 90^\circ \text{ F}$

**Figure 7.38 – Stress Increase (%) of End-Bearing Piles in 9 ft Deep Predrilled Holes of Bridges with 50 ft Spans due to Change in Radius from 800 ft to a Larger Radius**

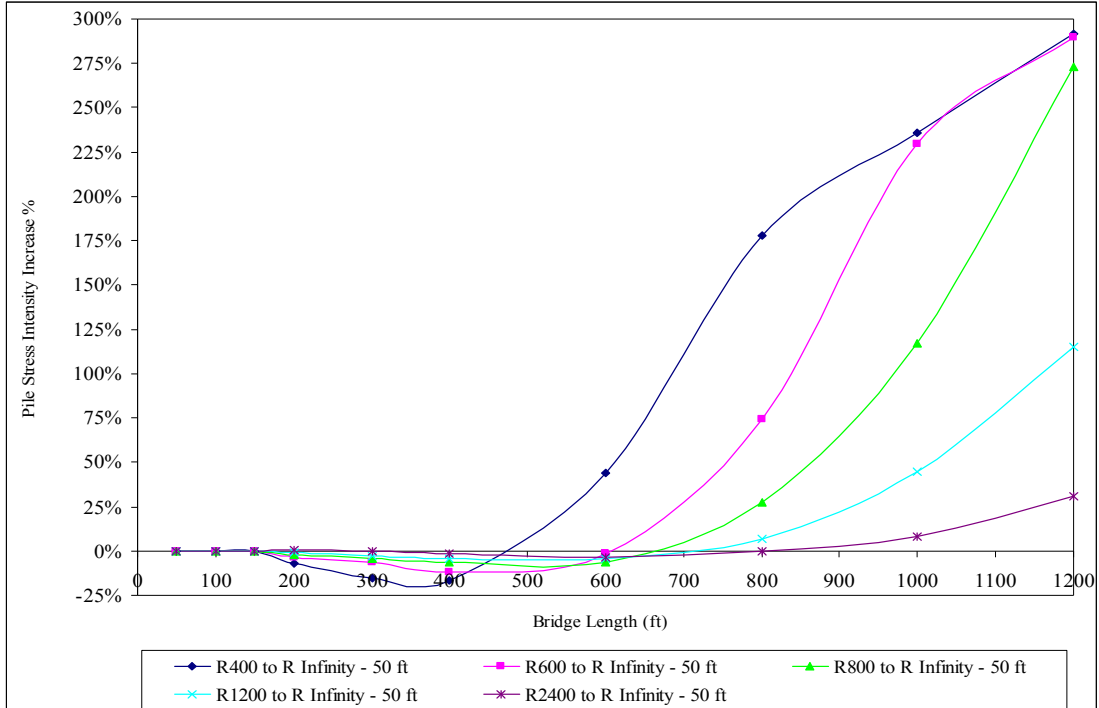


a)  $\Delta T_{\text{slab}} = 90^\circ \text{ F}$ ,  $\Delta T_{\text{the rest}} = 60^\circ \text{ F}$

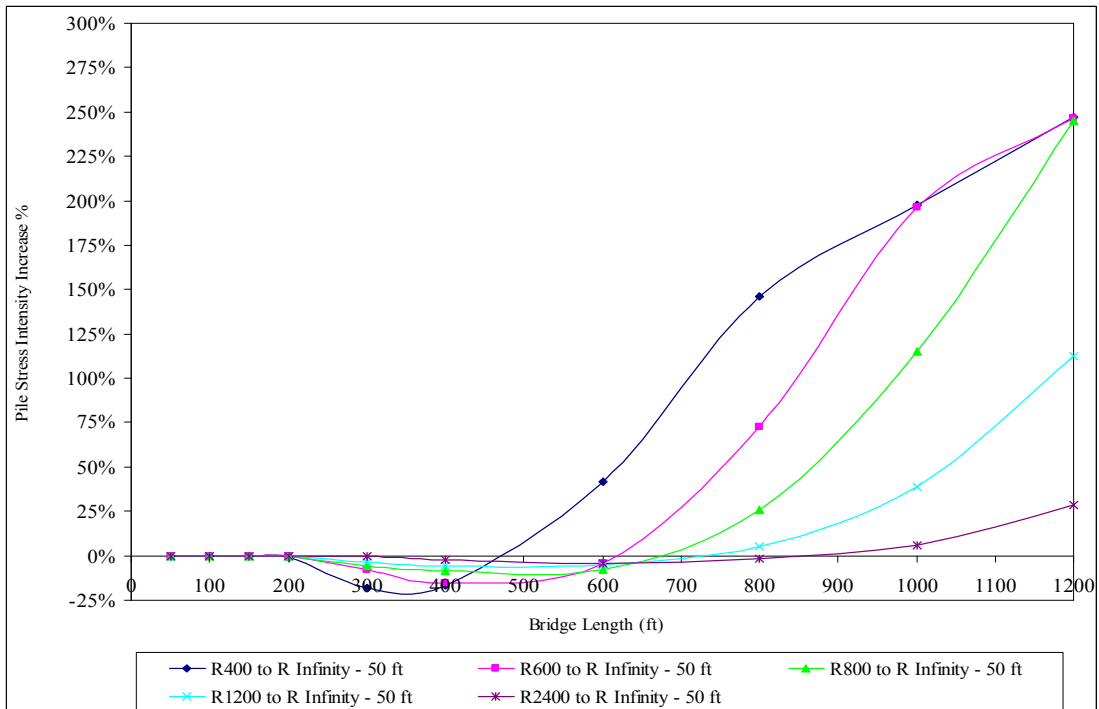


b)  $\Delta T_{\text{slab}} = 120^\circ \text{ F}$ ,  $\Delta T_{\text{the rest}} = 90^\circ \text{ F}$

**Figure 7.39 – Stress Increase (%) of End-Bearing Piles in 9 ft Deep Predrilled Holes of Bridges with 50 ft Spans due to Change in Radius from 1200 ft to a Larger Radius**

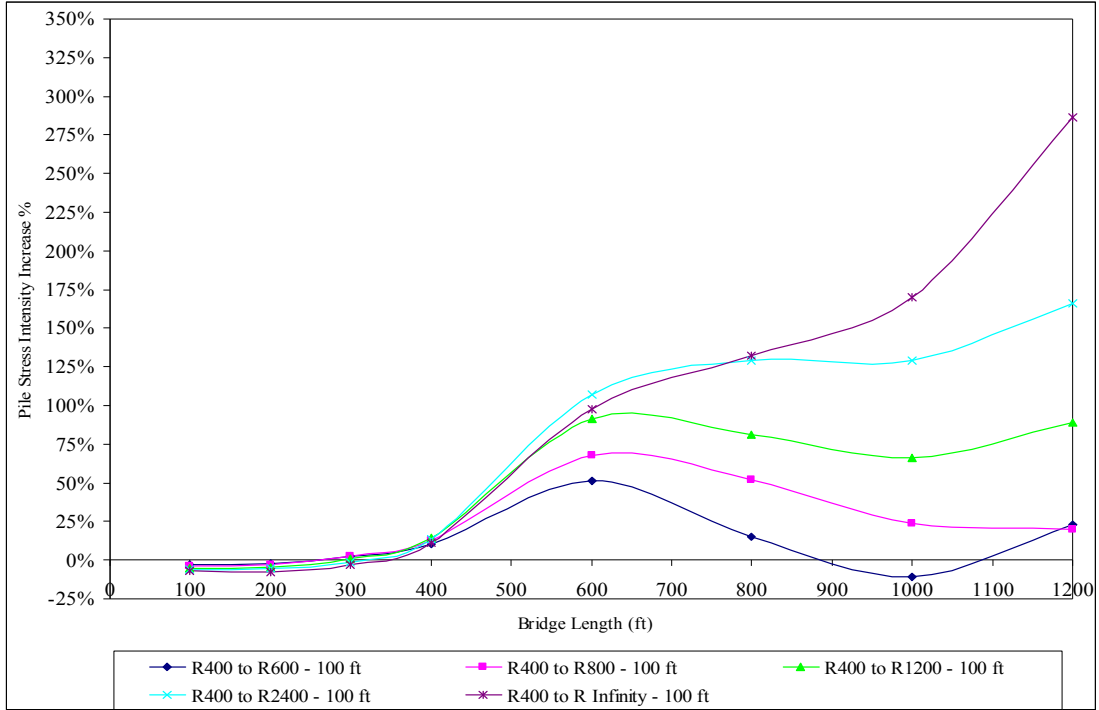


a)  $\Delta T_{\text{slab}} = 90^\circ \text{ F}$ ,  $\Delta T_{\text{the rest}} = 60^\circ \text{ F}$

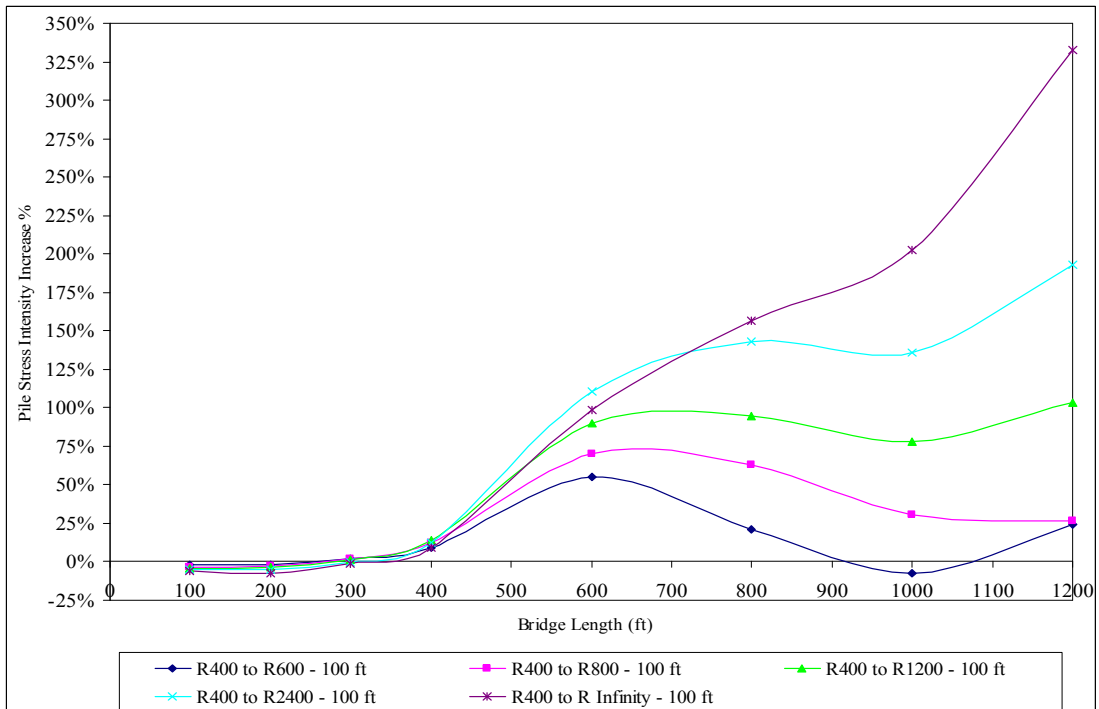


b)  $\Delta T_{\text{slab}} = 120^\circ \text{ F}$ ,  $\Delta T_{\text{the rest}} = 90^\circ \text{ F}$

**Figure 7.40 – Stress Increase (%) of End-Bearing Piles in 9 ft Deep Predrilled Holes of Bridges with 50 ft Spans due to Change in Radius from Different Values to Infinity**

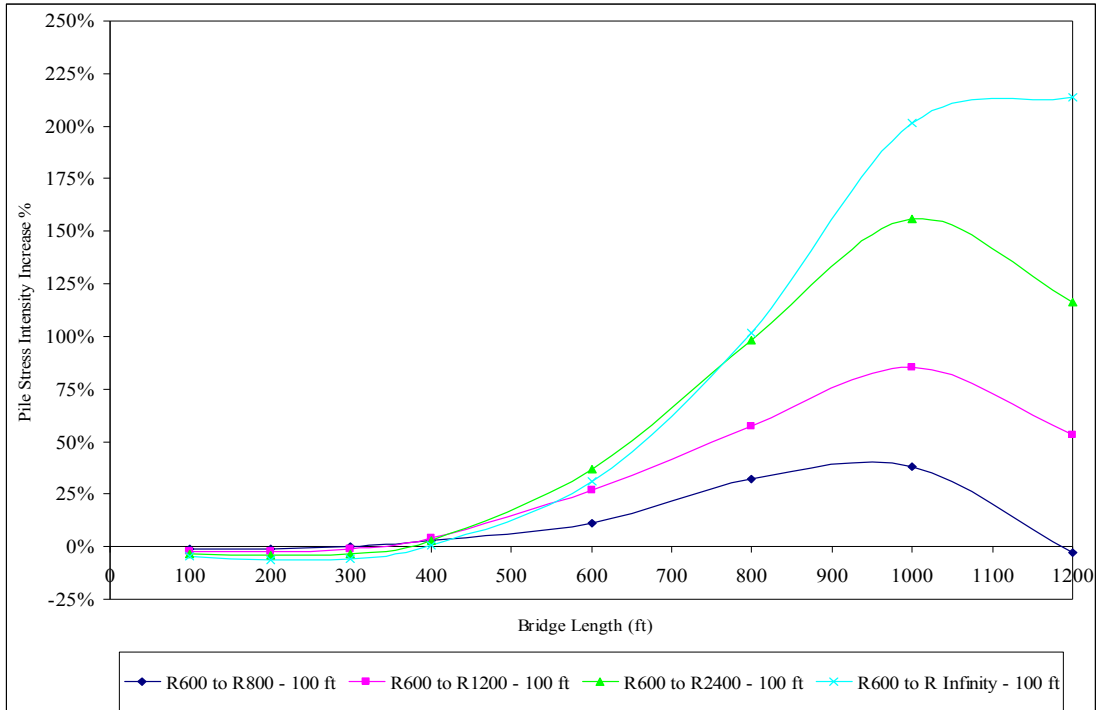


a)  $\Delta T_{\text{slab}} = 90^\circ \text{ F}$ ,  $\Delta T_{\text{the rest}} = 60^\circ \text{ F}$

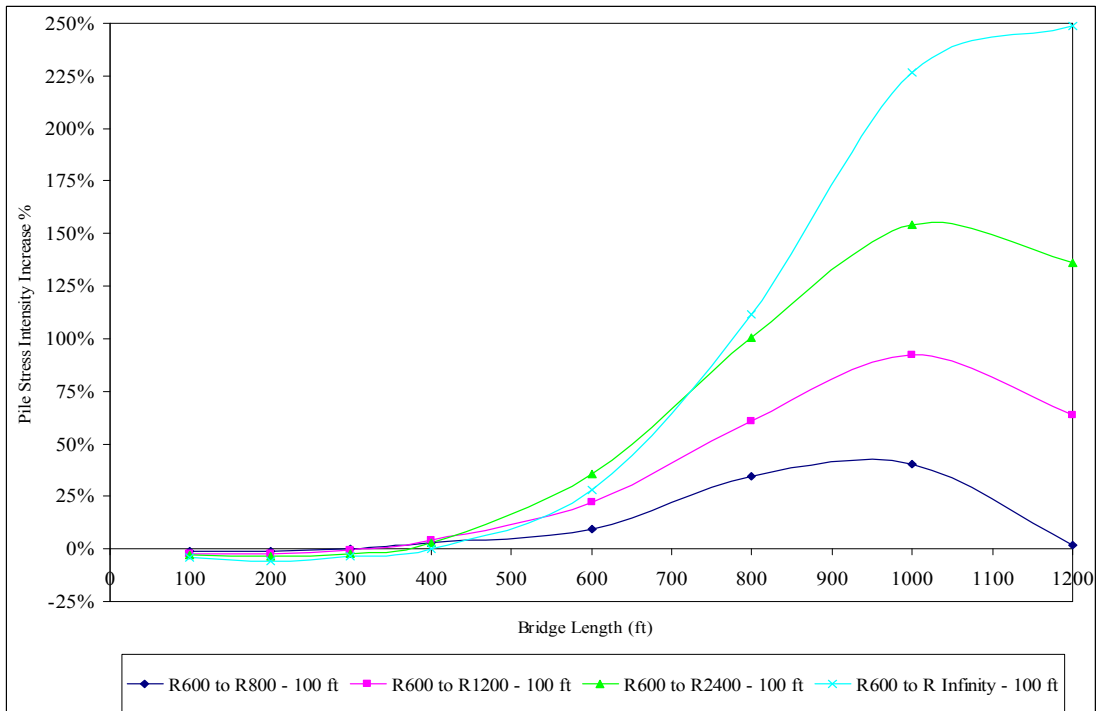


b)  $\Delta T_{\text{slab}} = 120^\circ \text{ F}$ ,  $\Delta T_{\text{the rest}} = 90^\circ \text{ F}$

**Figure 7.41 – Stress Increase (%) of End-Bearing Piles in Very Stiff Clay Soil Profile of Bridges with 100 ft Spans due to Change in Radius from 400 ft to a Larger Radius**

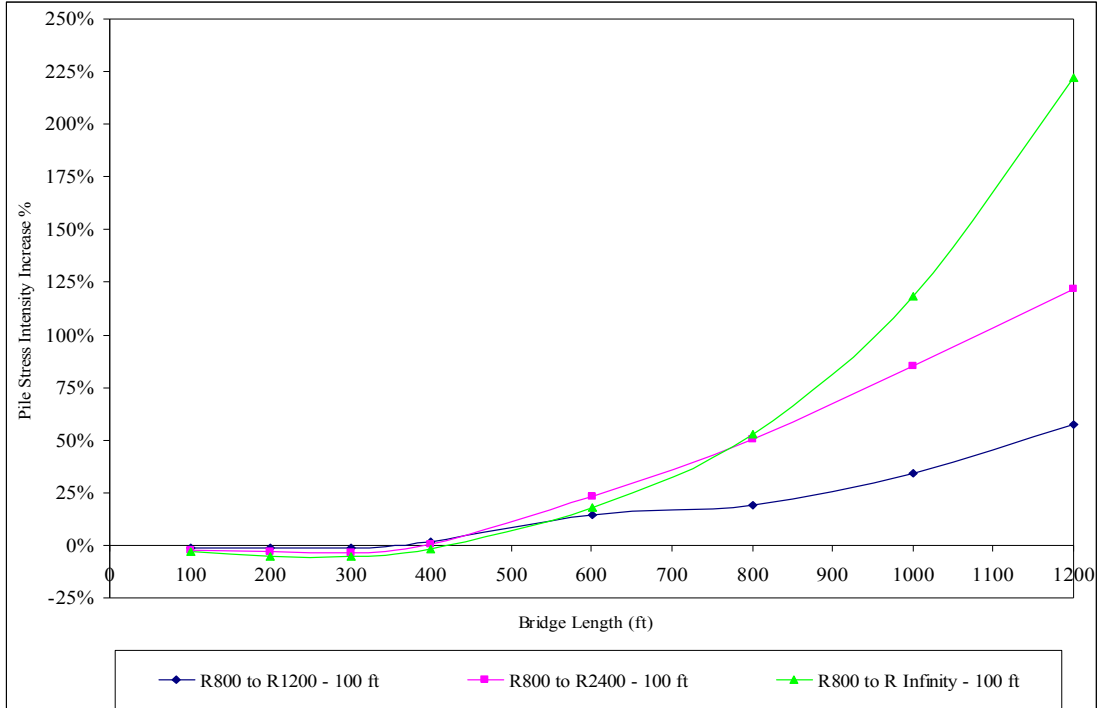


a)  $\Delta T_{\text{slab}} = 90^\circ \text{ F}$ ,  $\Delta T_{\text{the rest}} = 60^\circ \text{ F}$

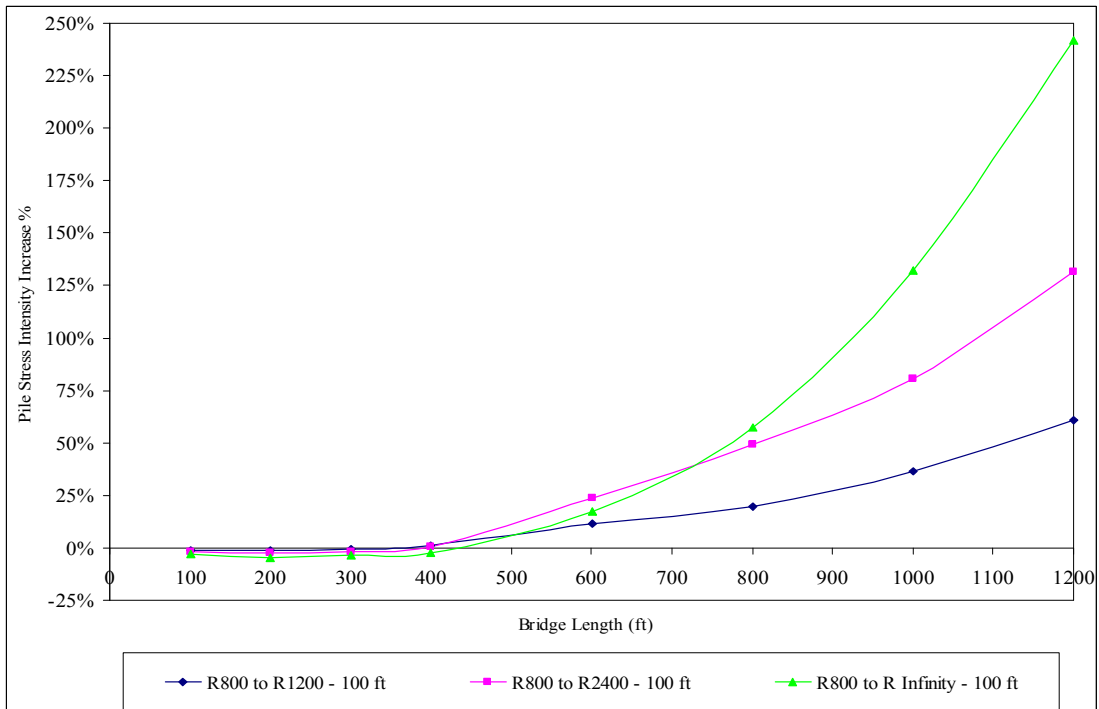


b)  $\Delta T_{\text{slab}} = 120^\circ \text{ F}$ ,  $\Delta T_{\text{the rest}} = 90^\circ \text{ F}$

**Figure 7.42 – Stress Increase (%) of End-Bearing Piles in Very Stiff Clay Soil Profile of Bridges with 100 ft Spans due to Change in Radius from 600 ft to a Larger Radius**

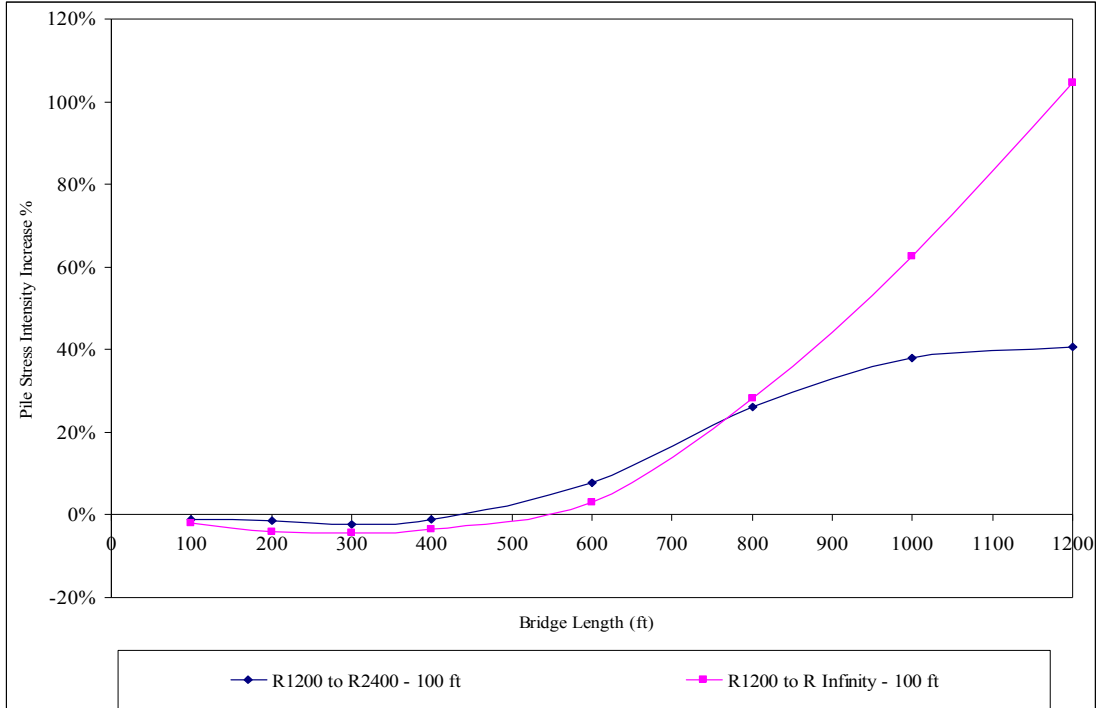


a)  $\Delta T_{\text{slab}} = 90^\circ \text{ F}, \Delta T_{\text{the rest}} = 60^\circ \text{ F}$

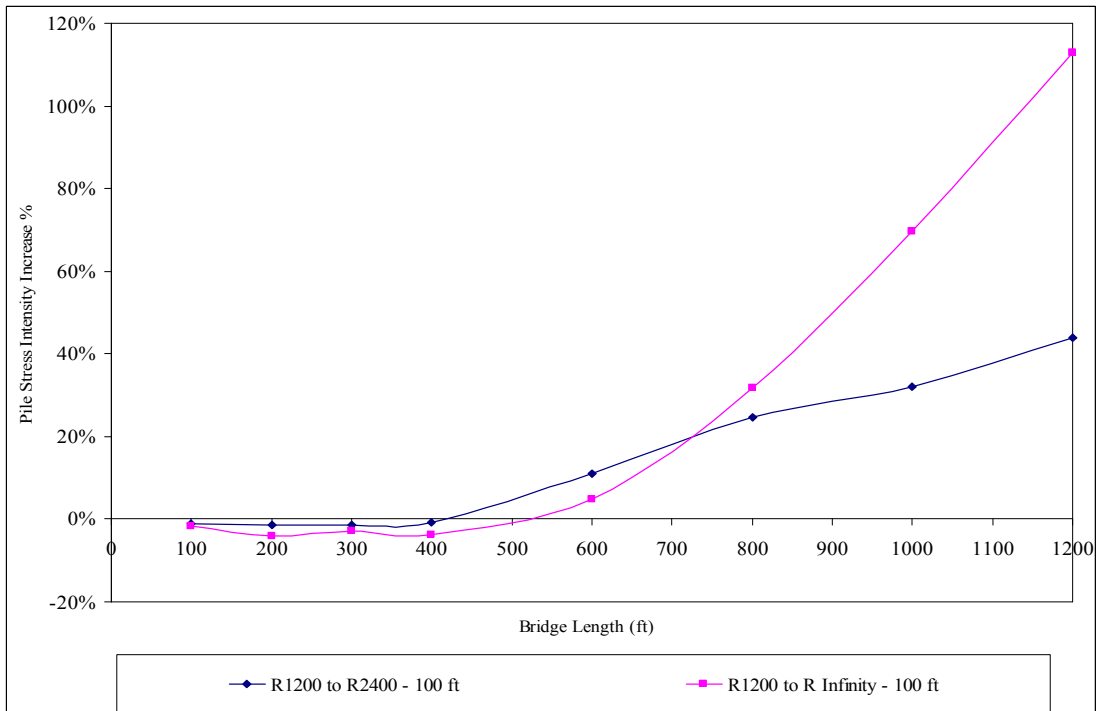


b)  $\Delta T_{\text{slab}} = 120^\circ \text{ F}, \Delta T_{\text{the rest}} = 90^\circ \text{ F}$

**Figure 7.43 – Stress Increase (%) of End-Bearing Piles in Very Stiff Clay Soil Profile of Bridges with 100 ft Spans due to Change in Radius from 800 ft to a Larger Radius**

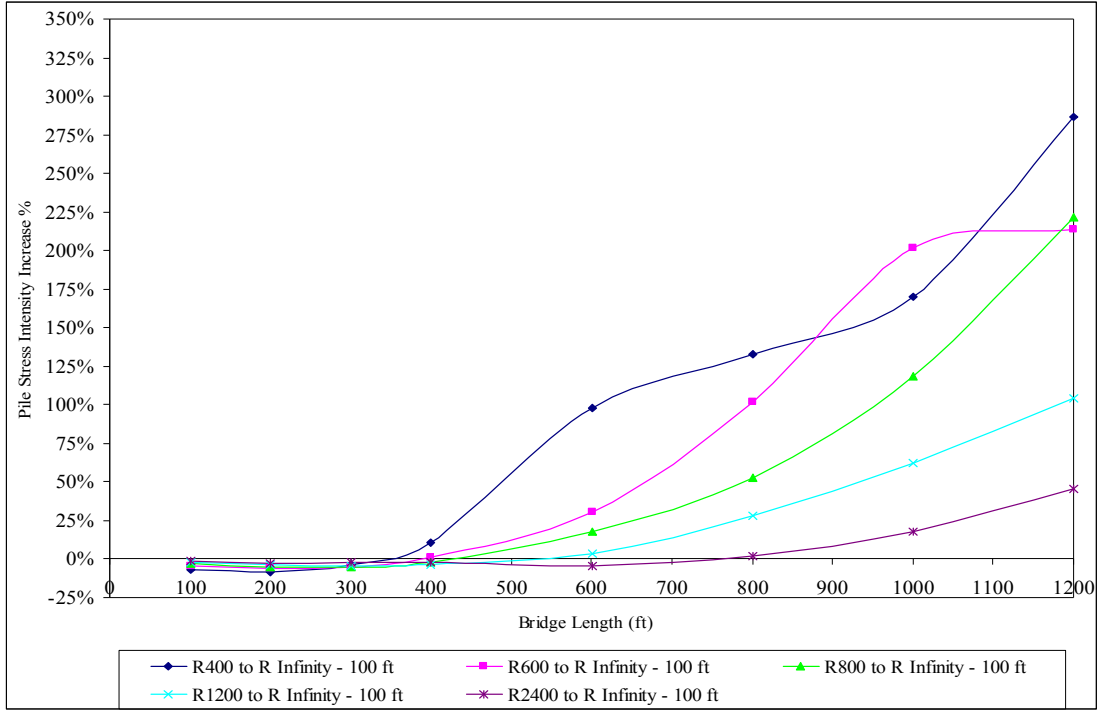


a)  $\Delta T_{\text{slab}} = 90^\circ \text{ F}, \Delta T_{\text{the rest}} = 60^\circ \text{ F}$

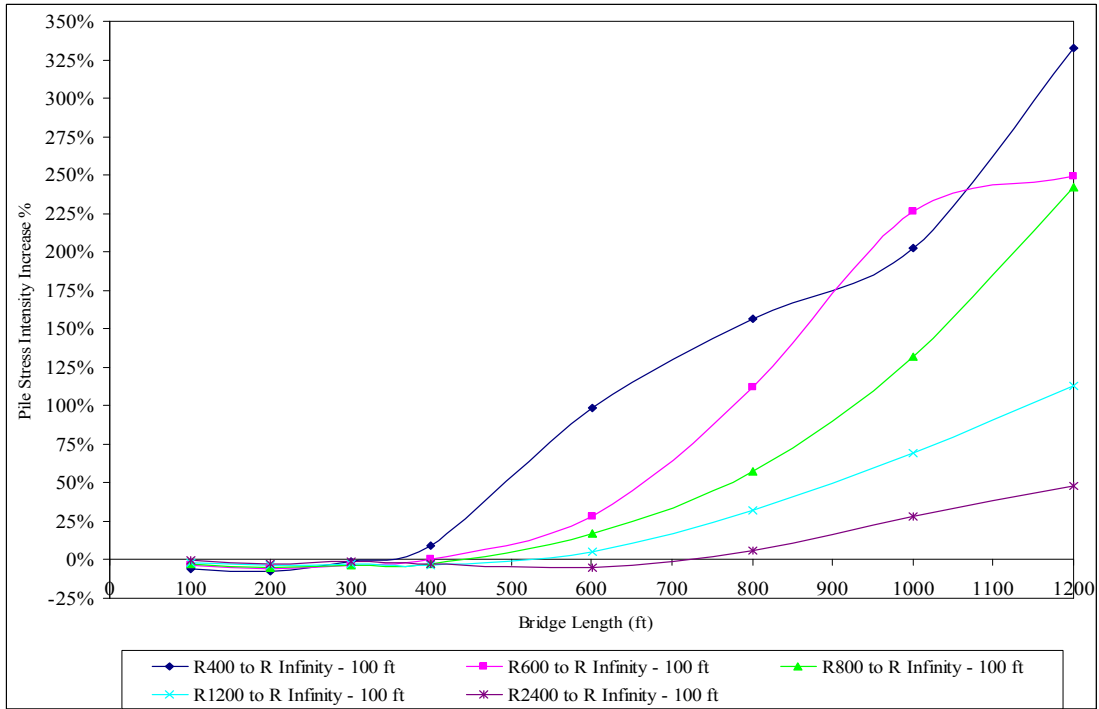


b)  $\Delta T_{\text{slab}} = 120^\circ \text{ F}, \Delta T_{\text{the rest}} = 90^\circ \text{ F}$

**Figure 7.44 – Stress Increase (%) of End-Bearing Piles in Very Stiff Clay Soil Profile of Bridges with 100 ft Spans due to Change in Radius from 1200 ft to a Larger Radius**



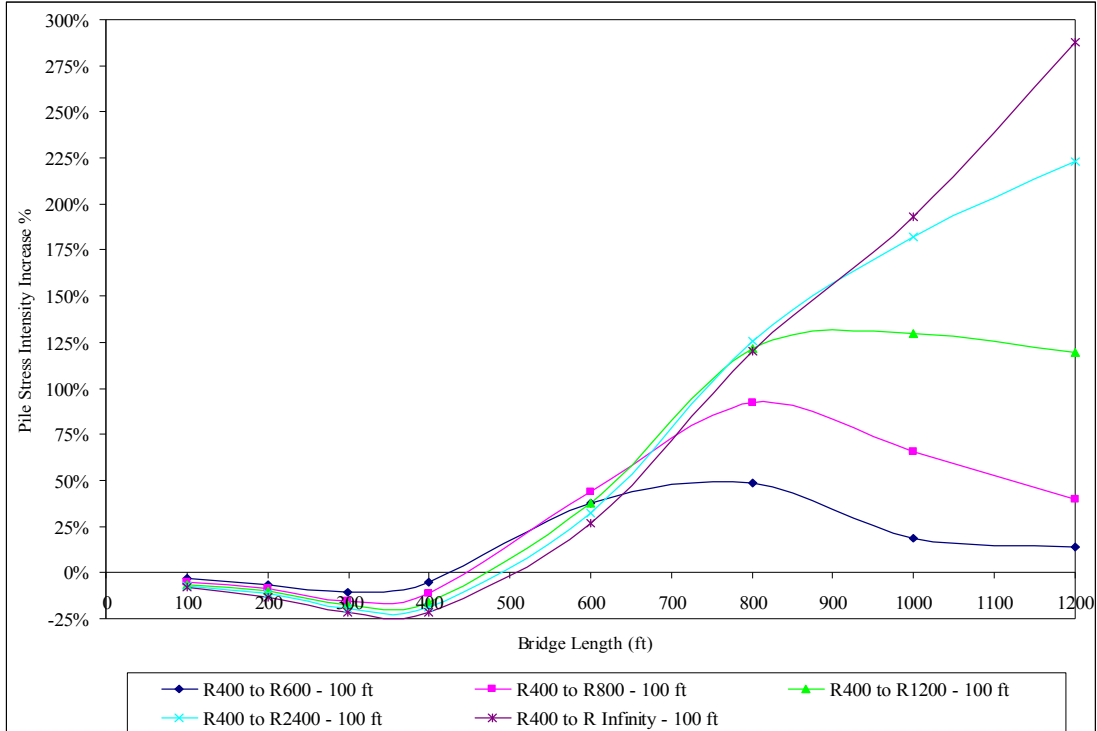
a)  $\Delta T_{\text{slab}} = 90^\circ \text{F}$ ,  $\Delta T_{\text{the rest}} = 60^\circ \text{F}$



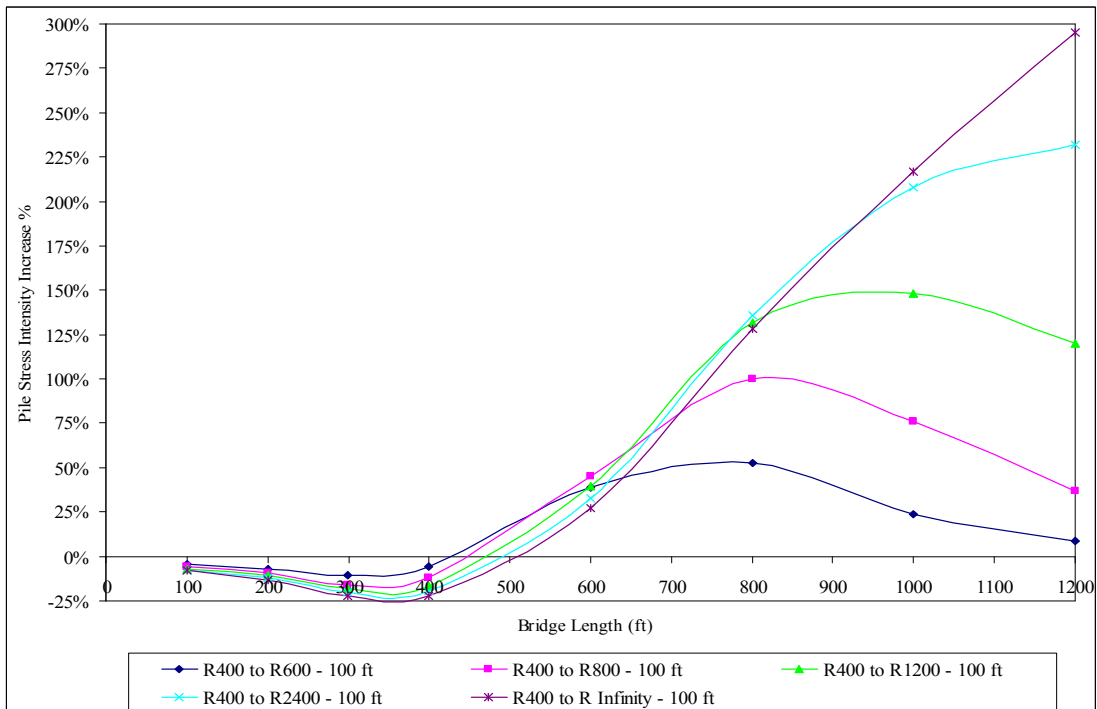
b)  $\Delta T_{\text{slab}} = 120^\circ \text{F}$ ,  $\Delta T_{\text{the rest}} = 90^\circ \text{F}$

**Figure 7.45 – Stress Increase (%) of End-Bearing Piles in Very Stiff Clay Soil Profile of Bridges with 100 ft Spans due to Change in Radius from Different Values to Infinity**



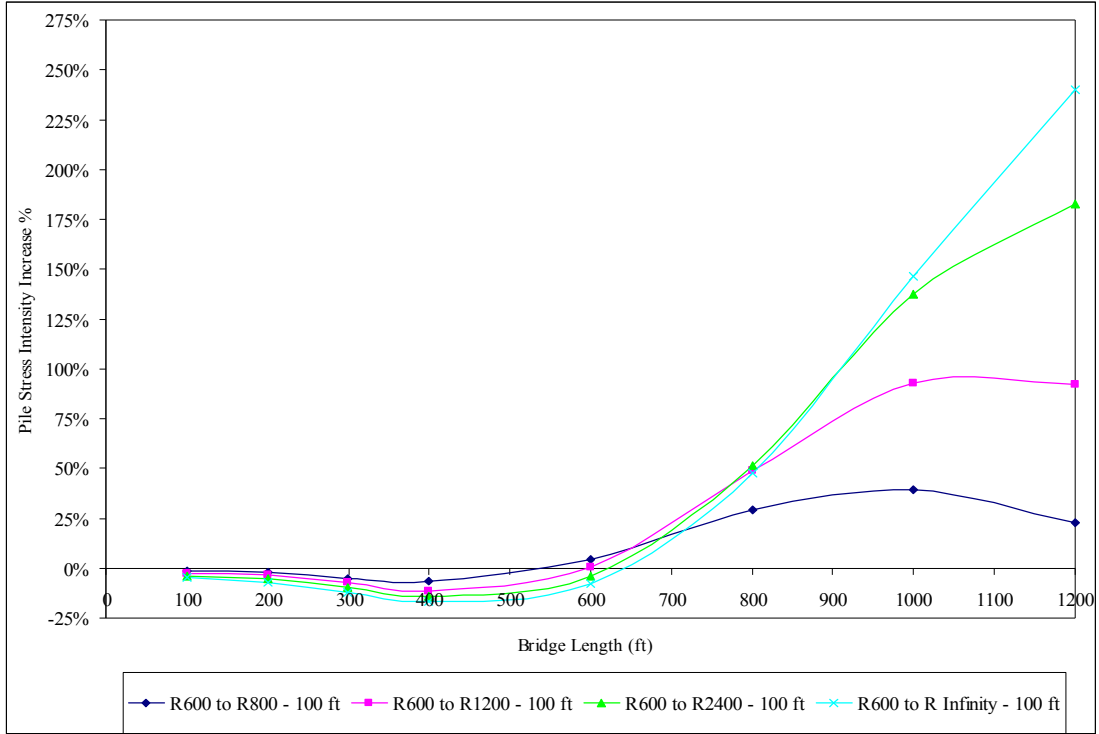


a)  $\Delta T_{\text{slab}} = 90^\circ \text{ F}$ ,  $\Delta T_{\text{the rest}} = 60^\circ \text{ F}$

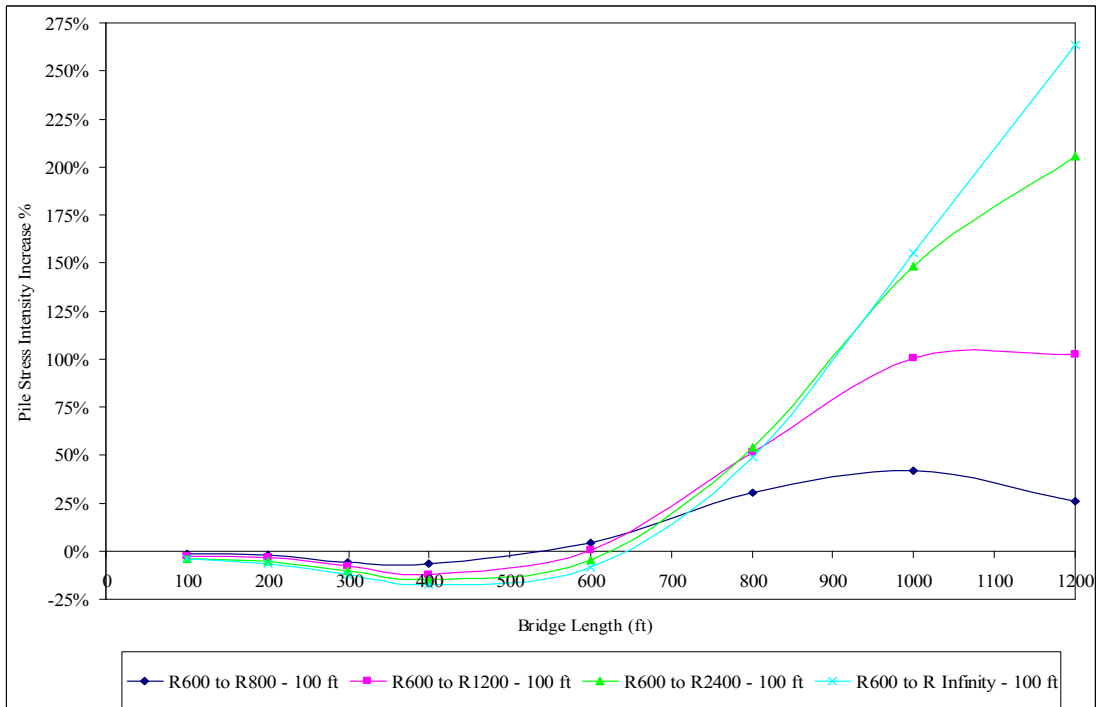


b)  $\Delta T_{\text{slab}} = 120^\circ \text{ F}$ ,  $\Delta T_{\text{the rest}} = 90^\circ \text{ F}$

**Figure 7.46 – Stress Increase (%) of End-Bearing Piles in 9 ft Deep Predrilled Holes of Bridges with 100 ft Spans due to Change in Radius from 400 ft to a Larger Radius**

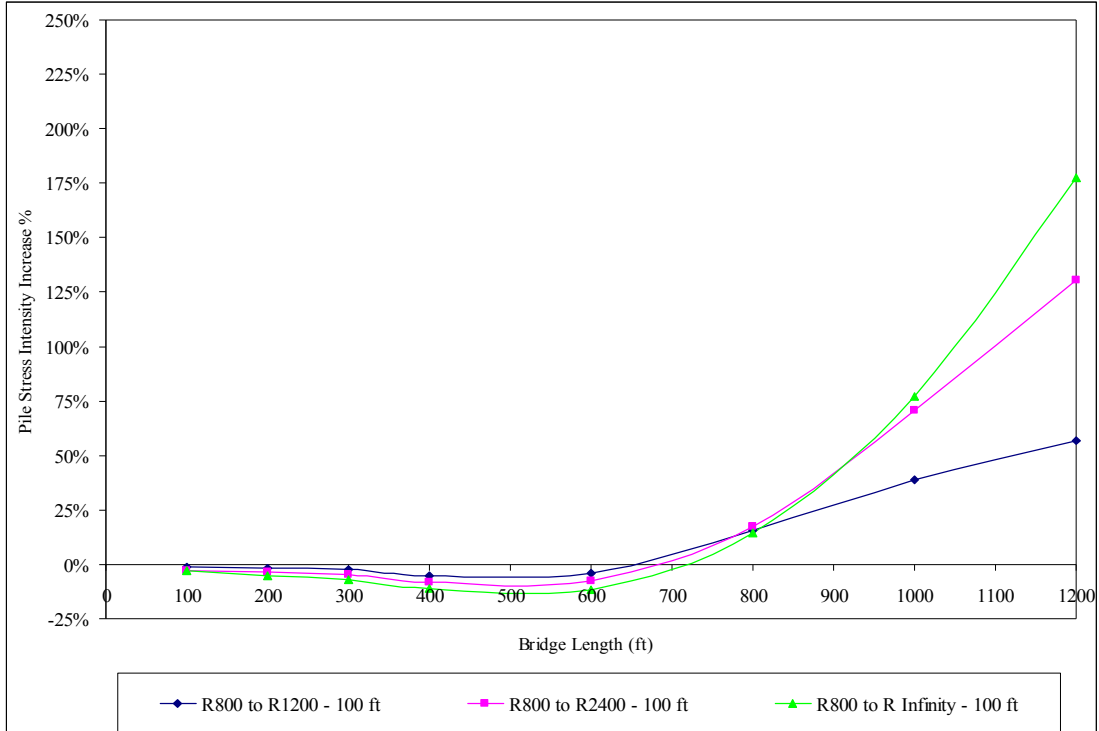


a)  $\Delta T_{\text{slab}} = 90^\circ \text{ F}, \Delta T_{\text{the rest}} = 60^\circ \text{ F}$

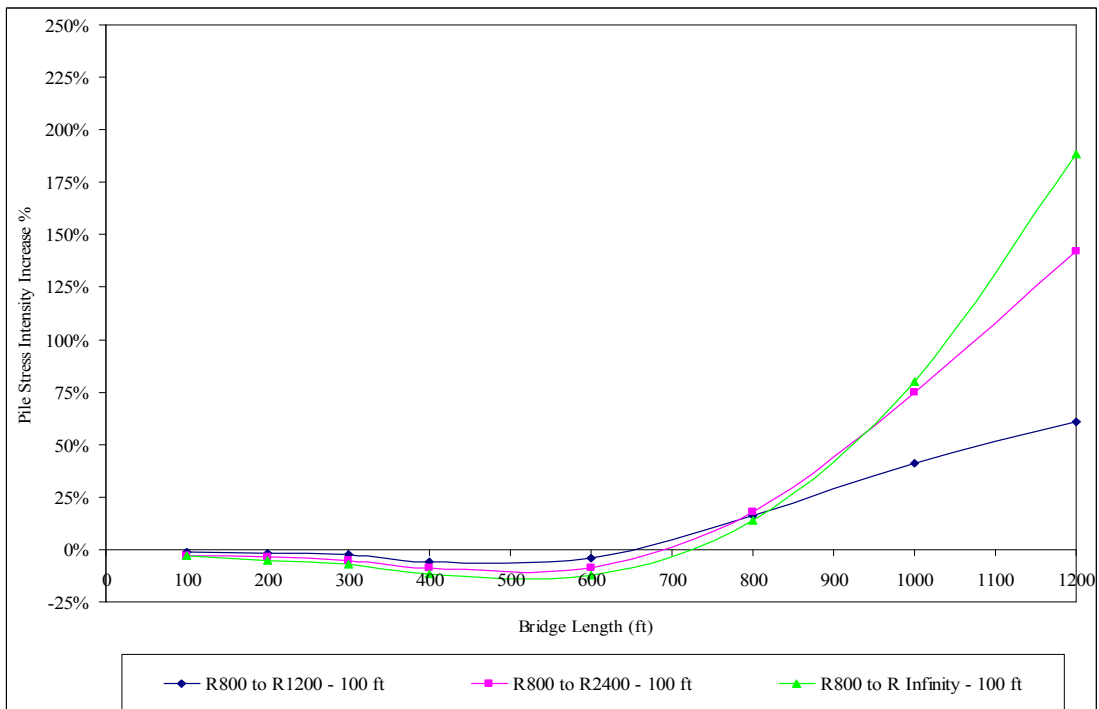


b)  $\Delta T_{\text{slab}} = 120^\circ \text{ F}, \Delta T_{\text{the rest}} = 90^\circ \text{ F}$

**Figure 7.47 – Stress Increase (%) of End-Bearing Piles in 9 ft Deep Predrilled Holes of Bridges with 100 ft Spans due to Change in Radius from 600 ft to a Larger Radius**

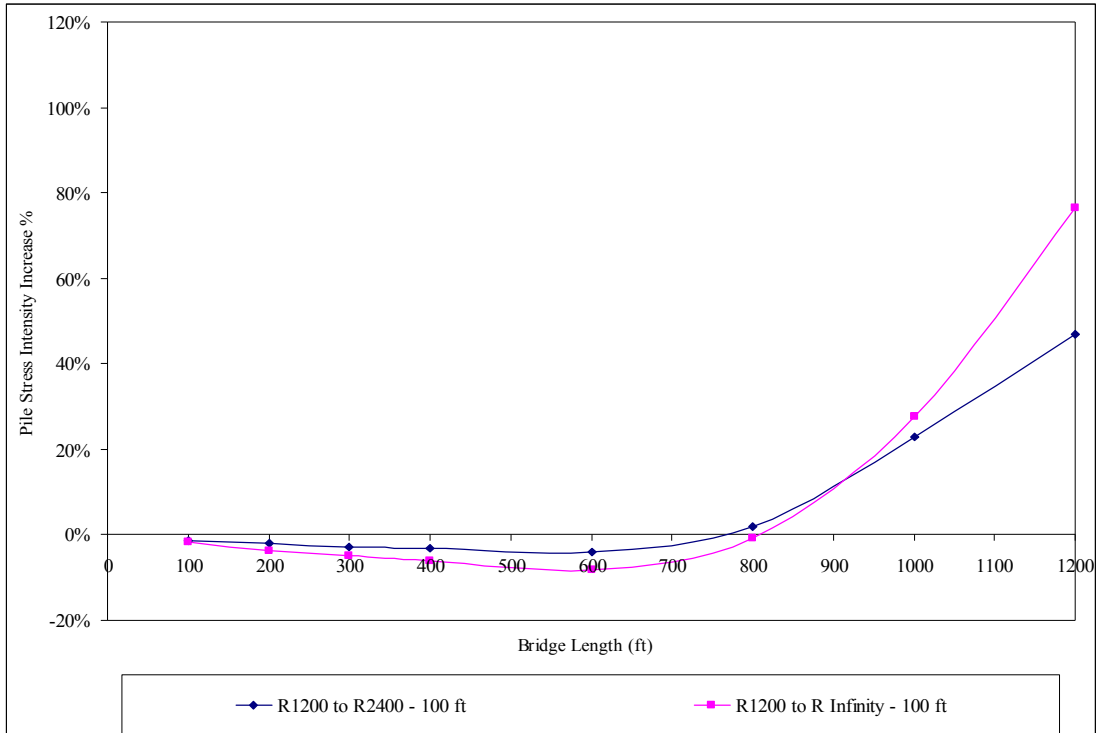


a)  $\Delta T_{\text{slab}} = 90^\circ \text{ F}, \Delta T_{\text{the rest}} = 60^\circ \text{ F}$

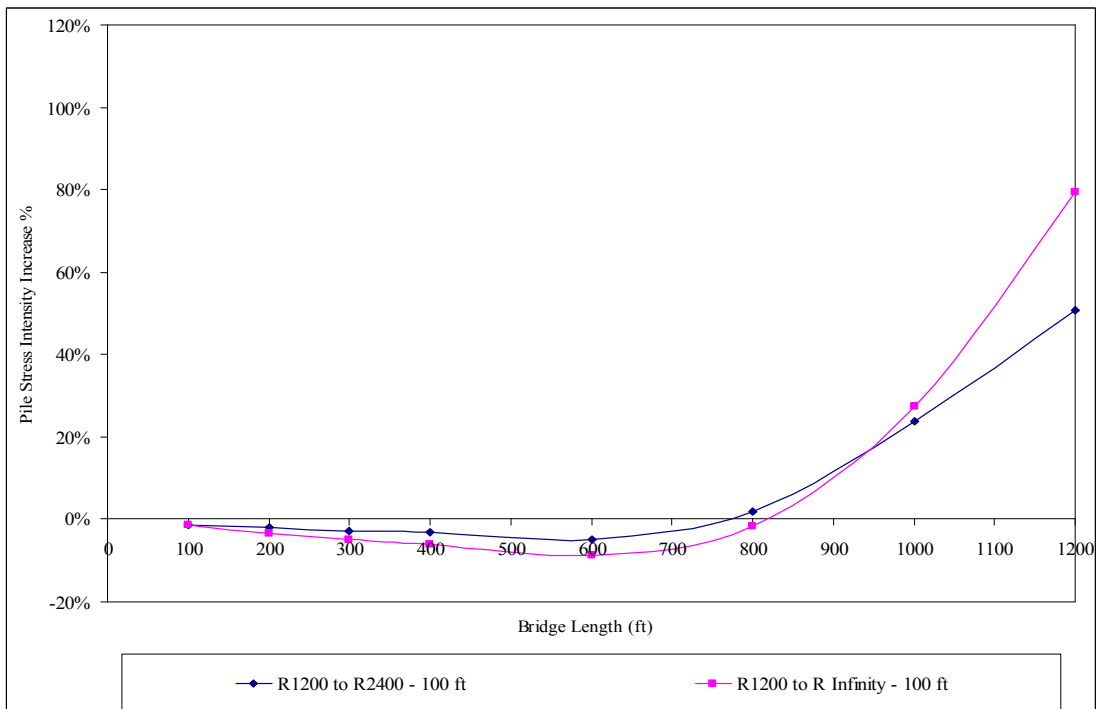


b)  $\Delta T_{\text{slab}} = 120^\circ \text{ F}, \Delta T_{\text{the rest}} = 90^\circ \text{ F}$

**Figure 7.48 – Stress Increase (%) of End-Bearing Piles in 9 ft Deep Predrilled Holes of Bridges with 100 ft Spans due to Change in Radius from 800 ft to a Larger Radius**

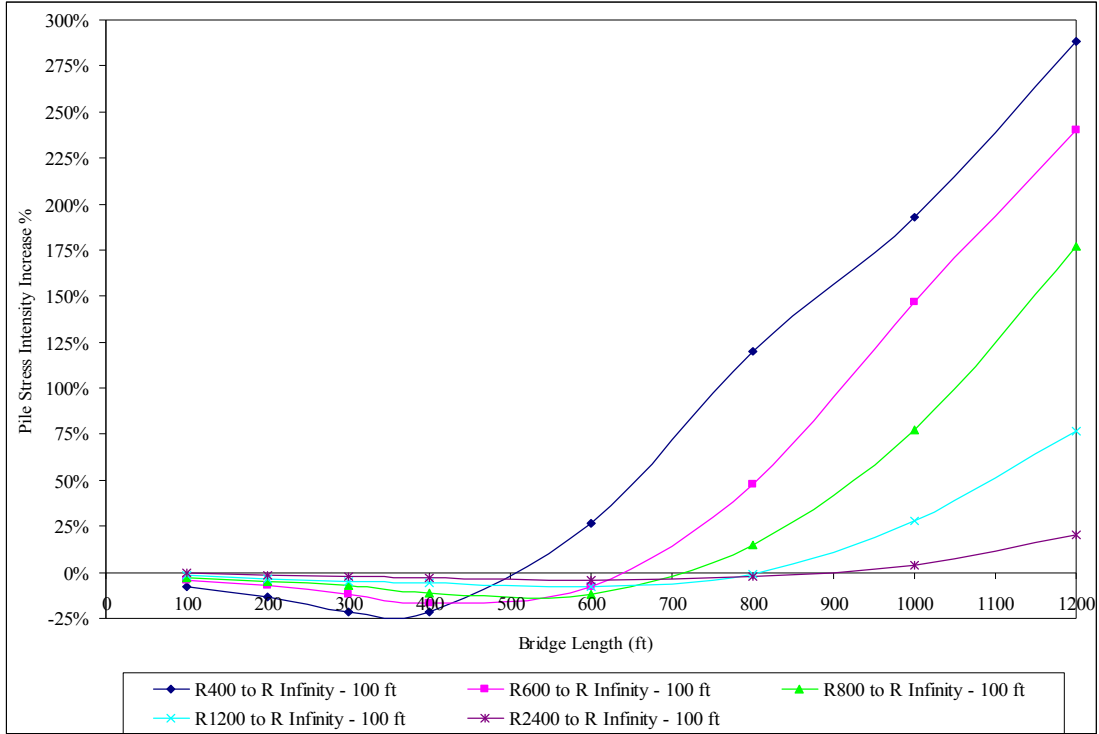


a)  $\Delta T_{\text{slab}} = 90^\circ \text{ F}, \Delta T_{\text{the rest}} = 60^\circ \text{ F}$

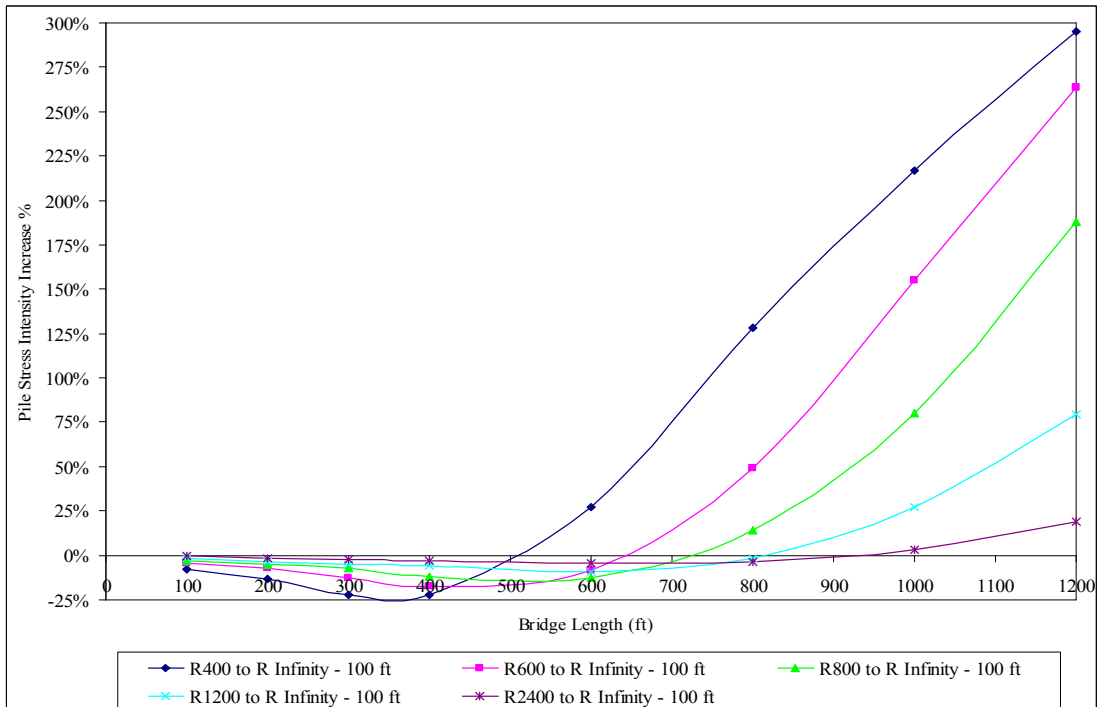


b)  $\Delta T_{\text{slab}} = 120^\circ \text{ F}, \Delta T_{\text{the rest}} = 90^\circ \text{ F}$

**Figure 7.49 – Stress Increase (%) of End-Bearing Piles in 9 ft Deep Predrilled Holes of Bridges with 100 ft Spans due to Change in Radius from 1200 ft to a Larger Radius**



a)  $\Delta T_{\text{slab}} = 90^\circ \text{ F}$ ,  $\Delta T_{\text{the rest}} = 60^\circ \text{ F}$



b)  $\Delta T_{\text{slab}} = 120^\circ \text{ F}$ ,  $\Delta T_{\text{the rest}} = 90^\circ \text{ F}$

**Figure 7.50 – Stress Increase (%) of End-Bearing Piles in 9 ft Deep Predrilled Holes of Bridges with 100 ft Spans due to Change in Radius from Different Values to Infinity**

## 7.6 Effect of Pile Type

Piles are designed either as friction or end-bearing piles. Friction piles are designed to resist axial load through the frictional area and the tip of the pile, while end-bearing piles are designed to resist axial load through the cross section.

From Tables 7.41 and 7.42, the increase in the maximum pile stress intensity (stress concentration) is in the range of 0.7% to 2.2% for curved IAB's with 50 ft spans, and in the range of 0.1% to 1.5% for curved IAB's with 100 ft spans when end-bearing piles are used instead of friction piles at two temperature levels.

Therefore, the difference in the maximum stress intensity between friction and end-bearing piles is relatively small.

**Table 7.41 – Mean and Standard Deviation of Stress Increase (%) of End-Bearing Piles Compared to Friction Piles of Bridges with 50 ft spans**

Description	Radius (ft)	$\Delta T_{\text{slab}} = 90^\circ \text{ F}$ $\Delta T_{\text{the rest}} = 60^\circ \text{ F}$				$\Delta T_{\text{slab}} = 120^\circ \text{ F}$ $\Delta T_{\text{the rest}} = 90^\circ \text{ F}$			
		Depth of Predrilled Holes (ft)							
		0	5	9	15	0	5	9	15
MEAN	400	1.2	1.8	1.9	1.9	0.8	1.1	1.1	1.4
	600	0.8	1.6	2.1	2.1	0.8	1.0	1.8	1.4
	800	0.6	2.0	2.2	1.9	0.7	1.0	1.6	1.4
	1200	1.0	1.2	1.9	1.9	1.1	0.8	1.9	1.9
	2400	1.1	1.7	1.6	1.4	1.2	1.1	1.1	1.0
	Infinity	0.9	1.5	1.5	1.3	0.8	1.0	1.0	0.9
STD	400	1.3	2.0	2.6	2.4	1.1	1.5	1.9	2.2
	600	1.4	1.8	2.0	2.3	1.7	1.2	2.3	1.8
	800	1.3	1.3	1.6	1.7	1.4	1.6	1.7	1.6
	1200	1.4	1.5	1.5	1.5	1.5	1.5	1.9	1.8
	2400	1.1	1.5	1.6	1.3	1.2	1.0	1.7	1.4
	Infinity	1.1	1.5	1.6	1.3	0.6	1.0	1.1	1.1

**Table 7.42 – Mean and Standard Deviation of Stress Increase (%) of End-Bearing Piles Compared to Friction Piles of Bridges with 100 ft spans**

Description	Radius (ft)	$\Delta T_{\text{slab}} = 90^\circ \text{ F}$ $\Delta T_{\text{the rest}} = 60^\circ \text{ F}$				$\Delta T_{\text{slab}} = 120^\circ \text{ F}$ $\Delta T_{\text{the rest}} = 90^\circ \text{ F}$			
		Depth of Predrilled Holes (ft)							
		0	5	9	15	0	5	9	15
MEAN	400	1.3	1.5	1.4	1.5	1.0	1.2	1.3	1.6
	600	0.8	1.1	1.2	1.4	0.8	1.1	1.2	1.4
	800	1.1	1.4	1.3	1.2	0.9	1.0	1.3	1.2
	1200	0.5	0.8	1.1	1.2	0.5	0.9	1.2	1.0
	2400	0.3	0.7	0.8	0.9	0.5	0.7	0.8	0.9
	Infinity	0.3	0.1	0.9	0.1	0.4	0.6	0.2	0.1
STD	400	1.1	0.8	0.9	1.1	0.6	0.9	1.0	1.0
	600	0.6	0.4	0.4	0.4	0.6	0.4	0.4	0.6
	800	1.4	0.9	0.6	0.4	1.2	0.3	0.8	0.4
	1200	0.4	0.2	0.7	0.5	0.4	0.3	0.9	0.3
	2400	0.2	0.2	0.2	0.3	0.3	0.3	0.3	0.3
	Infinity	0.2	0.6	2.7	0.5	0.4	1.4	0.3	0.4

Steel used in this study consists of grade 36 steel with a minimum yield stress of 36 ksi. The von Mises or equivalent stress is used in this study. Figure 7.51 shows the equivalent stress contour of friction and end-bearing piles in very stiff clay soil profile with 9 ft deep predrilled holes filled with loose sand of curved IAB's with 800 ft radius and 800 ft length at  $\Delta T_{\text{slab}}$  of  $120^\circ \text{ F}$  and  $\Delta T_{\text{the rest}}$  of  $90^\circ \text{ F}$ .

The pile at the right hand side (pile at the outermost radius) of friction and end-bearing pile groups shown in Figure 7.51 is investigated to determine the difference in the equivalent stress of friction and end-bearing piles. The equivalent stress in friction and end-bearing piles of curved IAB's with 50 ft and 100 ft spans is shown in Figure 7.52. The location of the partially plastic hinges in the piles is indicated in Table 7.43.





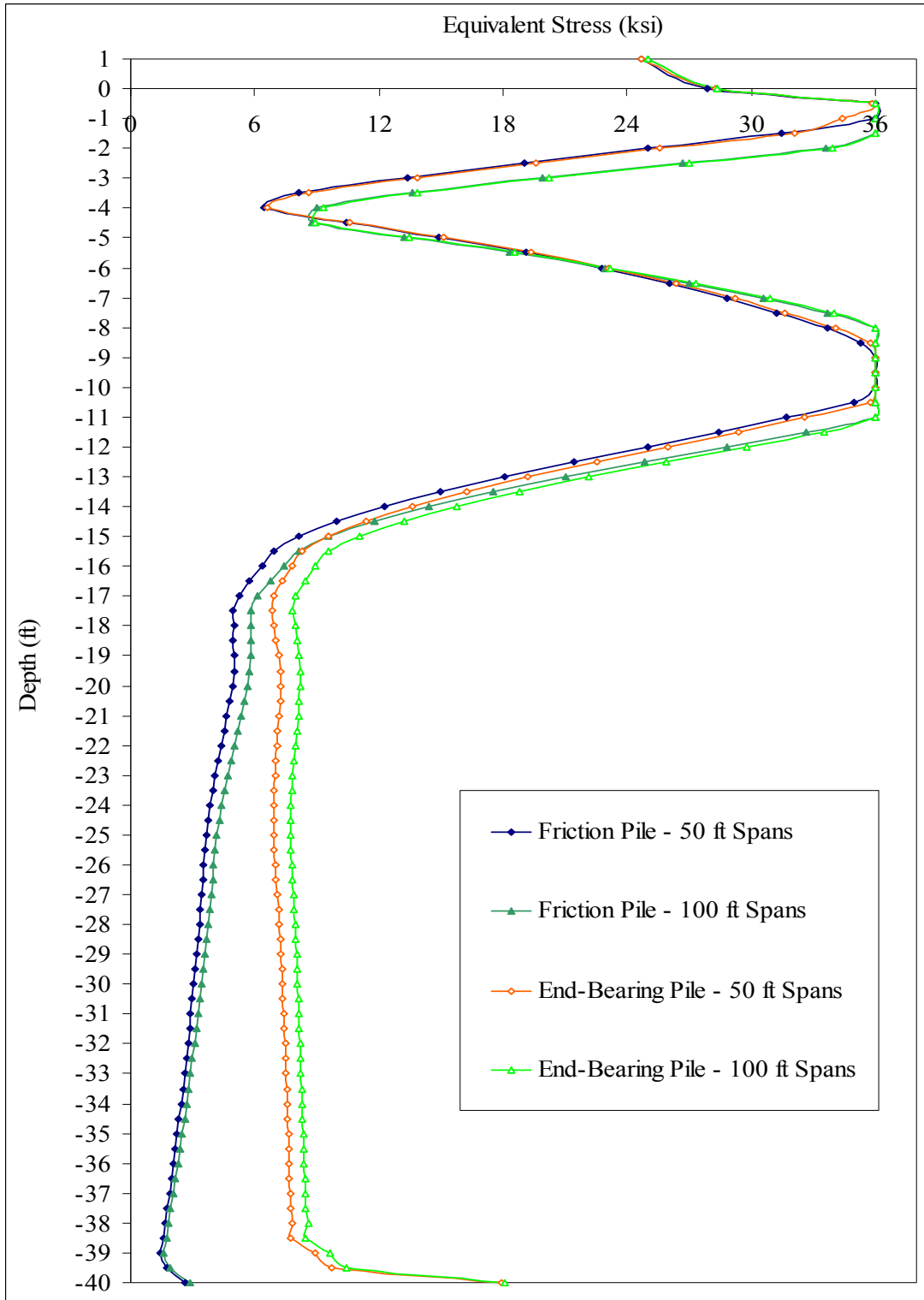
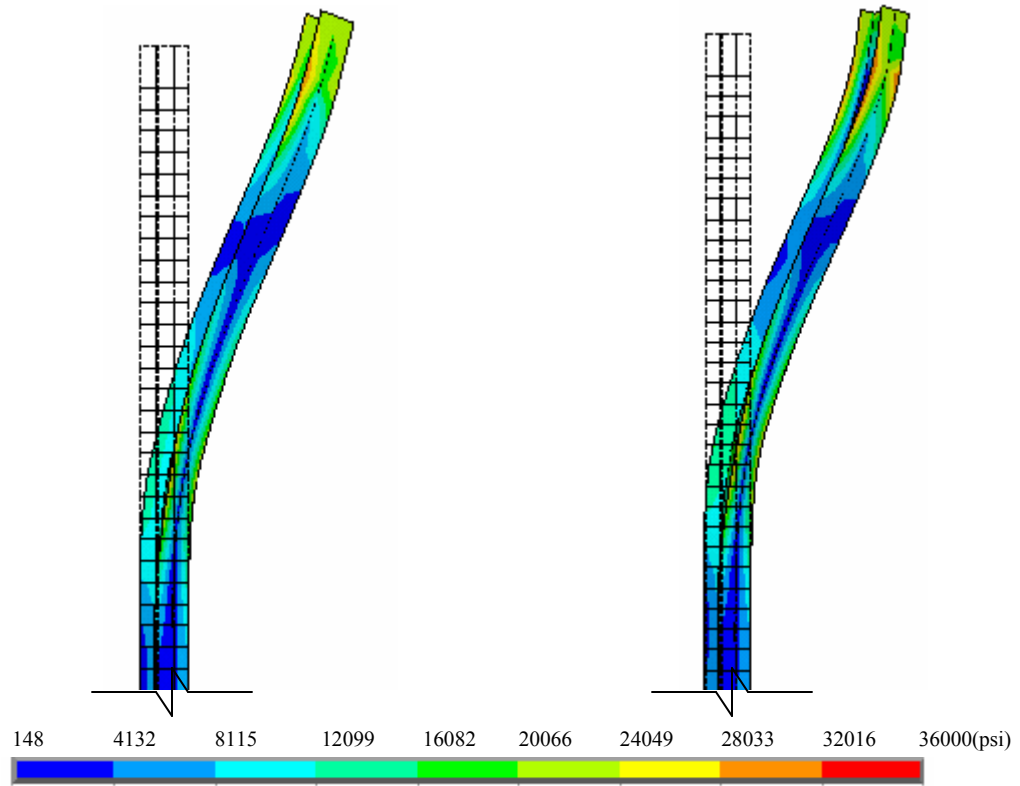


**Figure 7.52 – Comparison of Equivalent Stress in Friction and End-Bearing Piles in 9 ft Deep Predrilled Holes of Bridges with 800 ft Radius and 800 ft Length ( $\Delta T_{\text{slab}} = 120^{\circ} \text{ F}$ ,  $\Delta T_{\text{the rest}} = 90^{\circ} \text{ F}$ )**



a) 50 ft Spans

b) 100 ft spans

**Figure 7.53 – Equivalent Stress Contour with Deformed and Undeformed Shapes of Piles in 9 ft Deep Predrilled Holes of Bridges with 800 ft Radius and 800 ft Length ( $\Delta T_{\text{slab}} = 120^\circ \text{ F}$ ,  $\Delta T_{\text{the rest}} = 90^\circ \text{ F}$ )**

**Table 7.43 – Location of Partially Plastic Hinges in Piles**

Span Length (ft)	Depth Below the Bottom of the Abutment (ft)
50	0.5 – 1
	8.5 – 10.5
100	0.5 – 1.5
	8 – 11

Figures 7.52 and 7.53 and Table 7.43 indicate that the partially plastic hinges in friction and end-bearing piles are at the same location. The partially plastic region in the piles for curved IAB's with 100 ft spans is slightly longer compared to the partially plastic region for curved IAB's with 50 spans.

The equivalent stress in end-bearing piles is greater than that in friction piles from 10.5 ft to 40 ft below the bottom of the abutment. At the depth of 40 ft below the bottom of the abutment, the equivalent stress in end-bearing piles is greater than that of friction piles by 680% and 627% for curved IAB's with 50 ft and 100 ft spans, respectively.

Figure 7.54 indicates that the displacement at the end span of a bridge superstructure in lateral, longitudinal, and vertical directions causes the piles to displace in an upward direction for curved IAB's with both 50 ft and 100 ft spans.

Figures 7.55 and 7.56 indicate that the vertical displacement of friction piles is in an upward direction from 1 ft above the bottom of the abutment to 13 ft and 17 ft below the bottom of the abutment for curved IAB's with 100 ft and 50 ft spans, respectively. Below this depth, the vertical displacement of the piles is in a downward direction. The downward displacement in the piles of curved IAB's with 100 ft spans is greater than that of curved IAB's with 50 ft spans by 0.014 inch. For end-bearing piles, the vertical displacement is in an upward direction for curved IAB's with both 50 ft and 100 ft spans which results from a vertical deflection at the middle of the end span.

The vertical displacement in an upward direction of both friction and end-bearing piles of curved IAB's with 100 ft spans is less than that of piles of curved

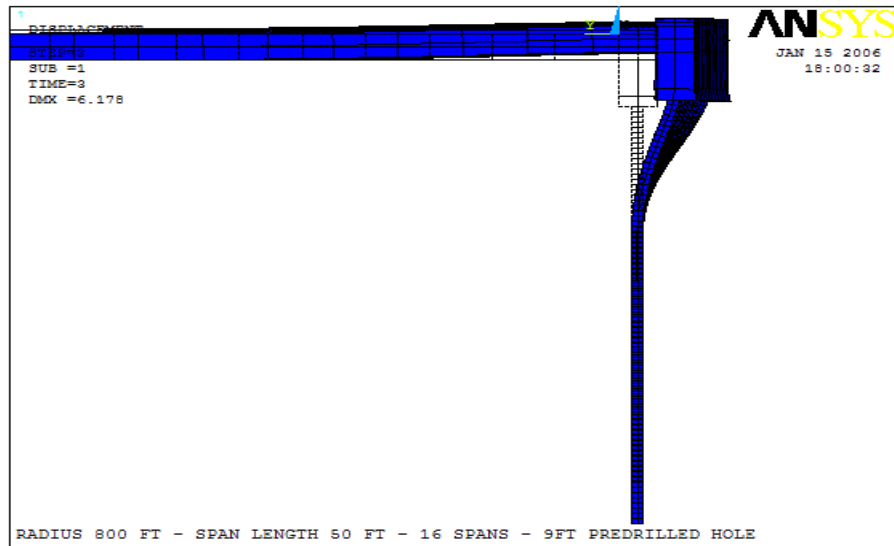
IAB's with 50 ft spans by 0.014 inch. It is, therefore, concluded that the vertical downward displacement of the piles of the longer span curved IAB's is greater than that of the piles of the shorter span curved IAB's as a result of the self weight of the bridge.

### **7.6.1 Conclusions**

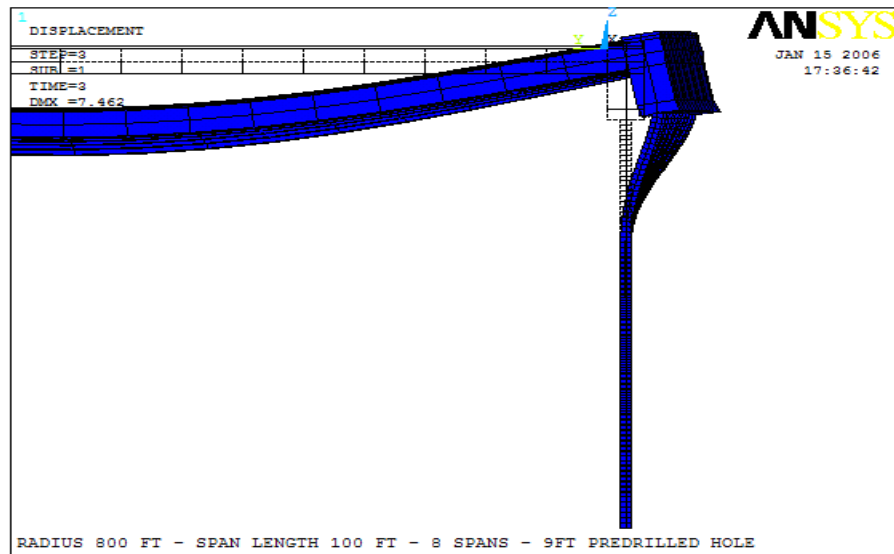
The following conclusions are drawn from the study of the effect of pile type on the maximum stress intensity (stress concentration) in the piles of curved IAB's investigated in this section:

1. The difference in the maximum stress intensity between friction and end-bearing piles of curved IAB's is relatively small.
2. The partially plastic region in the piles for curved IAB's with 100 ft spans is slightly longer compared to the partially plastic region for curved IAB's with 50 spans.
3. The von Mises or equivalent stress in end-bearing piles is greater than that in friction piles from 10.5 ft to 40 ft below the bottom of the abutment. At the depth of 40 ft below the bottom of the abutment, the equivalent stress in end-bearing piles is greater than that of friction piles by approximately 650%.
4. The displacement at the end span of a bridge superstructure in lateral, longitudinal, and vertical directions causes the piles to displace in an upward direction.

5. The vertical downward displacement of the piles of the longer span curved IAB's is greater than that of the piles of the shorter span curved IAB's as a result of the self weight of the bridge.

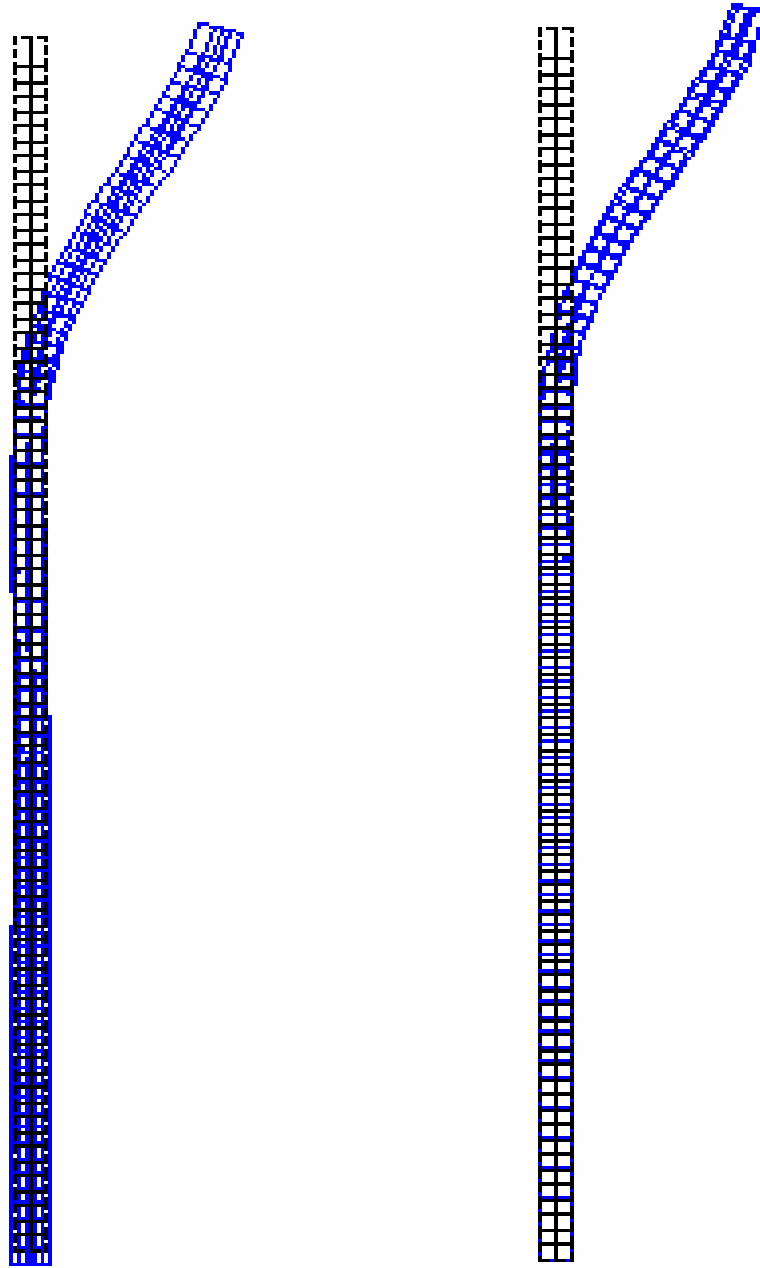


a) 50 ft Spans



b) 100 ft Spans

**Figure 7.54 – Deformed and Undeformed Shapes at the End Span of Bridges with 800 ft Radius and 800 ft Length and with Piles in 9 ft Deep Predrilled Holes ( $\Delta T_{\text{slab}} = 120^{\circ} \text{ F}$ ,  $\Delta T_{\text{the rest}} = 90^{\circ} \text{ F}$ )**



a) Friction Pile

b) End-Bearing Pile

**Figure 7.55 – Deformed and Undeformed Shapes of Friction and End-Bearing Piles in 9 ft Deep Predrilled Holes of Bridges with 800 ft Radius and 800 ft Length ( $\Delta T_{\text{slab}} = 120^{\circ} \text{ F}$ ,  $\Delta T_{\text{the rest}} = 90^{\circ} \text{ F}$ )**

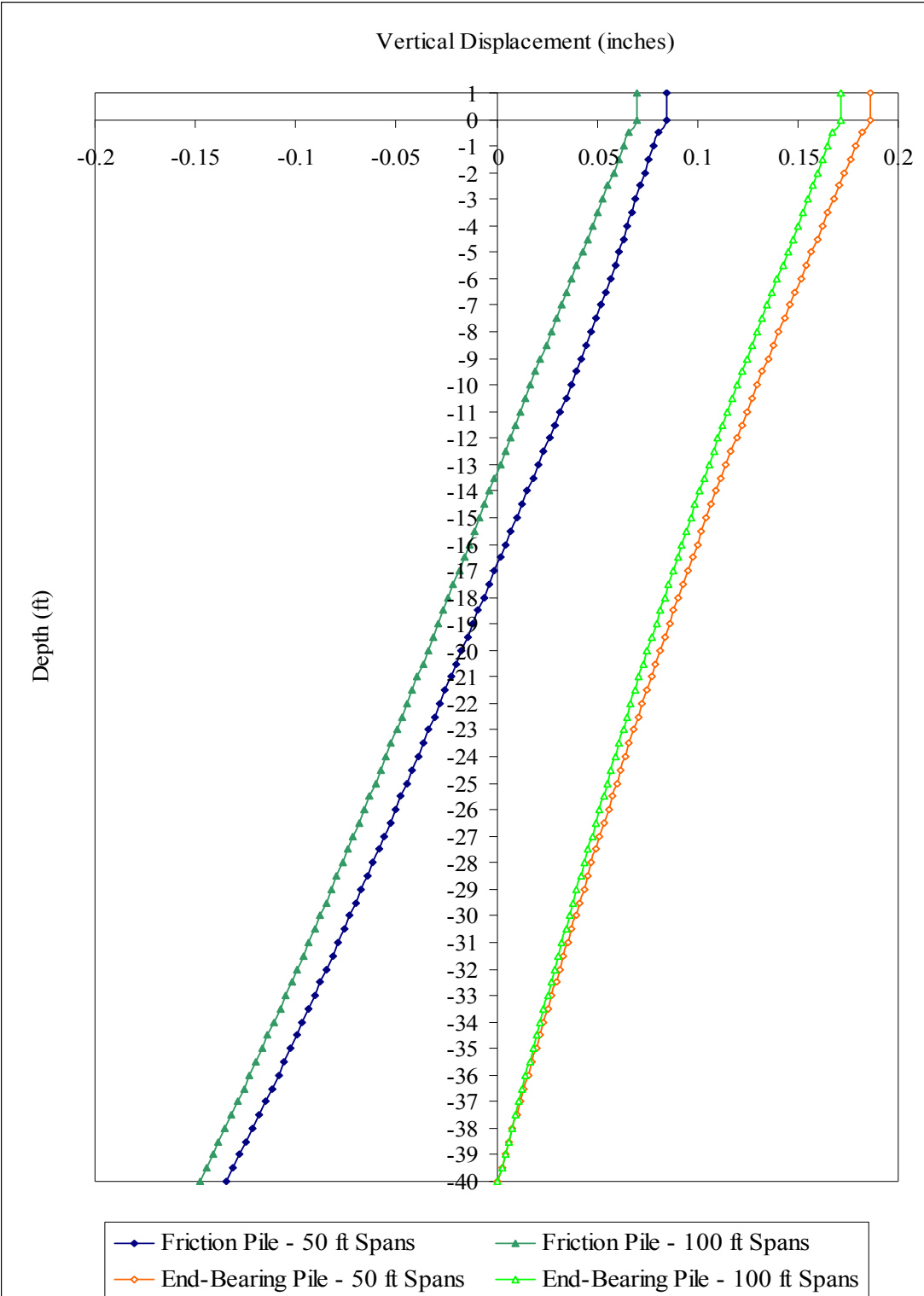


**Figure 7.56 – Vertical Displacement of Friction and End-Bearing Piles in 9 ft Deep Predrilled Holes of Bridges with 800 ft Radius and 800 ft Length ( $\Delta T_{\text{slab}} = 120^\circ \text{ F}$ ,  $\Delta T_{\text{the rest}} = 90^\circ \text{ F}$ )**

## CHAPTER 8

### PARAMETRIC STUDY OF LATERAL DISPLACEMENT OF CURVED INTEGRAL ABUTMENT BRIDGES

Over 1,700 models were analyzed using the ANSYS program. These models were broken into two categories based on the following differential temperatures:

- $\Delta T_{\text{slab}} = 90^{\circ} \text{ F}$  and  $\Delta T_{\text{the rest}} = 60^{\circ} \text{ F}$
- $\Delta T_{\text{slab}} = 120^{\circ} \text{ F}$  and  $\Delta T_{\text{the rest}} = 90^{\circ} \text{ F}$

The maximum lateral displacement in a radius direction of curved integral abutment bridges (hereafter referred to as curved IAB's) was investigated using the following parameters:

7. Effect of bridge length variation (from 50 ft to 1200 ft)
8. Effect of temperature increase (from  $\Delta T_{\text{slab}} = 90^{\circ} \text{ F}$  and  $\Delta T_{\text{the rest}} = 60^{\circ} \text{ F}$  to  $\Delta T_{\text{slab}} = 120^{\circ} \text{ F}$  and  $\Delta T_{\text{the rest}} = 90^{\circ} \text{ F}$ )
9. Effect of soil profile variation (very stiff clay soil profile, and very stiff clay soil profile with varying depths (5ft, 9ft, and 15 ft) of predrilled holes filled with loose sand (hereafter referred to as predrilled holes))
10. Effect of span length variation (50 ft and 100 ft)
11. Effect of radius variation (400 ft, 600 ft, 800 ft, 1200 ft, 2400 ft and Infinity)
12. Effect of pile type (end-bearing and friction piles)

Curved IAB's with end-bearing piles were considered throughout this study except when the parameter being considered is the effect of pile type.



## **8.1 Effect of Bridge Length Variation**

The analysis presented herein investigates the maximum lateral displacement in a radius direction of curved IAB's with an increasing bridge length from 50 ft to 1200 ft. Several different models with different radii, span lengths, soil profiles and temperature levels were created to investigate the effect of bridge length variation on the maximum lateral displacement developed in a bridge superstructure.

Figures 8.1 to 8.8 indicate that the maximum lateral displacement of curved IAB's of all radii, except an infinite radius (straight IAB's), is between 0.1 inch and 1.0 inch. This displacement range is for curved IAB's with piles in very stiff clay soil profile for a 50 ft to 300 ft bridge length. It is the same for curved IAB's with piles in predrilled holes for a 50 ft to 400 ft bridge length. Beyond these bridge lengths, the maximum lateral displacement starts to increase to its highest value at the bridge length indicated in Tables 8.1 and 8.2. After it reaches its highest value, some of the lateral displacement values start decreasing and continue to decrease as the bridge length is increased to 1200 ft.

Curved IAB's of an infinite radius (straight IAB's) have a maximum lateral displacement in the range of 0.11 inch to 0.41 inch for all bridge lengths, span lengths, temperature levels and piles in all soil profile types.

Tables 8.1 and 8.2 indicate that the highest lateral displacement of curved IAB's with both 50 ft and 100 ft spans is found at the same bridge length for two temperature levels.

The lengths of curved IAB's which have the highest lateral displacement from Tables 8.1 and 8.2 and from Figures 8.1 to 8.8 are plotted in Figure 8.9. The

maximum lateral displacement of curved IAB's of all radii with piles in very stiff clay profile (no predrilled holes) starts to increase from a 50 ft bridge length until it reaches its highest lateral displacement value at the bridge length indicated in Figure 8.9 (solid line). Beyond that bridge length, the highest lateral displacement value will start decreasing as the bridge length is increased (dashed and dotted lines).

For piles in predrilled holes, the maximum lateral displacement of curved IAB's of all radii starts to increase from a 50 ft bridge length until it reaches its highest lateral displacement value at the bridge length indicated in Figure 8.9 (dashed line). Beyond that bridge length, the highest lateral displacement value will start decreasing as the bridge length is increased (dotted line).

Figure 8.9 indicates that curved IAB's with radii of 1200 ft or larger have the highest lateral displacement at a 1200 ft length for piles in all soil profile types.

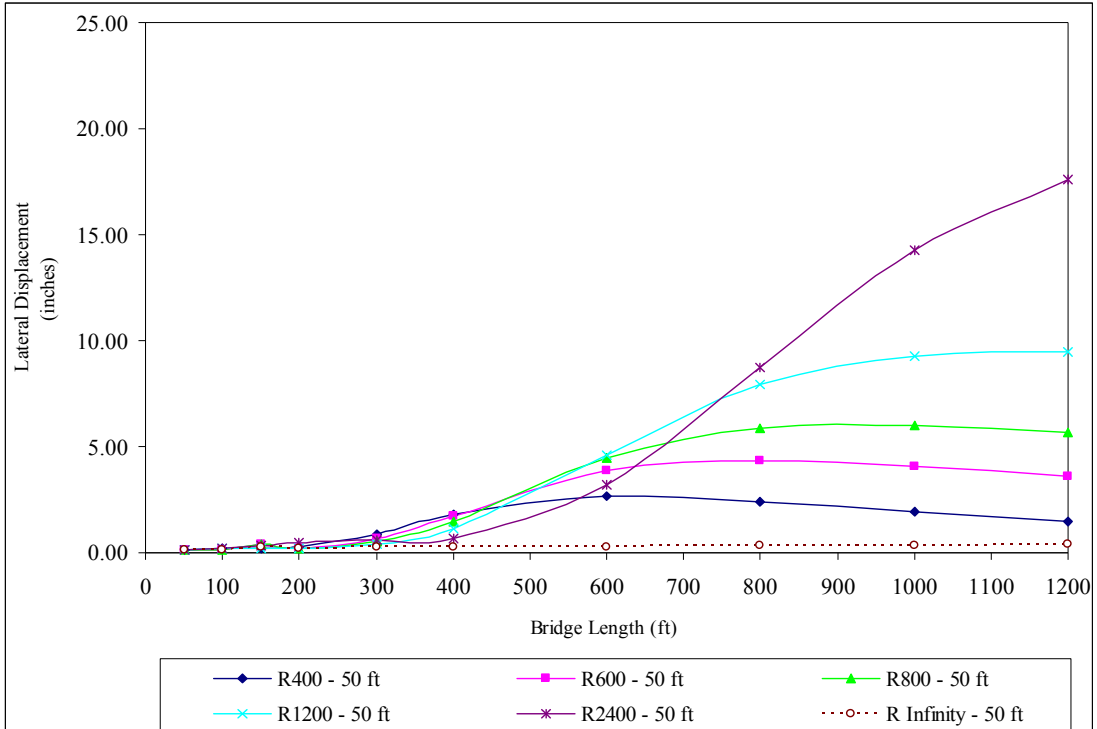
From Figures 8.1 to 8.8, the maximum lateral displacement of curved IAB's with a larger radius and with piles in very stiff clay soil profile is less than that of curved IAB's with a smaller radius for bridge lengths up to 400 ft. It is the same for curved IAB's with piles in predrilled holes for bridge lengths up to 600 ft. Beyond these bridge lengths, curved IAB's with a smaller radius, for the most part, have a maximum lateral displacement less than that of curved IAB's with a larger radius as the bridge length is increased to 1200 ft.

**Table 8.1 – Highest Lateral Displacement (inches) of Curved Integral Abutment Bridges of Different Radii with End-Bearing Piles in Very Stiff Clay Soil Profile**

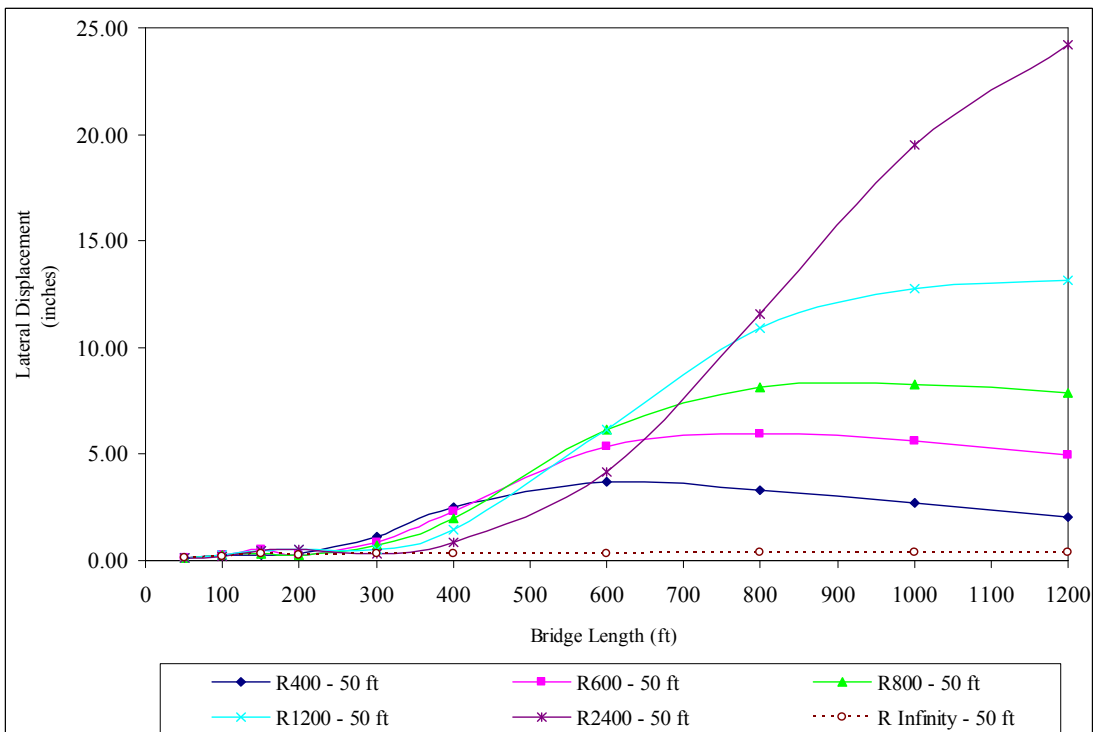
Span Length (ft)	Radius (ft)	Degree of Curve (Degrees)	Bridge Length (ft)	$\Delta T_{\text{slab}} = 90^\circ \text{ F}$ $\Delta T_{\text{the rest}} = 60^\circ \text{ F}$	$\Delta T_{\text{slab}} = 120^\circ \text{ F}$ $\Delta T_{\text{the rest}} = 90^\circ \text{ F}$
50	400	85.944	600	2.68	3.71
	600	76.394	800	4.33	5.98
	800	57.296	800	5.87	8.11
	1200	57.288	1200	9.50	13.13
	2400	28.648	1200	17.63	24.19
	Infinity	0	1200	0.37	0.41
100	400	85.944	600	3.40	4.39
	600	76.394	800	5.23	6.86
	800	57.296	800	7.07	9.24
	1200	57.288	1200	10.92	14.53
	2400	28.648	1200	19.77	26.15
	Infinity	0	1200	0.37	0.41

**Table 8.2 – Highest Lateral Displacement (inches) of Curved Integral Abutment Bridges of Different Radii with End-Bearing Piles in 9 ft Deep Predrilled Holes**

Span Length (ft)	Radius (ft)	Degree of Curve (Degrees)	Bridge Length (ft)	$\Delta T_{\text{slab}} = 90^\circ \text{ F}$ $\Delta T_{\text{the rest}} = 60^\circ \text{ F}$	$\Delta T_{\text{slab}} = 120^\circ \text{ F}$ $\Delta T_{\text{the rest}} = 90^\circ \text{ F}$
50	400	114.592	800	2.25	3.11
	600	95.493	1000	3.76	5.20
	800	85.944	1200	5.37	7.42
	1200	57.288	1200	8.26	11.39
	2400	28.648	1200	10.82	14.53
	Infinity	0	1200	0.13	0.17
100	400	114.592	800	2.86	3.71
	600	95.493	1000	4.63	6.07
	800	85.944	1200	6.38	8.42
	1200	57.288	1200	9.98	13.08
	2400	28.648	1200	12.81	16.38
	Infinity	0	1200	0.16	0.19

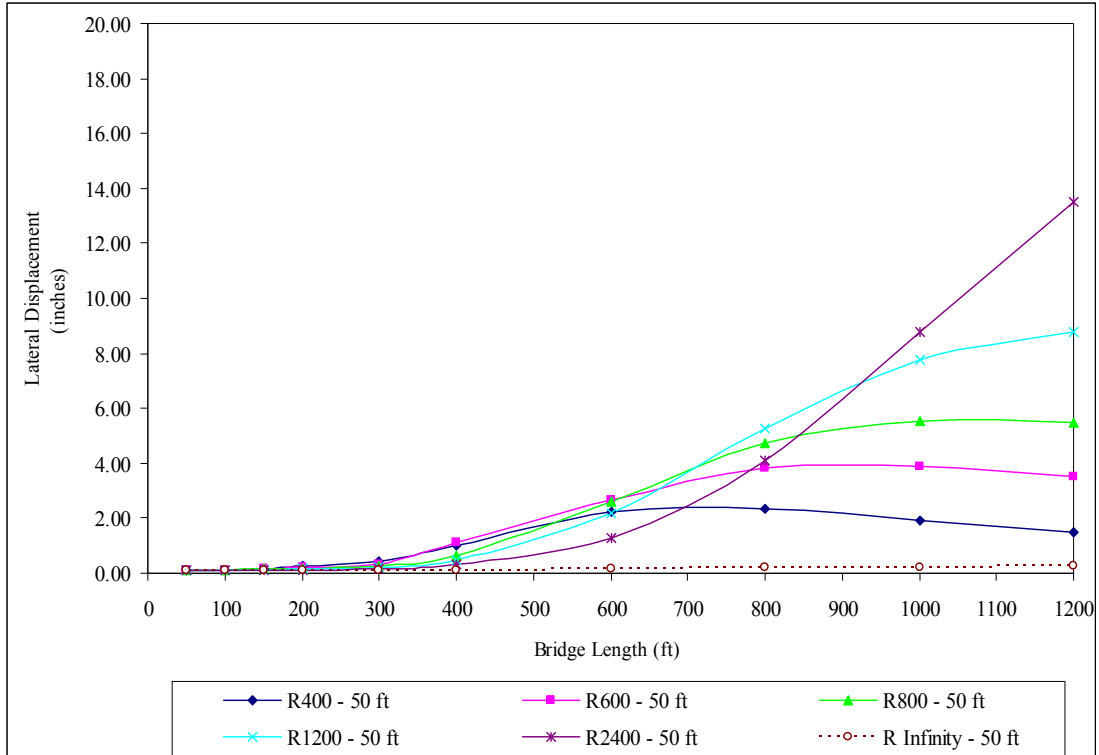


a)  $\Delta T_{\text{slab}} = 90^{\circ} \text{ F}$ ,  $\Delta T_{\text{the rest}} = 60^{\circ} \text{ F}$

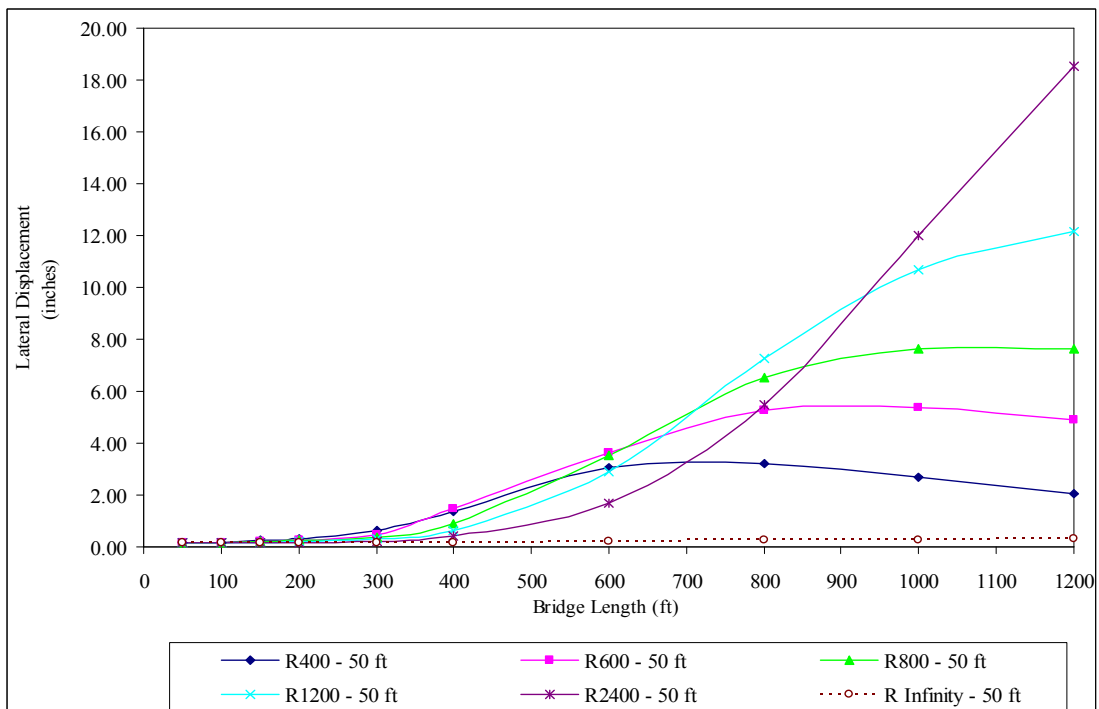


b)  $\Delta T_{\text{slab}} = 120^{\circ} \text{ F}$ ,  $\Delta T_{\text{the rest}} = 90^{\circ} \text{ F}$

**Figure 8.1 – Maximum Lateral Displacement of Bridges with 50 ft Spans and End-Bearing Piles in Very Stiff Clay Soil Profile**

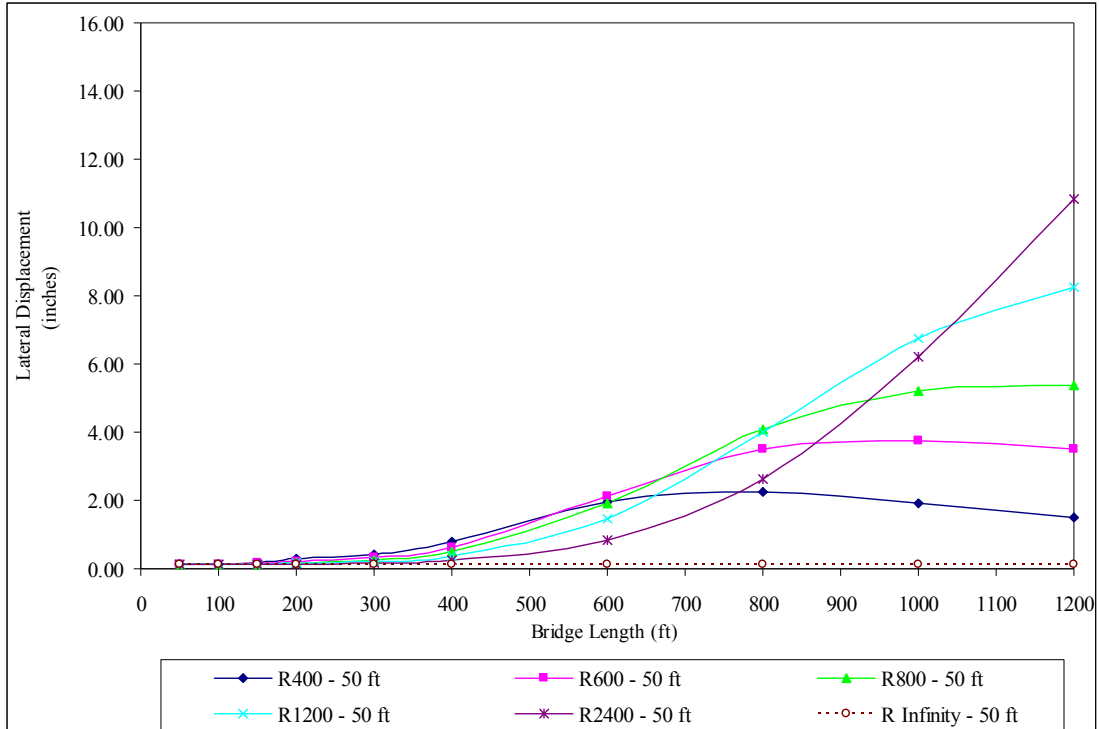


a)  $\Delta T_{\text{slab}} = 90^\circ \text{F}, \Delta T_{\text{the rest}} = 60^\circ \text{F}$

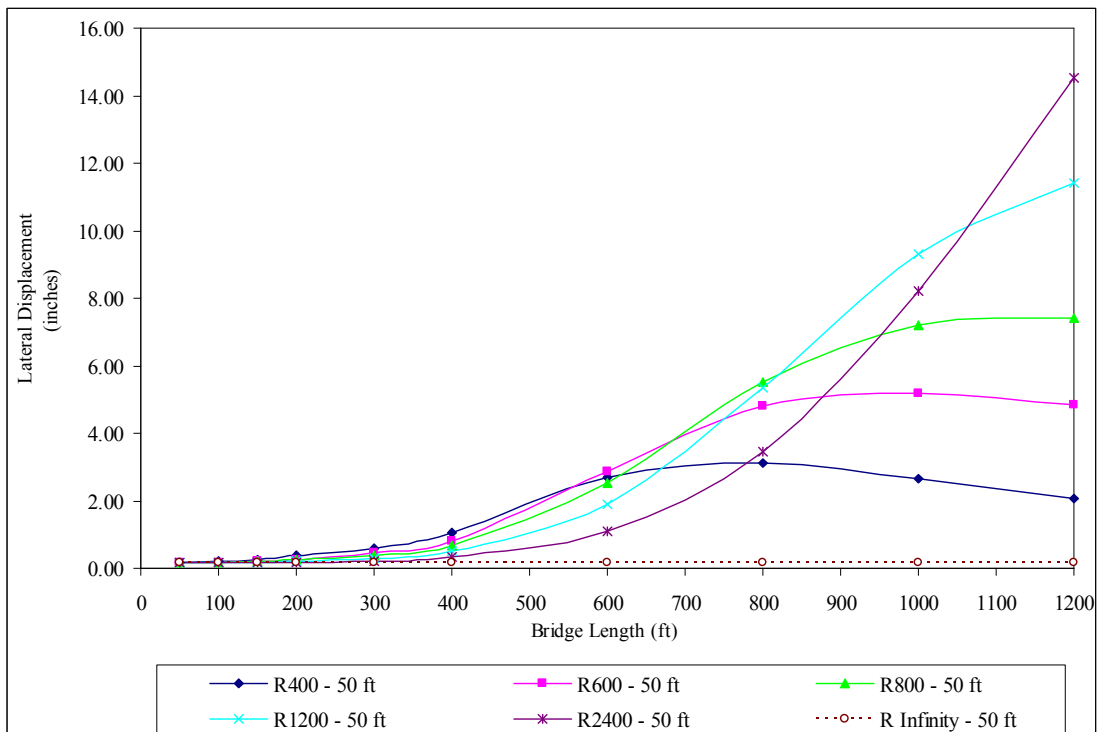


b)  $\Delta T_{\text{slab}} = 120^\circ \text{F}, \Delta T_{\text{the rest}} = 90^\circ \text{F}$

**Figure 8.2 – Maximum Lateral Displacement of Bridges with 50 ft Spans and End-Bearing Piles in 5 ft Deep Predrilled Holes**

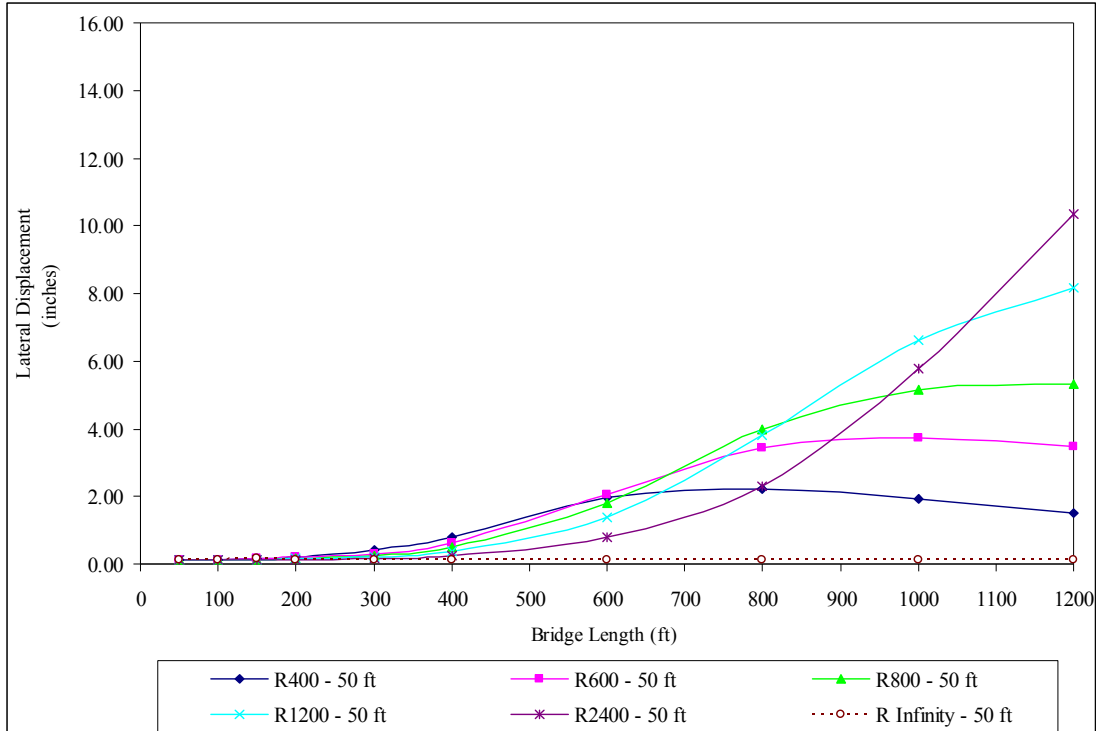


a)  $\Delta T_{\text{slab}} = 90^\circ \text{F}$ ,  $\Delta T_{\text{the rest}} = 60^\circ \text{F}$

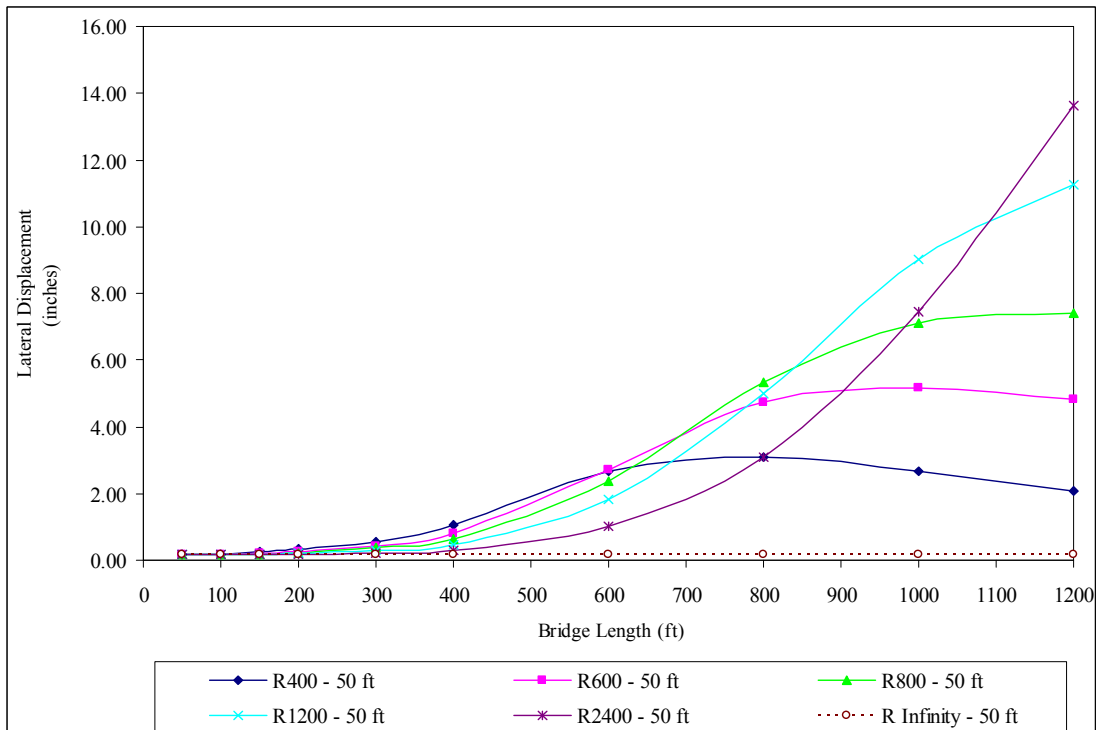


b)  $\Delta T_{\text{slab}} = 120^\circ \text{F}$ ,  $\Delta T_{\text{the rest}} = 90^\circ \text{F}$

**Figure 8.3 – Maximum Lateral Displacement of Bridges with 50 ft Spans and End-Bearing Piles in 9 ft Deep Predrilled Holes**

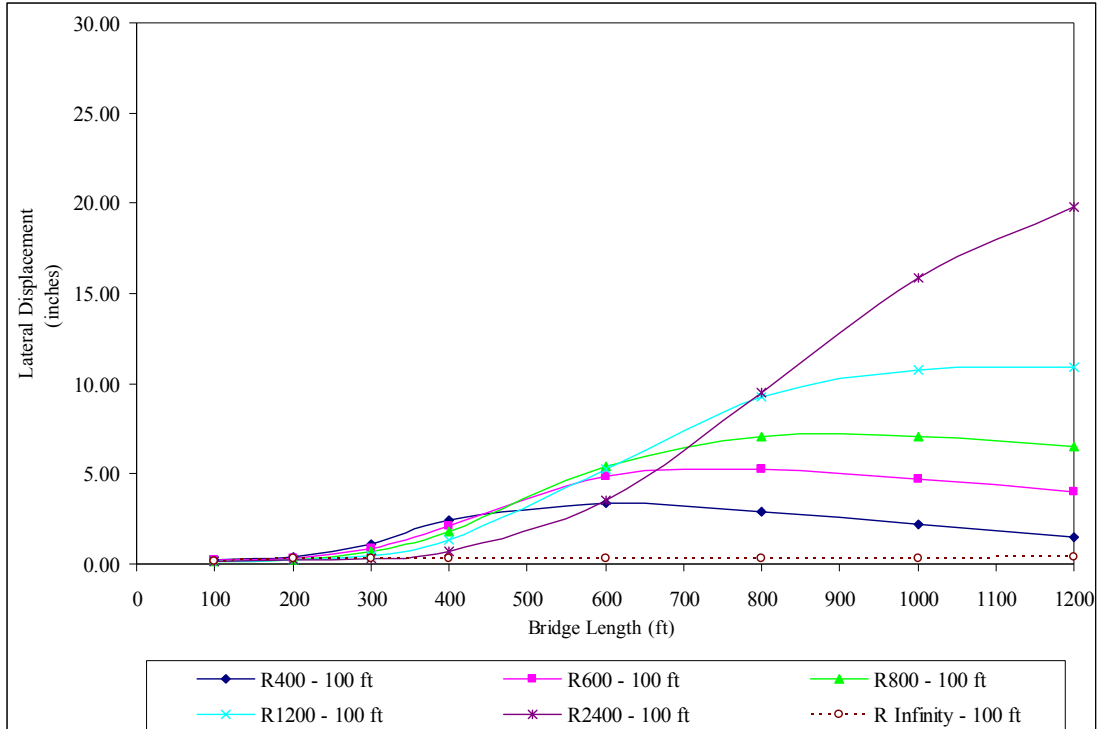


a)  $\Delta T_{\text{slab}} = 90^\circ \text{ F}, \Delta T_{\text{the rest}} = 60^\circ \text{ F}$

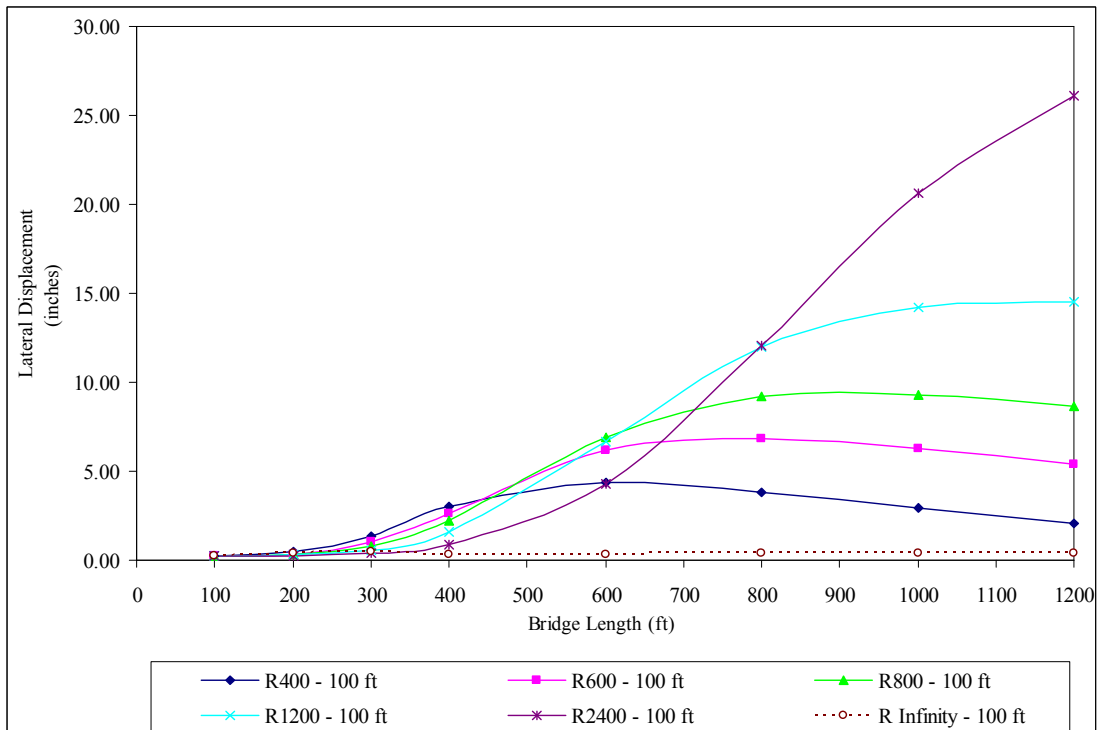


b)  $\Delta T_{\text{slab}} = 120^\circ \text{ F}, \Delta T_{\text{the rest}} = 90^\circ \text{ F}$

**Figure 8.4 – Maximum Lateral Displacement of Bridges with 50 ft Spans and End-Bearing Piles in 15 ft Deep Predrilled Holes**



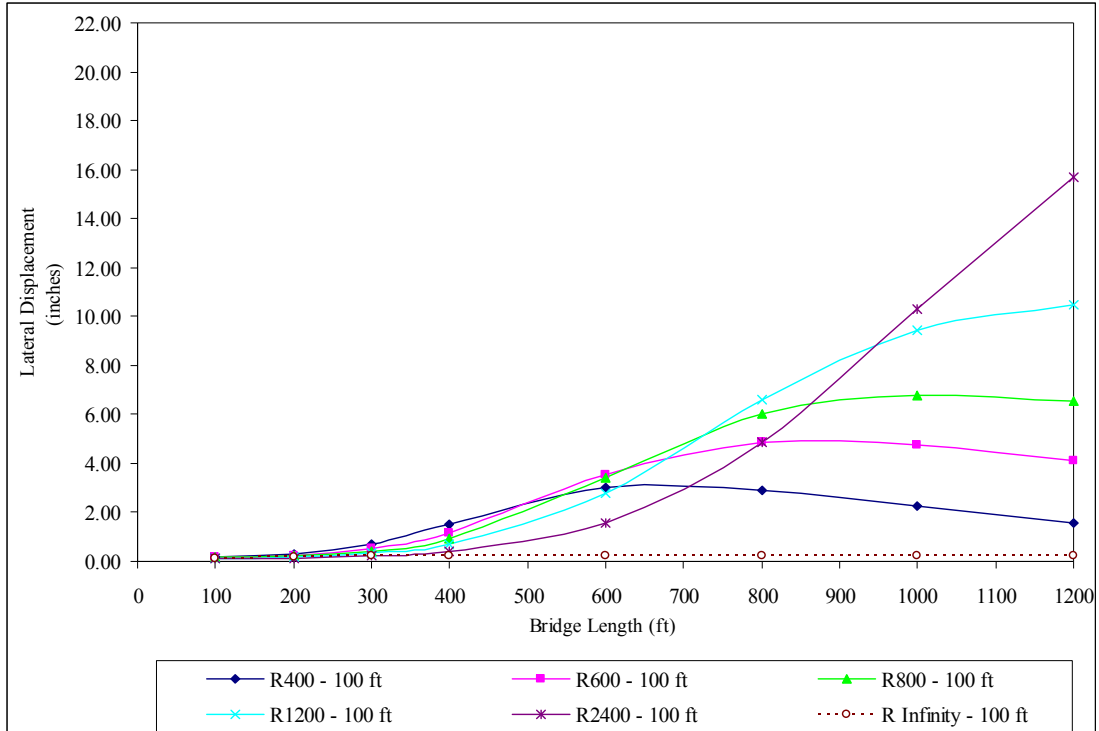
a)  $\Delta T_{\text{slab}} = 90^\circ \text{F}, \Delta T_{\text{the rest}} = 60^\circ \text{F}$



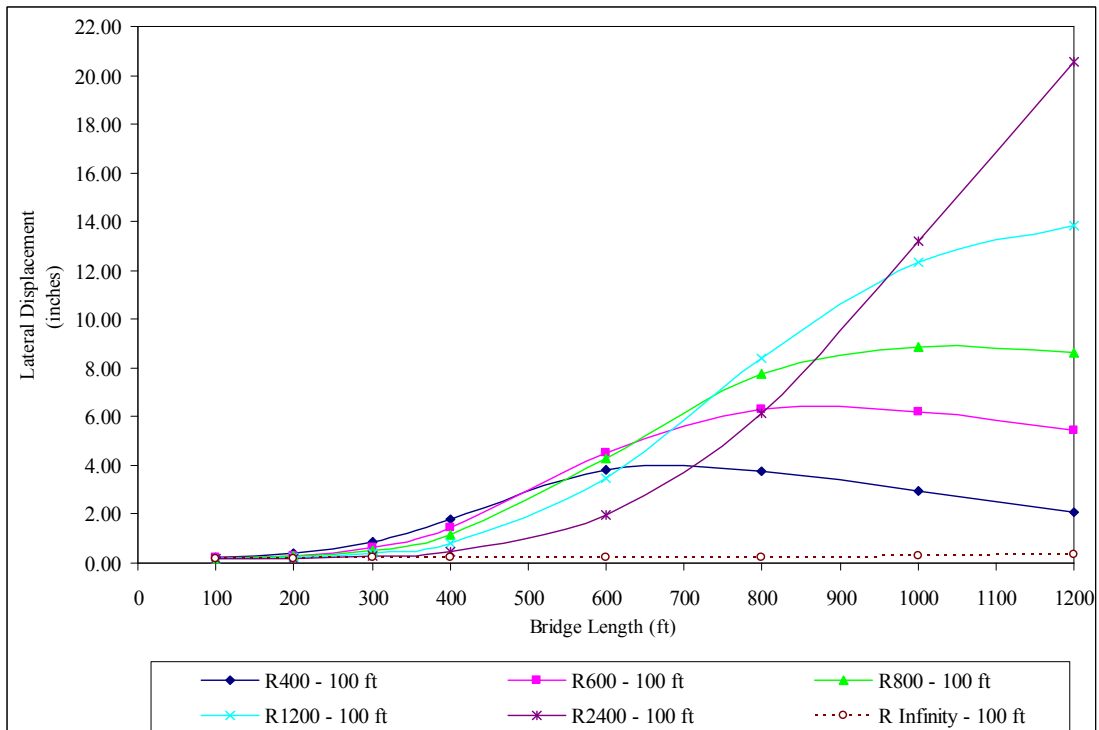
b)  $\Delta T_{\text{slab}} = 120^\circ \text{F}, \Delta T_{\text{the rest}} = 90^\circ \text{F}$

**Figure 8.5 – Maximum Lateral Displacement of Bridges with 100 ft Spans and End-Bearing Piles in Very Stiff Clay Soil Profile**



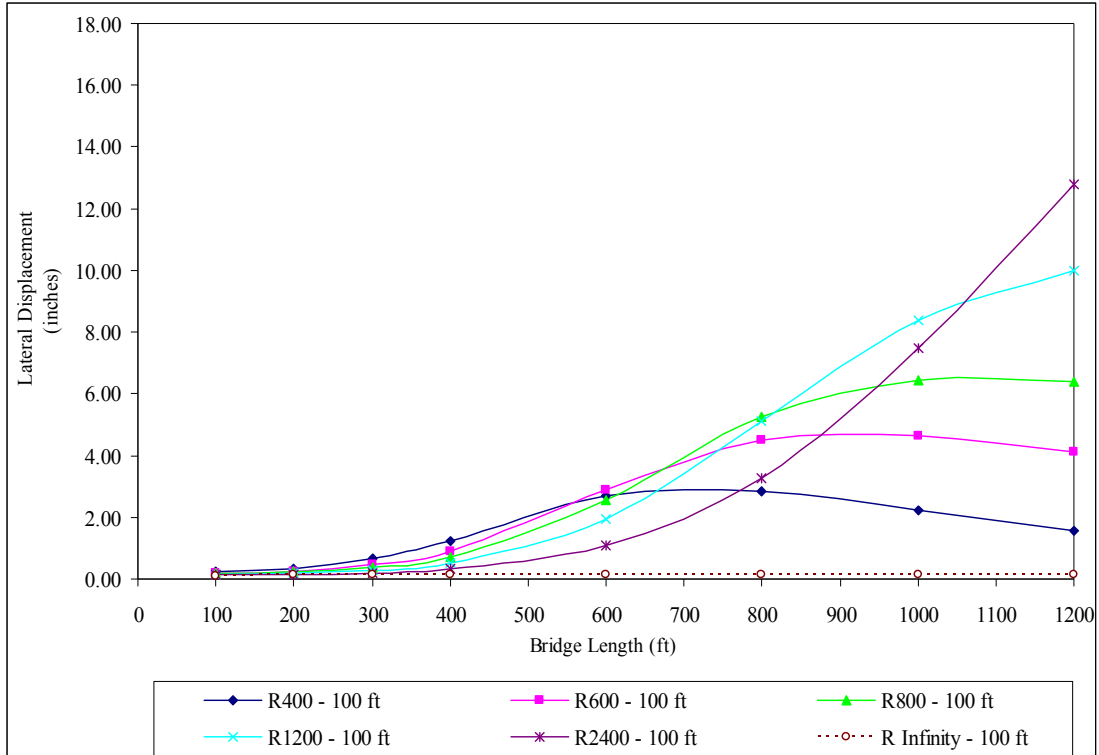


a)  $\Delta T_{\text{slab}} = 90^\circ \text{F}, \Delta T_{\text{the rest}} = 60^\circ \text{F}$

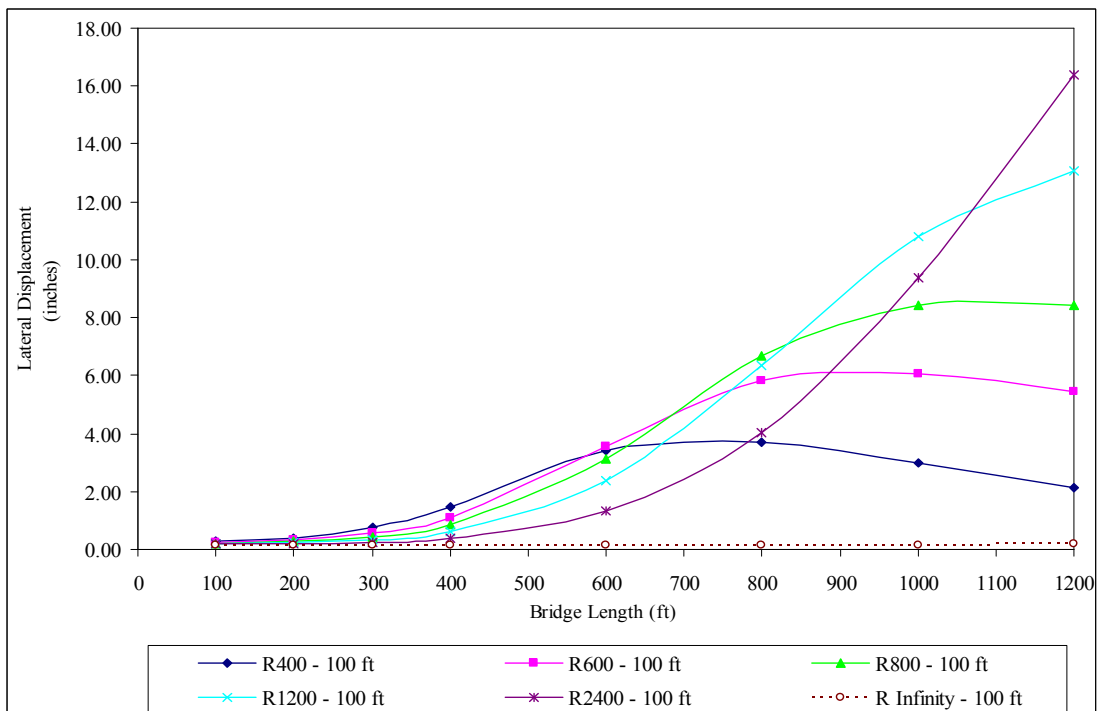


b)  $\Delta T_{\text{slab}} = 120^\circ \text{F}, \Delta T_{\text{the rest}} = 90^\circ \text{F}$

**Figure 8.6 – Maximum Lateral Displacement of Bridges with 100 ft Spans and End-Bearing Piles in 5 ft Deep Predrilled Holes**

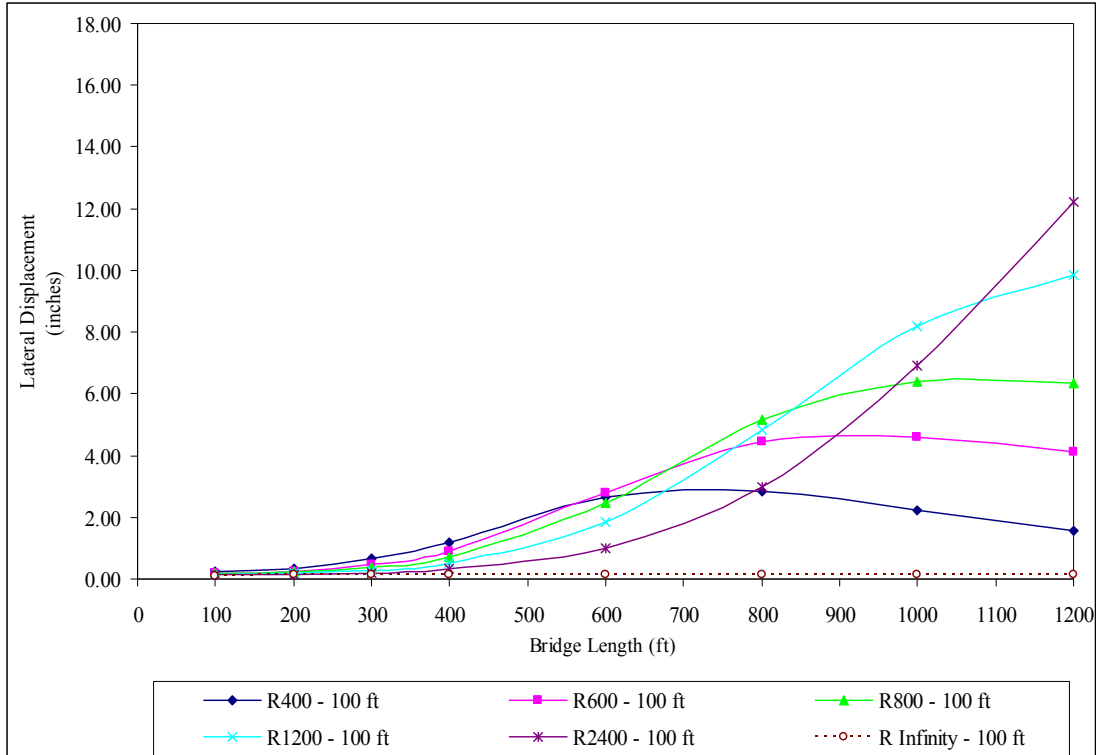


a)  $\Delta T_{\text{slab}} = 90^\circ \text{ F}$ ,  $\Delta T_{\text{the rest}} = 60^\circ \text{ F}$

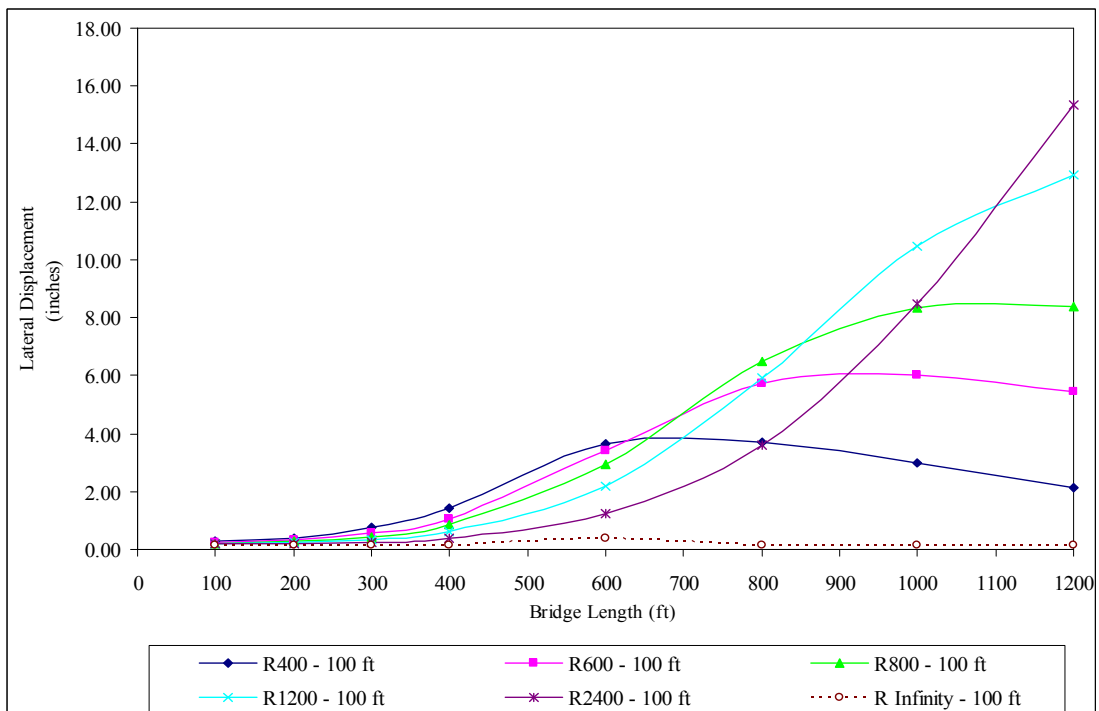


b)  $\Delta T_{\text{slab}} = 120^\circ \text{ F}$ ,  $\Delta T_{\text{the rest}} = 90^\circ \text{ F}$

**Figure 8.7 – Maximum Lateral Displacement of Bridges with 100 ft Spans and End-Bearing Piles in 9 ft Deep Predrilled Holes**



a)  $\Delta T_{\text{slab}} = 90^\circ \text{ F}$ ,  $\Delta T_{\text{the rest}} = 60^\circ \text{ F}$



b)  $\Delta T_{\text{slab}} = 120^\circ \text{ F}$ ,  $\Delta T_{\text{the rest}} = 90^\circ \text{ F}$

**Figure 8.8 – Maximum Lateral Displacement of Bridges with 100 ft Spans and End-Bearing Piles in 15 ft Deep Predrilled Holes**

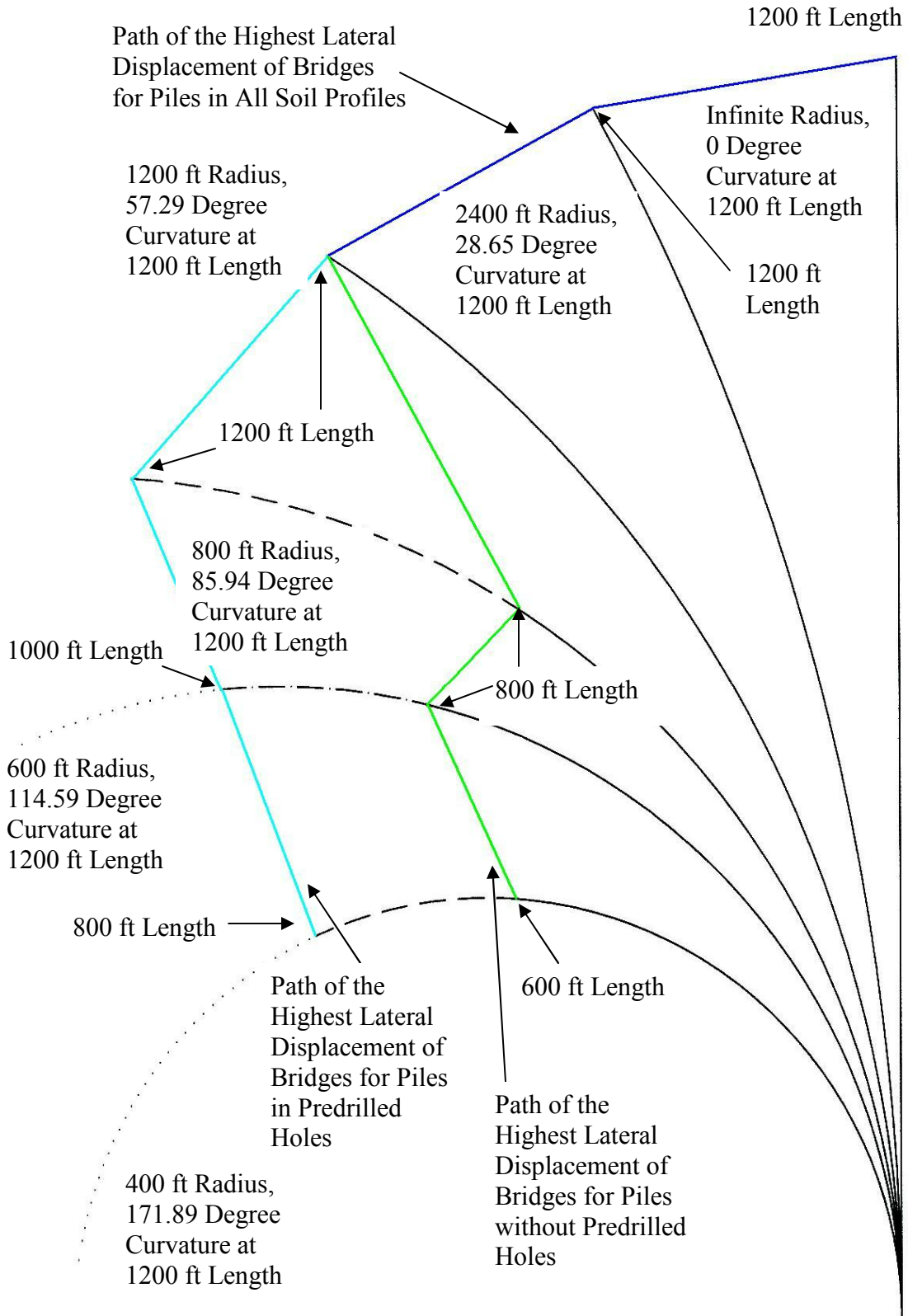


**Figure 8.9 – Highest Lateral Displacement of Curved Integral Abutment Bridges of Different Radii at Different Bridge Lengths**

## **8.2 Effect of Temperature Increase**

The effect of a temperature increase from  $\Delta T_{\text{slab}}$  of 90° F and  $\Delta T_{\text{the rest}}$  of 60° F to  $\Delta T_{\text{slab}}$  of 120° F and  $\Delta T_{\text{the rest}}$  of 90° F (temperature increase of 30° F) in curved IAB's is investigated in this study to determine the maximum lateral displacement increase in a bridge superstructure. All other parameters are held constant.

### **8.2.1 Curved Integral Abutment Bridges with 50 ft Spans**

For curved IAB's of all radii, except an infinite radius, with piles in very stiff clay soil profile, the lateral displacement increase due to the temperature increase is 36.4% at a 50 ft bridge length. It is between 26% and 36.8% at bridge lengths from 100 ft to 300 ft as shown in Figure 8.10. Beyond the 300 ft length, the lateral displacement increase rate starts increasing and continues to increase to its highest value of approximately 38% at a 1200 ft length.

In the case of straight IAB's (an infinite radius), the highest lateral displacement increase value due to the temperature increase is 36.4% at a 50 ft bridge length and decreases to its lowest value of 7.1% at a 400 ft length. After the lateral displacement increase reaches its lowest value, it increases to 20.7% at a 600 ft length. Beyond the 600 ft length, the lateral displacement increase rate due to the temperature increase starts to decrease to 10.8% at a 1200 ft length.

For curved IAB's of all radii with piles in predrilled holes, the lateral displacement increase due to the temperature increase varies in the range of 15.4% to 46.2% at bridge lengths from 50 ft to 400 ft. Beyond the 400 ft length, the lateral

displacement increase rate starts increasing and continues to increase to approximately 38% for a radius from 400 ft to 1200 ft, between 37.2% and 31.8% for a 2400 ft radius, and between 23.1% and 36.4% for an infinite radius as the bridge length is increased to 1200 ft.

The mean of the lateral displacement increase due to the temperature increase of curved IAB's of all radii with 50 ft spans is listed in Table 8.3 and plotted in Figure 8.12. It is shown that the mean of the lateral displacement increase due to the temperature increase is between 20.5% and 39.8% for bridge lengths from 50 ft to 400 ft. It starts to increase from 400 ft to 600 ft and is almost nearly constant in the range of 32.3% to 36.8% for bridge lengths from 600 ft to 1200 ft.

Table 8.4 indicates that curved IAB's with a smaller radius, for the most part, have the mean of the lateral displacement increase due to the temperature increase greater than that of curved IAB's with a larger radius. The mean of the lateral displacement increase due to the temperature increase of curved IAB's with piles in predrilled holes is greater than that of curved IAB's with piles without predrilled holes as indicated in Tables 8.3 and 8.4 as well as Figures 8.12 and 8.13.

**Table 8.3 – Mean and Standard Deviation of Lateral Displacement Increase (%)  
of Bridges with 50 ft Spans and End-Bearing Piles  
due to a 30° F Temperature Increase**

Span Length (ft)	Description	Bridge Length (ft)	Depth of Predrilled Holes (ft)			
			0	5	9	15
50	MEAN	50	36.4	35.9	35.9	35.9
		100	20.5	34.8	35.7	35.2
		150	21.7	35.8	35.1	29.1
		200	29.7	37.4	35.2	35.3
		300	29.8	35.1	39.8	37.8
		400	27.3	31.9	33.2	30.9
		600	33.1	34.3	35.5	32.3
		800	33.3	36.3	35.3	35.3
		1000	33.4	35.2	34.9	36.1
		1200	33.5	35.7	36.3	36.8
	STD	50	0.0	1.2	1.2	1.2
		100	10.6	2.8	3.6	2.7
		150	14.4	3.4	3.6	17.5
		200	5.2	3.9	5.8	2.9
		300	5.7	5.2	4.5	4.1
		400	11.6	8.2	1.9	3.1
		600	6.8	4.9	5.5	3.5
		800	9.1	2.7	2.7	2.7
		1000	10.8	6.7	5.4	3.6
		1200	11.1	6.2	3.1	2.6

**Table 8.4 – Mean and Standard Deviation of Lateral Displacement Increase (%)  
of Bridges of Different Radii with 50 ft Spans and End-Bearing Piles  
due to a 30° F Temperature Increase**

Span Length (ft)	Description	Radius (ft)	Depth of Predrilled Holes (ft)			
			0	5	9	15
50	MEAN	400	33.74	37.44	36.27	35.91
		600	35.61	37.21	36.00	37.39
		800	34.86	37.45	37.69	34.94
		1200	29.93	35.78	34.94	34.38
		2400	26.18	34.76	33.63	32.06
		Infinity	18.81	28.72	35.58	32.10
	STD	400	10.22	1.70	4.46	3.01
		600	2.70	2.92	3.23	2.87
		800	3.66	2.13	4.36	4.26
		1200	10.47	2.76	3.68	3.47
		2400	10.90	1.96	2.44	2.97
		Infinity	8.53	7.66	5.13	13.48



### **8.2.2 Curved Integral Abutment Bridges with 100 ft Spans**

For curved IAB's of all radii, except an infinite radius, with piles in very stiff clay soil profile, the lateral displacement increase due to the temperature increase is between 12% and 25% at bridge lengths from 100 ft to 300 ft as shown in Figure 8.11. Beyond the 300 ft length, the lateral displacement increase rate starts increasing and continues to increase to its highest value in the range of 32.3% to 36.8% as the bridge length is increased to 1200 ft.

In the case of straight IAB's (an infinite radius), the lateral displacement increase due to the temperature increase is 23.5% at a 100 ft bridge length and increases to 40.6% at a 300 ft length. Beyond the 300 ft length, the lateral displacement increase rate starts decreasing and continues to decrease to 10.8% as the bridge length is increased to 1200 ft.

For curved IAB's of all radii, except an infinite radius, with piles in predrilled holes, the lateral displacement increase due to the temperature increase varies in the range of 15.0% to 35.4% at bridge lengths from 100 ft to 400 ft. Beyond the 400 ft length, the lateral displacement increase rate starts increasing and continues to increase to approximately 36.5% for a 400 ft radius, between 31% and 32.8% for a radius from 600 ft to 1200 ft, and between 25.6% and 30.7% for a 2400 ft radius as the bridge length is increased to 1200 ft.

In the case of straight IAB's (an infinite radius), the lateral displacement increase due to the temperature increase varies in the range of 6.7% to 36.4% as the bridge length increases from 100 ft to 1200 ft.

The mean of the lateral displacement increase due to the temperature increase of curved IAB's of all radii with 100 ft spans is listed in Table 8.5 and plotted in Figure 8.12. It is shown that the mean of the lateral displacement increase due to the temperature increase is between 17% and 29.7% for bridge lengths from 50 ft to 400 ft. It starts increasing and continues to increase to its highest value of approximately 30.5% as the bridge length is increased to 1200 ft.

Table 8.6 indicates that curved IAB's with a smaller radius, for the most part, have the mean of the lateral displacement increase due to the temperature increase greater than that of curved IAB's with a larger radius. The mean of the lateral displacement increase due to the temperature increase of curved IAB's with piles in predrilled holes, for the most part, is less than that of curved IAB's with piles without predrilled holes as indicated in Tables 8.5 and 8.6 as well as Figures 8.12 and 8.13.

**Table 8.5 – Mean and Standard Deviation of Lateral Displacement Increase (%)  
of Bridges with 100 ft Spans and End-Bearing Piles  
due to a 30° F Temperature Increase**

Span Length (ft)	Description	Bridge Length (ft)	Depth of Predrilled Holes (ft)			
			0	5	9	15
100	MEAN	100	18.8	29.6	26.0	23.5
		200	23.8	18.9	21.7	22.7
		300	24.1	17.0	17.6	20.9
		400	20.9	29.7	17.6	19.7
		600	25.2	21.4	23.8	23.9
		800	27.6	23.8	23.4	25.4
		1000	28.7	27.0	25.8	28.2
		1200	30.0	31.7	29.8	30.4
	STD	100	4.0	4.9	6.9	8.5
		200	8.6	20.3	7.5	3.1
		300	8.2	13.0	5.6	3.4
		400	4.7	28.8	5.3	3.3
		600	4.8	10.6	3.0	7.0
		800	6.4	11.8	8.3	3.6
		1000	8.5	9.6	9.8	3.9
		1200	9.5	3.0	6.1	4.4

**Table 8.6 – Mean and Standard Deviation of Lateral Displacement Increase (%)  
of Bridges of Different Radii with 100 ft Spans and End-Bearing Piles  
due to a 30° F Temperature Increase**

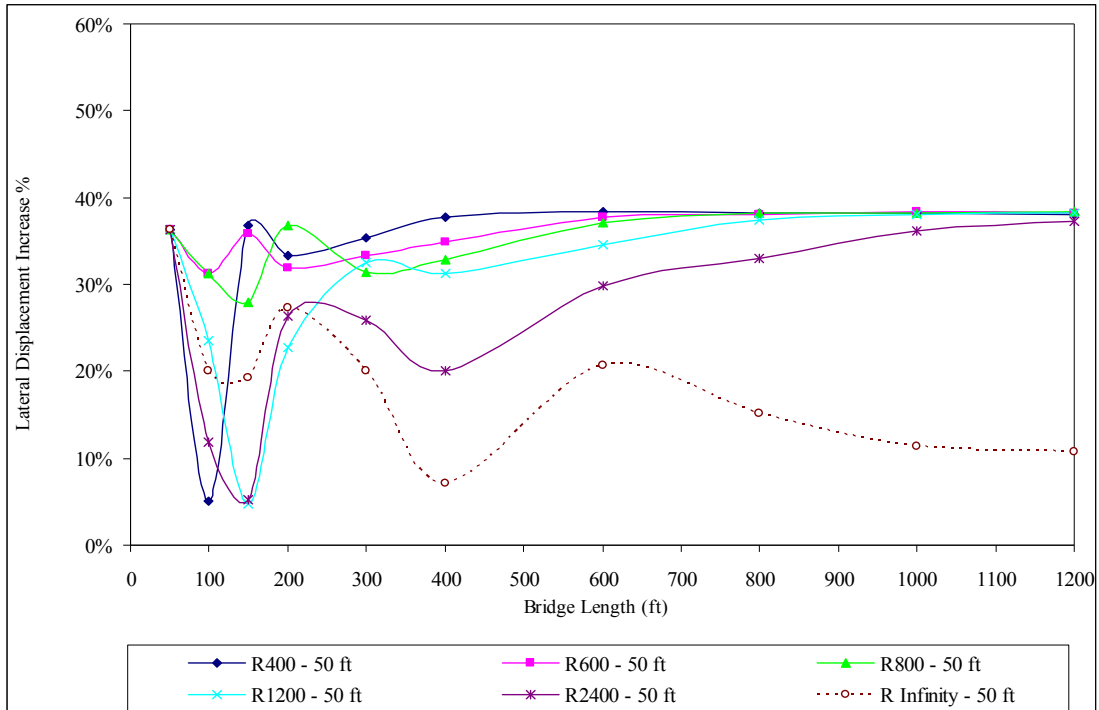
Span Length (ft)	Description	Radius (ft)	Depth of Predrilled Holes (ft)			
			0	5	9	15
100	MEAN	400	26.27	27.09	25.22	25.76
		600	26.10	33.57	25.00	23.45
		800	26.70	27.92	24.64	23.94
		1200	24.62	26.93	24.99	22.27
		2400	24.67	28.65	24.56	24.15
		Infinity	20.99	5.15	14.81	26.42
	STD	400	7.89	5.77	7.33	9.25
		600	6.74	21.51	5.16	6.58
		800	5.11	4.39	4.77	5.16
		1200	7.08	3.64	4.29	4.73
		2400	5.00	3.77	3.73	3.63
		Infinity	12.02	18.57	11.82	4.02

### 8.2.3 Conclusions

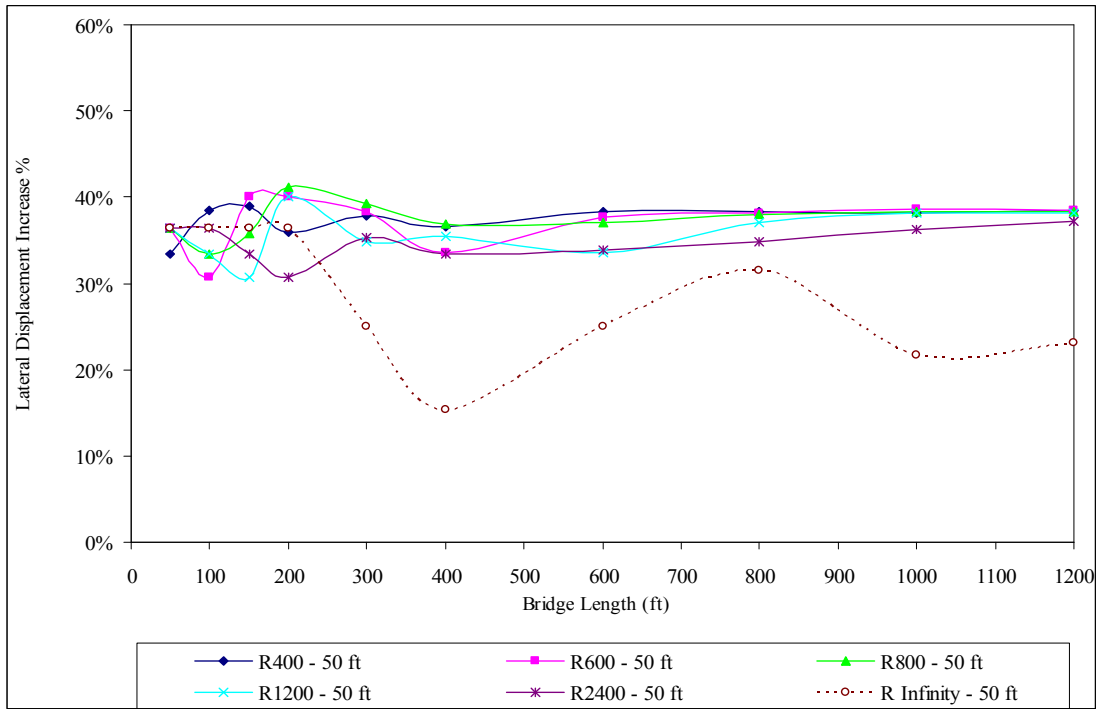
The following conclusions are drawn from the study of the effect of a temperature increase of 30° F in curved IAB's on the maximum lateral displacement increase in a bridge superstructure investigated in this section:

1. Curved IAB's with a smaller radius, for the most part, have the mean of the lateral displacement increase due to the temperature increase greater than that of curved IAB's with a larger radius.
2. Curved IAB's of all radii with 50 ft spans and with piles in all soil profile types have the mean of the lateral displacement increase due to the temperature increase between 20.5% and 39.8% for bridge lengths from 50 ft to 400 ft. It starts to increase from 400 ft to 600 ft and is almost nearly constant in the range of 32.3% to 36.8% for bridge lengths from 600 ft to 1200 ft.
3. Curved IAB's of all radii with 100 ft spans and with piles in all soil profile types have the mean of the lateral displacement increase due to the temperature increase between 17% and 29.7% for bridge lengths from 50 ft to 400 ft. It starts increasing and continues to increase to its highest value of approximately 30.5% as the bridge length is increased to 1200 ft.
4. The mean of the lateral displacement increase due to the temperature increase of curved IAB's with 50 ft spans and with piles in predrilled holes is greater than that of curved IAB's with piles without predrilled holes.

5. For curved IAB's with 100 ft spans, the mean of the lateral displacement increase due to the temperature increase of curved IAB's with piles in predrilled holes is less than that of curved IAB's with piles without predrilled holes.
6. Table 8.7 and Figure 8.14 indicate that the mean of the lateral displacement increase due to the temperature increase of curved IAB's with 50 ft spans is greater than that of curved IAB's with 100 ft spans because the self weight of curved IAB's with 100 ft spans is greater than that of curved IAB's with 50 ft spans. Therefore, curved IAB's with the longer span lengths will result in a smaller increase in the lateral displacement of curved IAB's due to the temperature increase when compared to curved IAB's with the shorter span lengths.

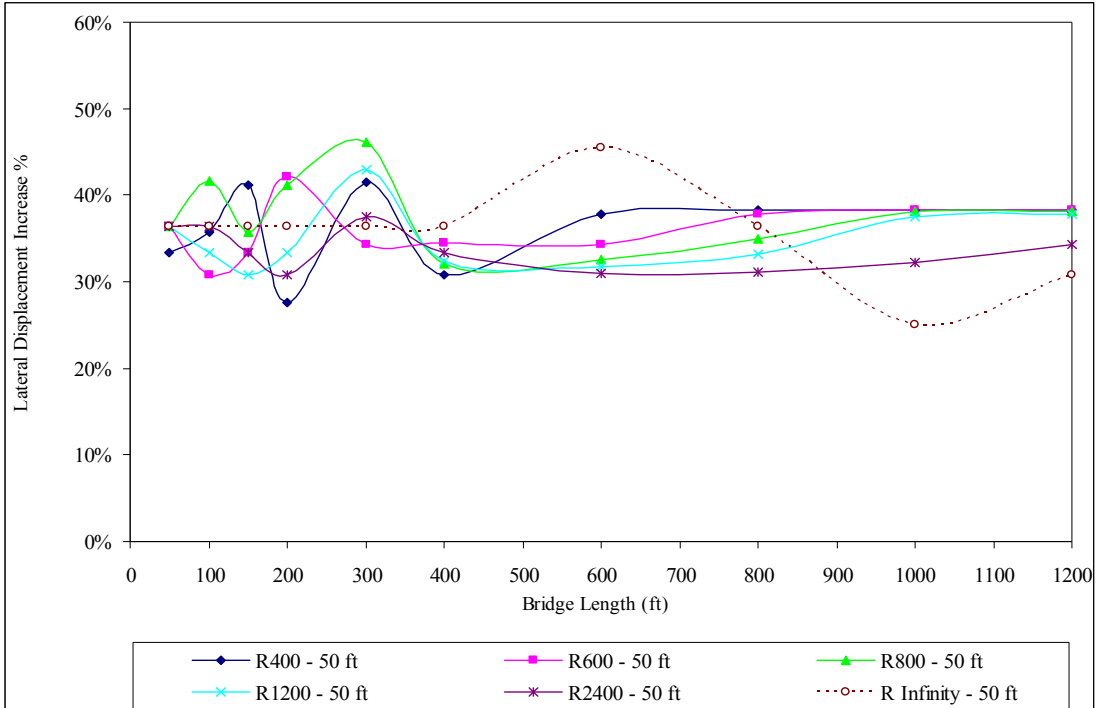


**a) Very Stiff Clay Soil Profile**

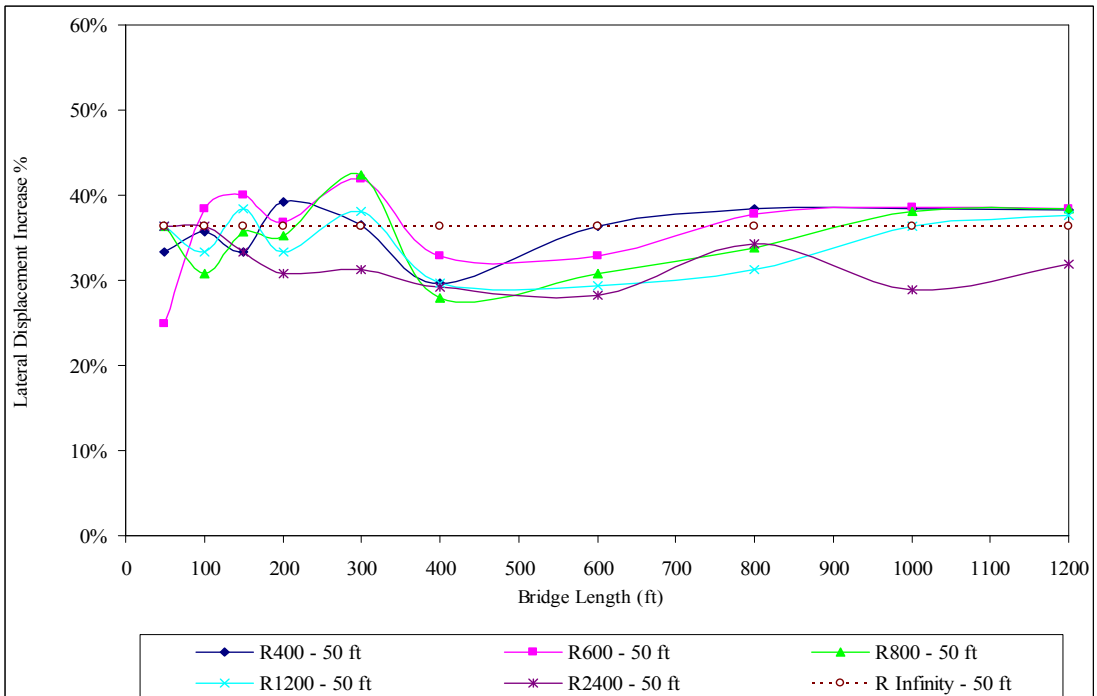


**b) Very Stiff Clay Soil Profile with 5 ft Deep Predrilled Holes Filled with Loose Sand**

**Figure 8.10 – Lateral Displacement Increase (%) of Bridges with 50 ft Spans and End-Bearing Piles due to a 30° F Temperature Increase**



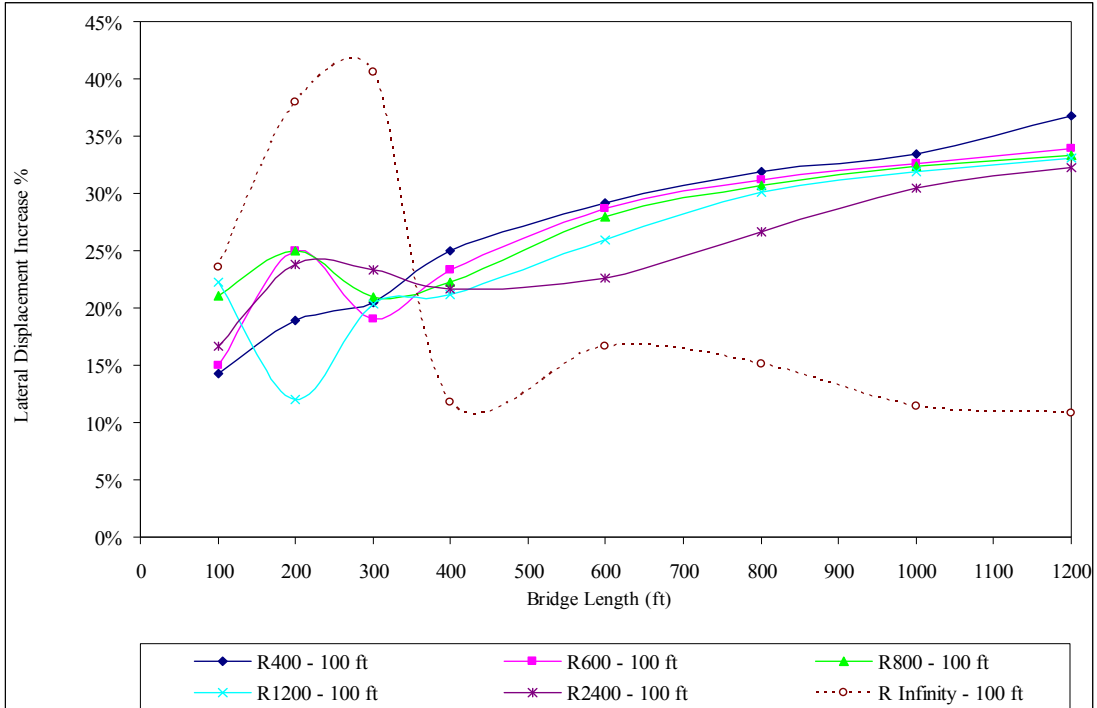
**c) Very Stiff Clay Soil Profile with 9 ft Deep Predrilled Holes Filled with Loose Sand**



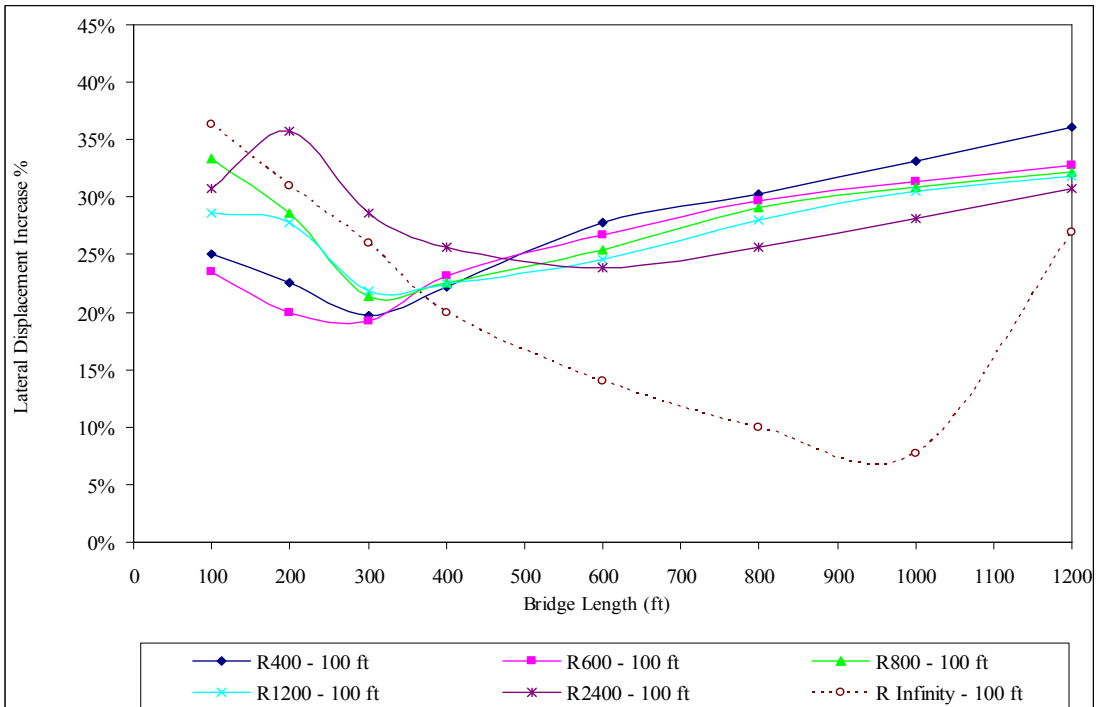
**d) Very Stiff Clay Soil Profile with 15 ft Deep Predrilled Holes Filled with Loose Sand**

**Figure 8.10 (Continued) – Lateral Displacement Increase (%) of Bridges with 50 ft Spans and End-Bearing Piles due to a 30° F Temperature Increase**



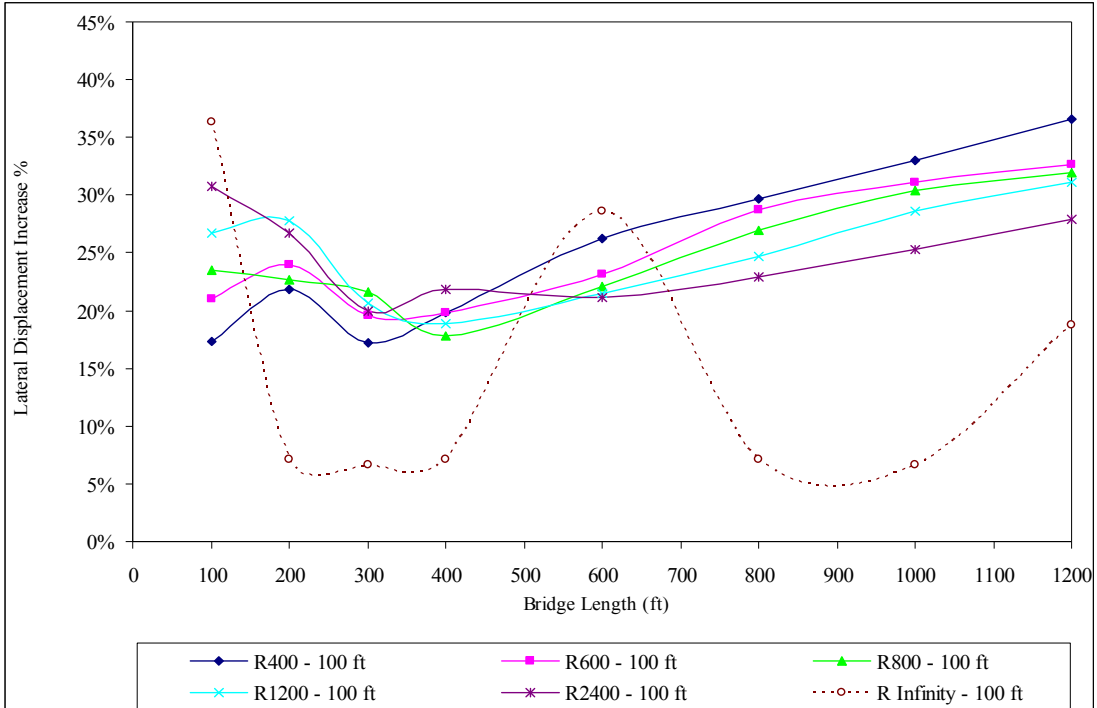


a) Very Stiff Clay Soil Profile

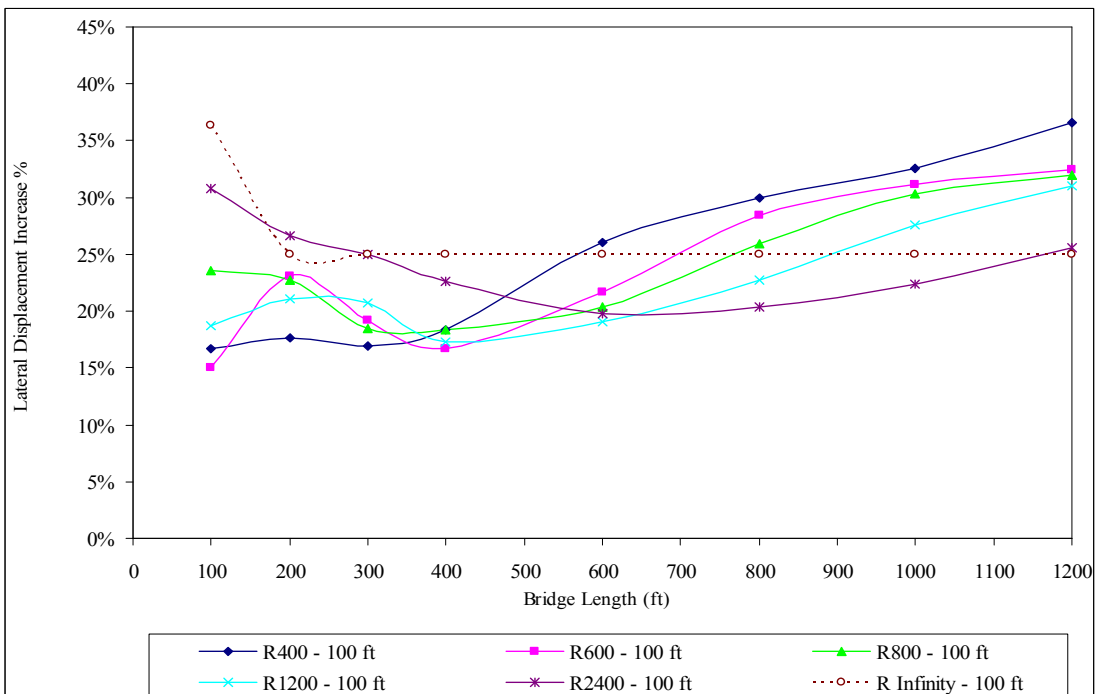


b) Very Stiff Clay Soil Profile with 5 ft Deep Predrilled Holes Filled with Loose Sand

Figure 8.11 – Lateral Displacement Increase (%) of Bridges with 100 ft Spans and End-Bearing Piles due to a 30° F Temperature Increase



**c) Very Stiff Clay Soil Profile with 9 ft Deep Predrilled Holes Filled with Loose Sand**



**d) Very Stiff Clay Soil Profile with 15 ft Deep Predrilled Holes Filled with Loose Sand**

**Figure 8.11 (Continued) – Lateral Displacement Increase (%) of Bridges with 100 ft Spans and End-Bearing Piles due to a 30° F Temperature Increase**

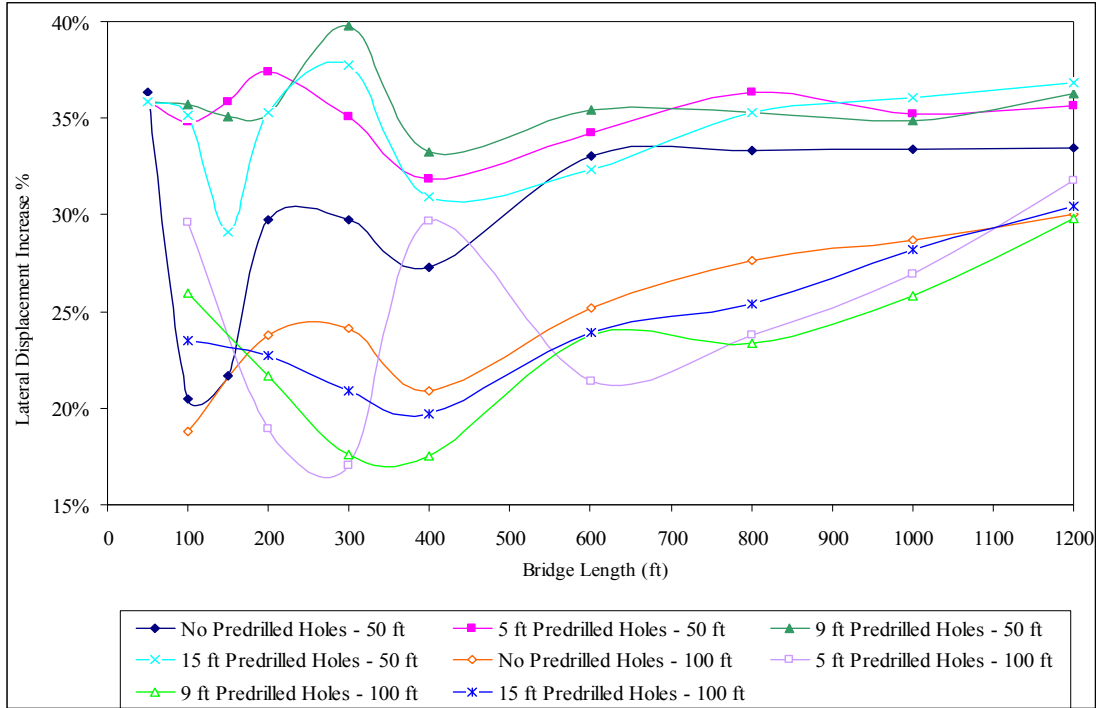


**Figure 8.12 – Mean of Lateral Displacement Increase (%) of Bridges with 50 ft and 100 ft Spans and End-Bearing Piles due to a 30° F Temperature Increase**

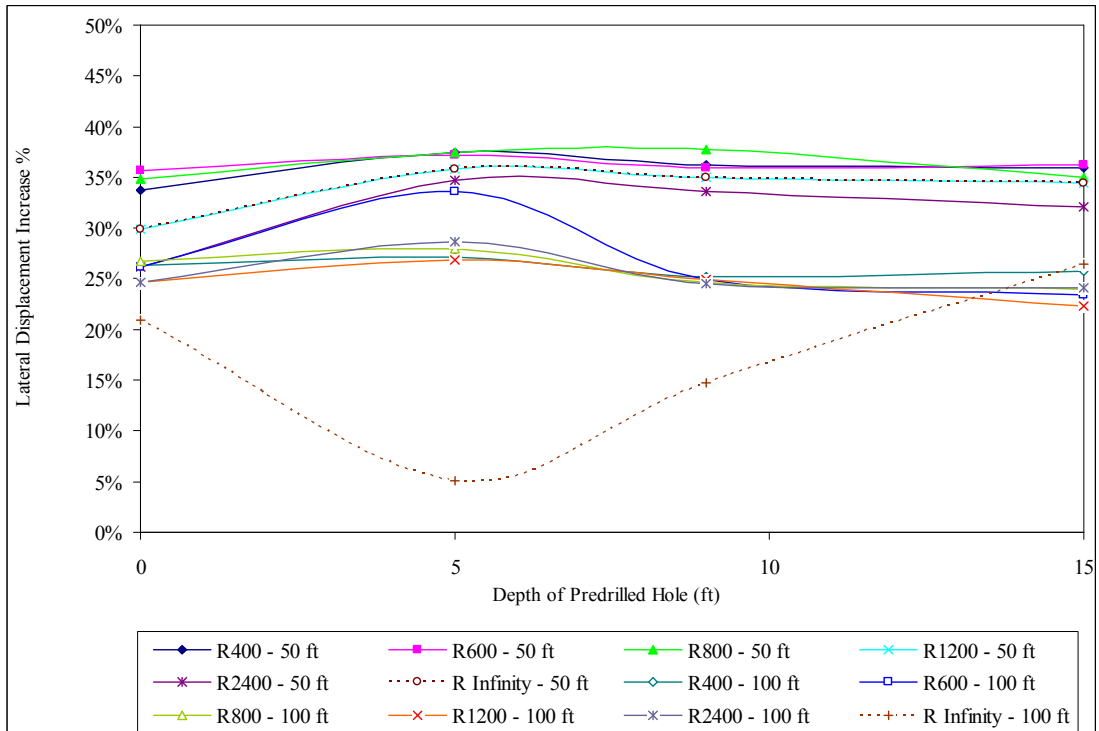


**Figure 8.13 – Mean of Lateral Displacement Increase (%) of Bridges of Different Radii and End-Bearing Piles due to a 30° F Temperature Increase**

**Table 8.7 – Difference in Lateral Displacement Increase (%) between Bridges with 50 ft and 100 ft Spans and End-Bearing Piles due to a 30° F Temperature Increase**

Description	Bridge Length (ft)	Depth of Predrilled Holes (ft)			
		0	5	9	15
MEAN	100	1.7	5.2	9.7	11.7
	200	5.9	18.5	13.5	12.6
	300	5.6	18.0	22.1	16.9
	400	6.4	2.2	15.7	11.2
	600	7.9	12.9	11.7	8.4
	800	5.7	12.6	11.9	9.9
	1000	4.7	8.3	9.1	7.9
	1200	3.5	3.9	6.5	6.4
STD	100	9.8	5.0	7.3	8.9
	200	9.1	20.8	10.0	5.6
	300	13.6	8.9	5.4	6.9
	400	7.5	26.6	6.8	3.1
	600	2.0	6.0	2.6	4.8
	800	2.8	9.3	8.5	2.3
	1000	2.3	3.0	4.7	2.0
	1200	2.2	4.1	3.3	3.1

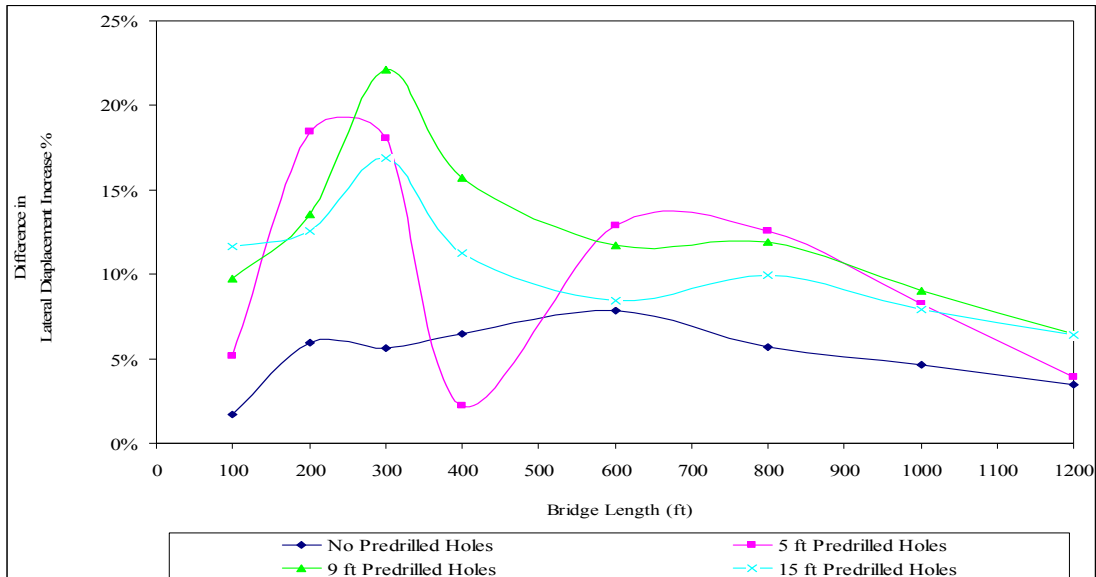


**Figure 8.14 – Difference in Lateral Displacement Increase (%) between Bridges with 50 ft and 100 ft Spans and End-Bearing Piles due to a 30° F Temperature Increase**

### **8.3 Effect of Soil Profile Variation**

Four different soil profiles are investigated in this study. Piles are driven 40 ft below the bottom of the abutment in each one of these four soil profiles. The first soil profile is a single layer of 40 ft deep very stiff clay below the abutment (equivalent to 0 ft predrilled hole). The other three soil profiles each consist of two layers combined to a total of 40 ft deep below the abutment. The top layer is loose sand to simulate predrilled holes filled with loose sand, while the bottom layer is very stiff clay. The difference between these three soil profiles is the depth of the predrilled holes, which is 5 ft, 9 ft, and 15 ft respectively. All other parameters are held constant.

#### **8.3.1 Curved Integral Abutment Bridges with 50 ft Spans**

Figures 8.15 to 8.17 indicate that there is no lateral displacement reduction of curved IAB's of all radii due to the introduction of predrilled holes for  $\Delta T_{\text{slab}}$  of 90° F and  $\Delta T_{\text{the rest}}$  of 60° F at a 50 ft bridge length.

For curved IAB's with a 400 ft radius, the lateral displacement of curved IAB's due to the introduction of predrilled holes does not decrease but increases by 9.1% at a 50 ft bridge length. The lateral displacement increases from 0.11 inch for piles without predrilled holes to 0.12 inch for piles in varying depths of predrilled holes.

Beyond the 50 ft length, the lateral displacement reduction rate starts to increase at bridge lengths between 100 ft and 150 ft. Beyond these lengths, the lateral displacement reduction rate decreases at a 200 ft length and then continues to increase to its highest value at the bridge length indicated in Table 8.8. After the lateral

displacement reduction rate reaches its highest value, it starts decreasing and continues to decrease as the bridge length is increased to 1200 ft.

It is shown in Figures 8.15 to 8.17 that the introduction of predrilled holes does not decrease the lateral displacement of curved IAB's with a 400 ft radius, but increases by 0.7% to 1.4% at bridge lengths between 1000 ft to 1200 ft. The lateral displacement reduction due to the introduction of predrilled holes of curved IAB's with a smaller radius decreases much more rapidly after reaching its highest value than that of curved IAB's with a larger radius as the bridge length is increased to 1200 ft.

The mean of the lateral displacement reduction of curved IAB's of all radii with 50 ft spans due to the introduction of predrilled holes is listed in Table 8.9 and plotted in Figure 8.18. It is shown that there is no lateral displacement reduction at a 50 ft bridge length. The mean of the lateral displacement reduction starts to increase from 50 ft to 150 ft lengths and decreases at a 200 ft length. Beyond the 200 ft length, it increases to its highest value at a 400 ft length. After the mean of the lateral displacement reduction reaches its highest value, it starts decreasing and continues to decrease as the bridge length is increased to 1200 ft.

**Table 8.8 – Lateral Displacement Reduction (%) of Bridges with 50 ft Spans and End-Bearing Piles in Varying Depths of Predrilled Holes Filled with Loose Sand ( $\Delta T_{\text{slab}} = 90^\circ \text{ F}$ ,  $\Delta T_{\text{the rest}} = 60^\circ \text{ F}$ )**

Radius (ft)	Highest Lateral Displacement Reduction (%) at Bridge Length (ft)		Lateral Displacement Reduction (%) at 1200 ft Length
400	47.1	300	-0.7
600	61.5	150	1.4
800	56.4	400	3.2
1200	57.1	400	7.5
2400	60.2	600	23.3
Infinity	57.7	150	29.7

**a) 5 ft Deep Predrilled Holes Filled with Loose Sand**

Radius (ft)	Highest Lateral Displacement Reduction (%) at Bridge Length (ft)		Lateral Displacement Reduction (%) at 1200 ft Length
400	55.7	400	-1.4
600	64.5	400	2.2
800	66.4	400	5.5
1200	68.3	600	13.1
2400	73.7	600	38.6
Infinity	66.7	800	64.9

**b) 9 ft Deep Predrilled Holes Filled with Loose Sand**

Radius (ft)	Difference between Depth of Predrilled Holes	
	9 ft – 5ft	15 ft – 9 ft
400	0 to 10.9	0 to 5.3
600	0 to 28.5	0 to 6.1
800	0 to 15.4	0 to 6.3
1200	0 to 16.3	0 to 2.4
2400	0 to 18.2	0 to 3.8
Infinity	0 to 35.1	0 to 5.4

**c) Difference in Lateral Displacement Reduction (%)**

For curved IAB's of different radii with 50 ft spans, it is found that curved IAB's with a smaller radius have the mean of the lateral displacement reduction due to the introduction of predrilled holes less than that of curved IAB's with a larger radius as indicated in Table 8.10 and Figure 8.19.

Tables 8.8c to 8.10 as well as Figures 8.15 to 8.19 indicate that curved IAB's with piles in 9 ft deep predrilled holes have a lateral displacement reduction in the range of 0% to 35.1% greater than that of curved IAB's with piles in 5 ft deep predrilled holes and in the range of 0% to 6.3% less than that of curved IAB's with piles in 15 ft deep predrilled holes. Therefore, it can be concluded that 9 feet deep predrilled holes filled with loose sand have a significant reduction in the lateral displacement of curved IAB's when compared with 5 ft deep predrilled holes filled with loose sand. The depth increase of predrilled holes deeper than 9 ft will further reduce the lateral displacement of curved IAB's, but the rate of reduction is much smaller than that of 9 ft deep predrilled holes.

From the analyses, it is shown that a temperature increase results in a lower lateral displacement reduction of curved IAB's. The mean of the lateral displacement reduction due to the introduction of predrilled holes of curved IAB's subjected to a temperature load of  $\Delta T_{\text{slab}}$  of 90° F and  $\Delta T_{\text{the rest}}$  of 60° F is greater than that of curved IAB's subjected to a temperature load of  $\Delta T_{\text{slab}}$  of 120° F and  $\Delta T_{\text{the rest}}$  of 90° F by 0.4% to 9.3%.



**Table 8.9 – Mean and Standard Deviation of Lateral Displacement Reduction (%) of Bridges with 50 ft Spans and End-Bearing Piles in Varying Depths of Predrilled Holes Filled with Loose Sand**

Description	Bridge Length (ft)	$\Delta T_{\text{slab}} = 90^\circ \text{ F}$ $\Delta T_{\text{the rest}} = 60^\circ \text{ F}$			$\Delta T_{\text{slab}} = 120^\circ \text{ F}$ $\Delta T_{\text{the rest}} = 90^\circ \text{ F}$		
		Depth of Predrilled Holes (ft)					
		5	9	15	5	9	15
MEAN	50	-1.5	-1.5	-1.5	-1.1	-1.1	-1.1
	100	28.4	27.5	26.5	19.8	18.2	17.4
	150	40.6	41.4	37.4	33.2	34.2	33.1
	200	23.4	21.7	25.4	19.1	18.9	22.4
	300	45.9	49.1	50.1	43.6	45.2	47.1
	400	50.8	63.4	63.4	49.2	61.3	61.9
	600	41.5	55.6	56.9	41.0	54.9	57.1
	800	27.3	40.4	41.9	25.8	40.0	41.6
	1000	16.8	28.3	29.8	15.7	27.9	29.1
	1200	10.7	20.5	22.1	9.4	19.7	21.4
STD	50	3.7	3.7	3.7	2.7	2.7	2.7
	100	6.3	5.6	6.6	3.9	4.9	5.1
	150	20.1	18.2	18.2	21.3	20.8	20.9
	200	17.2	20.2	15.2	16.8	18.2	14.3
	300	5.3	5.3	5.4	6.2	5.4	4.8
	400	8.6	4.3	4.3	7.2	6.5	6.8
	600	15.3	17.1	17.3	14.9	16.7	17.0
	800	18.9	25.8	26.4	17.7	24.7	25.4
	1000	16.1	27.0	28.3	15.0	26.2	27.0
	1200	12.7	26.0	28.1	10.7	24.1	26.2

**Table 8.10 – Mean and Standard Deviation of Lateral Displacement Reduction (%) of Bridges of Different Radii with 50 ft Spans and End-Bearing Piles in Varying Depths of Predrilled Holes Filled with Loose Sand**

Span Length (ft)	Description	Radius (ft)	$\Delta T_{\text{slab}} = 90^\circ \text{ F}$ $\Delta T_{\text{the rest}} = 60^\circ \text{ F}$			$\Delta T_{\text{slab}} = 120^\circ \text{ F}$ $\Delta T_{\text{the rest}} = 90^\circ \text{ F}$		
			Depth of Predrilled Holes (ft)					
			5	9	15	5	9	15
50	MEAN	400	15.1	16.4	18.2	12.8	14.8	16.5
		600	22.3	27.9	29.0	21.5	27.5	28.0
		800	25.6	30.5	30.3	24.5	29.0	30.2
		1200	30.8	37.1	37.7	27.6	34.3	34.9
		2400	37.3	44.9	46.0	32.8	40.9	42.6
		Infinity	39.1	51.0	49.9	34.2	45.0	45.7
	STD	400	20.1	23.6	22.4	18.7	22.6	22.3
		600	21.3	24.4	25.1	21.3	25.2	25.4
		800	20.6	23.4	23.8	19.9	23.5	23.6
		1200	18.5	21.8	21.9	18.3	22.6	23.5
		2400	17.6	22.2	23.0	18.2	24.3	25.4
		Infinity	17.3	21.4	22.4	17.3	20.3	20.9

### 8.3.2 Curved Integral Abutment Bridges with 100 ft Spans

Figures 8.20 to 8.22 indicate that the lateral displacement reduction of curved IAB's of all radii due to the introduction of predrilled holes for  $\Delta T_{\text{slab}}$  of  $90^\circ$  F and  $\Delta T_{\text{the rest}}$  of  $60^\circ$  F starts to increase from a 100 ft bridge length to its highest value at the bridge length indicated in Table 8.11. After the lateral displacement reduction rate reaches its highest value, it starts decreasing and continues to decrease as the bridge length is increased to 1200 ft.

For curved IAB's with a 400 ft radius, the lateral displacement of curved IAB's due to the introduction of predrilled holes does not decrease but increases by 9.5% and 14.3% for piles in 9 ft and 15 ft deep predrilled holes at a 100 ft bridge length, respectively. The lateral displacement increases from 0.21 inch for piles without predrilled holes to 0.23 inch and 0.24 inch for piles in 9 ft and 15 ft deep predrilled holes, respectively.

It is shown in Figures 8.20 to 8.22 that the introduction of predrilled holes does not decrease the lateral displacement of curved IAB's with radii of 400 ft and 600 ft, but increases by 2% to 2.6% at bridge lengths between 800 ft to 1200 ft for curved IAB's with a 400 ft radius and increases by 1.7% to 2% at bridge lengths between 1000 ft to 1200 ft for curved IAB's with a 600 ft radius. The lateral displacement reduction due to the introduction of predrilled holes of curved IAB's with a smaller radius decreases much more rapidly after reaching its highest value than that of curved IAB's with a larger radius as the bridge length is increased to 1200 ft.

**Table 8.11 – Lateral Displacement Reduction (%) of Bridges with 100 ft Spans and End-Bearing Piles in Varying Depths of Predrilled Holes Filled with Loose Sand ( $\Delta T_{\text{slab}} = 90^\circ \text{ F}$ ,  $\Delta T_{\text{the rest}} = 60^\circ \text{ F}$ )**

Radius (ft)	Lateral Displacement Reduction (%) at a 100 ft Length	Highest Lateral Displacement Reduction (%) at Bridge Length (ft)		Lateral Displacement Reduction (%) at 1200 ft Length
400	4.8	37.9	400	-2.0
600	15.0	45.8	400	-2.0
800	21.1	48.3	400	-0.3
1200	22.2	49.2	400	4
2400	27.8	54.6	600	20.5
Infinity	35.3	35.3	400	29.7

**a) 5 ft Deep Predrilled Holes Filled with Loose Sand**

Radius (ft)	Lateral Displacement Reduction (%) at a 100 ft Length	Highest Lateral Displacement Reduction (%) at Bridge Length (ft)		Lateral Displacement Reduction (%) at 1200 ft Length
400	-9.5	49.6	400	-2.6
600	5.0	57.5	400	-1.7
800	10.5	59.4	400	2.0
1200	16.7	63.0	600	8.6
2400	27.8	68.9	600	35.2
Infinity	35.3	58.8	400	56.8

**b) 9 ft Deep Predrilled Holes Filled with Loose Sand**

Radius (ft)	Difference between Depth of Predrilled Holes	
	9 ft – 5ft	15 ft – 9 ft
400	0 to 11.7	0 to 1.2
600	0 to 13.6	0 to 1.9
800	0 to 15.7	0 to 2.2
1200	0 to 16.0	0 to 2.8
2400	0 to 17.9	0 to 3.5
Infinity	0 to 33.3	0 to 7.8

**c) Difference in Maximum Lateral Displacement Reduction Ratio (%)**

The mean of the lateral displacement reduction of curved IAB's of all radii with 100 ft spans due to the introduction of predrilled holes is listed in Table 8.12 and plotted in Figure 8.18. It is shown that the mean of the lateral displacement reduction of curved IAB's starts to increase from a 100 ft bridge length to its highest value at a 400 ft length. After the mean of the lateral displacement reduction reaches its highest value, it starts decreasing and continues to decrease as the bridge length is increased to 1200 ft.

For curved IAB's of different radii with 100 ft spans, it is found that curved IAB's with a smaller radius have the mean of the lateral displacement reduction due to the introduction of predrilled holes less than that of curved IAB's with a larger radius as indicated in Table 8.13 and Figure 8.23.

Tables 8.11c to 8.13 as well as Figures 8.18 and 8.20 to 8.23 indicate that curved IAB's with piles in 9 ft deep predrilled holes have a lateral displacement reduction in the range of 0% to 33.3% greater than that of curved IAB's with piles in 5 ft deep predrilled holes and in the range of 0% to 6.3% less than that of curved IAB's with piles in 15 ft deep predrilled holes. Therefore, it can be concluded that 9 feet deep predrilled holes filled with loose sand have a significant reduction in the lateral displacement of curved IAB's when compared with 5 ft deep predrilled holes filled with loose sand. The depth increase of predrilled holes deeper than 9 ft will further reduce the lateral displacement of curved IAB's, but the rate of reduction is much smaller than that of 9 ft deep predrilled holes.

From the analyses, it is shown that a temperature increase results in a lower lateral displacement reduction of curved IAB's. The mean of the lateral displacement

reduction due to the introduction of predrilled holes of curved IAB's subjected to the temperature load of  $\Delta T_{\text{slab}}$  of 90° F and  $\Delta T_{\text{the rest}}$  of 60° F is greater than that of curved IAB's subjected to the temperature load of  $\Delta T_{\text{slab}}$  of 120° F and  $\Delta T_{\text{the rest}}$  of 90° F by 0.4% to 3.3%.

**Table 8.12 – Mean and Standard Deviation of Lateral Displacement Reduction (%) of Bridges with 100 ft Spans and End-Bearing Piles in Varying Depths of Predrilled Holes Filled with Loose Sand**

Description	Bridge Length (ft)	$\Delta T_{\text{slab}} = 90^\circ \text{ F}$ $\Delta T_{\text{the rest}} = 60^\circ \text{ F}$			$\Delta T_{\text{slab}} = 120^\circ \text{ F}$ $\Delta T_{\text{the rest}} = 90^\circ \text{ F}$		
		Depth of Predrilled Holes (ft)					
		5	9	15	5	9	15
MEAN	100	21.0	14.3	11.7	13.9	9.6	8.9
	200	22.5	23.5	22.5	24.2	23.3	22.5
	300	34.1	43.4	44.3	37.7	45.7	45.3
	400	44.0	57.0	58.7	40.4	58.2	59.1
	600	32.8	49.6	52.3	35.3	50.2	52.4
	800	20.4	34.6	37.2	22.9	36.6	38.4
	1000	12.4	23.2	25.8	13.5	24.7	26.5
	1200	8.3	16.4	19.0	7.3	16.8	19.4
STD	100	10.5	16.1	18.1	11.1	14.5	15.8
	200	10.7	16.3	19.9	19.6	20.2	20.8
	300	4.1	6.5	9.7	8.6	9.9	11.4
	400	5.9	3.8	4.9	11.3	3.6	3.5
	600	16.3	17.4	18.1	14.8	16.9	19.9
	800	17.6	25.5	27.1	18.1	25.6	26.3
	1000	15.1	26.0	28.9	15.5	26.5	27.8
	1200	13.5	24.3	28.2	10.5	23.2	26.9

**Table 8.13 – Mean and Standard Deviation of Lateral Displacement Reduction (%) of Bridges of Different Radii with 100 ft Spans and End-Bearing Piles in Varying Depths of Predrilled Holes Filled with Loose Sand**

Span Length (ft)	Description	Radius (ft)	$\Delta T_{\text{slab}} = 90^\circ \text{ F}$ $\Delta T_{\text{the rest}} = 60^\circ \text{ F}$			$\Delta T_{\text{slab}} = 120^\circ \text{ F}$ $\Delta T_{\text{the rest}} = 90^\circ \text{ F}$		
			Depth of Predrilled Holes (ft)					
			5	9	15	5	9	15
100	MEAN	400	12.8	14.0	12.9	11.9	14.3	13.0
		600	17.6	21.5	20.9	14.4	21.9	22.2
		800	21.7	26.4	27.0	20.9	27.3	28.3
		1200	28.3	35.5	35.4	26.9	34.8	36.1
		2400	37.2	46.1	47.7	34.9	45.7	47.3
		Infinity	29.1	53.0	59.8	37.5	54.7	57.6
	STD	400	16.5	22.1	22.9	17.5	23.3	23.9
		600	17.5	22.6	23.5	13.3	23.4	23.9
		800	17.4	22.7	22.9	17.6	23.0	23.5
		1200	15.7	19.9	21.4	16.1	21.3	22.1
		2400	11.8	16.8	17.8	13.3	18.6	20.1
		Infinity	5.7	7.6	10.3	14.3	11.7	12.0

### 8.3.3 Conclusions

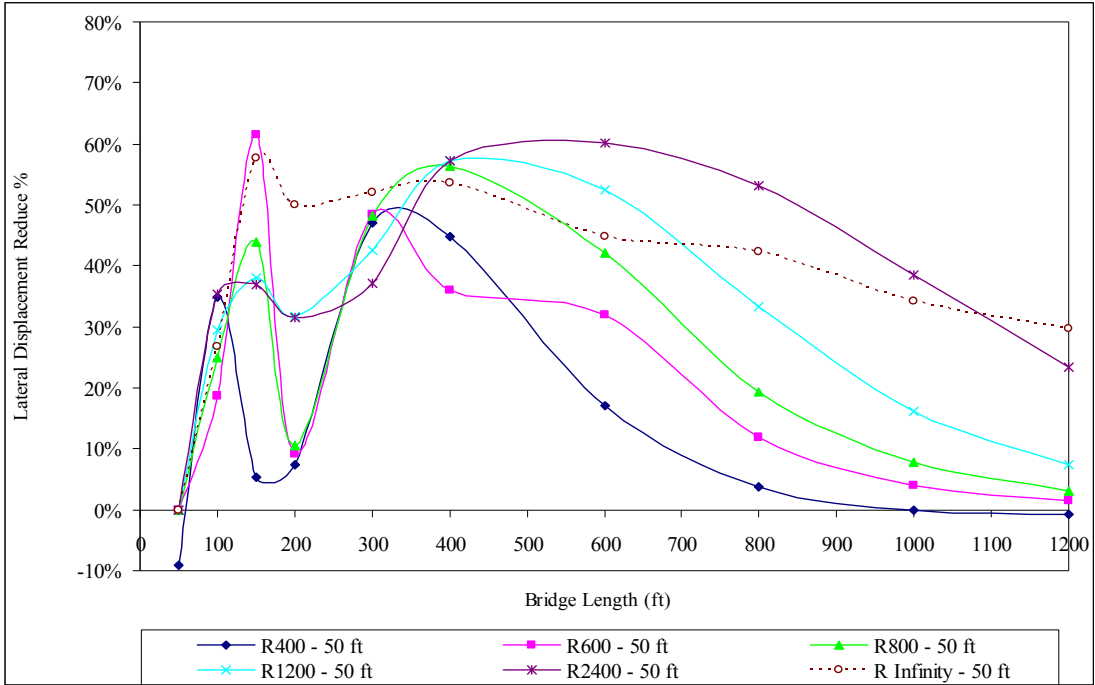
The following conclusions are drawn from the study of the effect of using varying depths of predrilled holes filled with loose sand instead of no predrilled holes on the maximum lateral displacement reduction in curved IAB's investigated in this section:

1. The lateral displacement reduction of curved IAB's due to the introduction of predrilled holes increases as the depth of the predrilled holes is increased.
2. Piles in 9 feet deep predrilled holes filled with loose sand have a significant reduction in the lateral displacement of curved IAB's when compared with piles in 5 ft deep predrilled holes filled with loose sand. The depth increase of predrilled holes deeper than 9 ft will further reduce the lateral displacement of curved IAB's, but the rate of reduction is much smaller than that of 9 ft deep predrilled holes.
3. Curved IAB's with a smaller radius have the mean of the lateral displacement reduction less than that of curved IAB's with a larger radius.
4. The mean of the lateral displacement reduction of curved IAB's of all radii with 50 ft spans due to the introduction of predrilled holes indicates that there is no lateral displacement reduction at a 50 ft bridge length. The mean of the lateral displacement reduction starts to increase from 50 ft to 150 ft lengths and decreases at a 200 ft length. Beyond the 200 ft length, it increases to its highest value at a 400 ft

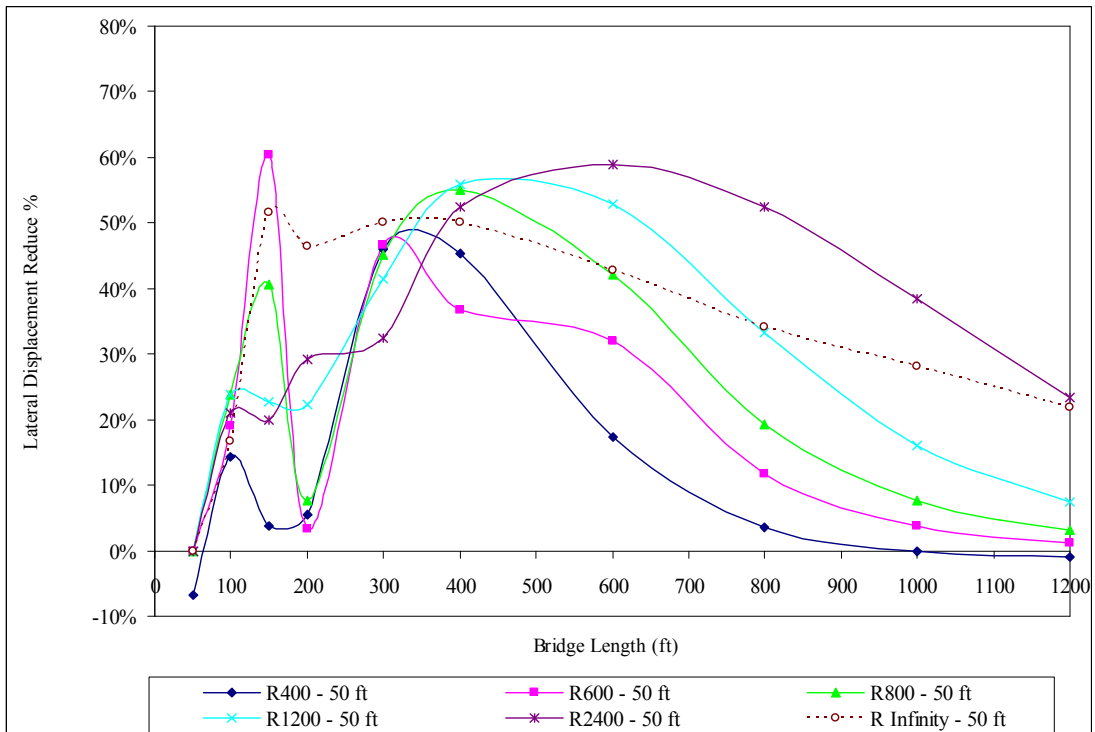


length. After the mean of the lateral displacement reduction reaches its highest value, it starts decreasing and continues to decrease as the bridge length is increased to 1200 ft.

5. For curved IAB's of all radii with 100 ft spans, the mean of the lateral displacement reduction due to the introduction of predrilled holes starts to increase from a 100 ft bridge length to its highest value at a 400 ft length. After the mean of the lateral displacement reduction reaches its highest value, it starts decreasing and continues to decrease as the bridge length is increased to 1200 ft.
6. The comparison of the mean of the lateral displacement reduction due to the introduction of predrilled holes between curved IAB's with 50 ft and 100 ft spans in Tables 8.9 and 8.12 indicates that curved IAB's with 50 ft spans have the mean of lateral displacement reduction greater than that of curved IAB's with 100 ft spans by 3.2% to 11.8%. The decrease in the span length results in the decrease in lateral and longitudinal displacements of the piles which decreases the lateral displacement of the bridge superstructure. Therefore, curved IAB's with the shorter span lengths will result in a smaller lateral displacement increase of curved IAB's when compared to curved IAB's with the longer span lengths.
7. A temperature increase results in a lower lateral displacement reduction of curved IAB's due to the introduction of predrilled holes.

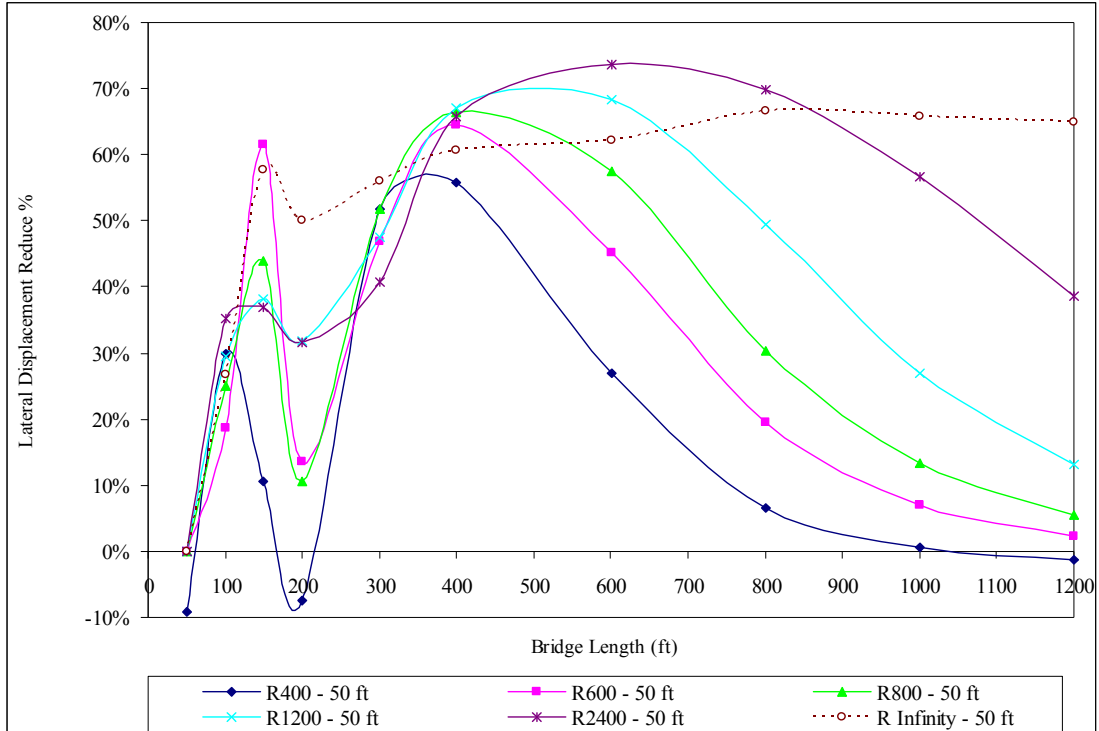


a)  $\Delta T_{\text{slab}} = 90^\circ \text{ F}$ ,  $\Delta T_{\text{the rest}} = 60^\circ \text{ F}$

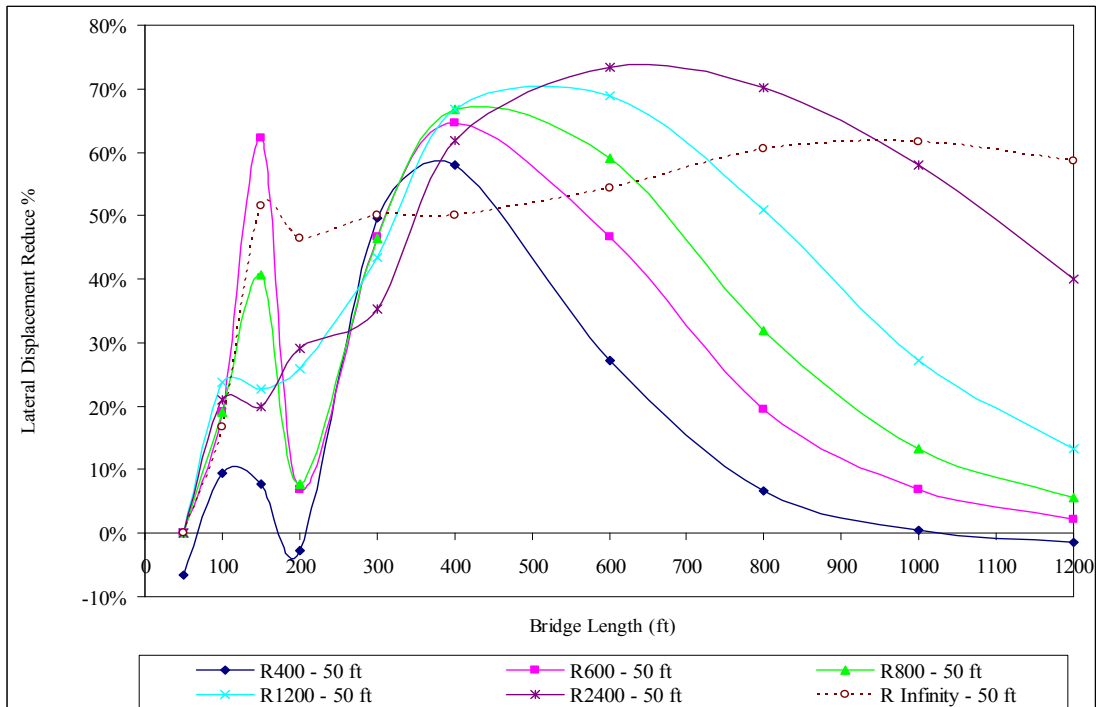


b)  $\Delta T_{\text{slab}} = 120^\circ \text{ F}$ ,  $\Delta T_{\text{the rest}} = 90^\circ \text{ F}$

Figure 8.15 – Lateral Displacement Reduction (%) of Bridges with 50 ft Spans and End-Bearing Piles in 5 ft Deep Predrilled Holes

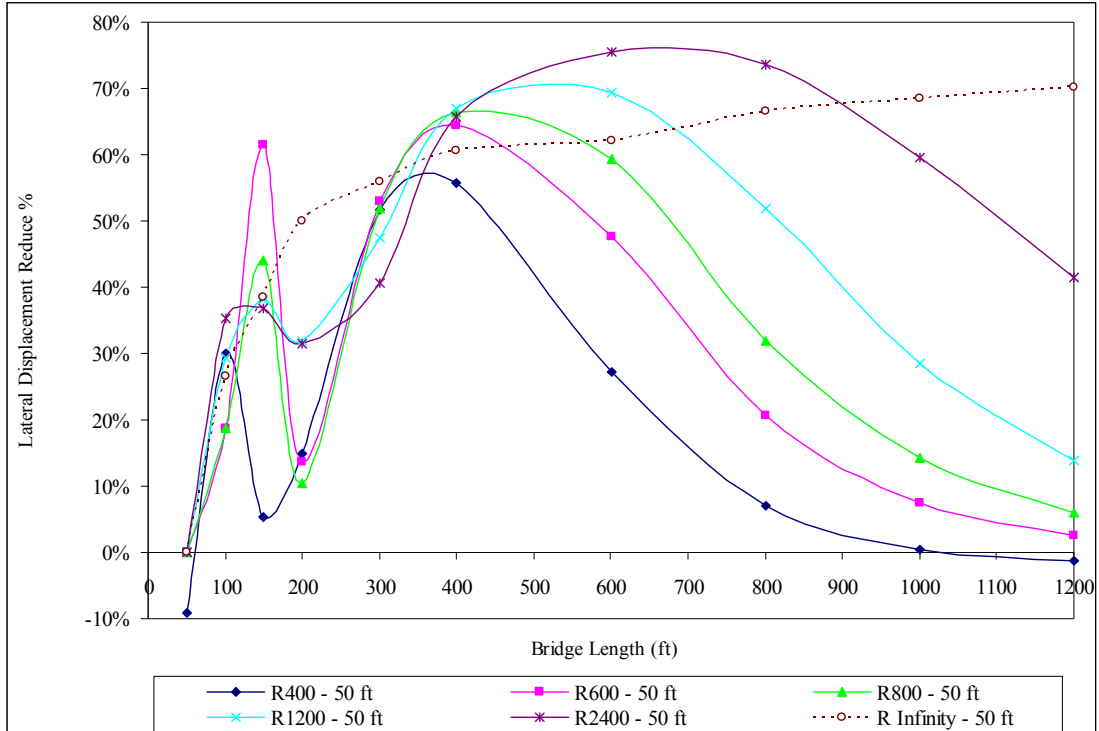


a)  $\Delta T_{\text{slab}} = 90^\circ \text{ F}$ ,  $\Delta T_{\text{the rest}} = 60^\circ \text{ F}$

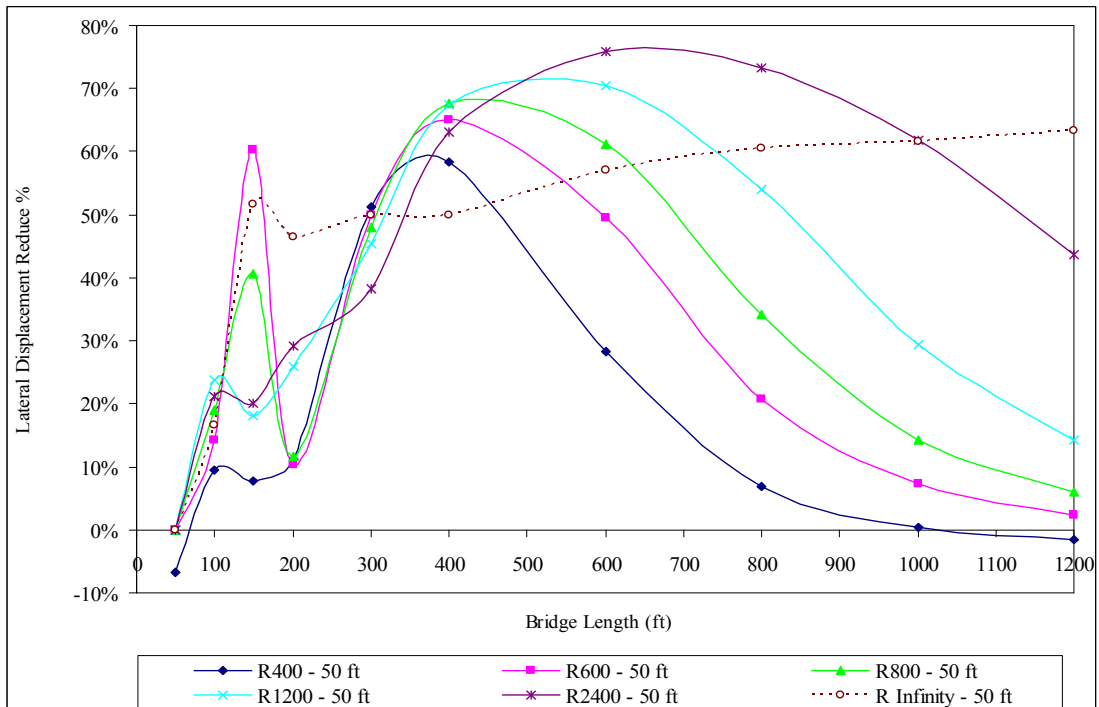


b)  $\Delta T_{\text{slab}} = 120^\circ \text{ F}$ ,  $\Delta T_{\text{the rest}} = 90^\circ \text{ F}$

Figure 8.16 – Lateral Displacement Reduction (%) of Bridges with 50 ft Spans and End-Bearing Piles in 9 ft Deep Predrilled Holes

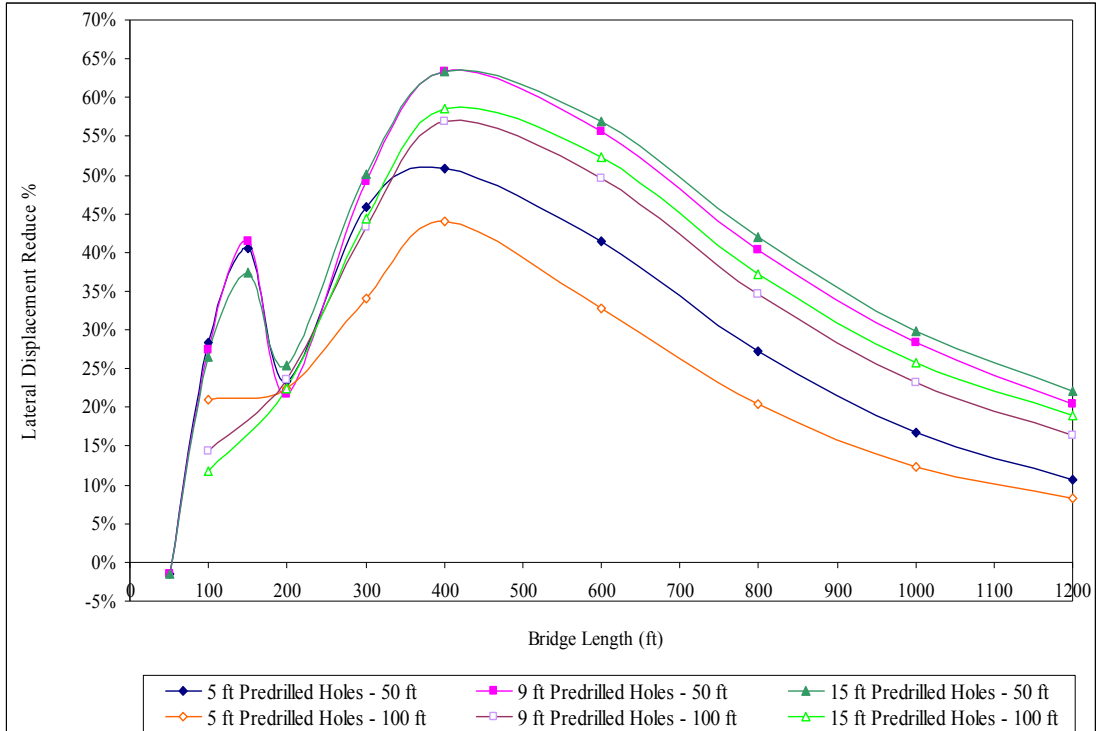


a)  $\Delta T_{\text{slab}} = 90^\circ \text{ F}$ ,  $\Delta T_{\text{the rest}} = 60^\circ \text{ F}$

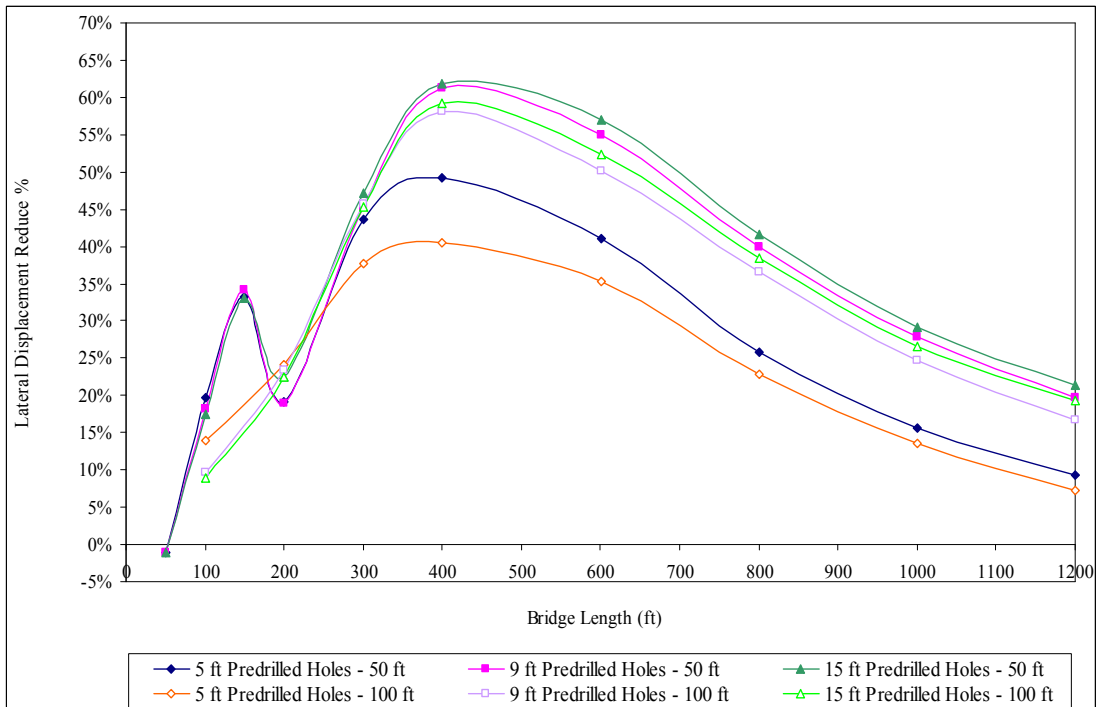


b)  $\Delta T_{\text{slab}} = 120^\circ \text{ F}$ ,  $\Delta T_{\text{the rest}} = 90^\circ \text{ F}$

Figure 8.17 – Lateral Displacement Reduction (%) of Bridges with 50 ft Spans and End-Bearing Piles in 15 ft Deep Predrilled Holes

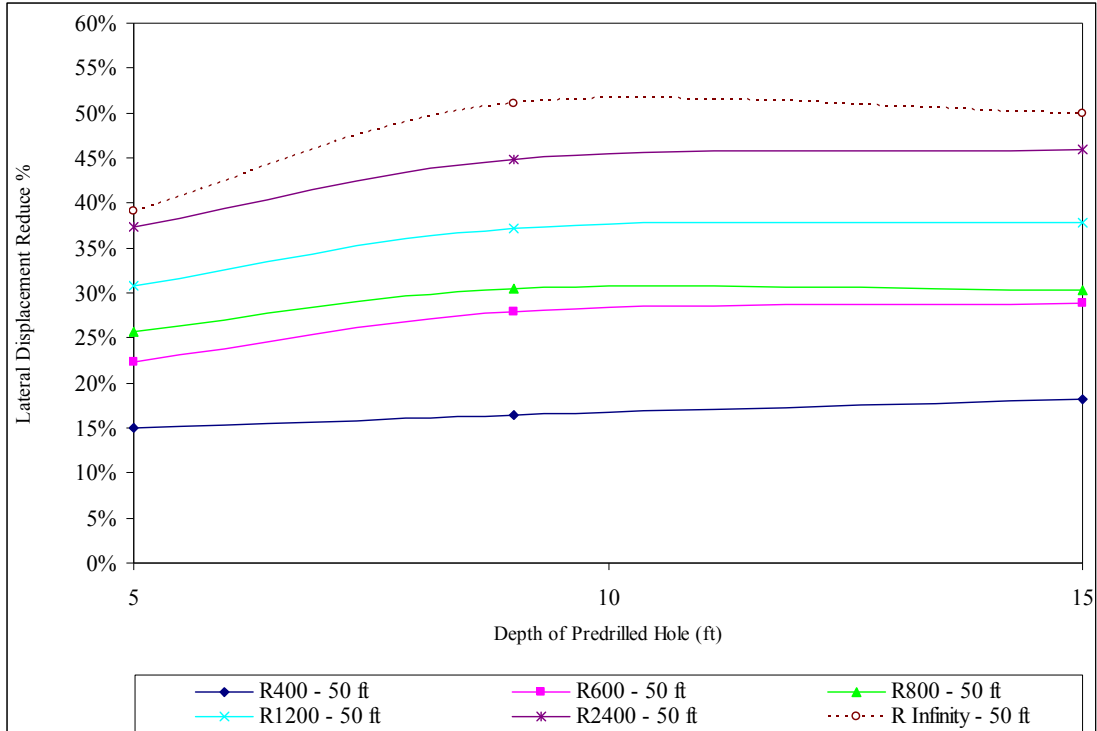


a)  $\Delta T_{\text{slab}} = 90^\circ \text{ F}$ ,  $\Delta T_{\text{the rest}} = 60^\circ \text{ F}$

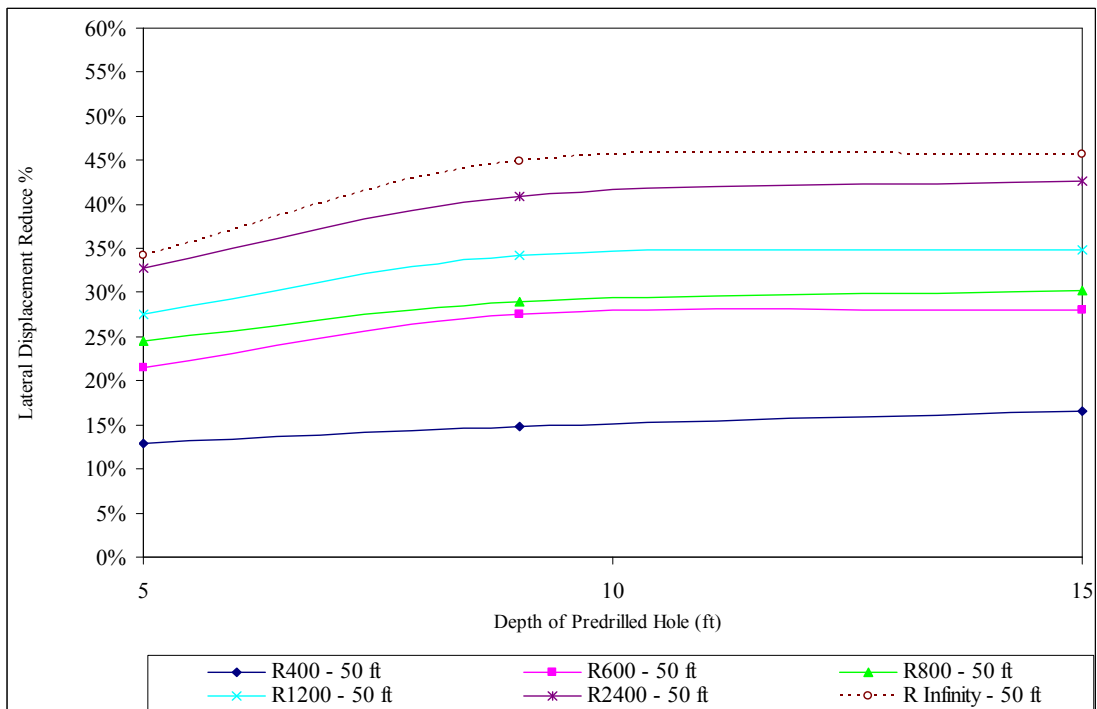


b)  $\Delta T_{\text{slab}} = 120^\circ \text{ F}$ ,  $\Delta T_{\text{the rest}} = 90^\circ \text{ F}$

**Figure 8.18 – Mean of Lateral Displacement Reduction (%) of Bridges with 50 ft and 100 ft Spans and End-Bearing Piles in Varying Depths of Predrilled Holes**

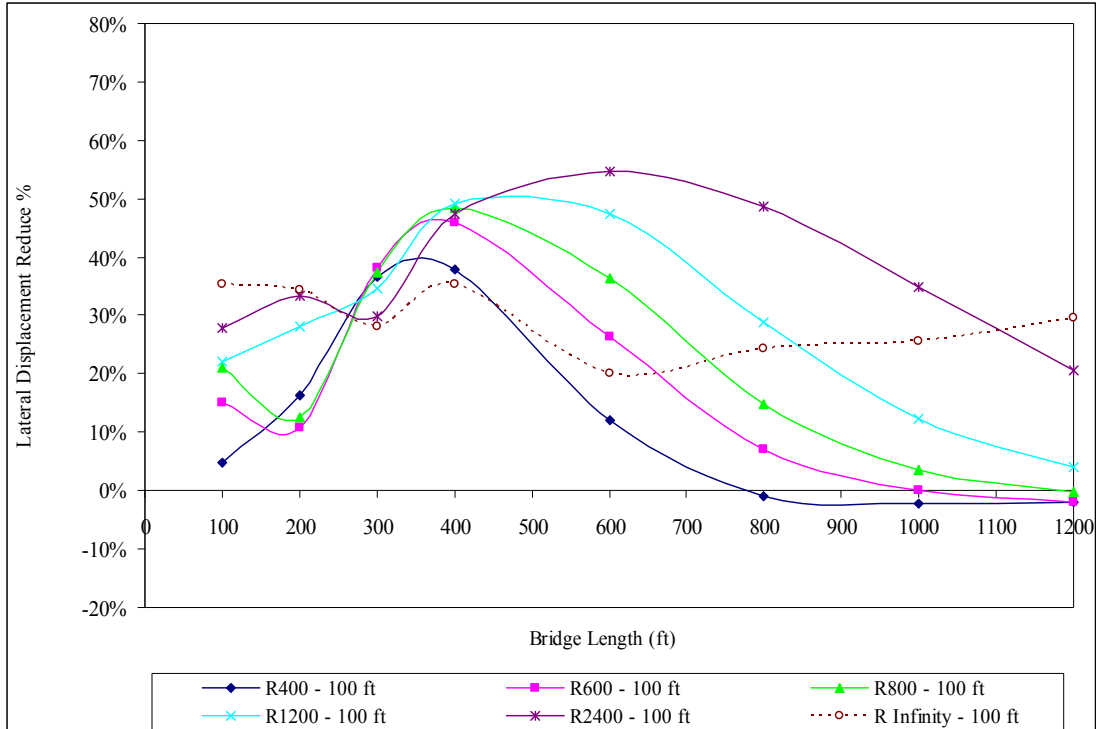


a)  $\Delta T_{\text{slab}} = 90^\circ \text{ F}$ ,  $\Delta T_{\text{the rest}} = 60^\circ \text{ F}$

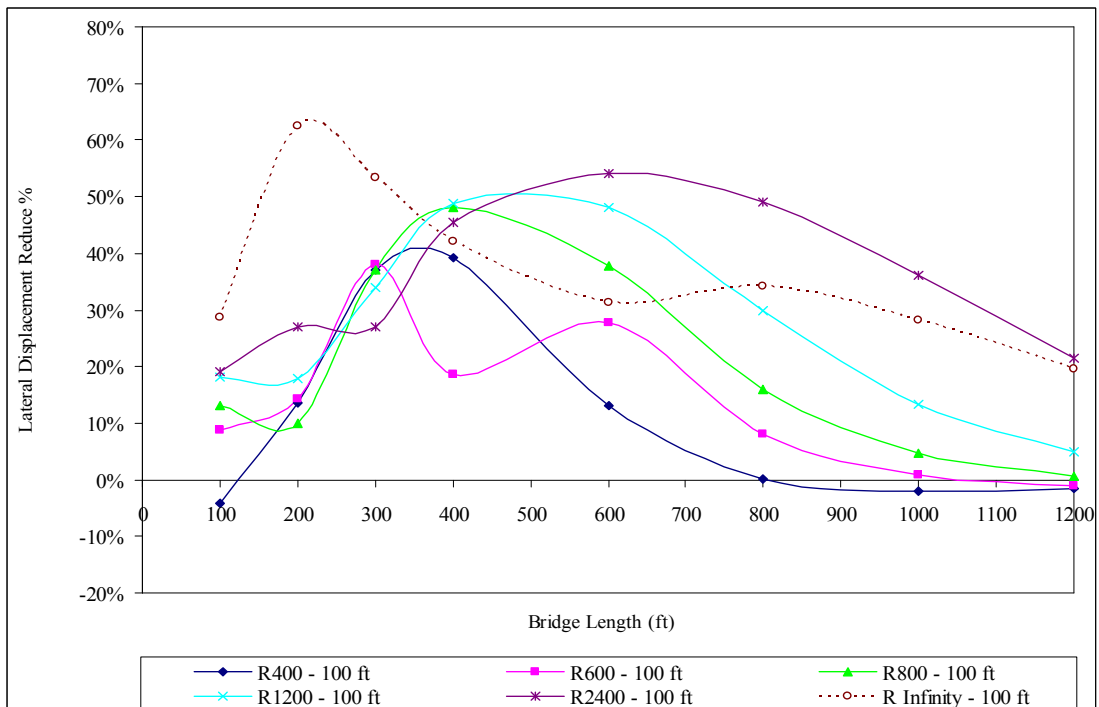


b)  $\Delta T_{\text{slab}} = 120^\circ \text{ F}$ ,  $\Delta T_{\text{the rest}} = 90^\circ \text{ F}$

**Figure 8.19 – Mean of Lateral Displacement Reduction (%) of Bridges of Different Radii with 50 ft Spans and End-Bearing Piles in Varying Depths of Predrilled Holes**

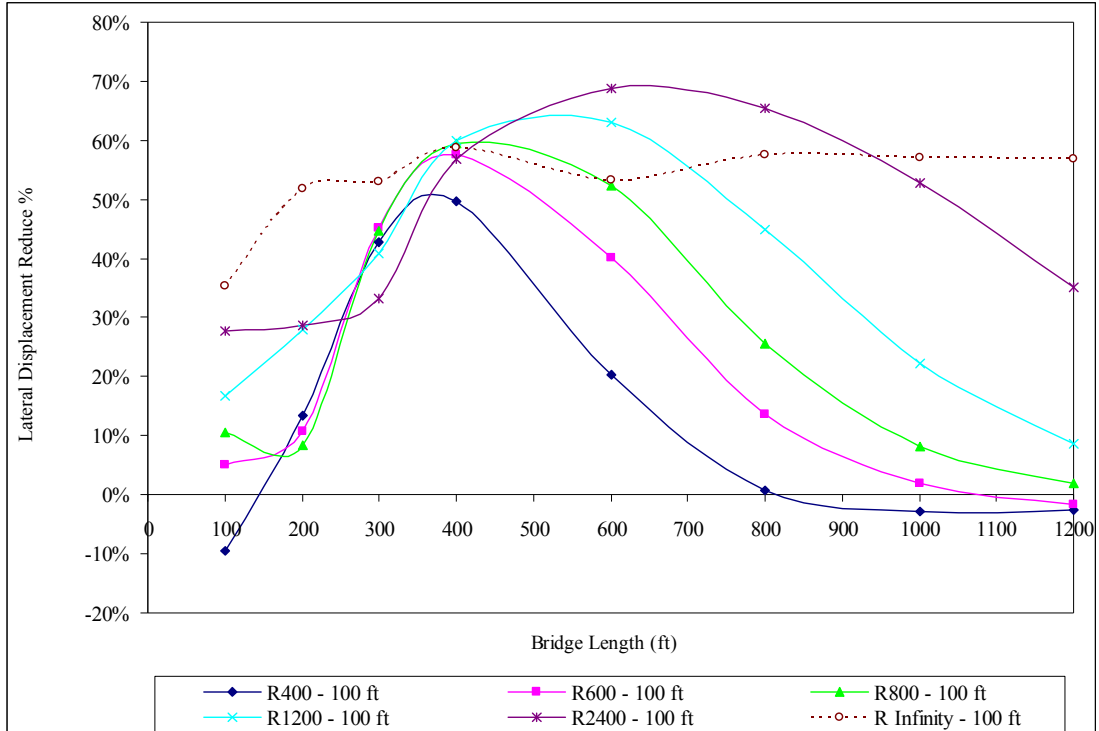


a)  $\Delta T_{\text{slab}} = 90^\circ \text{ F}$ ,  $\Delta T_{\text{the rest}} = 60^\circ \text{ F}$

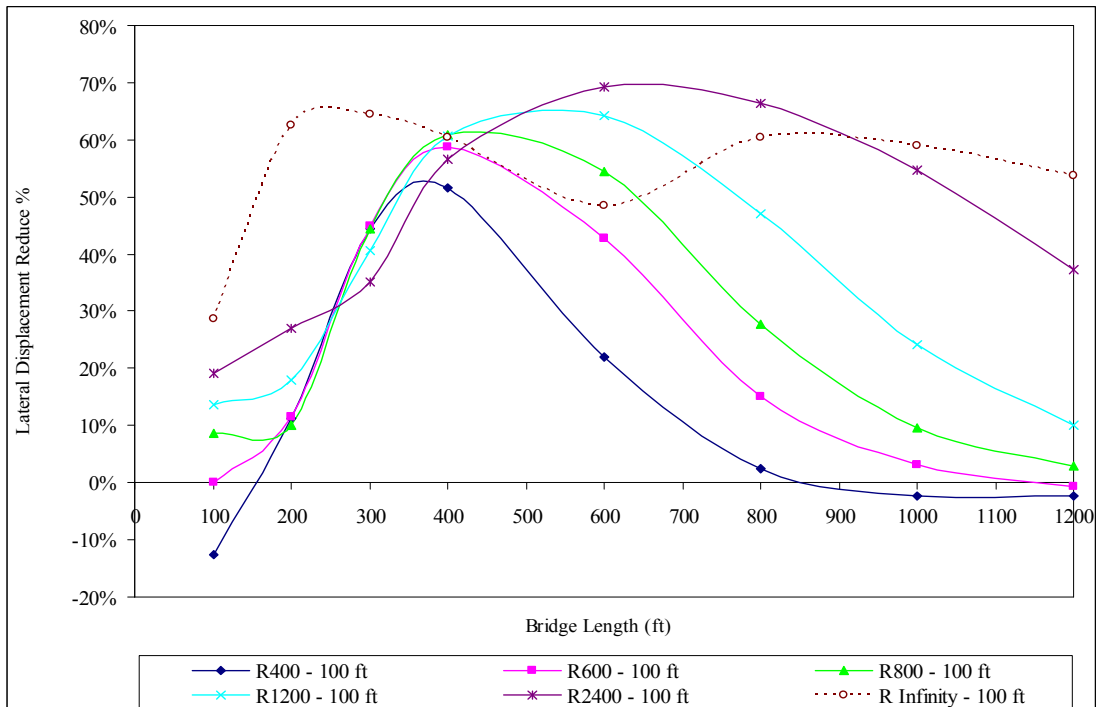


b)  $\Delta T_{\text{slab}} = 120^\circ \text{ F}$ ,  $\Delta T_{\text{the rest}} = 90^\circ \text{ F}$

**Figure 8.20 – Lateral Displacement Reduction (%) of Bridges with 100 ft Spans and End-Bearing Piles in 5 ft Deep Predrilled Holes**



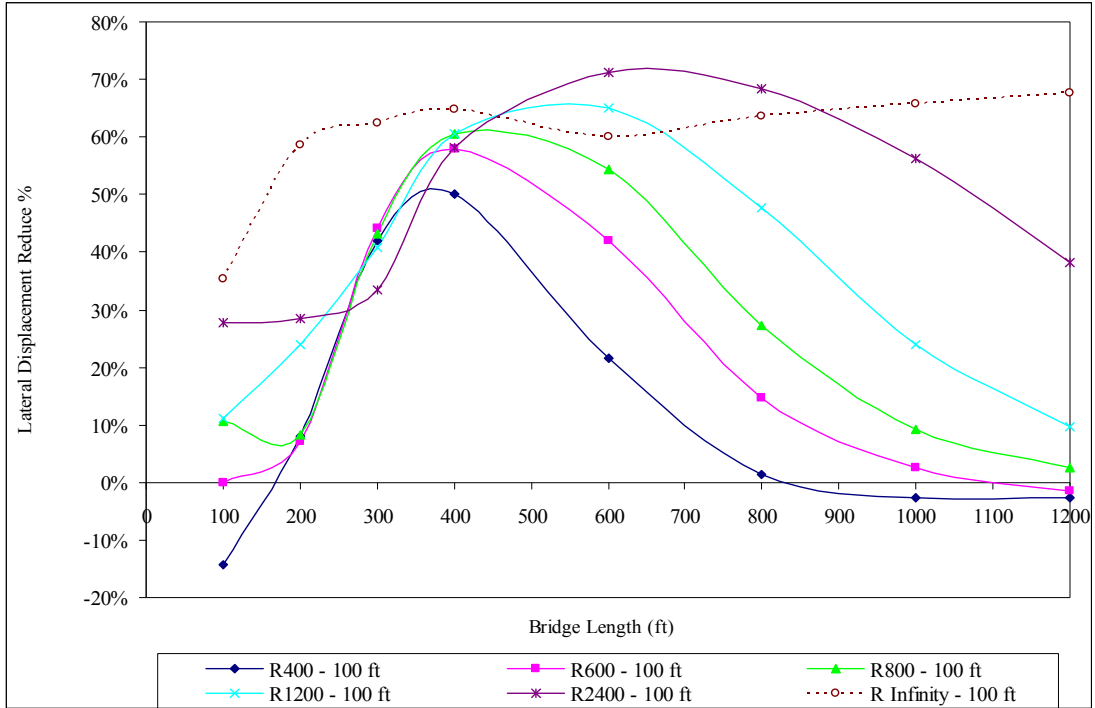
a)  $\Delta T_{\text{slab}} = 90^\circ \text{ F}$ ,  $\Delta T_{\text{the rest}} = 60^\circ \text{ F}$



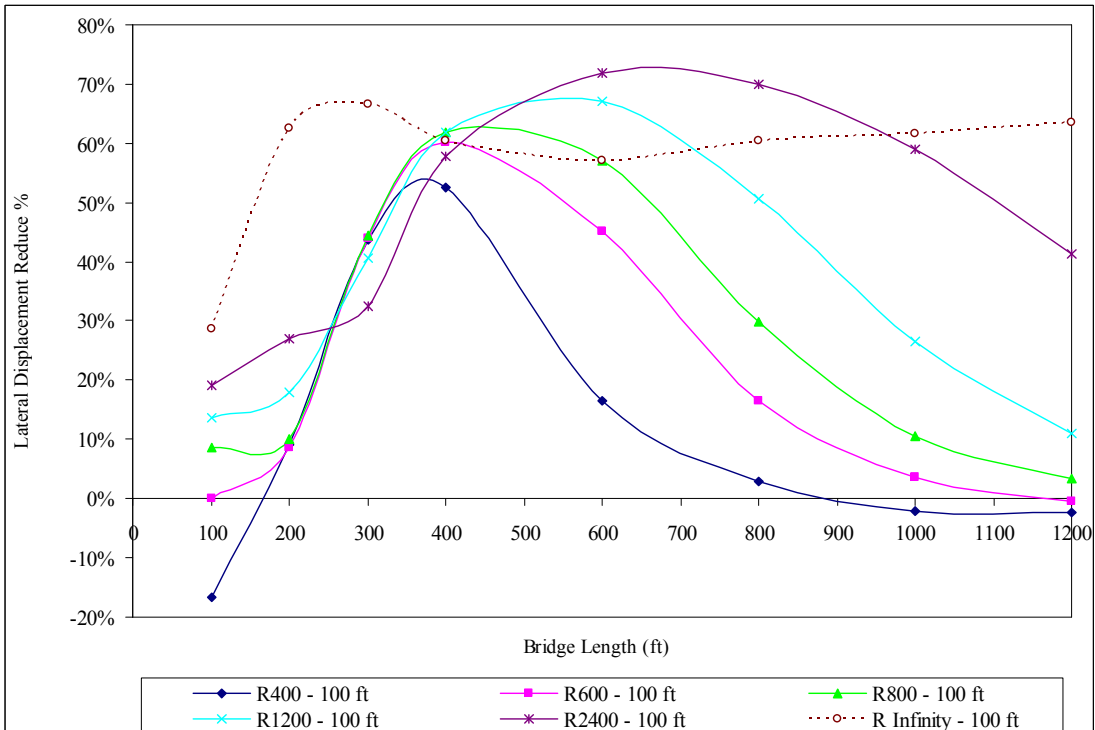
b)  $\Delta T_{\text{slab}} = 120^\circ \text{ F}$ ,  $\Delta T_{\text{the rest}} = 90^\circ \text{ F}$

Figure 8.21 – Lateral Displacement Reduction (%) of Bridges with 100 ft Spans and End-Bearing Piles in 9 ft Deep Predrilled Holes



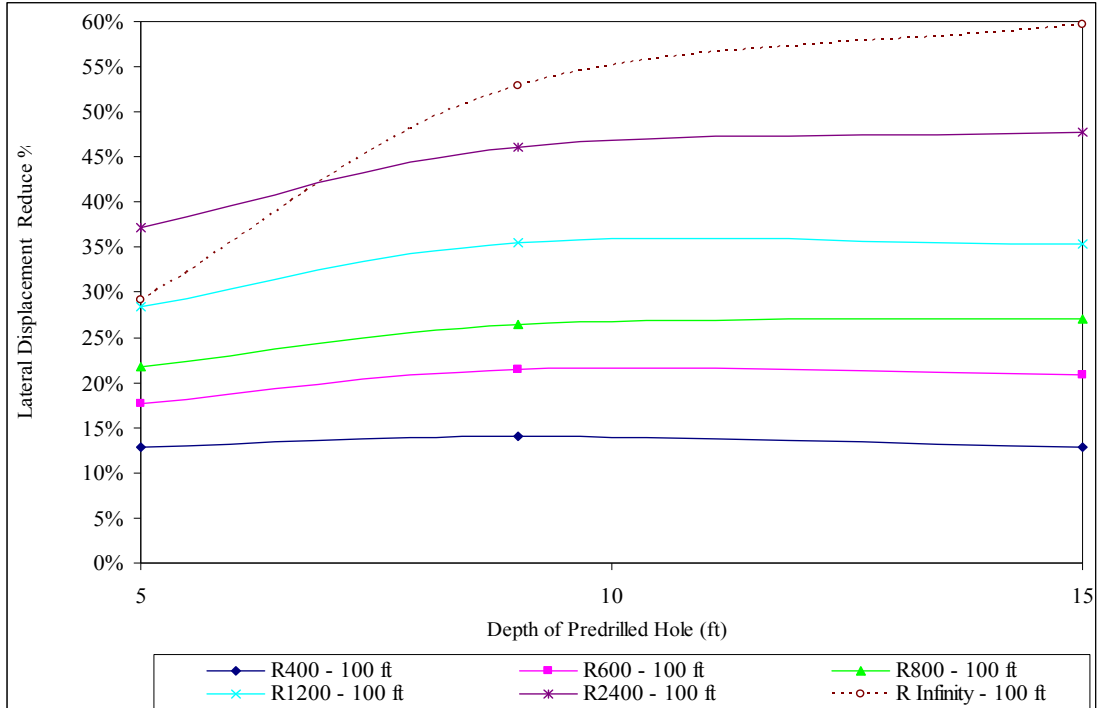


a)  $\Delta T_{\text{slab}} = 90^\circ \text{ F}$ ,  $\Delta T_{\text{the rest}} = 60^\circ \text{ F}$

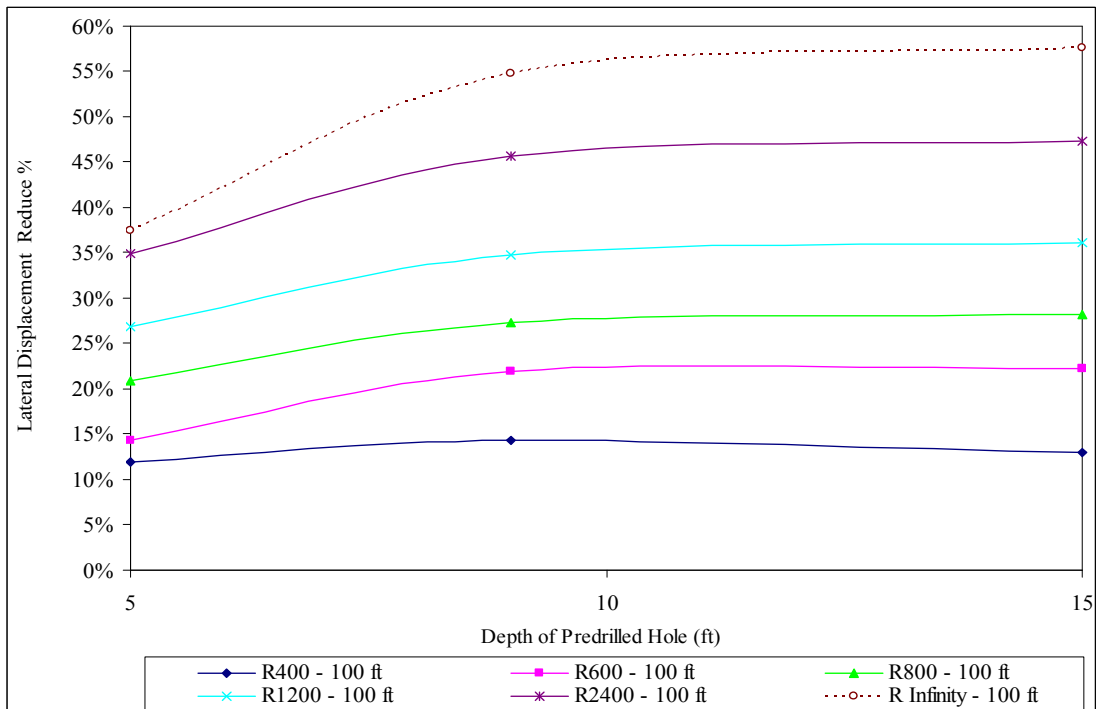


b)  $\Delta T_{\text{slab}} = 120^\circ \text{ F}$ ,  $\Delta T_{\text{the rest}} = 90^\circ \text{ F}$

Figure 8.22 – Lateral Displacement Reduction (%) of Bridges with 100 ft Spans and End-Bearing Piles in 15 ft Deep Predrilled Holes



a)  $\Delta T_{\text{slab}} = 90^\circ \text{F}, \Delta T_{\text{the rest}} = 60^\circ \text{F}$



b)  $\Delta T_{\text{slab}} = 120^\circ \text{F}, \Delta T_{\text{the rest}} = 90^\circ \text{F}$

**Figure 8.23 – Mean of Lateral Displacement Reduction (%) of Bridges of Different Radii with 100 ft Spans and End-Bearing Piles in Varying Depths of Predrilled Holes**

#### **8.4 Effect of Span Length Variation**

The effect of span length variation from 100 ft to 50 ft on the maximum lateral displacement reduction of curved IAB's is discussed in this section. All other parameters are held constant.

For piles in very stiff clay soil profile as shown in Figure 8.24, the lateral displacement reduction of curved IAB's due to the increase in the number of spans starts to increase from a 100 ft bridge length to its highest value at bridge lengths between 200 ft and 300 ft. Beyond these lengths, some of the lateral displacement reduction rates start decreasing and continue to decrease as the bridge length is increased to 1200 ft as indicated in Table 8.14.

For piles in 9 ft deep predrilled holes filled with loose sand as shown in Figure 8.25, the lateral displacement reduction due to the increase in the number of spans of curved IAB's of all radii (except an infinite radius) starts to decrease from a 100 ft bridge length to a 200 ft bridge length. Beyond the 200 ft length, the lateral displacement reduction rate starts to increase to its highest value at bridge lengths between 300 ft and 400 ft. Beyond these lengths, the lateral displacement reduction rate starts decreasing and continues to decrease as the bridge length is increased to 1200 ft as indicated in Table 8.15.

**Table 8.14 – Lateral Displacement Reduction (%) of Bridges and End-Bearing Piles in Very Stiff Clay Soil Profile due to the Increase in the Number of Spans**

Radius (ft)	Bridge Length (ft)	$\Delta T_{\text{slab}} = 90^\circ \text{ F}$ $\Delta T_{\text{the rest}} = 60^\circ \text{ F}$	$\Delta T_{\text{slab}} = 120^\circ \text{ F}$ $\Delta T_{\text{the rest}} = 90^\circ \text{ F}$
400	100	4.8	12.5
600	100	20.0	8.7
800	100	15.8	8.7
1200	100	5.6	4.5
2400	100	5.6	9.5
Infinity	100	11.8	14.3

**a) Lateral Displacement Reduction (%) at 100 ft Length**

Radius (ft)	Bridge Length (ft)	$\Delta T_{\text{slab}} = 90^\circ \text{ F}$ $\Delta T_{\text{the rest}} = 60^\circ \text{ F}$	$\Delta T_{\text{slab}} = 120^\circ \text{ F}$ $\Delta T_{\text{the rest}} = 90^\circ \text{ F}$
400	200	27.0	18.2
600	200	21.4	17.1
800	200	20.8	13.3
1200	300	18.4	10.2
2400	300	10.0	8.1
Infinity	300	21.9	33.3

**b) Highest Lateral Displacement Reduction (%)**

Radius (ft)	Bridge Length (ft)	$\Delta T_{\text{slab}} = 90^\circ \text{ F}$ $\Delta T_{\text{the rest}} = 60^\circ \text{ F}$	$\Delta T_{\text{slab}} = 120^\circ \text{ F}$ $\Delta T_{\text{the rest}} = 90^\circ \text{ F}$
400	1200	3.3	2.4
600	1200	11.4	8.5
800	1200	12.7	9.4
1200	1200	13.0	9.6
2400	1200	10.8	7.5
Infinity	1200	0.0	0.0

**c) Lateral Displacement Reduction (%) at 1200 ft Length**

**Table 8.15 – Lateral Displacement Reduction (%) of Bridges and End-Bearing Piles in 9 ft Deep Predrilled Holes due to the Increase in the Number of Spans**

Radius (ft)	Bridge Length (ft)	$\Delta T_{\text{slab}} = 90^\circ \text{ F}$ $\Delta T_{\text{the rest}} = 60^\circ \text{ F}$	$\Delta T_{\text{slab}} = 120^\circ \text{ F}$ $\Delta T_{\text{the rest}} = 90^\circ \text{ F}$
400	100	39.1	29.6
600	100	31.6	26.1
800	100	29.4	19.0
1200	100	20.0	15.8
2400	100	15.4	11.8
Infinity	100	0.0	0.0

**a) Lateral Displacement Reduction (%) at 100 ft Length**

Radius (ft)	Bridge Length (ft)	$\Delta T_{\text{slab}} = 90^\circ \text{ F}$ $\Delta T_{\text{the rest}} = 60^\circ \text{ F}$	$\Delta T_{\text{slab}} = 120^\circ \text{ F}$ $\Delta T_{\text{the rest}} = 90^\circ \text{ F}$
400	200	9.4	5.1
600	200	24.0	12.9
800	200	22.7	11.1
1200	200	16.7	13.0
2400	200	13.3	10.5
Infinity	200	21.4	0.0

**b) Lateral Displacement Reduction (%) at 200 ft Length**

Radius (ft)	Bridge Length (ft)	$\Delta T_{\text{slab}} = 90^\circ \text{ F}$ $\Delta T_{\text{the rest}} = 60^\circ \text{ F}$	$\Delta T_{\text{slab}} = 120^\circ \text{ F}$ $\Delta T_{\text{the rest}} = 90^\circ \text{ F}$
400	300	35.9	22.7
600	400	33.0	24.8
800	400	31.5	23.3
1200	400	30.2	22.2
2400	400	25.0	17.9
Infinity	200	26.7	6.3

**c) Highest Lateral Displacement Reduction (%)**

**Table 8.15 (Continued) – Lateral Displacement Reduction (%) of Bridges and End-Bearing Piles in 9 ft Deep Predrilled Holes due to the Increase in the Number of Spans**

Radius (ft)	Bridge Length (ft)	$\Delta T_{\text{slab}} = 90^{\circ} \text{ F}$ $\Delta T_{\text{the rest}} = 60^{\circ} \text{ F}$	$\Delta T_{\text{slab}} = 120^{\circ} \text{ F}$ $\Delta T_{\text{the rest}} = 90^{\circ} \text{ F}$
400	1200	4.5	3.3
600	1200	14.8	11.2
800	1200	15.8	11.9
1200	1200	17.2	12.9
2400	1200	15.5	11.3
Infinity	1200	18.8	10.5

**d) Lateral Displacement Reduction (%) at 1200 ft Length**

For curved IAB's with an infinite radius (straight IAB's), the lateral displacement reduction due to the increase in the number of spans of curved IAB's varies along the length of the bridge because the lateral displacement is in the range of 0.11 inch to 0.41 inch for all bridge lengths, span lengths, temperature levels and piles in all soil profile types. Therefore, a decrease of a few inches of the lateral displacement results in a higher increase in the lateral displacement reduction due to the increase in the number of spans of curved IAB's.

Table 8.16 and Figures 8.24 to 8.26 indicate that curved IAB's with a smaller radius, for the most part, have a lateral displacement reduction due to the increase in the number of spans greater than that of curved IAB's with a larger radius.

**Table 8.16 – Mean and Standard Deviation of Lateral Displacement Reduction (%) of Bridges of Different Radii and End-Bearing Piles in Various Soil Profile Types due to the Increase in the Number of Spans**

Description	Radius (ft)	$\Delta T_{\text{slab}} = 90^\circ \text{ F}$ $\Delta T_{\text{the rest}} = 60^\circ \text{ F}$				$\Delta T_{\text{slab}} = 120^\circ \text{ F}$ $\Delta T_{\text{the rest}} = 90^\circ \text{ F}$			
		Depth of Predrilled Holes (ft)							
		0	5	9	15	0	5	9	15
MEAN	400	16	23	23	26	12	17	17	20
	600	18	20	24	27	12	18	18	18
	800	17	23	25	24	11	17	17	17
	1200	13	20	22	23	8	14	16	16
	2400	9	16	19	19	7	12	13	14
	Infinity	10	25	19	7	12	10	4	0
STD	400	9	11	13	12	5	9	10	10
	600	4	9	6	7	3	8	6	4
	800	3	6	6	5	2	5	4	4
	1200	4	5	5	4	3	4	3	3
	2400	2	5	4	4	2	3	3	3
	Infinity	10	19	8	3	14	14	5	0

Table 8.16 and Figures 8.26 to 8.27 also indicate that the lateral displacement reduction due to the increase in the number of spans of curved IAB's with piles in predrilled holes is greater than that of curved IAB's with piles without predrilled holes. It is shown that piles in 9 feet deep predrilled holes filled with loose sand have a significant reduction in the lateral displacement of curved IAB's when compared with piles in 5 ft deep predrilled holes filled with loose sand. The depth increase of predrilled holes deeper than 9 ft will further reduce the lateral displacement of curved IAB's, but the rate of reduction is much smaller than that of 9 ft deep predrilled holes.

From the analyses, it is shown that a temperature increase results in a lower lateral displacement reduction. The mean of the lateral displacement reduction due to

the increase in the number of spans of curved IAB's of all radii subjected to a temperature load of  $\Delta T_{\text{slab}}$  of 120° F and  $\Delta T_{\text{the rest}}$  of 90° F is less than that of curved IAB's subjected to a temperature load of  $\Delta T_{\text{slab}}$  of 90° F and  $\Delta T_{\text{the rest}}$  of 60° F in the range of 1% to 13.7% as indicated in Table 8.17 and plotted in Figure 8.28.

**Table 8.17 – Difference in Lateral Displacement Reduction (%) of Bridges and End-Bearing Piles due to the Increase in the Number of Spans between  $\Delta T_{\text{slab}} = 120^\circ \text{ F}$ ,  $\Delta T_{\text{the rest}} = 90^\circ \text{ F}$  and  $\Delta T_{\text{slab}} = 90^\circ \text{ F}$ ,  $\Delta T_{\text{the rest}} = 60^\circ \text{ F}$**

Description	Bridge Length (ft)	Depth of Predrilled Holes (ft)			
		0	5	9	15
MEAN	100	-0.9	-3.0	-5.5	-6.7
	200	-4.2	-12.8	-9.1	-7.9
	300	-4.1	-10.1	-13.7	-10.0
	400	-4.1	-1.9	-9.8	-6.9
	600	-5.3	-8.1	-7.1	-5.5
	800	-3.7	-8.6	-7.9	-6.4
	1000	-3.1	-5.7	-6.1	-5.2
	1200	-2.3	-2.4	-4.3	-4.3
STD	100	7.2	2.7	3.9	4.8
	200	5.6	15.4	7.1	3.0
	300	8.1	5.0	3.7	3.5
	400	5.1	14.0	5.7	1.9
	600	1.0	4.2	1.6	3.1
	800	1.9	7.6	6.6	1.8
	1000	1.5	2.9	3.8	1.6
	1200	1.5	2.8	2.3	2.3



### 8.4.1 Conclusions

The following conclusions are drawn from the study of the effect of span length variation from 100 ft to 50 ft on the maximum lateral displacement reduction in curved IAB's investigated in this section:

1. Curved IAB's with a smaller radius, for the most part, have a lateral displacement reduction due to the increase in the number of spans greater than that of curved IAB's with a larger radius.
2. The lateral displacement reduction due to the increase in the number of spans of curved IAB's with piles in predrilled holes is greater than that of curved IAB's with piles without predrilled holes. It is shown that piles in 9 feet deep predrilled holes filled with loose sand have a significant reduction in the lateral displacement of curved IAB's when compared with piles in 5 ft deep predrilled holes filled with loose sand. The depth increase of predrilled holes deeper than 9 ft will further reduce the lateral displacement of curved IAB's, but the rate of reduction is much smaller than that of 9 ft deep predrilled holes.
3. A temperature increase results in a lower lateral displacement reduction due to the increase in the number of spans of curved IAB's.
4. Tables 8.18 and 8.19 as well as Figure 8.27 indicate that the mean of the lateral displacement reduction due to the increase in the number of spans of curved IAB's with piles in very stiff clay soil profile increases from a 100 ft bridge length to its highest value at a 200 ft length. Beyond the 200 ft length, the mean of the lateral displacement

reduction starts decreasing and continues to decrease to its lowest value as the bridge length is increased to 1200 ft.

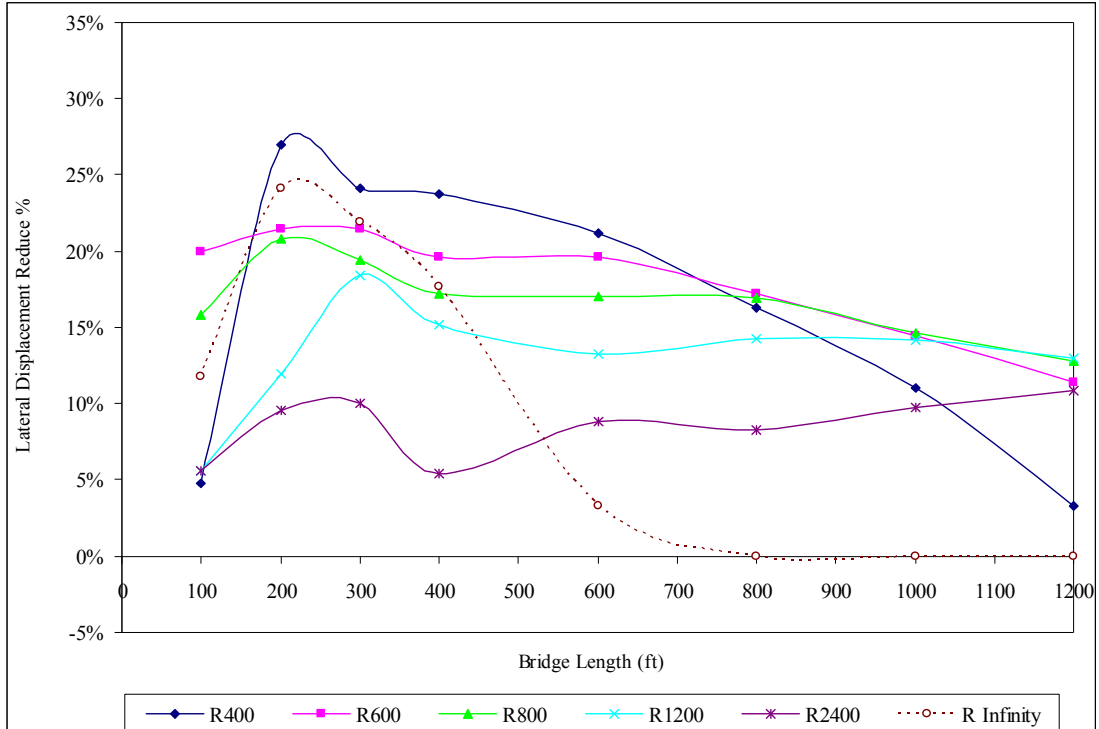
5. For curved IAB's with piles in predrilled holes, the mean of the lateral displacement reduction due to the increase in the number of spans of curved IAB's decreases from a 100 ft bridge length to a 200 ft bridge length. Beyond the 200 ft length, the mean of the lateral displacement reduction starts to increase to its highest value at bridge lengths between 300 ft and 400 ft. Beyond these lengths, the mean of the lateral displacement reduction starts decreasing and continues to decrease as the bridge length is increased to 1200 ft.

**Table 8.18 – Mean and Standard Deviation of Lateral Displacement Reduction (%) of Bridges and End-Bearing Piles in Various Soil Profile Types due to the Increase in the Number of Spans ( $\Delta T_{\text{slab}} = 90^\circ \text{ F}$ ,  $\Delta T_{\text{the rest}} = 60^\circ \text{ F}$ )**

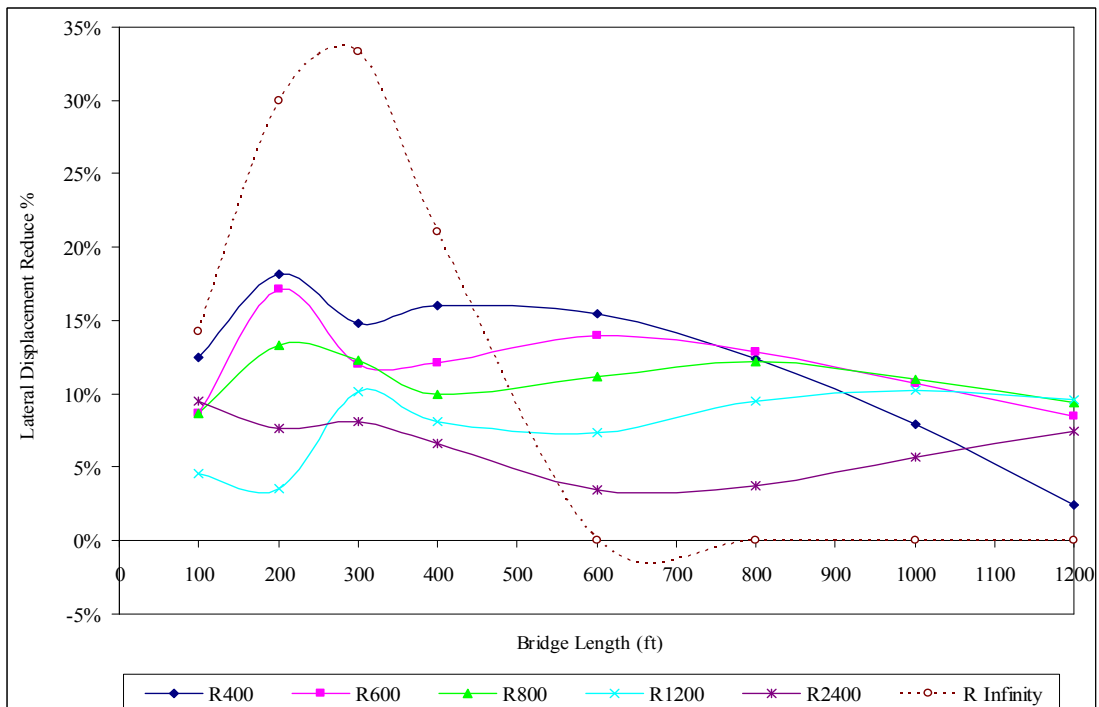
Description	Bridge Length (ft)	Depth of Predrilled Holes (ft)			
		0	5	9	15
MEAN	100	10.6	18.0	22.6	23.4
	200	19.2	20.7	17.9	20.8
	300	19.2	33.3	27.3	26.4
	400	16.5	26.6	29.0	25.7
	600	13.9	25.2	25.1	22.6
	800	12.2	20.5	21.5	19.9
	1000	10.7	15.5	18.1	16.0
	1200	8.5	10.8	14.4	12.7
STD	100	6.4	11.6	13.9	14.7
	200	6.9	11.5	5.8	8.8
	300	4.9	9.5	5.4	10.6
	400	6.1	12.0	4.8	9.2
	600	6.8	4.6	2.4	7.2
	800	6.8	2.6	1.0	5.7
	1000	5.6	2.9	2.3	4.3
	1200	5.5	6.8	5.1	5.1

**Table 8.19 – Mean and Standard Deviation of Lateral Displacement Reduction (%) of Bridges and End-Bearing Piles in Various Soil Profile Types due to the Increase in the Number of Spans ( $\Delta T_{\text{slab}} = 120^\circ \text{ F}$ ,  $\Delta T_{\text{the rest}} = 90^\circ \text{ F}$ )**

Description	Bridge Length (ft)	Depth of Predrilled Holes (ft)			
		0	5	9	15
MEAN	100	9.7	15.0	17.1	16.7
	200	15.0	7.9	8.8	12.9
	300	15.1	23.1	13.6	16.4
	400	12.3	24.8	19.2	18.7
	600	8.6	17.1	18.0	17.1
	800	8.4	11.9	13.6	13.5
	1000	7.6	9.8	12.0	10.8
	1200	6.2	8.3	10.2	8.4
STD	100	3.4	9.6	10.6	10.7
	200	9.2	4.2	5.2	7.2
	300	9.2	4.9	5.8	8.9
	400	5.4	5.7	9.9	9.5
	600	6.1	2.2	3.7	9.2
	800	5.4	6.2	6.7	6.7
	1000	4.2	5.2	3.2	5.5
	1200	4.1	4.3	3.5	5.4

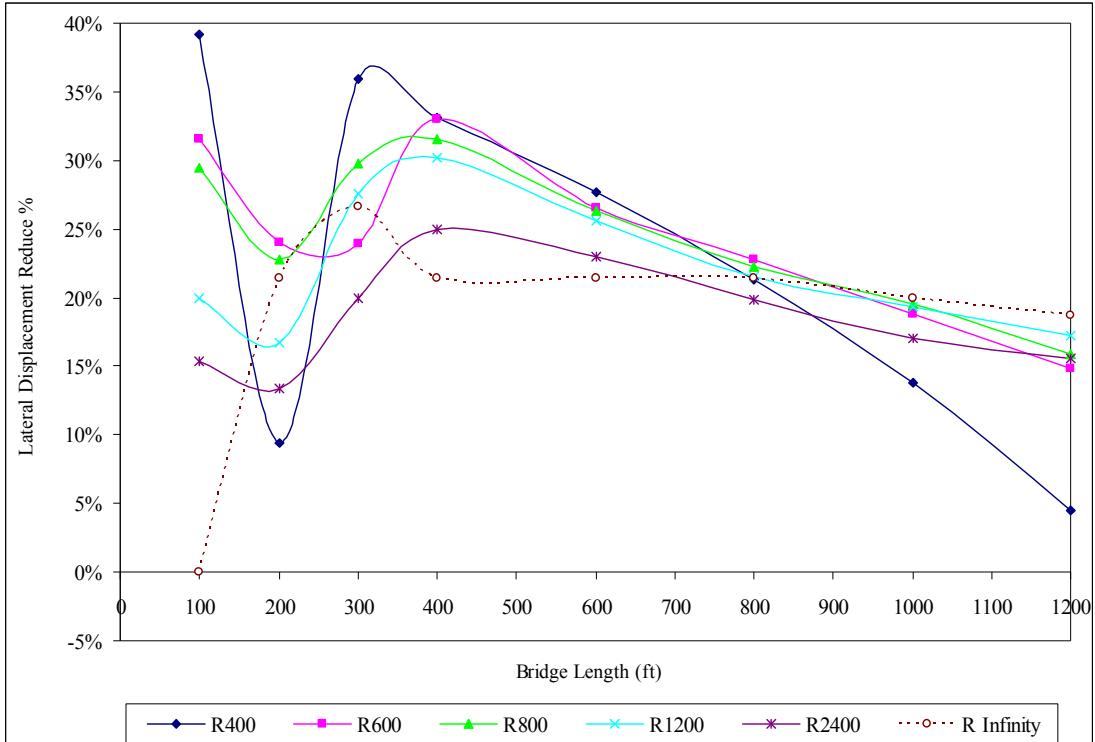


a)  $\Delta T_{\text{slab}} = 90^\circ \text{ F}$ ,  $\Delta T_{\text{the rest}} = 60^\circ \text{ F}$

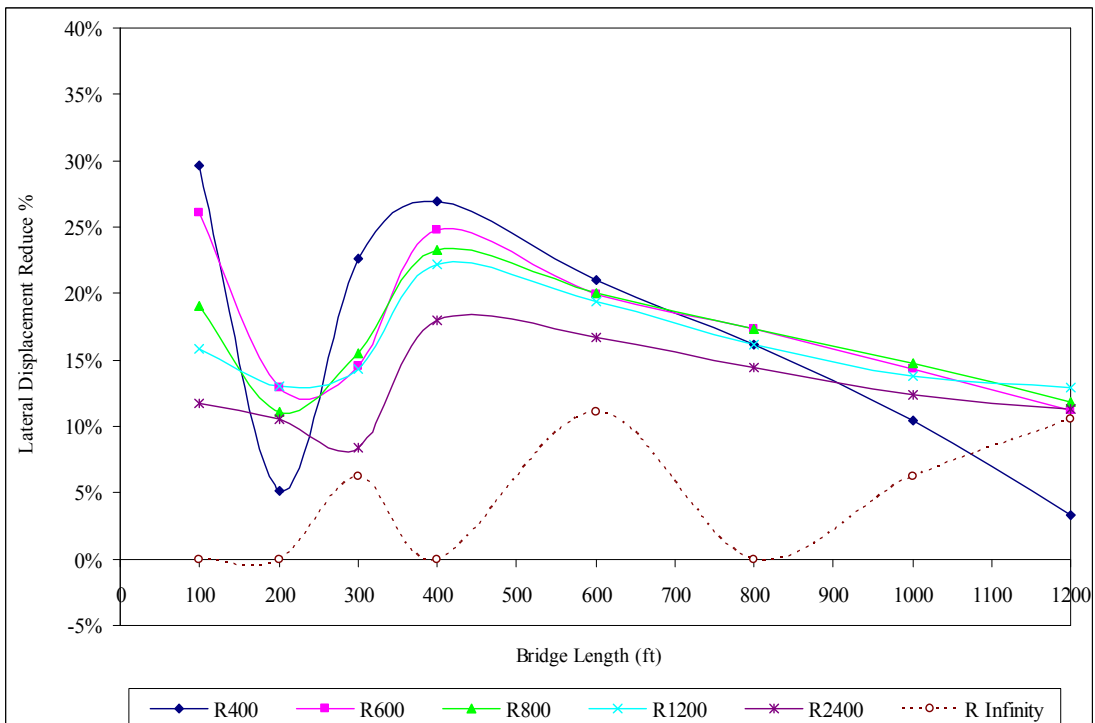


b)  $\Delta T_{\text{slab}} = 120^\circ \text{ F}$ ,  $\Delta T_{\text{the rest}} = 90^\circ \text{ F}$

**Figure 8.24 – Lateral Displacement Reduction (%) of Bridges and End-Bearing Piles in Very Stiff Clay Soil Profile due to the Increase in the Number of Spans**

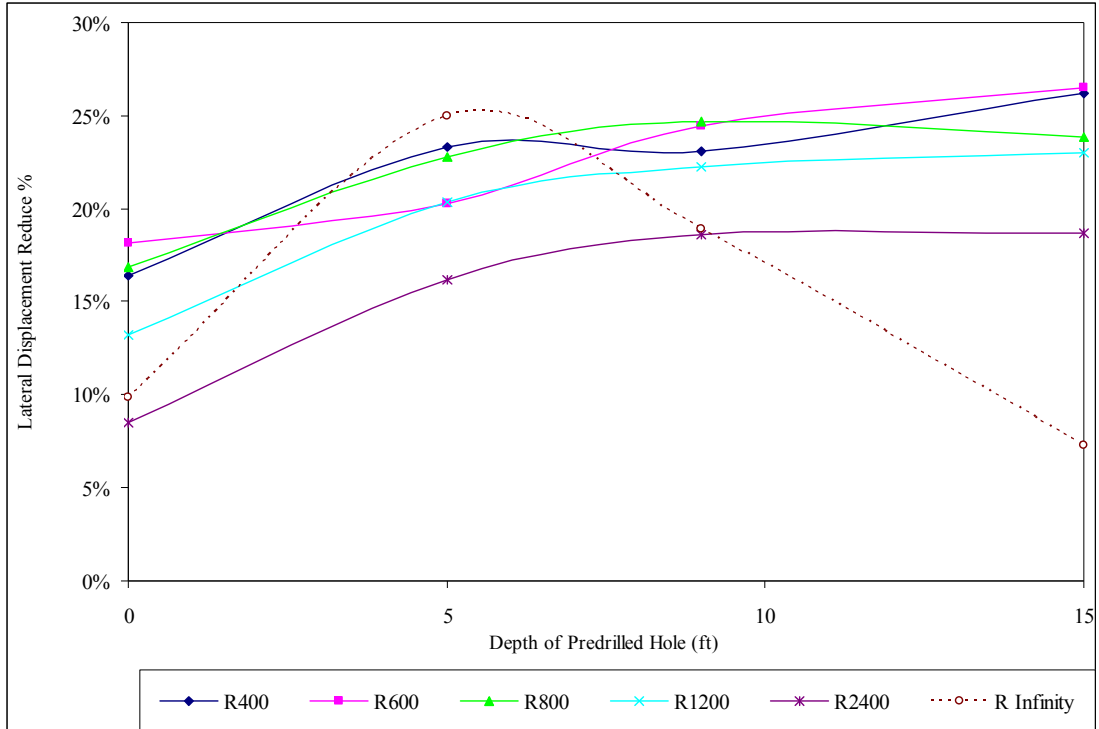


a)  $\Delta T_{\text{slab}} = 90^\circ \text{ F}$ ,  $\Delta T_{\text{the rest}} = 60^\circ \text{ F}$

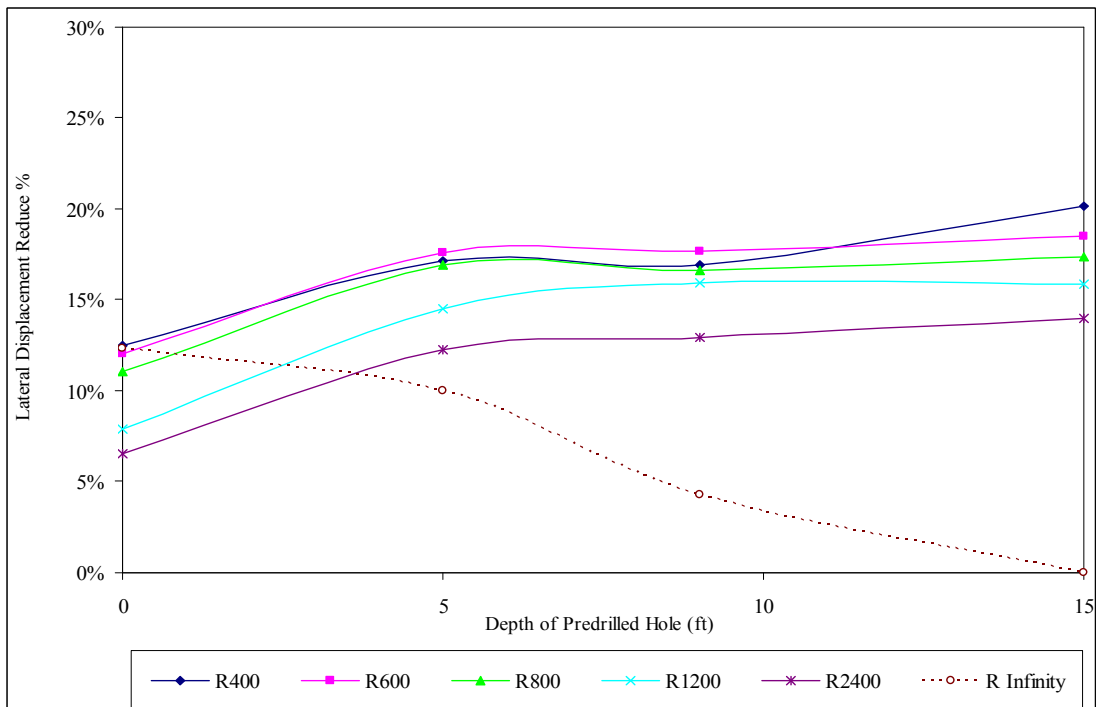


b)  $\Delta T_{\text{slab}} = 120^\circ \text{ F}$ ,  $\Delta T_{\text{the rest}} = 90^\circ \text{ F}$

**Figure 8.25 – Lateral Displacement Reduction (%) of Bridges and End-Bearing Piles in 9 ft Deep Predrilled Holes due to the Increase in the Number of Spans**

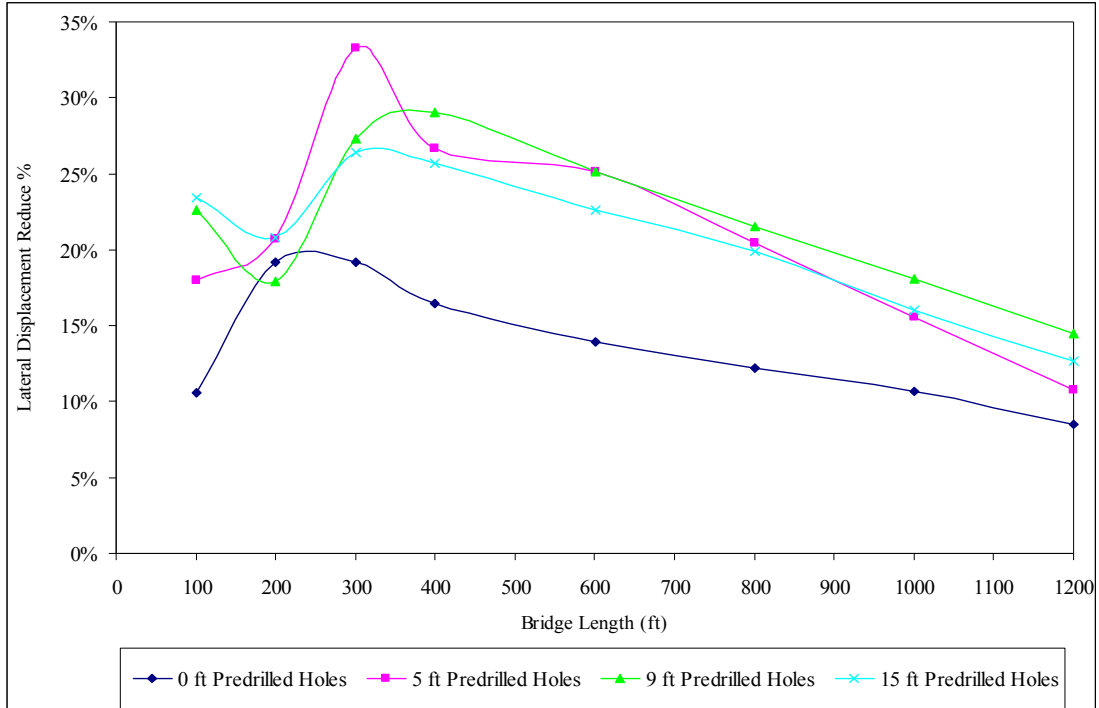


a)  $\Delta T_{\text{slab}} = 90^\circ \text{ F}, \Delta T_{\text{the rest}} = 60^\circ \text{ F}$

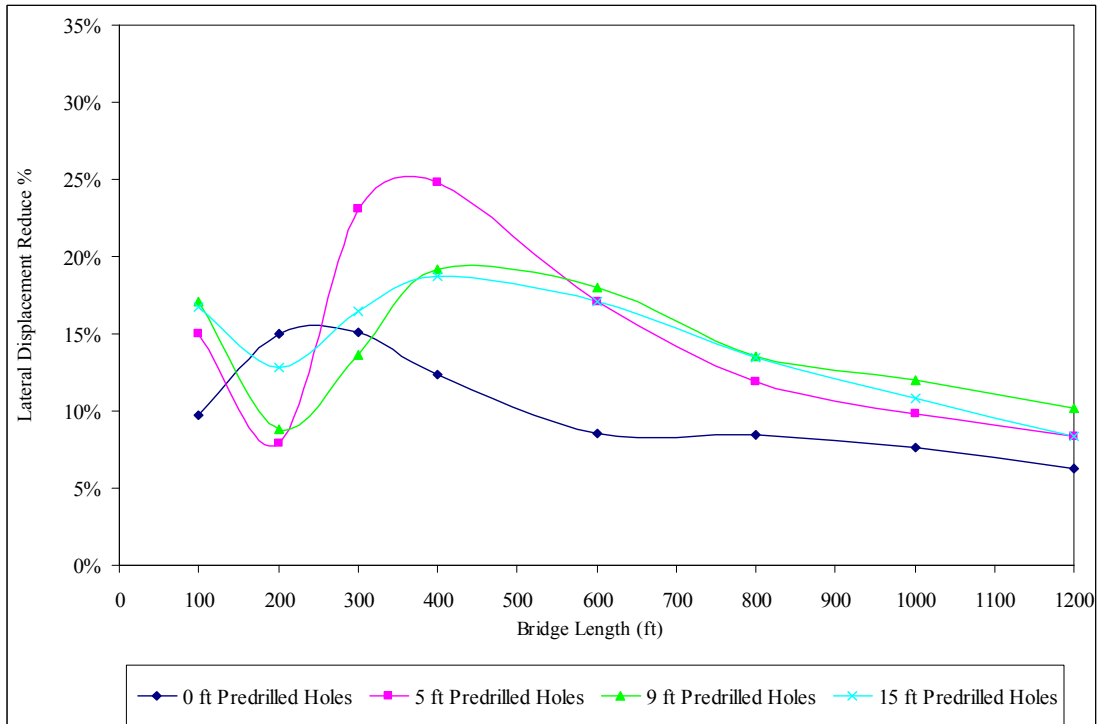


b)  $\Delta T_{\text{slab}} = 120^\circ \text{ F}, \Delta T_{\text{the rest}} = 90^\circ \text{ F}$

**Figure 8.26 – Mean of Lateral Displacement Reduction (%) of Bridges of Different Radii and End-Bearing Piles in Various Soil Profile Types due to the Increase in the Number of Spans**



a)  $\Delta T_{\text{slab}} = 90^\circ \text{ F}, \Delta T_{\text{the rest}} = 60^\circ \text{ F}$



b)  $\Delta T_{\text{slab}} = 120^\circ \text{ F}, \Delta T_{\text{the rest}} = 90^\circ \text{ F}$

**Figure 8.27 – Mean of Lateral Displacement Reduction (%) of Bridges and End-Bearing Piles in Various Soil Profile Types due to the Increase in the Number of Spans**

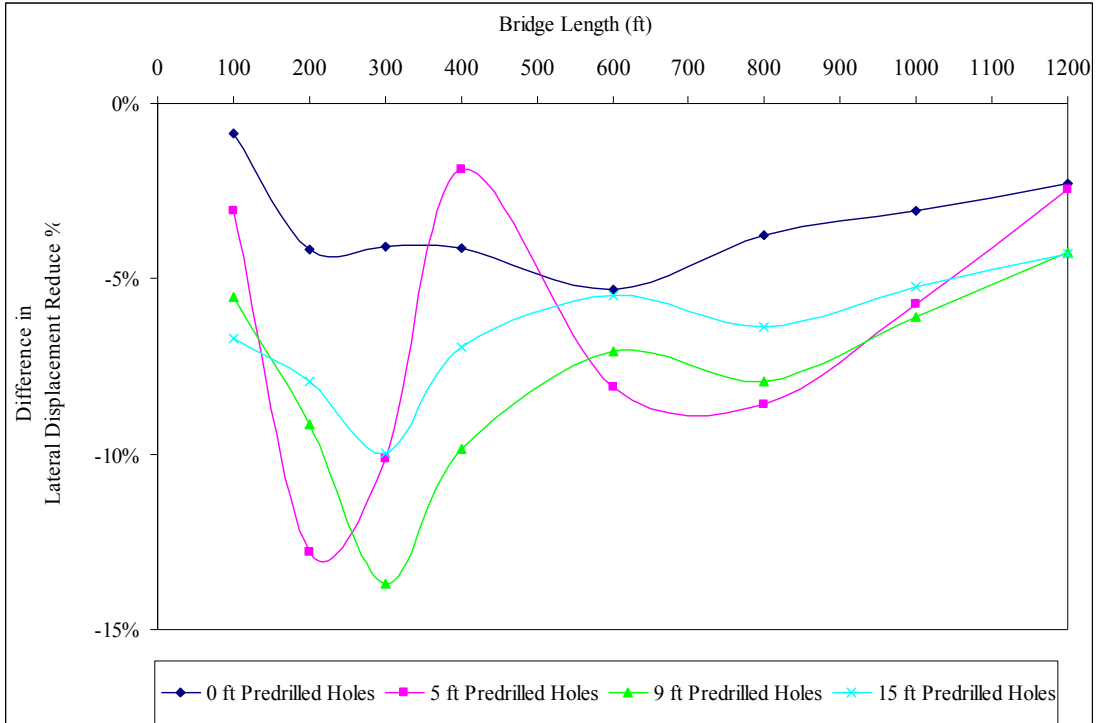


**Figure 8.28 – Difference in Lateral Displacement Reduction (%) of Bridges and End-Bearing Piles due to the Increase in the Number of Spans between  $\Delta T_{\text{slab}} = 120^\circ \text{ F}$ ,  $\Delta T_{\text{the rest}} = 90^\circ \text{ F}$  and  $\Delta T_{\text{slab}} = 90^\circ \text{ F}$ ,  $\Delta T_{\text{the rest}} = 60^\circ \text{ F}$**



## **8.5 Effect of Radius Variation**

The effect of radius variation on the maximum lateral displacement of curved IAB's is discussed in this section. All other parameters are held constant.

### **8.5.1 Curved Integral Abutment Bridges with 50 ft Spans**

Figures 8.29 to 8.33 indicate that the lateral displacement of curved IAB's with piles in very stiff clay soil profile at two temperature levels, for the most part, decreases as the radius is increased from 400 ft to 2400 ft for bridge lengths between 50 ft and 750 ft as indicated in Table 8.20. Curved IAB's with a smaller radius have a lateral displacement decrease due to change in radius at a shorter bridge length range than that of curved IAB's with a larger radius.

Beyond the lengths indicated in Table 8.20, the lateral displacement of curved IAB's starts increasing and continues to increase to its highest value as the bridge length is increased to 1200 ft as indicated in Table 8.21.

The lateral displacement of curved IAB's, in most cases, increases as the radius continues to increase to infinity (straight IAB's) at bridge lengths between 50 ft and 300 ft. It begins to decrease at bridge lengths between 200 ft and 300 ft and then remains nearly constant for bridge lengths from 600 ft to 1200 ft as indicated in Table 8.22.

**Table 8.20 – Lateral Displacement Decrease (%) of Bridges with 50 ft Spans and End-Bearing Piles in Very Stiff Clay Soil Profile due to Change in Radius**

Radius Increase from X ft to 2400 ft		
Radius X (ft)	Lateral Displacement Decrease (%)	Bridge Length (ft)
400	0.0 to 70.4	50 to 550
600	0.0 to 63.8	50 to 650
800	0.0 to 57.6	50 to 700
1200	0.0 to 42.9	50 to 750

**Table 8.21 – Lateral Displacement Increase (%) of Bridges with 50 ft Spans and End-Bearing Piles in Very Stiff Clay Soil Profile due to Change in Radius at 1200 ft Length ( $\Delta T_{\text{slab}} = 90^\circ \text{ F}$ ,  $\Delta T_{\text{the rest}} = 60^\circ \text{ F}$ )**

Increase Radius (ft)	400	600	800	1200	2400
To Radius (ft)					
600	143.5	-	-	-	-
800	286.4	58.7	-	-	-
1200	546.3	165.4	67.3	-	-
2400	1099.3	392.5	210.4	85.6	-

**Table 8.22 – Lateral Displacement Decrease (%) of Bridges with 50 ft Spans and End-Bearing Piles in Very Stiff Clay Soil Profile due to Change in Various Radii to Infinity at 1200 ft Length ( $\Delta T_{\text{slab}} = 90^\circ \text{ F}$ ,  $\Delta T_{\text{the rest}} = 60^\circ \text{ F}$ )**

Increase Radius (ft)	400	600	800	1200	2400
To Radius (ft)					
Infinity	74.8	89.7	93.5	96.1	97.9

For curved IAB's with piles in 9 ft deep predrilled holes filled with loose sand as shown in Figures 8.34 to 8.38, the lateral displacement of curved IAB's at two temperature levels decreases as the radius is increased from 400 ft to 2400 ft for bridge lengths between 50 ft and 1050 ft as indicated in Table 8.23. Curved IAB's with a smaller radius have a lateral displacement decrease due to change in radius at a shorter bridge length range than that of curved IAB's with a larger radius.

Beyond the lengths indicated in Table 8.23, the lateral displacement of curved IAB's starts increasing and continues to increase to its highest value as the bridge length is increased to 1200 ft as indicated in Table 8.24.

The lateral displacement of curved IAB's decreases as the radius continues to increase to infinity (straight IAB's). It begins to decrease at a 50 ft bridge length and then remains nearly constant for bridge lengths from 600 ft to 1200 ft as indicated in Table 8.25.

**Table 8.23 – Lateral Displacement Decrease (%) of Bridges with 50 ft Spans and End-Bearing Piles in 9 ft Deep Predrilled Holes due to Change in Radius**

Radius Increase from X ft to 2400 ft		
Radius X (ft)	Lateral Displacement Decrease (%)	Bridge Length (ft)
400	3.1 to 70.4	50 to 800
600	0.0 to 61.5	50 to 850
800	0.0 to 56.3	50 to 950
1200	0.0 to 42.4	50 to 1050

**Table 8.24 – Lateral Displacement Increase (%) of Bridges with 50 ft Spans and End-Bearing Piles in 9 ft Deep Predrilled Holes due to Change in Radius at 1200 ft Length ( $\Delta T_{\text{slab}} = 90^\circ \text{ F}$ ,  $\Delta T_{\text{the rest}} = 60^\circ \text{ F}$ )**

Increase Radius (ft)	400	600	800	1200	2400
To Radius (ft)					
600	134.9	-	-	-	-
800	260.4	53.4	-	-	-
1200	454.4	136.0	53.8	-	-
2400	626.2	209.1	101.5	31.0	-

**Table 8.25 – Lateral Displacement Decrease (%) of Bridges with 50 ft Spans and End-Bearing Piles in 9 ft Deep Predrilled Holes due to Change in Various Radii to Infinity at 1200 ft Length ( $\Delta T_{\text{slab}} = 90^\circ \text{ F}$ ,  $\Delta T_{\text{the rest}} = 60^\circ \text{ F}$ )**

Increase Radius (ft)	400	600	800	1200	2400
To Radius (ft)					
Infinity	91.3	96.3	97.6	98.4	98.8

Tables 8.20 and 8.23 indicate that the lateral displacement decrease due to change in radius of curved IAB's with piles in 9 ft deep predrilled holes filled with loose sand occurs at the bridge length ranges of 200 ft to 300 ft longer than that of curved IAB's with piles without predrilled holes.

Tables 8.21, 8.22, 8.24, 8.25, and Figures 8.29 to 8.38 indicate that the lateral displacement increase due to change in radius of curved IAB's with a smaller radius range, for the most part, is less than that of curved IAB's with a larger radius range. The highest lateral displacement increase value of curved IAB's due to change in radius from different radii to a 2400 ft radius is at a 1200 ft length. If the radius continues to increase to infinity, the lateral displacement increase of curved IAB's

due to change in radius will decrease until there is a relatively small increase in the lateral displacement of curved IAB's ( $\approx 0\%$ ).

Tables 8.22 and 8.25 also indicate that there is a significant decrease in the lateral displacement of curved IAB's due to change in radius from different radii to infinity by 74.8% to 98.8% at bridge lengths between 600 ft and 1200 ft.

The lateral displacement increase due to change in radius of curved IAB's with piles in predrilled holes is less than that of curved IAB's with piles without predrilled holes. It is shown that piles in 9 feet deep predrilled holes filled with loose sand have a significant reduction in the lateral displacement of curved IAB's when compared with piles in 5 ft deep predrilled holes filled with loose sand. The depth increase of predrilled holes deeper than 9 ft will further reduce the lateral displacement of curved IAB's, but the rate of reduction is much smaller than that of 9 ft deep predrilled holes as indicated in Table 8.26 and discussed in Section 8.3.

The lateral displacement increase due to change in radius of curved IAB's subjected to a temperature load of  $\Delta T_{\text{slab}}$  of  $120^\circ\text{ F}$  and  $\Delta T_{\text{the rest}}$  of  $90^\circ\text{ F}$  is less than that of curved IAB's subjected to a temperature load of  $\Delta T_{\text{slab}}$  of  $90^\circ\text{ F}$  and  $\Delta T_{\text{the rest}}$  of  $60^\circ\text{ F}$  by 1.64%. This is because with a temperature increase, the lateral displacement increase of curved IAB's with a smaller radius is greater than that of curved IAB's with a larger radius as discussed in Section 8.2.

**Table 8.26 – Difference in Lateral Displacement Increase (%) due to Change in Radius of Bridges with 50 ft Spans and End-Bearing Piles in Varying Depths of Predrilled Holes or End-Bearing Piles without Predrilled Holes**

( $\Delta T_{\text{slab}} = 90^\circ \text{ F}$ ,  $\Delta T_{\text{the rest}} = 60^\circ \text{ F}$ )

To Radius (ft)		600	800	1200	2400	Infinity
Increase Radius (ft)	Depth of Predrilled Holes (ft)					
400	5	-122	-54	-101	-286	-76
	9	-117	-70	-151	-473	-72
	15	-122	-74	-159	-506	-48
600	5	-	-28	-44	-127	-45
	9	-	-26	-68	-189	-42
	15	-	-26	-72	-200	-42
800	5	-	-	-28	-79	-51
	9	-	-	-37	-119	-51
	15	-	-	-40	-126	-51
1200	5	-	-	-	-41	-39
	9	-	-	-	-63	-39
	15	-	-	-	-67	-27
2400	5	-	-	-	-	-45
	9	-	-	-	-	-45
	15	-	-	-	-	-31

### 8.5.2 Curved Integral Abutment Bridges with 100 ft Spans

Figures 8.39 to 8.43 indicate that the lateral displacement of curved IAB's with piles in very stiff clay soil profile at two temperature levels decreases as the radius is increased from 400 ft to 2400 ft for bridge lengths between 100 ft and 800 ft as indicated in Table 8.27. Curved IAB's with a smaller radius have a lateral displacement decrease due to change in radius at a shorter bridge length range than that of curved IAB's with a larger radius.

Beyond the lengths indicated in Table 8.27, the lateral displacement of curved IAB's starts increasing and continues to increase to its highest value as the bridge length is increased to 1200 ft as indicated in Table 8.28.

The lateral displacement of curved IAB's, in most cases, increases as the radius continues to increase to infinity (straight IAB's) at bridge lengths between 100 ft and 300 ft. It begins to decrease at bridge lengths between 250 ft and 350 ft and then remains nearly constant for bridge lengths from 600 ft to 1200 ft as indicated in Table 8.29.

**Table 8.27 – Lateral Displacement Decrease (%) of Bridges with 100 ft Spans and End-Bearing Piles in Very Stiff Clay Soil Profile due to Change in Radius**

Radius Increase from X ft to 2400 ft		
Radius X (ft)	Lateral Displacement Decrease (%)	Bridge Length (ft)
400	2.3 to 73.2	100 to 600
600	0.0 to 65.9	100 to 650
800	2.4 to 59.1	100 to 700
1200	0.0 to 43.8	100 to 800

**Table 8.28 – Lateral Displacement Increase (%) of Bridges with 100 ft Spans and End-Bearing Piles in Very Stiff Clay Soil Profile due to Change in Radius at 1200 ft Length ( $\Delta T_{\text{slab}} = 90^\circ \text{ F}$ ,  $\Delta T_{\text{the rest}} = 60^\circ \text{ F}$ )**

Increase Radius (ft)	400	600	800	1200	2400
To Radius (ft)					
600	165.8	-	-	-	-
800	328.3	61.1	-	-	-
1200	618.4	170.3	67.7	-	-
2400	1200.7	389.4	203.7	81.0	-

**Table 8.29 – Lateral Displacement Decrease (%) of Bridges with 100 ft Spans and End-Bearing Piles in Very Stiff Clay Soil Profile due to Change in Various Radii to Infinity at 1200 ft Length ( $\Delta T_{\text{slab}} = 90^\circ \text{ F}$ ,  $\Delta T_{\text{the rest}} = 60^\circ \text{ F}$ )**

Increase Radius (ft)	400	600	800	1200	2400
To Radius (ft)					
Infinity	75.7	90.8	94.3	96.6	98.1

For curved IAB's with piles in 9 ft deep predrilled holes filled with loose sand as shown in Figures 8.44 to 8.48, the lateral displacement of curved IAB's at two temperature levels decreases as the radius is increased from 400 ft to 2400 ft for bridge lengths between 100 ft and 1050 ft as indicated in Table 8.30. Curved IAB's with a smaller radius have a lateral displacement decrease due to change in radius at a shorter bridge length range than that of curved IAB's with a larger radius.

Beyond the lengths indicated in Table 8.30, the lateral displacement of curved IAB's starts increasing and continues to increase to its highest value as the bridge length is increased to 1200 ft as indicated in Table 8.31.

The lateral displacement of curved IAB's decreases as the radius continues to increase to infinity (straight IAB's). It begins to decrease at a 100 ft bridge length and



then remains nearly constant for bridge lengths from 600 ft to 1200 ft as indicated in Table 8.32.

**Table 8.30 – Lateral Displacement Decrease (%) of Bridges with 100 ft Spans and End-Bearing Piles in 9 ft Deep Predrilled Holes due to Change in Radius**

Radius Increase from X ft to 2400 ft		
Radius X (ft)	Lateral Displacement Decrease (%)	Bridge Length (ft)
400	4.8 to 73.6	100 to 800
600	8.7 to 64.8	100 to 900
800	3.0 to 58.1	100 to 950
1200	0.0 to 44.3	100 to 1050

**Table 8.31 – Lateral Displacement Increase (%) of Bridges with 100 ft Spans and End-Bearing Piles in 9 ft Deep Predrilled Holes due to Change in Radius at 1200 ft Length ( $\Delta T_{\text{slab}} = 90^\circ \text{ F}$ ,  $\Delta T_{\text{the rest}} = 60^\circ \text{ F}$ )**

Increase Radius (ft)	400	600	800	1200	2400
To Radius (ft)					
600	163.5	-	-	-	-
800	309.0	55.2	-	-	-
1200	539.7	142.8	56.4	-	-
2400	721.2	211.7	100.8	28.4	-

**Table 8.32 – Lateral Displacement Decrease (%) of Bridges with 100 ft Spans and End-Bearing Piles in 9 ft Deep Predrilled Holes due to Change in Various Radii to Infinity at 1200 ft Length ( $\Delta T_{\text{slab}} = 90^\circ \text{ F}$ ,  $\Delta T_{\text{the rest}} = 60^\circ \text{ F}$ )**

Increase Radius (ft)	400	600	800	1200	2400
To Radius (ft)					
Infinity	89.7	96.1	97.5	98.4	98.8

Tables 8.27 and 8.30 indicate that the lateral displacement decrease due to change in radius of curved IAB's with piles in 9 ft deep predrilled holes filled with loose sand occurs at the bridge length ranges of 200 ft to 250 ft longer than that of curved IAB's with piles without predrilled holes.

Tables 8.28, 8.29, 8.31, 8.32, and Figures 8.39 to 8.48 indicate that the lateral displacement increase due to change in radius of curved IAB's with a smaller radius range, for the most part, is less than that of curved IAB's with a larger radius range. The highest lateral displacement increase value of curved IAB's due to change in radius from different radii to a 2400 ft radius is at a 1200 ft length. If the radius continues to increase to infinity, the lateral displacement increase of curved IAB's due to change in radius will decrease until there is a relatively small increase in the lateral displacement of curved IAB's ( $\approx 0\%$ ).

Tables 8.29 and 8.32 also indicates that there is a significant decrease in the lateral displacement of curved IAB's due to change in radius from different radii to infinity by 75.7% to 98.8% at bridge lengths between 600 ft and 1200 ft.

The lateral displacement increase due to change in radius of curved IAB's with piles in predrilled holes is less than that of curved IAB's with piles without predrilled holes. It is shown that piles in 9 feet deep predrilled holes filled with loose sand have a significant reduction in the lateral displacement of curved IAB's when compared with piles in 5 ft deep predrilled holes filled with loose sand. The depth increase of predrilled holes deeper than 9 ft will further reduce the lateral displacement of curved IAB's, but the rate of reduction is much smaller than that of 9 ft deep predrilled holes as indicated in Table 8.33 and discussed in Section 8.3.

The lateral displacement increase due to change in radius of curved IAB's subjected to a temperature load of  $\Delta T_{\text{slab}}$  of 120° F and  $\Delta T_{\text{the rest}}$  of 90° F is less than that of curved IAB's subjected to a temperature load of  $\Delta T_{\text{slab}}$  of 90° F and  $\Delta T_{\text{the rest}}$  of 60° F by 1.83%. This is because with a temperature increase, the lateral displacement increase of curved IAB's with a smaller radius is greater than that of curved IAB's with a larger radius as discussed in Section 8.2.

**Table 8.33 – Difference in Lateral Displacement Increase (%) due to Change in Radius of Bridges with 100 ft Spans and End-Bearing Piles in Varying Depths of Predrilled Holes or End-Bearing Piles without Predrilled Holes**  
( $\Delta T_{\text{slab}} = 90^\circ \text{ F}$ ,  $\Delta T_{\text{the rest}} = 60^\circ \text{ F}$ )

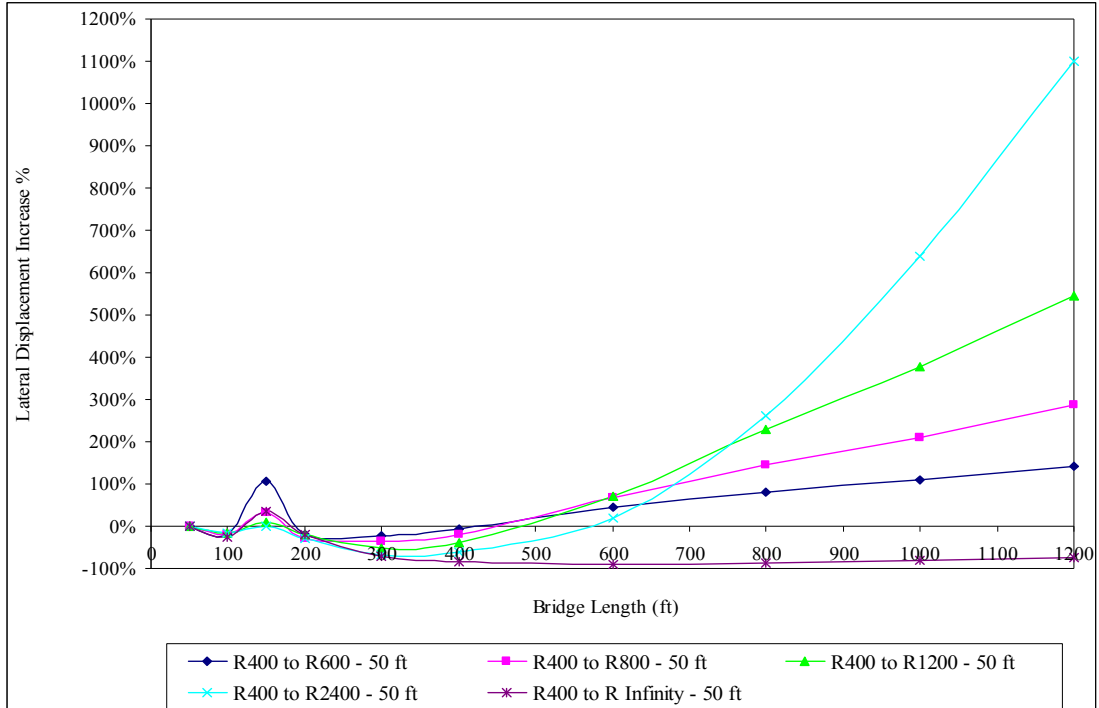
To Radius (ft)		600	800	1200	2400	Infinity
Increase Radius (ft)	Depth of Predrilled Holes (ft)					
400	5	-23	-44	-95	-287	-26
	9	-35	-64	-143	-480	-35
	15	-37	-67	-150	-518	-43
600	5	-	-15	-41	-117	-28
	9	-	-23	-64	-178	-48
	15	-	-24	-68	-192	-57
800	5	-	-	-21	-73	-30
	9	-	-	-34	-110	-57
	15	-	-	-37	-117	-66
1200	5	-	-	-	-38	-16
	9	-	-	-	-58	-38
	15	-	-	-	-63	-53
2400	5	-	-	-	-	-10
	9	-	-	-	-	-45
	15	-	-	-	-	-58

### 8.5.3 Conclusions

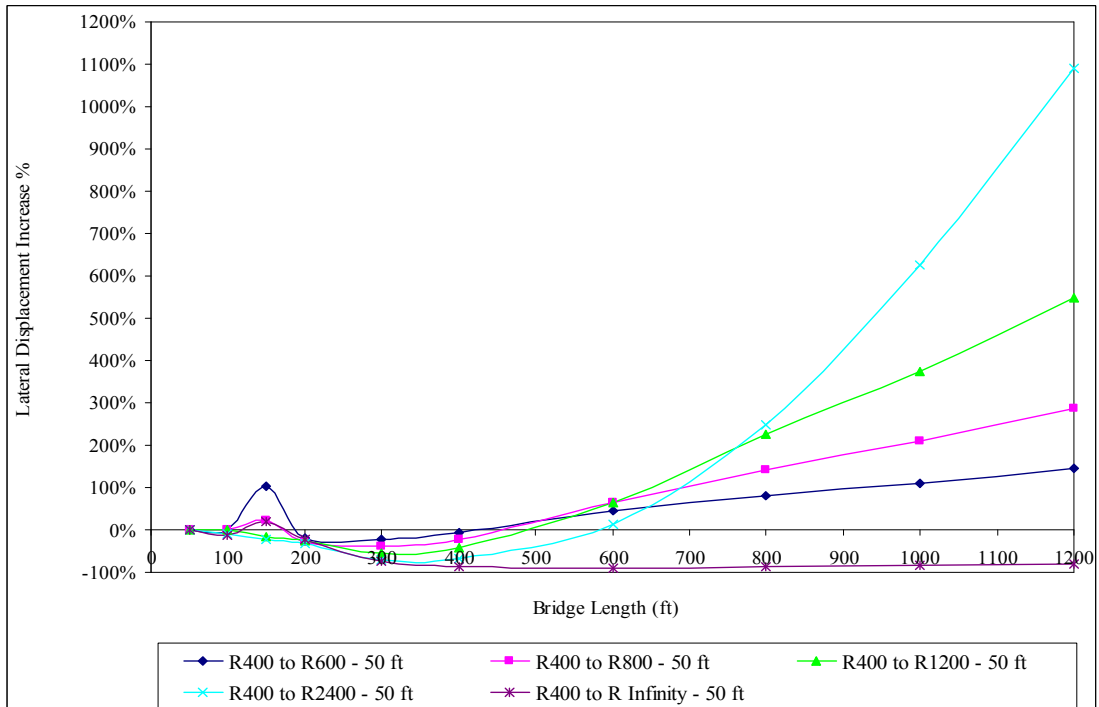
The following conclusions are drawn from the study of the effect of radius variation on the maximum lateral displacement in curved IAB's investigated in this section:

1. The lateral displacement of curved IAB's with both 50 ft and 100 ft spans and with piles in very stiff clay soil profile decreases as the radius is increased at bridge lengths between 50 ft and 800 ft. Beyond these lengths, the lateral displacement of curved IAB's starts to increase as the radius is increased.
2. Curved IAB's with piles in predrilled holes have a lateral displacement decrease due to change in radius occurring at the bridge length ranges of 200 ft to 300 ft longer than that of curved IAB's with piles without predrilled holes.
3. Curved IAB's with a smaller radius have a lateral displacement decrease due to change in radius at a shorter bridge length range than that of curved IAB's with a larger radius.
4. Curved IAB's with a smaller radius range, for the most part, have a lateral displacement increase due to change in radius less than that of curved IAB's with a larger radius range.
5. The highest lateral displacement increase value of curved IAB's due to change in radius from different radii to a 2400 ft radius is at a 1200 ft length.

6. If the radius continues to increase to infinity, the lateral displacement increase of curved IAB's due to change in radius will decrease until there is a relatively small increase in the lateral displacement of curved IAB's ( $\approx 0\%$ ). There is a significant decrease in the lateral displacement of curved IAB's due to change in radius from different radii to infinity by 74.8% to 98.8% at bridge lengths between 600 ft and 1200 ft.
7. The introduction of predrilled holes can reduce the lateral displacement increase of curved IAB's due to change in radius. It is shown that piles in 9 feet deep predrilled holes filled with loose sand have a significant reduction in the lateral displacement of curved IAB's when compared with piles in 5 ft deep predrilled holes filled with loose sand. The depth increase of predrilled holes deeper than 9 ft will further reduce the lateral displacement of curved IAB's, but the rate of reduction is much smaller than that of 9 ft deep predrilled holes.
8. The lateral displacement increase due to change in radius of curved IAB's subjected to a temperature load of  $\Delta T_{\text{slab}}$  of  $120^\circ\text{ F}$  and  $\Delta T_{\text{the rest}}$  of  $90^\circ\text{ F}$  is less than that of curved IAB's subjected to a temperature load of  $\Delta T_{\text{slab}}$  of  $90^\circ\text{ F}$  and  $\Delta T_{\text{the rest}}$  of  $60^\circ\text{ F}$  by 1.64% to 1.83%. This is because with a temperature increase, the lateral displacement increase of curved IAB's with a smaller radius is greater than that of curved IAB's with a larger radius as discussed in Section 8.2.

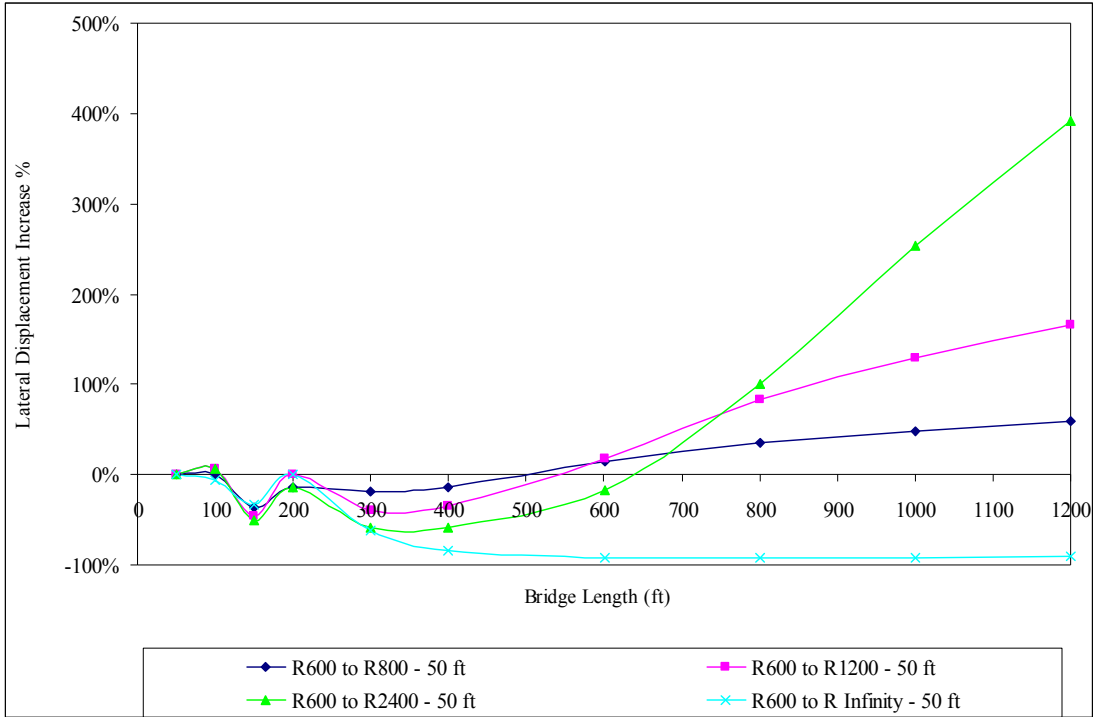


a)  $\Delta T_{\text{slab}} = 90^\circ \text{ F}$ ,  $\Delta T_{\text{the rest}} = 60^\circ \text{ F}$

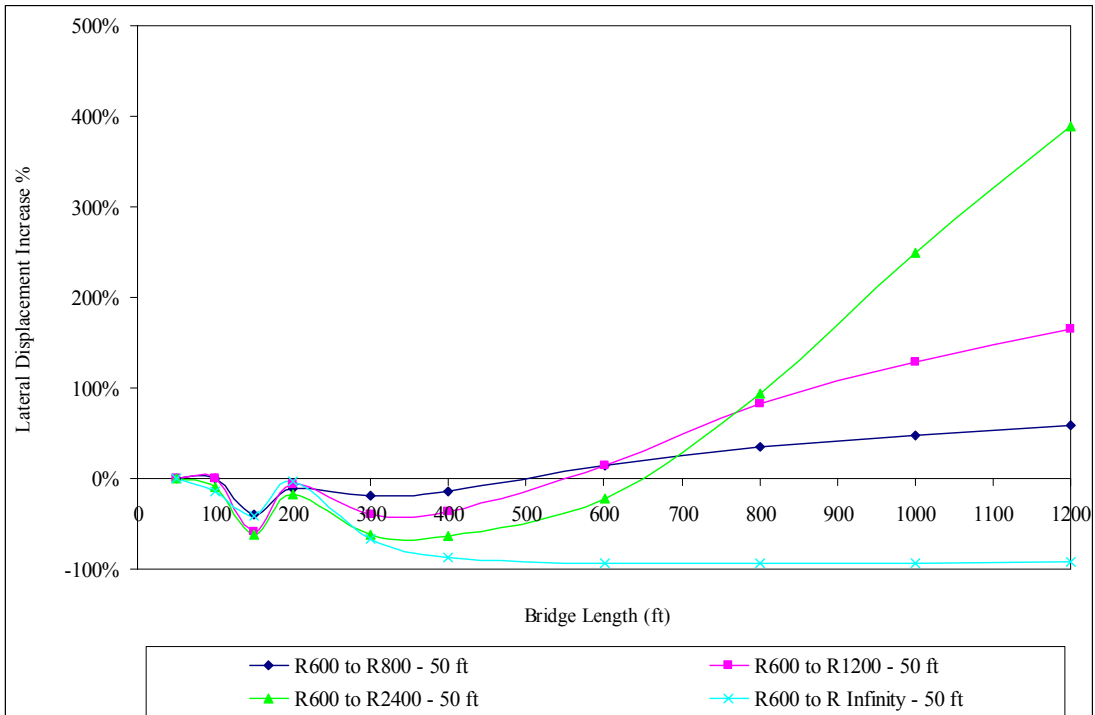


b)  $\Delta T_{\text{slab}} = 120^\circ \text{ F}$ ,  $\Delta T_{\text{the rest}} = 90^\circ \text{ F}$

**Figure 8.29 – Lateral Displacement Increase (%) of Bridges with 50 ft Spans and End-Bearing Piles in Very Stiff Clay Soil Profile due to Change in Radius from 400 ft to a Larger Radius**

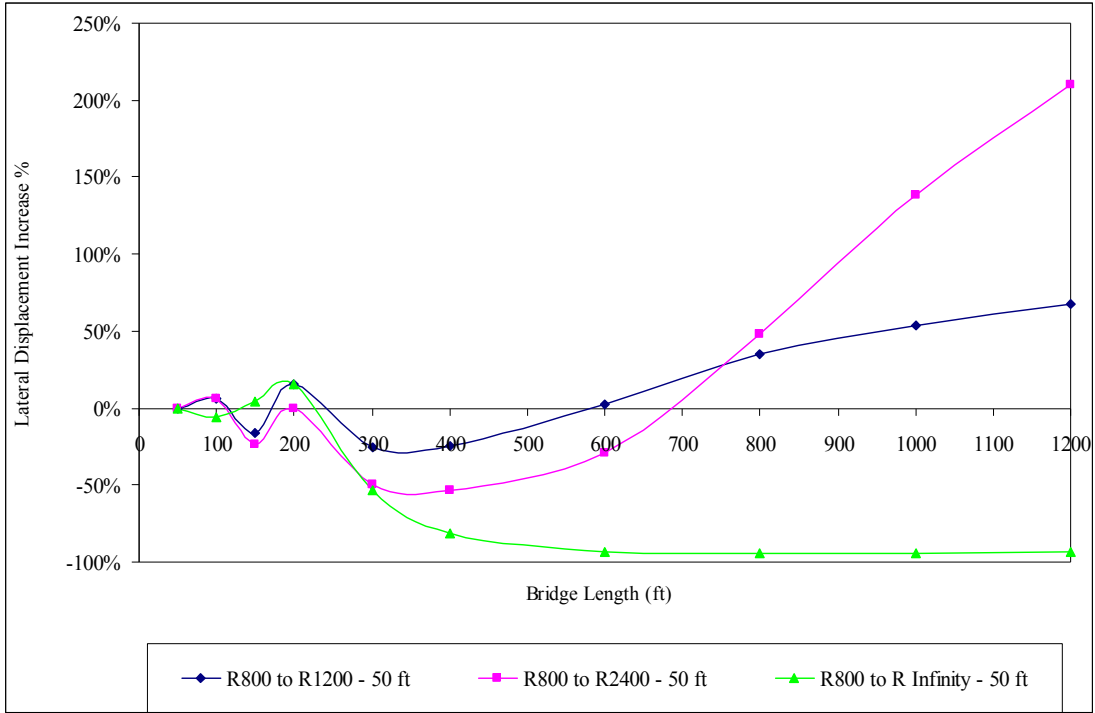


a)  $\Delta T_{\text{slab}} = 90^\circ \text{F}, \Delta T_{\text{the rest}} = 60^\circ \text{F}$

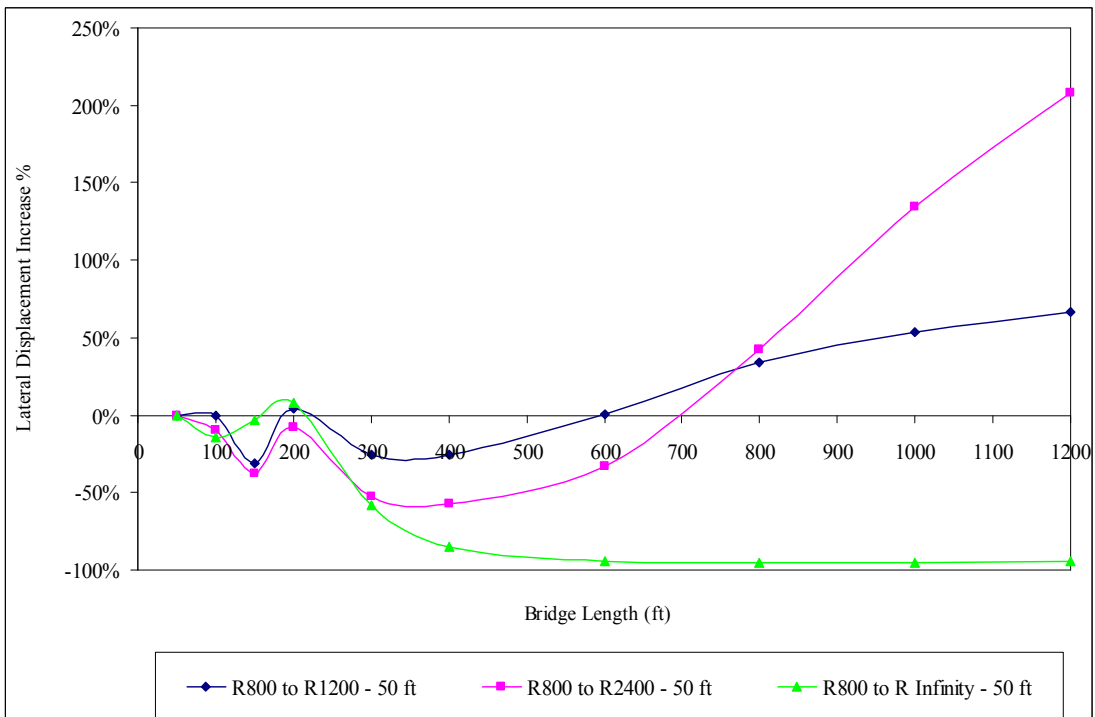


b)  $\Delta T_{\text{slab}} = 120^\circ \text{F}, \Delta T_{\text{the rest}} = 90^\circ \text{F}$

**Figure 8.30 – Lateral Displacement Increase (%) of Bridges with 50 ft Spans and End-Bearing Piles in Very Stiff Clay Soil Profile due to Change in Radius from 600 ft to a Larger Radius**



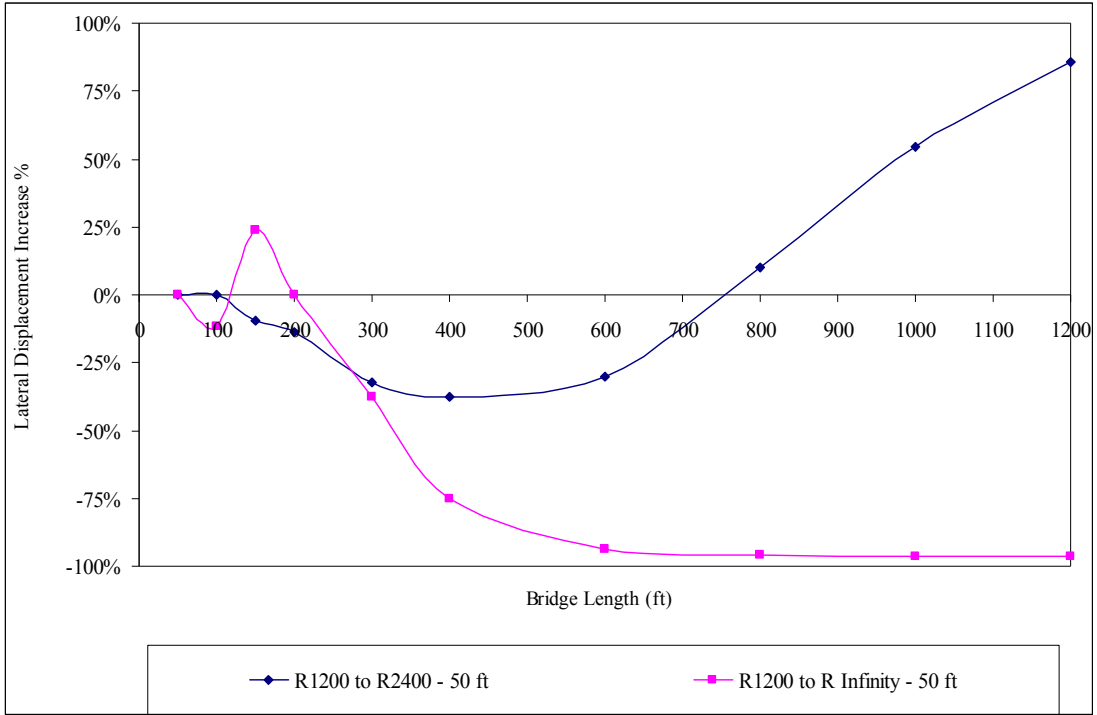
a)  $\Delta T_{\text{slab}} = 90^\circ \text{ F}, \Delta T_{\text{the rest}} = 60^\circ \text{ F}$



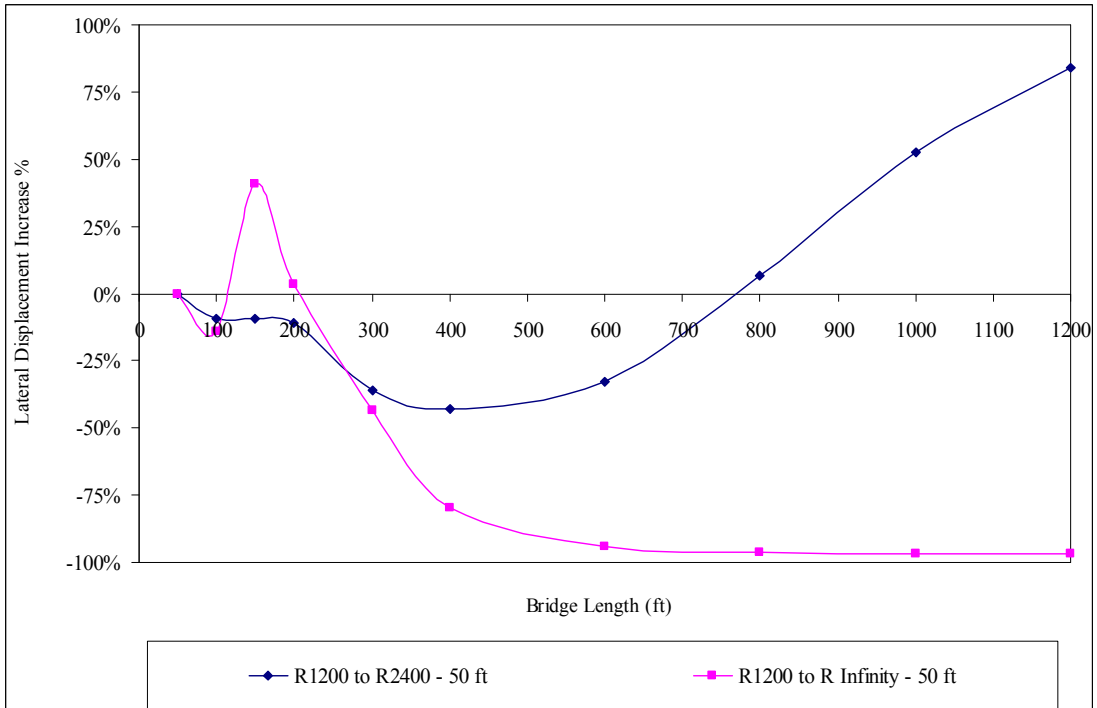
b)  $\Delta T_{\text{slab}} = 120^\circ \text{ F}, \Delta T_{\text{the rest}} = 90^\circ \text{ F}$

**Figure 8.31 – Lateral Displacement Increase (%) of Bridges with 50 ft Spans and End-Bearing Piles in Very Stiff Clay Soil Profile due to Change in Radius from 800 ft to a Larger Radius**



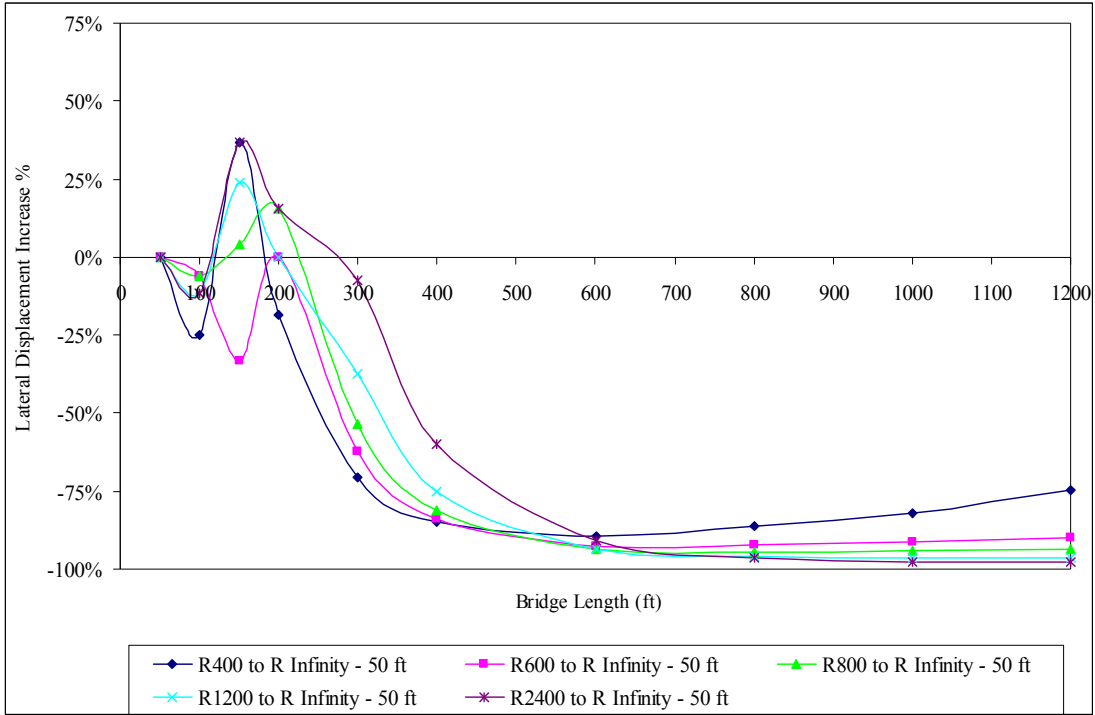


a)  $\Delta T_{\text{slab}} = 90^{\circ} \text{ F}$ ,  $\Delta T_{\text{the rest}} = 60^{\circ} \text{ F}$

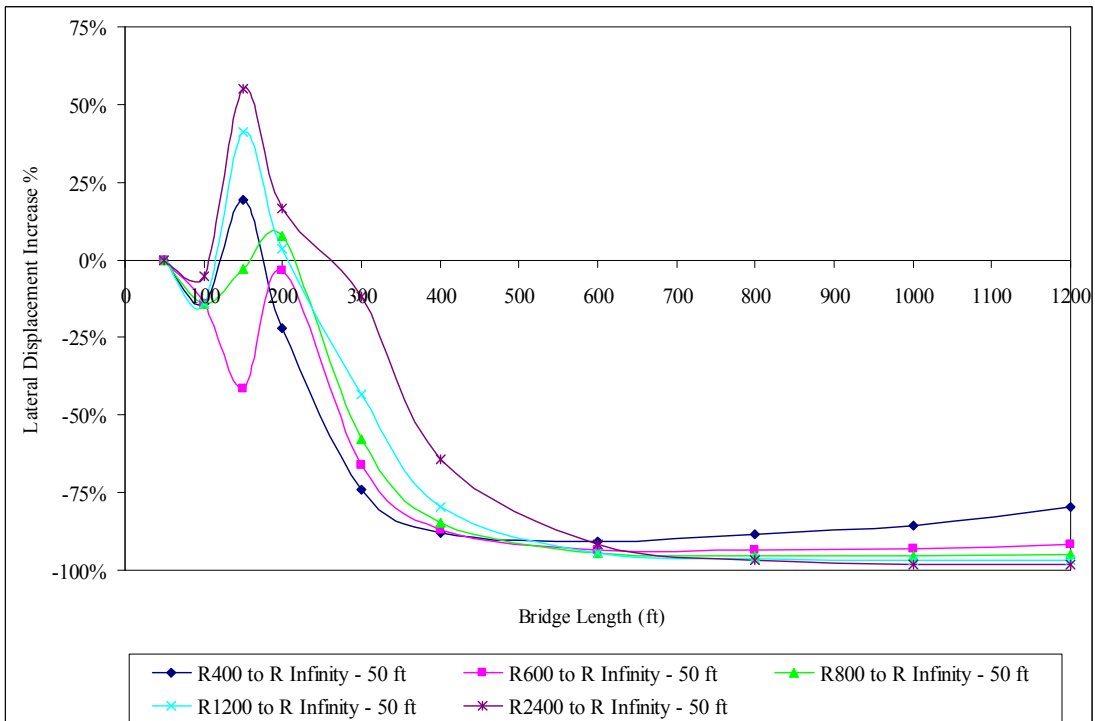


b)  $\Delta T_{\text{slab}} = 120^{\circ} \text{ F}$ ,  $\Delta T_{\text{the rest}} = 90^{\circ} \text{ F}$

**Figure 8.32 – Lateral Displacement Increase (%) of Bridges with 50 ft Spans and End-Bearing Piles in Very Stiff Clay Soil Profile due to Change in Radius from 1200 ft to a Larger Radius**

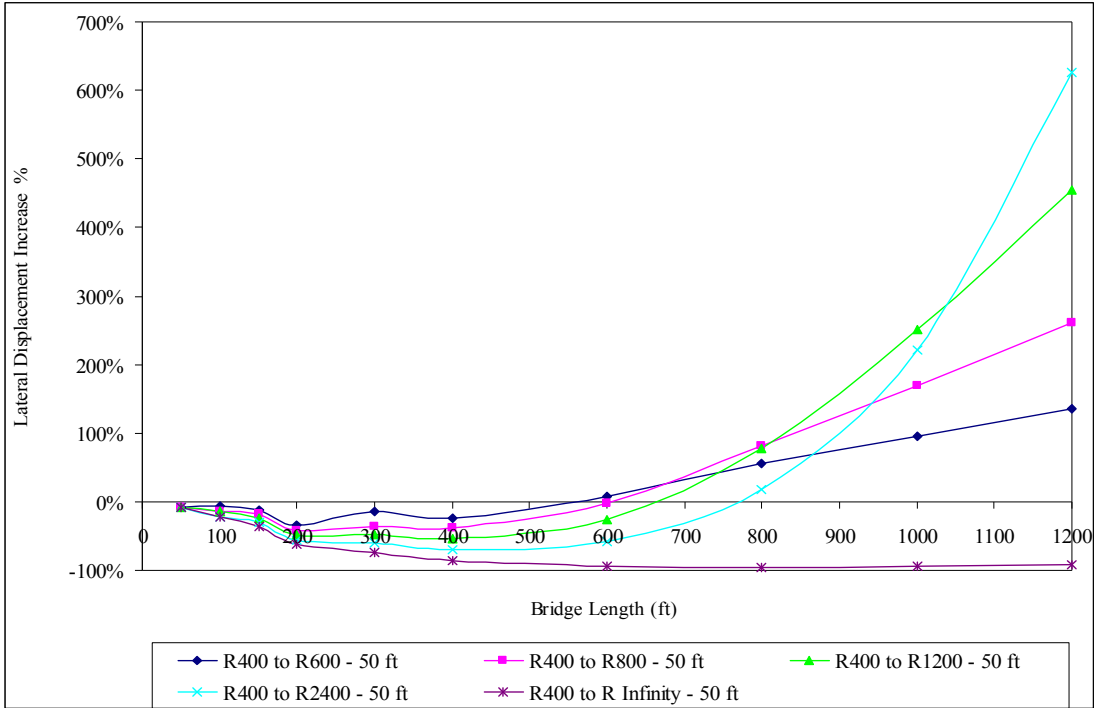


a)  $\Delta T_{\text{slab}} = 90^\circ \text{ F}$ ,  $\Delta T_{\text{the rest}} = 60^\circ \text{ F}$

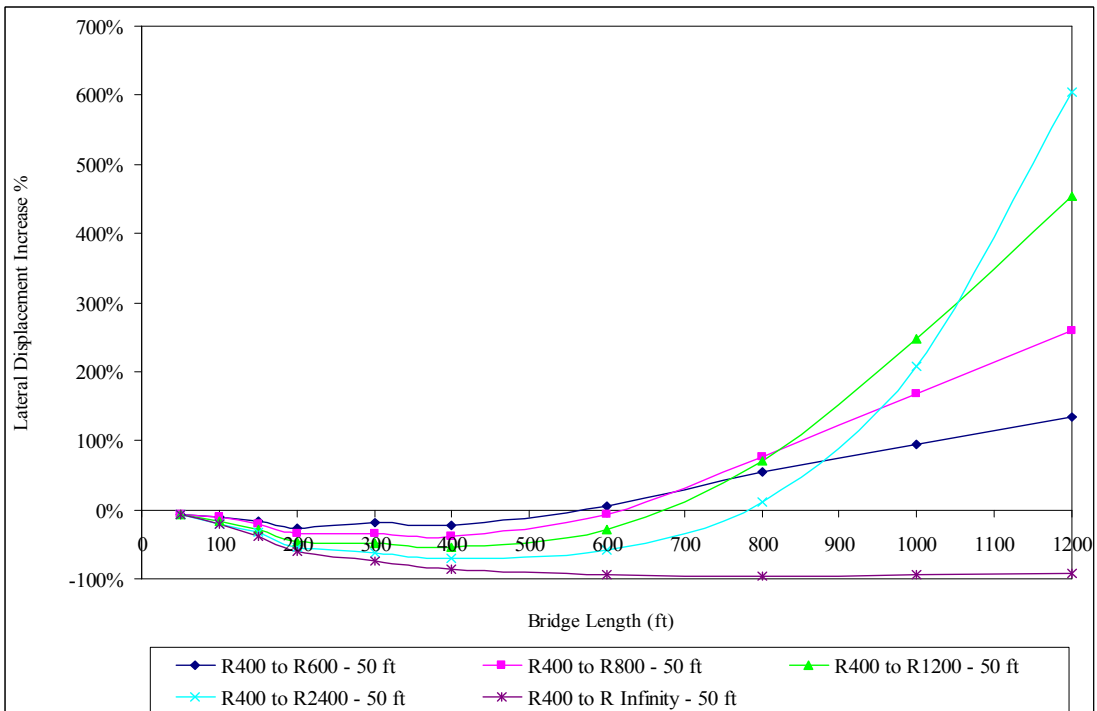


b)  $\Delta T_{\text{slab}} = 120^\circ \text{ F}$ ,  $\Delta T_{\text{the rest}} = 90^\circ \text{ F}$

**Figure 8.33 – Lateral Displacement Increase (%) of Bridges with 50 ft Spans and End-Bearing Piles in Very Stiff Clay Soil Profile due to Change in Radius from Different Values to Infinity**

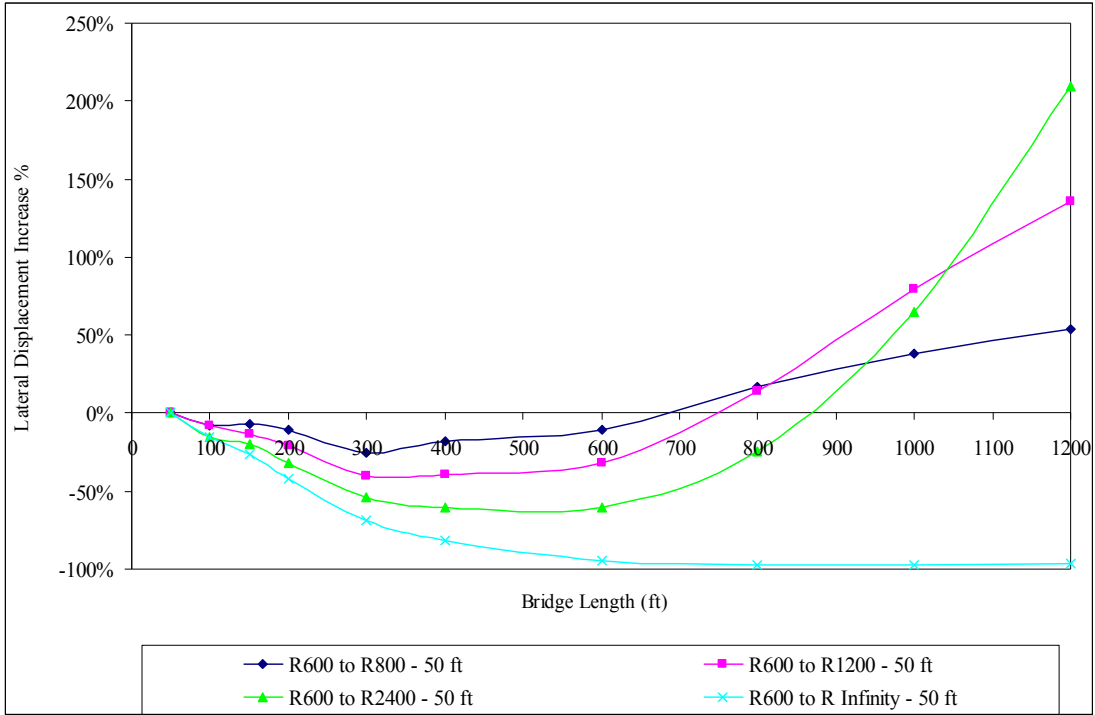


a)  $\Delta T_{\text{slab}} = 90^\circ \text{ F}$ ,  $\Delta T_{\text{the rest}} = 60^\circ \text{ F}$

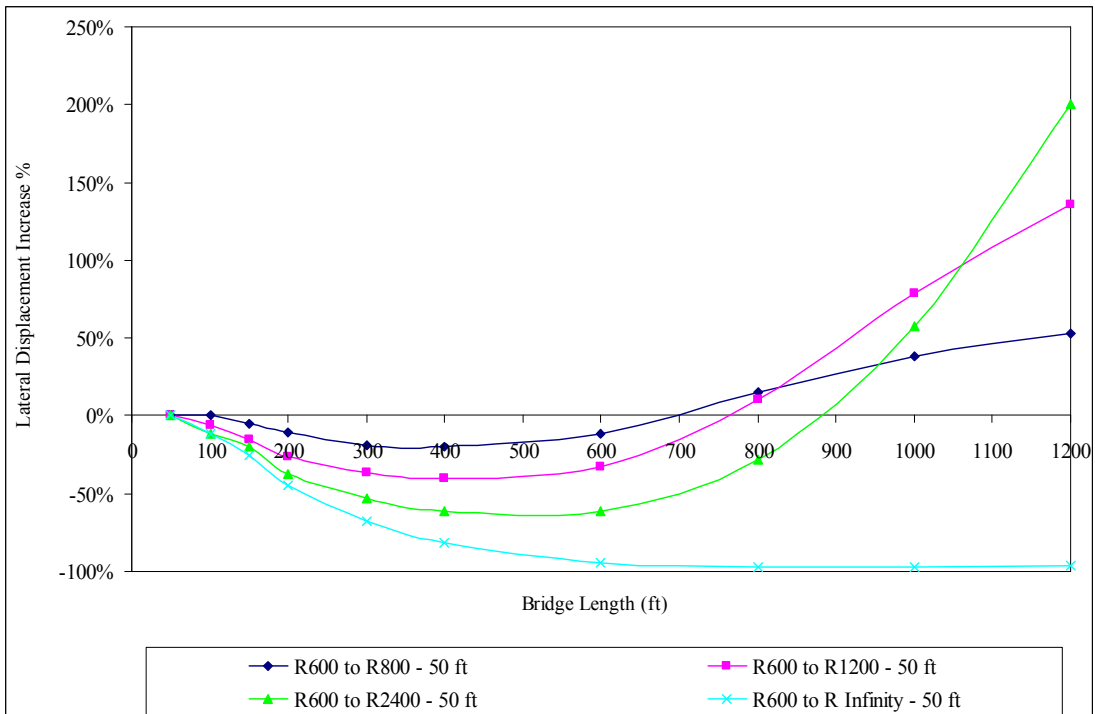


b)  $\Delta T_{\text{slab}} = 120^\circ \text{ F}$ ,  $\Delta T_{\text{the rest}} = 90^\circ \text{ F}$

**Figure 8.34 – Lateral Displacement Increase (%) of Bridges with 50 ft Spans and End-Bearing Piles in 9 ft Deep Predrilled Holes due to Change in Radius from 400 ft to a Larger Radius**

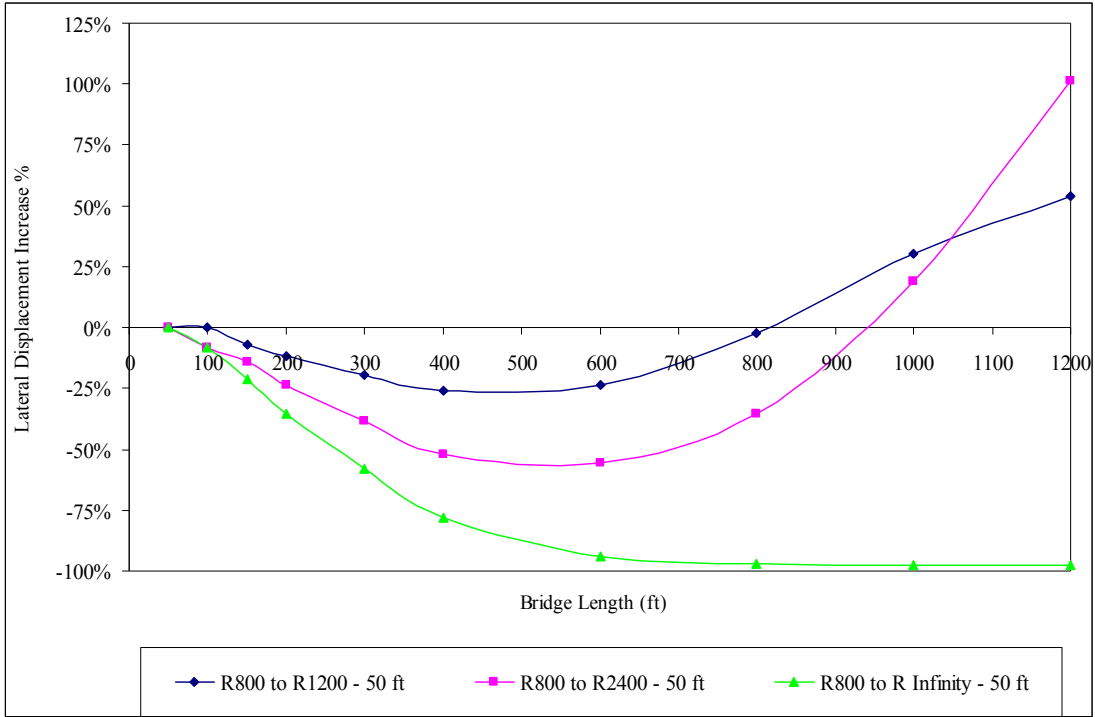


a)  $\Delta T_{\text{slab}} = 90^\circ \text{ F}$ ,  $\Delta T_{\text{the rest}} = 60^\circ \text{ F}$

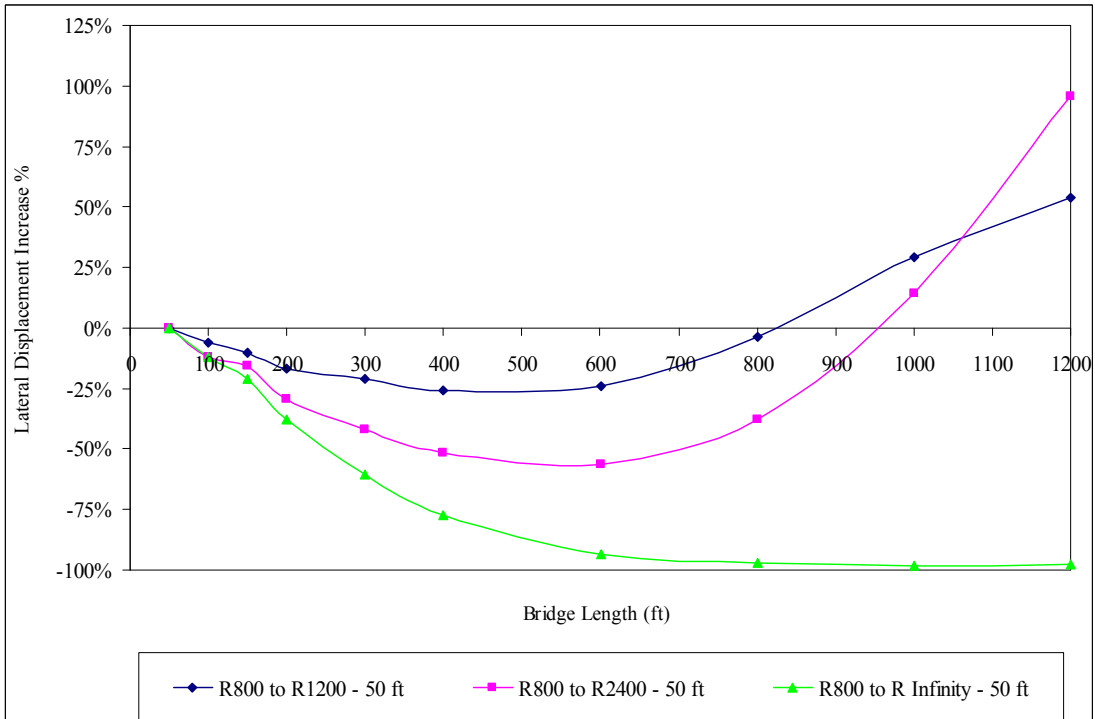


b)  $\Delta T_{\text{slab}} = 120^\circ \text{ F}$ ,  $\Delta T_{\text{the rest}} = 90^\circ \text{ F}$

**Figure 8.35 – Lateral Displacement Increase (%) of Bridges with 50 ft Spans and End-Bearing Piles in 9 ft Deep Predrilled Holes due to Change in Radius from 600 ft to a Larger Radius**

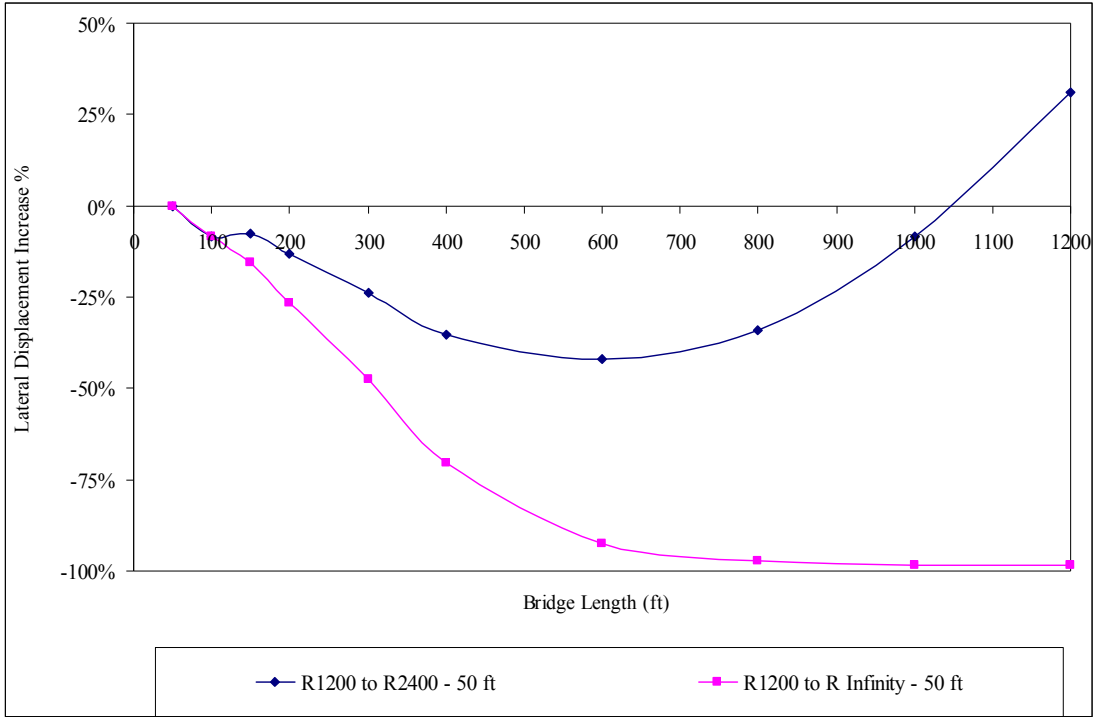


a)  $\Delta T_{\text{slab}} = 90^\circ \text{F}, \Delta T_{\text{the rest}} = 60^\circ \text{F}$

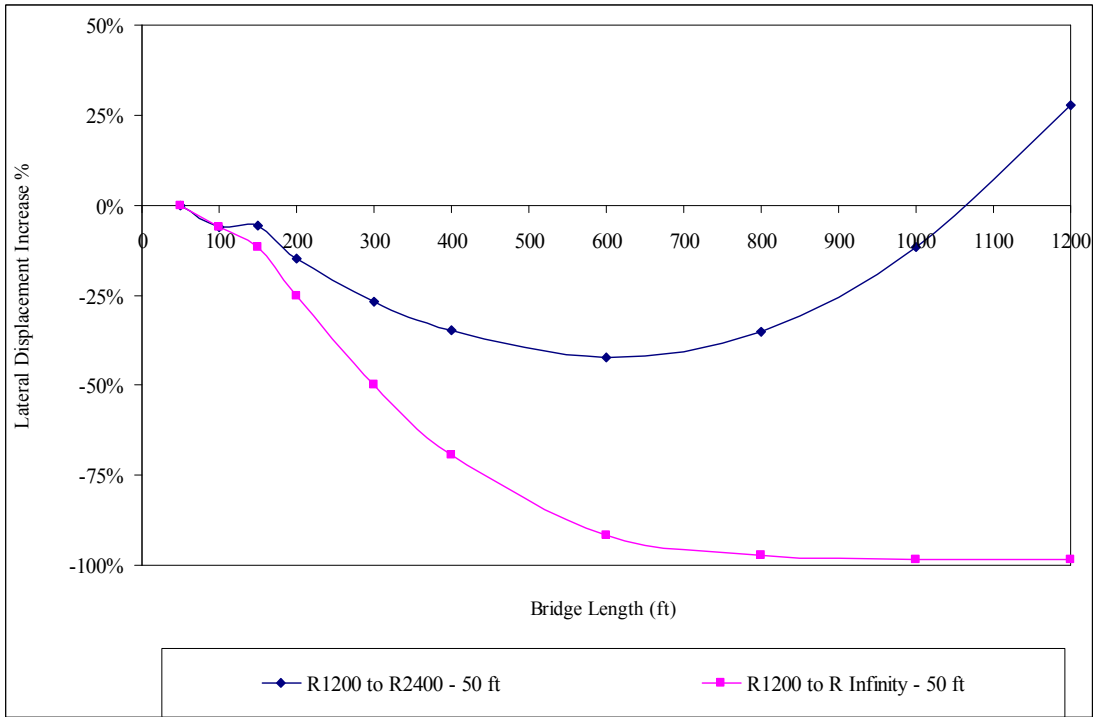


b)  $\Delta T_{\text{slab}} = 120^\circ \text{F}, \Delta T_{\text{the rest}} = 90^\circ \text{F}$

**Figure 8.36 – Lateral Displacement Increase (%) of Bridges with 50 ft Spans and End-Bearing Piles in 9 ft Deep Predrilled Holes due to Change in Radius from 800 ft to a Larger Radius**

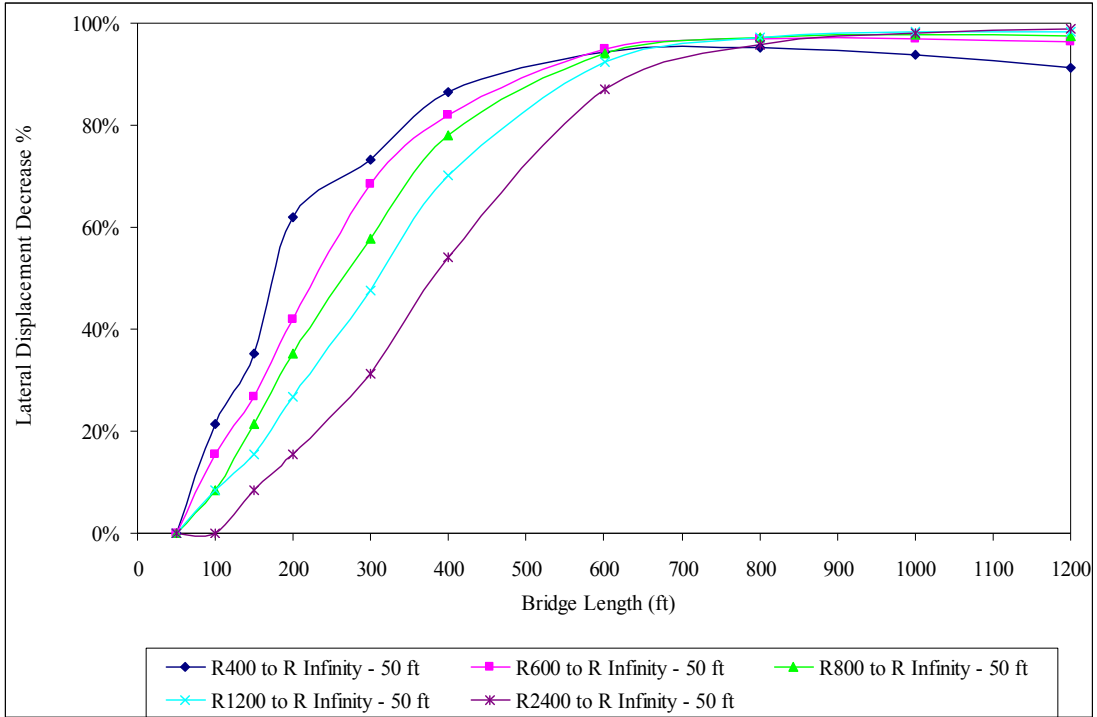


a)  $\Delta T_{\text{slab}} = 90^\circ \text{ F}$ ,  $\Delta T_{\text{the rest}} = 60^\circ \text{ F}$

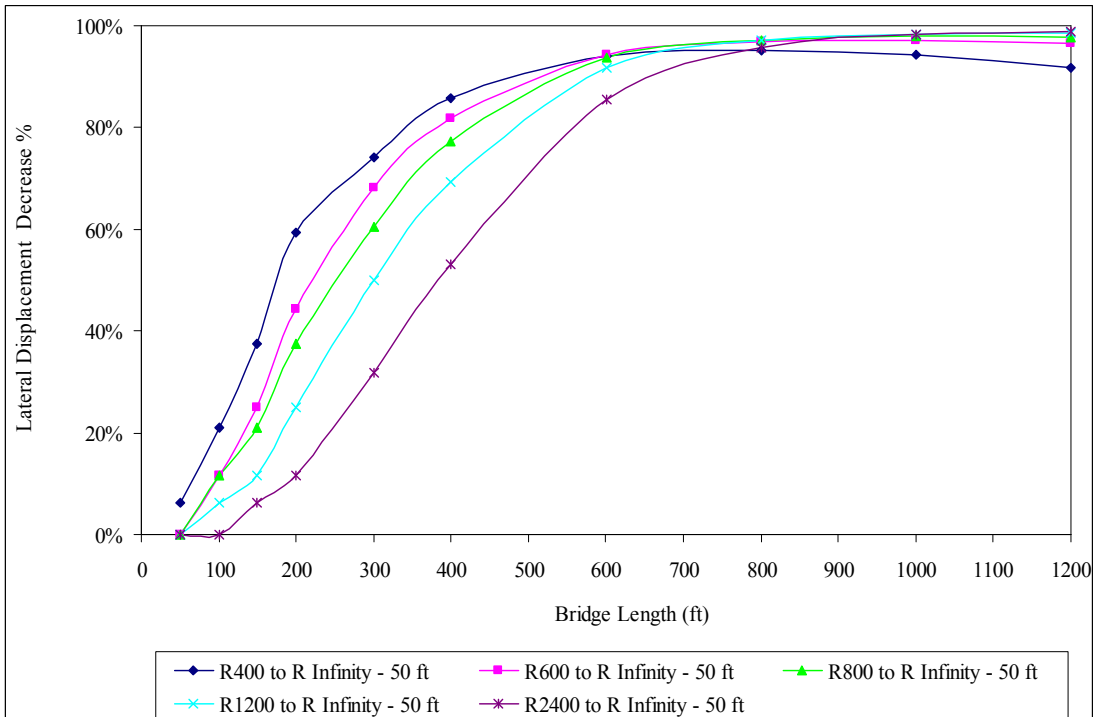


b)  $\Delta T_{\text{slab}} = 120^\circ \text{ F}$ ,  $\Delta T_{\text{the rest}} = 90^\circ \text{ F}$

**Figure 8.37 – Lateral Displacement Increase (%) of Bridges with 50 ft Spans and End-Bearing Piles in 9 ft Deep Predrilled Holes due to Change in Radius from 1200 ft to a Larger Radius**

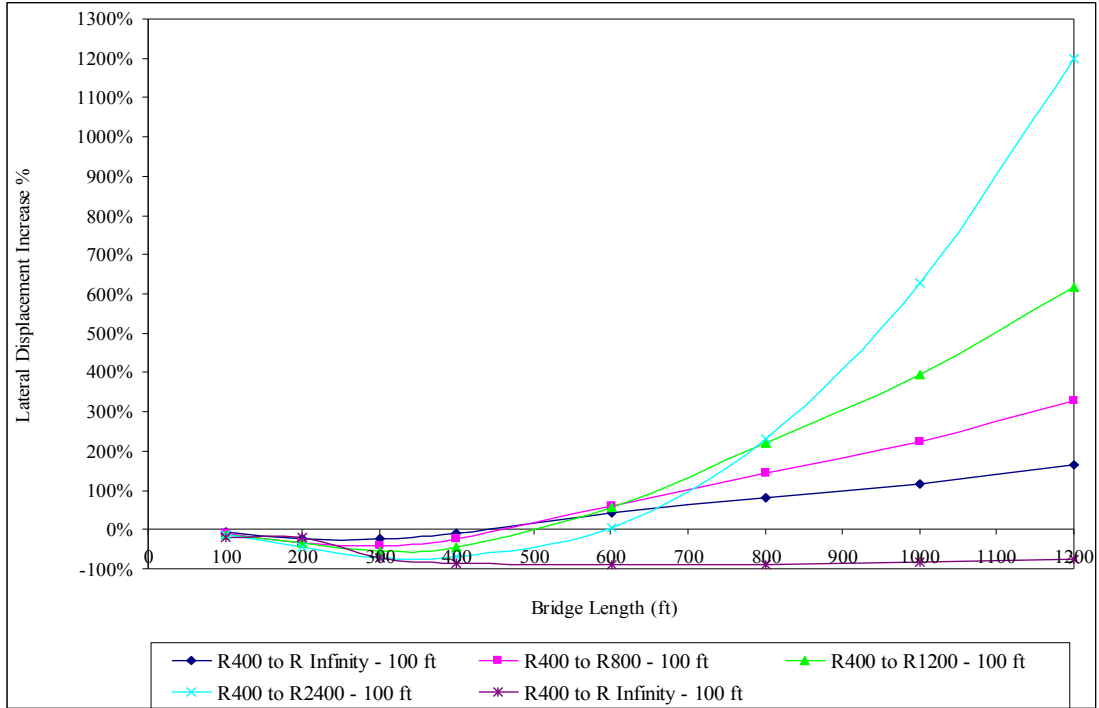


a)  $\Delta T_{\text{slab}} = 90^\circ \text{F}$ ,  $\Delta T_{\text{the rest}} = 60^\circ \text{F}$

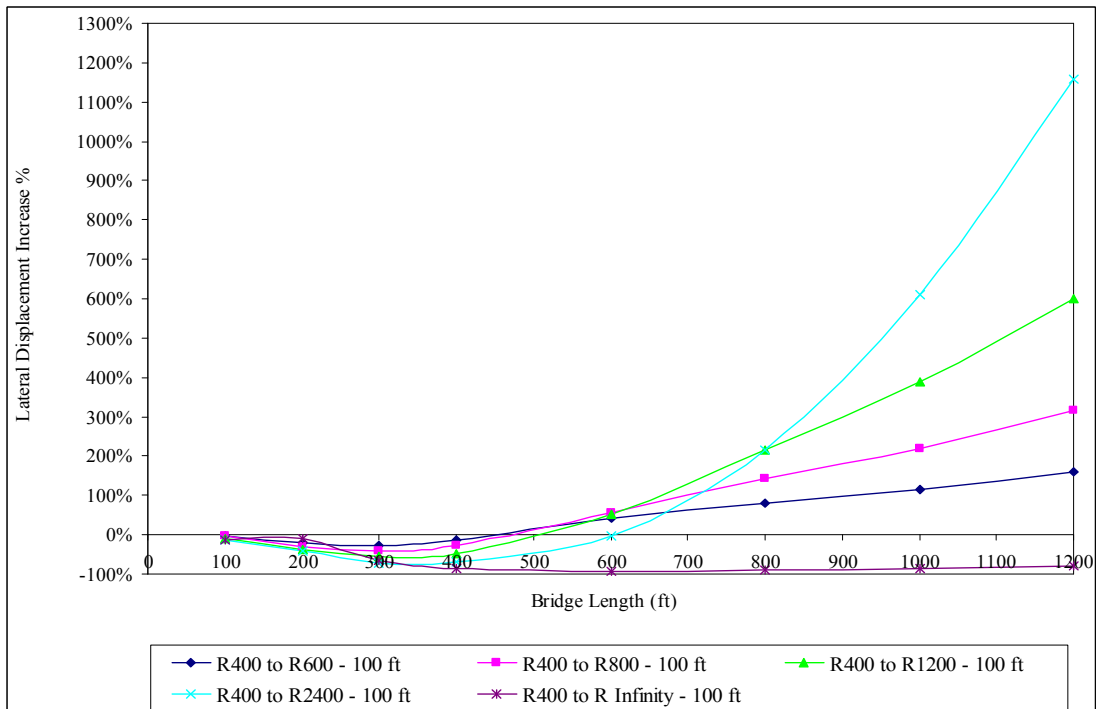


b)  $\Delta T_{\text{slab}} = 120^\circ \text{F}$ ,  $\Delta T_{\text{the rest}} = 90^\circ \text{F}$

**Figure 8.38 – Lateral Displacement Decrease (%) of Bridges with 50 ft Spans and End-Bearing Piles in 9 ft Deep Predrilled Holes due to Change in Radius from Different Values to Infinity**



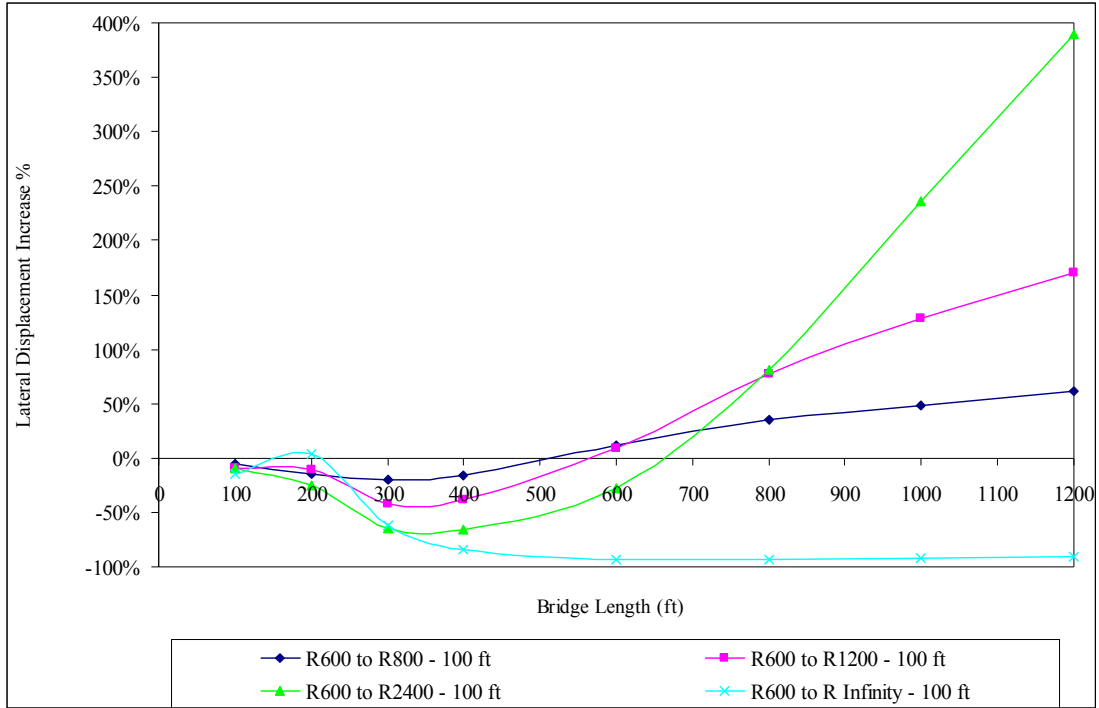
a)  $\Delta T_{\text{slab}} = 90^\circ \text{ F}, \Delta T_{\text{the rest}} = 60^\circ \text{ F}$



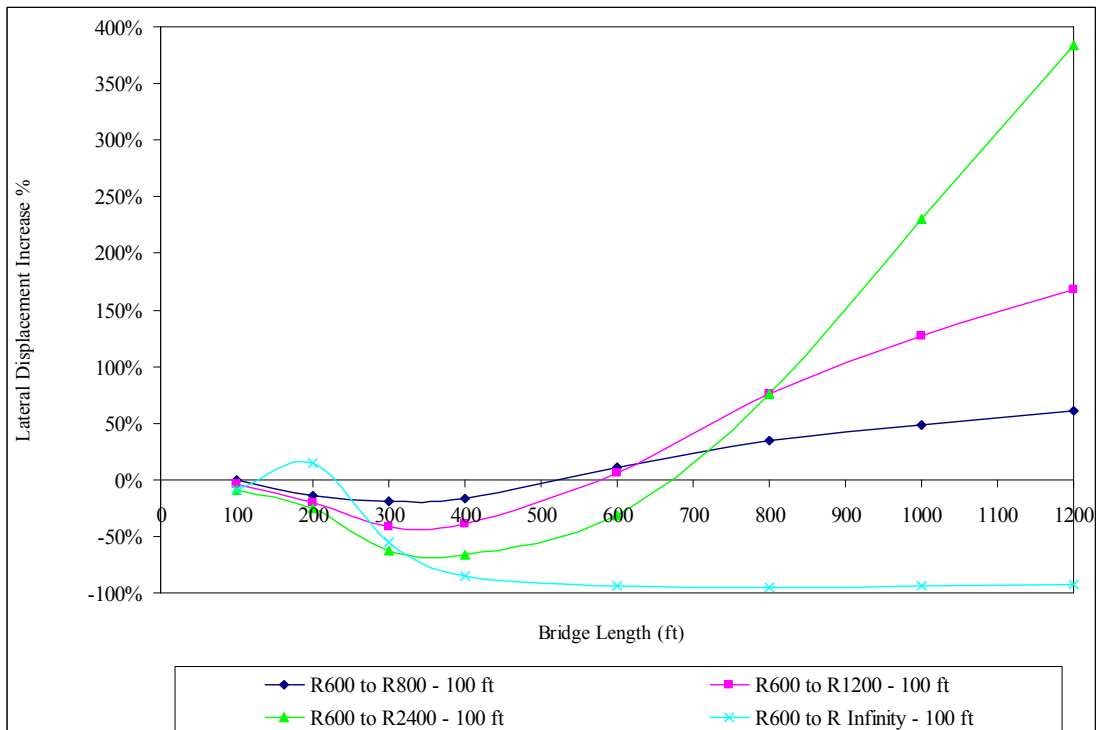
b)  $\Delta T_{\text{slab}} = 120^\circ \text{ F}, \Delta T_{\text{the rest}} = 90^\circ \text{ F}$

**Figure 8.39 – Lateral Displacement Increase (%) of Bridges with 100 ft Spans and End-Bearing Piles in Very Stiff Clay Soil Profile due to Change in Radius from 400 ft to a Larger Radius**



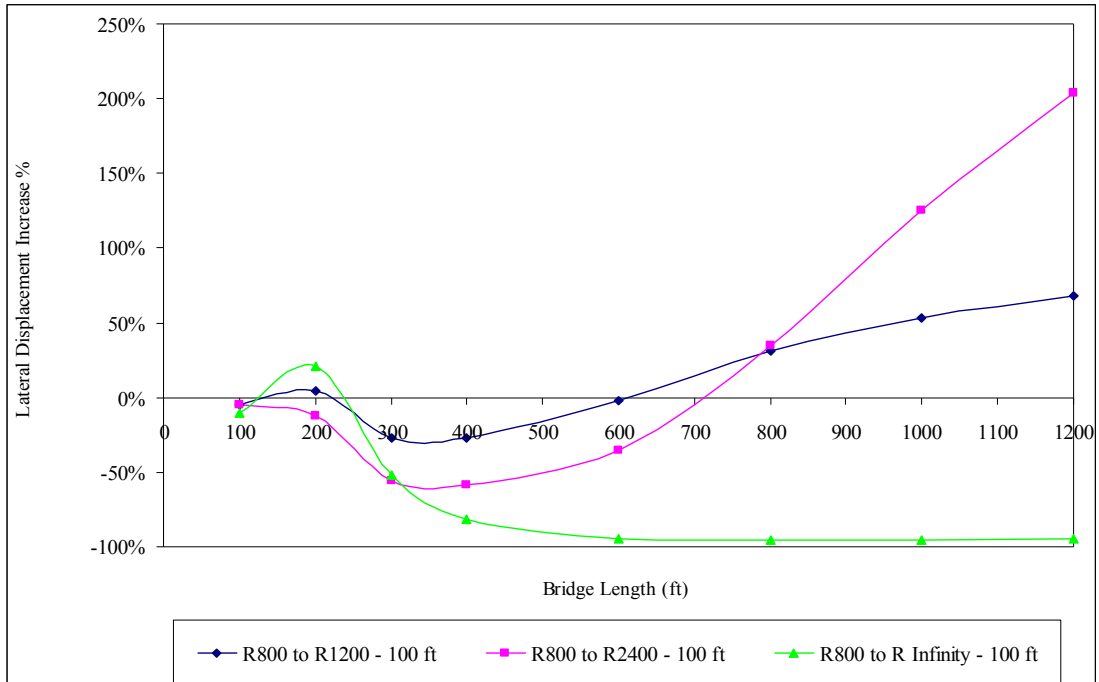


a)  $\Delta T_{\text{slab}} = 90^\circ \text{ F}$ ,  $\Delta T_{\text{the rest}} = 60^\circ \text{ F}$

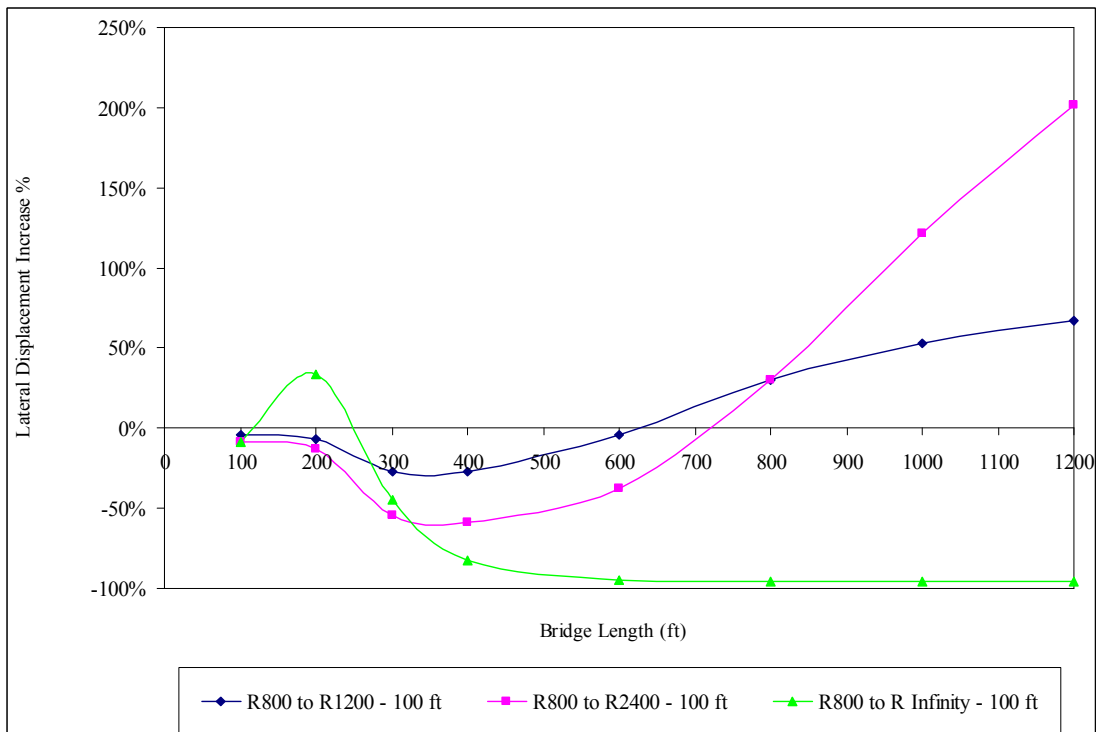


b)  $\Delta T_{\text{slab}} = 120^\circ \text{ F}$ ,  $\Delta T_{\text{the rest}} = 90^\circ \text{ F}$

**Figure 8.40 – Lateral Displacement Increase (%) of Bridges with 100 ft Spans and End-Bearing Piles in Very Stiff Clay Soil Profile due to Change in Radius from 600 ft to a Larger Radius**

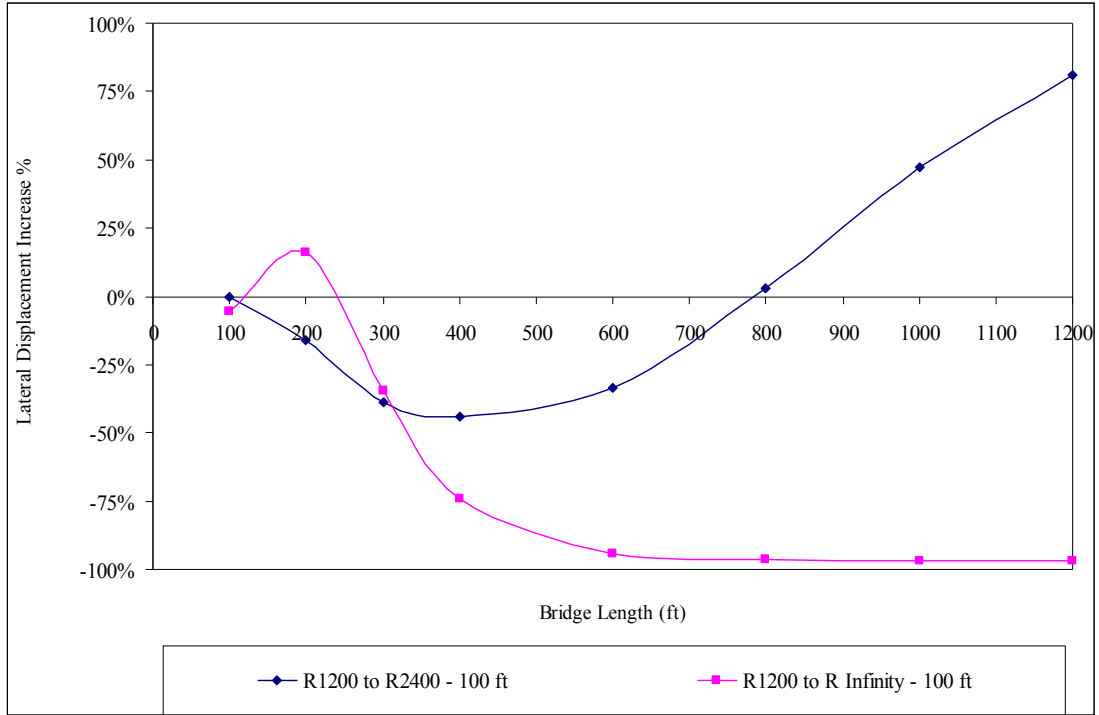


a)  $\Delta T_{\text{slab}} = 90^\circ \text{F}$ ,  $\Delta T_{\text{the rest}} = 60^\circ \text{F}$

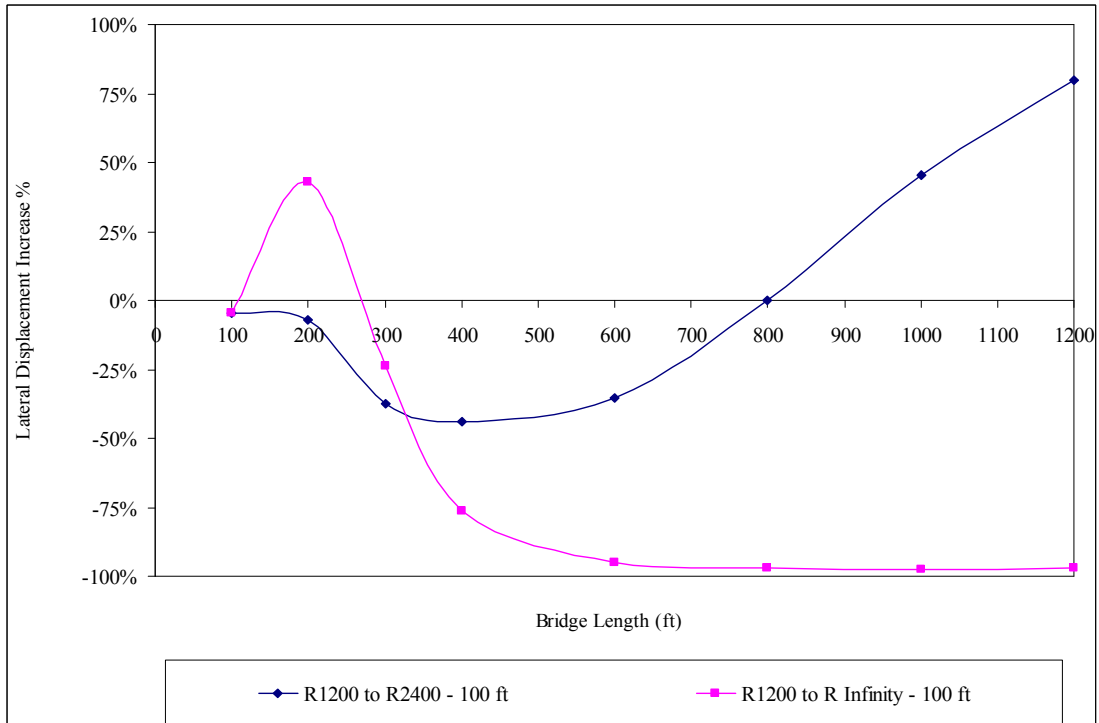


b)  $\Delta T_{\text{slab}} = 120^\circ \text{F}$ ,  $\Delta T_{\text{the rest}} = 90^\circ \text{F}$

**Figure 8.41 – Lateral Displacement Increase (%) of Bridges with 100 ft Spans and End-Bearing Piles in Very Stiff Clay Soil Profile due to Change in Radius from 800 ft to a Larger Radius**

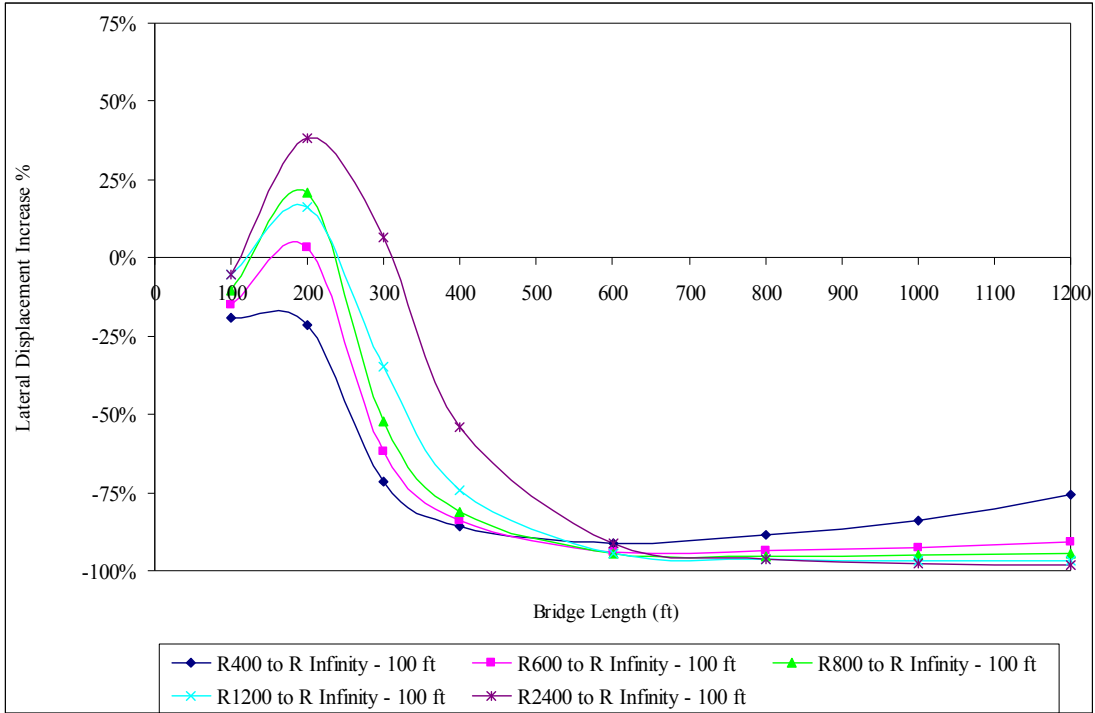


a)  $\Delta T_{\text{slab}} = 90^\circ \text{ F}, \Delta T_{\text{the rest}} = 60^\circ \text{ F}$

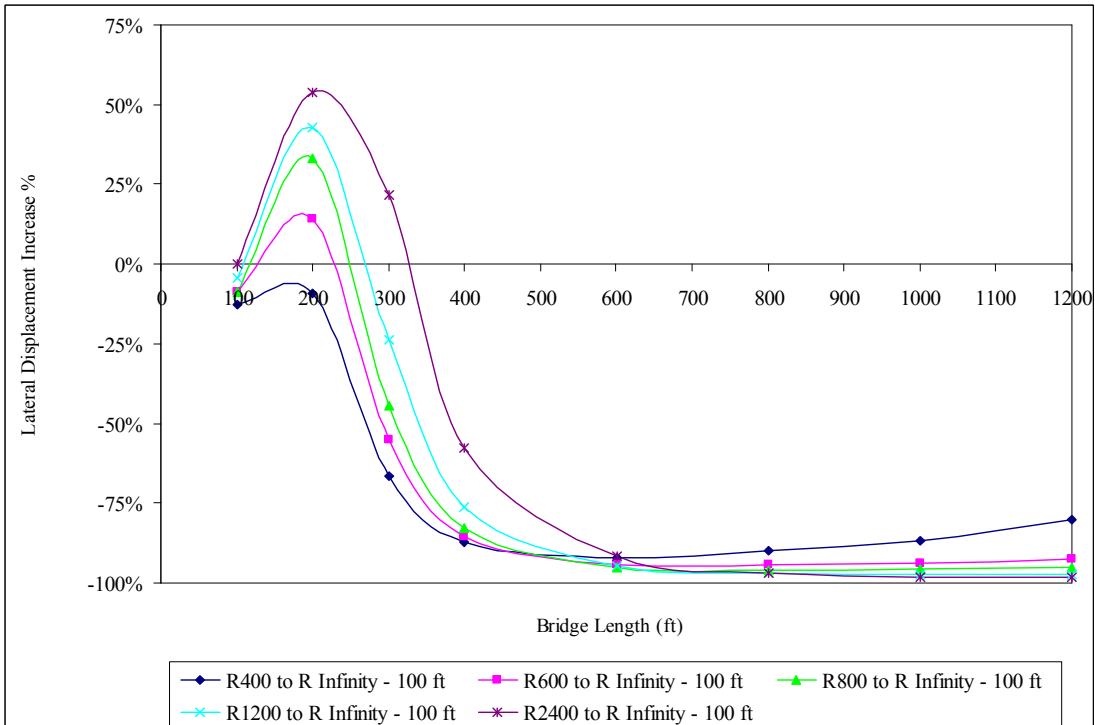


b)  $\Delta T_{\text{slab}} = 120^\circ \text{ F}, \Delta T_{\text{the rest}} = 90^\circ \text{ F}$

**Figure 8.42 – Lateral Displacement Increase (%) of Bridges with 100 ft Spans and End-Bearing Piles in Very Stiff Clay Soil Profile due to Change in Radius from 1200 ft to a Larger Radius**

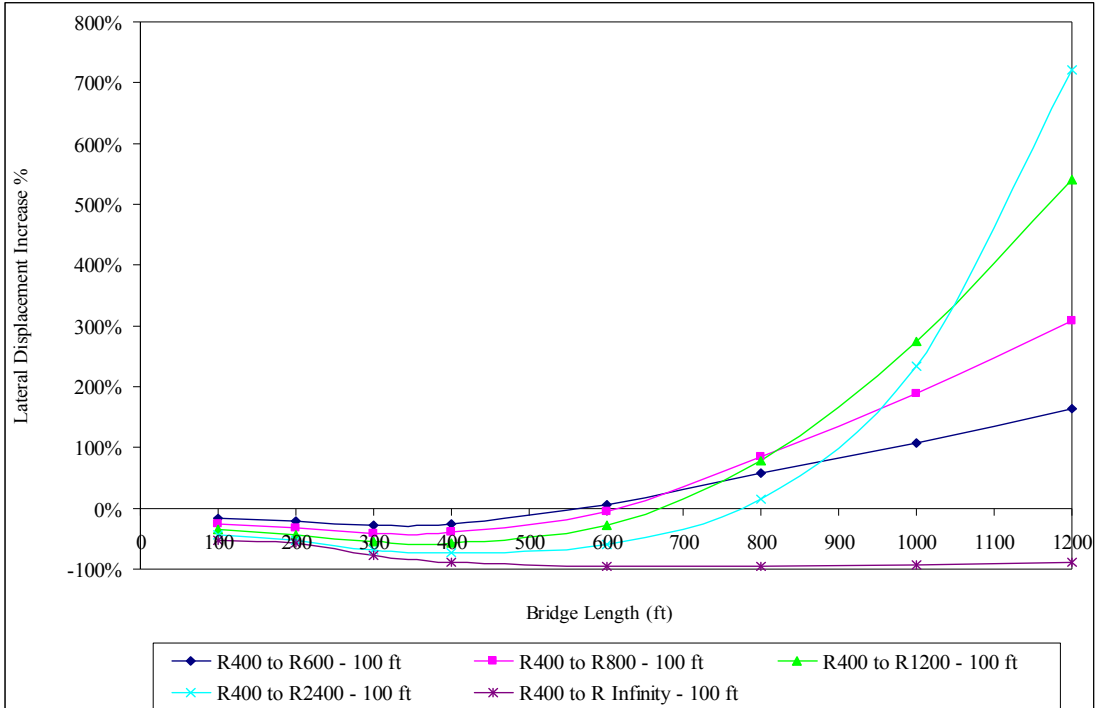


a)  $\Delta T_{\text{slab}} = 90^\circ \text{F}$ ,  $\Delta T_{\text{the rest}} = 60^\circ \text{F}$

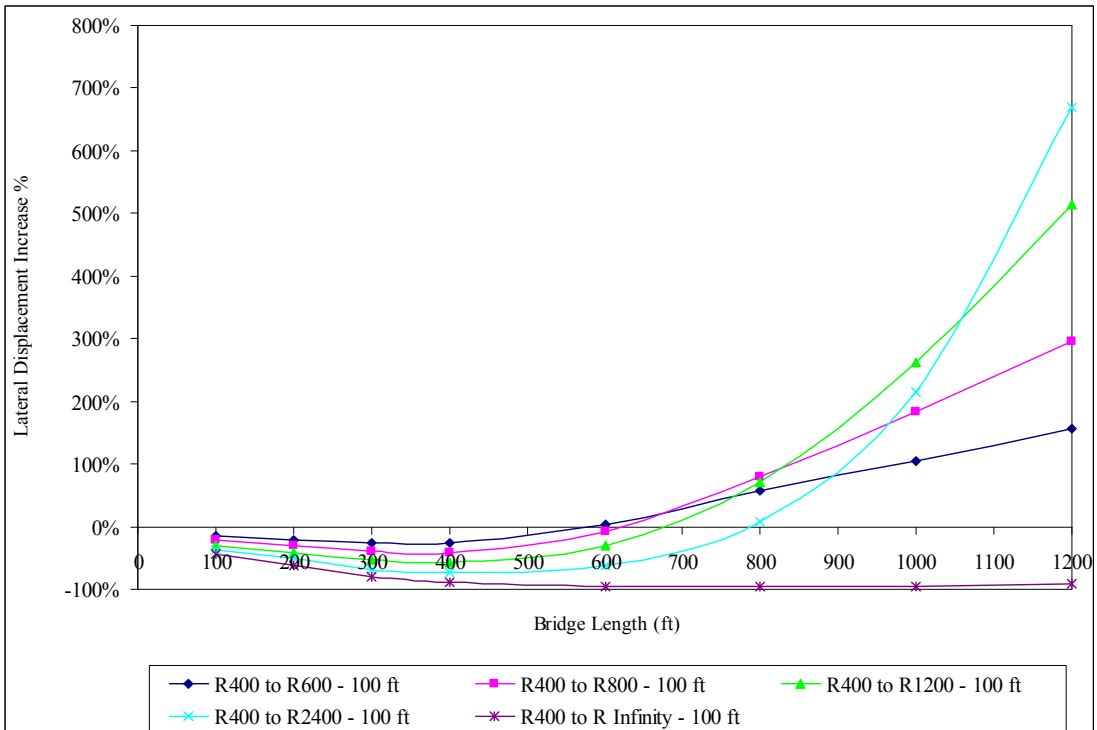


b)  $\Delta T_{\text{slab}} = 120^\circ \text{F}$ ,  $\Delta T_{\text{the rest}} = 90^\circ \text{F}$

**Figure 8.43 – Lateral Displacement Increase (%) of Bridges with 100 ft Spans and End-Bearing Piles in Very Stiff Clay Soil Profile due to Change in Radius from Different Values to Infinity**

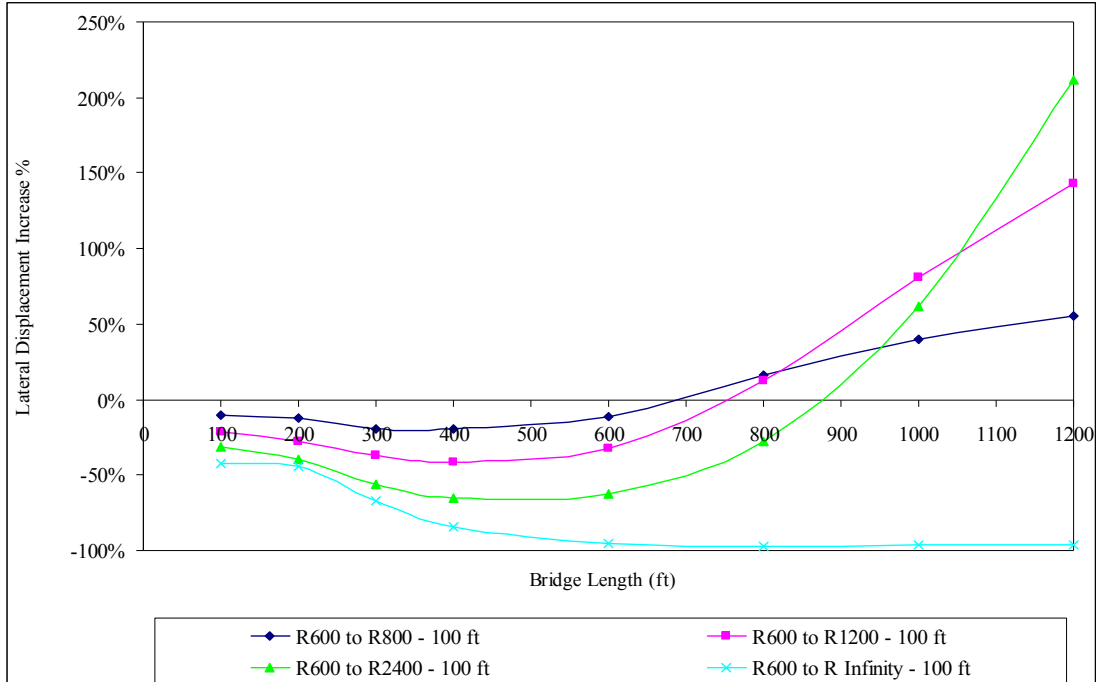


a)  $\Delta T_{\text{slab}} = 90^\circ \text{F}$ ,  $\Delta T_{\text{the rest}} = 60^\circ \text{F}$

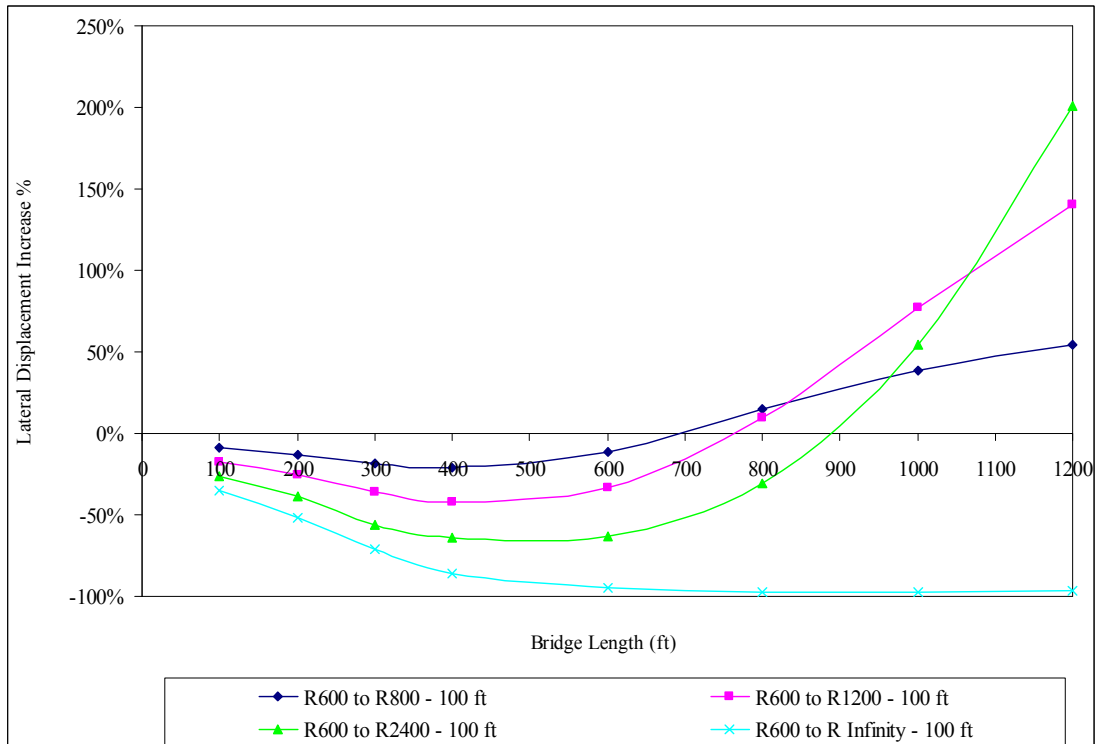


b)  $\Delta T_{\text{slab}} = 120^\circ \text{F}$ ,  $\Delta T_{\text{the rest}} = 90^\circ \text{F}$

**Figure 8.44 – Lateral Displacement Increase (%) of Bridges with 100 ft Spans and End-Bearing Piles in 9 ft Deep Predrilled Holes due to Change in Radius from 400 ft to a Larger Radius**

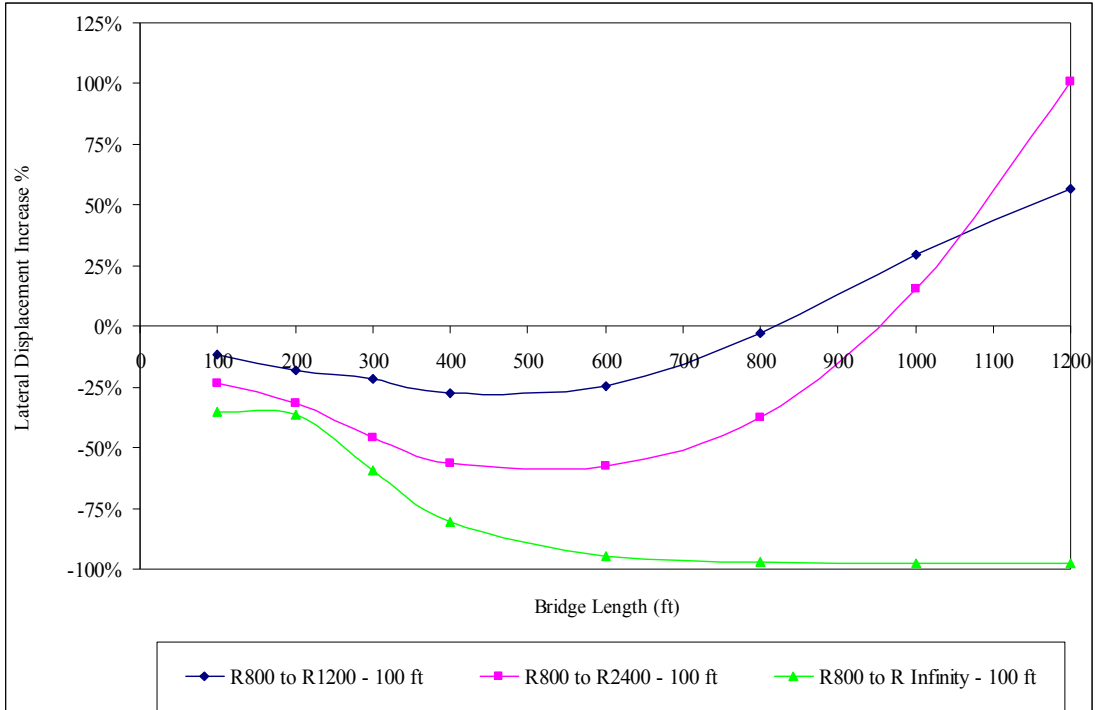


a)  $\Delta T_{slab} = 90^\circ F$ ,  $\Delta T_{the rest} = 60^\circ F$

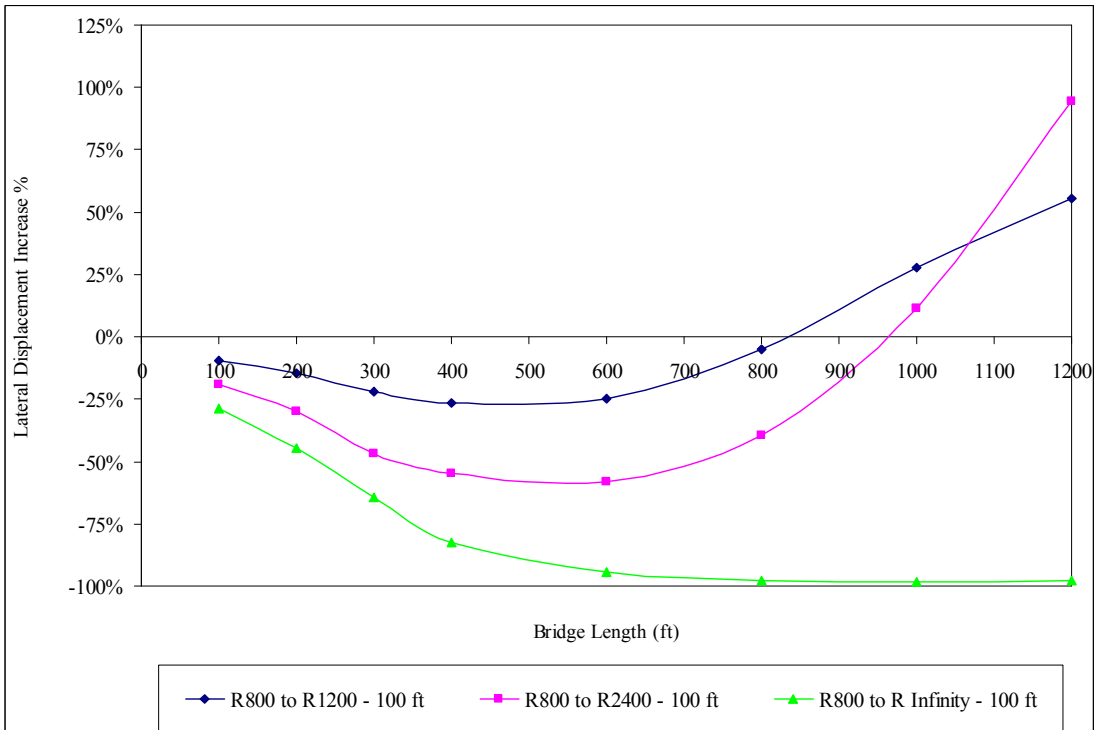


b)  $\Delta T_{slab} = 120^\circ F$ ,  $\Delta T_{the rest} = 90^\circ F$

**Figure 8.45 – Lateral Displacement Increase (%) of Bridges with 100 ft Spans and End-Bearing Piles in 9 ft Deep Predrilled Holes due to Change in Radius from 600 ft to a Larger Radius**

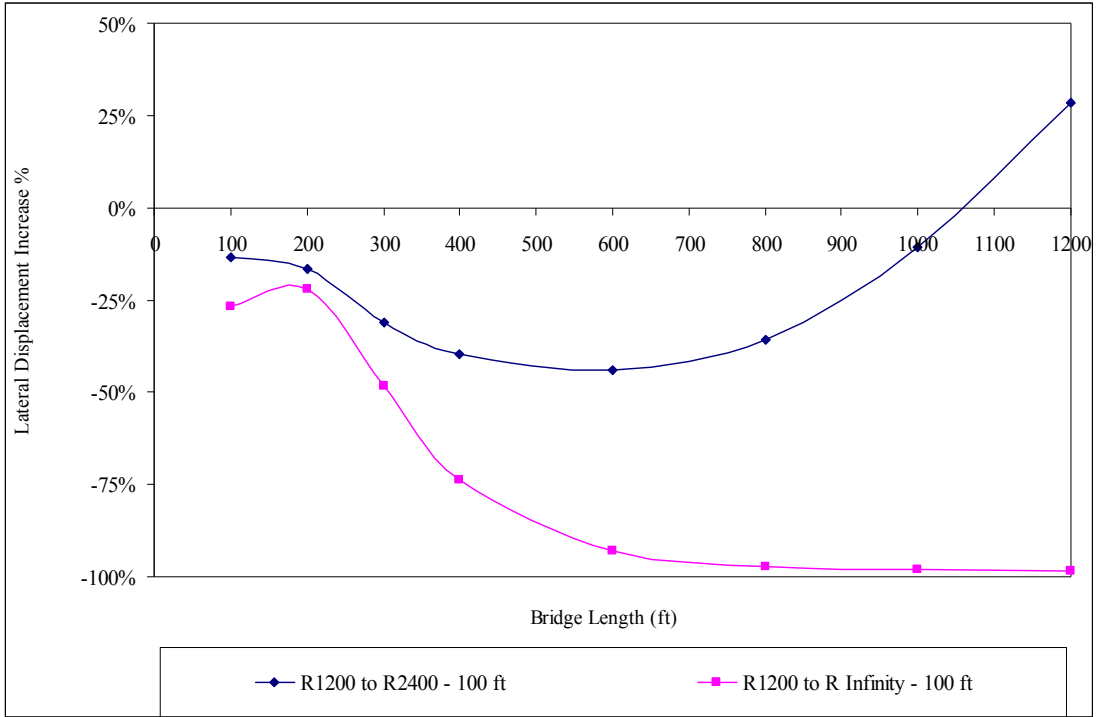


a)  $\Delta T_{\text{slab}} = 90^\circ \text{ F}$ ,  $\Delta T_{\text{the rest}} = 60^\circ \text{ F}$

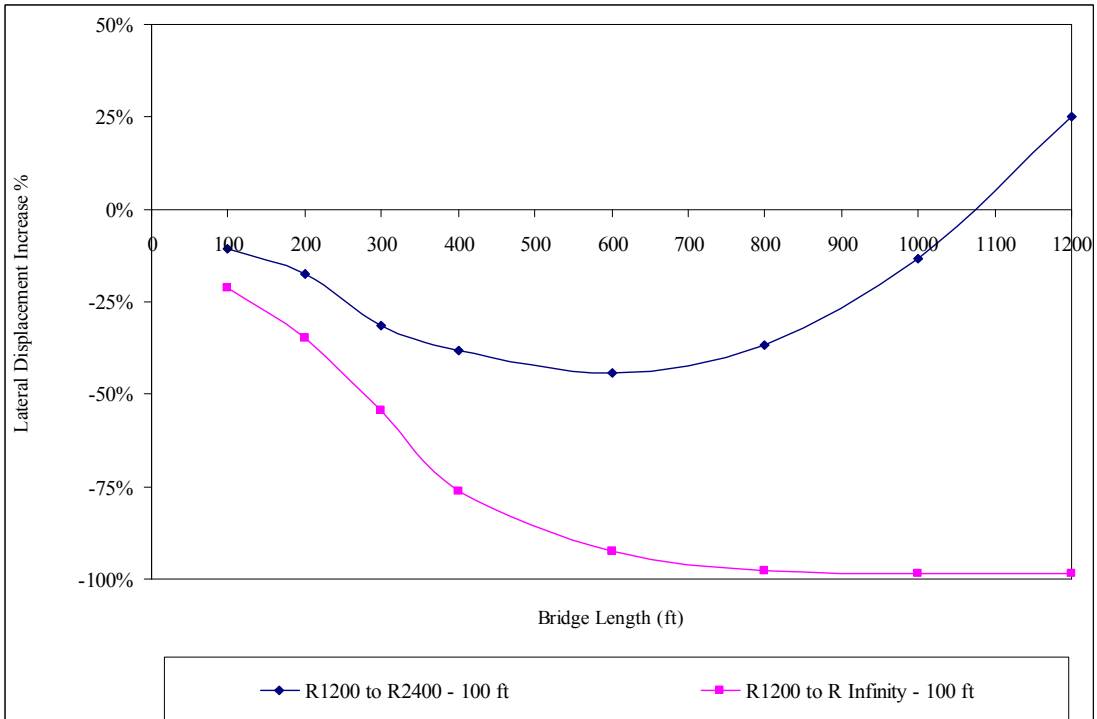


b)  $\Delta T_{\text{slab}} = 120^\circ \text{ F}$ ,  $\Delta T_{\text{the rest}} = 90^\circ \text{ F}$

**Figure 8.46 – Lateral Displacement Increase (%) of Bridges with 100 ft Spans and End-Bearing Piles in 9 ft Deep Predrilled Holes due to Change in Radius from 800 ft to a Larger Radius**



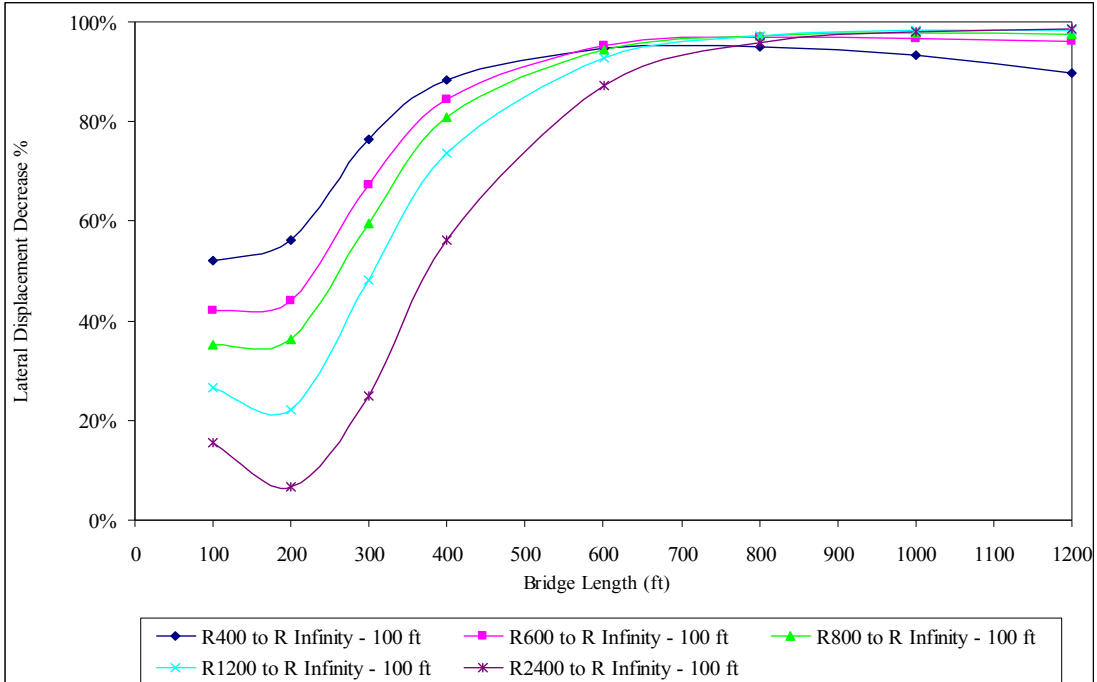
a)  $\Delta T_{\text{slab}} = 90^\circ \text{ F}$ ,  $\Delta T_{\text{the rest}} = 60^\circ \text{ F}$



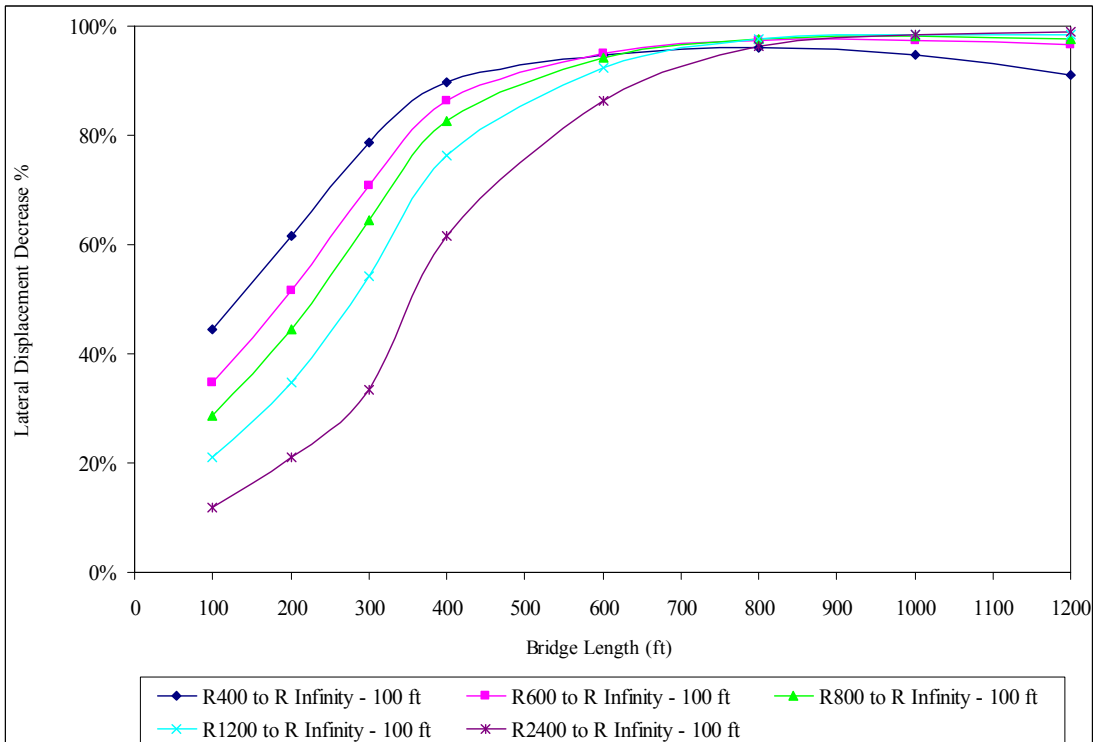
b)  $\Delta T_{\text{slab}} = 120^\circ \text{ F}$ ,  $\Delta T_{\text{the rest}} = 90^\circ \text{ F}$

**Figure 8.47 – Lateral Displacement Increase (%) of Bridges with 100 ft Spans and End-Bearing Piles in 9 ft Deep Predrilled Holes due to Change in Radius from 1200 ft to a Larger Radius**





a)  $\Delta T_{\text{slab}} = 90^\circ \text{ F}$ ,  $\Delta T_{\text{the rest}} = 60^\circ \text{ F}$



b)  $\Delta T_{\text{slab}} = 120^\circ \text{ F}$ ,  $\Delta T_{\text{the rest}} = 90^\circ \text{ F}$

**Figure 8.48 – Lateral Displacement Decrease (%) of Bridges with 100 ft Spans and End-Bearing Piles in 9 ft Deep Predrilled Holes due to Change in Radius from Different Values to Infinity**

## 8.6 Effect of Pile Type

The difference in the maximum lateral displacement of curved IAB's between friction and end-bearing piles is discussed in this section. Table 8.34 indicates that the maximum lateral displacement of curved IAB's with friction piles is greater than that of curved IAB's with end-bearing piles by 0.03 inch to 0.65 inch for curved IAB's with 50 ft spans. It is greater by 0.02 inch to 0.83 inch for curved IAB's with 100 ft spans. Therefore, the difference in the maximum lateral displacement of curved IAB's between friction and end-bearing piles is relatively small.

**Table 8.34 – Difference in Maximum Lateral Displacement (inch) of Curved Integral Abutment Bridges between Friction and End-Bearing Piles**

Span Length (ft)	Radius (ft)	$\Delta T_{\text{slab}} = 90^\circ \text{ F}$ $\Delta T_{\text{the rest}} = 60^\circ \text{ F}$				$\Delta T_{\text{slab}} = 120^\circ \text{ F}$ $\Delta T_{\text{the rest}} = 90^\circ \text{ F}$			
		Depth of Predrilled Holes (ft)							
		0	5	9	15	0	5	9	15
50	400	0.13	0.10	0.11	0.16	0.03	0.04	0.10	0.14
	600	0.21	0.31	0.08	0.11	0.29	0.08	0.06	0.17
	800	0.18	0.65	0.33	0.27	0.17	0.08	0.19	0.26
	1200	0.34	0.38	0.31	0.24	0.08	0.38	0.31	0.22
	2400	0.24	0.35	0.46	0.48	0.22	0.34	0.41	0.41
	Infinity	0.12	0.19	0.12	0.12	0.12	0.18	0.09	0.09
100	400	0.02	0.02	0.07	0.07	0.02	0.02	0.03	0.03
	600	0.12	0.03	0.08	0.13	0.04	0.06	0.03	0.11
	800	0.12	0.65	0.15	0.11	0.06	0.04	0.10	0.10
	1200	0.31	0.11	0.13	0.12	0.08	0.06	0.15	0.14
	2400	0.21	0.24	0.23	0.22	0.20	0.22	0.21	0.21
	Infinity	0.24	0.39	0.63	0.83	0.08	0.70	0.82	0.70

## CHAPTER 9

### PILES IN CURVED INTEGRAL ABUTMENT BRIDGES

The behavior of end-bearing piles in various soil profile types of curved integral abutment bridges (curved IAB's) with 800 ft radius and 800 ft length at  $\Delta T_{\text{slab}}$  of 120° F and  $\Delta T_{\text{the rest}}$  of 90° F is investigated in this chapter.

#### 9.1 Stress in Piles

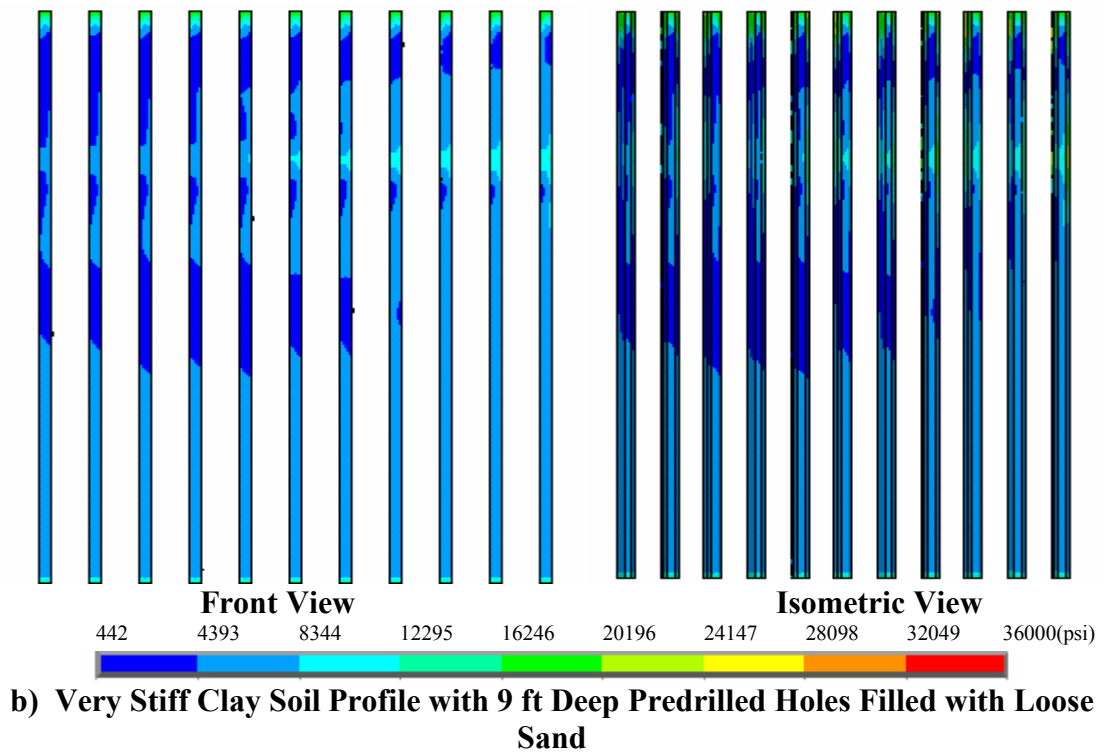
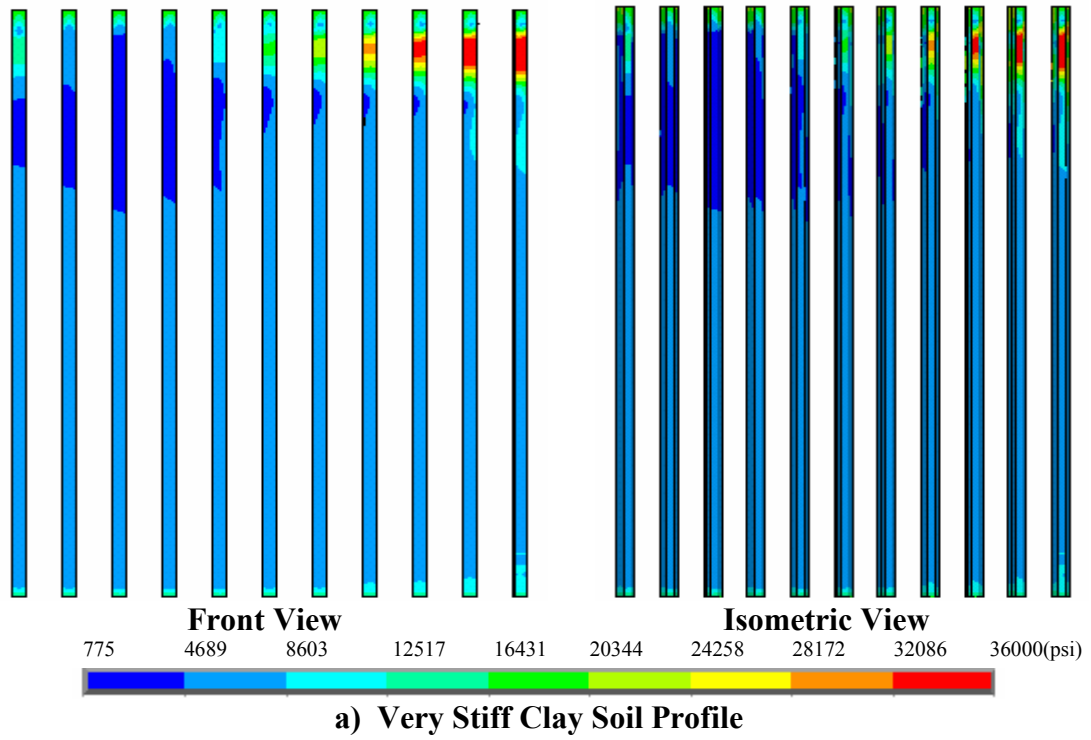
##### 9.1.1 Location of Partially Plastic Hinges

Steel used in this study consists of grade 36 steel with a minimum yield stress of 36 ksi. The von Mises or equivalent stress is used in this study. Figure 9.1 shows the equivalent stress contour of the piles in very stiff clay soil profile and in very stiff clay soil profile with 9 ft deep predrilled holes filled with loose sand of curved IAB's with 800 ft radius and 800 ft length.

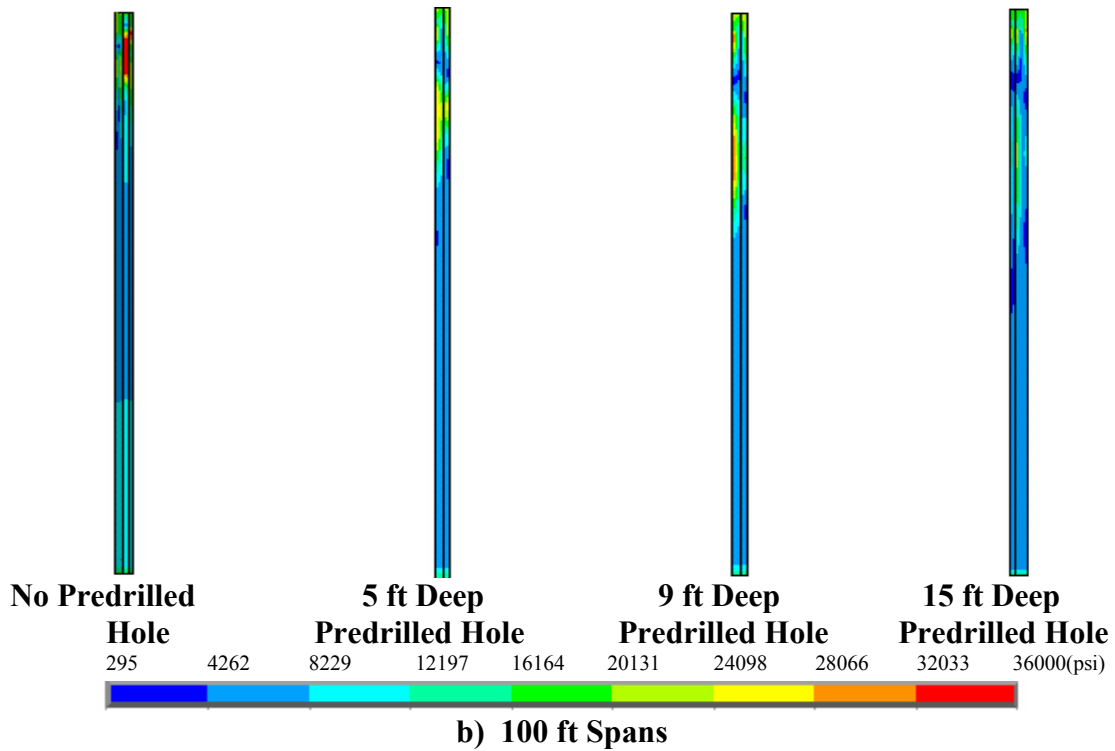
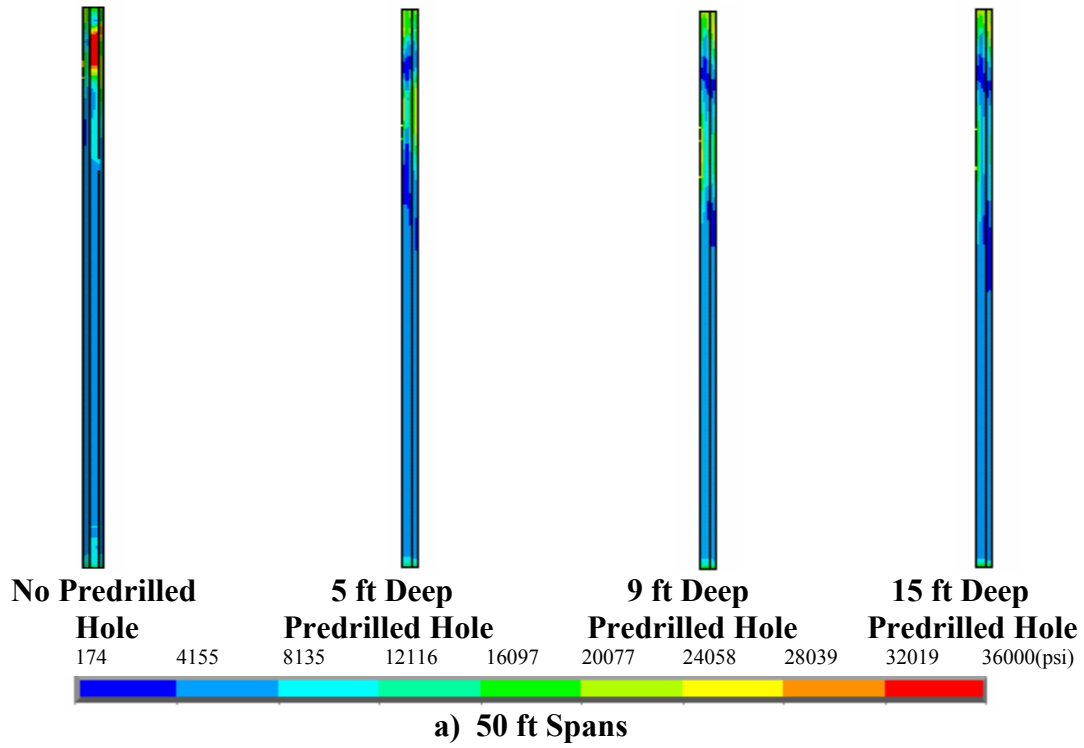
The von Mises or equivalent stress contour of the piles at the outermost radius, which is on the right hand side of the pile group, is shown in Figure 9.2. The equivalent stress in the piles in various soil profile types is plotted in Figures 9.3 to 9.5. Figure 9.5 indicates that the equivalent stress in the piles increases as the span length is increased. The introduction of predrilled holes can reduce the equivalent stress in the piles as discussed in Section 7.3.

Figure 9.6 shows the equivalent stress contour with deformed and undeformed shapes of the piles in various soil profile types with a deflection scale factor of 40.

The location of the partially plastic hinges is indicated in Table 9.1.



**Figure 9.1 – Equivalent Stress Contour in End-Bearing Piles of Bridges with 800 ft Radius and 800 ft Length ( $\Delta T_{\text{slab}} = 120^\circ \text{ F}$ ,  $\Delta T_{\text{the rest}} = 90^\circ \text{ F}$ )**



**Figure 9.2 – Equivalent Stress Contour in End-Bearing Piles in Various Soil Profile Types of Bridges with 800 ft Radius and 800 ft Length ( $\Delta T_{\text{slab}} = 120^\circ \text{ F}$ ,  $\Delta T_{\text{the rest}} = 90^\circ \text{ F}$ )**

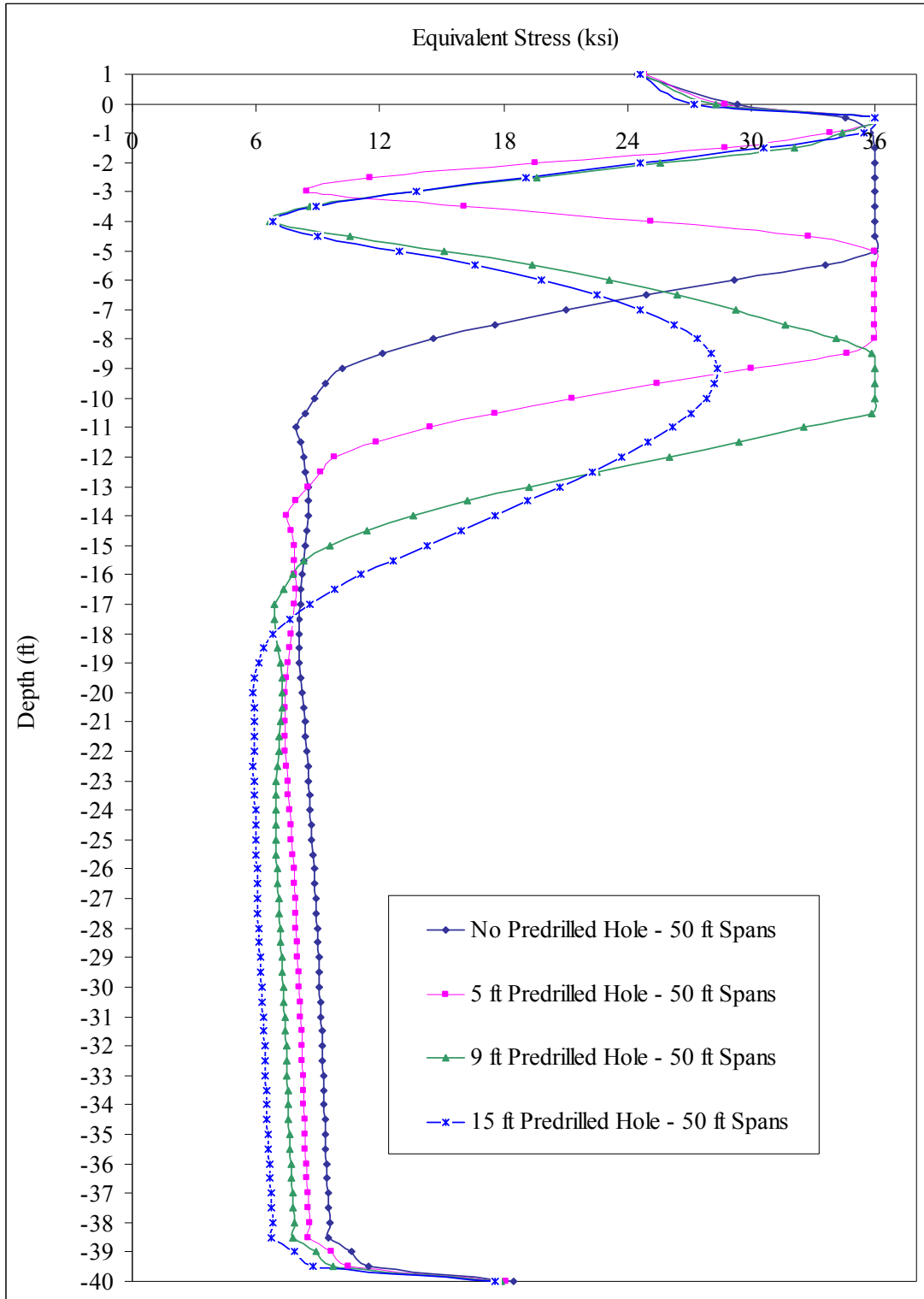


**Figure 9.3 – Equivalent Stress and Location of Partially Plastic Hinges in End-Bearing Piles in Various Soil Profile Types of a Bridge with 800 ft Radius and 16 - 50 ft Spans ( $\Delta T_{\text{slab}} = 120^\circ \text{ F}$ ,  $\Delta T_{\text{the rest}} = 90^\circ \text{ F}$ )**

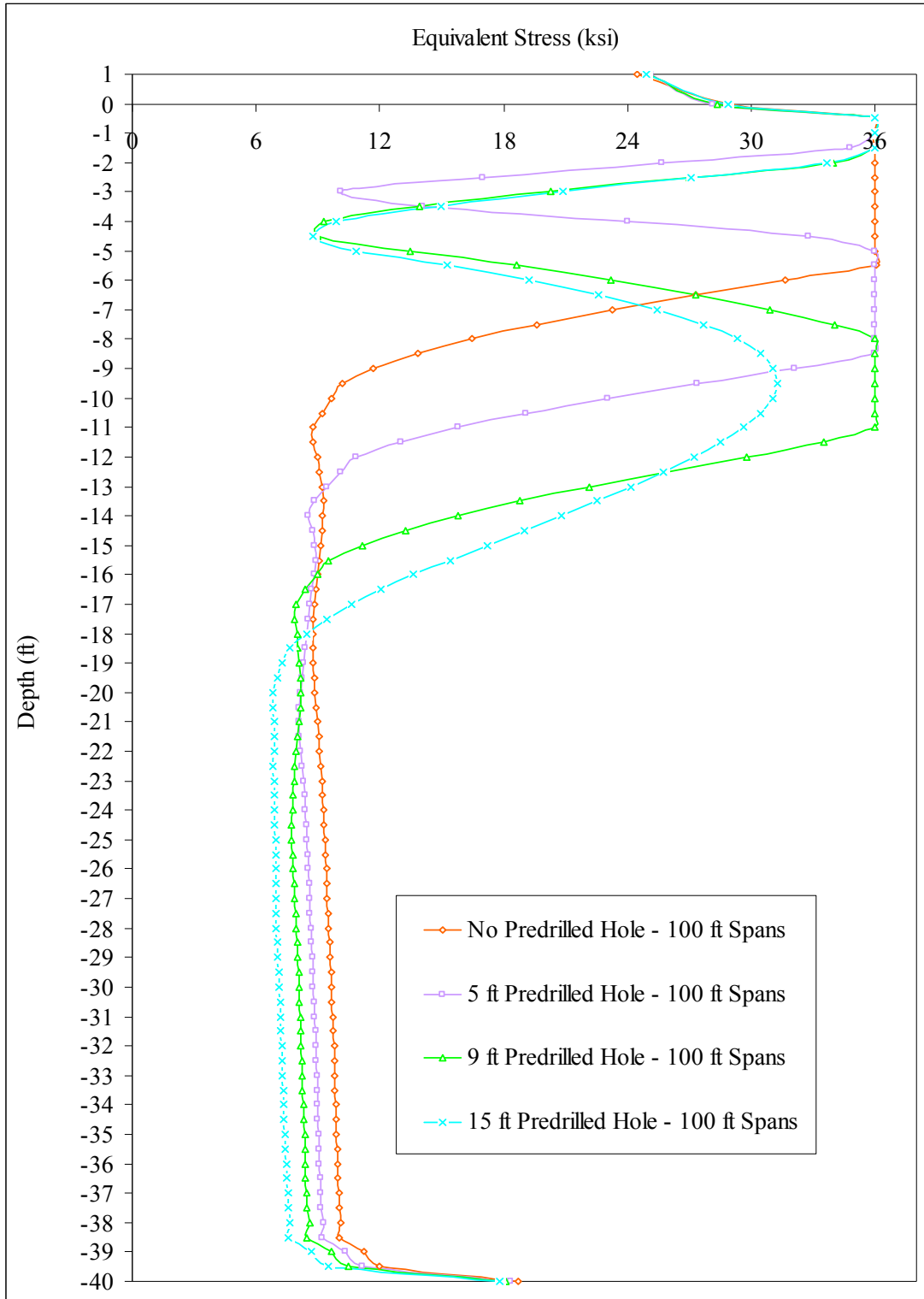


**Figure 9.4 – Equivalent Stress and Location of Partially Plastic Hinges in End-Bearing Piles in Various Soil Profile Types of a Bridge with 800 ft Radius and 8 - 100 ft Spans ( $\Delta T_{\text{slab}} = 120^\circ \text{ F}$ ,  $\Delta T_{\text{the rest}} = 90^\circ \text{ F}$ )**

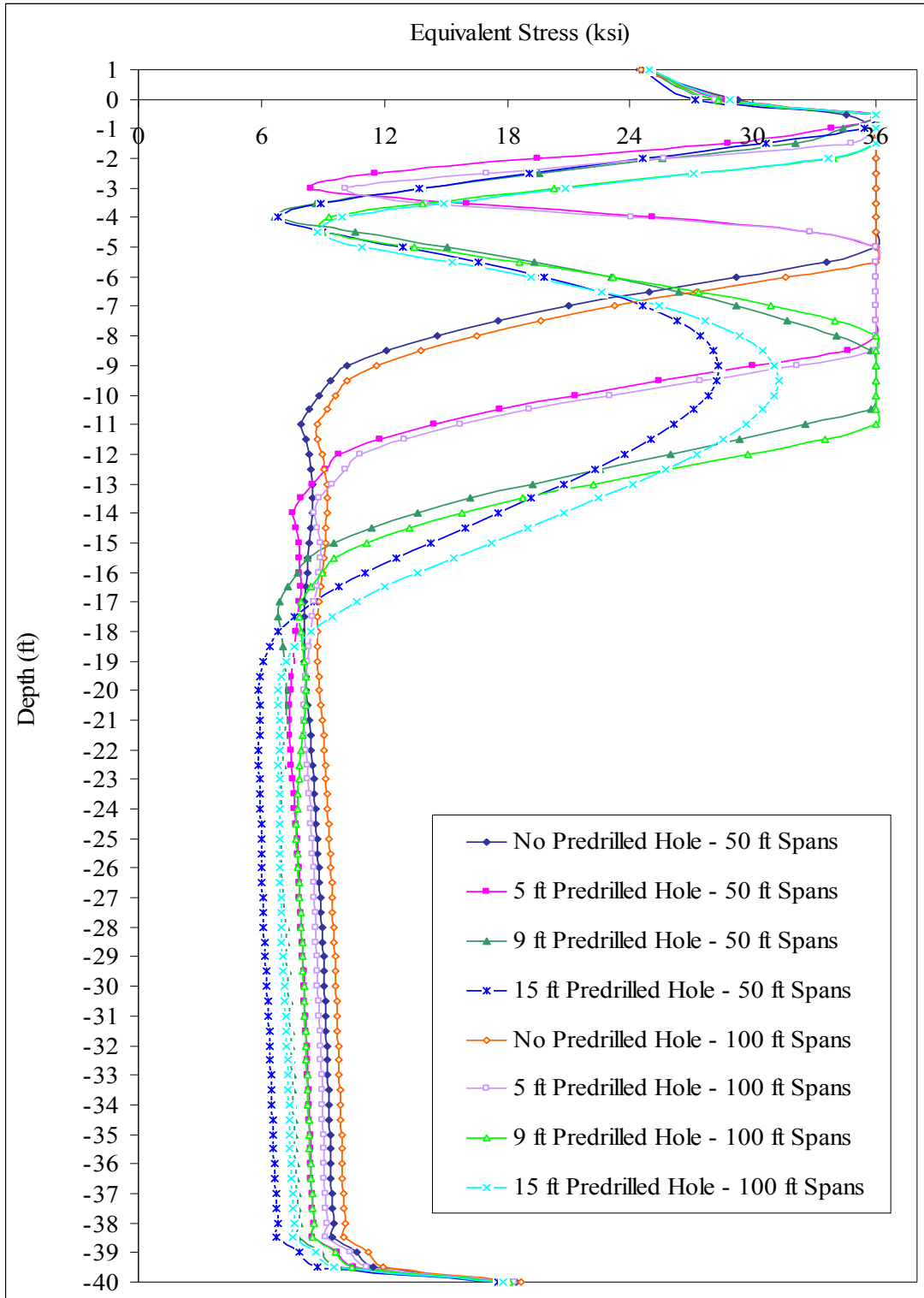


**Figure 9.5 – Comparison of Equivalent Stress and Location of Partially Plastic Hinges in End-Bearing Piles in Various Soil Profile Types between Bridges with 50 ft and 100 ft Spans with 800 ft Radius and 800 ft Length**  
 $(\Delta T_{\text{slab}} = 120^\circ \text{ F}, \Delta T_{\text{the rest}} = 90^\circ \text{ F})$



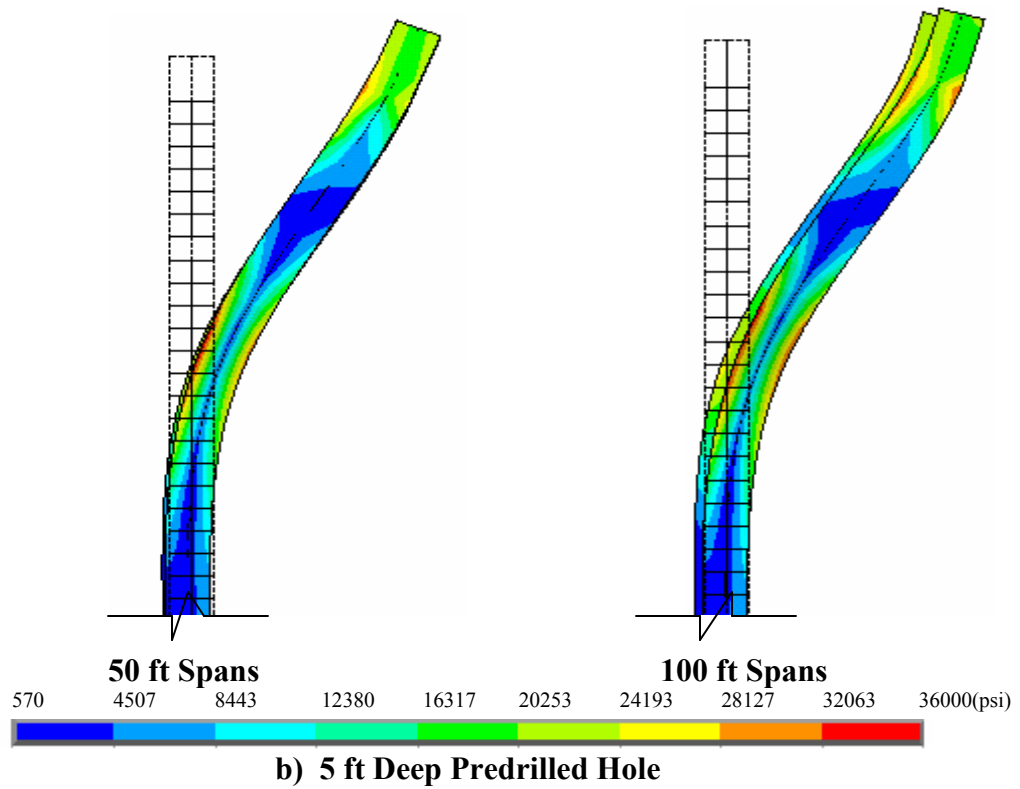
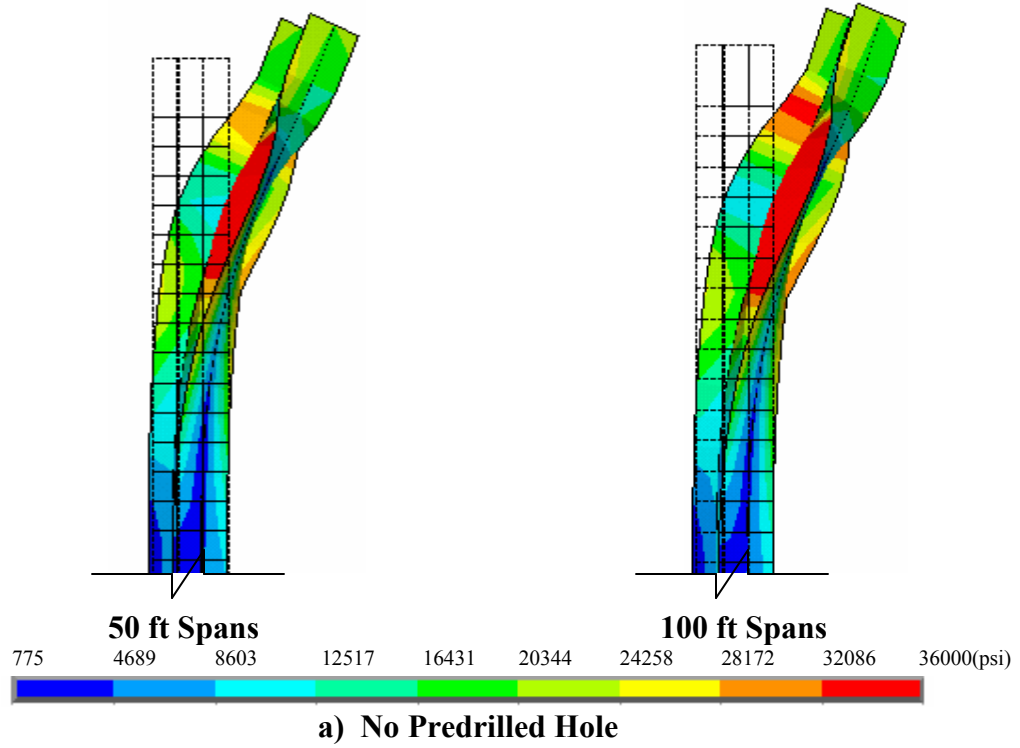


**Figure 9.6 – Equivalent Stress Contour with Deformed and Undeformed Shapes of End-Bearing Piles in Various Soil Profile Types of Bridges with 800 ft Radius and 800 ft Length ( $\Delta T_{\text{slab}} = 120^\circ \text{ F}$ ,  $\Delta T_{\text{the rest}} = 90^\circ \text{ F}$ )**

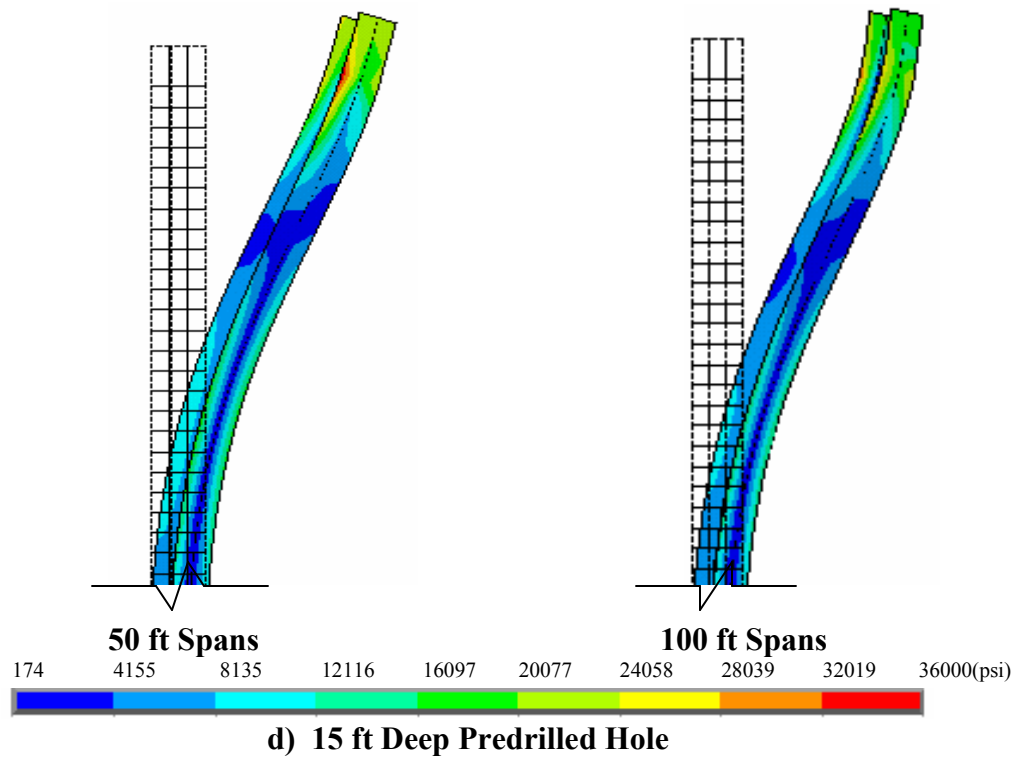
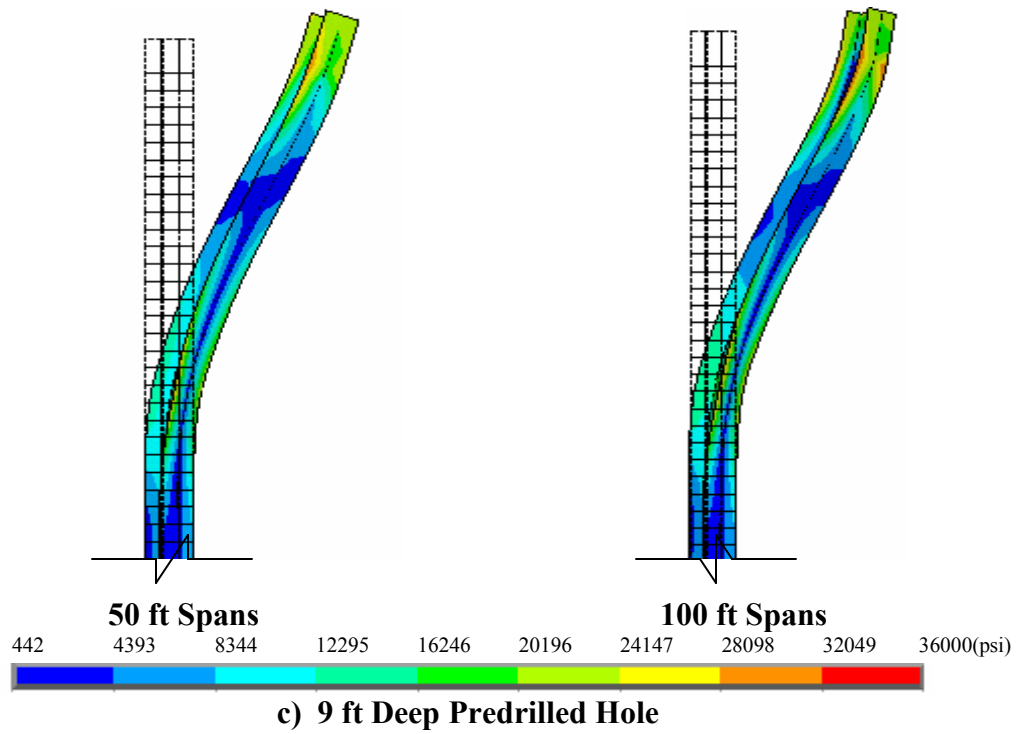


**Figure 9.6 (Continued) – Equivalent Stress Contour with Deformed and Undeformed Shapes of End-Bearing Piles in Various Soil Profile Types of Bridges with 800 ft Radius and 800 ft Length ( $\Delta T_{\text{slab}} = 120^\circ \text{ F}$ ,  $\Delta T_{\text{the rest}} = 90^\circ \text{ F}$ )**

**Table 9.1 – Location of Partially Plastic Hinges in End-Bearing Piles in Various Soil Profile Types of Bridges with 800 ft Radius and 800 ft Length**  
 ( $\Delta T_{\text{slab}} = 120^\circ \text{ F}$ ,  $\Delta T_{\text{the rest}} = 90^\circ \text{ F}$ )

Span Length (ft)	Depth Below the Bottom of the Abutment (ft)			
	Depth of Predrilled Holes (ft)			
	0	5	9	15
50	1 – 5	0.5	0.5	0.5
		5 – 8	8.5 – 10.5	
100	0.5 – 5.5	0.5 – 1	0.5 – 1.5	0.5 – 1.5
		5 – 8.5	8 – 11	

Table 9.1 indicates that the location of the partially plastic hinges in the piles for piles in 5 ft and 9 ft deep predrilled holes filled with loose sand is at two places. The first location is at 0.5 ft below the bottom of the abutment. The second location is at the connection between the loose sand layer and the very stiff clay layer.

For piles in very stiff clay soil profile and piles in 15 ft deep predrilled holes filled with loose sand, the location of the partially plastic hinges in the piles is at one place which starts at 0.5 ft to 1 ft below the bottom of the abutment. The partially plastic region in the piles for curved IAB's with 100 ft spans is slightly longer compared to the partially plastic region for curved IAB's with 50 ft spans.

Table 9.2 indicates that as the span length decreases from 100 ft to 50 ft, the von Mises or equivalent stress reduction in the piles without predrilled holes is relatively small. It continues to increase as the depth of the predrilled holes is increased. The difference in the pile stress reduction between piles in 9 ft deep predrilled holes and piles in 15 ft deep predrilled holes is 2.5% as the span length decreases. This confirms that the depth increase of predrilled holes deeper than 9 ft has a relatively small increase in pile stress reduction.

**Table 9.2 – Stress Reduction (%) of End-Bearing Piles in Various Soil Profile Types of Bridges with 800 ft Radius and 800 ft Length due to the Increase in the Number of Spans ( $\Delta T_{\text{slab}} = 120^\circ \text{ F}$ ,  $\Delta T_{\text{the rest}} = 90^\circ \text{ F}$ )**

Depth of Predrilled Holes (ft)			
0	5	9	15
0 to 12.8	0 to 32.3	0 to 38	0 to 40.5

Figures 9.3 to 9.5 indicate that the equivalent stress in the piles in all soil profile types of curved IAB's with 50 ft and 100 ft spans has almost the same stress value, which is approximately 25 ksi, at the top of the piles which are embedded 1 ft deep into the abutment. The equivalent stress in the piles then continues to increase to reach a yield stress of 36 ksi and the partially plastic hinges occur in the piles as indicated in Table 9.1.

For piles in very stiff clay soil profile, after the equivalent stress in the piles reaches the yield stress of 36 ksi indicated in Table 9.1, it starts to decrease to a new equivalent stress level at a certain depth and almost constant as the depth of the piles continues to increase to 38.5 ft below the bottom of the abutment as indicated in Table 9.3.

For piles in varying depths of predrilled holes filled with loose sand, after the equivalent stress in the piles reaches the yield stress of 36 ksi indicated in Table 9.1, it starts to decrease at a certain depth and increases again at the connection between the loose sand layer and the very stiff clay layer. Below that depth, it starts to decrease to a new equivalent stress level at a certain depth and almost constant as the depth of the piles continues to increase to 38.5 ft below the bottom of the abutment as indicated in Table 9.3.

In all soil profile types, the equivalent stress in the piles from 38.5 ft to 39.5 ft depth below the bottom of the abutment increases by 20% to 30%. From 39.5 ft to 40 ft depth below the bottom of the abutment, the equivalent stress in the piles increases significantly by 56% to 100%.

The equivalent stress in the piles in all soil profile types of curved IAB's with both 50 ft and 100 ft spans is approximately 18 ksi at a 40 ft depth below the bottom of the abutment.

**Table 9.3 – Equivalent Stress in End-Bearing Piles in Various Soil Profile Types  
of Bridges with 800 ft Radius and 800 ft Length  
( $\Delta T_{\text{slab}} = 120^\circ \text{ F}$ ,  $\Delta T_{\text{the rest}} = 90^\circ \text{ F}$ )**

Span Length (ft)	Depth of Predrilled Holes (ft)	Depth Below the Bottom of the Abutment (ft)	Equivalent Stress in Piles (ksi)
50	0	-1	24.5
		1 – 5	36.0
		11 – 38.5	8.0 – 9.5
		40	18.5
	5	-1	24.8
		0.5	36.0
		3	8.4
		5 – 8	36.0
		14 – 38.5	7.5 – 8.5
		40	18.1
	9	-1	24.7
		0.5	36.0
		4	6.6
		8.5 – 10.5	36.0
		17 – 38.5	7.0 – 8.0
		40	17.9
	15	-1	24.7
		0.5	36.0
		4	6.8
		9	28.3
19.5 – 38.5		6.1 – 6.7	
40		17.6	

**Table 9.3 (Continued) – Equivalent Stress in End-Bearing Piles in Various Soil Profile Types of Bridges with 800 ft Radius and 800 ft Length**  
 ( $\Delta T_{\text{slab}} = 120^\circ \text{ F}$ ,  $\Delta T_{\text{the rest}} = 90^\circ \text{ F}$ )

Span Length (ft)	Depth of Predrilled Holes (ft)	Depth Below the Bottom of the Abutment (ft)	Equivalent Stress in Piles (ksi)
100	0	-1	24.5
		0.5 – 5.5	36.0
		11 – 38.5	8.8 – 10.0
		40	18.7
	5	-1	25.1
		0.5 – 1	36.0
		3	10.0
		5 – 8.5	36.0
		14 – 38.5	8.6 – 9.2
		40	18.4
	9	-1	25.0
		0.5 – 1.5	36.0
		4.5	9.0
		8 – 11	36.0
		17 – 38.5	8.0 – 8.5
		40	18.1
	15	-1	24.9
		0.5 – 1.5	36.0
		4.5	8.8
		9.5	31.2
		19.5 – 38.5	7.0 – 7.5
40		17.8	

### 9.1.2 Stress in Piles at Different Locations in the Abutment

The equivalent stress in end-bearing piles in very stiff clay soil profile with 9 ft deep predrilled holes filled with loose sand at different locations in the abutment of curved IAB's with 800 ft radius and 800 ft length is investigated in this section. The equivalent stress of pile No. 1 (pile at the outermost radius), No. 6 (pile in the middle), and No. 11 (pile at the innermost radius) shown in Figure 9.7 is plotted in Figures 9.8 to 9.10.

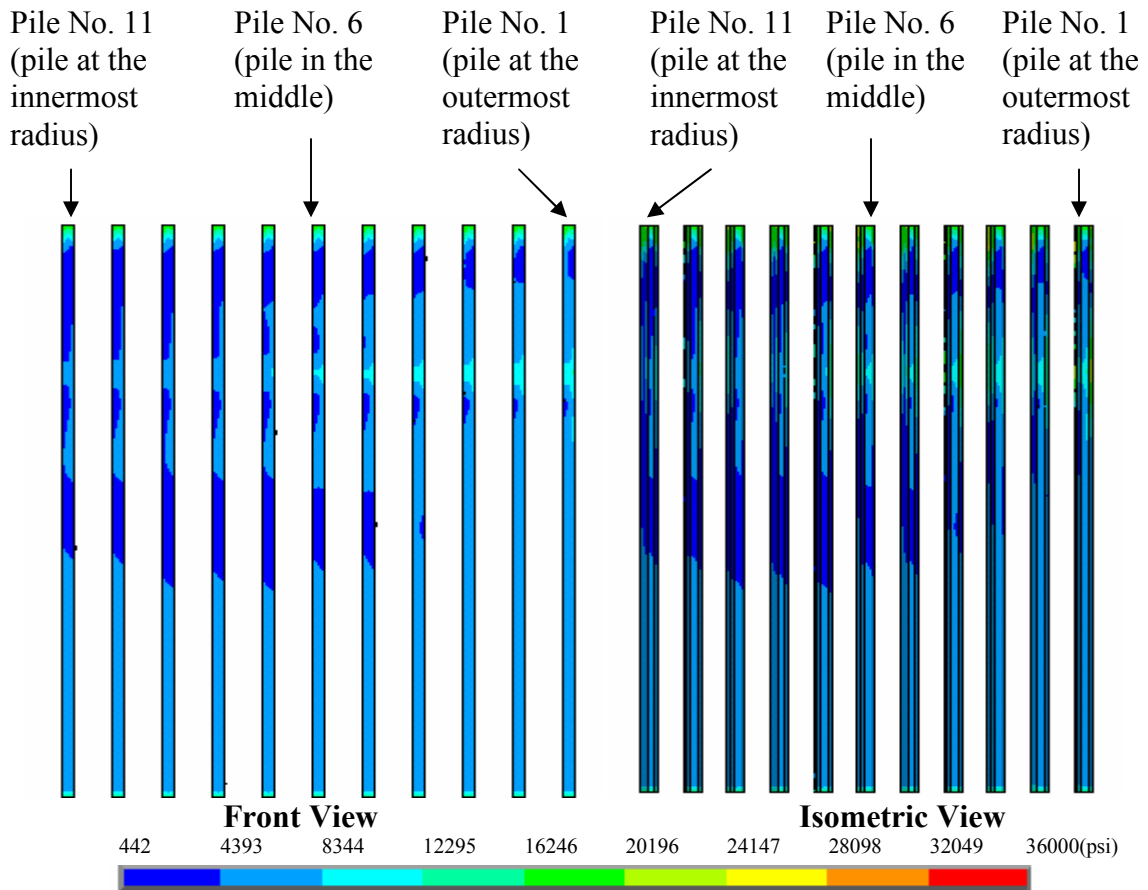


**Figure 9.7 – Equivalent Stress Contour in End-Bearing Piles in 9 ft Deep Predrilled Holes of Bridges with 800 ft Radius and 800 ft Length**  
 $(\Delta T_{\text{slab}} = 120^\circ \text{ F}, \Delta T_{\text{the rest}} = 90^\circ \text{ F})$



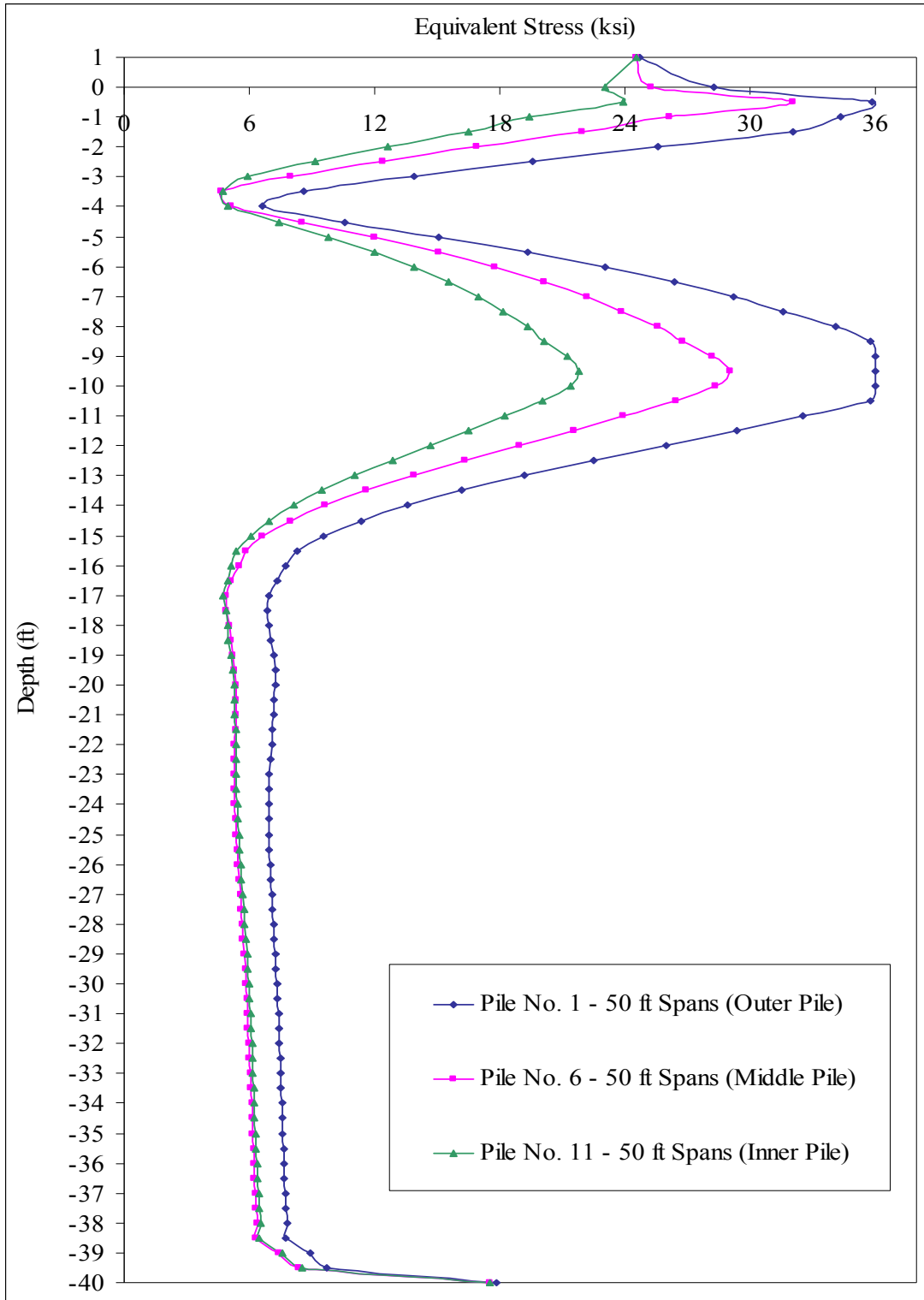


**Figure 9.8 – Equivalent Stress in End-Bearing Piles in 9 ft Deep Predrilled Holes at Different Locations in the Abutment of a Bridge with 800 ft Radius and 16 - 50 ft Spans ( $\Delta T_{\text{slab}} = 120^\circ \text{ F}$ ,  $\Delta T_{\text{the rest}} = 90^\circ \text{ F}$ )**

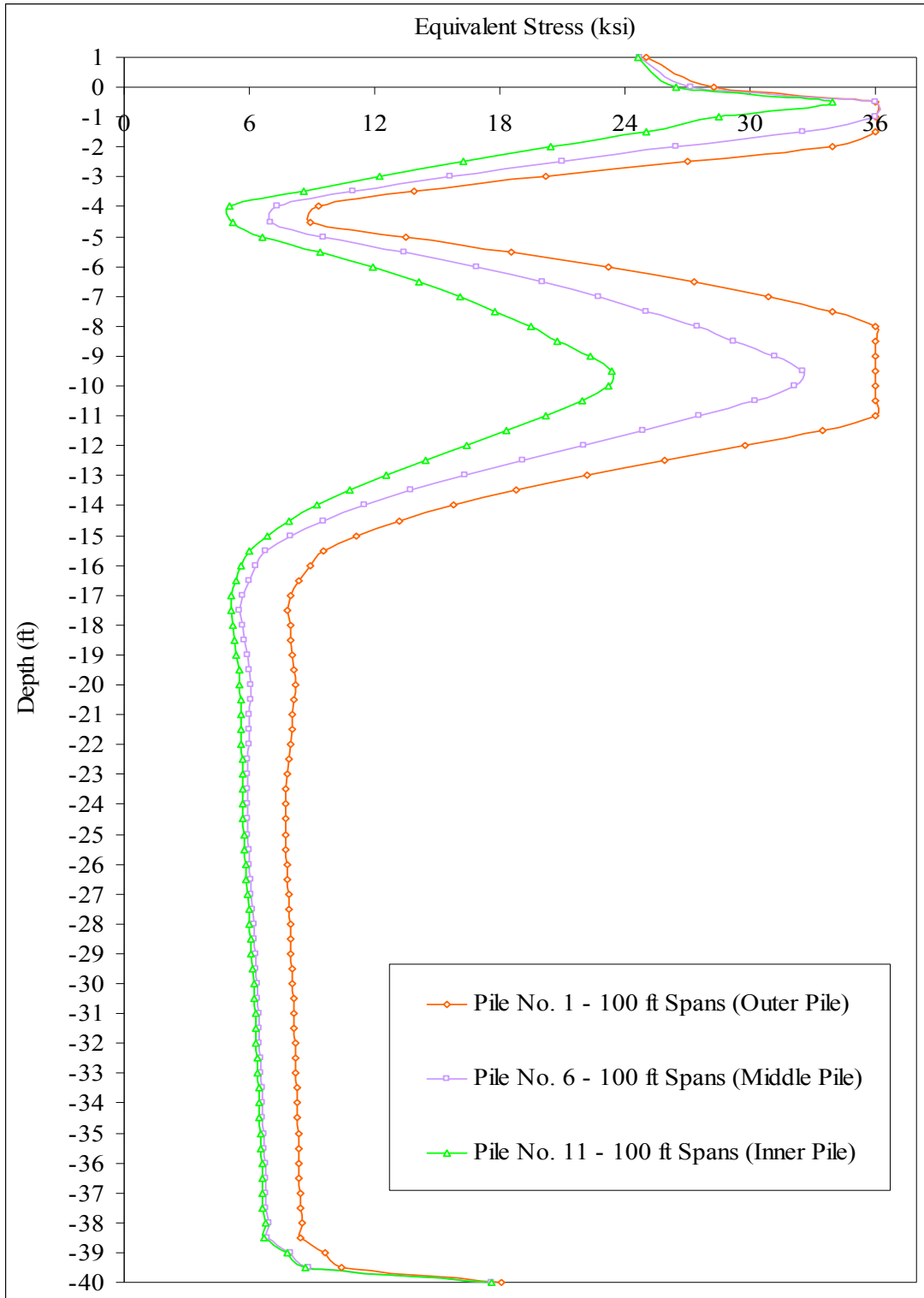


**Figure 9.9 – Equivalent Stress in End-Bearing Piles in 9 ft Deep Predrilled Holes at Different Locations in the Abutment of a Bridge with 800 ft Radius and 8 - 100 ft Spans ( $\Delta T_{\text{slab}} = 120^\circ \text{ F}$ ,  $\Delta T_{\text{the rest}} = 90^\circ \text{ F}$ )**

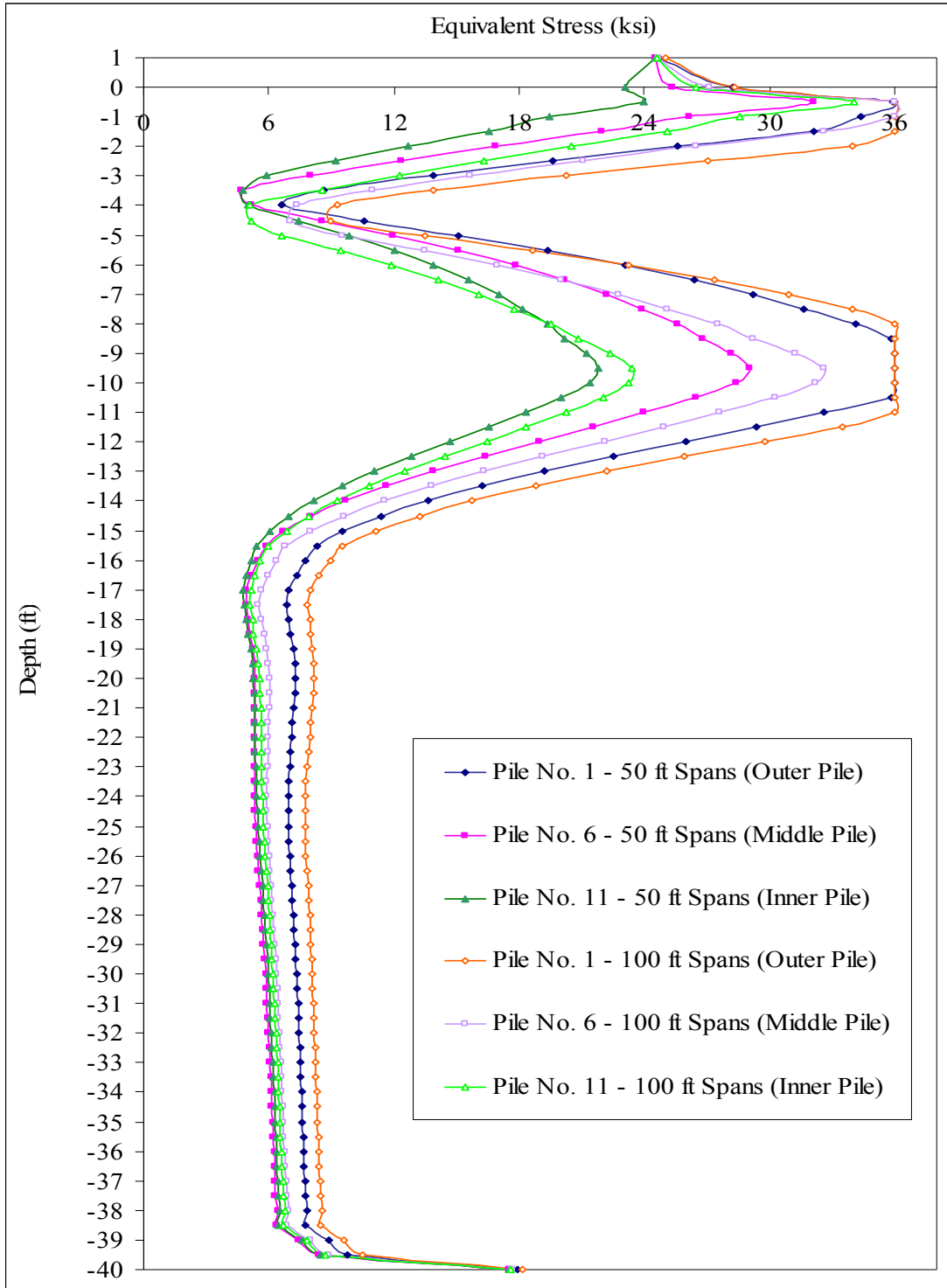


**Figure 9.10 – Comparison of Equivalent Stress in End-Bearing Piles in 9 ft Deep Predrilled Holes at Different Locations in the Abutment between Bridges with 50 ft and 100 ft Spans with 800 ft Radius and 800 ft Length**  
 $(\Delta T_{\text{slab}} = 120^\circ \text{ F}, \Delta T_{\text{the rest}} = 90^\circ \text{ F})$

Figures 9.8 to 9.10 indicate that the highest von Mises or equivalent stress is in pile No. 1 (pile at the outermost radius). It continues to decrease to the lowest equivalent stress in pile No. 11 (pile at the innermost radius) as indicated in Table 9.4. The partially plastic hinges are found in pile No. 1 (pile at the outermost radius) for curved IAB's with 50 ft spans and are found in pile No. 1 (pile at the outermost radius), and pile No. 6 (pile in the middle). for curved IAB's with 100 ft spans as indicated in Table 9.5. The partially plastic region in piles for curved IAB's with 100 ft spans is slightly longer compared to the partially plastic region for curved IAB's with 50 ft spans.

**Table 9.4 – Equivalent Stress Decrease (%) of End-Bearing Piles in 9 ft Deep Predrilled Holes between Piles at Different Locations in the Abutment ( $\Delta T_{\text{slab}} = 120^\circ \text{ F}$ ,  $\Delta T_{\text{the rest}} = 90^\circ \text{ F}$ )**

Span Length (ft)	Comparison between Piles		
	No. 1 with No. 6	No. 1 with No. 11	No. 6 with No. 11
50	0 to 46	0 to 57	0 to 26
100	0 to 30	0 to 51	0 to 30

**Table 9.5 – Location of Partially Plastic Hinges in End-Bearing Piles in 9 ft Deep Predrilled Holes at Different Locations in the Abutment ( $\Delta T_{\text{slab}} = 120^\circ \text{ F}$ ,  $\Delta T_{\text{the rest}} = 90^\circ \text{ F}$ )**

Span Length (ft)	Depth Below the Bottom of the Abutment (ft)		
	Pile Number		
	1	6	11
50	0.5	–	–
	8.5 – 10.5		
100	0.5 – 1.5	0.5 – 1	–
	8 – 11		

The equivalent stress in all three piles in very stiff clay soil profile with 9 ft deep predrilled holes filled with loose sand of curved IAB's with 50 ft and 100 ft spans has almost the same stress value, which is approximately 25 ksi, at the top of the piles which are embedded 1 ft deep into the abutment. The equivalent stress in the piles then continues to increase to reach a yield stress of 36 ksi and the partially plastic hinges occur in the piles as indicated in Table 9.5. After the equivalent stress in the piles reaches the yield stress of 36 ksi indicated in Table 9.5, it starts to decrease at a certain depth and increases again at the connection between the loose sand layer and the very stiff clay layer. Below that depth, it starts to decrease to a new equivalent stress level at a certain depth and almost constant as the depth of the piles continues to increase to 38.5 ft below the bottom of the abutment as indicated in Table 9.6.

The equivalent stress in all three piles from 38.5 ft to 39.5 ft depth below the bottom of the abutment increases by 23% to 32%. From 39.5 ft to 40 ft depth below the bottom of the abutment, the equivalent stress in all three piles increases significantly by 74% to 110%.

The equivalent stress in all three piles of curved IAB's with both 50 ft and 100 ft spans and piles in very stiff clay soil profile with 9 ft deep predrilled holes filled with loose sand is approximately 18 ksi at a 40 ft depth below the bottom of the abutment. Piles No. 6 (pile in the middle) and No. 11 (pile at the innermost radius) at 17 ft to 40 ft depth below the bottom of the abutment have almost the same equivalent stress value.

**Table 9.6 – Equivalent Stress in End-Bearing Piles in 9 ft Deep Predrilled Holes at Different Locations in the Abutment of Bridges with 800 ft Radius and 800 ft Length ( $\Delta T_{\text{slab}} = 120^\circ \text{ F}$ ,  $\Delta T_{\text{the rest}} = 90^\circ \text{ F}$ )**

Span Length (ft)	Pile Number	Depth Below the Bottom of the Abutment (ft)	Equivalent Stress in Piles (ksi)
50	1 (pile at the outermost radius)	0.5	36.0
		4	6.6
		8.5 – 10.5	36.0
		17 – 38.5	6.9 – 7.8
		40	17.9
	6 (pile in the middle)	0.5	32.0
		3.5	4.7
		9.5	29.0
		17 – 38.5	4.9 – 6.4
		40	17.5
	11 (pile at the innermost radius)	0.5	24.0
		3.5	4.8
		9.5	21.8
		17 – 38.5	4.8 – 6.5
		40	17.5
100	1 (pile at the outermost radius)	0.5 – 1.5	36.0
		4.5	9.0
		8 – 11	36.0
		17 – 38.5	8.0 – 8.5
		40	18.1
	6 (pile in the middle)	0.5 – 1	36.0
		4.5	7.0
		9.5	32.6
		17 – 38.5	5.7 – 6.9
		40	17.6
	11 (pile at the innermost radius)	0.5	34.0
		4	5.1
		9.5	23.4
		17 – 38.5	5.1 – 6.7
		40	17.6

## 9.2 Displacement of Piles

Figure 9.11 shows the deformed (light line) and undeformed (dark line) shapes of curved IAB's with 800 ft radius and 800 ft length with end-bearing piles in very stiff clay soil profile with 9 ft deep predrilled holes filled with loose sand at  $\Delta T_{\text{slab}}$  of 120° F and  $\Delta T_{\text{the rest}}$  of 90° F. The deflection scale factor of 40 is used to enlarge the displacement in this study. The deformed and undeformed shapes of curved IAB's at the right abutment are shown in Figures 9.12 to 9.14. Figures 9.12 and 9.13 indicate that the displacement at the end span of a bridge superstructure in lateral, longitudinal, and vertical directions causes the piles to displace in an upward direction for curved IAB's with both 50 ft and 100 ft spans.

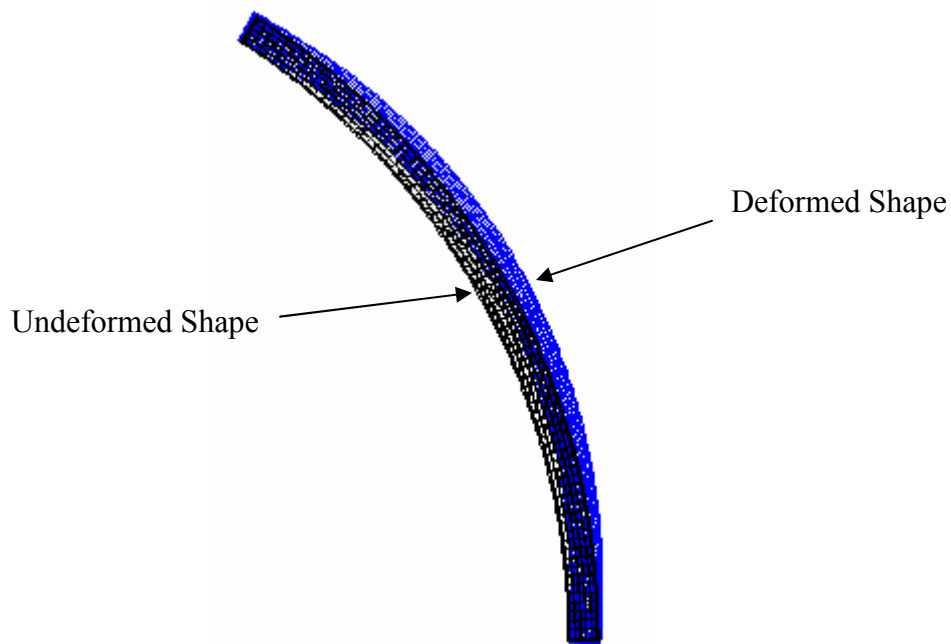
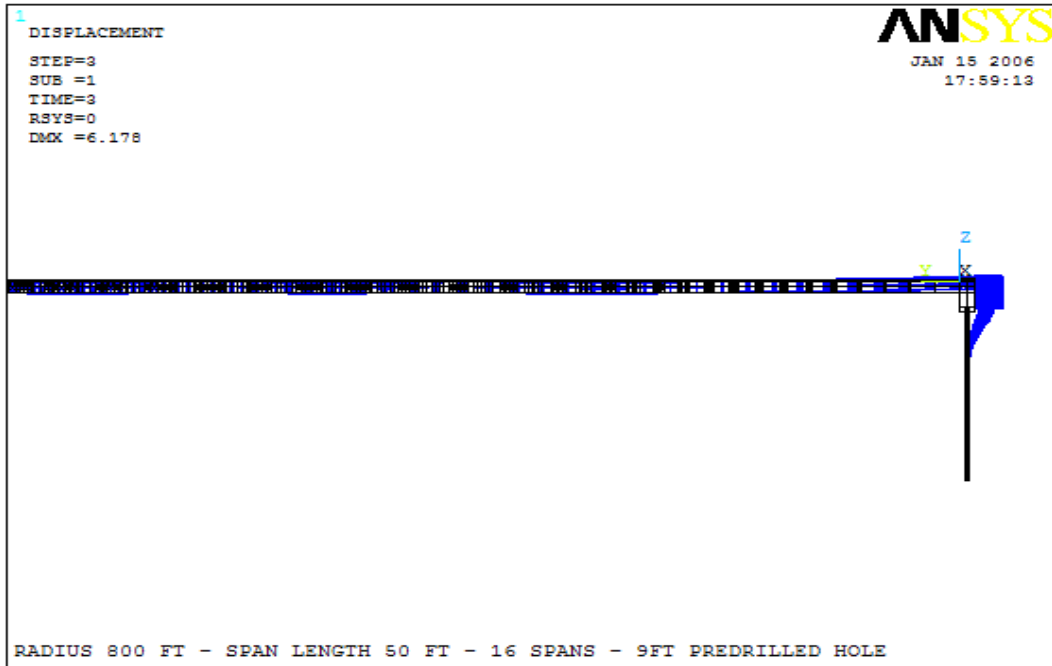
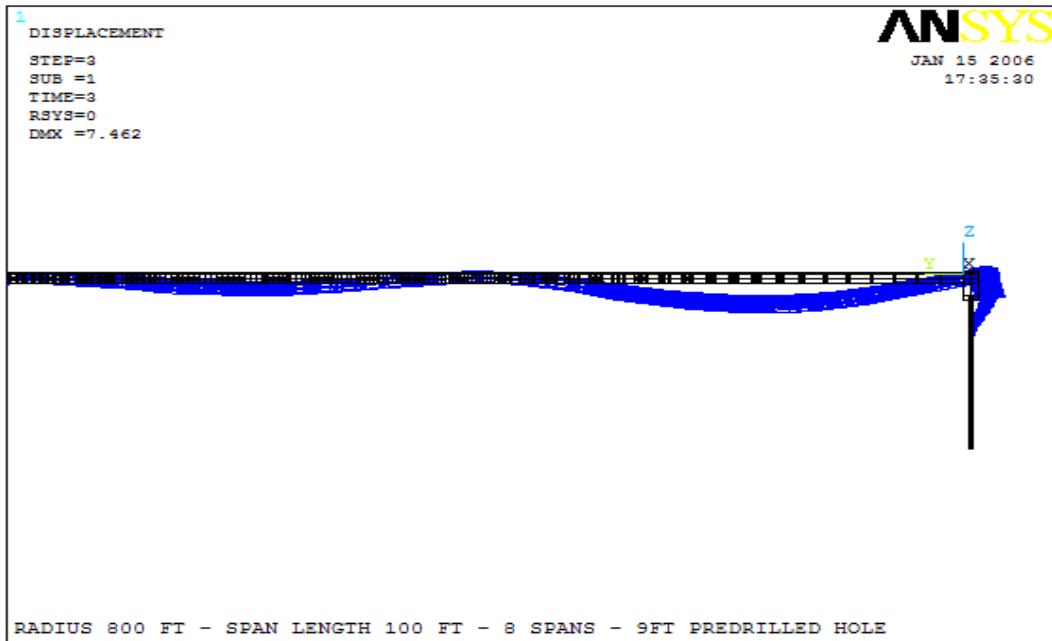


**Figure 9.11 – Deformed and Undeformed Shapes of Bridges with 800 ft Radius and 800 ft Length with End-Bearing Piles in 9 ft Deep Predrilled Holes ( $\Delta T_{\text{slab}} = 120^{\circ}$  F,  $\Delta T_{\text{the rest}} = 90^{\circ}$  F)**



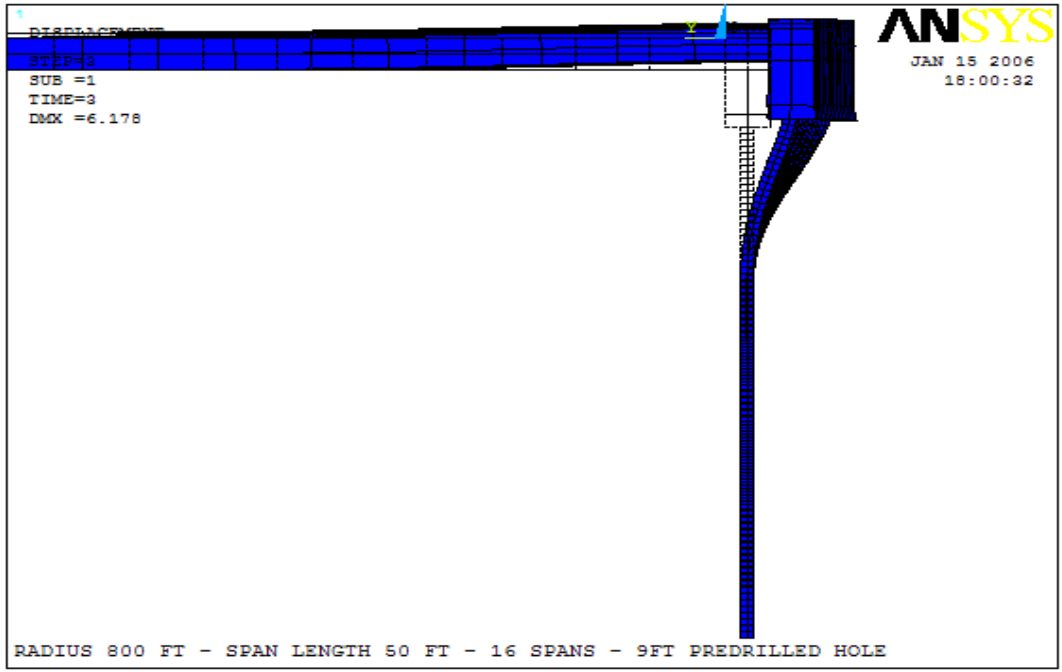
a) 50 ft Spans



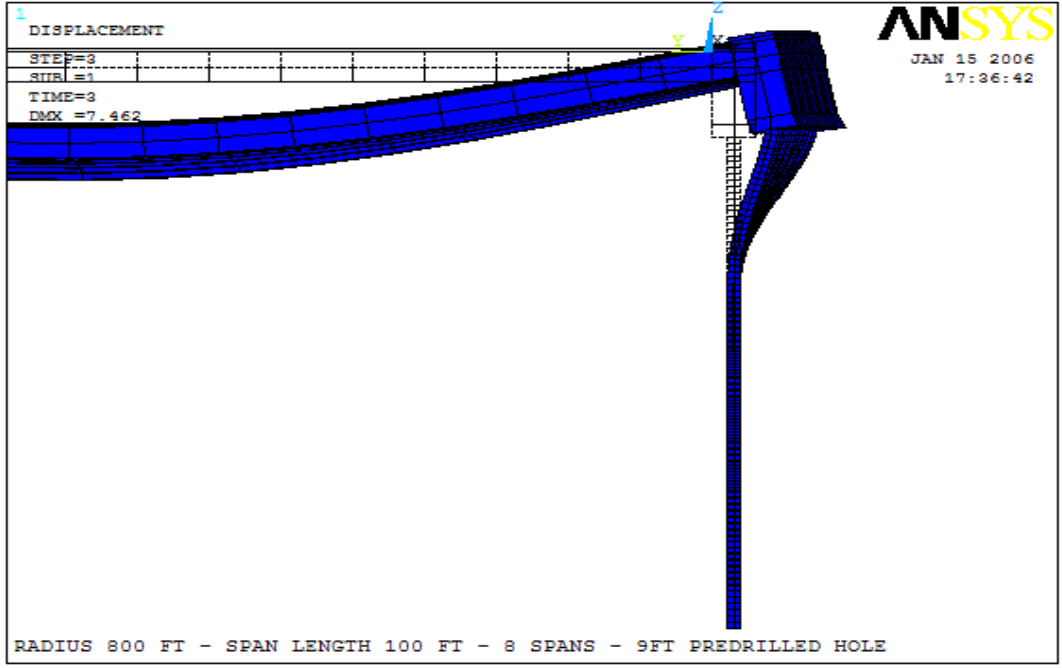
b) 100 ft Spans

**Figure 9.12 – Front View of Deformed and Undeformed Shapes at the Right Abutment of Bridges with 800 ft Radius and 800 ft Length with End-Bearing Piles in 9 ft Deep Predrilled Holes ( $\Delta T_{\text{slab}} = 120^\circ \text{ F}$ ,  $\Delta T_{\text{the rest}} = 90^\circ \text{ F}$ )**



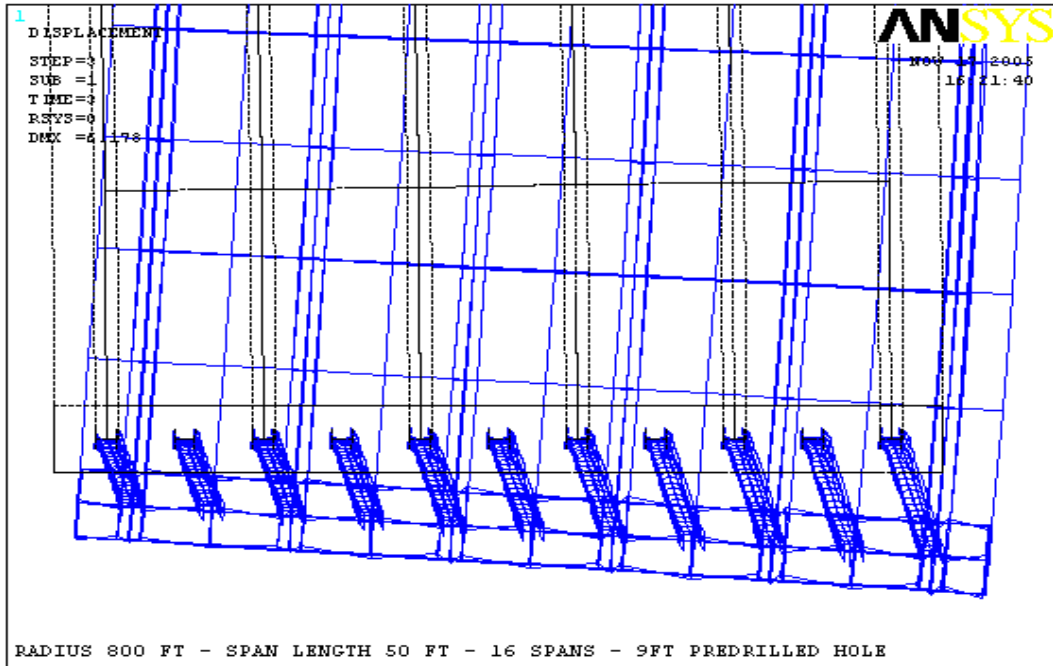


a) 50 ft Spans

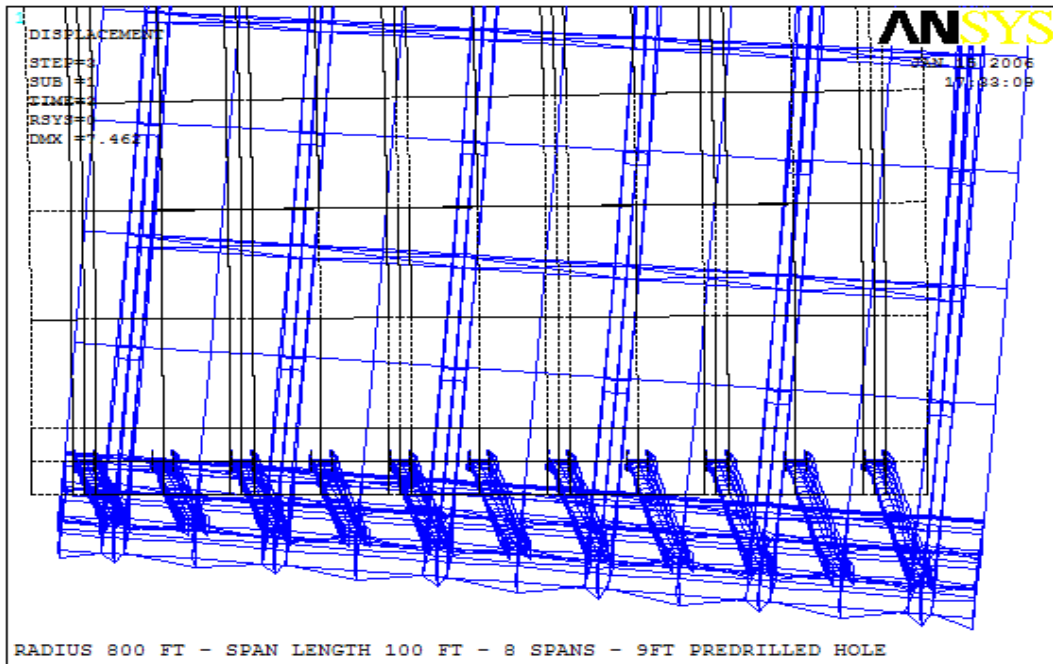


b) 100 ft Spans

**Figure 9.13 – Zoom View of Deformed and Undeformed Shapes at the Right Abutment of Bridges with 800 ft Radius and 800 ft Length with End-Bearing Piles in 9 ft Deep Predrilled Holes ( $\Delta T_{\text{slab}} = 120^\circ \text{ F}$ ,  $\Delta T_{\text{the rest}} = 90^\circ \text{ F}$ )**



a) 50 ft Spans



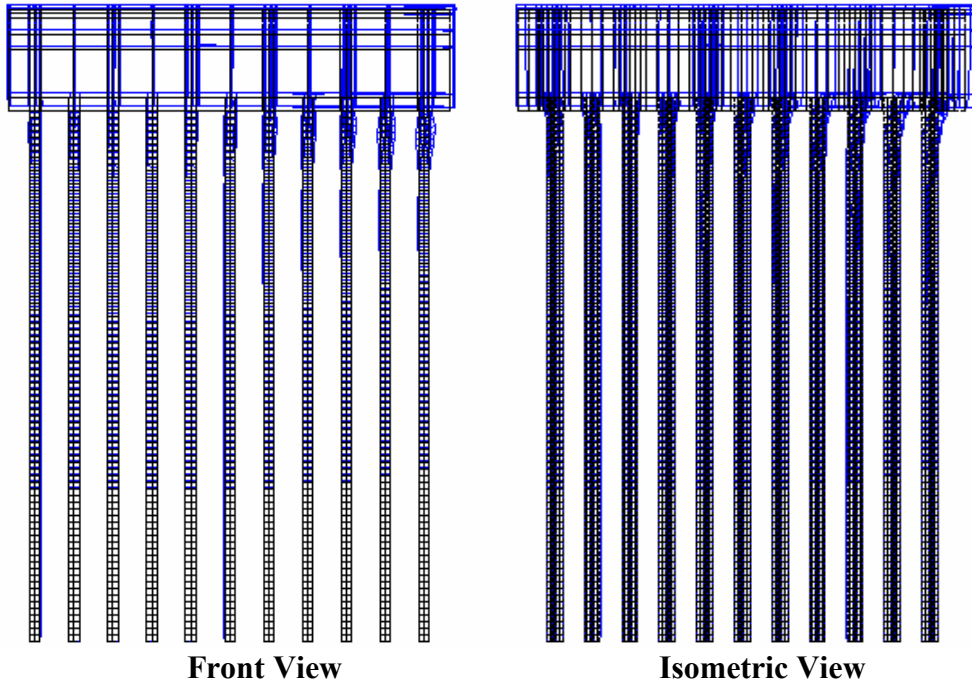
b) 100 ft Spans

**Figure 9.14 – Top View of Deformed and Undeformed Shapes at the Right Abutment of Bridges with 800 ft Radius and 800 ft Length with End-Bearing Piles in 9 ft Deep Predrilled Holes ( $\Delta T_{\text{slab}} = 120^\circ \text{ F}$ ,  $\Delta T_{\text{the rest}} = 90^\circ \text{ F}$ )**

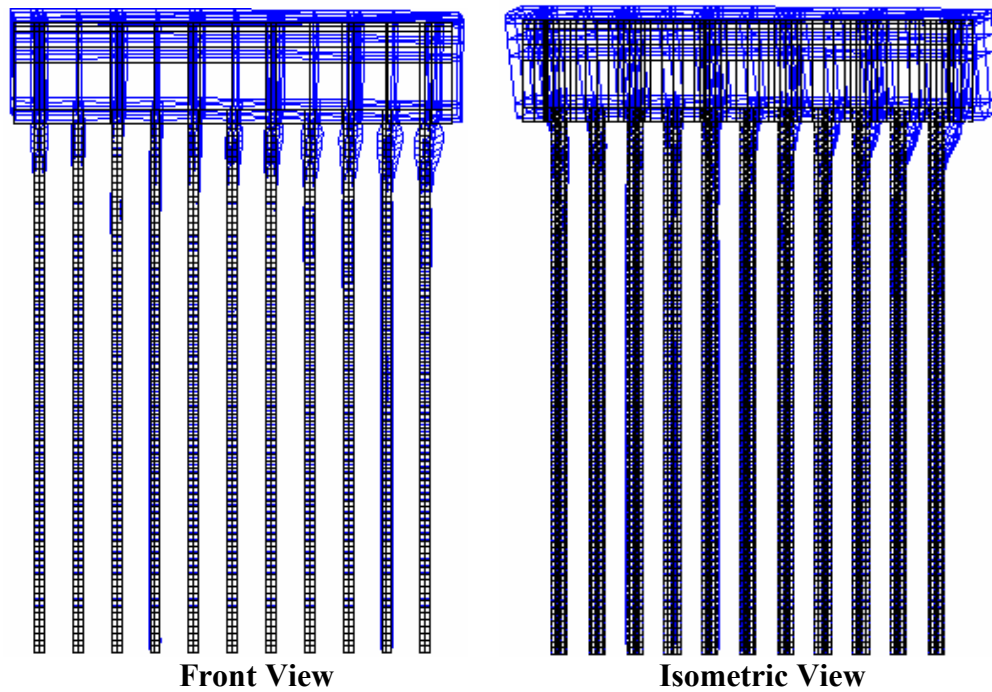
The deformed (light line) and undeformed (dark line) shapes of abutment with piles in very stiff clay soil profile and in very stiff clay soil profile with 9 ft deep predrilled holes filled with loose sand are shown in Figures 9.15 and 9.16, respectively. The deformed (light line) and undeformed (dark line) shapes of the piles without abutment for piles in very stiff clay soil profile and piles in very stiff clay soil profile with 9 ft deep predrilled holes filled with loose sand are shown in Figures 9.17 to 9.20.

Figures 9.17 to 9.20 indicate that the displacement of the piles in curved IAB's with 50 ft and 100 ft spans is the same. In very stiff clay soil profile, the maximum displacement is in expansion and is in the pile on the right hand side of the pile group (the pile at the outermost radius). The displacement continues to decrease to the lowest value which is in contraction and is in the pile on the left hand side of the pile group (the pile at the innermost radius).

In very stiff clay soil profile with 9 ft deep predrilled holes filled with loose sand, the displacement of all piles is in expansion. The maximum displacement is in the pile on the right hand side of the pile group (the pile at the outermost radius). The displacement continues to decrease to the lowest value in the pile on the left hand side of the pile group (the pile at the innermost radius).

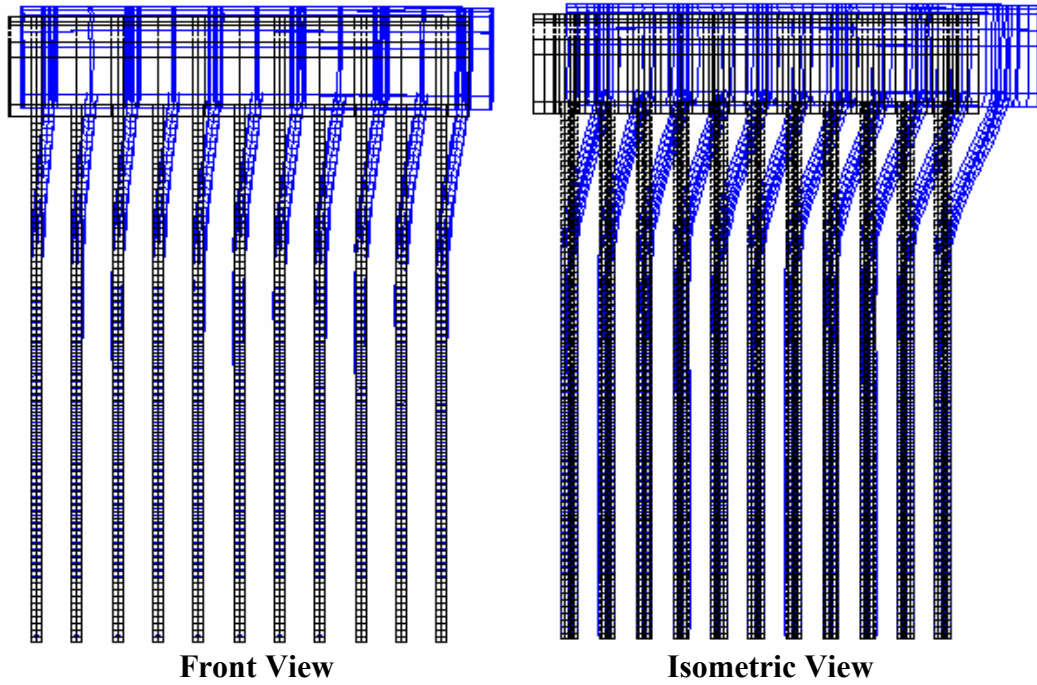


a) 50 ft Spans

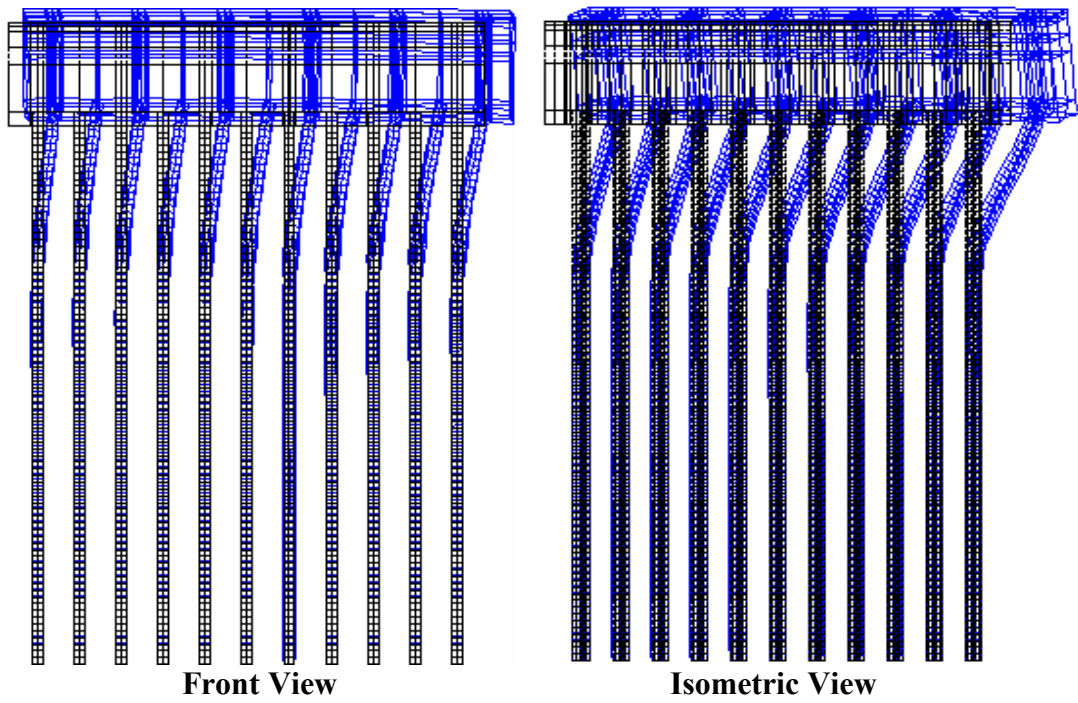


b) 100 ft Spans

**Figure 9.15 – Deformed and Undeformed Shapes of Abutment with End-Bearing Piles in Very Stiff Clay Soil Profile of Bridges with 800 ft Radius and 800 ft Length ( $\Delta T_{\text{slab}} = 120^\circ \text{ F}$ ,  $\Delta T_{\text{the rest}} = 90^\circ \text{ F}$ )**

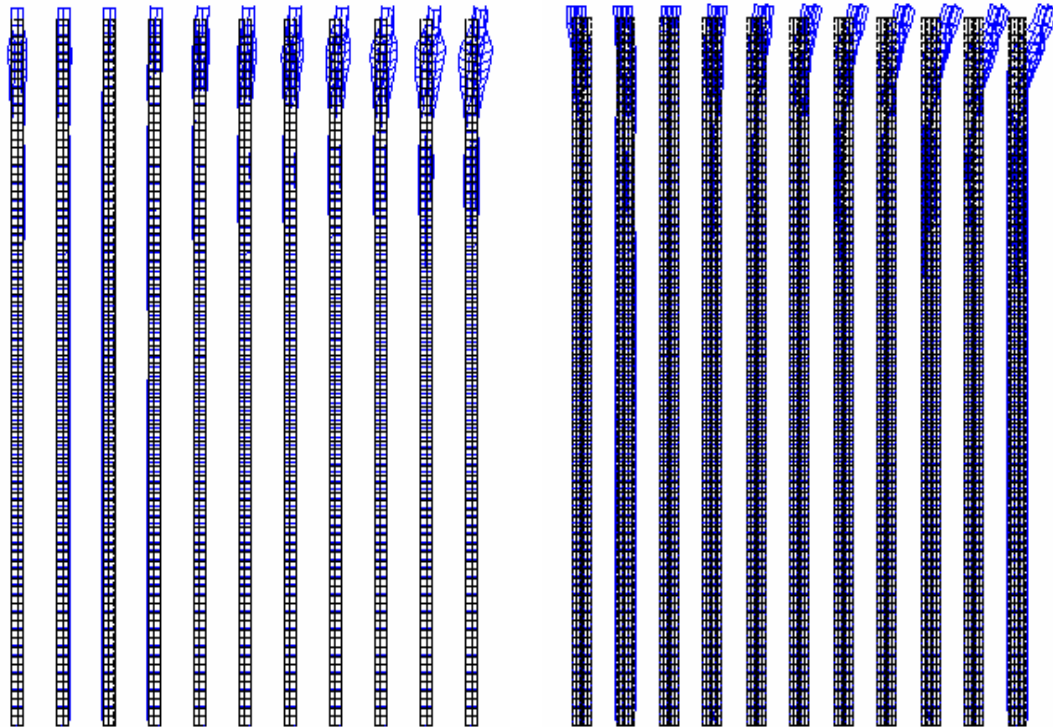


a) 50 ft Spans



b) 100 ft Spans

**Figure 9.16 – Deformed and Undeformed Shapes of Abutment with End-Bearing Piles in 9 ft Deep Predrilled Holes of Bridges with 800 ft Radius and 800 ft Length ( $\Delta T_{\text{slab}} = 120^\circ \text{ F}$ ,  $\Delta T_{\text{the rest}} = 90^\circ \text{ F}$ )**



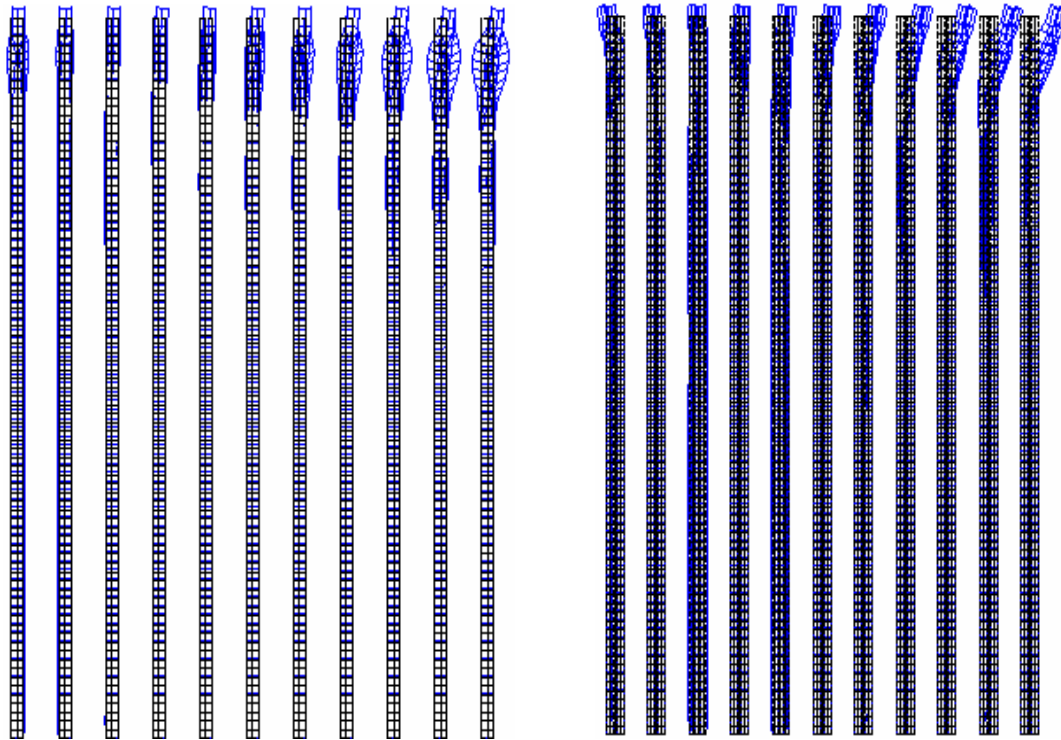
a) Front View

b) Isometric View



c) Top View

**Figure 9.17 – Deformed and Undeformed Shapes of End-Bearing Piles in Very Stiff Clay Soil Profile of a Bridge with 800 ft Radius and 16 - 50 ft Spans ( $\Delta T_{\text{slab}} = 120^\circ \text{ F}$ ,  $\Delta T_{\text{the rest}} = 90^\circ \text{ F}$ )**



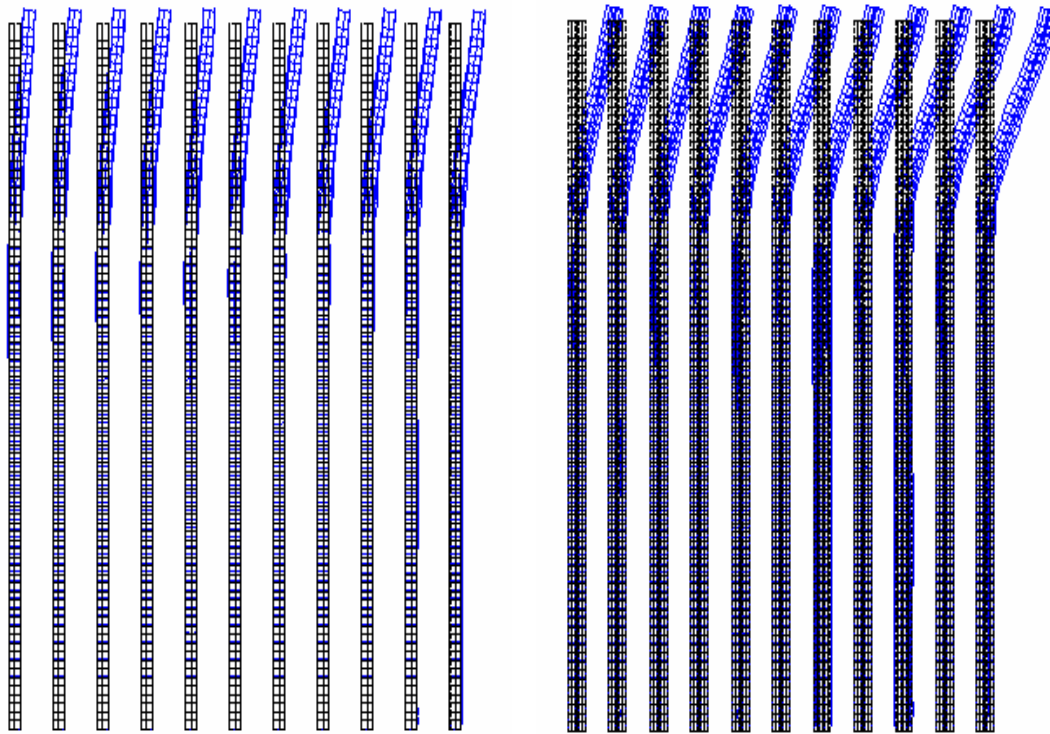
a) Front View

b) Isometric View



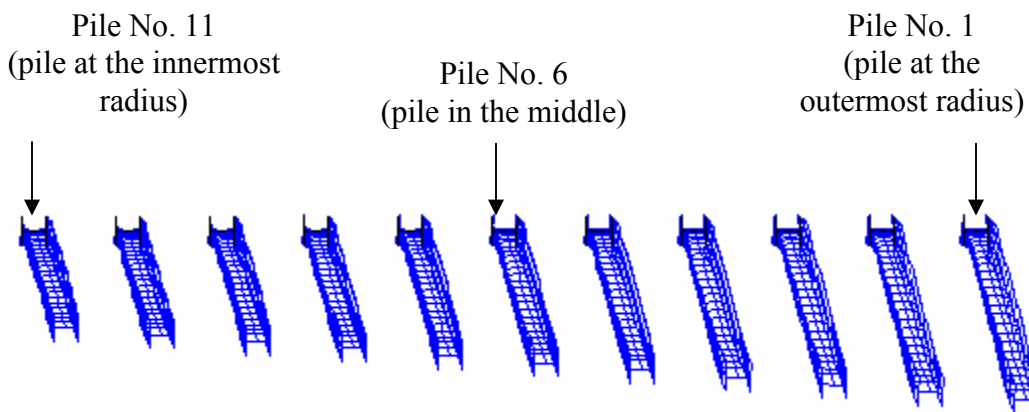
c) Top View

**Figure 9.18 – Deformed and Undeformed Shapes of End-Bearing Piles in Very Stiff Clay Soil Profile of a Bridge with 800 ft Radius and 8 - 100 ft Spans**  
 $(\Delta T_{\text{slab}} = 120^\circ \text{ F}, \Delta T_{\text{the rest}} = 90^\circ \text{ F})$



**a) Front View**

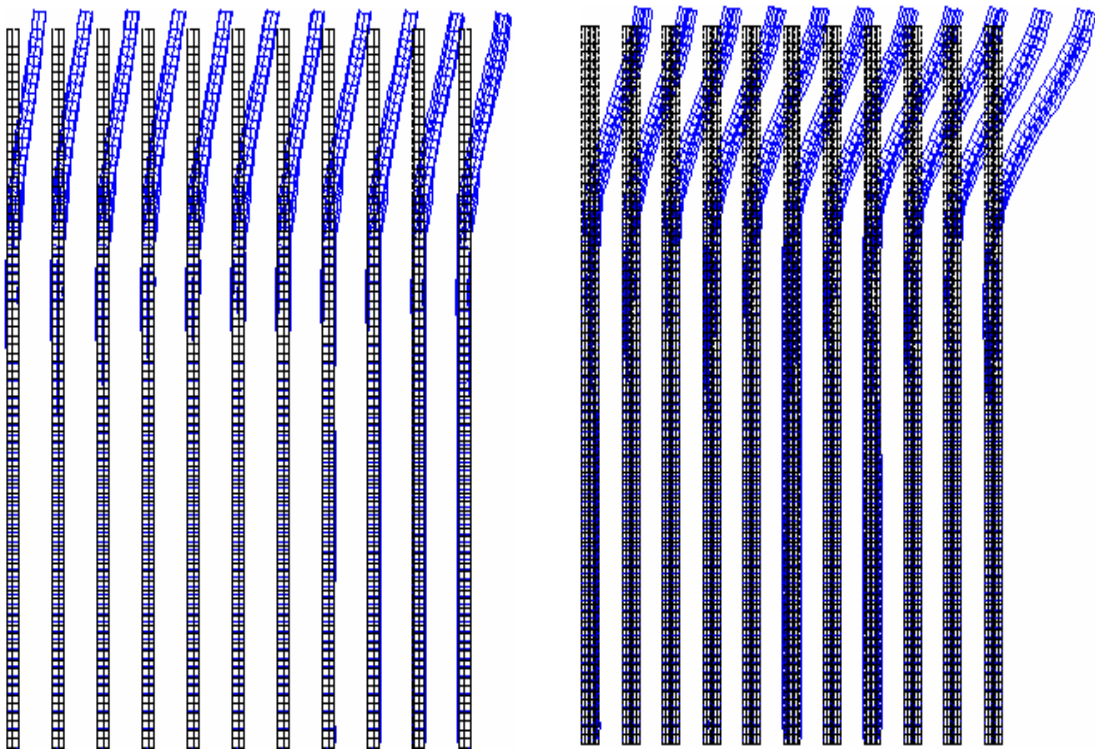
**b) Isometric View**



**c) Top View**

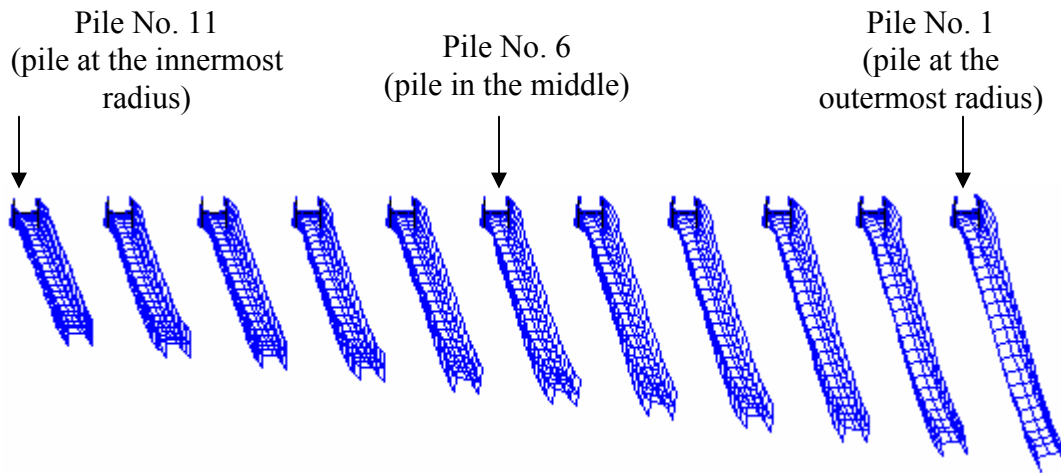
**Figure 9.19 – Deformed and Undeformed Shapes of End-Bearing Piles in 9 ft Deep Predrilled Holes of a Bridge with 800 ft Radius and 16 - 50 ft Spans ( $\Delta T_{\text{slab}} = 120^\circ \text{ F}$ ,  $\Delta T_{\text{the rest}} = 90^\circ \text{ F}$ )**





a) Front View

b) Isometric View



c) Top View

**Figure 9.20 – Deformed and Undeformed Shapes of End-Bearing Piles in 9 ft Deep Predrilled Holes of a Bridge with 800 ft Radius and 8 - 100 ft Spans ( $\Delta T_{\text{slab}} = 120^\circ \text{ F}$ ,  $\Delta T_{\text{the rest}} = 90^\circ \text{ F}$ )**

The deformed (light line) and undeformed (dark line) shapes of the piles on the right hand side of the pile group (the pile at the outermost radius) in various soil profile types are shown in Figures 9.21 and 9.22. The lateral and longitudinal displacements of the piles on the right hand side of the pile group in various soil profile types are plotted in Figures 9.23 and 9.24, respectively.

Figures 9.23 and 9.24 indicate that the maximum displacement in both lateral and longitudinal directions of the piles in all soil profile types of curved IAB's with 50 ft and 100 ft spans is at the top of the piles which are embedded 1 ft deep into the abutment. It is indicated in Table 9.7.

Table 9.7 indicates that the maximum lateral and longitudinal displacements as well as the point of fixity of piles for curved IAB's with 50 ft and 100 ft spans increase as the depth of the predrilled holes is increased.

**Table 9.7 – Displacements and Point of Fixity of End-Bearing Piles in Various Soil Profile Types of Bridges with 800 ft Radius and 800 ft Length**  
( $\Delta T_{\text{slab}} = 120^\circ \text{ F}$ ,  $\Delta T_{\text{the rest}} = 90^\circ \text{ F}$ )

Span Length (ft)	Depth of Predrilled Holes (ft)	Maximum Lateral Displacement (inches)	Maximum Longitudinal Displacement (inches)	Point of Fixity Below the Bottom of the Abutment (ft)
50	0	0.182	0.760	14.0
	5	0.360	1.291	17.5
	9	0.489	1.609	20.5
	15	0.539	1.655	23.5
100	0	0.193	0.764	14.0
	5	0.406	1.294	17.5
	9	0.564	1.645	21.0
	15	0.622	1.705	23.5

The maximum longitudinal displacement of the piles is greater than the maximum lateral displacement of the piles in all soil profile types as indicated in Table 9.8. As the depth of the predrilled holes is increased, the difference in the maximum longitudinal displacement and the maximum lateral displacement of the piles increases. The difference in the maximum longitudinal displacement and the maximum lateral displacement of piles in 9 ft deep predrilled holes and piles in 15 ft deep predrilled holes is almost the same value. Therefore, for the depth increase of predrilled holes deeper than 9 ft, the difference in the maximum lateral displacement and the maximum longitudinal displacement of the piles is similar to the piles in 9 ft deep predrilled holes.

The maximum lateral and longitudinal displacements of the piles increase as the span length is increased from 50 ft to 100 ft which is indicated in Table 9.9. The increase in the lateral and longitudinal displacements of the piles is relatively small by 0.003 inch to 0.083 inch.

**Table 9.8 – Difference in Longitudinal and Lateral Displacements of End-Bearing Piles in Various Soil Profile Types of Bridges with 800 ft Radius and 800 ft Length ( $\Delta T_{\text{slab}} = 120^\circ \text{ F}$ ,  $\Delta T_{\text{the rest}} = 90^\circ \text{ F}$ )**

Span Length (ft)	Depth of Predrilled Holes (ft)	Difference in Displacement (inches)
50	0	0.578
	5	0.931
	9	1.120
	15	1.116
100	0	0.571
	5	0.888
	9	1.081
	15	1.083

**Table 9.9 – Difference in Displacements and Point of Fixity of End-Bearing Piles in Various Soil Profile Types between Bridges with 100 ft and 50 ft Spans with 800 ft Radius and 800 ft Length ( $\Delta T_{\text{slab}} = 120^\circ \text{ F}$ ,  $\Delta T_{\text{the rest}} = 90^\circ \text{ F}$ )**

Depth of Predrilled Holes (ft)	Difference in Lateral Displacement (inch)	Difference in Longitudinal Displacement (inch)	Difference in Point of Fixity Below the Bottom of the Abutment (ft)
0	0.011	0.004	0.0
5	0.046	0.003	0.0
9	0.075	0.036	0.5
15	0.083	0.050	0.0

Piles No. 1 (pile at the outermost radius), No. 6 (pile in the middle), and No. 11 (pile at the innermost radius) shown in Figures 9.19 and 9.20 are chosen to study the displacement of the piles at different locations in the abutment of curved IAB's with 800 ft radius and 800 ft length with end-bearing piles in very stiff clay soil profile with 9 ft deep predrilled holes filled with loose sand. The lateral and longitudinal displacements of the piles at different locations in the abutment are

plotted in Figures 9.25 and 9.26. The maximum lateral and longitudinal displacements as well as the point of fixity of the piles at different locations in the abutment are indicated in Table 9.10.

Table 9.10 indicates that the maximum lateral and longitudinal displacements as well as the point of fixity of the piles in curved IAB's with both 50 ft and 100 ft spans have the highest values in pile No.1 (pile at the outermost radius). They continue to decrease to the lowest values in pile No. 11 (pile at the innermost radius).

Table 9.11 as well as Figures 9.25 and 9.26 indicate that the maximum lateral displacement of all three piles increases by 0.075 inch when the span length is increased from 50 ft to 100 ft.

As the span length increases from 50 ft to 100 ft, the maximum longitudinal displacement of the piles is as follows:

- For pile No.1 (pile at the outermost radius), the maximum longitudinal displacement increases in expansion.
- For pile No.6 (pile in the middle), the maximum longitudinal displacement decreases in contraction at the top of the pile which is embedded 1 ft deep into the abutment. It begins to increase in expansion at the bottom of the abutment.
- For pile No.11 (pile at the innermost radius), the maximum longitudinal displacement decreases in contraction from the top of the pile which is embedded 1 ft deep into the abutment. It begins to increase in expansion at the depth of 3 ft below the bottom of the abutment.

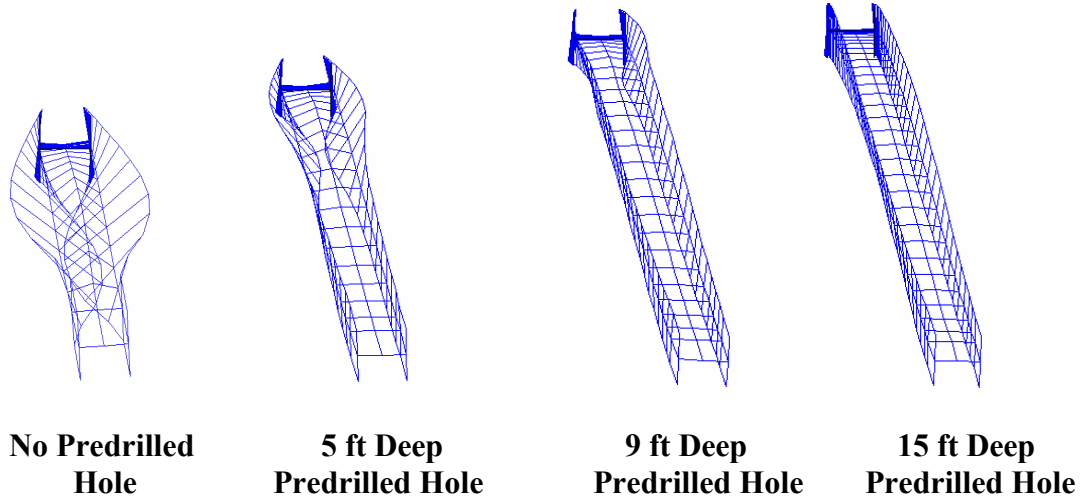
The point of fixity of all three piles is 0.5 ft deeper when the span length is increased from 50 ft to 100 ft.

**Table 9.10 – Displacements and Point of Fixity of End-Bearing Piles in 9 ft Deep Predrilled Holes at Different Locations in the Abutment of Bridges with 800 ft Radius and 800 ft Length ( $\Delta T_{\text{slab}} = 120^\circ \text{ F}$ ,  $\Delta T_{\text{the rest}} = 90^\circ \text{ F}$ )**

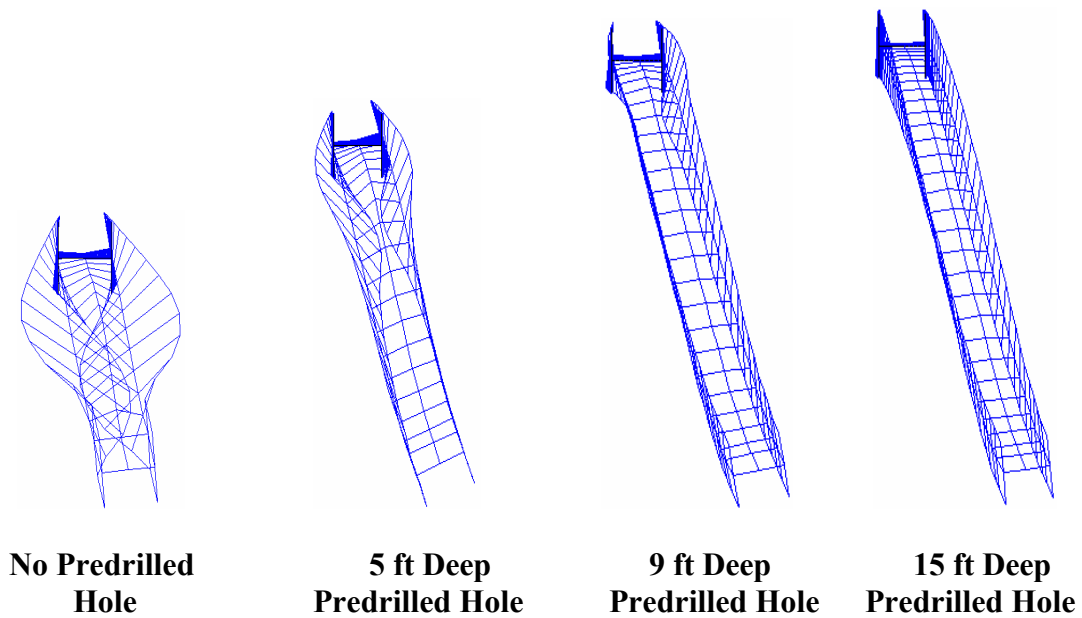
Span Length (ft)	Pile Number	Maximum Lateral Displacement (inches)	Maximum Longitudinal Displacement (inches)	Point of Fixity Below the Bottom of the Abutment (ft)
50	1	0.489	1.609	20.5
	6	0.400	1.252	20.0
	11	0.301	0.922	20.0
100	1	0.564	1.645	21.0
	6	0.475	1.214	20.5
	11	0.376	0.812	20.5

**Table 9.11 – Difference in Displacements and Point of Fixity of End-Bearing Piles in 9 ft Deep Predrilled Holes at Different Locations in the Abutment between Bridges with 100 ft and 50 Spans with 800 ft Radius and 800 ft Length ( $\Delta T_{\text{slab}} = 120^\circ \text{ F}$ ,  $\Delta T_{\text{the rest}} = 90^\circ \text{ F}$ )**

Pile Number	Difference in Lateral Displacement (inch)	Difference in Longitudinal Displacement (inch)	Difference in Point of Fixity Below the Bottom of the Abutment (ft)
1	0.075	0.036	0.5
6	0.075	-0.038	0.5
11	0.075	-0.110	0.5

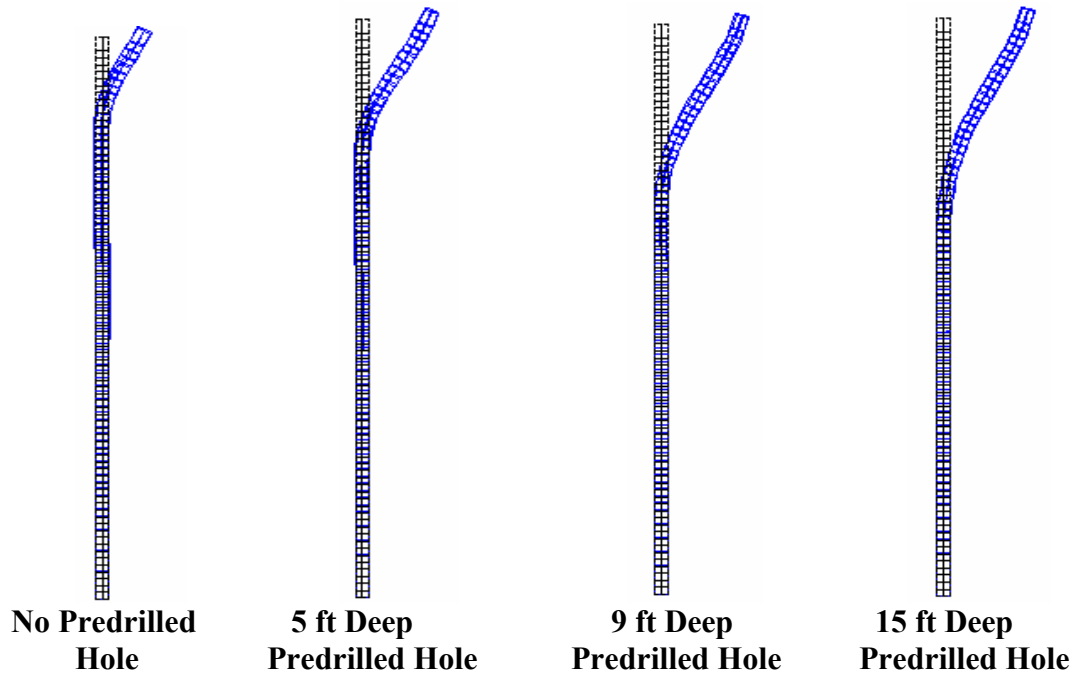


**a) 50 ft Spans**

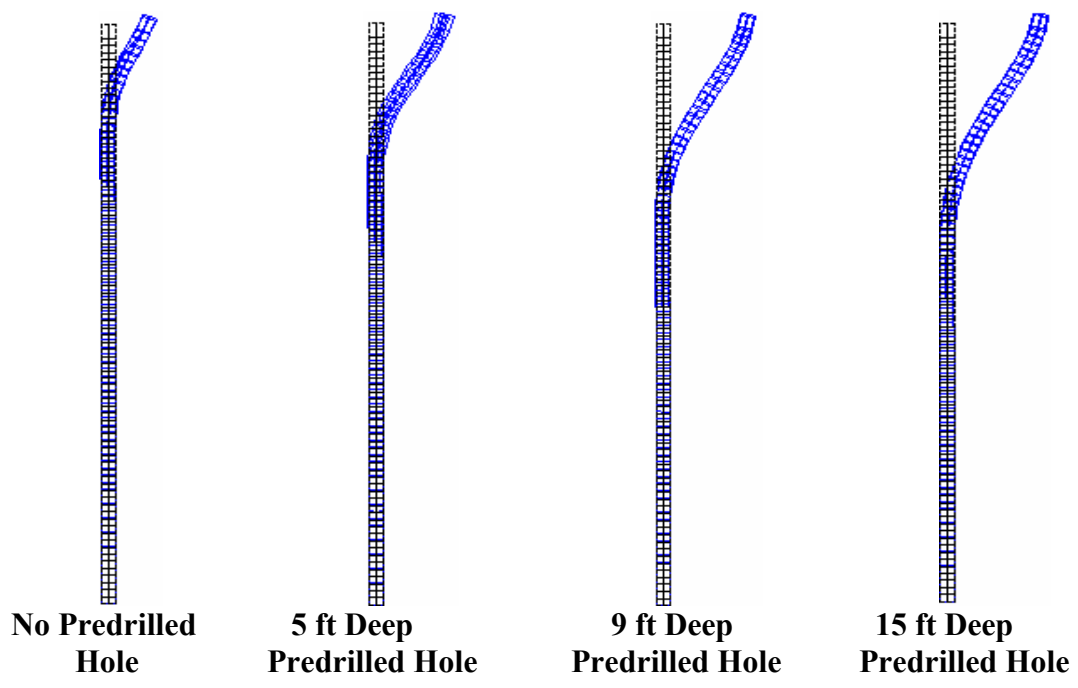


**b) 100 ft Spans**

**Figure 9.21 – Top View of Deformed and Undeformed Shapes of End-Bearing Piles in Various Soil Profile Types of Bridges with 800 ft Radius and 800 ft Length ( $\Delta T_{\text{slab}} = 120^\circ \text{ F}$ ,  $\Delta T_{\text{the rest}} = 90^\circ \text{ F}$ )**



a) 50 ft Spans



b) 100 ft Spans

**Figure 9.22 – Deformed and Undeformed Shapes of End-Bearing Piles in Various Soil Profile Types of Bridges with 800 ft Radius and 800 ft Length ( $\Delta T_{\text{slab}} = 120^\circ \text{ F}$ ,  $\Delta T_{\text{the rest}} = 90^\circ \text{ F}$ )**



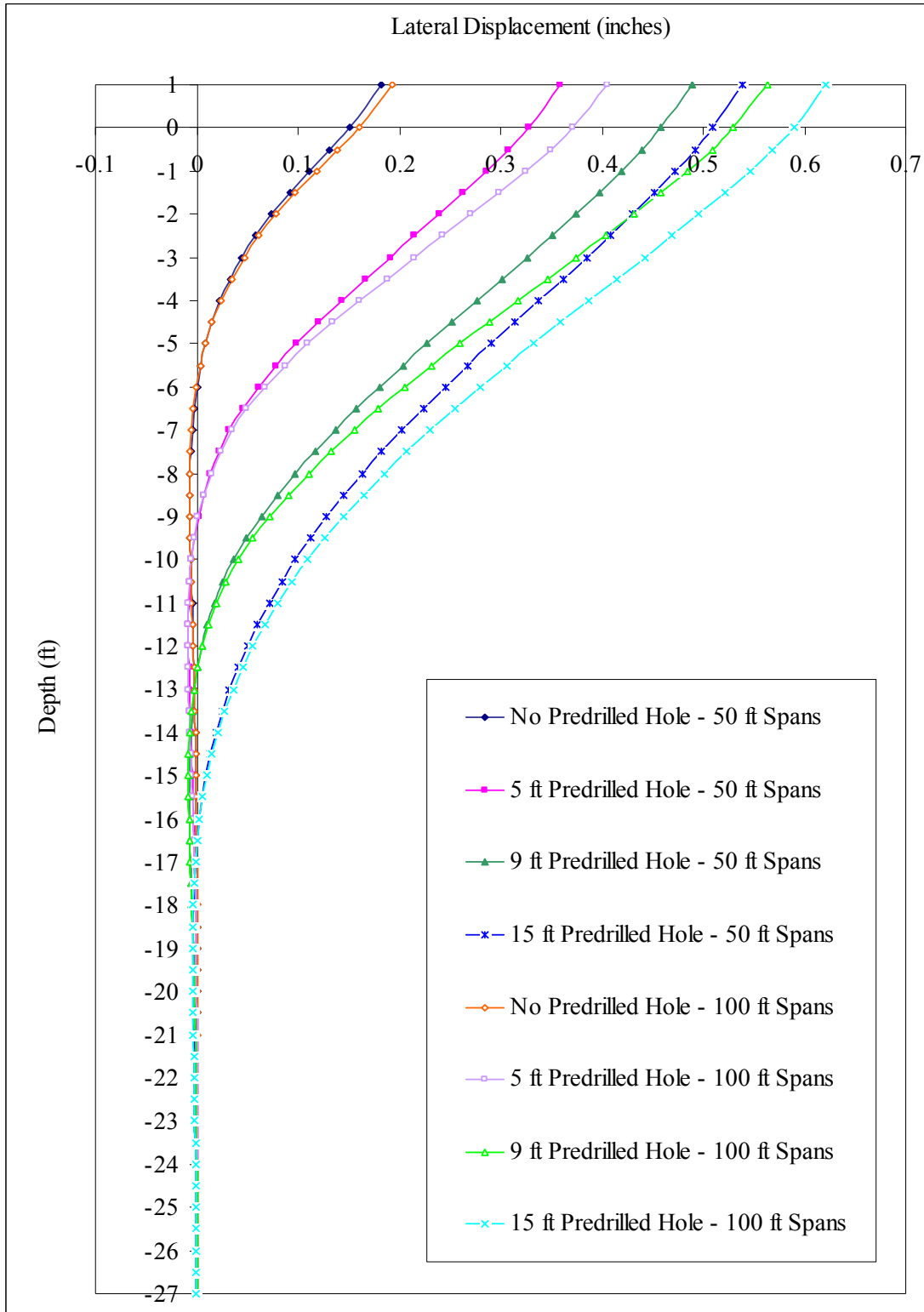


**Figure 9.23 – Lateral Displacement of End-Bearing Piles in Various Soil Profile Types of Bridges with 800 ft Radius and 800 ft Length**  
 $(\Delta T_{\text{slab}} = 120^\circ \text{ F}, \Delta T_{\text{the rest}} = 90^\circ \text{ F})$

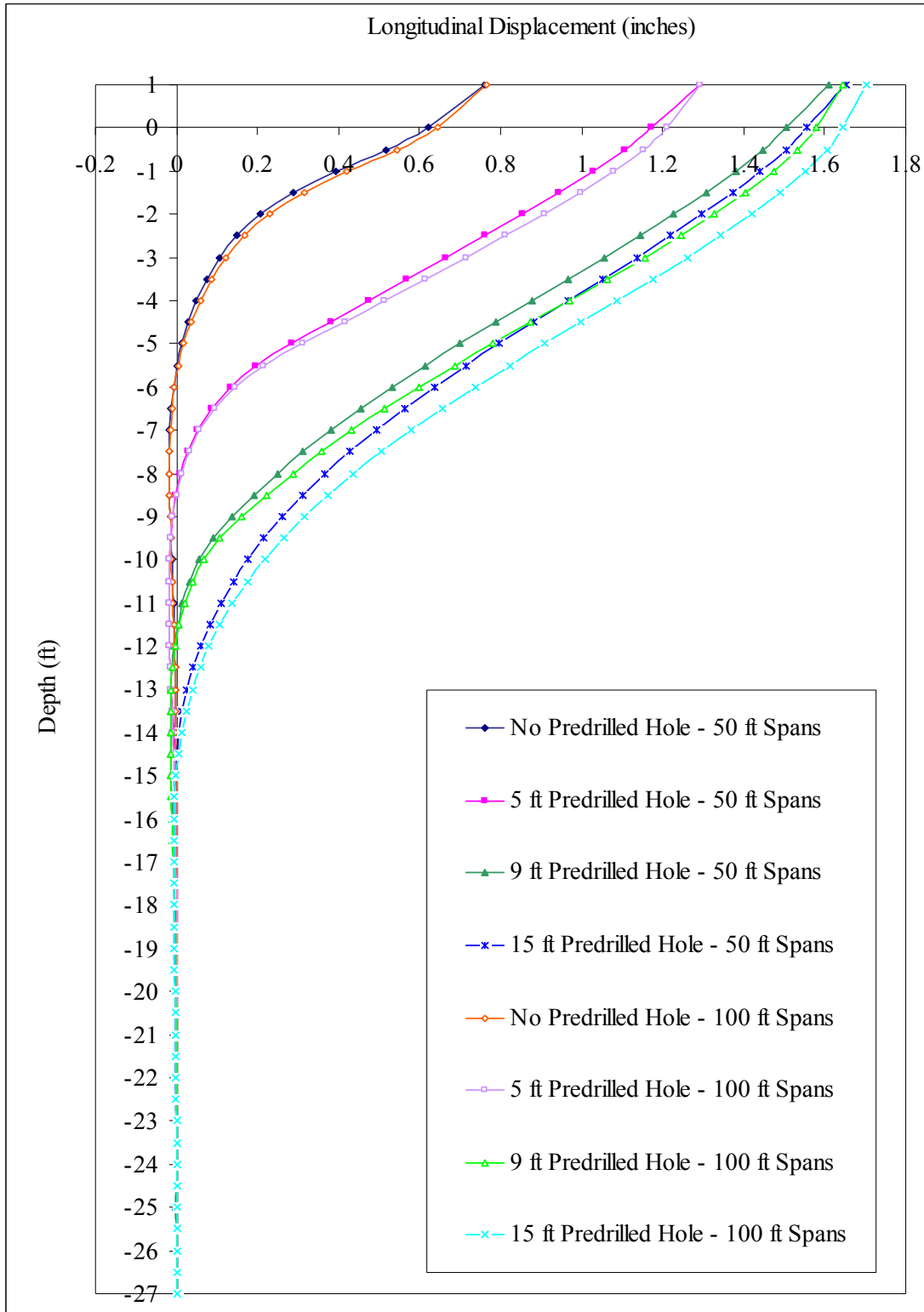


**Figure 9.24 – Longitudinal Displacement of End-Bearing Piles in Various Soil Profile Types of Bridges with 800 ft Radius and 800 ft Length**  
 $(\Delta T_{\text{slab}} = 120^\circ \text{ F}, \Delta T_{\text{the rest}} = 90^\circ \text{ F})$

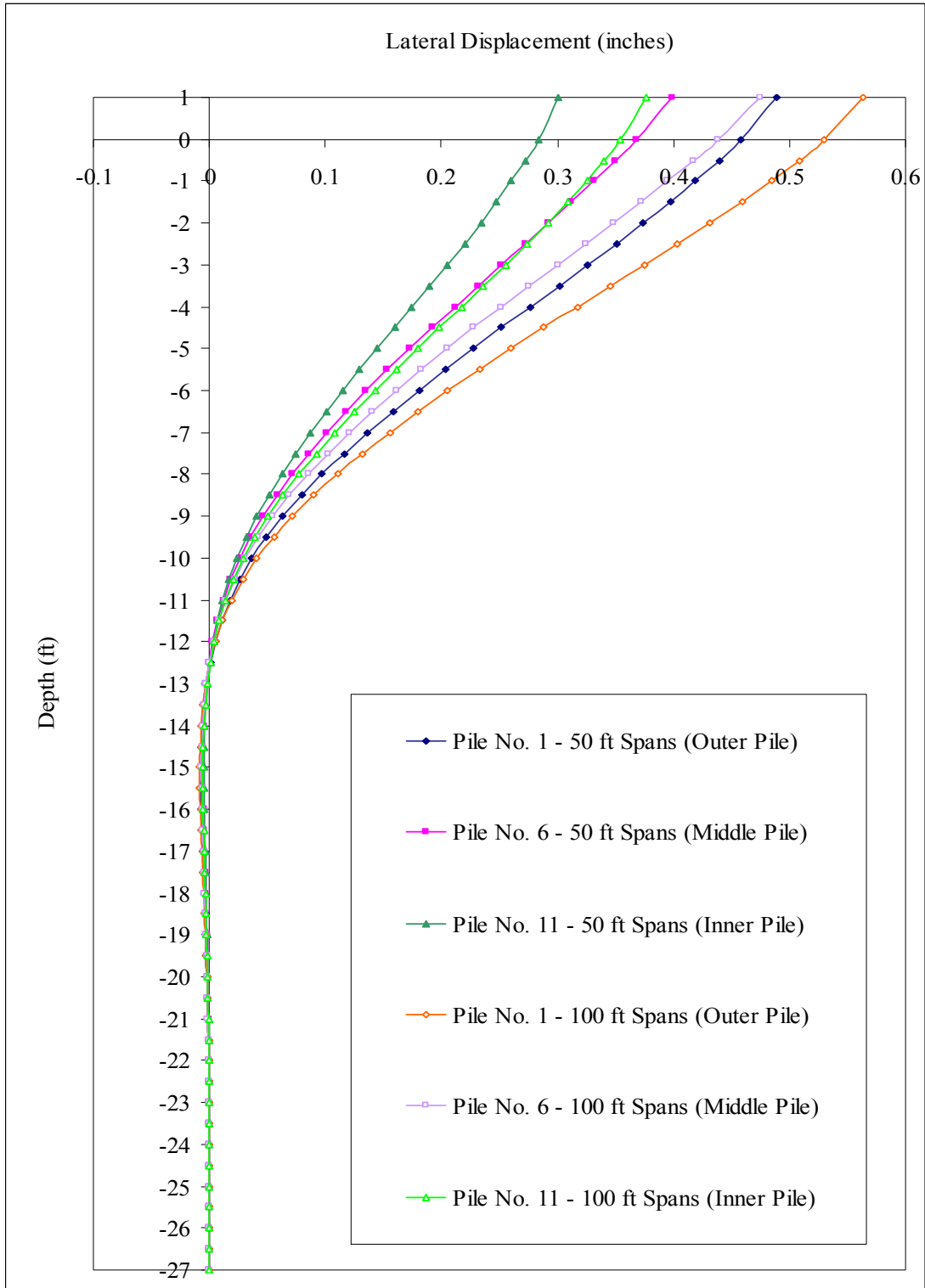


**Figure 9.25 – Lateral Displacement of End-Bearing Piles in 9 ft Deep Predrilled Holes at Different Locations in the Abutment of Bridges with 800 ft Radius and 800 ft Length ( $\Delta T_{\text{slab}} = 120^\circ \text{ F}$ ,  $\Delta T_{\text{the rest}} = 90^\circ \text{ F}$ )**

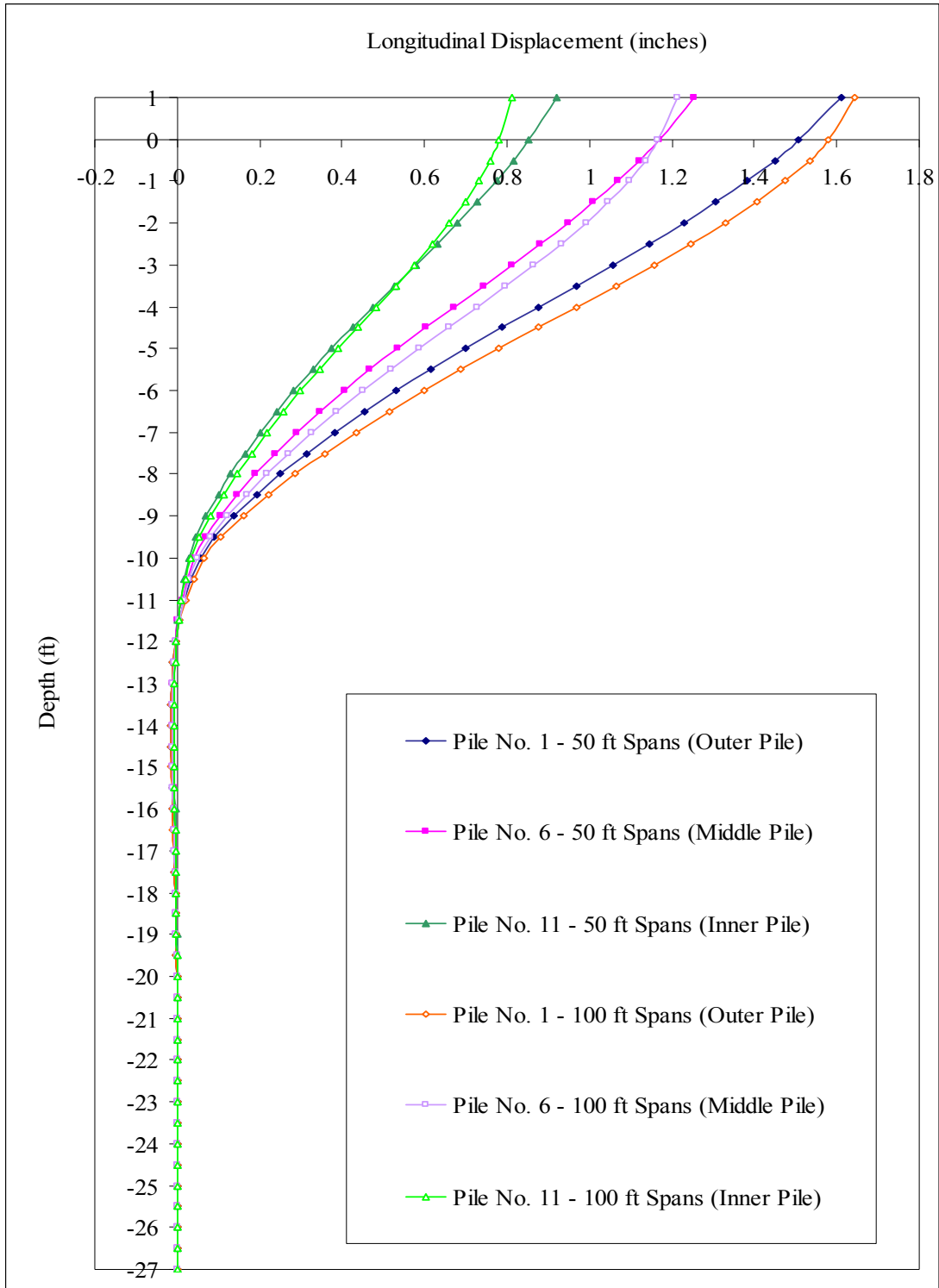


**Figure 9.26 – Longitudinal Displacement of End-Bearing Piles in 9 ft Deep Predrilled Holes at Different Locations in the Abutment of Bridges with 800 ft Radius and 800 ft Length ( $\Delta T_{\text{slab}} = 120^\circ \text{ F}$ ,  $\Delta T_{\text{the rest}} = 90^\circ \text{ F}$ )**

### 9.3 Conclusions

The following conclusions are drawn from the study of the behavior of end-bearing piles in various soil profile types of curved IAB's investigated in this chapter:

1. Curved IAB's with both 50 ft and 100 ft spans and with piles in very stiff clay soil profile or with piles in 15 ft deep predrilled holes filled with loose sand have partially plastic hinges at one place in the piles starting at a location of 0.5 ft to 1 ft below the bottom of the abutment.
2. For piles in 5 ft and 9 ft deep predrilled holes filled with loose sand, the location of the partially plastic hinges in the piles is at two places. The first location is at 0.5 ft below the bottom of the abutment. The second location is at the connection between the loose sand layer and the very stiff clay layer.
3. The partially plastic region in the piles for curved IAB's with 100 ft spans is slightly longer compared to the partially plastic region for curved IAB's with 50 ft spans.
4. An increase in the number of spans can reduce the maximum equivalent stress in the piles and the maximum lateral displacement of a bridge superstructure.
5. The introduction of predrilled holes filled with loose sand can reduce the von Mises or equivalent stress and the displacements in the piles. It is shown that piles in 9 feet deep predrilled holes filled with loose sand have a significant reduction in the equivalent stress and the displacements in the piles when compared with piles in 5 ft deep

predrilled holes filled with loose sand. The depth increase of predrilled holes deeper than 9 ft will further reduce the equivalent stress and the displacements in the piles but the rate of reduction is much smaller than that of 9 ft deep predrilled holes.

6. The pile at the outermost radius of the abutment experiences the highest equivalent stress as well as the highest lateral and longitudinal displacements. These values start to decrease to the lowest values for a pile which is at the innermost radius of the abutment.

## CHAPTER 10

### CONCLUSIONS AND RECOMMENDATIONS

Based on the finite element analyses of the three-dimensional models of different types of curved integral abutment bridges (hereafter referred to as curved IAB's) and piles, the following conclusions and a summary table are drawn for the design and construction of curved IAB's:

1. The radius of curved IAB's is an important parameter in their design and construction. Curved IAB's with a larger radius and with piles in very stiff clay soil profile have a maximum stress intensity (stress concentration) in the piles less than that of curved IAB's with a smaller radius for bridge lengths up to 300 ft. It is the same for curved IAB's with piles in predrilled holes for bridge lengths up to 400 ft. Beyond those bridge lengths, curved IAB's with a smaller radius and with piles in all soil profile types, for the most part, have a maximum stress intensity in the piles less than that of curved IAB's with a larger radius as the bridge length is increased to 1200 ft.
2. The maximum lateral displacement of curved IAB's with a larger radius and with piles in very stiff clay soil profile is less than that of curved IAB's with a smaller radius for bridge lengths up to 400 ft. It is the same for curved IAB's with piles in predrilled holes for bridge lengths up to 600 ft. Beyond those bridge lengths, curved IAB's with a smaller radius, for the most part, have a maximum lateral displacement

less than that of curved IAB's with a larger radius as the bridge length is increased to 1200 ft.

3. Based on a 1200 ft bridge length, the maximum stress intensity (stress concentration) in the piles increases with an increase in radius. It will have the highest stress intensity value at an infinite radius (straight IAB's). The maximum lateral displacement of a bridge superstructure increases as the radius is increased until it reaches the highest lateral displacement value at a radius which is known to be larger than 2400 ft but is not determined in the scope of this study. The lateral displacement then starts to decrease to the lowest value at an infinite radius.
4. For straight IAB's, the maximum stress intensity (stress concentration) in the piles increases as the bridge length is increased. In the case of curved IAB's, the maximum stress intensity in the piles begins to increase at a shorter bridge length. As the bridge length is increased, the stress intensity in the piles continues to increase until it reaches its highest stress intensity value at a certain bridge length. Beyond that bridge length, it starts decreasing and continues to decrease as the bridge length is increased.
5. The maximum lateral displacement of a bridge superstructure of curved IAB's with a smaller radius begins to increase at a shorter bridge length. As the bridge length is increased, the lateral displacement continues to increase until it reaches its highest lateral



displacement value at a certain bridge length. Beyond that bridge length, it starts decreasing and continues to decrease as the bridge length is increased. As the radius becomes larger (a 1200 ft radius or larger in this study), the maximum lateral displacement continues to increase with the increase in bridge length.

6. A temperature increase of 30° F results in increasing both the maximum stress intensity (stress concentration) in the piles and the lateral displacement of a bridge superstructure. The increase in the maximum stress intensity in the piles of curved IAB's with 50 ft spans is greater than that of curved IAB's with 100 ft spans. The stress intensity increase in the piles of curved IAB's with 50 ft spans and a smaller radius is greater than that of curved IAB's with a larger radius. As the span length is increased from 50 ft to 100 ft, the stress intensity increase in the piles of curved IAB's with a smaller radius is less than that of curved IAB's with a larger radius.
7. The maximum lateral displacement increase of curved IAB's with 50 ft spans due to the temperature increase is greater than that of curved IAB's with 100 ft spans. Curved IAB's with a smaller radius have a maximum lateral displacement increase due to the temperature increase greater than that of curved IAB's with a larger radius.
8. The introduction of predrilled holes filled with loose sand can reduce both the maximum stress intensity (stress concentration) in the piles and the maximum lateral displacement of a bridge superstructure.

From the analyses, it is shown that 9 feet deep predrilled holes filled with loose sand have a significant reduction in the pile stress intensity and the lateral displacement of a bridge superstructure when compared with 5 ft deep predrilled holes filled with loose sand. The depth increase of predrilled holes deeper than 9 ft will further reduce the stress intensity in the piles and the lateral displacement of a bridge superstructure, but the rate of reduction is much smaller than that of 9 ft deep predrilled holes. Curved IAB's with a smaller radius have a reduction rate less than that of curved IAB's with a larger radius. Curved IAB's with 50 ft spans have a reduction rate greater than that of curved IAB's with 100 ft spans.

9. In some cases, the maximum stress intensity (stress concentration) in the piles will increase when predrilled holes are introduced, especially for curved IAB's with 100 ft spans and a smaller radius. According to Greimann, Amde, and Yang [1.45], the displacements of the piles decrease the vertical load carrying capacity of the piles. While the vertical load (self weight of a bridge superstructure) is constant, the displacements in lateral, longitudinal, and twisting of the piles in predrilled holes are greater than that of the piles without predrilled holes which result in the increase in the pile stress intensity at some bridge lengths of curved IAB's. Therefore, it can be concluded that a difference in the arrangement of pile groups due to different bridge lengths of curved IAB's with different radii results in the stress

intensity increase in the piles in predrilled holes, at some bridge lengths, when compared to the piles without predrilled holes. It is shown that the increase in the radius and in the depth of predrilled holes decreases the stress intensity increase in the piles due to the introduction of predrilled holes.

10. An increase in the number of spans can reduce both the maximum stress intensity (stress concentration) in the piles and the maximum lateral displacement of a bridge superstructure. Curved IAB's with a smaller radius, for the most part, have a reduction rate greater than that of curved IAB's with a larger radius. Therefore, it is recommended to increase the number of spans or decrease the span length wherever it is considered feasible.
11. The difference in the maximum stress intensity (stress concentration) in the piles and the maximum lateral displacement of a bridge superstructure between friction and end-bearing piles in curved IAB's is relatively small. The difference in the maximum stress intensity between two types of piles is approximately 2%. The difference in the maximum lateral displacement of a bridge superstructure between two types of piles is between 0.02 inch and 0.83 inch.
12. Curved IAB's with both 50 ft and 100 ft spans and with piles in very stiff clay soil profile or with piles in 15 ft deep predrilled holes filled with loose sand have partially plastic hinges in the piles at one place starting at a location of 0.5 ft to 1 ft below the bottom of the abutment.

For piles in 5 ft and 9 ft deep predrilled holes filled with loose sand, the location of the partially plastic hinges in the piles is at two places. The first location is at 0.5 ft below the bottom of the abutment. The second location is at the connection between the loose sand layer and the very stiff clay layer. The partially plastic region in the piles for curved IAB's with 100 ft spans is slightly longer compared to the partially plastic region for curved IAB's with 50 ft spans.

13. The pile at the outermost radius of the abutment experiences the highest stress intensity as well as the highest lateral and longitudinal displacements. These values start to decrease to the lowest values for a pile which is at the innermost radius of the abutment.
14. It is recommended that piles in curved IAB's should be oriented about their weak axis and perpendicular to the bridge center line to allow for bending primarily about the weak axis.
15. The current study considered two soil profiles. Other soil profiles different than those included in this study need to be investigated.
16. Approach slabs seem to be a major concern to the highway agencies in the United States and abroad. Future studies should investigate the connection between the approach slab and the abutment at one end and between the approach slab and approach roadway at the other end.
17. Curved IAB's with skewed abutments should be studied because, in some cases, the abutments of curved IAB's will not be perpendicular to the bridge center line as in this study.

**Table 10.1 – Summary of Curved Integral Abutment Bridges**

Parameter	Stress Intensity in the Piles	Lateral Displacement of Bridge Superstructure
Bridge Length Increase	<ul style="list-style-type: none"> <li>• Curved IAB's with a larger radius have a stress intensity in the piles less than that of curved IAB's with a smaller radius for bridge lengths up to 300 ft and 400 ft.</li> <li>• Beyond these bridge lengths, curved IAB's with a smaller radius, for the most part, have a stress intensity in the piles less than that of curved IAB's with a larger radius as the bridge length is increased to 1200 ft.</li> </ul>	<ul style="list-style-type: none"> <li>• Curved IAB's with a larger radius have a lateral displacement less than that of curved IAB's with a smaller radius for bridge lengths up to 400 ft and 600 ft.</li> <li>• Beyond these bridge lengths, curved IAB's with a smaller radius, for the most part, have a lateral displacement less than that of curved IAB's with a larger radius as the bridge length is increased to 1200 ft.</li> </ul>
Temperature Increase	<ul style="list-style-type: none"> <li>• For 50 ft spans, curved IAB's with a smaller radius have a pile stress intensity increase greater than that of curved IAB's with a larger radius.</li> <li>• For 100 ft spans, curved IAB's with a smaller radius have a pile stress intensity increase less than that of curved IAB's with a larger radius.</li> <li>• Curved IAB's with 50 ft spans have a pile stress intensity increase greater than that of curved IAB's with 100 ft spans.</li> </ul>	<ul style="list-style-type: none"> <li>• Curved IAB's with a smaller radius have a lateral displacement increase greater than that of curved IAB's with a larger radius.</li> <li>• Curved IAB's with 50 ft spans have a lateral displacement increase greater than that of curved IAB's with 100 ft spans.</li> </ul>

**Table 10.1 (Continued) – Summary of Curved Integral Abutment Bridges**

Parameter	Stress Intensity in the Piles	Lateral Displacement of Bridge Superstructure
Introduction of Predrilled Holes	<ul style="list-style-type: none"> <li>• Curved IAB's with a smaller radius have a pile stress intensity reduction less than that of curved IAB's with a larger radius.</li> <li>• Curved IAB's with 50 ft spans have a pile stress intensity reduction greater than that of curved IAB's with 100 ft spans.</li> </ul>	<ul style="list-style-type: none"> <li>• Curved IAB's with a smaller radius have a lateral displacement reduction less than that of curved IAB's with a larger radius.</li> <li>• Curved IAB's with 50 ft spans have a lateral displacement reduction greater than that of curved IAB's with 100 ft spans.</li> </ul>
Increase Number of Spans	<ul style="list-style-type: none"> <li>• Curved IAB's with a smaller radius, for the most part, have a pile stress intensity reduction greater than that of curved IAB's with a larger radius.</li> </ul>	<ul style="list-style-type: none"> <li>• Curved IAB's with a smaller radius, for the most part, have a lateral displacement reduction greater than that of curved IAB's with a larger radius.</li> </ul>
Pile Type	<ul style="list-style-type: none"> <li>• The difference in the maximum stress intensity in the piles between friction and end-bearing piles of curved IAB's is relatively small.</li> </ul>	<ul style="list-style-type: none"> <li>• The difference in the maximum lateral displacement of a bridge superstructure between friction and end-bearing piles of curved IAB's is relatively small.</li> </ul>

**Table 10.1 (Continued) – Summary of Curved Integral Abutment Bridges**

Parameter	Stress Intensity in the Piles	Lateral Displacement of Bridge Superstructure
Radius Increase	<ul style="list-style-type: none"> <li>• Curved IAB's with a smaller radius have a pile stress intensity decrease at a shorter bridge length range than that of curved IAB's with a larger radius.</li> <li>• Curved IAB's with a smaller radius range, for the most part, have a pile stress intensity increase less than that of curved IAB's with a larger radius range.</li> <li>• If the radius continues to increase from a radius larger than 2400 ft to infinity, the pile stress intensity increase will decrease until there is a relatively small increase in the pile stress intensity (<math>\approx 0\%</math>).</li> </ul>	<ul style="list-style-type: none"> <li>• Curved IAB's with a smaller radius have a lateral displacement decrease at a shorter bridge length range than that of curved IAB's with a larger radius.</li> <li>• Curved IAB's with a smaller radius range, for the most part, have a lateral displacement increase less than that of curved IAB's with a larger radius range.</li> <li>• If the radius continues to increase to infinity, the lateral displacement increase will decrease until there is a relatively small increase in the lateral displacement of curved IAB's (<math>\approx 0\%</math>).</li> </ul>

# BIBLIOGRAPHY

## CHAPTER 1

- 1.1 McMillan, R. K., and Henry, A. (1979). "Bridge Deck Joint-Sealing Systems, Evaluation and Performance Specification." *National Cooperative Highway Research Program Report 204*, Transportation Research Board, National Research Council, Washington, D.C.
- 1.2 Burke, M. P., Jr., Hopwood, T., Kazakavich, V., Keegan, C., Kratochvil, J., Lisle, F. N., Lwin, M., McKeel, W. T., Nicholson, R., Puccio, G. S., and Romack, G. P. (2003). "Bridge Deck Joint Performance." *National Cooperative Highway Research Program Report 319*, Transportation Research Board, National Research Council, Washington, D.C.
- 1.3 Wolde-Tinsae, A. M. (Amde M. Amde), Klinger, J. E., and Mullangi, R. (1988). "Bridge Deck Joint Rehabilitation or Retrofitting." AW089-327-046, FHWA/MD-89/12.
- 1.4 Burke, M. P., Jr. (1990). "Integral Bridges." *Transportation Research Record 1275*, Transportation Research Board, National Research Council, Washington, D.C., pp. 53-61.
- 1.5 Husain, I., and Bagnariol, D. (2000). "Design and Performance of Jointless Bridges in Ontario." *Transportation Research Record 1696*, Transportation Research Board, National Research Council, Washington, D.C., pp. 109-121.
- 1.6 Wolde-Tinsae, A. M. (Amde M. Amde), and Klinger, J. E. (1987). "The State-of-the-Art in Integral Abutment Bridge Design and Construction." AW087-313-046, FHWA/MD-87/04.



- 1.7 Wolde-Tinsae, A. M. (Amde M. Amde), et al. (1987). “*Performance and Design of Jointless Bridges.*” U.S. Department of Transportation, Federal Highway Administration.
- 1.8 Wolde-Tinsae, A. M. (Amde M. Amde), and Greimann, L.F. (1988). “General Design Details for Integral Abutment Bridges.” *Journal of Civil Engineering Practice*, BSCE/ASCE, ISSN: 0886-9685, Vol. 3, No. 2, pp. 7-20.
- 1.9 Wolde-Tinsae, A.M. (Amde M. Amde), Greimann, L.F., and Johnson, B. (1983). “Performance of Bridge Abutments.” *The Journal of the International Association for Bridge and Structural Engineering*, IABSE PERIODICA, pp. 17-34.
- 1.10 Wolde-Tinsae, A.M. (Amde M. Amde), Aggour, M.S., and Chini, S.A. (1987). “*Structural and Soil Provisions for Approaches to Bridges, Phase I.*” Maryland Department of Transportation.
- 1.11 Wolde-Tinsae, A.M. (Amde M. Amde), Aggour, M.S., Moumena, L., and Chini, S.A. (1989). “*Structural and Soil Provisions for Approaches to Bridges.*” AW089-321-046, FHWA/MD-89/12.
- 1.12 Wolde-Tinsae, A.M. (Amde M. Amde), and Aggour, M.S. (1990). “*Structural and Soil Provisions for Approaches to Bridges.*” AW089-321-046, FHWA/MD-90/01.
- 1.13 Moumena, L., Wolde-Tinsae, A.M. (Amde M. Amde), and Aggour, M.S. (1990). “Analysis of Approaches to Bridges.” *Proceedings of the Second NSF Sponsored Workshop on Bridge Engineering Research in Progress*, University of Nevada, Reno.

- 1.14 Moumena, L., and Wolde-Tinsae, A.M. (Amde M. Amde). (1991). "Plasticity Analysis of Abutment Lateral Effect on Bridge Approaches." *Proceedings of the 13th Canadian Congress of Applied Mechanics*, Winnipeg, Manitoba, Canada.
- 1.15 Wolde-Tinsae, A.M. (Amde M. Amde), Chini, S.A., and Moumena, L. (1993). "Finite Element Representation of Approach Slabs." *Proceedings of the Fifth International Conference on Computing in Civil and Building Engineering*, Anaheim, California, pp. 184-188.
- 1.16 Chini, S.A., Amde, A.M., and Aggour, M.S. (1993). "Drainage and Backfill Provisions for Approaches to Bridges." *Transportation Research Record 1425*, Transportation Research Board, National Research Council, Washington, D.C., pp. 45-53.
- 1.17 Burke, M. P., Jr. (1994). "Semi-Integral Bridges: Movements and Forces." *Transportation Research Record 1460*, Transportation Research Board, National Research Council, Washington, D.C., pp. 1-7.
- 1.18 Burke, M. P., Jr. (1996). "Elementalistic and Holistic Views for the Evaluation and Design of Structure Movements Systems." *Transportation Research Record 1541*, Transportation Research Board, National Research Council, Washington, D.C., pp. 1-7.
- 1.19 Burke, M. P., Jr., and Gloyd, C. S. (1997). "Emergence of Semi-Integral Bridges." *Transportation Research Record 1594*, Transportation Research Board, National Research Council, Washington, D.C., pp. 179-186.

- 1.20 Burke, M. P., Jr. (1997). "Structure Movement Systems Approach to Effective Bridge Design." *Transportation Research Record 1594*, Transportation Research Board, National Research Council, Washington, D.C., pp. 147-153.
- 1.21 Wolde-Tinsae, A. M. (Amde M. Amde), Greimann, L. F., and Johnson, B. (1983). "Performance of Integral Abutment Bridges." *Proceeding IABSE, International Association for Bridge and Structural Engineering*, Zurich, Switzerland, pp. 17-34.
- 1.22 Wolde-Tinsae, A. M. (Amde M. Amde), Klinger, J. E., and White, E. J. (1988). "Performance of Jointless Bridges." *Journal of Performance of Construction Facilities*, ASCE, Vol. 2, No. 2, pp. 111-125.
- 1.23 Burke, M. P., Jr. (1993). "Integral Bridges: Attributes and Limitations." *Transportation Research Record 1393*, Transportation Research Board, National Research Council, Washington, D.C., pp. 1-8.
- 1.24 Oesterle, R. G., Refai, T. M., Volz, J. S., Scanlon, A., and Weiss, W. J. (2002). "*Jointless and Integral Abutment Bridges: Analytical Research and Proposed Design Procedures*." Final Report to FHWA, Washington, D.C.
- 1.25 Wolde-Tinsae, A.M. (Amde M. Amde), Greimann, L.F., and Yang, P.S. (1982). "Non-linear Pile Behavior in Integral Abutment Bridges." HR-227, ISU-ERI-Ames 82123.
- 1.26 Yang, P.S., Wolde-Tinsae, A.M. (Amde M. Amde), and Greimann, L.F. (1982). "Non-linear Finite Element Study of Piles in Integral Abutment Bridges." ERI 1501, ISU-ERI-Ames-83068.

- 1.27 Greimann, L.F., Edwards, S., and Wolde-Tinsae, A.M. (Amde M. Amde). (1985). "Simplified Model for Piles in Integral Abutment Bridges." *1985 Canadian Society for Civil Engineering Annual Conference*, Saskatoon, Saskatchewan.
- 1.28 Greimann, L. F., Wolde-Tinsae, A. M. (Amde M. Amde), and Yang, P.S. (1987). "Finite Element Model for Soil-Pile Interaction in Integral Abutment Bridges." *International Journal of Computers and Geotechnics*, Elsevier Applied Science Publishers Ltd., England, Vol. 4, pp. 127-149.
- 1.29 Greimann, L. F., and Wolde-Tinsae, A. M. (Amde M. Amde). (1988). "Design Model for Pile in Jointless Bridges." *Journal of Structural Engineering*, ASCE, Vol. 114, No. 6, pp. 1354-1371.
- 1.30 Amde, A.M., Chini, S.A., and Mafi, M. (1997). "Experimental Study of Piles in Integral Abutment Bridges." *International Journal of Geotechnical and Geological Engineering*, Vol. 15, pp. 343-355.
- 1.31 Abendroth, R. E., Greimann, L. F., and Ebner, P. B. (1989). "Abutment Pile Design for Jointless Bridges." *Journal of Structural Engineering*, ASCE, Vol. 115, No. 11, pp. 2914-2929.
- 1.32 Lawver, A., French, C., and Shield, C. K. (2000). "Field Performance of Integral Abutment Bridge." *Transportation Research Record 1740*, Transportation Research Board, National Research Council, Washington, D.C., pp. 108-117.

- 1.33 Soltani, A. A., and Kukreti, A. R. (1992). "Performance Evaluation of Integral Abutment Bridges." *Transportation Research Record 1371*, Transportation Research Board, National Research Council, Washington, D.C., pp. 17-25.
- 1.34 Thippeswamy, H. K., and Gangarao, H. V. S. (1995). "Analysis of In-Service Jointless Bridges." *Transportation Research Record 1476*, Transportation Research Board, National Research Council, Washington, D.C., pp. 162-170.
- 1.35 Alampalli, S., and Yannotti, A. P. (1998). "In-Service Performance of Integral Bridges and Jointless Decks." *Transportation Research Record 1624*, Transportation Research Board, National Research Council, Washington, D.C., pp. 1-7.
- 1.36 Wasserman, E. P. (1987). "Jointless Bridge Decks." *AISC Engineering Journal*, Vol. 24, No. 3, pp. 93-100.
- 1.37 Kunin, J., and Alampalli, S. (2000). "Integral Abutment Bridges: Current Practice in United States and Canada." *Journal of Performance of Construction Facilities*, ASCE, Vol. 14, No. 3, pp. 104-111.
- 1.38 Jorgenson, J. L. (1983). "Behavior of Abutment Piles in an Integral Abutment in Response to Bridge Movements." *Transportation Research Record 903*, Transportation Research Board, National Research Council, Washington, D.C., pp. 72-79.
- 1.39 Burke, M. P., Jr. (1990). "Integral Bridge Design Is on the Rise." *Modern Steel Construction*, AISC, Vol. 30, No. 4, pp. 9-11.

- 1.40 Greimann, L. F., Wolde-Tinsae, A. M. (Amde M. Amde), and Yang, P. S. (1988). "End-Bearing Pile in Jointless Bridges." *Journal of Structural Engineering*, ASCE, Vol. 114, No. 8, pp. 1870-1884.
- 1.41 Burke, M. P., Jr. (1987). "Bridge Approach Pavements, Integral Bridges, and Cycle Control Joints." *Transportation Research Record 1113*, Transportation Research Board, National Research Council, Washington, D.C., pp. 54-65.
- 1.42 Griton, D. D., Hawkinson, T. R., and Greimann, L. F. (1991). "Validation of Design Recommendations for Integral-Abutment Piles." *Journal of Structural Engineering*, ASCE, Vol. 117, No. 7, pp. 2117-2134.
- 1.43 Burke, M. P., Jr. (1993). "The Design of Integral Concrete Bridges." *Concrete International*, Vol. 15, No. 6, pp. 37-42.
- 1.44 Arockiasamy, M., Butrieng, N., and Sivakumar, M. (2004). "State-of-the-Art Integral Abutment Bridges: Design and Practice" *Journal of Bridge Engineering*, ASCE, Vol. 9, No. 5, pp. 497-506.
- 1.45 Greimann, L. F., Wolde-Tinsae, A. M. (Amde M. Amde), and Yang, P. S. (1985). "Effects of Predrilling and Layered Soils on Piles." *Journal of Geotechnical Engineering*, ASCE, Vol. 111, No. 1, pp. 18-31.
- 1.46 Faraji, S., Ting, J. M., Crovo, D. S., and Ernst, H. (2001). "Nonlinear Analysis of Integral Bridges: Finite-Element Model." *Journal of Geotechnical and Geoenvironmental Engineering*, ASCE, Vol. 127, No. 5, pp. 454-461.
- 1.47 Greimann, L. F., Wolde-Tinsae, A. M. (Amde M. Amde), and Yang, P. S. (1983). "Skewed Bridges with Integral Abutments." *Transportation Research*

*Record 903*, Transportation Research Board, National Research Council, Washington, D.C., pp. 64-72.

- 1.48 Haj-Najib, R. (2002). “*Integral Abutment Bridges with Skew Angles.*” PhD thesis, University of Maryland, College Park.
- 1.49 Oesterle, R. G., Tabatabai, H., and Lawson, T. J. (2002). “*Jointless and Integral Abutment Bridges: Experimental Research and Field Studies.*” Final Report to FHWA, Washington, D.C.

## CHAPTER 2

- 2.1 Reynolds, J. C., and Emanuel, J. H. (1974). “Thermal Stresses and Movements in Bridges.” *Journal of the Structural Division*, ASCE, Vol. 100, No. 1, pp. 63-78.
- 2.2 Berwanger, C. (1970). “Thermal Stresses in Composite Bridges.” *Proceedings, ASCE Specialty Conference on Steel Structures*, Engineering Extension Series, NO. 15, University of Missouri-Columbia, Columbia, Mo., pp. 27-36.
- 2.3 Emerson, M. (1973). “Bridge Temperatures for Setting Bearings and Expansion Joints.” *TRRL Report LR561*, Department of Transport, Crowthorne, England.
- 2.4 Emerson, M. (1976). “Bridge Temperatures Estimated from Shade Temperatures.” *TRRL Report LR696*, Department of Transport, Crowthorne, England.

- 2.5 Emerson, M. (1981). "Thermal Movements in Concrete Bridges Field Measurements and Method of Prediction." *ACI Publication Sp-70*, Vol. 1.
- 2.6 Roeder, C.W., and Moorty, S. (1990). "Thermal Movements in Bridges." *Transportation Research Record 1290*, Transportation Research Board, National Research Council, Washington, D.C., pp. 135-143.
- 2.7 Krauss, P. D., and Rogalla, E. A. (1996). "Transverse Cracking in Newly Constructed Bridge Decks." *National Cooperative Highway Research Program Report 380*, Transportation Research Board, National Research Council, Washington, D.C.
- 2.8 Abendroth, R. E., and Greimann, L. F. (1989). "A Rational Design Approach for Integral Abutment Bridge Piles." *Transportation Research Record 1223*, Transportation Research Board, National Research Council, Washington, D.C., pp. 12-23.
- 2.9 Imbsen, R. A., Vandershaf, D. E., Schamber, R. A., and Nutt, R. V. (1985). "Thermal Effects in Concrete Bridge Superstructures." *National Cooperative Highway Research Program Report 276*, Transportation Research Board, National Research Council, Washington, D.C.
- 2.10 *Climatic Atlas of the United States*. (1968). U.S. Department of Commerce, Ashville, North Carolina.
- 2.11 Dilger, W. H., Ghali, A., Chan, M. S., and Maes, M. A. (1983). "Temperature-Induced Stressess in Composite Box-Girder Bridges." *Journal of Structural Engineering*, ASCE, Vol. 109, No. 6, pp. 1460-1478.



- 2.12 Fu, H. C., Ng, S. F., and Cheung, M. S. (1990). "Thermal Behavior of Composite Bridges." *Journal of Structural Engineering*, ASCE, Vol. 116, No. 12, pp. 3302-3323.
- 2.13 Duffie, J. A., and Beckman, W. A. (1974). "*Solar Energy Thermal Processes*." John Wiley and Sons, Inc., New York, N.Y.
- 2.14 Elbadry, M. M., and Ghali, A. M. (1983). "Temperature Variations in Concrete Bridges." *Journal of Structural Engineering*, ASCE, Vol. 109, No. 10, pp. 2355-2374.
- 2.15 Kreith, F. (1973). "*Principles of Heat Transfer*." 3<sup>rd</sup> Edition, Intext Educational Publishers, New York, N.Y.
- 2.16 Emanuel, J. H., and Hulsey, J. L. (1978). "Temperature Distributions in Composite Bridges." *Journal of the Structural Division*, ASCE, Vol. 104, No. 1, pp. 65-78.
- 2.17 Zuk, W. (1965). "Thermal Behavior of Composite Bridges-Insulated and Uninsulated." *Highway Research Record*, No. 76, pp. 231-253.
- 2.18 Narouka, M., Hirai, I., and Yamaguti, T. (1957). "Measurement of the Temperature of the Interior of the Reinforced Concrete Slab of the Shigita Bridge and Presumption of Thermal Stress." *Symposium of the Stress Measurements for Bridge and Structures*, Japan Society for the Promotion of Science, Proceeding, Tokyo, Japan, pp. 106-115.
- 2.19 Barber, E. S. (1957). "Calculation of Maximum Pavement Temperatures from Weather Reports." *Highway Research Board Bulletin 168*, pp. 1-8.

- 2.20 Zuk, W. (1965). "Simplified Design Check of Thermal Stresses in Composite Highway Bridges." *Highway Research Record*, No. 103, pp. 10-13.
- 2.21 Churchward, A., and Sokal, Y. J. (1981). "Prediction of Temperatures in Concrete Bridges." *Journal of the Structural Division*, ASCE, Vol. 107, No. 11, pp. 2163-2176.
- 2.22 Berwanger, C. (1983). "Transient Thermal Behavior of Composite Bridges." *Journal of Structural Engineering*, ASCE, Vol. 109, No. 10, pp. 2325-2339.
- 2.23 Ho, D., and Liu, C. H. (1989). "Extreme Thermal Loadings in Highway Bridges." *Journal of Structural Engineering*, ASCE, Vol. 115, No. 7, pp. 1681-1696.
- 2.24 Moorty, S., and Roeder, C.W. (1992). "Temperature Dependent Bridge Movements." *Journal of the Structural Division*, ASCE, Vol. 118, No. 4, pp. 1090-1105.
- 2.25 Roeder, C.W. (2003). "Proposed Design Method for Thermal Bridge Movements." *Journal of Bridge Engineering*, ASCE, Vol. 8, No. 1, pp. 12-19.
- 2.26 Moorty, S. (1991). "*Thermal Movements in Bridges*." PhD thesis, University of Washington, Seattle.
- 2.27 Soliman, M. H., and Kennedy, J. B. (1986). "Simplified Method for Estimating Thermal Stresses in Composite Bridges." *Transportation Research Record 1072*, Transportation Research Board, National Research Council, Washington, D.C.
- 2.28 Zuk, W. (1961). "Thermal and Shrinkage Stresses in Composite Beams." *Journal of American Concrete Institute*, Vol. 58, No. 3, pp. 327-340.

- 2.29 Liu, Y. N., and Zuk, W. (1963). "Thermoelastic Effects in Prestressed Flexural Members." *Journal of Prestressed Concrete Institute*, Vol. 8, No. 3, pp. 64-85.
- 2.30 Houk, I. E., Paxton, J. A., and Houghton, D. L. (1970). "Prediction of Thermal Stress and Strain Capacity of Concrete by Tests on Small Beams." *Journal of American Concrete Institute*, Vol. 67, No. 3, pp. 253-261.
- 2.31 Priestly, M. J. N. (1978). "Design of Concrete Bridges for Temperature Gradients." *Journal of American Concrete Institute*, No. 5, pp. 209-217.
- 2.32 Radolli, M., and Green, R. (1975). "Thermal Stresses in Concrete Bridge Superstructures under Summer Conditions." *Transportation Research Record* 547, Transportation Research Board, National Research Council, Washington, D.C., pp. 23-36.
- 2.33 Juhl, H. G. (1970). "Horizontal Thermal Movement of Curved Bridge Decks." *Journal of the Structural Division*, ASCE, Vol. 96, No. 10, pp. 2037-2044.

### CHAPTER 3

- 3.1 Gillespie, J. (1968). "Analysis of Horizontally Curved Bridges." *AISC Engineering Journal*, Vol. 5, No. 4, pp. 137-143.
- 3.2 Yoo, C. H., and Littrell, P. C. (1986). "Cross-Bracing Effects in Curved Stringer Bridges." *Journal of Structural Engineering*, ASCE, Vol. 112, No. 9, pp. 2127-2140.

- 3.3 Davidson, J. S., Keller, M. A., and Yoo, C. H. (1996). "Cross-Frame Spacing and Parametric Effects in Horizontally Curved I-Girder Bridges." *Journal of Structural Engineering*, ASCE, Vol. 122, No. 9, pp. 1089-1096.
- 3.4 Albaijet, H. M. O. (1999). "*Behavior of Horizontally Curved Bridges under Static Load and Dynamic Load from Earthquakes.*" PhD thesis, Illinois Institute of Technology, Chicago.
- 3.5 DeSantiago, E., Mohammadi, J., and Albaijat, H. M. O. (2005). "Analysis of Horizontally Curved Bridges Using Simple Finite-Element Models." *Practice Periodical on Structural Design and Construction*, ASCE, Vol. 10, No. 1, pp. 18-21.

#### CHAPTER 4

- 4.1 Bowles, J. E. (1997). "*Foundation Analysis and Design.*" McGraw-Hill Companies, Inc., New York, N.Y.
- 4.2 Xanthakos, P. P. (1995). "*Bridge Substructure and Foundation Design.*" Prentice-Hall, Inc., New Jersey.

#### CHAPTER 5

- 5.1 Powrie, W. (1997). "*Soil Mechanics: Concepts and Applications.*" Chapman & Hall, New York, N.Y.
- 5.2 Greimann, L. F., and Wolde-Tinsae, A. M. (Amde M. Amde) (1988). "Design Model for Pile in Jointless Bridges." *Journal of Structural Engineering*, ASCE, Vol. 114, No. 6, pp. 1354-1371.

- 5.3 Greimann, L. F., Wolde-Tinsae, A. M. (Amde M. Amde), and Yang, P. S. (1986). "Nonlinear Analysis of Integral Abutment Bridges." *Journal of Structural Engineering*, ASCE, Vol. 112, No. 10, pp. 2263-2280.
- 5.4 Greimann, L. F., Yang, P. S., Edmunds, S. K., and Wolde-Tinsae, A. M. (Amde M. Amde). (1984). "*Design of Piles for Integral Abutment Bridges.*" Final Report, Iowa DOT Project HR-252, ISU-ERI-Ames 80026, Iowa State University, Ames.
- 5.5 Haj-Najib, R. (2002). "*Integral Abutment Bridges with Skew Angles.*" PhD thesis, University of Maryland, College Park.
- 5.6 Wolde-Tinsae, A. M. (Amde M. Amde), Greimann, L. F., and Yang, P. S. (1988). "End-Bearing Pile in Jointless Bridges." *Journal of Structural Engineering*, ASCE, Vol. 114, No. 8, pp. 1870-1884.